Département de Chimie
Université de Fribourg (Suisse)

Synthesis and Investigation of New Large Self-Assembled Supramolecules as Potential Electron Emitters

THESE

Présentée à la Faculté des Sciences de l'Université de Fribourg (Suisse) pour l'obtention du grade de *Doctor rerum naturalium*

Par

Bassam Alameddine
de Beyrouth (Liban)

Thèse N° 1440
Hélio-cop SA, Fribourg
2004

Acceptée par la Faculté des Sciences de l'Université de Fribourg (Suisse) sur la proposition du Prof. Dr. Titus A. Jenny, Dr. Niklaus Bühler (Ciba specialty chemicals), Prof. Dr. Robert Deschenaux (Université de Neuchâtel, Suisse) et Prof. Dr. Carl-Wilhelm Schläpfer, président du jury.

Fribourg, le 16 mars 2004

Le directeur de thèse :
Titus Jenny
Prof. Dr. Titus A. Jenny

Le doyen :
D. Baeriswyl
Prof. Dr. Dionys Baeriswyl

To Abed, Amira, Bilal, Houssam, and Khaled

نصف ما أقوله لك لا معنى له لكنني أقوله ليكتمل معنى النصف الآخر

جبران خليل جبران

‘Half of what I say is meaningless but I say it so that the other half may reach you’

Gibran Khalil Gibran

Acknowledgment

I would like to express my gratefulness to Professor Dr. Titus A. Jenny for accepting me in his research group, for his guidance and for the valuable advices as well as all the discussions we had during the PhD period. I am also indebted to him for the insightful comments that helped me to improve the quality and readability of this manuscript.

I would also like to extend my gratitude to Dr. Niklaus Bühler and Professor Dr. Robert Deschenaux for the time they spent for reading this work and to their valuable feedback.

The present and the previous heads of the department; Professors Thomas Bally, Carl-Wilhelm Schläpfer, and Albert Gossauer are acknowledged for confining me, during all this stay, the assistantship position. Priv. Doc. Dr. Norbert Engel is kindly appreciated for organizing the students' practical courses.

I wish to express my sincere appreciation to Oliver Scheidegger (analytical service, ETHZ) who carried out the MALDI-TOF characterization of the final products. Special thanks to Dr. Massoud Dadras and Mireille LeBoeuf (Institute of Microtechnology, University of Neuchâtel) for their joint collaboration and the SEM micrographs they provided. Dr. Jens Dittmer (Prof. Bodenhausen's group, EPFL) is thanked for the non-negligible effort and the practical courses he gave me on the solid state NMR instrument. I am also grateful to Fabien Tran (Prof. Wesolowski's group, University of Geneva) for the numerical calculations he did. I am thankful to David Scanu (Prof. Deschenaux's group, University of Neuchâtel) for the DSC and the POM investigations he carried out.

Many thanks go to the analytical service at Fribourg University, in particular, Freddy Nyddegger, Inge Müller (Mass spectra) as well as Felix Fehr (NMR spectra).

Christophe Eggertswyler, Roger Mafua, Ludwig Muster, Martine Poffet, and Olivier Aebischer are all admired for their patience to review the manuscript. Krzysztof Piech is acknowledged for fixing the computer.

My thanks will also extend to those who participated to this project: Zeinab Cheiab, Jöel Kühni, Claire-Lise Ciana (Advanced Practical work), and particularly to both Olivier Aebischer (Diploma work) as well as Corinne Savary.

My appreciation goes to all the Chemistry department members in general and to the organic section in particular. All of those whose kind support greatly facilitated this work are thanked: Christophe Allemann, Fosca Gattoni, Vroni Hüber, Tibor Kiss, Fabrice Levrat, Geraldine Martin, Jaime Lage Robles, Simona Ruccareanu, and Anne Schuwey. Christophe Eggertswyler and Roger Mafua esteemed for their encouragement, in addition to the good moments and the fruitful discussions we had over the period of this PhD stay.

Last but not the least my gratitude goes to Philippe Rime, Noelle Chassot, Lucienne Rouillet, Xavier Hanselmann, Bernadette Kuhn-Piccand, and Hubert Favre of the central service for the distribution of chemicals. Many thanks to Emerith Brügger, Marie-Thérèse Dafflon, and Verena Schwalm (secretary) for making the administrative work goes smoothly. Alphonse Crottet (mechanical atelier) is acknowledged for his disposition and to the many services he offered.

This project was supported by the Swiss National Science Foundation.

Contents

List of abbreviations

Summary 1

Résumé 3

I. Theoretical part 5

---

1. Introduction 7

2. Self-organization 9

2.1 An efficient tool for supramolecular control 9

2.2 Hydrogen bonding 11

2.2.1 Introduction 11

2.2.2 Selected examples 11

2.3 Metal complexes 14

2.4 Arene-Arene interaction 16

2.4.1 Introduction 16

2.4.2 Disc-shaped molecules 18

2.4.3 Twisted PAHs 22

2.5 Combined systems 25

2.5.1 Introduction 25

2.5.2 π- and H- Bonding 25

2.5.3 π-stacking and Metal complexes 28

3. Field electron emission (FEE) 31

3.1 Introduction 31

3.2 Advantages and future perspectives 31

3.3 FEE Theory 32

3.4 Field Emission displays (FED) 34

4. Organic flat panel displays 39

4.1 General considerations 39

4.2 Field emission from diamond and diamond like films 40

4.2.1 FEE from good quality diamond films 40

4.2.2 FEE from DLC films 41
4.2.3 FEE from Diamond coatings 41
4.2.4 Conclusion 42
4.3 CNTs field emitters 42
4.3.1 FEE from CNT films 43
4.3.2 FEE from well-dispersed CNTs 45
4.3.3 Conclusion 46
5. Design features of a new organic FED 47
5.1 Toward a self-assembled field emitter 47
5.2 Investigation of new nitrogen-containing PAH 49

II. Results and Discussion 51

6. General strategies to produce HBC 53
6.1 Symmetrical synthesis pathway 58
6.1.1 Tolane synthesis from stilbene 58
6.1.2 Tolane synthesis in a step-by-step Sonogashira cross-coupling 59
6.1.3 Tolane synthesis from a one-pot Sonogashira cross-coupling 60
6.1.4 Trimerization of tolane derivative **25** 61
6.2 Asymmetrical synthesis pathway 61
6.3 One-pot synthesis of HBC derivative 63
6.4 Development of a new precursor 64
7. Primers syntheses 67
7.1 Introduction 67
7.2 HBC with R = CF_3 67
7.3 HBC with R = 4-$PhCF_3$ and 3,5-$Ph(CF_3)_2$ 75
7.3.1 Syntheses of the brominated precursors 76
7.3.2 Synthesis of 4,4'-bis-(trifluoromethyl)diphenylacetylene (To-$PhCF_3$) 79
7.3.3 Synthesis of 3,3',5,5'-tetrakis-(trifluoromethyl)diphenylacetylene (To-3,5$PhCF_3$) 80
7.3.4 HBC with R=3,5-$Ph(CF_3)_2$ 82
7.4 HBC with R = OCF_3 85
7.5 HBC with R = SCF_3 88
7.5.1 Synthetical approach 88
7.5.2 SEM investigation 90
7.6 Conclusion 92
8. HBCs bearing long perfluorinated chains 95
8.1 Introduction 95

8.2 HBC with R = PhRf$_6$ 95

9. Perfluorinated HBCs with alkyl intercalators 101

9.1 HBC with R = Rf$_{2,8}$ and PhRf$_{2,8}$ 101

9.1.1 Synthetical strategy 101

9.1.2 DSC investigation of HBC-Rf$_{2,8}$ and HBC-PhRf$_{2,8}$ 110

9.2 HBC with R = Rf$_{4,8}$ and Rf$_{6,6}$ 111

9.2.1 Synthetical approach 111

9.2.2 Calorimetric analyses of HBC-Rf$_{4,8}$ and HBC-Rf$_{6,6}$ 118

9.2.3 Optical microscopy study of HBC-Rf$_{4,8}$ and HBC-Rf$_{6,6}$ 120

9.2.4 SEM investigation of HBC-Rf$_{4,8}$ and HBC-Rf$_{6,6}$ 122

10. HBCs with perfluoroalkyl alkoxy side chains 133

10.1 Synthetical attempt of HBC with R = ORf$_{4,8}$ 133

10.2 HBCs with phenoxy alkylated perfluoroalkyl substituents 136

10.2.1 Introduction 136

10.2.2 Tolane synthesis via Kumada and Suzuki cross-coupling 137

10.2.3 Tolane synthesis via Sonogashira cross-coupling 138

10.2.4 Trimerization and cyclodehydrogenation of **123** and **130** 140

10.2.5 DSC investigation of HBC-PhORf$_{4,8}$ and HBC-PhORf$_{6,6}$ 144

10.3 Conclusion 145

11. Nitrogen-containing polycondensed aromatic systems 147

11.1 Introduction 147

11.2 Synthesis of the perfluoroalkyl substituted precursors 150

11.3 Synthetical attempts of the perfluoroalkyl substituted trinaphthyl amine 151

11.3.1 Via a one-pot reaction 151

11.3.2 Using binaphthyl amine **144** as starting material 153

11.3.3 Oxidative cyclization of binaphthyl amine **144** 157

11.4 Conclusion 163

III. Conclusions and outlooks 165

12.1 HBCs bearing perfluorinated groups 167

12.2 N-containing PAH 168

IV. Experimental part 171

13. Analytical tools for characterizing PAHs 173

13.1 Optical spectroscopy 173
13.2 MALDI-TOF mass spectrometry 176
13.3 Solid-state NMR 183
14. General remarks 185
15. Synthesis of the HBC primers 187
15.1 HBC with R = CF_3 187
15.2 Tolane with R = *p*-$PhCF_3$ 191
15.3 HBC with R = 3,5-$Ph(CF_3)_2$ 194
15.4 HBC with R = OCF_3 197
15.5 HBC with R = SCF_3 201
16. Synthesis of the HBCs with long perfluorinated chains 205
16.1 Attempted synthesis of HBC with R = *p*-PhC_6F_{13} 205
16.2 HBC with R = $(CH_2)_2C_8F_{17}$ 209
16.3 Tolane with R = *p*-$Ph(CH_2)_2C_8F_{17}$ 213
16.4 HBC with R = $(CH_2)_4C_8F_{17}$ 220
16.5 HBC with R = $(CH_2)_6C_6F_{13}$ 223
16.6 Attempted synthesis of HBC with R = $O(CH_2)_4C_8F_{17}$ 226
16.7 HBC with R = *p*-$PhO(CH_2)_4C_8F_{17}$ 231
16.8 HBC with R = *p*-$PhO(CH_2)_6C_6F_{13}$ 239
17. Attempted synthesis of nitrogen-containing PAH 245
17.1 Synthesis of the perfluorinated binaphthyl amine compound 144 245
17.2 Attempted syntheses of the *N,N,N*-tris[4-(3,3,4,4,5,5,6,6,7,7,8,8,9,9,10,10-heptadecafluorodecyl)-1-naphthyl]amine 135 250
17.3 Synthesis of perfluorinated aryl amine derivatives 253

V. Annexes 255

A.1 Calorimetric data from DSC measurements 257
A.2 SEM micrographs of HBC-SCF_3 (71) 258
A.3 SEM micrographs of HBC-$Rf_{4,8}$ (114) 260
A.4 SEM micrographs of HBC-$Rf_{6,6}$ (115) 285

VI. References 293

VII. Curriculum Vitae 311

List of abbreviations

1,2,4-TCB	1,2,4-Trichlorobenzene
Ac	Acetyl
AFM	Atomic force microscopy
BTACl	Benzyltriethylammonium chloride
BTF	Benzyltrifluoride
CNT	Carbon nanotube
Col	Columnar
CP	Cross-polarization
CRT	Cathode ray tube
CVD	Chemical vapor deposition
D	Discotic
DLC	Diamond like carbon
DMA	*N, N*-Dimethylacetamide
DMF	*N, N*-Dimethylformamide
EI	Electron impact
ESI	Electrospray ionization
FC-72	Perfluoro-n-hexane
FEA	Field emission array
FED	Field emission display
FEE	Field electron emission
GC/MS	Gas capillary chromatography / mass spectrometry
HBC	Hexabenzo[*bc,ef,hi,kl,no,qr*]coronene
HPB	Hexaphenylbenzene
hpdec	High-power ^{1}H-decoupling
LC	Liquid crystalline
LCD	Liquid crystal displays
M	Molar
MALDI-TOF	Matrix-assisted laser desorption ionization-time of flight
MAS	Magic angle spinning
MWNT	Multiwalled nanotube
NEA	Negative electron affinity

NMR	Nuclear magnetic resonance
NQS	Non-quaternary suppression
OFET	Organic field effect transistors
OLED	Organic light emitting diodes
OTf	Triflate, trifluoromethanesulfonate
PAH	Polycyclic aromatic hydrocarbon
POM	Polarized optical microscopy
$Rf_{n,m}$	Perfluoroalkylated alkyl (*with n: number of aliphatic carbons, and m: number of perfluorinated carbons*)
SEM	Scanning electron microscopy
SS-NMR	Solid state nuclear magnetic resonance
SWNT	Single walled nanotube
TBABr	Tetrabutyl ammonium bromide
TEM	Transmission electron microscopy
T_g	Glass transition temperature
THF	Tetrahydrofuran
TLC	Thin layer chromatography
TMS	Trimethylsilyl
TMSA	Trimethylsilylacetylene
To	Tolane, Diphenylacetylene
UV	Ultraviolet
VIS	Visible

Summary

Nanotechnology, a research area that covers many scientific disciplines such as Medicine, Biology, Physics and Chemistry has found a great interest in research institutions and wide applications in industries. This is due to many reasons; from these we note the control down to the molecular level providing thereby a greatest efficiency and an important added value as a reason of the low cost of the fabricated molecules and devices. Molecular self-assembly, a phenomenon which employs weak, non-covalent molecular interactions to form well-defined supramolecular architectures is a promising trend that could be applied in nanotechnology to render the constituent molecules 'smarter' offering them the feature of self-organizing into functional nano-devices without having the necessity to be bound chemically to each other and allowing, therefore, for a self-healing property permitting the correction of any error that could arise during the assembly.

This work is interested in synthesizing specially designed disc-shaped polycyclic aromatic molecules that self-assemble by π-stacking into columnar architectures forming, therefore, nanometer-sized conductors. These latter can be applied in the domain of materials for the fabrication of many functional devices such as low cost field emission flat panel displays that excel over existing ones due to the ease of their manufacturing process, in addition to better properties expected, for instance, a free defect architectures, a lower power consumption, a higher brightness and a larger viewing angle.

In the first part of this work, large polycyclic aromatic disc shaped molecules; known as hexabenzocoronene derivatives (HBCs), which self assemble to one-dimensional conducting structures, have been synthesized and characterized. These compounds were decorated laterally with perfluoroalkylated alkyl chains offering them a teflon-like clad to avoid any lateral interaction between neighboring stacks. Different scanning electron microscopy techniques as well as calorimetric measurements have revealed a tremendous possibility of obtaining singular columnar stacks. Additionally, calorimetric measurement showed a high thermal and chemical stability of these compounds.

However, in order to immobilize these nano-sized columnar stacks on the electrode surface, specially designed primer molecules of HBC, bearing at their ends atoms like oxygen and sulfur atoms, were synthesized. Upon deposition of a monolayer of these molecules, the heteroatoms are expected to act as anchoring groups by chemically binding to the electrode surface assuring, therefore, a good adhesion between the substrate and the molecule on one hand and serving as a pattern or a template molecule for the remaining HBCs bearing long perfluorinated tails, on the other hand.

As a prospective extension to this work, another project that consisted of synthesizing a nitrogen-containing polyaromatic hydrocarbon (PAH) was also initiated. The advantage of such type of molecules is the low oxidation potential of the nitrogen atom with respect to carbon which will facilitate the electron emission and eventually the hole transport in the column leading to less power consumption.

Several synthetic strategies for this hitherto unknown target have been employed during this work but none of them led to the desired product so far due to the high steric hindrance in an intermediate product. Nevertheless, two perfluoroalkylated triaryl amine derivatives were synthesized, both products showing potential for an application as hole transport molecules in organic light emitting diodes (OLED).

Résumé

La nanotechnologie, domaine de recherche qui couvre plusieurs branches scientifiques en Médecine, Biologie, Physique et Chimie, est en pleine expansion dans les institutions de recherche et suscite un vif intérêt dans l'industrie vu ses prometteuses applications. Ceci est dû à plusieurs raisons, parmi lesquelles, on note le control à une échelle moléculaire ce qui augmente l'efficacité du procédé et diminue le coût en matière première. L'auto-assemblage moléculaire, phénomène qui implique les faibles interactions moléculaires non-covalentes, permet de former des architectures supramoléculaires bien définies. Cette propriété peut servir la nanotechnologie en rendant les molécules plus 'intelligentes' en leur offrant cette propriété d'auto-organisation en nanostructures fonctionnelles sans avoir besoin de former des liaisons chimiques entre elles, permettant donc une autocorrection de tout défaut qui pourrait avoir lieu durant l'assemblage.

Le but principal de ce travail est de synthétiser des molécules aromatiques polycycliques en forme de disques qui s'auto-assemblent par des interactions secondaires de leurs orbitaux π, formant alors des structures colonnaires qui pourraient être utilisées comme des nano-émetteurs d'électrons. Ces dernières peuvent avoir des applications potentielles dans le domaine des matériaux pour la fabrication de plusieurs outils fonctionnels comme, par exemple, des écrans plats à émission de champs. Ceux-ci surpassent les écrans plats qui s'appuient sur d'autres principes, comme par exemple, les cristaux liquides, grâce à leur facilité de fabrication, et de propriétés additionnelles telles que leurs structures sans défaut, une consommation d'énergie plus faible ou un angle de vision plus large.

Dans la première partie de cette étude, nous décrivons la synthèse et la caractérisation de dérivés d'une molécule aromatique en forme de disque, connue sous le nom de hexabenzocornène (HBC), qui s'auto-assemblent en structures colonnaires permettant une conductivité unidimensionnelle des électrons. Ces dérivés ont été décorés latéralement avec des chaînes perfluoroalkylées servant "d'enveloppe" au centre aromatique grâce à leurs propriétés anti-adhésives (Téflon) empêchant toute interaction intercolonnaire. Diverses mesures de microscopie électronique à balayage (MEB) ont révélé la possibilité d'obtenir des nanofilaments. De plus, des mesures calorimétriques (calorimétrie différentielle à balayage) ont montré la grande stabilité thermique et chimique de ces dérivés HBC.

Pourtant, afin d'assurer une fixation optimale de ces colonnes sur la surface de l'électrode, des dérivés HBC, portant des atomes d'oxygène et de soufre sur leurs extrémités, ont été synthétisés pour servir de molécules 'premières'. Une fois la couche monomoléculaire déposée sur la surface du substrat, les hétéroatomes vont agir comme des agents d'ancrages en se liant chimiquement au substrat, ce qui offrira alors une bonne adhésion entre l'électrode et la molécule. D'autre part, le centre polycyclique de ces HBC d'interface servira de base sur laquelle s'empileront les dérivés perfluoroalkylés qui seront déposés ultérieurement.

Un autre projet, considéré comme une extension prospective, a été exploré. Il consiste à synthétiser une molécule aromatique, en forme de disque, mais qui contient un atome d'azote. L'avantage principal apporté par une telle modification est le faible potentiel d'oxydation de l'azote par rapport au carbone, ce qui faciliterait l'émission électronique et, éventuellement, le transport cationique dans les colonnes et donc diminuerait l'énergie nécessaire au fonctionnement.

Plusieurs stratégies de synthèse de cette molécule, inconnue jusqu'à présent, ont été employées pendant ce travail, mais aucune d'entre elles n'a fourni le produit désiré, à cause de l'encombrement stérique d'un des produits intermédiaires. Néanmoins deux dérivés de triaryl amines contenant des chaînes perfluoroalkylés ont été synthétisés. Ces derniers montrent un grand potentiel comme molécules de transport cationique dans le domaine de diodes organiques émetteur de lumière (DOEL).

I. Theoretical part

1. Introduction

Supramolecular chemistry[1] or ‘chemistry beyond the molecule’ is a wide term that covers an immense new field of chemistry based on synthesizing and studying molecules whose cooperation affords totally new properties to the entire system. This interesting domain of research can also be considered as the most prominent imitation of nature that shows various examples emerging from cooperation between different constituents[2, 3]. The concepts developed in supramolecular chemistry are increasingly used in fields like materials science, surface science, sensor technology and nanotechnology[4].

However, to achieve the best efficacy, the cooperation between the different molecules involved must be precise in such a way that each one has a definite role and assembles in a ‘smart’ manner. An idea that gave rise to self-organization which employs weak, non-covalent molecular interactions to form well-defined supramolecular architectures, providing, therefore, novel properties with beforehand determined functionalities.

Contrarily to covalently bonded systems whose dissociation is irreversible, the advantages of non-covalently self-assembled molecules are reversibility and error correction; two properties that assure an immediate reassembly of the supramolecular entity after being exposed to an external influence[4, 5]. Several self-assembled chemical systems have been synthesized and investigated so far, from these we highlight some functional devices possessing promising applications in biology, mechanics, photonics, electronics, and catalysis[6].

The leading idea behind this work comprises a multidisciplinary research approach lying at the intersection between chemistry, physics and materials science. From a chemical point of view, we are interested in developing and synthesizing new large disc-shaped aromatic molecules that self-assemble into columnar like structures. Possessing good charge carrier mobilities, these nanometer-sized stacks can be employed as cold electron emitter sources and can, therefore, find many industrial applications in molecular electronics field such as the simple fabrication of flat panel displays.

We will summarize in the following chapters some important concepts that constitute the bases of this project: in the first part we will have an insight on self-organization phenomena showing the different types of non-covalent interactions, focusing on π-

stacking. In the second chapter we will evoke the theory of field electron emission revealing the advantages of it, summarizing the most important applications that can be based on this concept and concentrating on emerging commercially available field emission flat panel displays. Finally we will give emphasis to the organic devices used so far as promising candidates for field emission flat panel displays as well as the major drawbacks encountered when using them.

2. Self-organization

2.1 An efficient tool for supramolecular control

Self-assembly of organic molecules in solution and in the solid state leading to well-defined supramolecular architectures has revealed the paramount importance of weak reversible non-covalent interactions in constructing and controlling materials down to the molecular level. These interactions comprise mainly hydrogen bonding, metal coordination and π-stacking; three different types of weak bonding whose lone or combined presence affords outstanding properties to the supramolecular system. Self-organization relies upon complementary of size, shape, and varying the number of chemical functionalities capable of performing non-covalent bonding[7] giving rise to newly different chemical and physical properties as compared to the single building block, as we will see in the following sections. Furthermore, the reversibility of the non-covalent bonding excels that of the covalent ones, since the former can be restructured by simple changing of the medium parameters such as the concentration or the nature of solvent, when they are present in solution, and the substrate or the deposition technique, when they are engineered in the solid state to construct a variety of synthetic architectures[8]. Thus, self-assembly by weak interactions offers the possibility of a 'self-healing' network that can reassemble after being subjected to any external changing[5].

This class of novel materials has brought together supramolecular chemistry and materials science[9] opening new perspectives to chemists and physicists toward a nanometric control of materials and leads researchers to name it "supramolecular polymers" defining this new term as '*polymeric arrays of monomeric units that are brought together by reversible and highly directional secondary interactions, resulting in polymeric properties in dilute and concentrated solutions, as well as in the bulk. The monomeric units of the supramolecular polymers themselves do not possess a repetition of chemical fragments. The directionality and strength of the supramolecular bonding are important features of systems that can be regarded as polymers and that behave according to well-established theories of polymer physics*"[10].

In spite of the extreme efforts exerted by several chemists, since two decades, that have led to generate a wide variety of self-assembled supramolecules[8], we are still far from paving a way toward a suitable function of high importance to this new class of materials that surpasses the scientific curiosities. Only few applications are foreseen for some types of hydrogen bonded molecules as efficient polymers[11] on one hand, and for other promising discotic molecules in the field of molecular electronics, due to their strong π-interactions allowing their columnar structures to bear high charge carrier mobilities[12-14], on the other hand.

It is noteworthy that the most useful functions of self-assembly are found in nature[3, 15, 16]. Figure 2.1 illustrates one of the well-known examples on self-organization found in human body: microtubules. These latter have a crucial role in the organism since they control the movement of subcellular structures such as the separation of sister chromatids during mitosis, the transportation of proteins in neurons from the cell body down the axon to the synaptic region, etc. The most fascinating property in these proteins is the fact that they are dynamic: once the cell enters mitosis, the array is disassembled whereas the mitotic spindle is assembled as the cell prepares itself for chromatid separation and subsequent division. These microtubules are composed of individual protein subunit dimers known as tubulin that are arranged in a cylindrical and helical form in such a way to create a single microtubule[17].

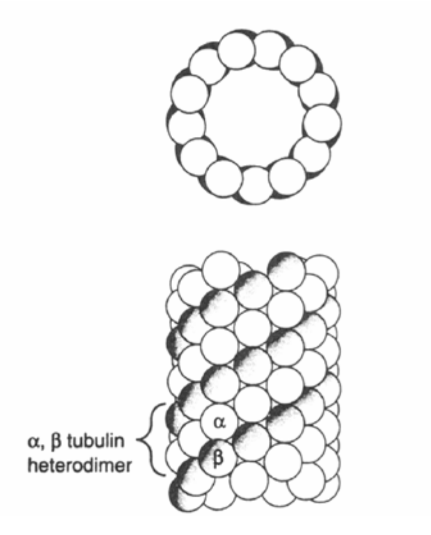

Figure 2.1. The assembled α, β-tubulin heterodimer. The top structure is a view of the microtubule from above, whereas the bottom structure is a view from the side.

We will present in the next sections a short overview on the three non-covalent interactions we evoked previously in addition to some examples showing few combined systems of these latter. It is worthwhile to note, however, that neither the biological systems[2, 3, 15, 16] nor the supramolecular assemblies held together by topological controls [18-20], as in rotaxanes or catenanes, will be discussed.

2.2 Hydrogen bonding

2.2.1 Introduction

Even though hydrogen bonds are fairly weak, they are one of the most widely used interaction principle in self-assembly due to their directionality, versatility, as well as its biological relevance[21]. Their weak force can be multiplied by increasing the number of interacting sites or by additional forces, such as liquid crystalline properties and phase separation; both properties that exclude the volume interaction[22]. Hydrogen bonding is based on the formation of donor-acceptor functions (D-A); hence, the strength of this type of interactions depends on the nature and the arrangement of the donors and the acceptors and mostly on the solvent nature, when they are present in solution[9]. Supramolecular chemists widely employ two-dimensional hydrogen bonded networks, which are usually composed of rigid, flat and heterocyclic molecules[7]. Various hydrogen bonded network have been obtained, so far, using the hitherto mentioned principle of donor-acceptor functions (D-A), from these we note: zeolites-like[23], stacked columns[24, 25], interpenetrating molecular ladders[26], capsules[7, 27] as well as various molecules assembled in the solid state[28].

2.2.2 Selected examples

Very stable hydrogen-bonded complexes have been first made by the association of linear arrays bearing three hydrogen bonding sites[21, 22, 29]. The association constant of these molecules have been found to be dependent on the arrangement of the donor-acceptor positions where, as figure 2.2 depicts, the complex DDD-AAA has the highest association constant ($>10^5$ M^{-1}) due to the lack of any secondary interactions; that occur when diagonally opposed sites of the same type repel each other[10]. The most stable complexes synthesized so far are the quadruple hydrogen bonded systems[30, 31] whose hydrogen-bonding sites arrangements offer the possibility of having a broad spectrum of association constants, ranging from 10^2-10^8 M^{-1}[32], and hence, allowing these systems to exhibit interesting polymer-like properties[33]. Moreover, some of these latter have shown potential electronic properties[34] whereas others were found to be acting as 'smart materials' changing reversibly their degree of association when subjected to UV light[35].

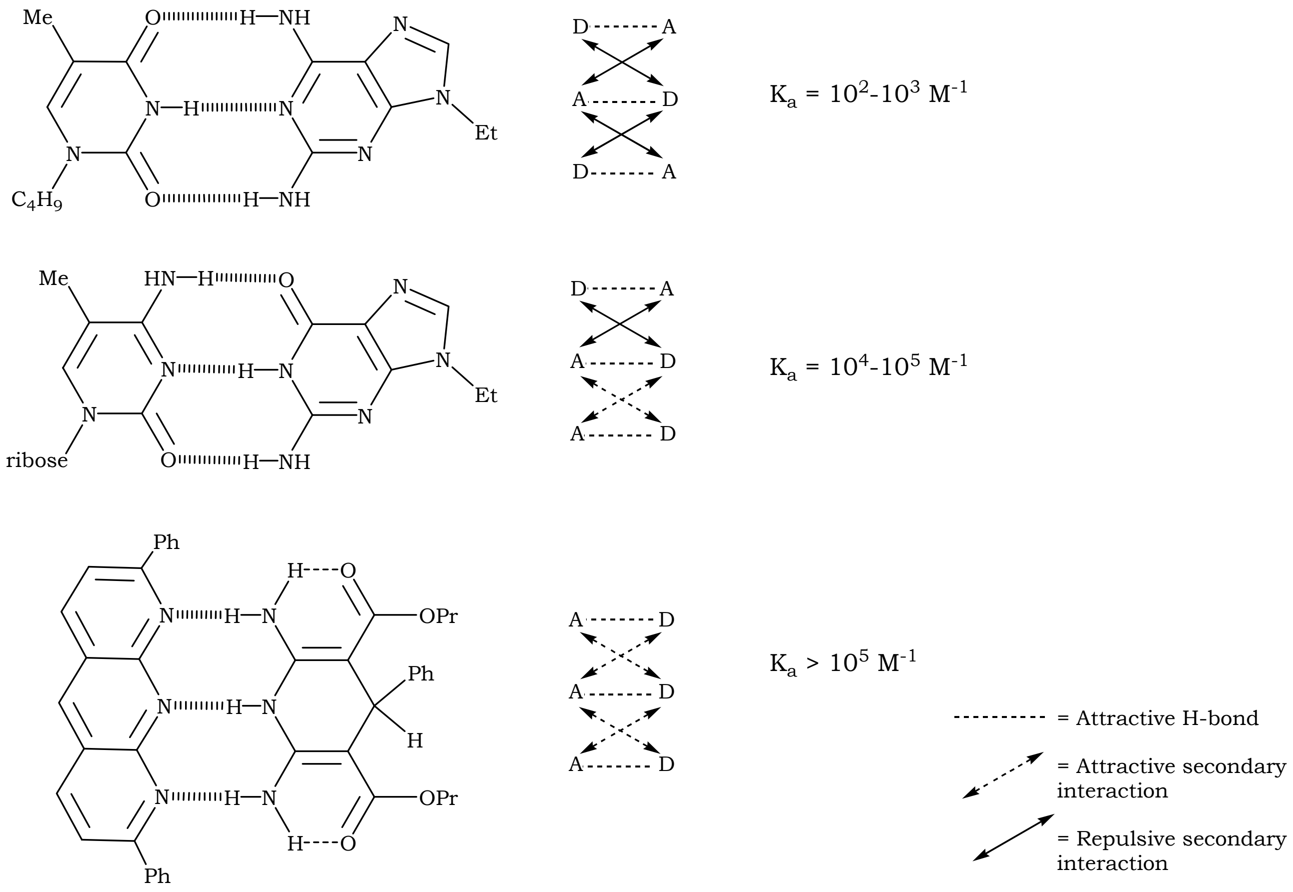
Me
C4H9
Et
D A
A D
D A
Ka = 10²-10³ M⁻¹
Me
ribose
Et
D A
A D
A D
Ka = 10⁴-10⁵ M⁻¹
Ph
OPr
Ph
H
OPr
Ph
A D
A D
A D
Ka > 10⁵ M⁻¹
= Attractive H-bond
= Attractive secondary interaction
= Repulsive secondary interaction

Figure 2.2. Influence of donor-acceptor sites positions on the association constant[10].

Nevertheless, the major drawback of the quadruple hydrogen-bonded complexes is their tendency to tautomerize leading to loss of complexation either due to the increase of secondary repulsive interactions or due to the loss of complementarity. Recently, Zimmerman et al. have reported the synthesis of a new quadruple system in which all the tautomers can dimerize[36] (figure 2.3).

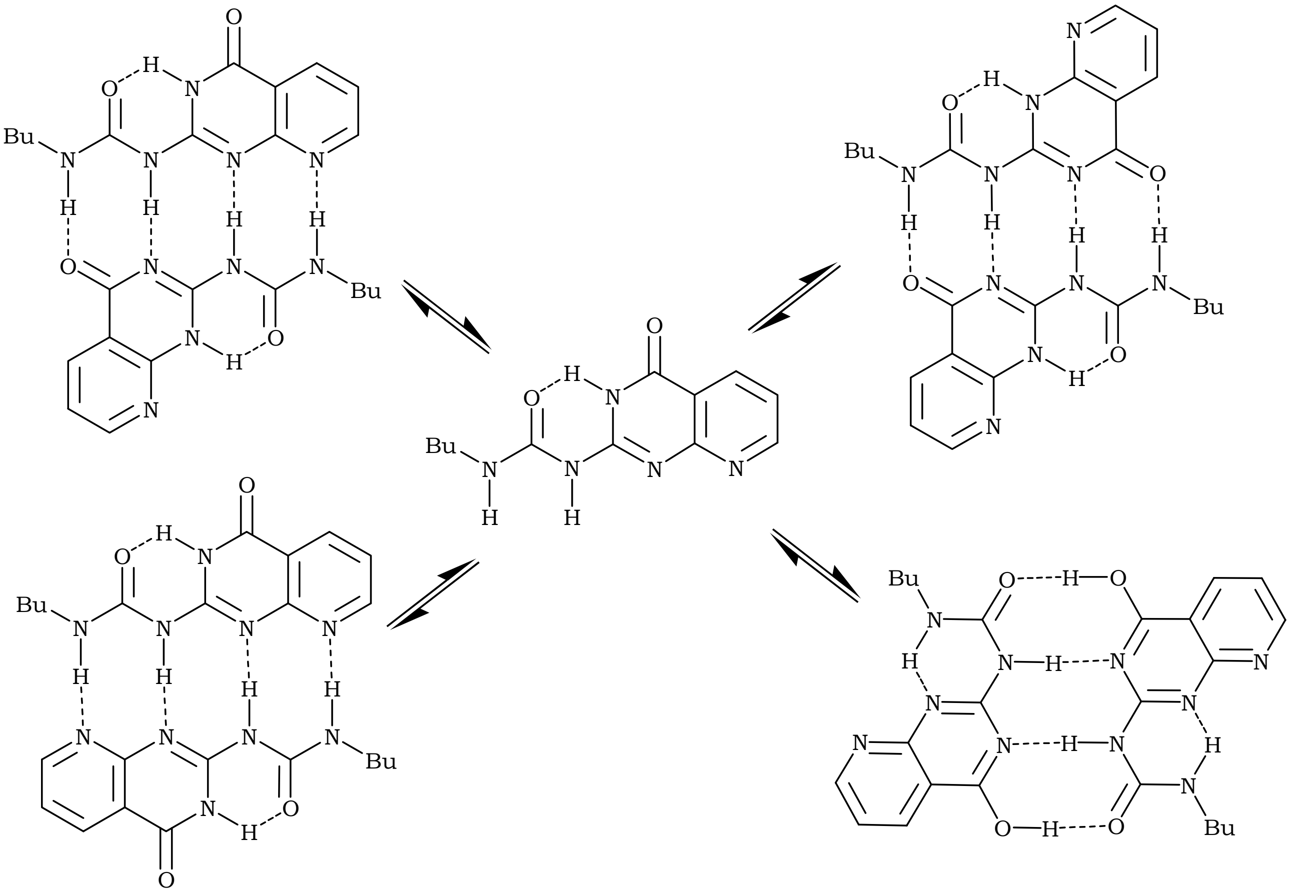

Figure 2.3. Tautomers dimerization of quadruple hydrogen bonding system.

Lehn and coworkers were the first who developed triple hydrogen bonding complexes that, when are separated, don't exhibit any liquid crystalline property but whose 1:1 mixture affords thermotropic liquid crystallinity[37]. When a rigid core replaces the aliphatic chains in these molecules, lyotropic liquid crystals have been obtained instead[38, 39]. Other research groups have reduced the synthetical complexity by using single or double hydrogen bonding sites instead of triple ones[40-44]. The wide majority of these groups have obtained highly ordered liquid crystalline supramolecules either by simply incorporating small molecules such as benzoic acid derivatives and pyridine moieties to the system[45] or by introducing chiral groups[46].

It is worthwhile to note that the combination of hydrogen bonding and liquid crystallinity shows extraordinary polymer-like properties such as the possibility of drawing fibers from the melt[47] and memory effects where the crystalline order decreases when the material is kept in the isotropic state for a long time[48].

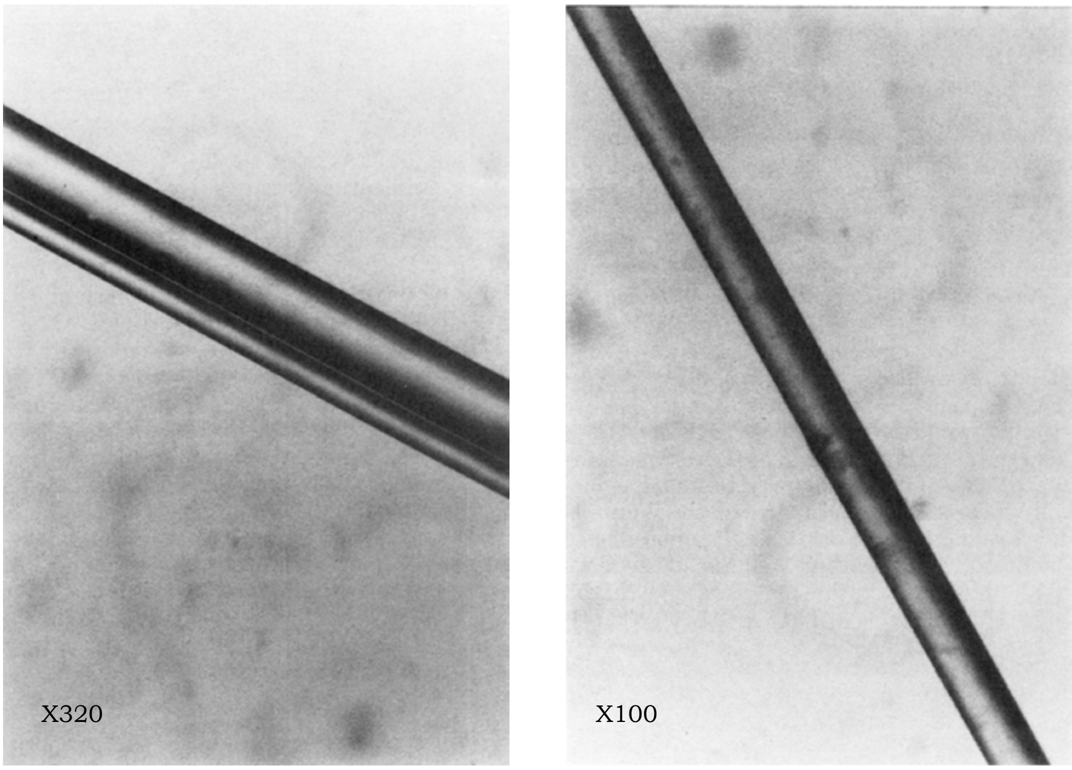

Figure 2.4. Optical microscopy micrographs of fibers pulled from melt of two different products[47].

Alternatively, Lillya et al. have found that upon capping poly(tetramethylene oxide) (PTHF) with molecules capable of forming a crystalline domain, such as benzoic acid derivatives, the strength of the hydrogen bond increases drastically giving rise to astonishing polymeric properties[49].

2.3 Metal complexes

Numerous supramolecular coordination compounds have been reported in the literature[50, 51]. These assemblies have a wide scope of structures starting from simple complexes to remarkable geometries comprising star-shaped, ladders, grids, boxes and helices. Likewise, many research groups have focused on synthesizing supramolecular coordination polymers comprising one dimensional linear[52-55] as well as dendritic moieties[56]. Nevertheless, all these complexes, which have been isolated and studied either in the solid state or in solution, don't exhibit any dynamic reversibility; a property which was first reported by van Koten and coworkers after synthesizing a Cu(I) and Ag(I) complexes with a peptide derivative polydentate ligand[57]. A more interesting compound has been synthesized by Velten et al. in which a phenanthroline-based ligand has been complexed by Cu(I) in a 1:1 ratio, forming the polymer coordination compound **1** illustrated in Figure 2.5 below. It is important to note, however, that **1** could have been obtained only after using a non-complexing solvent that doesn't promote ligand exchange with the phenanthroline derivative.

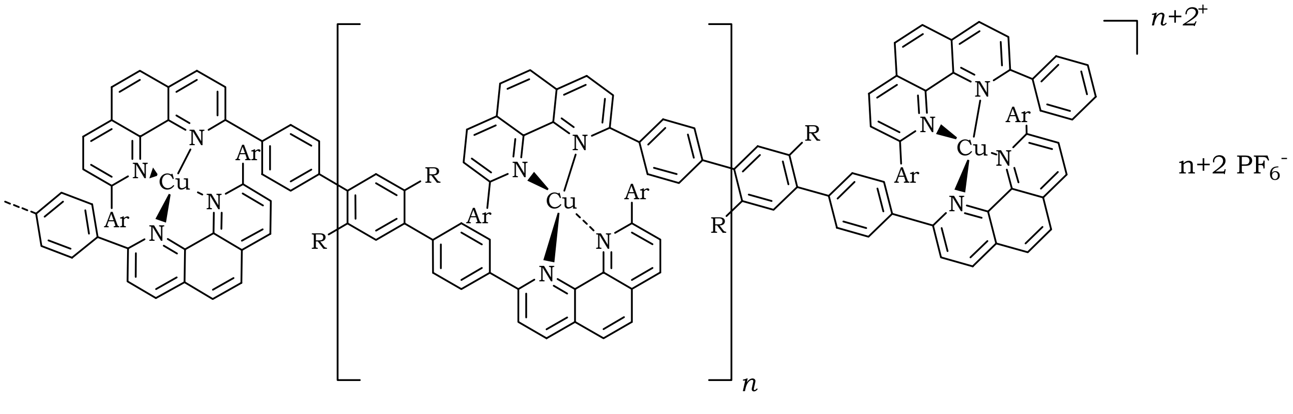

1

Figure 2.5. Cu(I) coordination polymer.

Hunter et al. has also reported the synthesis of a high molecular weight coordination polymer based on porphyrin[58]: The addition of two pendant pyridine groups to the latter compound allowed the complexation of the nitrogen atom of the hitherto mentioned molecule to the central cobalt metal which; consequently, leads to the formation of **3** as figure 2.6 depicts.

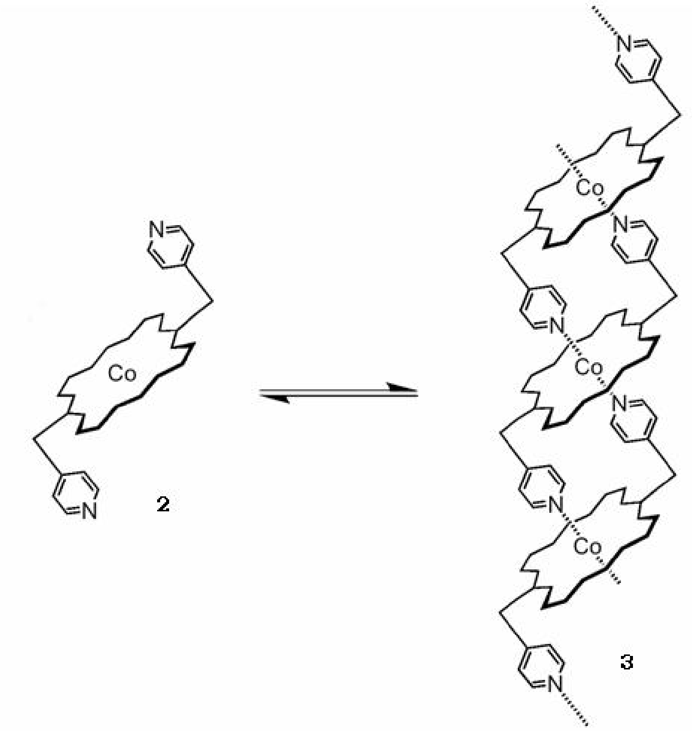

Figure 2.6. Coordination polymer from porphyrin derivative **2**.

2.4 Arene-Arene interaction

2.4.1 Introduction

This type of interaction, also called π-stacking, is based on the secondary bonding that occurs between π-orbitals of neighboring molecules. The structure of these aromatic species is usually made up of planar disc-shaped polyaromatic hydrocarbon (PAH) core having three-, four-, or six-fold rotational symmetry leading to the formation of stacked columns. Nevertheless, the high insolubility of such systems has prompted the researchers to functionalize these discotic molecules with flexible aliphatic chains rendering them highly soluble. Consequently, the anisotropy stimulated by the ditopic structures of these molecules (rigid core and flexible chains), gives rise to the formation of thermotropic liquid crystalline mesophases, as figure 2.7 illustrates, ranging from the least ordered nematic phase to the highly packed columnar one[59].

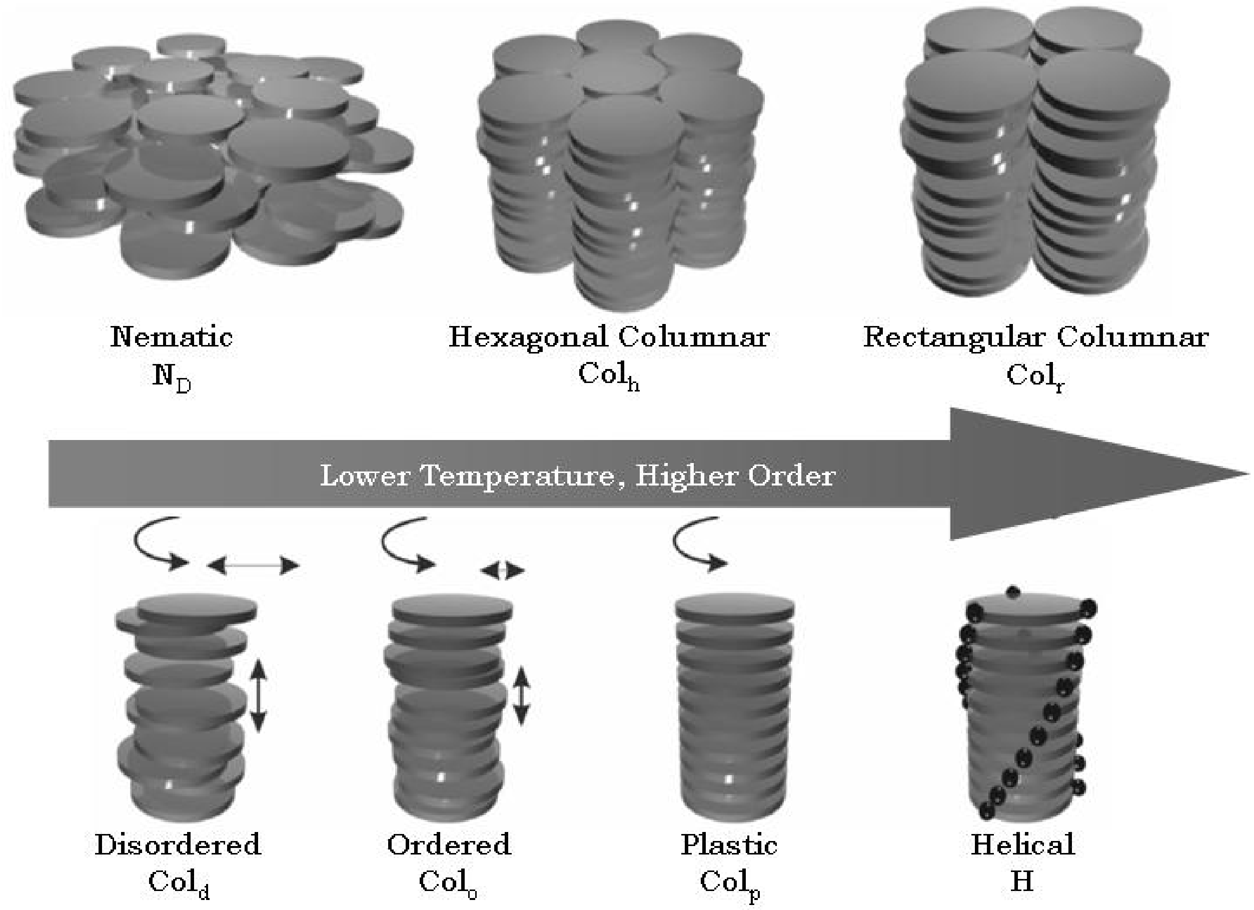
Nematic
N_D
Hexagonal Columnar
Col_h
Rectangular Columnar
Col_r
Lower Temperature, Higher Order
Disordered
Col_d
Ordered
Col_o
Plastic
Col_p
Helical
H

Figure 2.7. The mesophases of the disc-shaped molecules are characterized by their various degrees of positional order and symmetry (top). The columnar mesophases are sub-classified according to their degree of order and the dynamics of the molecules within the column (bottom)[60].

In fact, this type of molecules is the only type of liquid crystals able to generate linear architectures in dilute solution due to the strong π-interaction between the different discogens, which permits a high tendency to form columnar arrays in both polar and apolar solvents. Nevertheless, upon increasing the concentration, the interaction between the different columnar stacks increases leading, in some cases, to the formation of gels in medium concentration and to an aggregation when the medium is further concentrated. The same behavior is also formed in the solid state but to a higher extent with a significant occurrence since the intercolumnar interactions are much stronger which causes further packing and, hence, a higher degree of aggregation promoted by the high crystal packing of the lateral aliphatic chains[10].

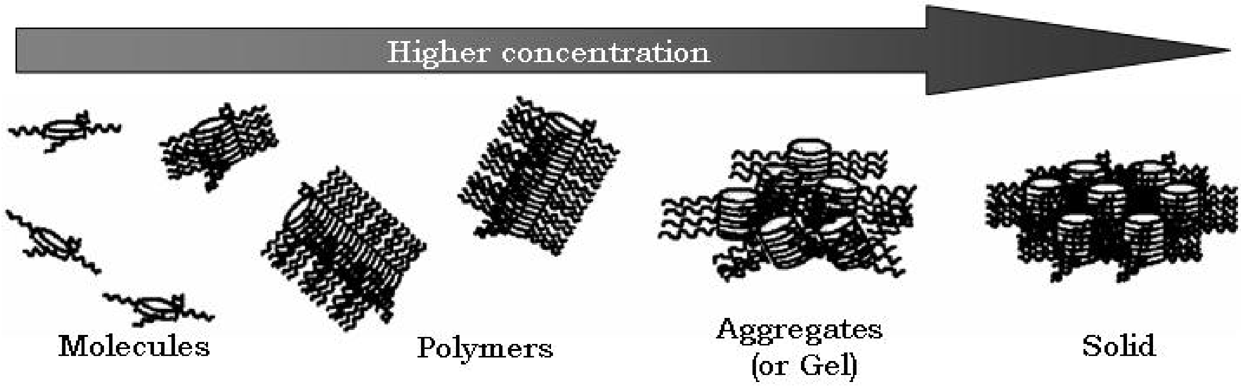

Figure 2.8. Self-assembly of discotic molecules into columnar stacks as a function of concentration.

The unique linear stacking behavior of discotic molecules has encouraged many researchers to study their luminescence and electronic properties among others where some compounds show high charge carrier mobilities allowing them to be potential candidates in the field of organic optoelectronic devices as we will see in the next section. Very recently, Nakano and coworkers have synthesized π-stacked oligomers owing very good emission properties[61] whereas Wang and coworkers have showed that the emission of a perylene derivative can be tuned from green to red depending on its concentration in the medium[62].

2.4.2 Disc-shaped molecules

Triphenylene **4** and phthalocyanine **5** derivatives were among the first disc-shaped molecules which have been synthesized and whose stacking has been deeply investigated because the majority of them exhibit thermotropic liquid crystalline properties[63, 64]. Even though it has a small core size, triphenylenes bearing alkoxy side chains **4a** form columns but with loose stacking and with an interdisc distance of 6 Å instead of 3.5 Å allowing, therefore, the molecules to undergo rotational and lateral translation within the column[10]. The replacement of the alkoxy groups by amphiphilic aliphatic chains yields the water soluble product **4b** that forms columnar micelles. Upon increasing the concentration of the latter product in water, it forms lyotropic liquid crystals[65]. The same behavior has been recorded when employing the ionic species **4c**[10]. Due to the low packing, we have mentioned previously, the introduction of a chiral aliphatic chain to the molecule didn't show any supramolecular chirality[10]. Helical triphenylene stacks have only been obtained after intercalating the discs with a bulky chiral electron acceptor[66]. Closely packed triphenylene columns have been detected only when preparing an equimolar amount of the donor-acceptor derivatives **4a** and **4d** in apolar solvents[67, 68]. The resulting alternating stacks show unidirectional charge transport through the column upon excitation[69]. Alternatively, fluorescence studies show that upon increasing the concentration of a triphenylene derivative, its radiative lifetime also increases supposing that this is due to the formation of longer columns, which requires more time for the mobile exciton to move through them[10]. Furthermore, the increase of the column length has been proved by means of small angle neutron scattering (SANS) as well as the broadening and the increase of the absorbance in the UV-Vis spectrum when a higher concentration of **4** is present in solution[66]. Last but not least, the charge carrier mobility for various triphenylene moieties was found to be relatively high[70, 71].

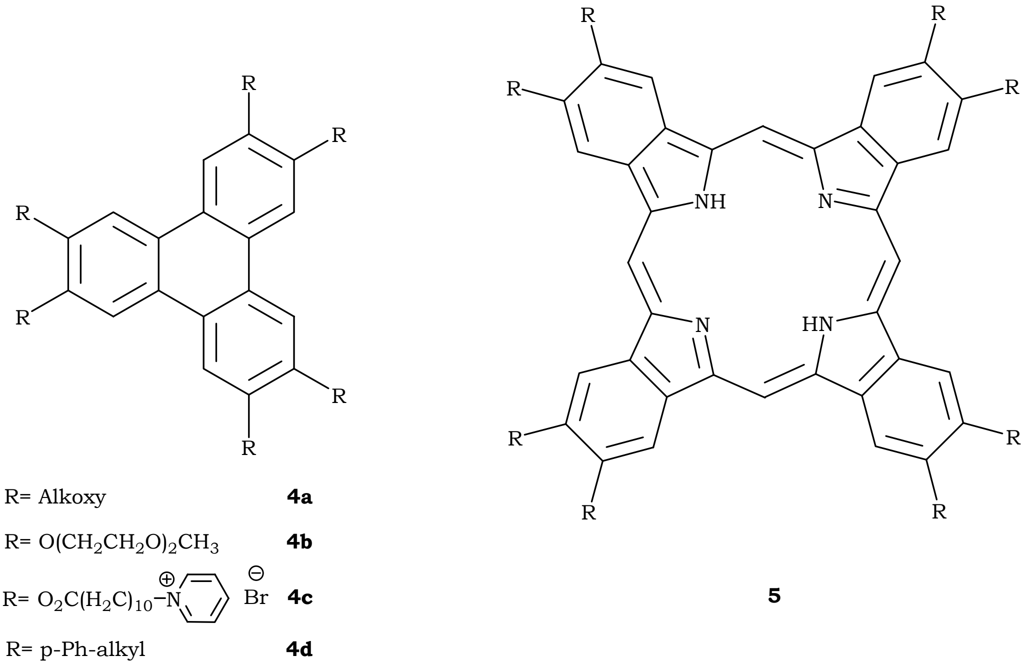

R= Alkoxy **4a**
R= $O(CH_2CH_2O)_2CH_3$ **4b**
R= $O_2C(H_2C)_{10}-N^{\oplus}$ $Br^{\ominus}$ **4c**
R= p-Ph-alkyl **4d**

5

Figure 2.9. Triphenylene and phthalocyanine derivatives.

On the other hand, phthalocyanines **5** have prompted researchers to study their stacking behavior due to their large core and because the incorporation of a metal tunes the optical and electronic properties. Conversely, phthalocyanines rather prefer to dimerize in solution and don't form aggregates unless much higher concentrated[72-74]. Nevertheless, long supramolecular architectures of species of type **5** were only detected after the use of phase separation systems or in the solid state[75]. Helical supramolecules of **5** derivatives have also been reported after locking the positions of these latter with chiral aliphatic chains to prevent their rotation[76]. The replacement of the chiral chains by crown ethers[77, 78] has opened the possibility to turn off the helicity after the addition of a potassium salt[79]. It is noteworthy that these helical structures form fibrous materials at very high concentration. Similar to phthalocyanines, porphyrins also dimerize in solution[80, 81] and form aggregates in the solid state that in some cases lead to the formation of fibers[82].

The interest in large disc-shaped molecules led to the syntheses of various *m*-phenylenes ethynylene macrocycles as figure 2.10 depicts. All these derivatives have a strong π-interaction and, consequently, they form thermotropic mesophases[83, 84]. New generation of these rigid molecules bearing butadiyne bridged with benzene **7** or with pyridine **8** has also been studied showing the formation of columnar structures as well[85, 86].

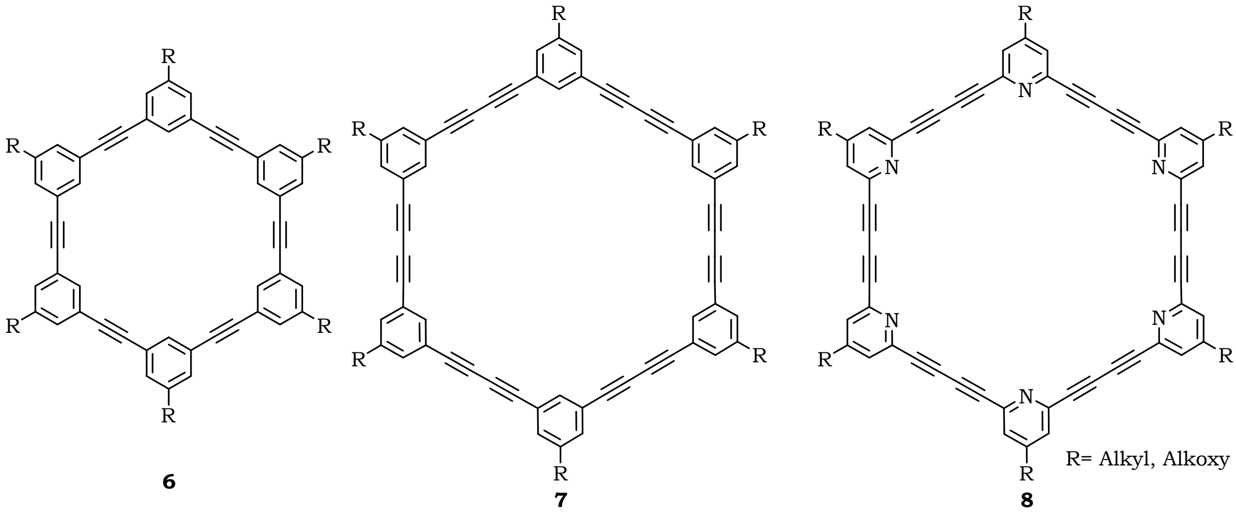

6 **7** **8**

R= Alkyl, Alkoxy

Figure 2.10. Various *m*-phenylenes ethynylene macrocycles.

The relatively good columnar arrangement of triphenylene moieties and the interesting properties they show, among others their good charge carrier mobility, have encouraged many researchers to investigate the more extended polyaromatic hydrocarbons (PAH). Müllen and coworkers have improved a synthetical method in which large PAHs can be produced in a few steps and in very good yields[87-92]. The most prominent of these extended benzene structures is hexa-*peri*-hexabenzocoronene **9** (HBC, R = H) illustrated in figure 2.11 on the next page. The decoration of the latter molecule with aliphatic side chains makes the otherwise highly insoluble product soluble in common organic solvents and bestows it with thermotropic liquid crystalline properties over a wide range of temperatures depending on the length and on the nature of the lateral groups attached[93-97].

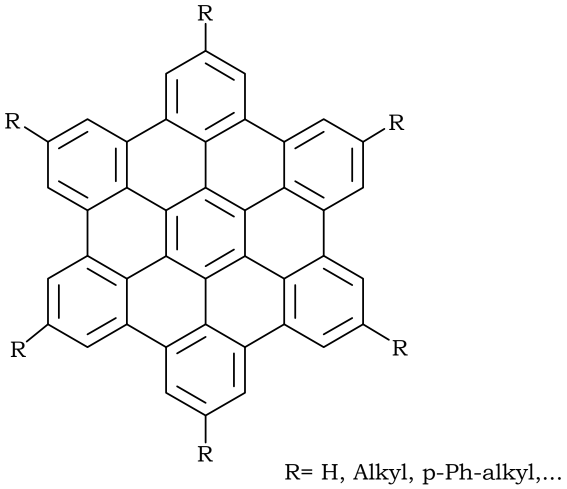

9

Figure 2.11. Structure of hexa-peri-hexabenzocoronene.

Extensive studies on the stacking behavior of various HBC species have been carried out so far. In solution, the molecules form columnar aggregates even at low concentration and the length of the stacks can be increased by increasing the concentration of HBC moieties in the medium[98]. On the other hand, the aggregation of these molecules in the solid state affords closely packed columnar arrays due to the high intercolumnar interaction besides the high degree of crystallization and packing order of the aliphatic side chains[99]. However, the alignment of these columnar arrays greatly depends on the deposition conditions: they usually align in a planar fashion (discs edge-on the surface or vertical) as they can be deposited homeotropically (discs flat-on to the surface or horizontal) in a herringbone structure resembling to that of graphite[100]. Nevertheless, electron microscopy characterization of ultrathin layers of **9** (5-8 molecules in thickness) on Cu(111) or Au(111) surfaces revealed that the columns are perfectly aligned showing little translation[101]. Very recently, helical columnar mesophases have been produced by adding acetylene between the phenyl moiety and the side group[102, 103].

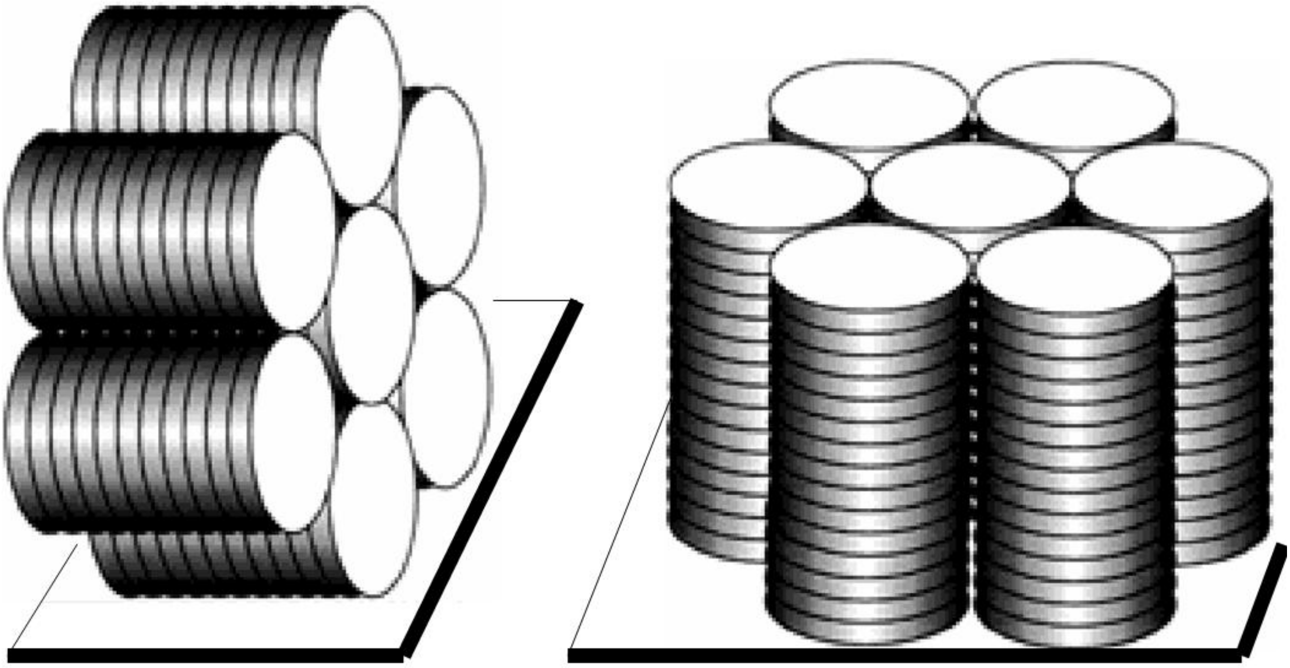

Figure 2.12. Planar (left) and homeotropic (right) alignment of columns.

It is noteworthy that HBC derivatives exhibit the highest charge carrier mobility recorded so far for any disc-shaped molecules in both liquid crystalline mesophase and in the solid state[13, 14, 104], which opens the way for their employment for many electronic devices[105, 106]. Additionally, new room temperature liquid crystalline HBC derivatives exhibit promising optoelectronic properties[107].

2.4.3 Twisted PAHs

The investigation of the rigid, twisted, nonracemic helicene[108, 109] **10a** has shown that it self-assembles in solution into helical structures and it forms fibers over long ranges in the solid state[110]. The study of these fibrous structures has revealed interesting optical properties[111]. Furthermore, the derivatization of **10a** into the room temperature liquid crystalline, nonracemic compound **10b** resulted in the formation of corkscrew-shaped columns at high concentrations[112].

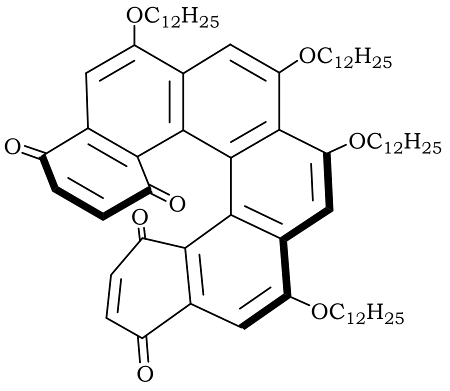
OC12H25
OC12H25
OC12H25
OC12H25
O
O
O
O

10a

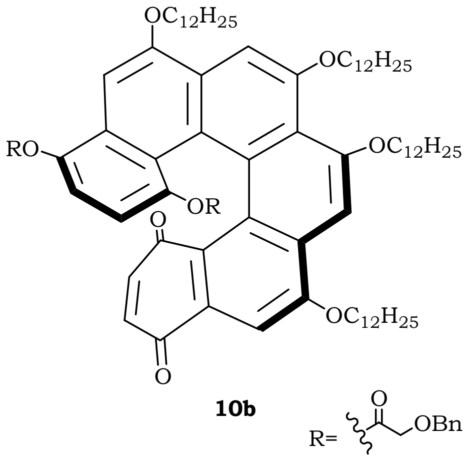
OC12H25
OC12H25
OC12H25
OC12H25
RO
OR
O
O
R=
O
OBn

10b

Figure 2.13. Structure of helicene **10a** and its RT liquid crystalline derivative **10b**.

Based on the same conceptual structure of helicenes, pyridine-pyridazine oligomers **11** have also been synthesized and the study of its self-organization has showed that they arrange into helices as well[113, 114].

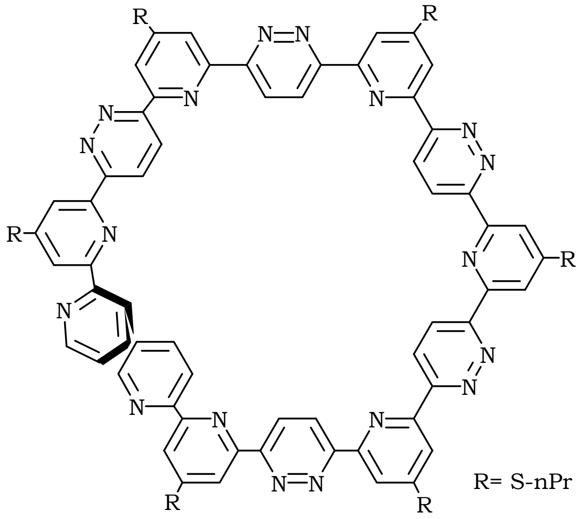
R
R
R
R
R
R
N=N
N=N
N
N
N
N
R= S-nPr

11

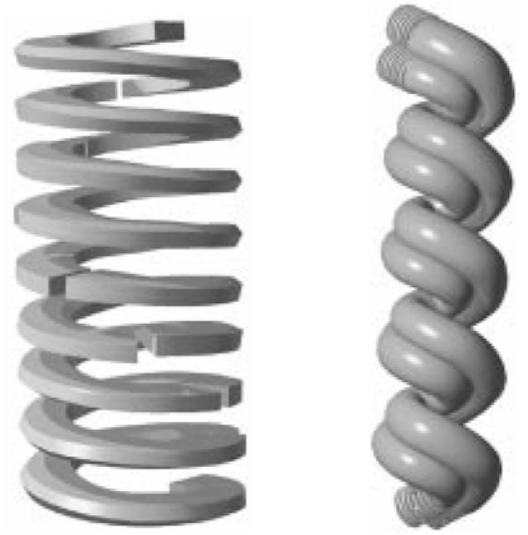

Figure 2.14. Pyridine-pyridazine oligomer and its proposed mode of aggregation into helical columns and fibers[113].

Helical structures can also be obtained from flexible molecules like *m*-phenylene ethynylene oligomers **12a-d**, illustrated in figure 2.15, whereupon employing a poor solvent, they self-organize into helices leading to the formation of corkscrew-shaped columns whereas the use of a good solvent leads to the formation of stacked lamellae[115-

118]. However, **12b** self-assembles into columnar helices in the liquid crystalline state due to the methyl group it bears (X= Me)[119].

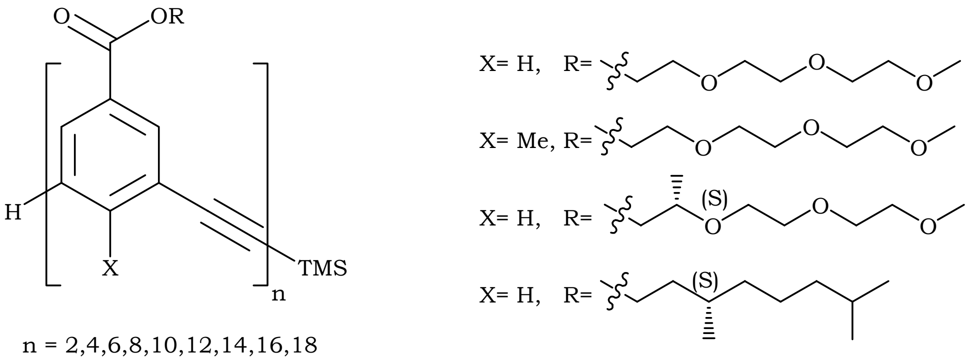
O
OR
H
X
TMS
n
n = 2,4,6,8,10,12,14,16,18
X= H, R=
X= Me, R=
X= H, R=
X= H, R=
O
(S)

12a
12b
12c
12d

Figure 2.15. Various *m*-phenylenes ethynylene oligomers.

Likewise, the same architecture can be generated from linear oligo-isophthalamide strand upon binding with a cyanuric acid derivative. This latter causes a template effect folding the molecule into a helical configuration and into fibers at higher concentrations[120] (figure 2.16).

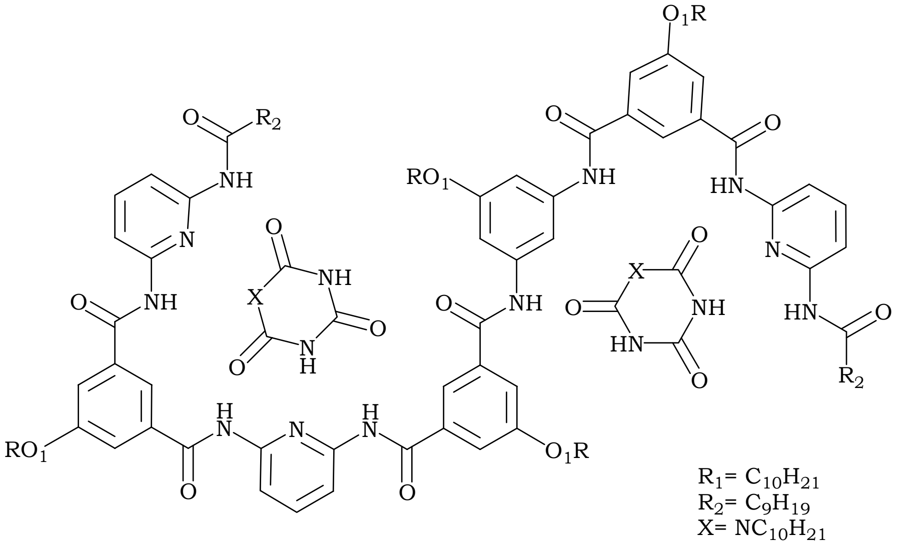
O₁R
RO₁
O
R₂
NH
HN
N
H
X
R₁= C₁₀H₂₁
R₂= C₉H₁₉
X= NC₁₀H₂₁

Figure 2.16. Folding effect of the cyanuric acid derivative on the oligo-isophthalamide.

2.5 Combined systems

2.5.1 Introduction

The mutual combination of two or more types of secondary interactions was found to be a versatile tool to circumvent the problems encountered upon building a supramolecular architecture based on one type of weak bonding only. The cooperation between the different interacting systems usually results in the formation of closely packed arrangements with special conformational features.

2.5.2 π- and H- Bonding

Contrarily to π-stacked assemblies that arrange in solution regardless of the solvent employed, the formation of hydrogen bonded molecular arrays occurs in apolar solvents only. On the other hand, we have showed previously that a good arene-arene stacking necessitates the use of a relatively large core to form closely packed structures. To circumvent these limitations, many molecules bearing both types of bonding have been synthesized. This synthetical strategy has allowed the formation of highly ordered supramolecular arrays even with small molecules like 1,3,5-benzene triamide derivatives[121] **13**, for example, that self-organize into helical columns whose order can be biased by adding a small amount of **13b** that bears chiral aliphatic chains[122].

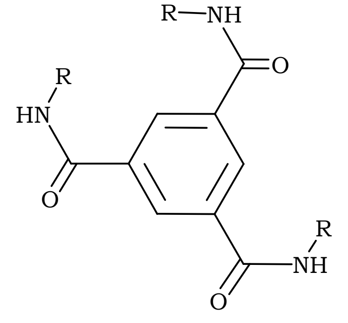

R= Aliphatic chain **13a**

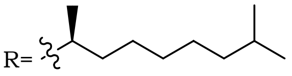

13b

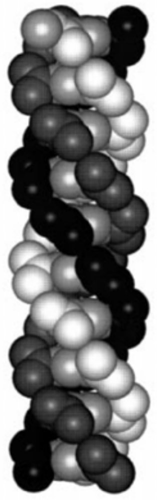

Figure 2.17. 1,3,5-benzene triamide derivatives and the graphical representation of the helical columns they form in the solid state[121] .

The replacement of terminal alkyl chains of **13** by bulky aryl groups results in the formation of the propeller-like[123] **14** that self-assembles into a helical columnar order. Interestingly, the presence of only one chiral molecule **14a** per 80 achiral ones **14b**, induces the columns to have a well-defined helicity[124]. The substitution of the apolar side chains with polar ones affords the water soluble, lyotropic products **14c** and **14d** that form helical assemblies in various polar solvents and whose helicity can also be tuned by adding a small amount of the chiral discs **14d** with respect to the achiral derivative **14c**[125, 126].

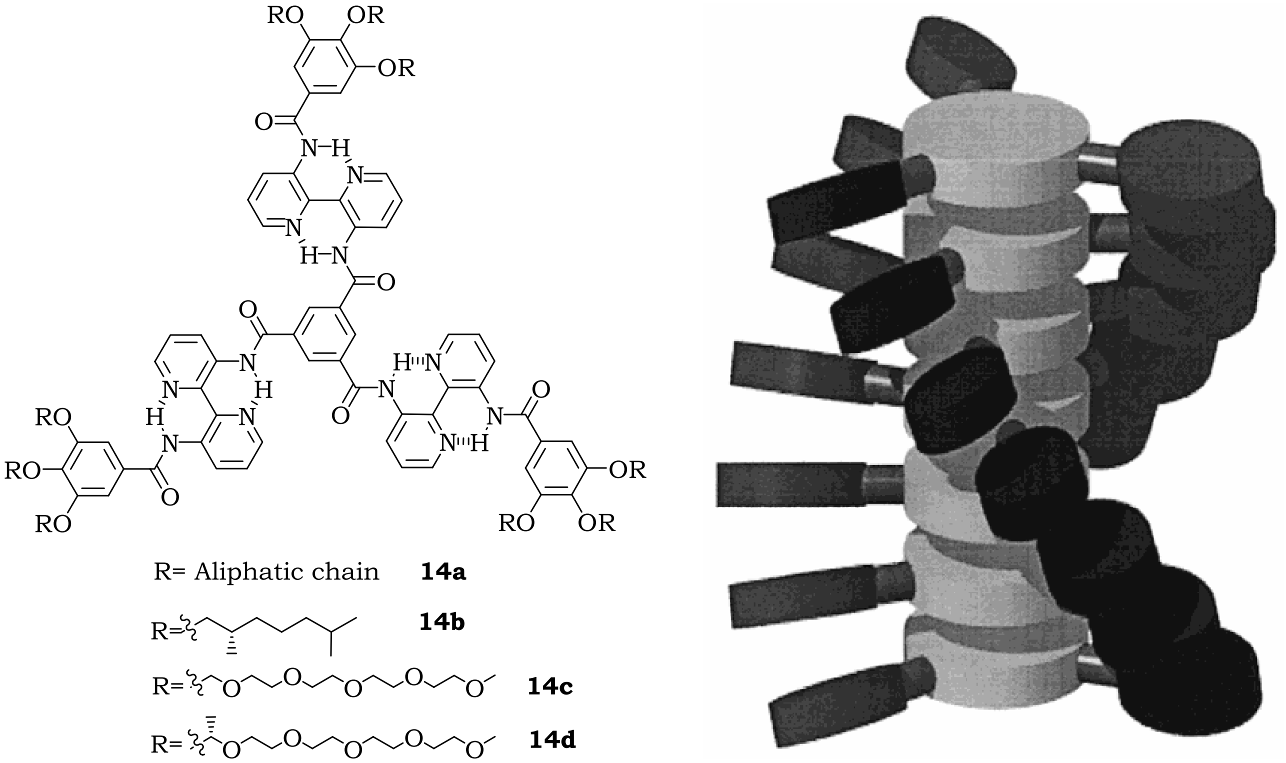

Figure 2.18. Structure of the propeller-like **14** and the graphical representation of the helical columns they form in the solid state[127].

Meijer and coworkers have synthesized the ureiditriazine species **15** that dimerize via the quadruple hydrogen bonds into a discotic core first, followed by their self-organization into columnar molecules by π-interaction. Product **16**, formed upon interconnection of a dimer with an aliphatic spacer, gives rise to helical columns because the free rotation of the discogens is locked[128].

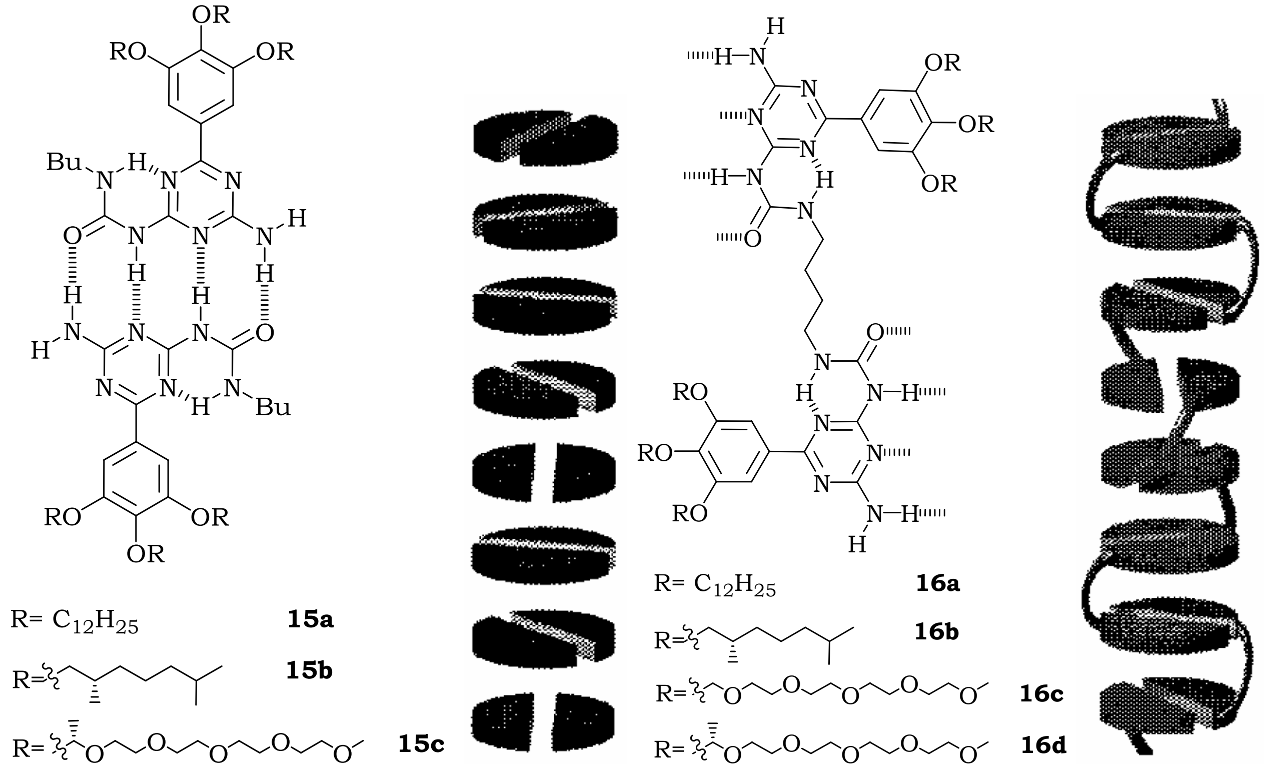

Figure 2.19. Structures of ureiditriazine monomer **15** and its interconnected dimer homologue **16**. The graphical representations reveal the columnar packing of the former and the columnar helical for the latter[128].

Very recently, the growth of helical columnar structures of *p*-phenylenevinylenes oligomers **17** in apolar solvents has been reported showing that monolayers of this latter form cyclic twisted structures via hydrogen bonding first and suggesting that the formation of helical stacks is due to a subsequent π–interaction. Fibers and lamellae can also be grown in the solid state from solution depending on the substrate employed[129, 130].

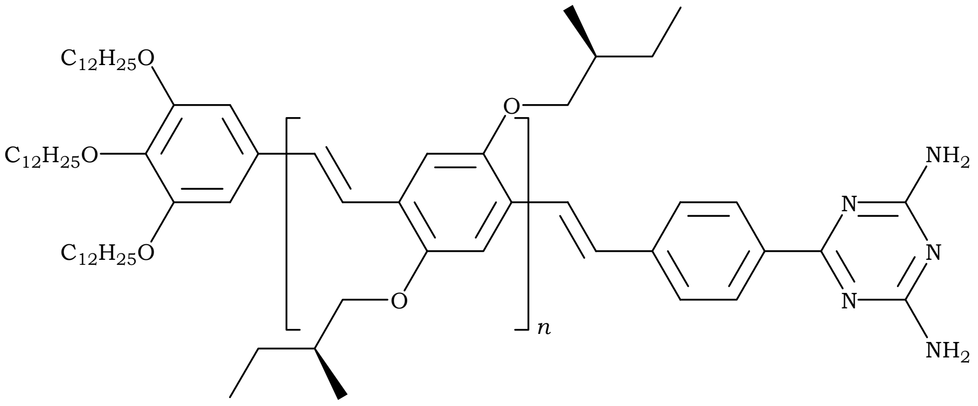

17

Figure 2.20. *p*-phenylenevinylenes oligomers.

2.5.3 π-stacking and metal complexes

Based on the same principle we mentioned in the previous section i.e. combining the secondary interactions to strengthen the supramolecular packing, the interest in this type of combination has been growing in the aim of finding new functional organic devices possessing many properties especially catalytical and optical ones.

The complexation of the nickel macrocycle bearing pyridine pendants **18** with different ligands has afforded two- and three-dimensional structures depending on the nature of the ligand used: the reaction of **18** and isonicotinate affords the complex **19** where the ligand coordinates to Ni atom, and perform a face-to-face π-stacking with the neighboring isonicotinate forming, therefore, a linear one-dimensional array. The linear chains are linked to each other via arene-arene interaction between the pendant pyridine units leading, therefore, to the formation of a two-dimensional sheet[131].

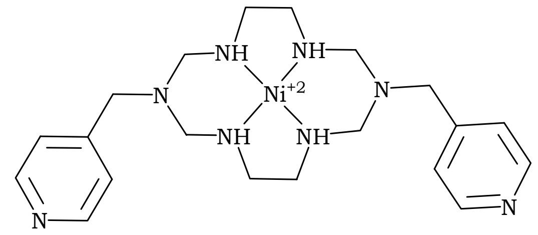

18

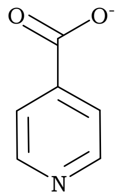

isonicotinate

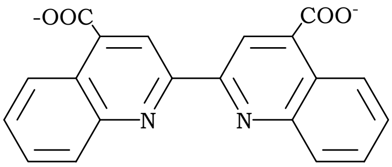

BQDC^{-2}

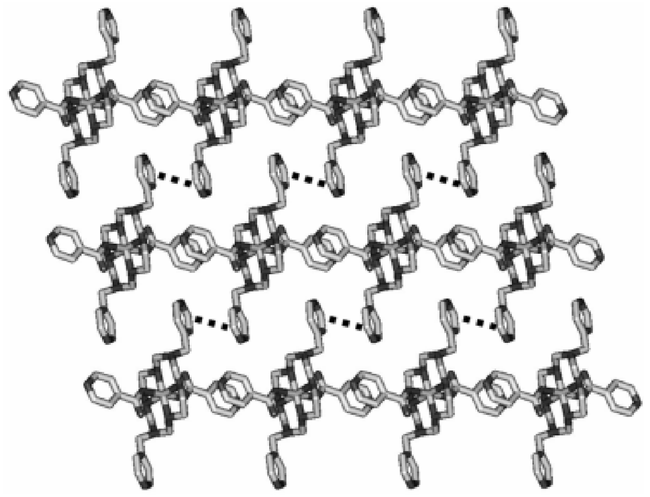

Figure 2.21. Nickel macrocycle, isonicotinate, and BQDC structures (left). Extended 2D structure of **19** showing the face-to-face π-interaction between pyridine units (right).

The replacement of isonicotinate by the bulkier 2,2’-biquinoline-4,4’-dicarboxylate (BQDC^{2-}) yields compound **20** that forms a three-dimensional network because, BQDC^{2-} can undergo π-stacking with its homologue as well as with the pendant pyridine[131].

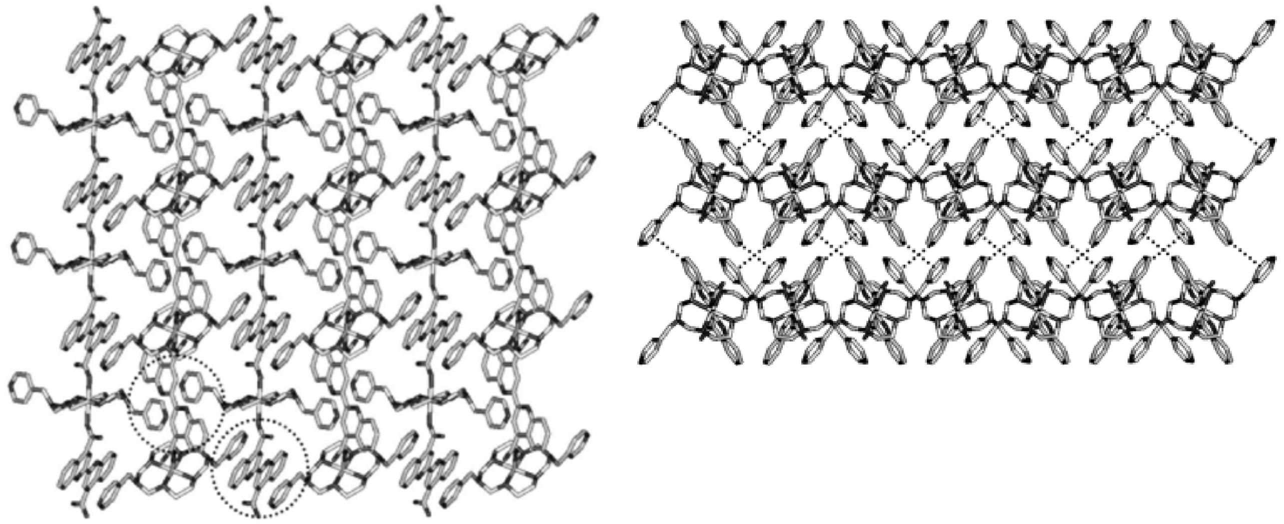

Figure 2.22. Extended 2D structure of **20** showing the face-to-face π-interaction between aryl units (left). Side view of the packed structure of **20** showing herringbone π-interaction between the 2D layers (right).

Tsuda and coworkers have reported recently a π-extended zinc porphyrin complex with a metal legating 3-pyridyl group **21** that exhibits interesting thermochromic properties changing from green to yellow to red on heating from 0 to 50 to 100°C respectively. The structural study of this compound reveals that it adopts a cyclic tetramer configuration via the axial coordination of 3-pyridyl groups to the zinc species where the inner pyridyl are in contact with one another via arene-arene interaction[132] (Figure 2.23).

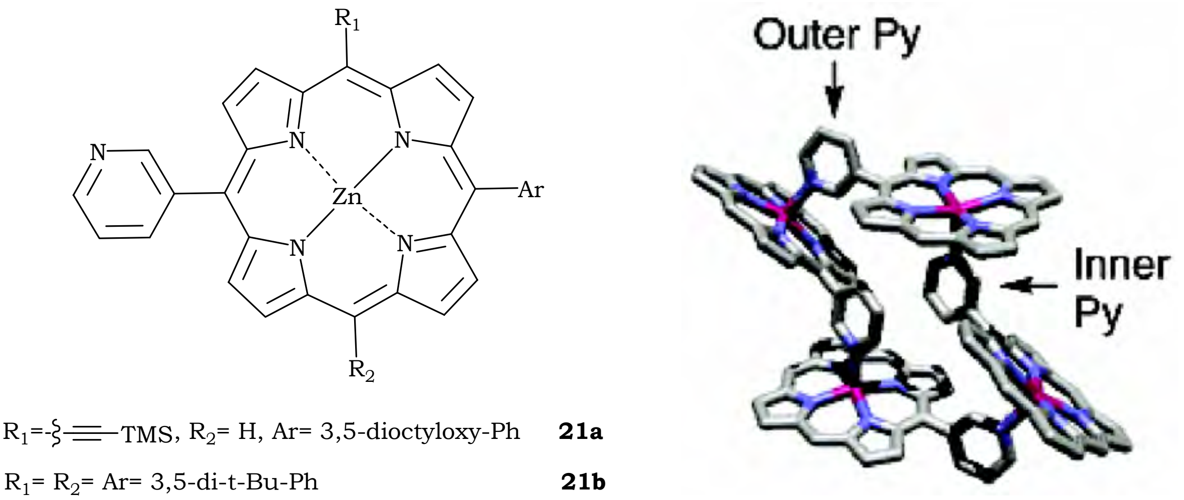

R_1=-ξ-≡-TMS, R_2= H, Ar= 3,5-dioctyloxy-Ph **21a**

R_1= R_2= Ar= 3,5-di-t-Bu-Ph **21b**

Figure 2.23. Structure of the thermochromic compounds and the X-ray crystal structure of **21b**.

3. Field electron emission (FEE)

3.1 Introduction

Field electron emission (FEE) is an exceptional quantum-mechanical effect of electrons tunneling from a condensed matter into vacuum. FEE is known to have a very high current density and that no energy is consumed by the emission process. Contrarily to solid-state microelectronics that necessitates scattering-dominated electron transport in semiconducting solids, vacuum microelectronics relies on the scattering-free, ballistic motion of electrons in vacuum. All these properties allowed field emission to find wide applications as ‘cold cathodes’ in the area of high resolution electron spectroscopy such as Auger spectroscopy, atomic-resolution electron holography and other areas of superfine characterization of atomic surfaces. FEE is also a process capable of generating high-power electron beams (thousands and millions of amperes) through a phenomenon called explosion electron emission[133].

We will develop in this section the advantages of FEE, the theory behind as well as we will introduce the most prominent application based on this property i.e. field emission displays. Nevertheless, it is important to note that this work presents FEE from a chemist point a view interested in this particular phenomenon for designing and synthesizing organic devices that could find application in FED.

3.2 Advantages and future perspectives

Many research works have tried since the 1960s[134] to introduce the FEE concept as electron sources in some devices which are used in everyday life like the cathode ray tubes (CRT) in television sets, X-ray generators and microwave amplifiers. Generally, these devices use thermionic emitters as electron sources operating at very high temperatures (between 950-2000°C). Even though thermionic emitters represent many advantages, such as, their high current densities and the fact that they are relatively inexpensive, they do possess many drawbacks: they are power-controlled electron sources and therefore, direct variation of the electron emission is slow. Also, the high temperatures used cause a relatively high energy consumption and, the impossibility of miniaturization to micro- or nano-emitters because of insufficient heat dissipation[135].

On the other hand, vacuum microelectronics is seen as the new technological generation to replace thermionic sources and this is due to many reasons[133]:

- Each field emitter is used as an active element in such a device and consequently this opens the possibility of reducing the size of these active elements to the nanometer scale. Once reached, the small dimensions of these emitters permit achieving a very high density of 10^6-10^9 cm^{-2}.
- Lower voltages are required for electronic devices based on FEE than thermionic ones.
- No dissipation of energy occurs during electron transport since it is carried out in vacuum.
- The lack of inertia in the field emission process enables such devices to act in a high speed which permits designing of fast-acting high-frequency devices.

All these advantages are expected to promote the use of cold cathodes in many technological applications such as flat panel displays, high-power radio frequency amplifiers, electron guns for traveling wave tubes and data storage devices[136].

3.3 FEE Theory

FEE is a phenomenon described by quantum mechanics revealing the physical effect of electrons tunneling from the surface of the solid into vacuum when very high electric field (~3000 $V\mu m^{-1}$) are present at the surface[137]. In order to produce such high electric fields using reasonable potentials, a needle-like emitter also known as the 'Spindt' emission tip, is usually used (figure 3.1). The conical shape of the Spindt emitter will enhance the applied electric field by a factor β called the field enhancement factor. Therefore; for an emitter having a cylindrical shape of height h and an apex radius r, the field enhancement factor β equals, at first approximation, to h/r[138]. This means that for a Spindt emitter with a height of 6µm and an apex radius of 30 nm exhibits a field enhancement of 200 (figure 3.1). Consequently an applied electrical field of 15 $V\mu m^{-1}$ will be amplified 200 times at the apex of the emitter to produce 3000 $V\mu m^{-1}$ for FEE to occur.

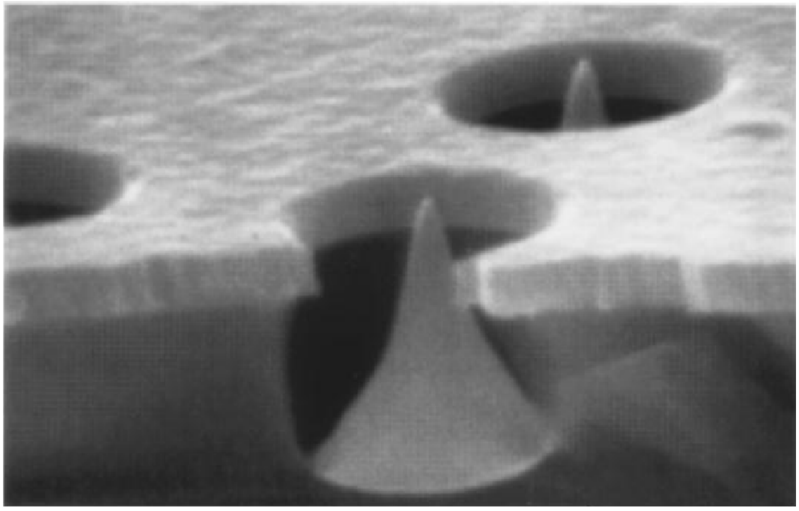

Figure 3.1. The Spindt type field emission tip[139].

The Fowler-Nordheim theory[140, 141] is the best quantitative description of the FEE process. According to this theory the FEE current *j* is a function of the electric field *E* and the emitter work function ϕ according to the equation:

$$j = \frac{e^3}{4(2\pi)^2 \hbar\phi} E^2 \exp\left(-\frac{4\sqrt{2m_e}}{3\hbar eE} \phi^{1.5} \right) \tag{1}$$

In equation 1 the Fowler-Nordheim elliptical function, correcting for the image charge contribution to the tunneling barrier, has been taken to be unity. The total energy distribution *P(ε)* of the field-emitted electrons near the Fermi energy level can be written as:

$$P(\varepsilon) = f(\varepsilon, \varepsilon_F, T) B(E, \phi) \exp\left[C_v \frac{\theta^{0.5}}{E} (\varepsilon - \varepsilon_F) \right] \tag{2}$$

Where ε denotes the electron energy, ε_F the Fermi energy of the emitter, ϕ the emitter work function, E the electric field, f(ε, ε_F, T) the Fermi-Dirac distribution at temperature T and B(E, ϕ) is an energy independent intensity factor.

Figure 3.2 illustrates schematically the situation at a metal surface under FEE conditions[142]. On the left, the metal-vacuum interface is depicted where the vertical axis stands for the energy relative to the Fermi energy. The electron density of the metal is supposed to be the Fermi-Dirac distribution at T = 300K. As shown in the middle section, under the presence of a strong electric field, 2700 Vμm^{-1} in this case, the surface potential step confining the electrons to the solid becomes a triangular shaped barrier. Close to the surface the shape of the barrier is influenced by the image charge potential. Under these conditions, the probability that electrons near the Fermi energy can tunnel quantum mechanically through the barrier is sufficiently high to let them escape into vacuum. The sketch on the right hand side depicts the resulting energy distribution of the emitted electrons.

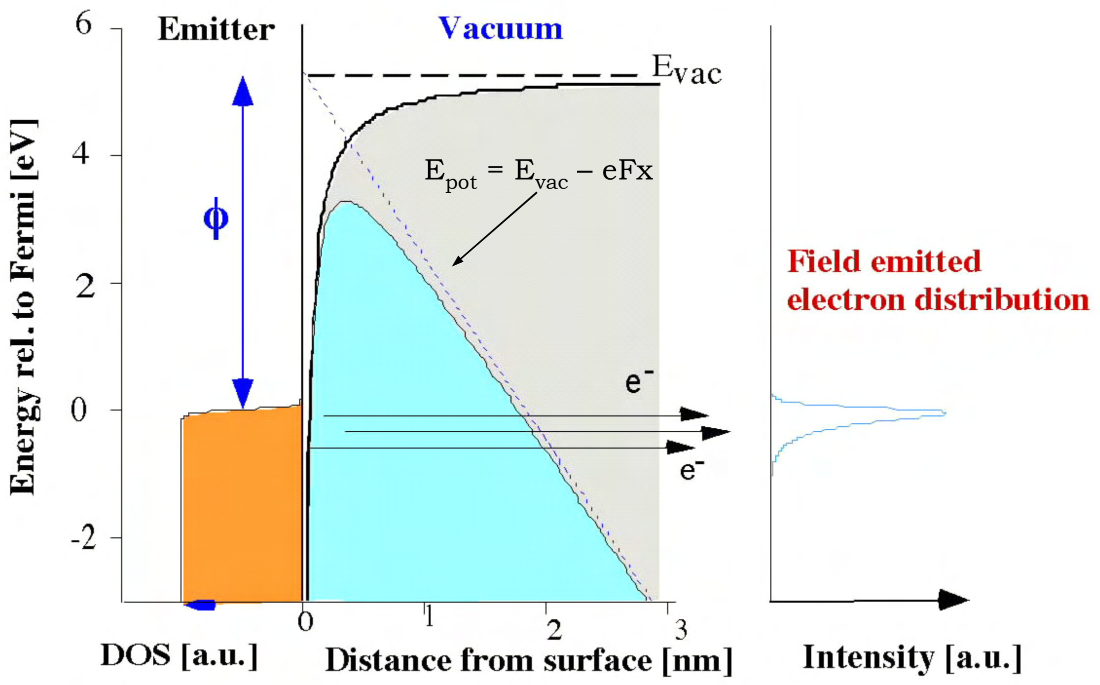
Energy rel. to Fermi [eV]
6
4
2
0
-2
Emitter
Vacuum
E_{vac}
φ
$E_{pot} = E_{vac} - eFx$
e^-
e^-
Field emitted electron distribution
0
1
2
3
DOS [a.u.]
Distance from surface [nm]
Intensity [a.u.]

Figure 3.2. Schematic of the FEE from a metal surface with a work function of 5.3 eV and an electric field E = 2.7 Vnm^{-1}. Diagram on the right shows the resulting emitted total energy electron distribution according to equation 2[138].

3.4 Field Emission displays (FED)

The field emission display is a device based on vacuum electronics and it has many common features with cathode ray tube (CRT) since the image is created by impinging electrons from a cathode onto a phosphor coated screen. Nevertheless, CRT uses thermionic power operating at high temperatures (950 -2000°C) whereas FED's electron source consists of a matrix-addressed array of millions of cold emitters (figure 3.3). It is noteworthy that both diode and triode types FEDs have been realized so far; the difference between these two is that the latter bears an additional gate electrode.

Therefore; in a diode type FED, the brightness of a pixel is controlled by varying the potential between emitter and phosphor screen, which is in the order of several kilovolts. Alternatively, a triode configuration uses the control electrode situated just above the tip emitter that monitors the electron emission by modulating the potential between cathode and control electrode[143] (figure 3.3). Although it requires additional steps and more complex fabrication process than the diode type FED, the triode type offers a higher gray scale and a better modulation of electron emission[144].

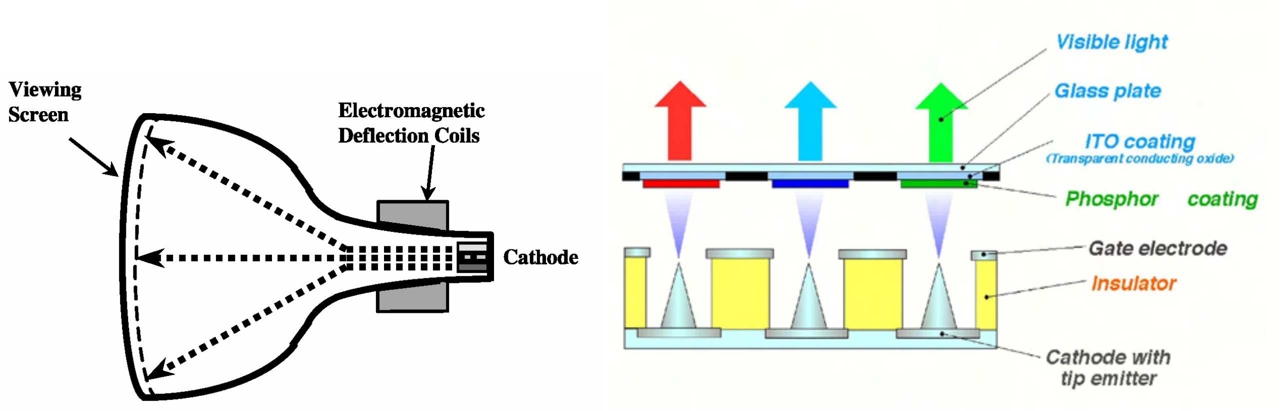
Viewing Screen
Electromagnetic Deflection Coils
Cathode
Visible light
Glass plate
ITO coating
(Transparent conducting oxide)
Phosphor coating
Gate electrode
Insulator
Cathode with tip emitter

Figure 3.3. CRT Vs. FED. Both include a glass vacuum envelope, a cathode electron source and a phosphor coating anode.

The idea of a field emission array (FEA) was first proposed by Shoulders[145] at the Stanford research institute (SRI). The first operating FEAs were developed by Spindt[146] also from the SRI. Spindt applied the semiconductor manufacturing concept to fabricate micron-sized, conical-shaped, tungsten or molybdenum arrays where each emitter is surrounded by a metal gate[147] (Figure 3.4) The first commercialized prototype of FED was however fabricated by Meyer[148] from the Laboratoire d'Electronique de Technologie et d'Instrumentation (LETI). Two companies, Motorola and Candescent, have developed Mo-based FEA for using them as cold cathodes in FEDs.

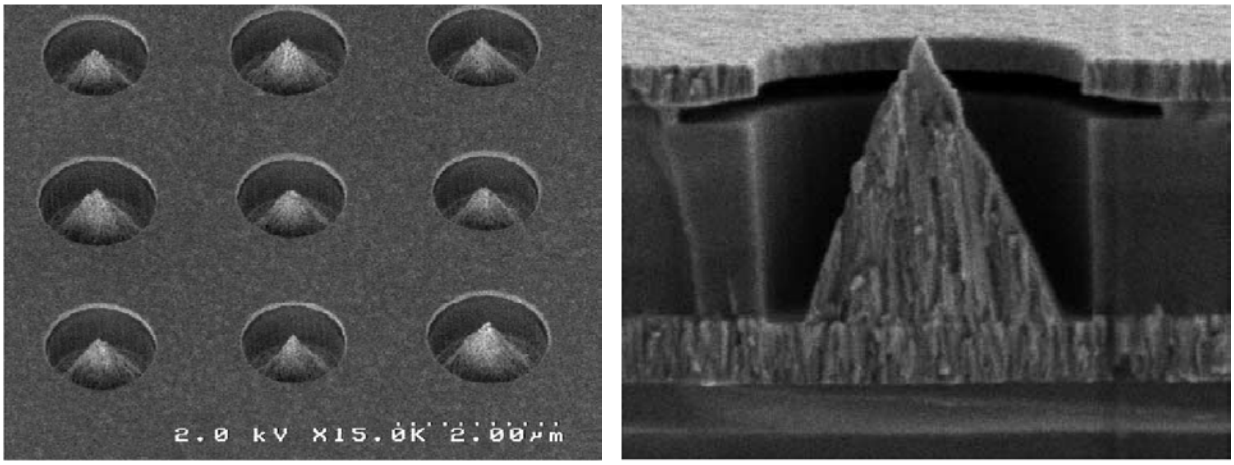

Figure 3.4. SEM of Spindt type field emitters manufactured at Motorola showing a top view of an array of nine tips (left) and a cross-section of one emitter (right).

Currently, two companies, Pixtech and Futuba, are producing FEDs for commercial use[149] but still many requirements associated with producing FEDs with competitive prices, and large scalability are not attained[150-152] and this is due to the use of the expensive semiconductor manufacturing processes to produce the emitters. In addition, FEAs technology based on metallic tips suffers from many other severe drawbacks such as the high operating voltages and the short lifetime due to the emission degradation caused by the sputter erosion and the chemical contamination of the Mo tips[139, 153]. On top of that, the relatively large surface occupied by the base of the cones prevents reaching a higher density of the emitting tips (10^6-10^8 cm^{-2}) capable of increasing the emission current density and, consequently of improving the image quality[138]. Therefore; the key for reaching planar field emitter of high current density (~1 Acm^{-2}) resides in the integration of a large number of field-enhancing tips on a surface and this necessitates the scaling down to submicron dimensions.

In summary, the design of the first generation FEDs based on the Spindt type metallic emitters constituted a major technological breakthrough but they suffer from many limitations that prevented their effective commercialization, such as, long, sophisticated, and costly production processes, high difficulty to produce large area displays, high operating voltages, poor color quality and low brightness. To overcome these problems, many researchers have been designing a second generation FEDs focusing on the replacement of the Spindt type field emitters with alternate ones which are mostly based on organic materials as we will see in the next chapter. The advantage in using such type of materials is that their film deposition requires less sophisticated techniques than the ones used for the metallic tips on one hand as well as they will permit scaling down to nanometric dimensions on the other hand.

4. Organic flat panel displays

4.1 General considerations

Given our interest in FED as the basis of this work, we will only focus in this chapter on the organic materials that are used so far for this application only, keeping in mind that a wide range of organic molecules have found application in other types of displays based on totally different concepts[154, 155] such as liquid crystal displays (LCD) and organic light emitting diodes (OLED). The former has been widely studied and developed by industrialists[156] while the latter has been lately introduced to the market because it surpasses LCD's with a wider viewing angle, higher brightness and lower power consumption but it still has a shorter lifetime[157-159]. We must point out that both latter applications have been exhaustively developed for being used in this field employing organic-based liquid crystals (LCs) but with totally different properties and prerequisites for each one among others the conjugation and the viscosity extents in addition to the hole mobility[105]. On the other hand, FED technology excels both LCD and OLED due to its high performance, good environmental characteristics and scalability as well as price that is expected to drastically decrease once a cost-effective process is found and applied in industry[133, 149, 160].

Nevertheless, the ongoing interest in fabricating a second generation of cold emitters that excel the Spindt type ones has been growing since many years due to the limitations met by the metallic tips; as we have pointed out in the previous chapter. Hence, the ideal new cold cathode has to fulfill several conditions[161]:

- The electron source must be chemically and physically stable and its emitting area must be precisely defined.
- The source should emit high current densities in such a way that the total current emitted from a small area is sufficient for device operation. It is worthwhile to note that a current of 1 µA from 1 μm^2 area requires a current density of 100 Acm^{-2}. A current density of 10 Acm^{-2} is a lower limit for a source to reach wide applications in vacuum microelectronic devices.
- The emission current should be voltage controllable.
- The energy spread from the emitted electrons should be comparable to thermionic cathodes (< 0.5 eV).

- To attain an acceptable device lifetime, the emission characteristics should be reproducible for all the sources and must have a good stability over a long period of time ($\geq 10^4$ hours)
- The manufacturing process must be cost-effective, simple, and adaptable for various applications.

Once these requirements are met, cold cathodes can then find their way towards many potential and interesting electronic applications. Nowadays, researchers are focusing mainly on the field electron emission from carbon structures such as diamond and diamond-like thin films on one hand, and carbon nanotubes (CNT) on the other hand.

4.2 Field emission from diamond and diamond like films

Field electron emission from diamond was first reported in 1991 by Djubua et al.[162] and since then hundreds of papers have been published studying the emission property of chemical vapor deposited (CVD) diamond[163-167] and diamond like (DLC) thin films[168]. The great interest in these two materials is because emission occurs at relatively low applied fields[163, 164]. Additionally, they exhibit excellent mechanical and chemical properties in addition to their low negative electron affinity (NEA) that is, unlike other materials, stable in a residual gas ambient[169-171]. NEA means that the vacuum level lies below the bottom of the conduction band and hence, electrons in this latter band gain energy when leaving the surface. To demonstrate the feasibility of carbon emitters, Motorola created a carbon-based triode FED in 1997[149]. Nevertheless, little is known about the mechanism of FEE from CVD diamond and DLC films where several emission models have been proposed[172-174] but none of them was experimentally confirmed to this date.

4.2.1 FEE from good quality diamond films

Gröning et al[175] showed that when high quality diamond films containing low defect density and few grain boundaries are deposited on a silicon substrate, unstable emission starts to occur at an applied electric field of 200 Vμm^{-1} with a breakdown of the emission above 300 Vμm^{-1} whereas when bad quality diamond films with high defect density and many grain boundaries are deposited, good emission properties are detected starting from an applied electric field of 3.5 Vμm^{-1} with a work function of 6 eV; values which are close to that of Spindt type metallic emitters. Also, when diamond films contain hydrogens at their surfaces, emission occurs while upon replacement of hydrogens by oxygen atoms, the film becomes insulator[176]. It is worthwhile to note that the emission was not homogeneous in all the cases. Additionally, when nanocrystallites of diamond were deposited, it was found that the FEE originates from well-separated individual spots where many parameters such as size, chemical and structural nature of these spots are still unknown.

4.2.2 FEE from DLC films

An important observation was recorded upon measuring the emission of several DLC films having different sp^2/ sp^3 carbon ratios: The low sp^2 containing films showed no emission until an applied field of 145 $V\mu m^{-1}$ where a sudden increase in FEE occurs and reaches saturation at 100 nA. Alternatively, DLC films with high sp^2 content show strong non-activated emission. This supposes the formation of inclusions containing long conductive channels that go down to substrate and act like emitters under the Fowler-Nordheim theory[168]. In agreement with this study, homogeneous emission was also observed from clusters of a nitrogen-containing DLC film on a silicon wafer showing a field enhancement factor β of these clusters in the range of 150-300 and revealing the importance of sp^2 bonded carbon structures in the emission process[177]. Nevertheless, the emission is always recorded from inclusions and surface irregularities and not from a homogeneous surface[176].

4.2.3 FEE from diamond coatings

Several tips coated with diamond by different deposition methods have been tested[178, 179]. The emitters showed different emission behavior depending on the coating technique employed, particle size and particle size distribution. Nonetheless, the preparation of such type of films requires the use of highly sophisticated semiconductor fabrication techniques to deposit the tip-like arrays first.

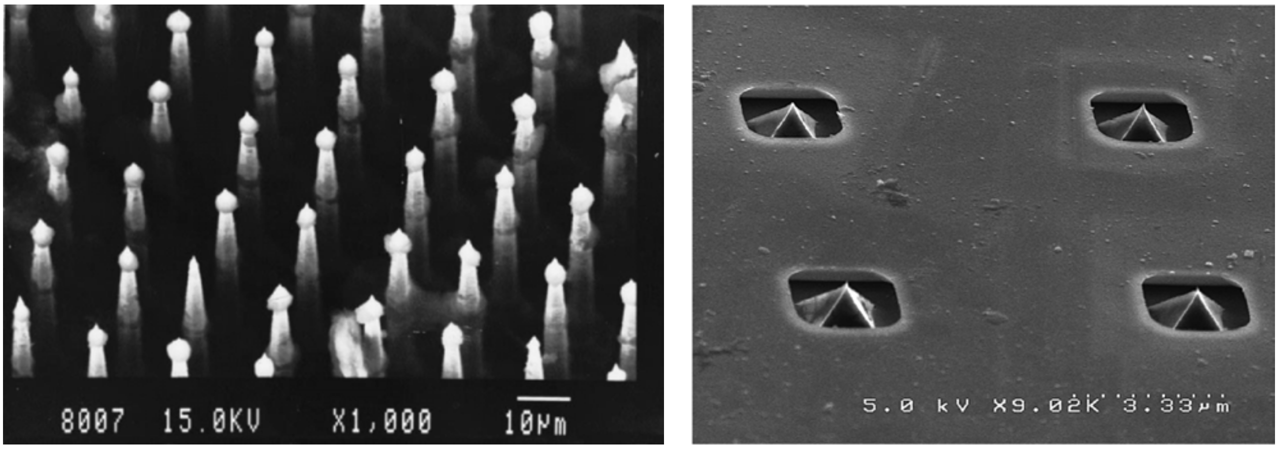

Figure 4.1. SEM of nanodiamond coated Si tips [178] (left) and a 2 x 2 array of gated diamond emitter[179] (right).

4.2.4 Conclusion

Although several interesting observations have been reported on the emission of diamond and DLC films relating the good field emission properties to the high content of sp^2 carbon centers and to the formation of inclusions containing conductive channels, the identification of the emission mechanism of diamond and DLC thin films is still ambiguous leading to fundamental difficulties in analyzing and improving their field emission. Consequently, the FEE of this type of materials is inhomogeneous all along the entire surface, which is in opposition to the Spindt type metal emitters where the emission site is well localized at the apex of the tip allowing its accurate calculations and exhaustive study. Diamond-coated tips, on the other hand, show different emission properties, ranging from good to bad ones, depending on several parameters such as the deposition technique used as well as the structural and the chemical properties of the diamond employed. Nonetheless, this latter method uses even more sophisticated deposition techniques for fabrication of the arrays than the Spindt type ones.

4.3 CNTs field emitters

After Utsumi[180] has concluded that the best emission tip should be whisker-like, industrialists and researchers have been showing an increasing interest in single and multiwalled CNTs as field emission electron sources for flat panel displays[181]. Unlike diamond and DLC films, field emission mechanism of CNTs is well-known and is governed by geometric field enhancement according to the Fowler-Nordheim theory where the field enhancement factor $\beta = h/r$ with $h >> r$ (h = height and r = radius). As a consequence, CNTs are ideally suited for field emission applications since they exhibit exceptional high aspect ratios with a length in the micrometer region and a diameter of a few tens of nanometers permitting therefore high values of β when singular CNTs are tested. This has led Smalley et al.[182] to assume (to date there is no follow-up) ballistic motion of electrons in a CNT is due to the formation of an atomic wire formed by sp carbons at the tip end. Recently, Samsung has produced several prototypes of FEDs based on CNT with a diode configuration[144] but whose costs and lifetime are still critical[149]. We present herein the recent advances in field emission from CNTs (SWNTs and MWNTs) films as well as from micro-dispersed ones. It is important to note that we designate by the term "CNT films" the results obtained when CNTs were deposited either in thin films or when they were grown in bundles on a micrometer sized metal pattern forming arrays while we mean by "well-dispersed" CNTs those that were grown on nano sized metal patterns whose dispersion on the substrate is of high uniformity.

4.3.1 FEE from CNT films

Extensive studies of FEE from CNTs films have been carried out since the last decade using different conditions and many deposition techniques[181, 183-185]. Mentioning these latter will exceed the aim of this work that is only concerned in the major problems encountered when using CNTs for FEDs applications.

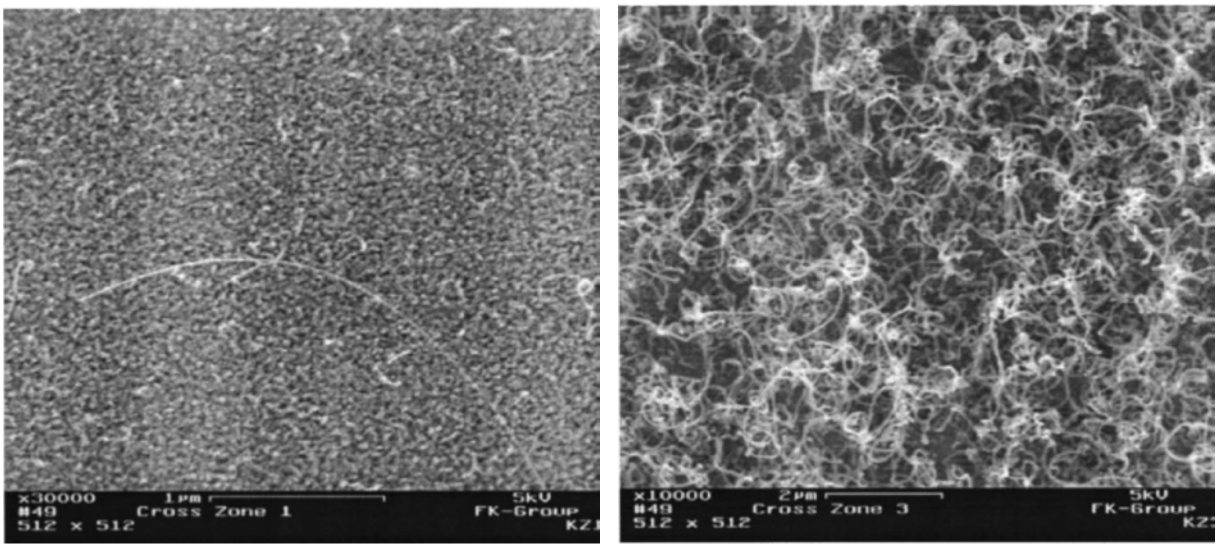

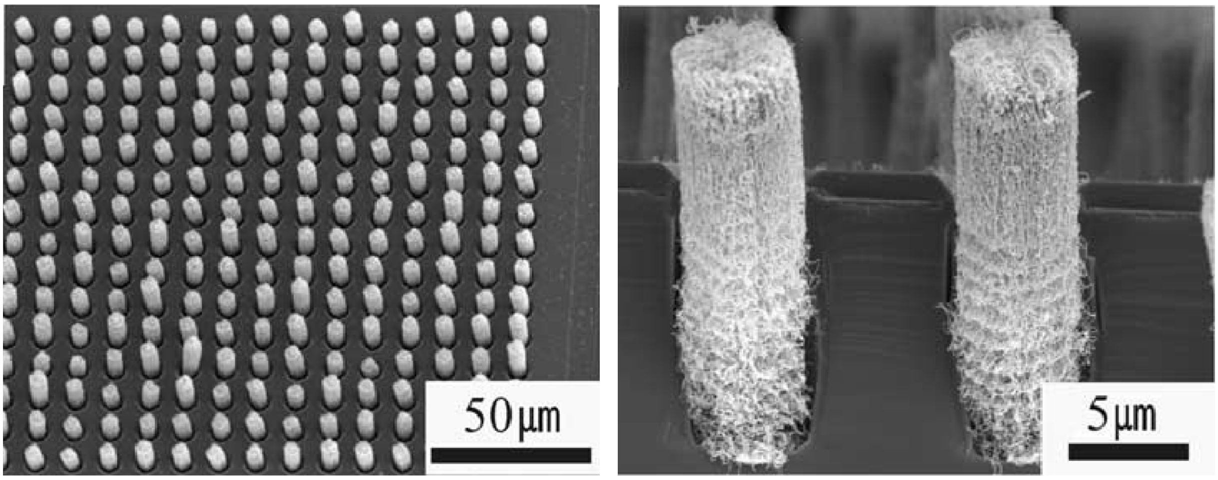

Figure 4.2. HRSEM images of cross-shaped patterned CNT film[142] (up) and CNTs grown on hole patterns[186] (down).

Isolated MWNT and SWNT exhibit exceptional emitting properties with a very good chemical stability[182] but when the emission of a group of CNTs is tested, the FEE behaves differently showing many sources of emission degradation. To better understand the mechanism of this latter, Nilsson et al.[187] have developed a scanning anode field emission microscope (SAFEM) capable of analyzing the individual emission sites and allowing, consequently, the retrieval of many information about the damage phenomenon. Two main types of degradation have been detected [188, 189]: the first occurs at very low emission current and seems to be driven by the electric field while the second is current driven and occurs above 300 nA/emitter. The former is typically seen during the first emission scan and is believed to be caused by the presence of different adsorbates, like amorphous carbon remaining from deposition. On the other hand, the current driven degradation is due to interaction and heat dissipation during solid state transport of a high current density through the CNT, at the CNT-substrate interface or at the CNT apex. It should be noted that the first is caused by the high internal resistance in the CNT due to the defects it might contain while the second is for the reason that the interface contact plays an important role in heat dissipation where a poor electric contact provides the main obstacle in the electron transport evolving an impressive amount of heat, high enough to melt the substrate.

Different CNTs based FEDs with diode and triode configurations have been fabricated[144, 184], as figure 4.3 on the next page depicts, showing instable emission caused by fluctuations in emission current where some CNTs decomposed at high currents[186]. On top of that, when bundles of CNTs are used as the emitting source, electric field were strongly enhanced at the edges causing, therefore, a non-uniformity in the illumination of the screen[144].

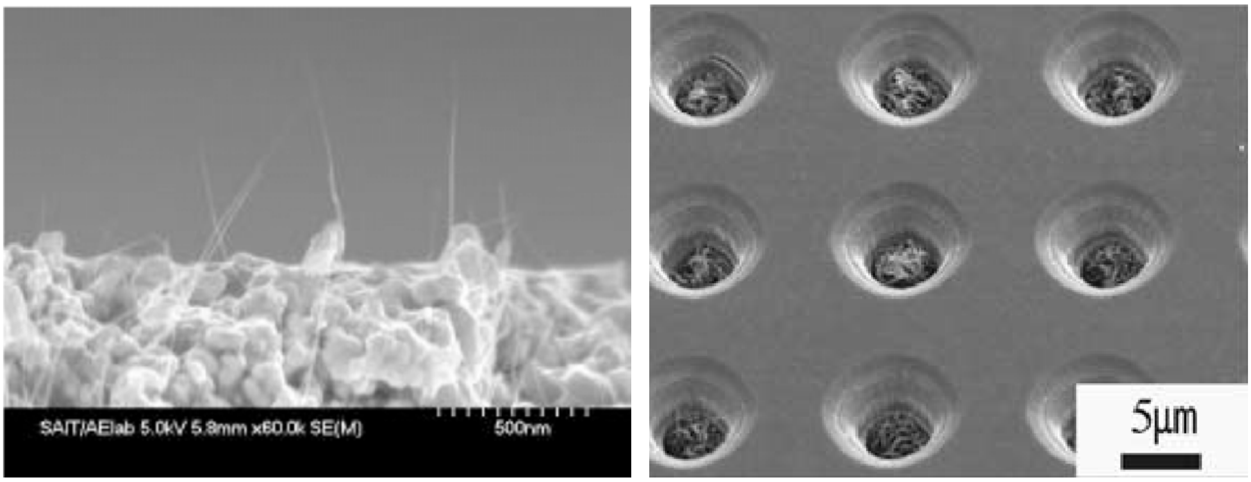

Figure 4.3. SEM images of the CNTs based diode structure[144] (left) and triode one[186] (right).

Another problem has been detected during the study of the CNTs arrays; low density CNTs films have shown superior emission than high density ones, a phenomenon caused by the screening effect of the neighboring CNTs which are shielding the electric field and consequently decreasing the field enhancement factor[143] β. To overcome this effect, researchers have proved that a maximum emission is achieved when the CNTs are separated by a distance d that is equal to twice their height[142] ($d = 2 \times h$ with d the distance between two CNTs).

4.3.2 FEE from well-dispersed CNTs

Recently, Milne et al. have succeeded in growing vertically aligned MWNTs on nano-dispersed Fe and Ni patterns after using a suitable deposition technique[190, 191]. These upright CNTs arrays exhibit a high degree of uniformity, as figure 4.4 illustrates. Field emission examination of these latter showed that they are conductive in nature, having current densities of 10^7-10^8 A/cm^2, and an average field enhancement factor β of 242 with a deviation of 7.5%. Nevertheless, the maximum emission current extracted (~10µA) from these structures, which is still 100 fold less than a single MWNT, causes irreversible degradation of the CNTs. In fact, these latter were found to be up-rooted due to electrostatic force at the interface substrate-CNT.

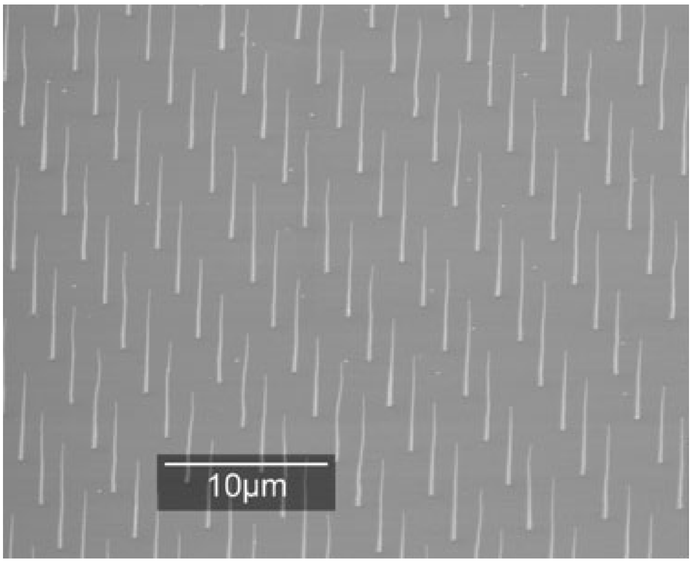

Figure 4.4. SEM of well-dispersed CNTs arrays.

4.3.3 Conclusion

CNTs show exceptional emission properties when they are present in isolated form due to their quasi one dimensional structures, with a length of a few micrometers and a diameter of a few nanometers, giving rise to a high field enhancement factor. Nevertheless, CNTs suffer from many drawbacks when deposited on a substrate for a FED application, from these we note: the non-uniformity of the CNTs heights and radii, the defects present in CNTs during the growing process, the poor contact at the interface with the substrate as well as the shielding effect caused by neighboring CNTs. All these latter cause severe damages like non-uniform emission as well as irreversible degradation. It could be easily noticed that all these inconveniences originate from the growing and the deposition processes used so far and that employ ‘physical’ techniques without any employment of chemical engineering that could be useful in building such nano devices.

5. Design features of a new organic FED

5.1 Toward a self-assembled field emitter

We have shown previously (chapter 2) that self-assembly by weak, non-covalent interactions affords a 'self-healing' supramolecular network that, because of its reversibility, can reassemble after applying an external distortion whereas the rigidity of covalently bonded systems results in an irreparable damage. Consequently, we have foreseen to replace the rigid columnar CNTs field emitters by disk-shaped molecules that self-organize into pillars. Although these latter molecules are synthesized chemically and therefore, their structures and purity are well-controlled, they must fulfill many requirements for their investigation as good emitters, from these we note, a good charge carrier mobility through the column, an adequate environmental stability, a chemical functionality that prevents a lateral coagulation of the stacks, and last but not least, a perfect adhesion on the substrate.

The candidate that best fits these requirements are the HBC derivatives: they self-assemble into columns with an outstanding degree of order in the solid state[101, 106, 192] and they exhibit the highest charge carrier mobility recorded so far for a disc shaped molecule both in solid and in liquid crystalline states[13, 104]. Additionally, these 'super benzene' structures show very good chemical stability as well as high decomposition temperatures (>350°C in air)[14, 96, 193].

Nevertheless, the main drawback of HBC derivatives for such an application is the lateral interaction between adjacent stacks brought about by the high crystalline packing of their aliphatic side chains, as figure 5.1 illustrates. This latter feature is expected to cause a severe drop of the field electronic emission due to the screening effect we evoked lately (section 4.3.1). Additionally, most of HBCs bearing aliphatic chains are liquid crystalline at room temperature, which constitutes a second disadvantage since it induces a drastic decrease of their charge carrier mobilities[14].

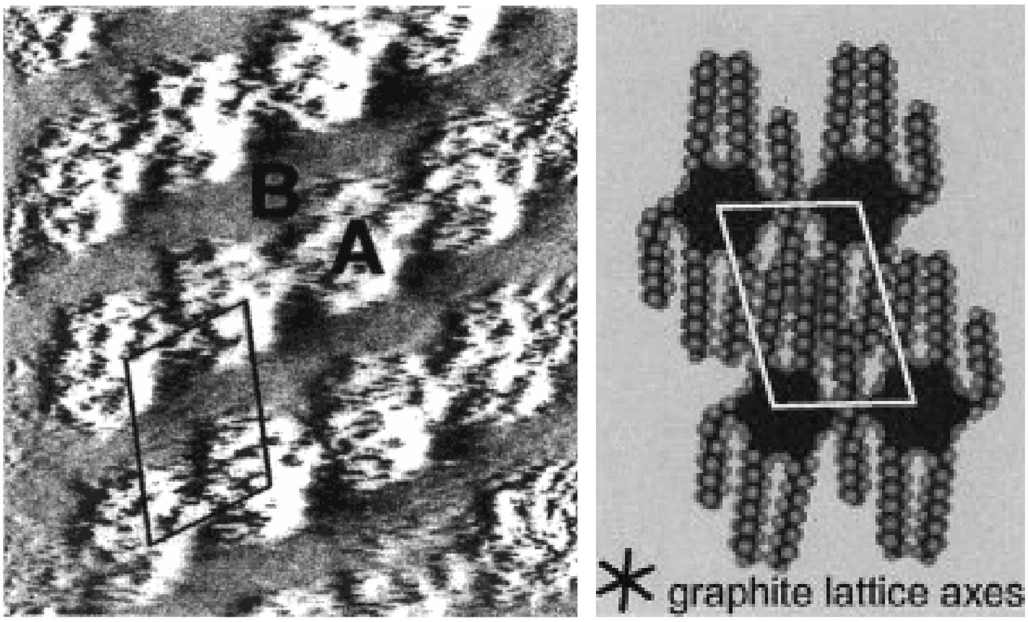

Figure 5.1. STM image of HBC-C_{12} on HOPG[99] (left) and packing model of a two-dimensional crystal of HBC-C_{12}[94] (right).

To prevent the intercolumnar interactions, and hence increase the one dimensional electronic emission, long perfluorinated side chains will have to replace their alkyl homologues. The former groups are well-known for their Teflon-like properties such as, high volatility, low solubility, high thermal stability and low aggregation tendency due to their low Van der Waals interactions as well as to the fact that they hardly ever make hydrogen bonds[194]. Besides inhibiting the intercolumnar interactions, the perfluorinated chains will constitute a ‘mantle’ around the central core, which will also facilitate their self-organization, in all types of solvents, into single dispersed columns.

Moreover, to assure a good adhesion between the HBCs ‘towers’ and the substrate, syntheses of primer molecules should be used. These specially designed HBC derivatives will be deposited onto the substrate as the foremost monolayer, being fixed to the electrode surface and acting as hosts for the other long perfluorinated chains bearing HBC’s, during their deposition process, since these latter will prefer to self-assemble onto the primers in a column like ordered structure rather than depositing onto the ‘uncovered’ metallic substrate. Figure 5.2 on the next page illustrates the idea of a diode-type FED based on perfluorinated HBCs.

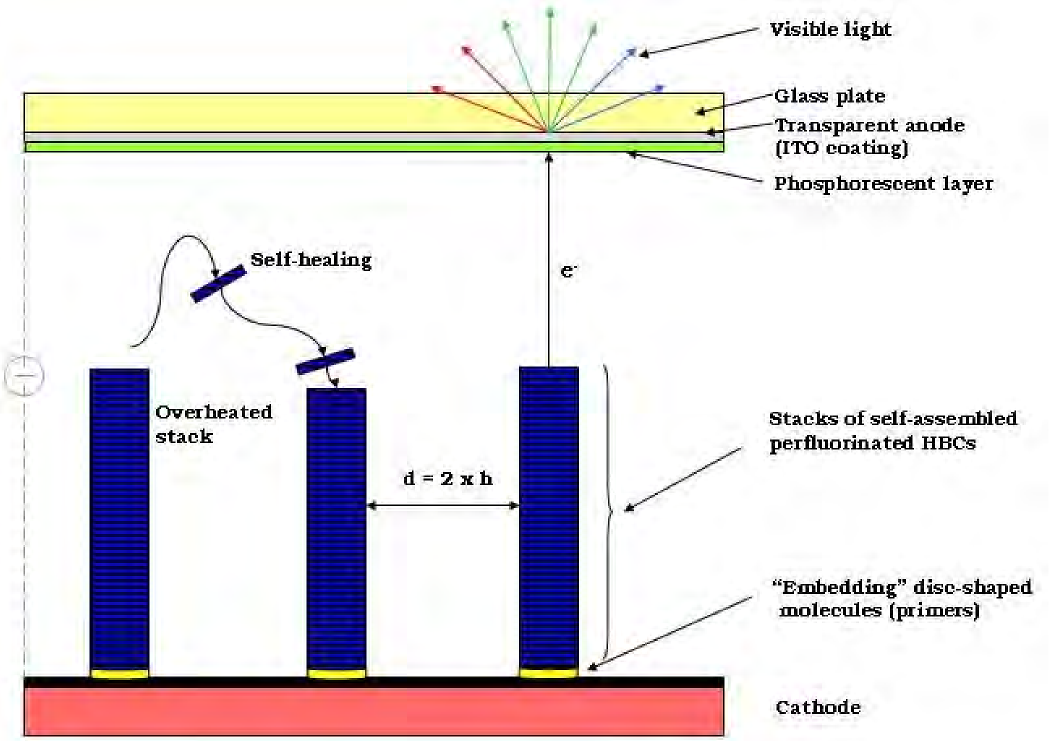
Visible light
Glass plate
Transparent anode (ITO coating)
Phosphorescent layer
Self-healing
e-
Overheated stack
d = 2 x h
Stacks of self-assembled perfluorinated HBCs
"Embedding" disc-shaped molecules (primers)
Cathode

Figure 5.2. Descriptive sketch of the perfluorinated HBCs based diode structure; with d the distance between two columns and h the column height (arbitrary dimensions).

5.2 Investigation of new nitrogen-containing PAH

The objective of this project can be considered as a logical evolution of the one presented in the previous section. The idea relies on finding a synthetical strategy to construct a disc-shaped HBC-like molecule bearing a nitrogen atom in its center. Because of the free lone pair of electron it bears, the nitrogen atom has a low oxidation potential which will enhance the electron donating property in such a way that the columnar stacks formed by auto-assembly of these molecules will be not only more efficient hole conductors than their HBCs homologues, but also much better emitters from the top most molecule.

For this purpose, synthesis of two completely unknown molecules will be initiated: the symmetrical naphth-annelated cyclazine **22** and the less symmetrical one, lacking six peripheral sp^2 carbon atoms, **23**. Both products will also be decorated with perfluorinated chains for the same reasons we have stated previously (section 5.1).

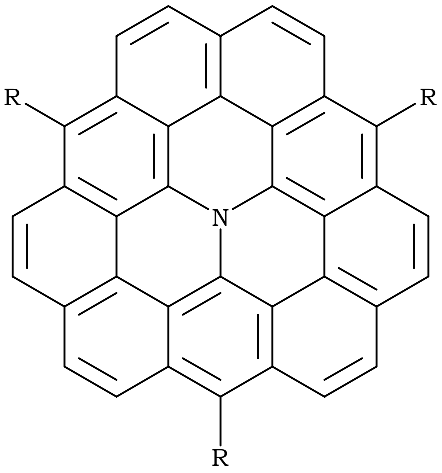

22

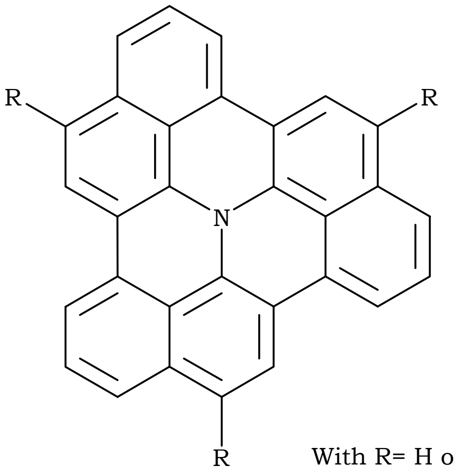

With R= H or perfluorinated
chain

23

Figure 5.3. Structure of the symmetrical nitrogen-containing PAH **22** and the less symmetrical one **23**.

II. Results and Discussion

6. General strategies to produce HBC

Hexa-peri-hexabenzocoronene (HBC) **9** moieties can be obtained by two main synthetical pathways: the first is favorable when the target molecule bears the same lateral functional groups yielding a completely symmetrical molecule[93, 195, 196] while the second is preferable when synthesis of an asymmetrical HBC is envisaged[87, 94, 96]. We will also discuss two new strategies for synthesizing symmetrical HBCs: a one-pot reaction published recently[197] and a new strategy explored and developed in our laboratory. It must be pointed out that all the multistep reactions mentioned above lead to the formation of a hexaphenyl benzene derivative **24** first, which will be converted to the desired product, in a final key step, by cyclodehydrogenation reaction using one of the conditions listed in figure 6.1 below[90].

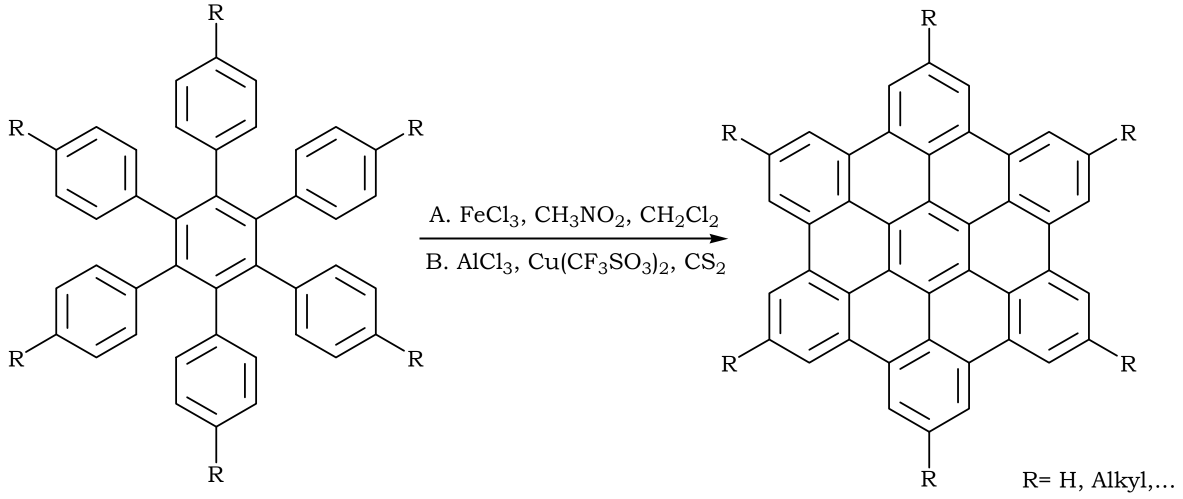

24

9

Figure 6.1. Synthesis of HBC via cyclodehydrogenation of hexaphenylbenzene.

It is worthwhile to note that besides the conditions used above[198], one finds a lot of oxidative cyclodehydrogenation conditions in literature using, for example, vanadium(V) salts[199, 200], thallium(III) salts[201, 202], as well as photochemical cyclodehydrogenation using elemental iodine[59, 203]. Palladium(0)-catalyzed cyclodehydrogenation at high temperatures up to 400°C or higher has been also reported. Never the less, the yield of this last process is very low[204]. The first HBC obtained by oxidative cyclodehydrogenation of hexaphenylbenzene was reported by Halleux et al.[205], using the well-known $AlCl_3$/NaCl melt as reagent[206], but affording HBC in a very low yield.

Recently, Müllen et al.[88] have applied Kovacic's conditions[207, 208], which employ $AlCl_3/CuCl_2$ for benzene polymerization to *p*-polyphenyl, where $AlCl_3$ acts as a Lewis acid catalyst while $CuCl_2$ is the oxidant reagent. Reacting this latter combination of Lewis acid/oxidant with hexaphenylbenzene derivative **24** at room temperature, affords HBC derivatives **9** in a quantitative yield. Nonetheless, for alkyl substituted hexaphenyl benzene moieties, it was found that the $AlCl_3/CuCl_2$ mixture causes migration or even cleavage of the alkyl chains[90] and in some cases, it generates the chlorination of some partially oxidized derivatives, especially upon using bulkier oligophenylenes[64, 87]. For these reasons, iron(III) chloride known to be a mild Lewis acid and an oxidant at the same time[209], is used[210] instead of $AlCl_3/CuCl_2$ combination. The use of nitromethane or nitroethane in the medium, to enhance the reaction and to provide a higher yield has been also reported[211, 212]. In case the mild iron(III) chloride was not efficient as a Friedel-Crafts catalyst, it can be replaced by the $AlCl_3/Cu(OTf)_2$ combination, the latter is used instead of $CuCl_2$ to avoid any contamination of the final product by chlorine[93, 99, 213].

It was proven that the cyclodehydrogenation reaction evolves HCl and reduces iron(III) species to iron(II)[210]. Therefore, the reaction balance of the cyclodehydrogenation reaction can be written as shown in scheme I below.

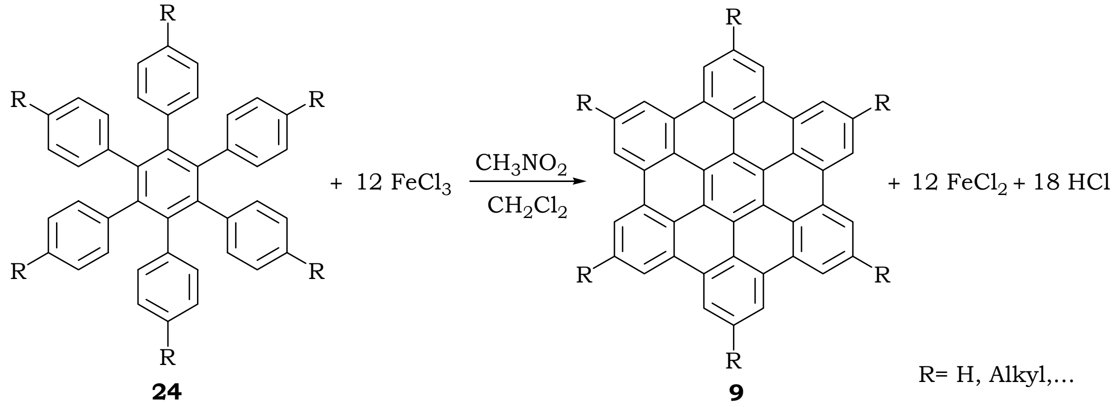

Scheme I. Equilibrium reaction of the cyclodehydrogenation reaction.

The mechanism of the dehydrogenation reaction using the Lewis acid-oxidant combination, in general, was the subject of many propositions since it is not fully understood yet. Nevertheless, two principal pathways have been proposed[214]: the radical cation route, presented in scheme II and the σ complex pathway shown in scheme III. It has also been reported[215] that one of these mechanisms takes place depending on the type of the substrate and on the reaction conditions applied, as well as both can even be valid in some cases.

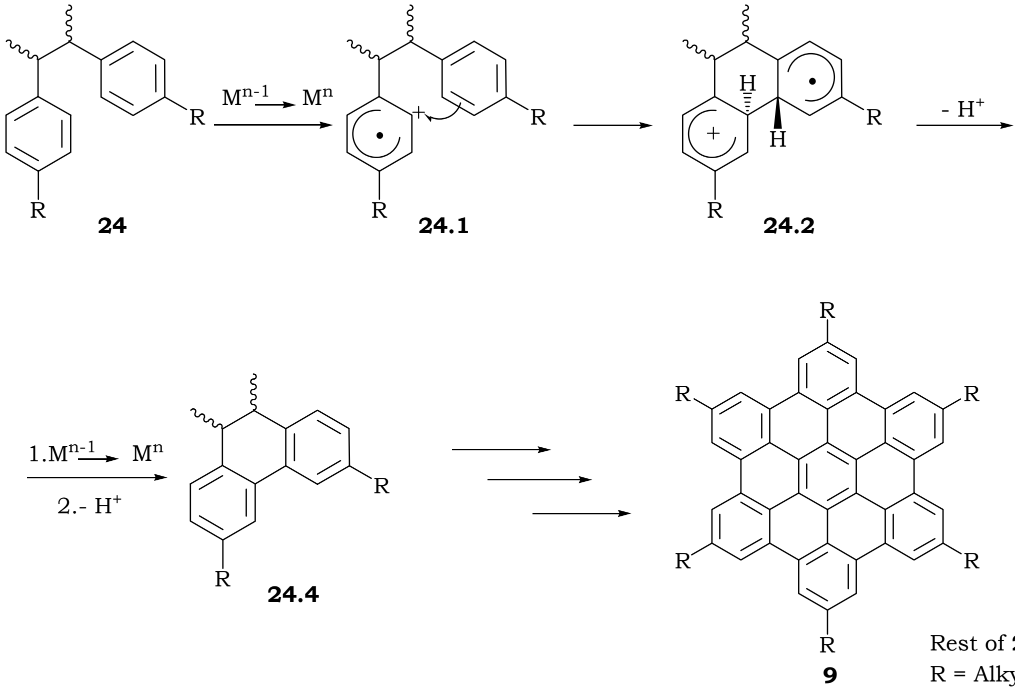
R
24
M^{n-1} → M^n
R
24.1
H
H
R
24.2
- H^+
H
R
24.3
1.M^{n-1} → M^n
2.- H^+
R
24.4
R
9

Rest of **24** is omitted for clarity
R = Alkyl or *p*-substitued-phenyl
M^{n-1} = Fe(III), Cu(II)

Scheme II. Proposed mechanism of the cyclodehydrogenation reaction by the formation of a radical cation in a first step.

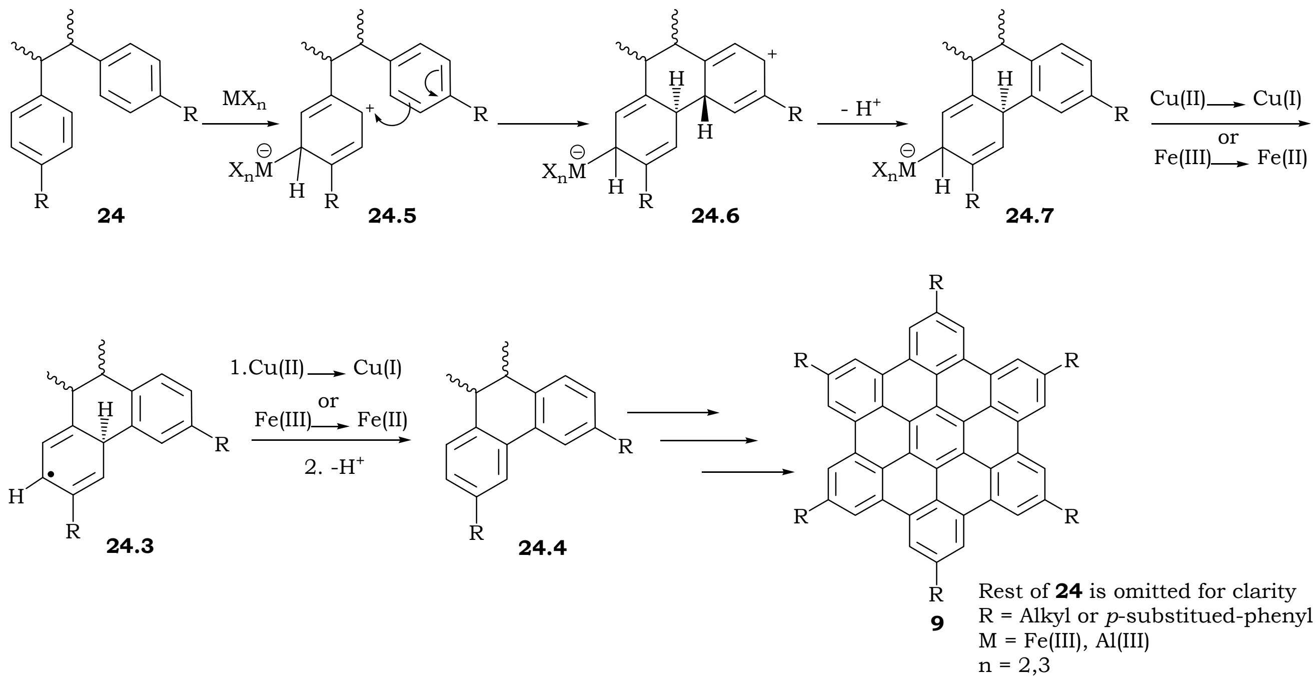

Rest of **24** is omitted for clarity
R = Alkyl or *p*-substitued-phenyl
M = Fe(III), Al(III)
n = 2,3

Scheme III. Proposed mechanism of the cyclodehydrogenation reaction by the formation of a Friedel-Crafts complex in a first step.

It must be pointed out that there is considerable support for the formation of monocation radical **24.2** presented in scheme II due to many demonstrations on a variety of systems[216]. However, the latter scheme represents an oversimplification of the mechanism that can take place. Scheme IV shows an extrapolation of this mechanism; instead of the formation of the radical species **24.3**, the radical cation **24.2** undergoes subsequent oxidation forming, therefore, the dication moiety **24.8**. Though, this process is associated with the more stable species and was found in many highly delocalized systems, such as perylene and thianthrene derivatives[216]. On the other hand, the evidence for scheme III occurrence is the fact that the presence of HCl was found to be crucial in many cases, where upon the elimination of that latter by a stream of an inert gas, the reaction ceases but resumed on reintroduction of the protonic acid[217].

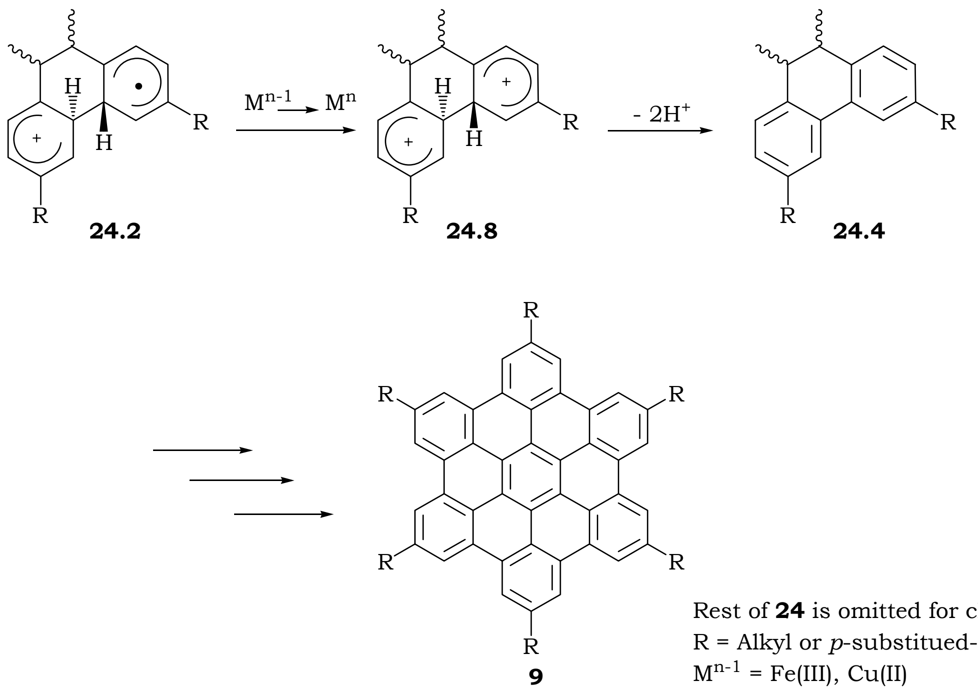

Rest of **24** is omitted for clarity
R = Alkyl or *p*-substitued-phenyl
M^{n-1} = Fe(III), Cu(II)

Scheme IV. Proposed mechanism of the cyclodehydrogenation reaction by the formation of a dication followed by extrusion of two protons.

From all this discussion above, we can conclude that the cyclodehydrogenation mechanism of hexaphenyl benzene species, are more favorable to the mechanisms described in schemes II and IV than to the one shown in scheme III for several reasons: first, the reaction is done in absence of any trace of water, which is crucial to produce the protonic acid needed to initiate the reaction and, second upon doing the reaction, HCl that forms in the medium is immediately extruded by a stream of argon without preventing the reaction from proceeding further. As a result to this assumption, we might assign to nitromethane the role of radical intermediates stabilizer rather than the role of a Brönsted acid needed to initiate the reaction, in the case of a radical initiation process as it has been proposed by Kovacic[211, 212] (scheme III). Following the same analogy, we suppose that the reaction conditions employing $AlCl_3/Cu(OTf)_2$ combination is more favorable towards schemes II and IV since the reaction is done after heating the latter the mixture at a high temperature to remove any trace of water from the medium, bubbling the reaction medium with a stream of argon would be interesting to see whether the reaction stops or not in this case.

6.1 Symmetrical synthesis pathway

As a reason of its symmetrical structure, the synthetical approach herein is based on building the para-substituted tolane derivative in a first step **25** followed by trimerization of the alkyne moiety to yield the hexaphenylbenzene species **24** which will be oxidized in a later step to the desired HBC derivative **9** as mentioned previously. Synthesis of the tolane species **25** can be achieved via three different pathways: the first is made by the dehydrohalogenation of a 1,2-diphenyl dihaloethane derivative, the second is done in a step-by-step Sonogashira cross-coupling and the third uses the same coupling type but in a one-pot synthesis.

6.1.1 Tolane synthesis from stilbene[218]

The tolane derivative **25** is obtained in a two step reaction as shown in figure 6.2 below: after the bromination (or the iodination) of the stilbene derivative **26**, the resulting product **27** is transformed by dehydrohalogenation, with a solution of sodium hydroxide in ethanol, to the desired tolane derivative in a moderate to good yield (depending on the type of the para-substituted products).

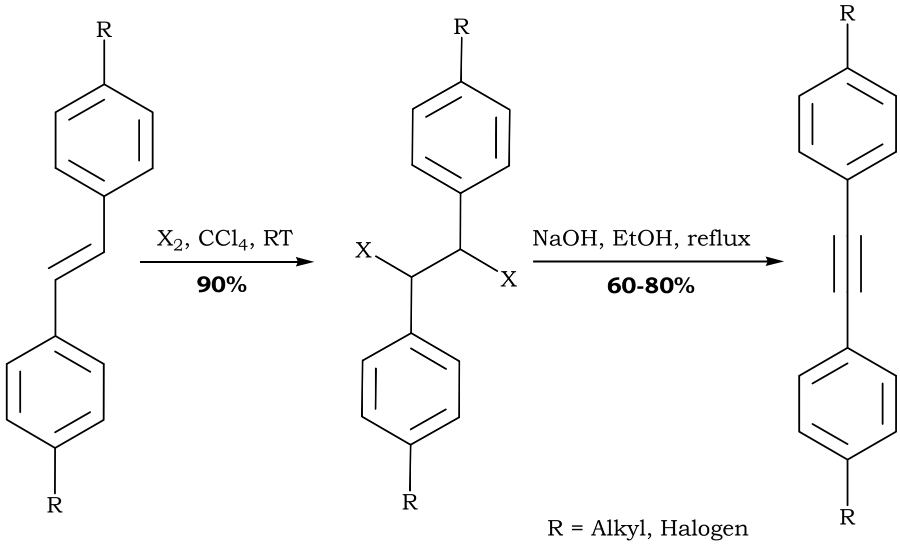

26 **27** **25**

Figure 6.2. Tolane synthesis by dehydrohalogenation of stilbene derivative.

6.1.2 Tolane synthesis in a step-by-step Sonogashira cross-coupling[219]

This method uses the standard Sonogashira coupling reaction conditions that will be further discussed in the following chapters. As it can be noticed from figure 6.3 below, the benzene derivative **28** is reacted with trimethylsilyl acetylene (TMSA) in a first step to afford the trimethylsilylated alkynylbenzene moiety **29** that is then deprotected under basic conditions to its alkyne homologue **30**. This latter is reacted, in a third step, with product **28** in presence of a suitable palladium catalyst to yield the desired tolane derivative **25**. The overall yield varies drastically depending on the nature of the terminal groups.

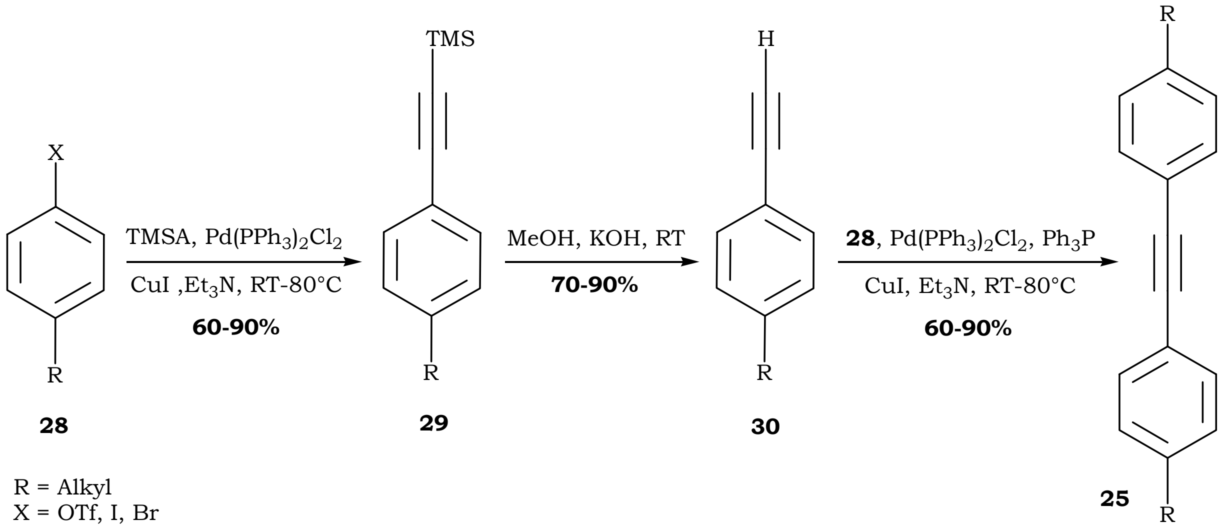

R = Alkyl
X = OTf, I, Br

Figure 6.3. Tolane synthesis via a step-by-step Sonogashira reaction.

It is noteworthy that the nature of the leaving group highly affects the reaction: on one hand triflate and iodine are better leaving groups than bromine thus a higher yield is obtained and milder reaction conditions are employed; the reaction is run at room temperature instead of heating it to 80°C upon using bromine. But on the other hand, triflate and iodine are reactive to such extent that homocoupling byproducts of **28** and **30** could form during the reaction (figure 6.4).

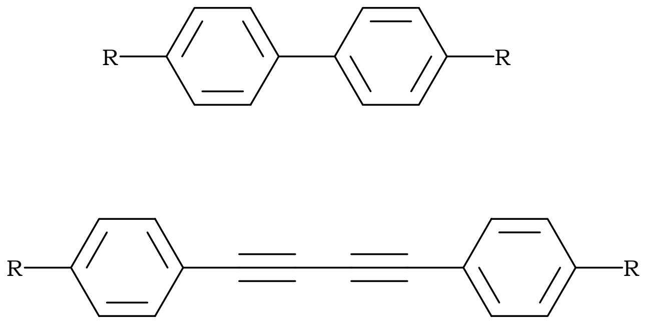

Figure 6.4. Homocoupling products of **28** (up) and **30** (down).

6.1.3 Tolane synthesis from a one-pot Sonogashira cross-coupling[220, 221]

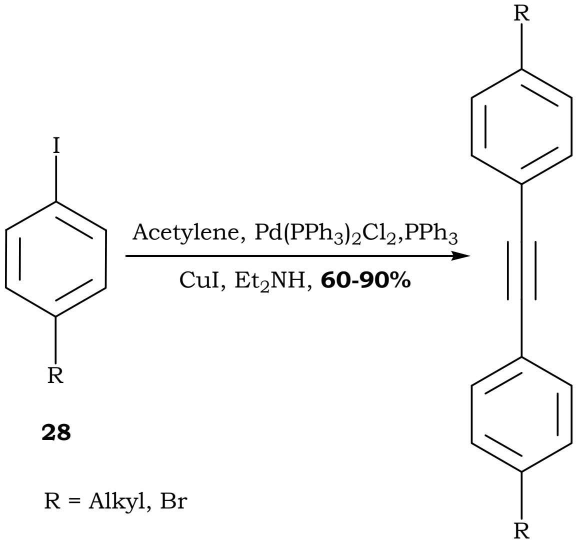

Acetylene, $Pd(PPh_3)_2Cl_2$, PPh_3; CuI, Et_2NH, **60-90%**

28

R = Alkyl, Br

25

Figure 6.5. Tolane synthesis via a one-pot Sonogashira reaction.

It is probably the easiest way to obtain symmetrical tolane derivatives. Nonetheless, it is not a reaction whose conditions could be applied to all the benzene derivatives **28** as it will be shown in the in the next sections and this is due to the fact that the functional group in the para position has great influence on both the formation of byproducts and on the yield of the desired tolane species. Recently researchers succeeded to obtain a wide range of tolane derivatives by changing the reaction conditions after replacing acetylene gas, palladium catalyst and diethyl amine by TMSA, Pd(0) and amidine base respectively[222]. Nevertheless, traces of monosubstituted and homocoupling products were still detected.

6.1.4 Trimerization of tolane derivative **25**

Once synthesized and isolated, the tolane derivative **25** could be trimerized using one of both cobalt catalysts well known for this type of reaction. Therefore, the alkyne moiety is refluxed in a suitable solvent in presence of either octacarbonyldicobalt, $Co_2(CO)_8$, or dicarbonyl(cyclopentadienyl)cobalt(I)[223-228], $CoCp(CO)_2$ to yield the hexaphenylbenzene **24** (figure 6.6). Lately, other catalysts that could also be used for trimerizing such type of molecules were found from these we note tetrakis(triphenylphosphine)-nickel(0)[229], $Ni(PPh_3)_4$ and hexachlorodisilane[230], Si_2Cl_6.

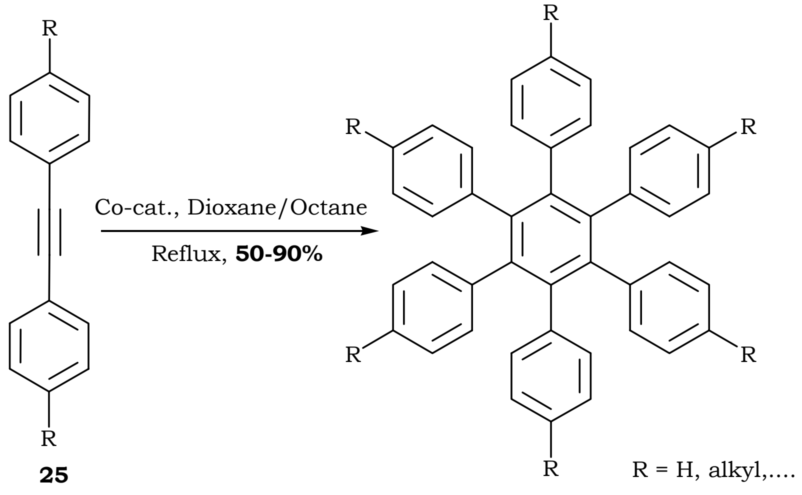

25

24

Figure 6.6. Synthesis of hexaphenylbenzene by trimerization of tolane.

6.2 Asymmetrical synthesis pathway

This synthetical route is used when an HBC bearing different terminal groups is needed. In this case the asymmetrical hexaphenylbenzene **24** derivative is produced, in a fairly good yield, after a [4+2]-cycloaddition reaction of tetraarylcyclopentadienone **31** and tolane **25** derivative in refluxing diphenylether. It is noteworthy that each of those starting materials could bear two different functional groups at their ends yielding, thereby, an HBC having a maximum of four different groups.

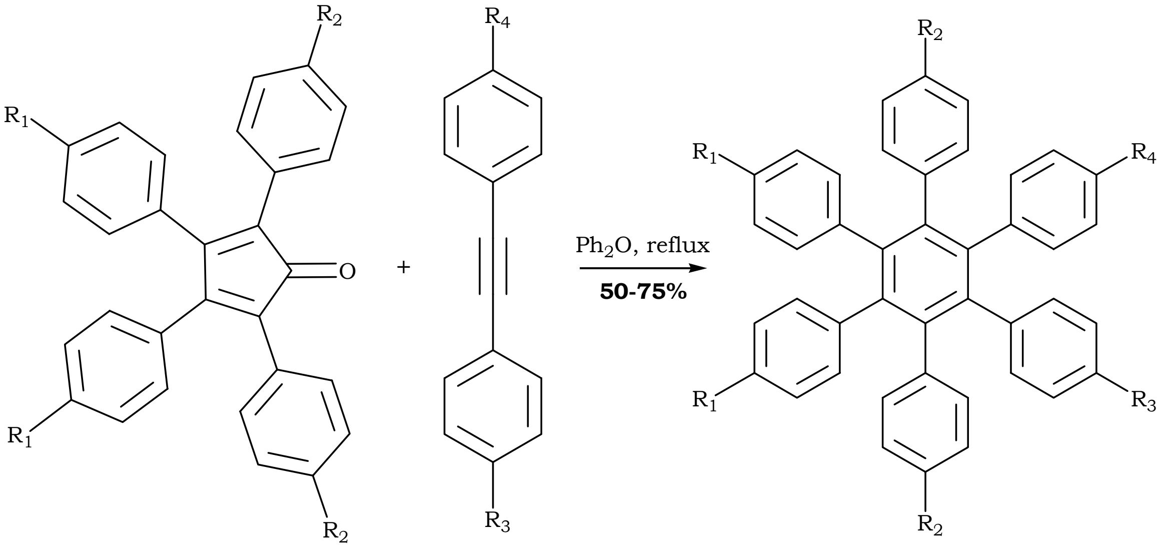

31 **25** **24**

Figure 6.7. Synthesis of hexaphenylbenzene by a [4+2] cycloaddition reaction.

Nonetheless, product **31** is obtained after a series of different multistep reactions as it can be noticed from figure 6.8 on the next page: tolane species is oxidized with iodine in DMSO to yield **32**[231] whereas condensation of the benzyl halide precursor **33** with $Fe(CO)_5$ in presence of a phase transfer catalyst affords the 1,3-diarylacetone derivative **34**[232]. A two-fold Knoevenagel condensation between this latter and the 1,2-diketone derivative **32** yields the desired tetraarylcyclopentadienone **31**[94]. It must be pointed out that the overall yield can vary from moderate to good depending on the nature of the terminal functional groups.

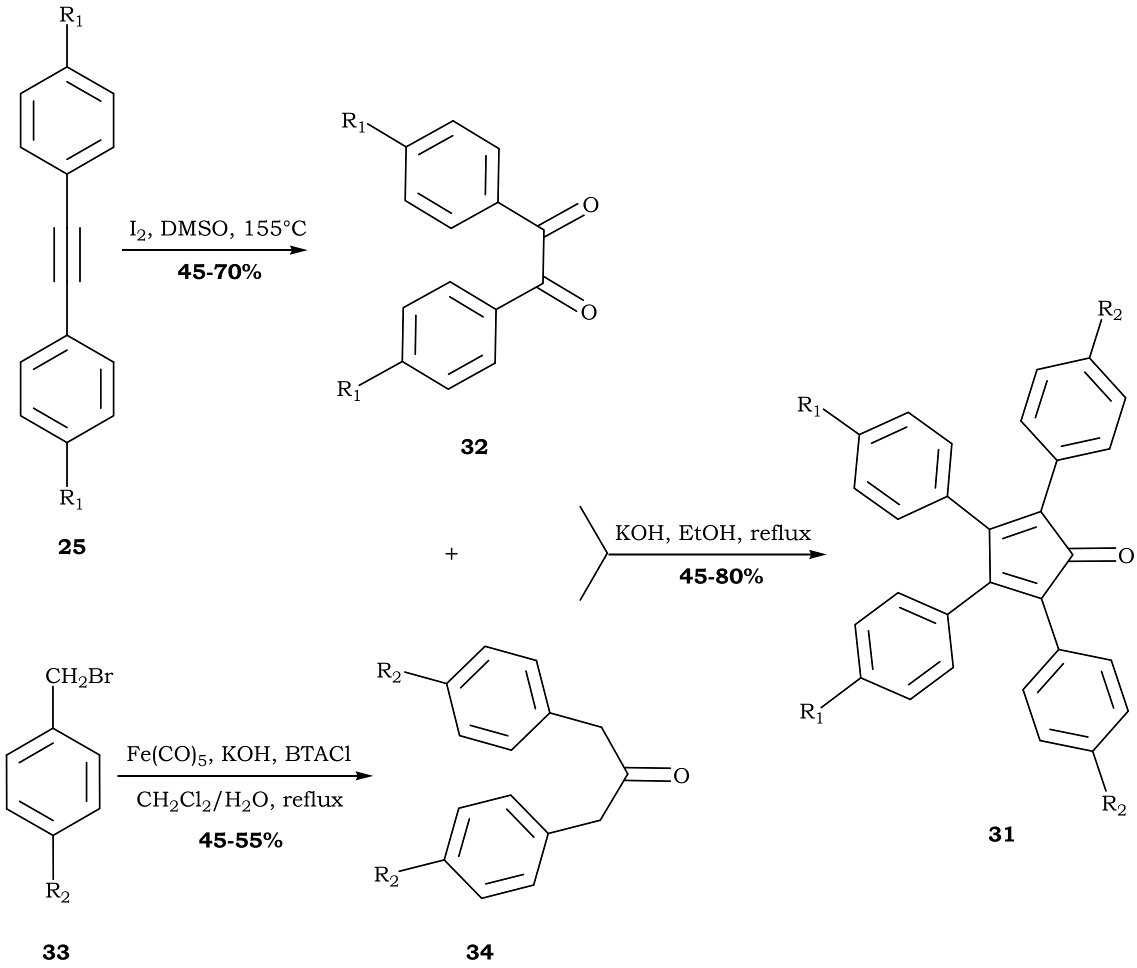
R1
R1
25
I2, DMSO, 155°C
45-70%
R1
O
O
R1
32
+
KOH, EtOH, reflux
45-80%
R1
R2
O
R1
R2
31
CH2Br
R2
33
Fe(CO)5, KOH, BTACl
CH2Cl2/H2O, reflux
45-55%
R2
O
R2
34

Figure 6.8. Synthesis of the tetraarylcyclopentadienone precursor.

The advantage of this synthetical strategy is that it allows a decoration of the HBC moieties **9** with different functional groups, which consequently widens the prospect of obtaining new HBC groups. Nevertheless, this approach requires additional steps and more starting materials to be done.

6.3 One-pot synthesis of HBC derivative

Recently Rathore et al.[197] have developed a synthetical method in which hexa-*tert*-butyl HBC derivative **35** is produced in a high yield by reacting the commercially available hexaphenylbenzene with an excess of *tert*-butylchloride in presence of excess iron(III) chloride. This latter has a double role; it acts as a Lewis acid for the Friedel-Crafts alkylation first, followed by acting as a Lewis acid/oxidant providing, therefore, the desired HBC derivative **35** as it was proven in the reference mentioned previously; whereupon using a catalytic amount of $FeCl_3$, a high amount of partially alkylated hexaphenylbenzene derivatives were isolated in addition to the hexa- substituted hexaphenyl benzene product (30%) and traces of HBCs.

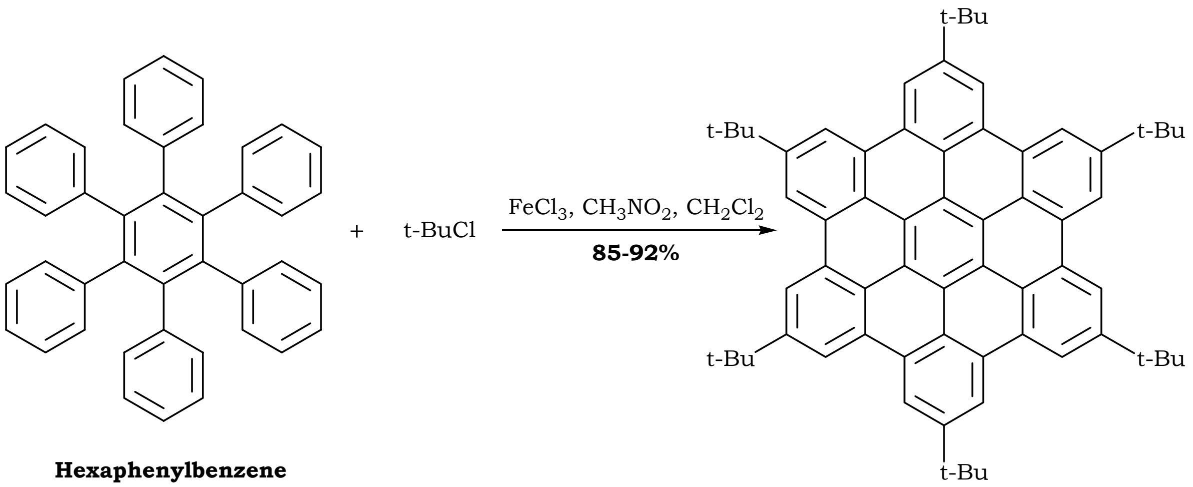

Hexaphenylbenzene (HPB)

35

Figure 6.9. One-pot synthesis of HBC bearing t-butyl group.

This reaction would be of great interest if it is generalized to produce a wide range of hexa-alkylated HBCs. However, preliminary attempts in our laboratory turned out to be negative as we will see in the following chapters. The reason of this failure is due to the fact that the alkyl group used by Rathore et al. is a tertiary one which is much more active in Friedel-Crafts reactions than a primary alkyl chain. Moreover, the high bulkiness of tert-butyl group prevents any aggregate formation during the reaction leading to product **35** known for its high solubility due to the disability to form stacks[233] whereas upon using an n-alkyl chain, the aggregation leads then to the formation of a mixture of substituted alkylated HBCs, as a reason of the insolubility of the aggregates.

6.4 Development of a new precursor

As it could be noticed from the strategies shown above, even when the HBC derivative is a symmetrical one, its synthesis requires a multistep reaction whose yield increases or decreases drastically depending on the type of the terminal functional group it bears. This has led us to work on the design of a new precursor that could be used as a basic substrate to produce, in two or less steps, the desired HBC candidates instead of going many steps back at each time we want to synthesize a new derivative. Consequently, we have tried to functionalize the material we always need to get any HBC moiety i.e. hexaphenylbenzene with good leaving groups able to react via the standard C-C coupling reactions to afford the desired hexaphenylbenzene derivatives which will be oxidized in a next step to the desired HBC derivatives. Therefore, trimerization reaction of 4,4'-dibromodiphenyl acetylene **36** using a catalytic amount of cobalt carbonyl in refluxing dioxane was done affording hexakis(4-bromophenyl)benzene **37** in a moderate yield.

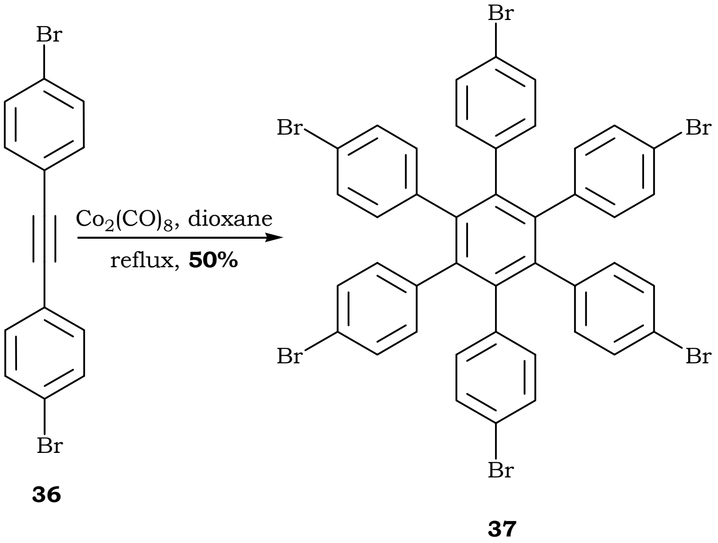

36

37

Figure 6.10. Synthesis of the hexabrominated hexaphenylbenzene **37**.

This synthesis has an advantage over the one we found in literature[234] and in which hexaphenylbenzene is reacted with excess bromine in chilled EtOH to afford the desired product after a six fold bromination reaction which causes contamination by incompletely brominated hexaphenylbenzene species.

Despite the fact that all the HBC derivatives we have produced are symmetrical, we will see in the next sections that the main reason for not using **37** as a general precursor in this work is the high insolubility of the intermediate products, which will certainly prevent the six fold coupling reaction to be accomplished and will consequently afford many incomplete substituted species. Unfortunately, this assumption has been proved and published by Wu et al.[102] since he employed **37** for synthesizing many soluble alkylated HBCs but, on the other hand, he has reported the high difficulty to synthesize derivatives having low solubility.

In conclusion, the synthetical strategies we have used to produce HBC derivatives were strongly dependent of the nature of the perfluorinated chain we wanted to insert since the reactivity of that latter changed drastically from one group to another. Consequently, many synthetical pathways were used, mainly the step-by-step Sonogashira cross-coupling and the one-pot synthesis of tolane **25**. The synthetical route using tetraarylcyclopentadienone **31** was not attempted since no asymmetrical synthesis of HBC derivatives was envisaged.

7. Primers syntheses

7.1 Introduction

As we have mentioned previously, the idea behind the synthesis of primers was firstly in the aim of designing an HBC moiety bearing small perfluorinated functional groups at their ends which, after choosing a suitable substrate, will be deposited onto it as the foremost monolayer. The primers are expected to act as hosts for the HBC derivatives, bearing long perfluorinated chains, during their deposition process since these latter will prefer to self-assemble onto the primers in column like ordered structures rather than depositing onto the ‘’uncovered” metallic substrate. Syntheses of many potential candidates of the first generation primers have been attempted via different synthetic routes as described later on. Nonetheless, a major problem was neglected during the synthetical trials of those first generation primers: they are mostly constituted of carbon and fluorine only which will cause a poor adhesion between these structures and metallic surfaces after deposition process. This problem is frequently encountered especially during characterization with electronic microscopy tools like scanning tunneling microscopy (STM) and atomic force microscopy[92, 99, 235, 236] (AFM). Consequently, a second generation primers has been envisaged to overcome this problem. These improved HBCs will have an additional feature over their predecessors since they will bear atoms, such as oxygen and sulfur, known for their good adhesion to metallic surfaces[237]. As a result, good adsorption on the substrate on one hand and good stacking on the other hand are expected from them.

Some of the first generation primers were successfully isolated while the others weren’t due to different reasons developed in the next section. Yields of the desired products varied drastically depending on the synthetic pathway chosen to obtain them.

7.2 HBC with R = CF_3

Synthesis of the target molecule **39** has been envisaged via a step-by-step Sonogashira coupling starting from the commercially available 1-bromo-4-(trifluoromethyl)benzene **38**.

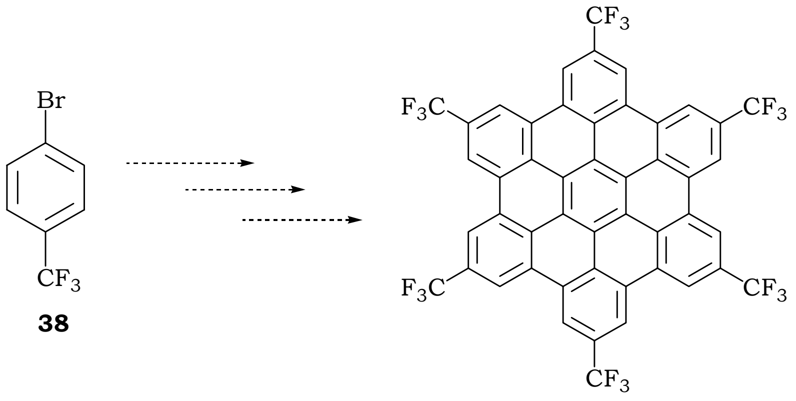

38

39

Figure 7.1. HBC bearing trifluoromethyl groups.

The Sonogashira conditions generally employ a suitable palladium catalyst which could be a Pd(II) or a Pd(0) with a wide choice of ligands. The most frequently used ligands are either phosphine[219] or imidazole[238, 239]. Copper(I) iodides or bromides are used as a co-catalyst[219, 240], they can be replaced by zinc species[241] or even omitted[242]. The commonly used base in this type of coupling is a secondary or a tertiary amine, inorganic bases like carbonates were also employed recently[243]. The solvent could vary depending on the solubility of the substrates the most commonly used are THF and toluene, recently a new method has been developed in which Sonogashira couplings are done in aqueous systems[220, 244-247]. As we have mentioned earlier (6.1.2), the leaving group could be triflate, iodide or bromide. The first two afford a high yield and are run at room temperature whereas the last one requires harsher conditions i.e. heating at 80°C. Nevertheless, the high reactivity of good leaving groups represents, in some cases, a major drawback since it increases the possibility of obtaining homocoupled by-products, a problem that we have faced as we will see in the next section. In our case, we have used either Pd(II) or Pd(0), depending on the degree of difficulty we have estimated for the reaction to take place, but generally the former was used for coupling with TMSA while the latter was employed upon tolane formation reaction. Piperidine acts as a base and was used as the solvent too; it is well known that this type of cyclic secondary amine base excels the primary, secondary and tertiary alkyl amines[248] for this type of coupling reactions.

The conventional mechanism[249] of Sonogashira cross-coupling reaction is shown in scheme V on the next page, it proposes that upon using a Pd(II) source as catalyst, a two fold catalytical amount of the homocoupling diyne product forms in order to reduce the palladium catalyst, into the active Pd(0) species. This was observed in our case when coupling the halogenated derivatives with TMSA using bis(triphenylphosphine)-palladium(II) dichloride ($Pd(PPh_3)_2Cl_2$) as catalyst, whereupon work-up isolation of a byproduct and its analysis by GC/MS revealed it to be the homocoupled TMSA. Once activated, the Pd(0) catalyst undergoes an oxidative addition with the halogenated species. The intermediate product formed will then react with the transmetallated alkyne product and the resulting intermediate species will then afford the desired alkyne regenerating the Pd(0) catalyst by a reductive elimination process.

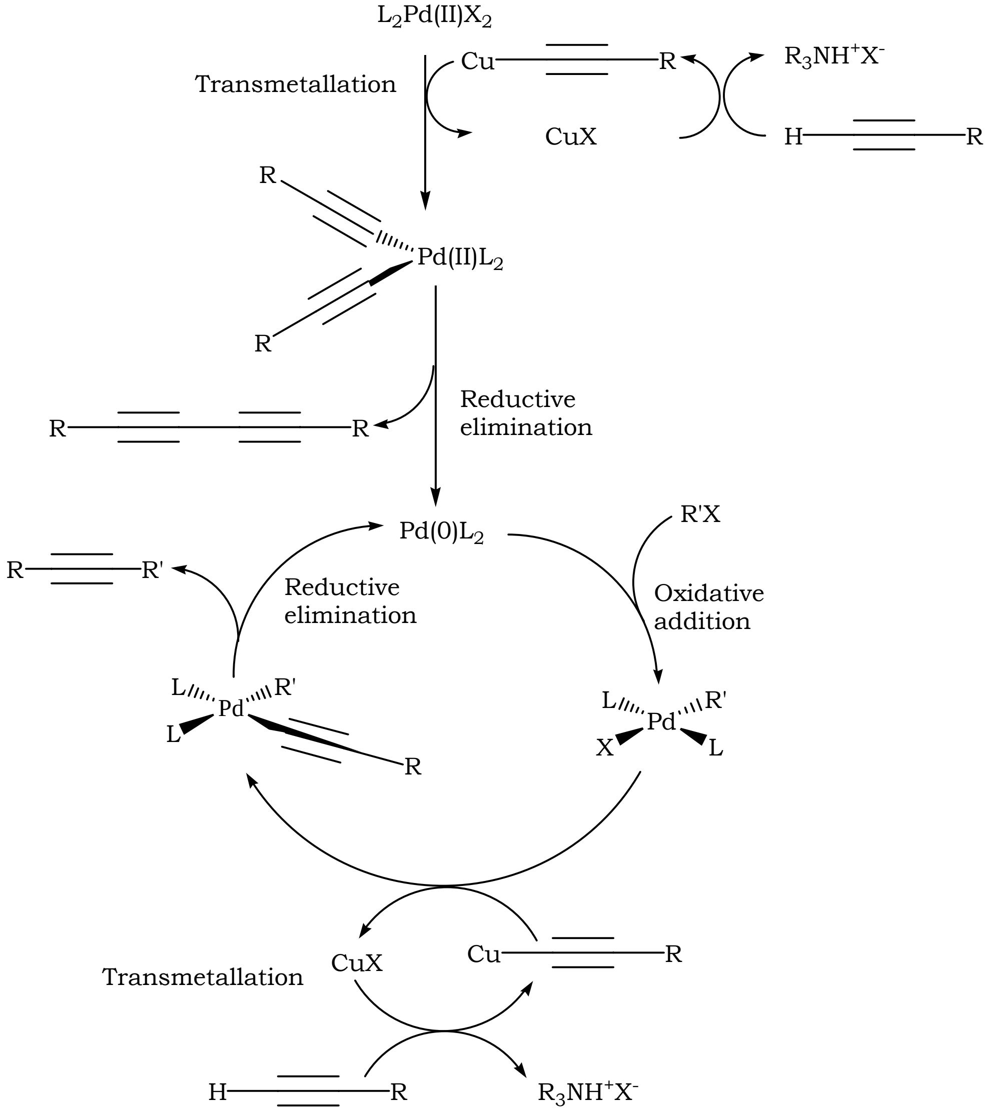
$L_2Pd(II)X_2$
Transmetallation
Cu
R
$R_3NH^+X^-$
CuX
H
R
Pd(II)L₂
R
R
R
R
Reductive
elimination
Pd(0)L₂
R'X
R
R'
Reductive
elimination
Oxidative
addition
L
Pd
R'
L
R
L
Pd
R'
X
L
Transmetallation
CuX
Cu
R
H
R
$R_3NH^+X^-$

Scheme V. Mechanism of the Sonogashira cross-coupling reaction.

Product **38** was coupled with trimethylsilylacetylene (TMSA), using Sonogashira coupling reactions (Figure 7.2) to afford the trimethyl protected acetylene in a 96% yield.

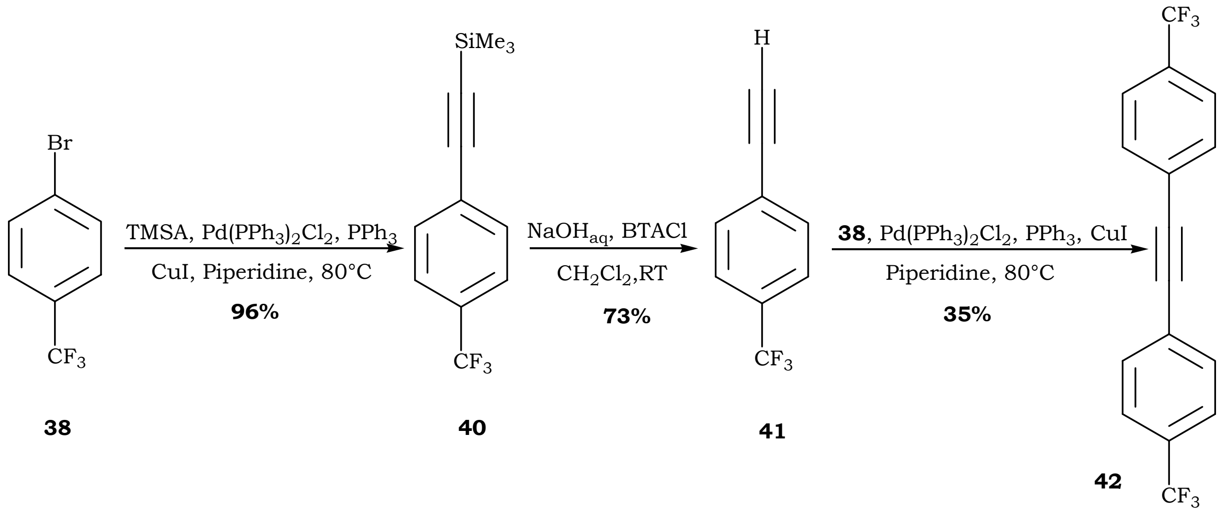

Figure 7.2. Synthesis of the tolane bearing trifluoromethyl groups **42**.

Deprotection of the trimethylsilyl group (TMS) has been achieved by dissolving **40** in the minimum amount of CH_2Cl_2 then stirring it with a saturated aqueous solution of sodium hydroxide in presence of benzyltriethylammonium chloride (BTACl) as a phase transfer catalyst to afford **41** in a good yield. The hydrolysis conditions used herein are a result of several optimization attempts we have tried on another perfluorinated substrate as we will see in section 9. The isolated product **41** was then reacted with **38** under the Sonogashira cross-coupling reaction conditions listed in table 1 below giving the desired trifluoromethyl tolane species **42** (To-CF_3) as an off-white product in a low yield (35%) and which is soluble in common organic solvents. Even though the relatively high catalytical amount of Pd(II) species used and the long reaction time required (entry 2), the low yield of the To-CF_3 can only be explained by a lower activity of Pd(II) than Pd(0) for this type of synthesis and this was confirmed by the recovery of the starting materials.

Table 1. Synthesis of tolane **42** via step-by-step Sonogashira couplings[a,b].

Entry	Substrate (eq.)	Catalyst (Mol%)	Co-cat. (Mol%)	Ligand (Mol%)	Base[c]	T (°C)	T (h)	Product (%Yld)
1	TMSA (1.3)	$Pd(PPh_3)_2Cl_2$ (3)	CuI (6)	PPh_3 (6)	Piperidine	80	24	**40** (96)
2	41 (1)	$Pd(PPh_3)_2Cl_2$ (6)	CuI (12)	PPh_3 (12)	Piperidine	80	48	**42** (35)

a: reactions were done under argon atmosphere. b: equivalents are w.r.t 38. c: as solvent.

The tolane species To-CF_3 was reacted, in a later step, with a catalytical amount of $Co_2(CO)_8$ in refluxing dioxane as shown in figure 7.3 below. The trimerization reaction has yielded 67% of an off-white precipitate whose solubility was weak in common organic solvents except in $CHCl_3$ which dissolves the trimer **43** (HPB-CF_3) very well.

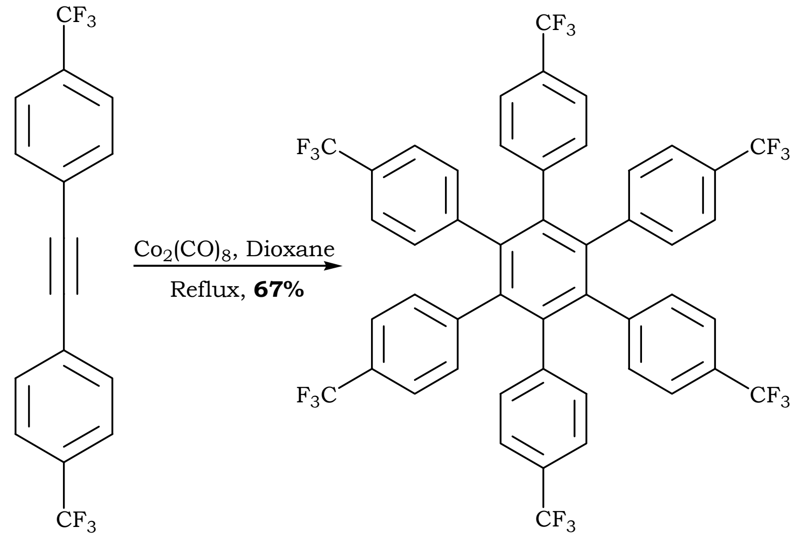

42 **43**

Figure 7.3. Synthesis of hexaphenyl benzene bearing trifluoromethyl groups.

The trimerization reaction of alkynes in presence of cobalt species like $CoCp(CO)_2$ and $Co_2(CO)_8$ is well-known as we have mentioned in section 6.1.4. Nevertheless, the proposed mechanism for $Co_2(CO)_8$ cyclotrimerization is not fully understood yet[250] and it is believed to be a complex process involving several organometallic species[251-254]. However, it is proven that upon reacting a stoichiometric amount $Co_2(CO)_8$ and alkyne species **25** under mild conditions the readily isolated stable intermediate complex **25.1** is formed[255] which upon heating, reacts with an additional alkyne to form the intermediate **25.2** that contains a cobalt-cyclopentadiene unit π-bonded to the other cobalt atom[256]. Additional reaction with **25** gives the intermediate **25.3** which has been isolated and characterized by X-ray crystallography showing a bridging unit linking the three alkynes units in a so-called 'flyover' arrangement[257]. Heating the latter product **25.3** affords the desired benzene product **24** and regenerates the active cobalt species. The conventional mechanism[258] of the cyclotrimerization reaction is presented in Scheme VI.

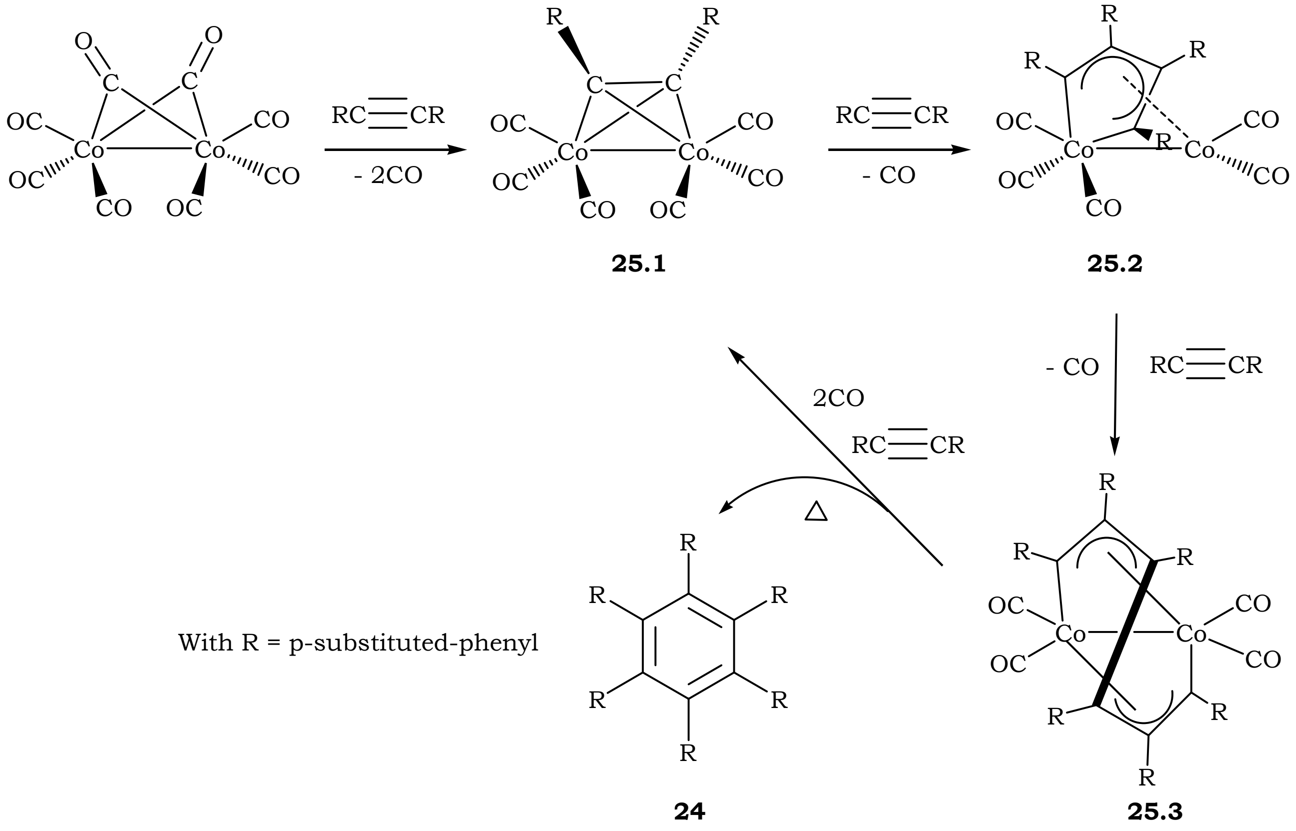
RC≡CR
- 2CO
25.1
RC≡CR
- CO
25.2
- CO
RC≡CR
25.3
2CO
RC≡CR
△
24
With R = p-substituted-phenyl

Scheme VI. Trimerization mechanism using dicobalt carbonyl.

The isolated hexaphenyl benzene derivative **43** was subjected to many cyclodehydrogenation attempts that didn't yield the hexa-substituted trifluoromethyl HBC **39** (HBC-CF_3) as shown in figure 7.4 on the next page.

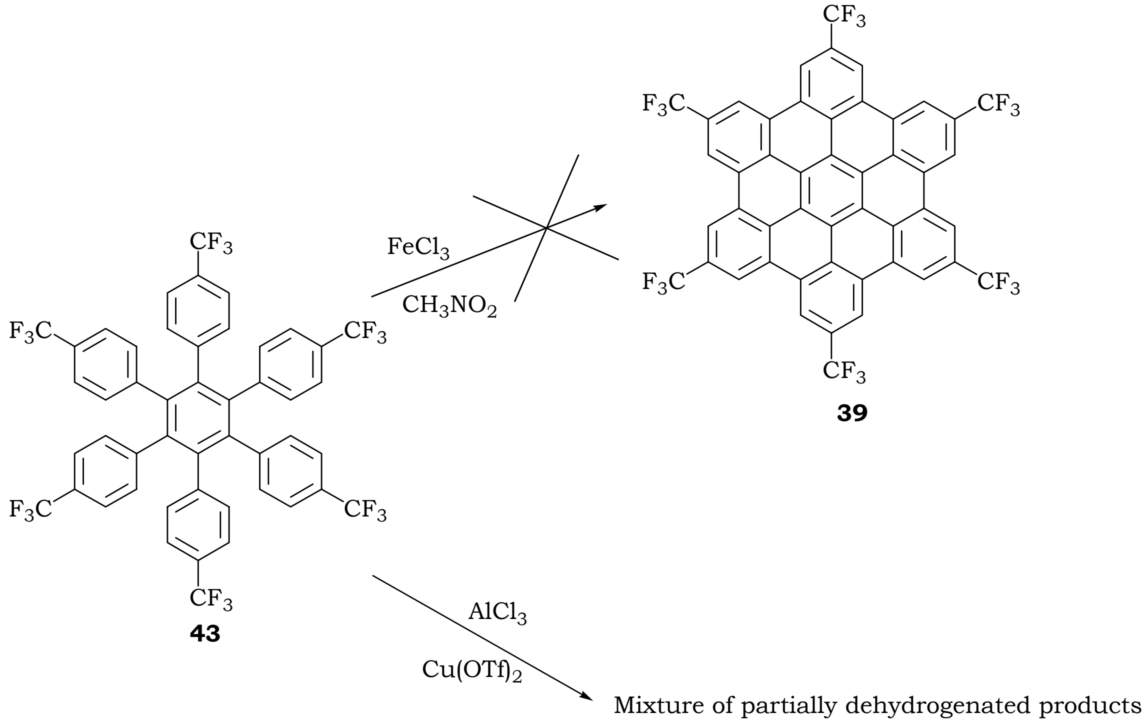

Figure 7.4. Cyclodehydrogenation trials of HPB-CF$_3$.

The data listed in table 2 on the next page reveal many important indications regarding this type of reaction. Entry 1, which uses the standard cyclodehydrogenation reaction conditions employing FeCl$_3$ and CH$_3$NO$_2$ in CH$_2$Cl$_2$, affords the starting material HPB-CF$_3$ even after 24 hours of reaction. This led us to think first, that the low solubility of the hexaphenyl benzene derivative **43** might be the major reason for this failure. Therefore THF, which was revealed to be a better solvent for HPB-CF$_3$ than CH$_2$Cl$_2$ (entry 2), was used instead while keeping the other conditions without any change. Even though the good solubility observed in the medium during the reaction, no trace of the desired product HBC-CF$_3$ was observed and most of the starting material **43** was recovered. This result brings to light another parameter, which is the mild Lewis acid property of FeCl$_3$, probably insufficient to oxidize a molecule bearing an electronegative group such as trifluoromethyl one. Consequently, FeCl$_3$ was replaced by the stronger and more efficient 1:1 mixture of AlCl$_3$/Cu(OTf)$_2$ Lewis acid-oxidant combination, as shown in entry 3. Nonetheless, this latter has afforded a mixture of partially cyclodehydrogenated species mostly lacking 6 protons in ~10% yield. Since many isomers of the partially oxidized moieties lacking 4, 6 and 8 protons are possible, we were interested in knowing their structures to better understand the cyclodehydrogenation mechanism but this was very difficult as a reason of their very weak solubility and consequently to the difficulty to separate and characterize them. Therefore, MALDI-TOF mass spectrometry was the only technique available to reveal the presence of this mixture of partially oxidized products (figure 7.5).

Table 2. Cyclodehydrogenation conditions applied to HPB-CF_3.

Entry	**Reagent (Nb of eq/H)**	**Additive**	**Solvent**	**Temp. (°C)**	**Time (h)**	**Product**
1	$FeCl_3$(7.5)	CH_3NO_2	CH_2Cl_2	RT	24^a	**43**
2	$FeCl_3$(6.5)	CH_3NO_2	THF	RT	5^b	**43**
3	$AlCl_3$(3)	Cu(OTf)$_2$	CS_2	30°C	24	**43**,...

a: argon was bubbled for 8 hrs. b: argon was bubbled throughout the reaction.

It is important to note that it has been reported in the literature[214], the failure of many cyclodehydrogenation reactions of aryl derivatives bearing electron-withdrawing substituents. This corroborates with our result since it is well-known that trifluoromethyl is an electron withdrawing group. Consequently, this latter prevents the cyclodehydrogenation reaction to occur upon using $FeCl_3$ on one hand, and yields only partially dehydrogenated products upon using a stronger Lewis acid ($AlCl_3$) even after a relatively long reaction time, on the other hand.

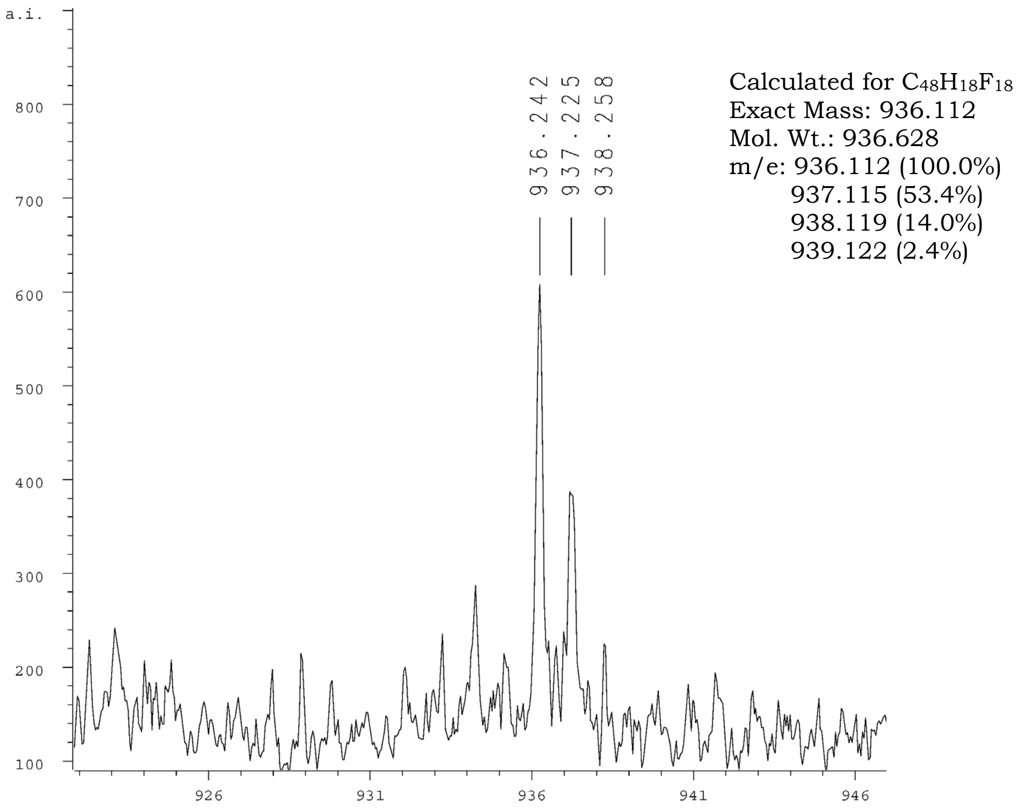

Calculated for $C_{48}H_{18}F_{18}$
Exact Mass: 936.112
Mol. Wt.: 936.628
m/e: 936.112 (100.0%)
937.115 (53.4%)
938.119 (14.0%)
939.122 (2.4%)

Figure 7.5. MALDI-TOF spectra of partially oxidized products of **43**.

7.3 HBC with R = 4-$PhCF_3$ and 3,5-$Ph(CF_3)_2$

To circumvent the problem with the electron withdrawing groups we have faced during the attempted synthesis of the hexakis-trifluoromethyl HBC **39**, we have thought about inserting a phenyl spacer between the hexaphenyl benzene and the trifluoromethyl moiety to form species **44** (HBC-$PhCF_3$) depicted in figure 7.6 on the next page. Moreover, we have tried the synthesis of hexakis-(3,5-bis-trifluoromethyl-phenyl)-HBC **45** (HBC-3,5$PhCF_3$) because the position of the trifluoromethyl groups forces the phenyl spacer to tilt preventing the tolane from forming a rigid rod-like insoluble structure.

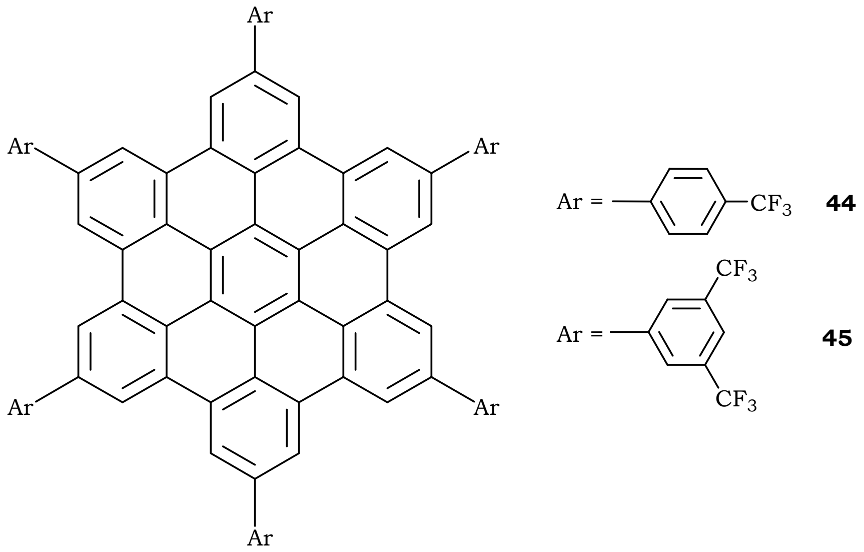
Ar
Ar
Ar
Ar
Ar
Ar
Ar =
CF3
44
Ar =
CF3
CF3
45

Figure 7.6. HBC primers with phenyl spacers.

7.3.1 Syntheses of the brominated precursors

The synthetical strategy focuses in a first place on the synthesis of the brominated biphenyl derivatives **50** and **51** (figure 7.7). These latter are used as the major precursors needed for the formation of HBC-PhCF_3 and HBC-3,5PhCF_3 via the step-by-step Sonogashira cross-coupling pathway. For this reason, the carbon-carbon Suzuki coupling of **38**[259] and **46**[260] with the phenylboronic acid **47** was performed affording the corresponding biphenyl derivatives **48** and **49** in a quantitative yield upon using the reaction conditions listed in table 3.

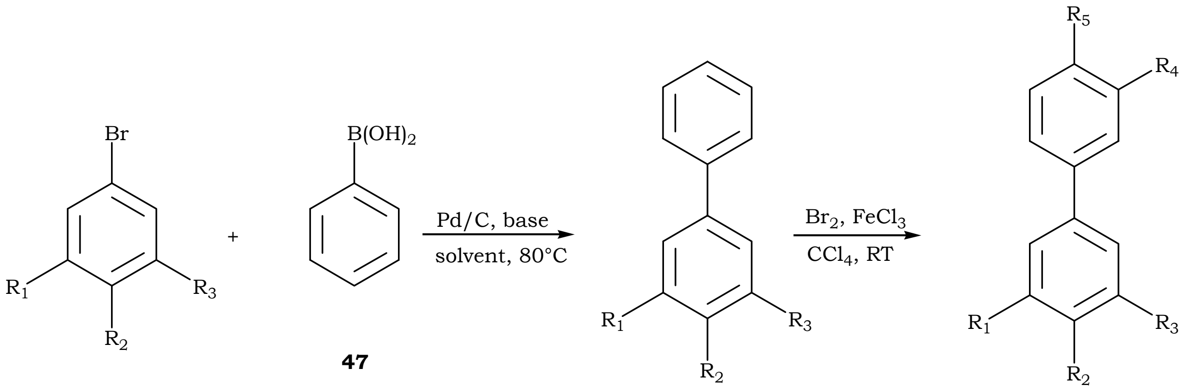
Br
R1
R3
R2
+
B(OH)2
47
Pd/C, base
solvent, 80°C
R1
R3
R2
Br2, FeCl3
CCl4, RT
R5
R4
R1
R3
R2

R_1=R_3=H, R_2=CF_3 **38**
R_2=H, R_1=R_3=CF_3 **46**

R_1=R_3=H, R_2=CF_3 **48**
R_2=H, R_1=R_3=CF_3 **49**

R_1=R_3=R_4=H, R_2=CF_3, R_5=Br **50**
R_2=R_4=H, R_1=R_3=CF_3, R_5=Br **51**
R_2=R_5=H, R_1=R_3=CF_3, R_4=Br **52**

Figure 7.7. Synthesis of the brominated precursor **50** and **51**.

Table 3. Suzuki cross-coupling conditions[a] of **38** and **46** with **47**.

Entry	Substrate (eq.)	Catalyst (Mol%)	Base (eq.)	Solvent	Temp. (°C)	Time (h)	Product (%Yld)
1	38 (0.83)	Pd/C (5)	K_2CO_3 (1.6)	DMA/H_2O [b]	80	24	**48** (100)
2	46 (0.83)	Pd/C (5)	Na_2CO_3 (3)	EtOH	80	24	**49** (97)

a: reactions were done under argon atmosphere. b: DMA/H_2O ratio is 20:1 by volume

It is worthwhile to note that the Suzuki coupling is one of the most recent C-C cross-coupling reactions and it uses boron as the organometallic species. This latter is known to be easily accessible[261-264], stable and having a low toxicity contrarily to other organometallic species such as tin[265]. Basically, Suzuki reaction conditions necessitate the presence of a halogenated aryl group, a boron-containing aryl species (boronic acid, boronate or trifluoroborate), a palladium catalyst, a suitable ligand, and a base all in a suitable organic solvent. However many developments in the latest years have been brought to this type of coupling: halogenated groups(iodo- and bromo- compounds) have been replaced with chlorides[266, 267], triflates[268], tosylates[269] and diazonium salts[270, 271]. These new groups have permitted a new type of alkyl-aryl Suzuki coupling[272]. Recently, different palladium sources have shown a very high activity[273-277] in addition to some promising nickel catalysts[278, 279]. The former and the latter are most frequently used under ligandless conditions[280-282]. Concerning the nature of the base, carbonates and hydroxides are the most frequently used. Recent developments have also shown that the Suzuki reaction occurs in aqueous medium[283, 284].

The mechanism of Suzuki coupling[285] is similar to Sonogashira one in the major steps as it can be noticed from scheme VII: 1) generation of an active palladium species, 2) oxidative addition, 3) transmetallation, and 4) reductive elimination.

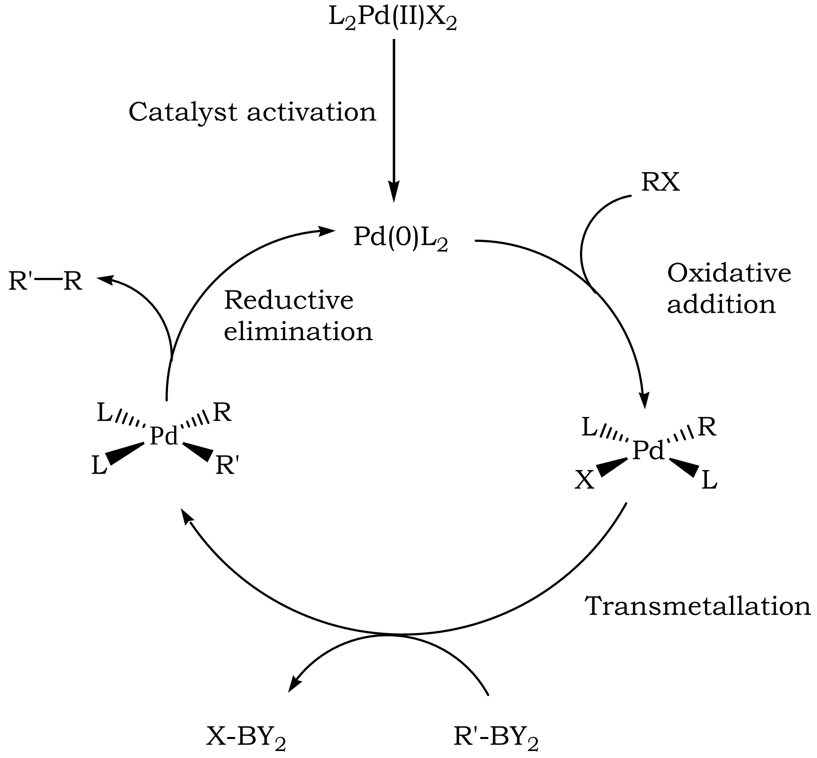
L2Pd(II)X2
Catalyst activation
Pd(0)L2
RX
Oxidative addition
Reductive elimination
R'—R
L
Pd
R
L
R'
L
Pd
R
X
L
Transmetallation
X-BY2
R'-BY2

Scheme VII. Mechanism of the Suzuki cross-coupling reaction.

However, it has been proven[285] that the rate determining step depends on the nature of the halogen: if X = I, the r.d.s is the transmetallation and if X = Br, then the oxidative addition is the r.d.s. The base has a major role in this coupling reaction; two different mechanisms are proposed to explain its function[286]: The first one is based on the fact that the electronegativity difference between carbon and boron is very small and, therefore, the R' group is not very reactive. But in the presence of a base, the boron species will react with it yielding the more active borate derivative (Scheme VIII).

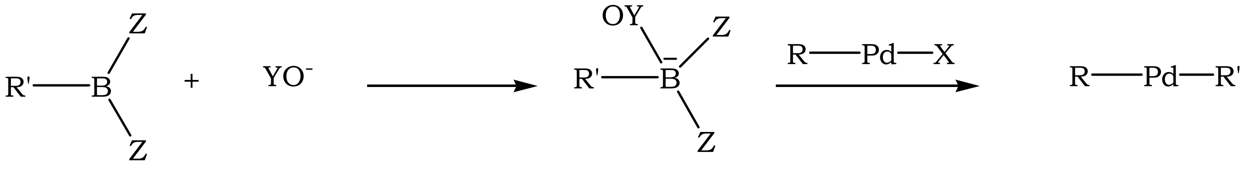
Z
R'
B
Z
+
YO-
OY
Z
R'
B
Z
R—Pd—X
R—Pd—R'

Z = OH, OR, alkyl

Scheme VIII. Activation of the boronic acid by the base.

The second mechanism involves the formation of an alkoxy-palladium derivative; it is formed when using weak bases unable to react with boron to afford an organoborate species (Scheme IX).

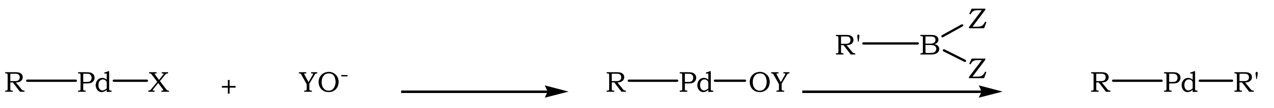

Z = OH, OR, alkyl

Scheme IX. Formation of an alkoxy palladium species.

Table 4 summarizes the reaction conditions employed for the bromination of **48** and **49**. The former has yielded the desired bromo- derivative **50** in a good yield, whereas the latter has yielded a mixture of α- and β- bromo-substituted products (**51** & **52**) in a ratio of ~95:5 respectively. Despite the low amount of the by-product present, all usual purification methods such as column chromatography, distillation, or recrystallization, have failed to isolate **51** in a pure form.

Table 4. Bromination of **48** and **49**.

Entry	**Substrate (eq.)**	**Eq. of $FeCl_3$**	**Eq. of Br_2**	**Solvent**	**Temp. (°C)**	**Time**	**Product (%Yld)**
1	40 (1)	0.25	1	CCl_4	RT	2d	**50** (78)
2	41 (1)	0.25	1	CCl_4	RT	1d	**51** (90)[a] **52** (5)[a]
3	41 (1)	0.25	1	CCl_4	RT	4hrs	**51** (73)[a] **52** (4)[a]

a: yields determined from ^{1}H-NMR spectra.

The results shown in entries 2 and 3 above prompted us to explore another synthetical approach. This latter, described in section 6.1.3, is based on the synthesis of a functionalized tolane derivative bearing good leaving groups, allowing it to react with the 3,5-bis(trifluoromethyl)benzene derivative, via a suitable C-C cross-coupling reaction, to afford the desired tolane species. Before developing this, we will first describe the synthesis of tolane derivative obtained from **50**.

7.3.2 Synthesis of 4,4'-bis-(trifluoromethyl)diphenylacetylene (To-PhCF$_3$)

Starting from **50**, the corresponding tolane derivative was obtained in a good yield via the step-by-step Sonogashira coupling (figure 7.8). The first step affords the trimethylsilylated acetylene species **53** in a good yield. Deprotection of this latter, provides highly pure **54** in 83% yield. Coupling of **50** and **54**, using the conditions shown in figure 7.8 below, yields To-PhCF$_3$ as a white precipitate which is obtained after a series of washings to remove a yellow by-product with common organic solvents. As expected, the rigid rod-like structure of **55** renders it insoluble in nearly all the common organic solvents, such as, hexane, pentane, CHCl$_3$, CH$_2$Cl$_2$, THF, dioxane and benzyltrifluoride (BTF). This high insolubility of To-PhCF$_3$ has led us to explore the pathway, mentioned previously, that involves the formation of a functionalized tolane derivative which will be subjected to an additional reaction to afford 3,3',5,5'-tetrakis(trifluoromethyl)-diphenylacetylene (To-3,5PhCF$_3$).

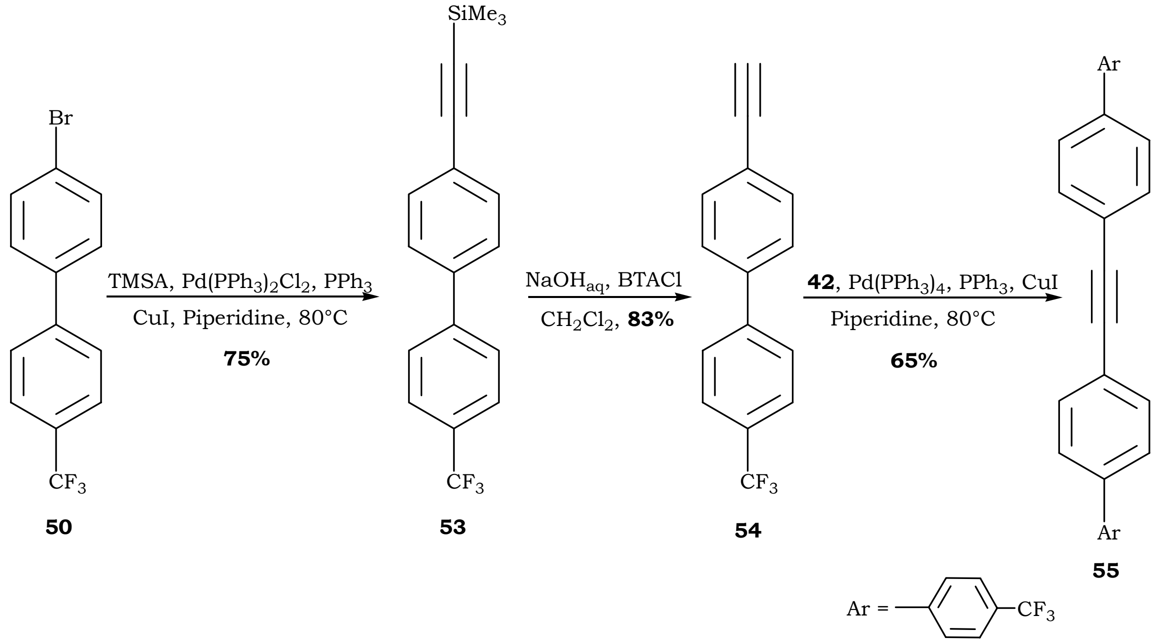

Figure 7.8. Synthesis of To-PhCF$_3$ via step by step Sonogashira coupling.

7.3.3 Synthesis of 3,3',5,5'-tetrakis-(trifluoromethyl)diphenylacetylene (To-3,5PhCF$_3$)

Since all the attempts, mentioned in section 7.3.1, have failed to get the bromo- species **51** in a sufficient pure form to carry on the step-by-step Sonogashira coupling, a new synthetical route has been tried; it consists of synthesizing 4,4'-dibromotolane **36**, first, by reacting the commercially available 1-bromo-4-iodobenzene **56** with acetylene at room temperature in presence of a palladium/copper catalyst (Figure 7.9).

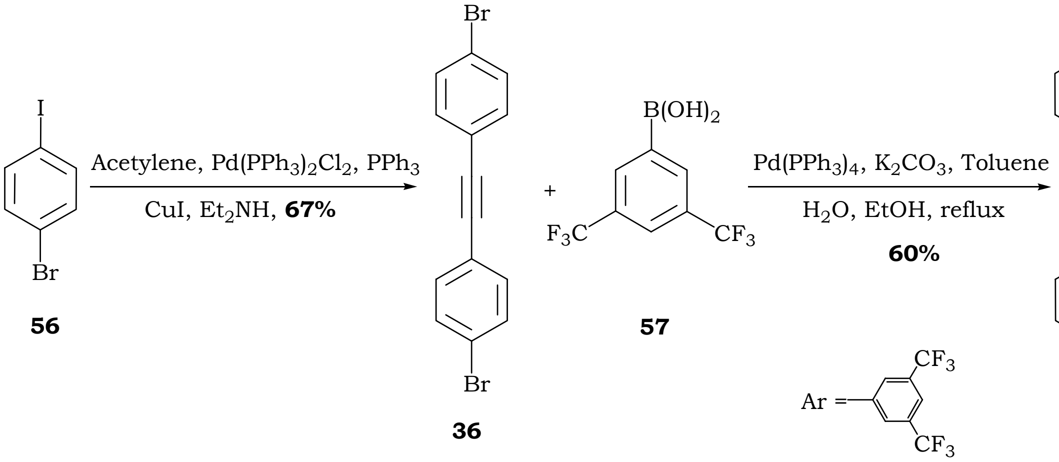
Acetylene, Pd(PPh3)2Cl2, PPh3
CuI, Et2NH, 67%
56
36
57
Pd(PPh3)4, K2CO3, Toluene
H2O, EtOH, reflux
60%
Ar =
58

Figure 7.9. Synthesis of tolane building block To-3,5PhCF$_3$.

Table 5 lists the different conditions used for both the Sonogashira and the Suzuki coupling reactions types. As it can be noticed from entry 1, **36** is obtained under suitable Sonogashira coupling conditions in 67% yield. The reaction between **36** and **57** under Suzuki cross-coupling conditions that employs a Pd/C catalyst, potassium carbonate as base, and a DMA/H_2O solvent mixture[259] doesn't afford To-3,5PhCF$_3$ (entry 2). Applying harsher Suzuki coupling reaction conditions[261, 264, 287] that use a Pd(PPh$_3$)$_4$ catalyst, potassium carbonate as a base, in a refluxing mixture of toluene/water/ethanol, provides the desired tolane derivative **58** in a 60% yield (entry 3).

Table 5. Syntheses[a] of **36** and **58**.

Entry	Sub. 1 (eq.)	Sub. 2 (eq.)	Catalyst (Mol%)	Co-Cat. (Mol%)	Base (eq.)	Solvent	T (°C)	t (h)	Pdt (%Yld)
1	56 (1)	acetylene[b]	$Pd(PPh_3)_4$ (1.4)	CuI (1)	Et_2NH[c]	-	RT	24	**36** (67)
2	56 (1)	57 (2.4)	Pd/C (5)	-	K_2CO_3 (4)	DMA/ H_2O[d]	80	24	**-**
3	56 (1)	57 (2)	$Pd(PPh_3)_4$ (10)	-	K_2CO_3 (16)	toluene/ H_2O/ EtOH[e]	reflux	48	**58** (60)

a: all the reactions were done under argon atmosphere. b: acetylene was bubbled for 7.5 hrs. c: as solvent. d: DMA/H_2O ratio is 20:1 by volume. e: toluene/H_2O/EtOH ratio is 4:2:1 by volume.

Contrarily to 4,4'-bis-(trifluoromethyl)diphenylacetylene **55**, product **58** shows a very good solubility ranging from the non-polar solvents, such as hexane and pentane, to the polar ones like chloroform and CH_2Cl_2.

7.3.4 HBC with R=3,5-Ph$(CF_3)_2$

Trimerization of the tolane species To-3,5PhCF_3 to its hexaphenyl derivative **59** (HBC-3,5PhCF_3) was successful yielding 83% of this latter when employing the conditions listed in table 6 on the next page. Nevertheless, HPB-3,5PhCF_3 was found to be insoluble in common organic solvents but very scarcely soluble in chloroform and THF. Therefore the latter solvent was used for the cyclodehydrogenation reaction using $FeCl_3$ as shown in table 6.

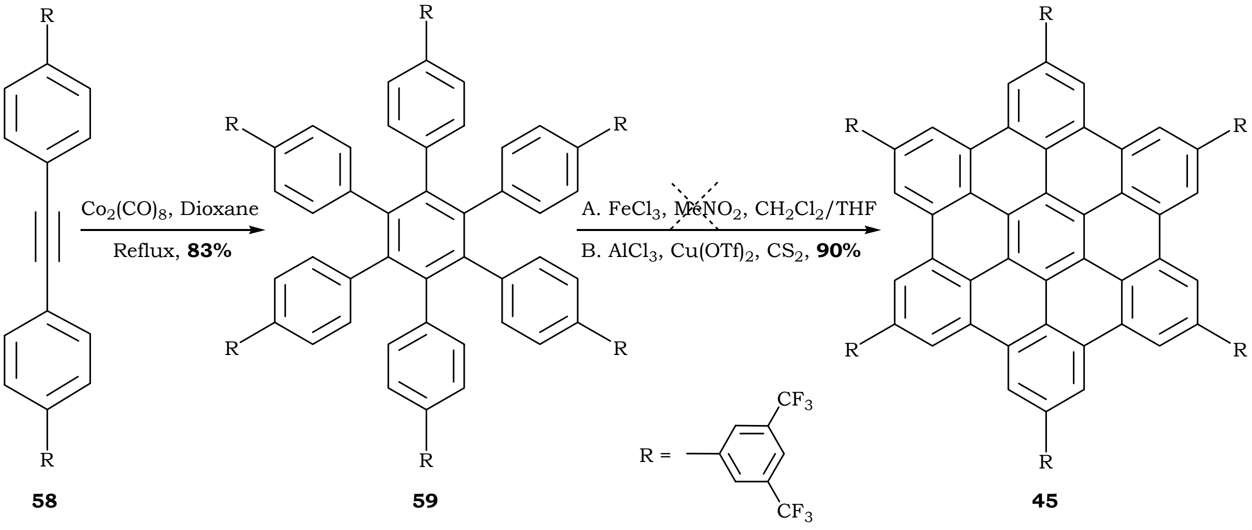

Figure 7.10. Synthesis of HBC primer **45**.

Cyclodehydrogenation reaction of HPB-3,5PhCF$_3$ has been carried out using different conditions as it can be noticed from table 6 on the next page: the first reaction (entry 2) done, using FeCl$_3$/MeNO$_2$ in THF at room temperature, gave only the starting material **59**. Thus, we have applied the same reaction conditions but with adding CH$_2$Cl$_2$ as a co-solvent in a 1:2.5 mixture with respect to THF. Unfortunately, neither the reaction at room temperature (entry 3) nor at reflux (entry 4) has afforded any trace of the desired product HBC-3,5PhCF$_3$, only **59** has been recovered instead. Entry 5, shows that upon using AlCl$_3$/Cu(OTf)$_2$ mixture, the reaction occurs affording the HBC derivative **45** as a yellow-green insoluble product in 90% yield. From these results we can think about two factors responsible of the failure upon using the FeCl$_3$/CH$_3$NO$_2$ combination: on one hand, the electron-withdrawing effect induced by the trifluoromethyl groups are still high, even through a phenyl spacer and, consequently are preventing the oxidation reaction to occur. On the other hand, THF could have formed a complex with iron(III) chloride, which has prevented the oxidation reaction to take place. Both assumptions stand for true and could be involved at the same time; however the second one is more favorable in this case particularly because even at reflux (entry 4), no traces of partially oxidized products has been detected. The use of the Al(III)/Cu(II) reagent (entry 5) seems to be more efficient than Fe(III) ones, especially that there is no risk of displacing the perfluorinated chains since they are inert towards Friedel-Crafts reactions.

Table 6. Trimerization and cyclodehydrogenation reactions conditions[a].

Entry	Reagent (nb. eq/ H)	Additive	Solvent	Temp. (°C)	Time (h)	Product (%Yld)
1	$Co_2(CO)_8$[b]	-	Dioxane	reflux	24	**59** (83)
2	$FeCl_3$(6.5)	CH_3NO_2	THF	RT	9[c]	**59**
3	$FeCl_3$(6.5)	CH_3NO_2	THF/CH_2Cl_2[d]	RT	16	**59**
4	$FeCl_3$(6.5)	CH_3NO_2	THF/CH_2Cl_2[d]	reflux	1	**59**
5	$AlCl_3$(3)[e]	$Cu(OTf)_2$	CS_2	35	39	**45** (90)

a: all the reactions were done under argon. b: cobalt used catalytically (10 mol%). c: argon was bubbled throughout the reaction. d: THF/CH_2Cl_2 ratio is 2.5:1 by volume. e: equimolar amount of Al/Cu.

The desired product was isolated after a series of washings with several solvents to remove any trace of metallic species first, followed by many sequences of refluxing-filtrating-washing of the crude product with several solvents such as THF, CH_2Cl_2, and $CHCl_3$ to remove the starting materials and the partially dehydrogenated species. Figure 7.11 on the next page shows the MALDI-TOF spectrum of HBC-3,5PhCF$_3$, it can be noticed that the peak corresponds to the exact mass within the margin error of the spectrometer (1-3 ppm) of the desired product and shows the absence of any trace of HPB-3,5PhCF$_3$ and the partially cyclodehydrogenated products.

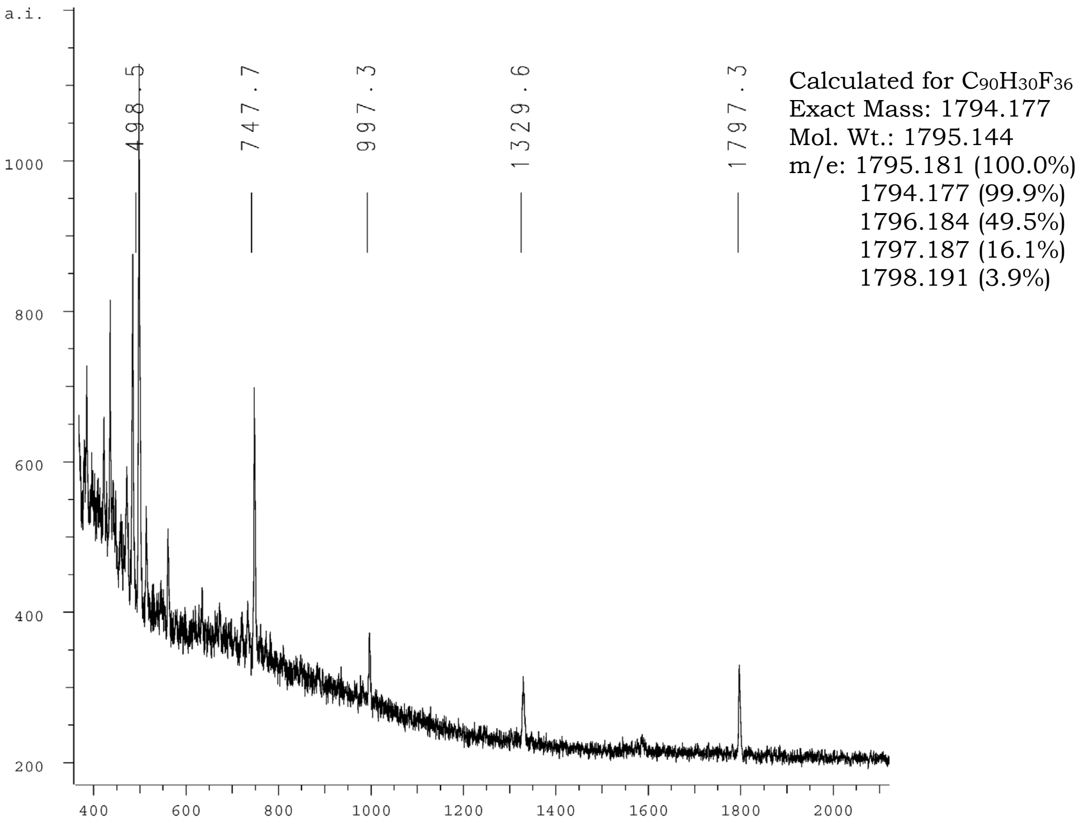

Figure 7.11. MALDI-TOF spectra of HBC-3,5PhCF$_3$.

7.4 HBC with R = OCF$_3$

As we have discussed previously (section 7.1), in order to improve the adhesion of the HBC primers at the substrate's surface, we have thought about replacing the trifluoromethyl group by an alkoxy one. However, Weiss and co-workers have shown that the synthesis of an HBC bearing alkoxy groups isn't possible because during the cyclodehydrogenation step quinonoid derivatives form instead[288]. Therefore, we have diverted the idea by using an 'inert' group that doesn't contain protons, such as the trifluoromethoxy group. This latter is expected to prevent the formation of quinonoids leading to the HBC derivative **65** (HBC-OCF$_3$, figure 7.13) in its place. Additionally, the main reason which has prevented the synthesis of HBC bearing trifluoromethyl groups **39** i.e. the electron-withdrawing effect, is expected not to occur or to be less effective herein due to the presence of the oxygen atom. However, to have a better understanding of these types of reactions and to be able to make a comparison between the chemical behavior of trifluoromethyl and its methoxy derivative, we have chosen to perform the same synthetical route we applied to synthesize HBC-CF$_3$ i.e. the step-by-step coupling (figure 7.12).

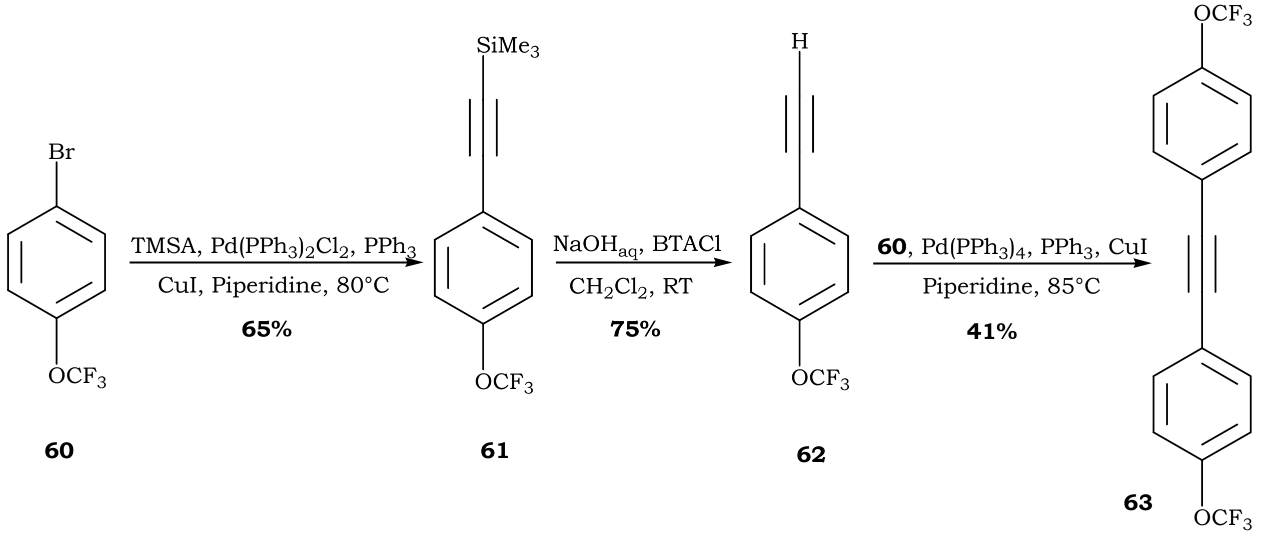

Figure 7.12. Synthesis of trifluoromethoxy tolane derivative **63**.

Synthesis of the tolane derivative **63** (To-OCF$_3$) has been done using the reactions conditions listed in table 7 below. The starting material **60** was reacted with TMSA under suitable Sonogashira coupling reaction conditions to afford **61** in a fair yield (entry 1). It must be pointed out that ~5-10% of **60** were recovered indicating that the reaction was incomplete even after 24 hours, the same time required for the trifluoromethyl derivative **46** to be completely converted. This result shows that the trifluoromethoxy substituent acts as an electron donating group which deactivates the bromine and hence decreases the rate of palladium oxidative addition to **60**. Reaction of the deprotected acetylene species **62** with an equimolar amount of **60** (entry 2) affords To-OCF$_3$ in 41% yield in addition to recovered starting material. This low yield can be explained by the same reason mentioned before i.e. the deactivating effect of the trifluoromethoxy group.

Table 7. Synthesis of To-OCF$_3$ via step-by-step Sonogashira coupling[a].

Entry	**Substrate (eq.)[b]**	**Catalyst (Mol%)**	**Co-catalyst (Mol%)**	**Ligand (Mol%)**	**Base[c]**	**Temp. (°C)**	**Time (h)**	**Product (%Yld)**
1	TMSA(1.3)	Pd(PPh$_3$)$_2$Cl$_2$ (3)	CuI (6)	PPh$_3$ (6)	Piperidine	80	24	**61** (65)
2	62 (1)	Pd(PPh$_3$)$_4$ (3)	CuI (6)	-	Piperidine	85	48	**63** (41)

a: reactions were done under argon atmosphere. b: equivalents are w.r.t 60. c: as solvent.

Trimerization of the tolane derivative **63** was then done using the reaction conditions shown in figure 7.13. The hexaphenyl benzene moiety **64** (HPB-OCF_3) is obtained in 71% yield (table 8, entry 1) as a white product soluble in most common organic solvent.

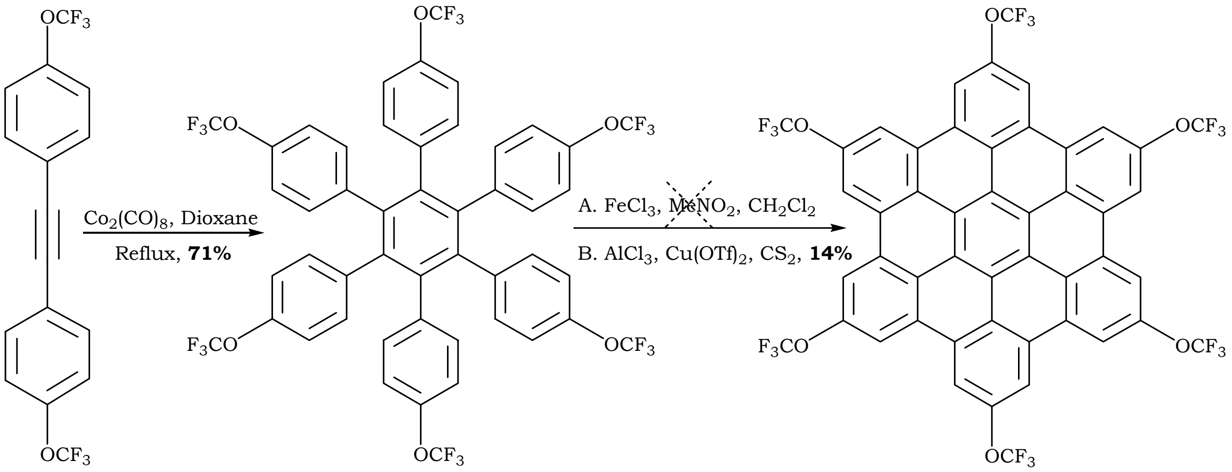

OCF_3
F_3CO
$Co_2(CO)_8$, Dioxane
Reflux, **71%**
A. $FeCl_3$, $MeNO_2$, CH_2Cl_2
B. $AlCl_3$, $Cu(OTf)_2$, CS_2, **14%**

63 **64** **65**

Figure 7.13. Synthesis of HBC-OCF_3 **65**.

The cyclodehydrogenation reaction of HPB-OCF_3 has been carried out using $FeCl_3$ (entry 2) and Al/Cu conditions (entry 3). The former were found not to be efficient enough to oxidize the hexaphenylbenzene species **64** that was recovered at the end of the reaction. But even, the latter conditions have afforded HBC-OCF_3 in 14% yield only. This low amount isolated is most probably due to a loss of a large fraction of the product during the work-up that necessitates washings with harsh reagents such as aqueous hydrochloric acid and 10% ammonia solution to eliminate all the metallic salts which also cause the hydrolysis of a non negligible part of HBC-OCF_3.

Table 8. Trimerization and cyclodehydrogenation reactions conditions[a] of **63**.

Entry	**Reagent (nb. eq/ H)**	**Additive**	**Solvent**	**Temp. (°C)**	**Time (h)**	**Product (%Yld)**
1	$Co_2(CO)_8$[b]	-	Dioxane	reflux	48	**64** (71)
2	$FeCl_3$(6)	CH_3NO_2	CH_2Cl_2[c]	RT	8	**no rxn**
3[d]	$AlCl_3$(3.3)	$Cu(OTf)_2$	CS_2	35°C	24	**65** (14)

a: all the reactions were done under argon. b: cobalt used catalytically (5 mol%).

c: argon was bubbled throughout the reaction. d: equimolar amount of Al/Cu.

7.5 HBC with R = SCF_3

7.5.1 Synthetical approach

Synthesis of the HBC **71** (HBC-SCF_3, figure 7.15) bearing a sulfur atom instead of an oxygen, for better binding to electrodes such as gold, has been first envisaged via the step-by-step Sonogashira coupling reaction. Product **66** has been reacted with TMSA to afford the trimethylsilylated acetylene derivative **67** in 36% yield only due to the unexpected volatility of the desired product. Deprotection of the TMS group, under the conditions shown in figure 7.14, affords **68** in 92% yield as it has been estimated from the ^1H NMR spectrum of the crude reaction mixture. Again, the high volatility of this latter product leads to its loss when distilling off CH_2Cl_2 and pentane from the medium.

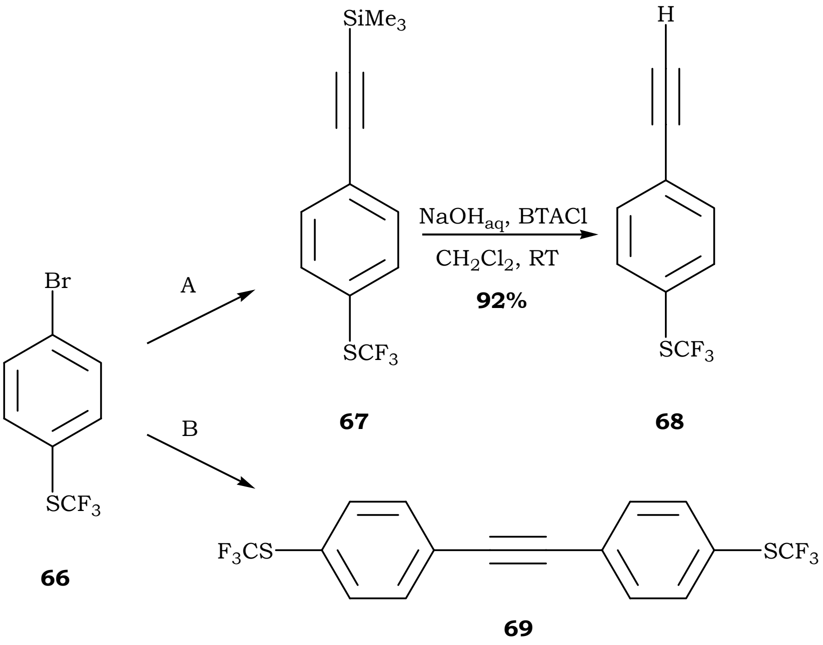

A: TMSA, $Pd(PPh_3)_2Cl_2$, PPh_3, CuI, Piperidine, 80°C, **36%**
B: Acetylene, $Pd(PPh_3)_2Cl_2$, PPh_3, CuI, Piperidine, 80°C, **57%**

Figure 7.14. Different synthetical attempts to produce **69** (To-SCF_3).

The high volatility of **68** has prompted us to change the synthetical pathway toward the one-pot tolane one using an improved procedure to the one we have found in literature[289]: reaction of **66** and acetylene at high temperature in presence of a palladium catalyst affords To-SCF_3 in a 57% yield as shown in entry 3 of table 9 on the next page.

Table 9. Synthesis of tolane **69**[a-c].

Entry	Substrate (eq.)	Catalyst (Mol%)	Co-catalyst (Mol%)	Ligand (Mol%)	Base	T (°C)	t (h)	Product (%Yld)
1	TMSA(1.3)	$Pd(PPh_3)_2Cl_2$ (3)	CuI (6)	PPh_3 (6)	Piperidine	80	24	**67** (36)
2	acetylene[d]	$Pd(PPh_3)_2Cl_2$ (2)	CuI (3)	PPh_3 (3)	Piperidine	80	24	**69** (57)

a: reactions were done under argon atmosphere. b: equivalents are w.r.t 66. c: base used as solvent too. d: acetylene was bubbled in the reaction medium for 6 hours.

Trimerization of To-SCF_3 using dicobalt carbonyl yields the hexaphenyl benzene moiety **70** (HPB-SCF_3) in 86% yield as entry 1 of table 10 depicts. Entry 2 shows that the cyclodehydrogenation of the latter product affords the desired HBC derivative HBC-SCF_3 in a 66% yield.

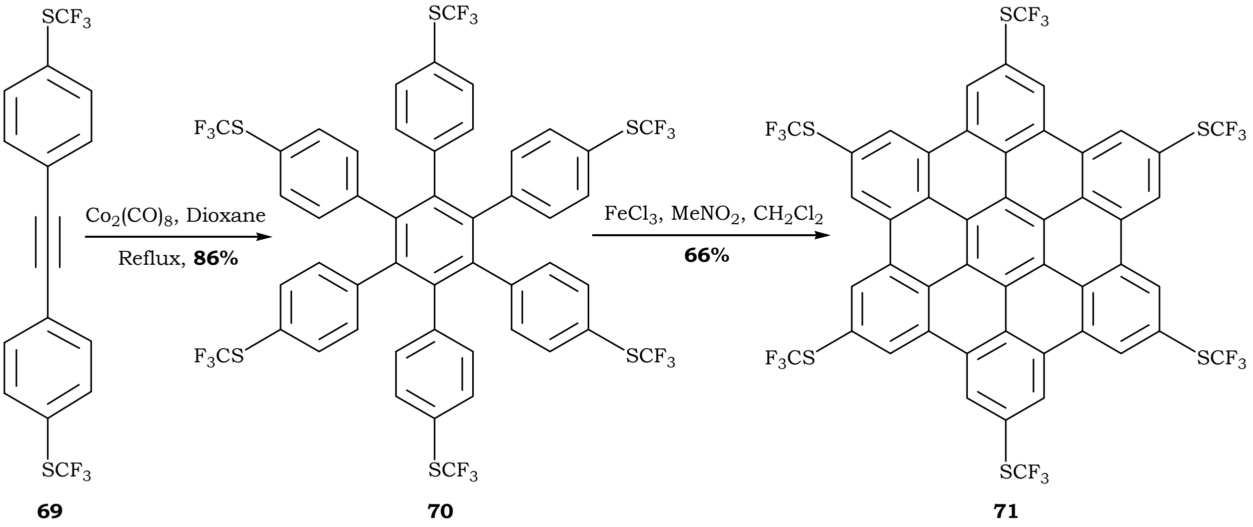

Figure 7.15. Synthesis of sulfur-containing HBC moiety **71**.

Several sequences of reflux-filtration-washing, with different solvents known to dissolve **70** and the partially oxidized byproduct, have been performed until no trace of these latter products were detected by ^1H NMR in the filtrate.

Table 10. Trimerization and cyclodehydrogenation reactions conditions[a].

Entry	Reagent (nb. eq/ H)	Additive	Solvent	Temp. (°C)	Time (h)	Product (%Yld)
1	$Co_2(CO)_8$[b]	-	Dioxane	reflux	48	**70** (86)
2	$FeCl_3$(6.5)	CH_3NO_2	CH_2Cl_2	RT	5[c]	**71**(66)

a: all the reactions were done under argon. b: cobalt used catalytically (5 mol%). c: argon was bubbled throughout the reaction.

Nevertheless, characterization of the isolated species with MALDI-TOF technique, in solid state and in 1,2,4-TCB solution, hasn't revealed either the starting material HPB-SCF_3 or the HBC derivative **71**. This is probably due to the weak S-C bond that breaks during the characterization process which causes the absence of the desired peak from the spectrum. On the other hand, UV-VIS has detected the presence of the characteristic peaks of the HBCs aggregates, in 1,2,4-TCB, at 351, 391, and 422 nm as shown in figure 7.16.

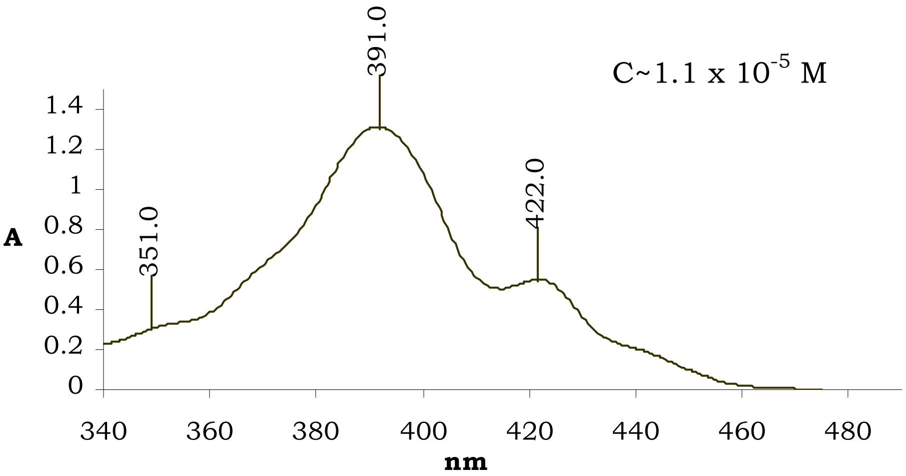

Figure 7.16. UV-Vis spectrum of HBC-SCF_3.

7.5.2 SEM investigation

Scanning electron microscopy (SEM) investigation of HBC-SCF_3, under low pressure (2.9 Torr), has been performed. The bulk yellow precipitate shows dispersed particles of inhomogeneous sizes, varying from few hundreds of nanometers to few microns (figure 7.17).

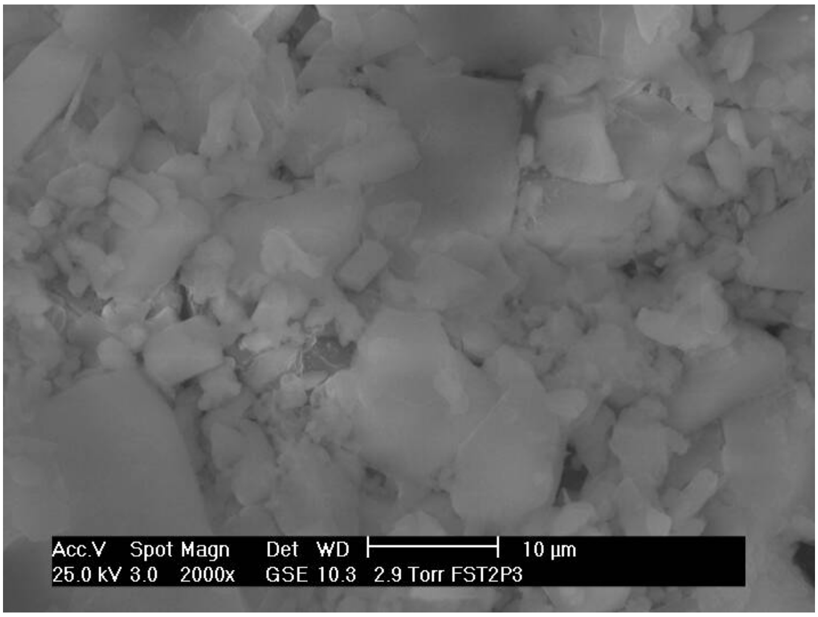
Acc.V Spot Magn Det WD 10 µm
25.0 kV 3.0 2000x GSE 10.3 2.9 Torr FST2P3

Figure 7.17. SEM micrograph of the precipitate HBC-SCF_3.

These results have prompted us to investigate preliminarily the morphological changing of the product when it is deposited on a substrate by evaporation from solution. Thus, deposition has been performed by placing a droplet of a ~5 x 10^{-4} M solution of HBC-SCF_3 in 1,2,4-TCB on a Si(100) substrate. The wafer was put in a vacuum chamber and the solvent was evaporated at ~10^{-4} Torr. The resulting deposit was sputtered with gold to form a ~5 nm thick conducting film. SEM investigation (figure 7.18) has revealed the formation of a thin, smooth, homogenous film of the HBC-SCF_3 over a relatively large area on Si(100). It is noteworthy that the continuous film was detected mainly at the center of the evaporated droplet. However, upon moving the electron beam to the edges of the film, long columnar dendrites whose main chain length is ~16-24 µm, were observed. This basic study shows that HBC-SCF_3 forms homogeneous films with relatively good adherence on the substrate on one hand and that the film is grown in a high degree of order as a reason of the columnar dendritic nature of the product, on the other hand. From these promising observations we can draw out some future perspectives, such as, finding a suitable and more sophisticated deposition technique, from solution, to form monolayered or ultrathin films that allow the use of HBC-SCF_3 as a primer. The main advantage of deposition from solution is the facility to monitor the parameters that influence this process; from these factors we note: the concentration of the solution that controls the thickness of the layer, the nature of the solvent which effects the deposition time, as well as both the type and the surface preparation of the substrate. It is worth noting that the use of a polished Au substrate should be used primarily since it is expected to enhance a face to face deposition of the products on the support instead of an edge to face one due to the presence of the sulfur groups (see figure 2.12 in chapter 2).

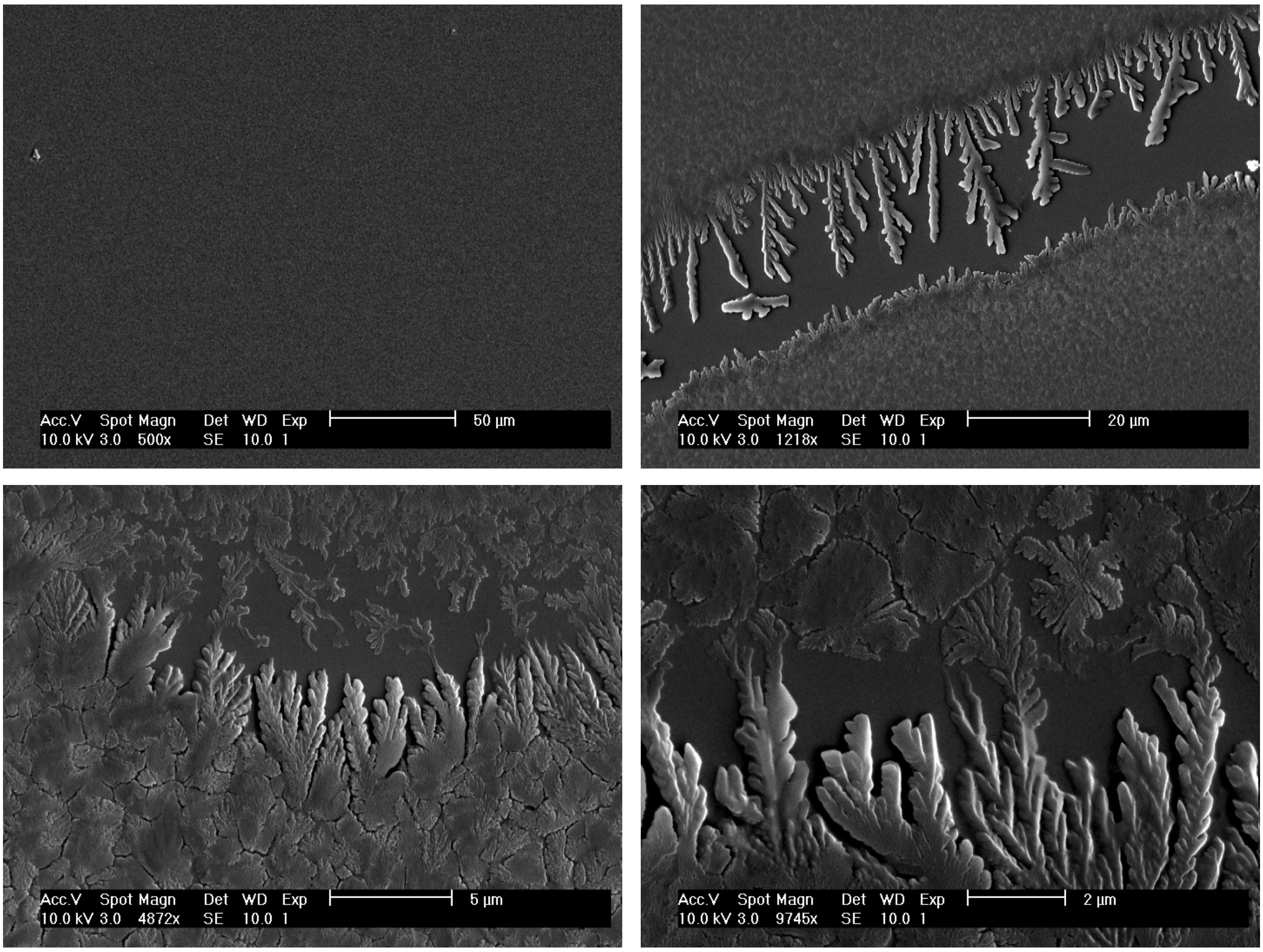
Acc.V Spot Magn Det WD Exp 50 µm
10.0 kV 3.0 500x SE 10.0 1
Acc.V Spot Magn Det WD Exp 20 µm
10.0 kV 3.0 1218x SE 10.0 1
Acc.V Spot Magn Det WD Exp 5 µm
10.0 kV 3.0 4872x SE 10.0 1
Acc.V Spot Magn Det WD Exp 2 µm
10.0 kV 3.0 9745x SE 10.0 1

Figure 7.18. SEM micrograph of HBC-SCF$_3$ deposited on Si(100) showing the formation of a homogeneous thin film at the centre of the substrate (upper left), the columnar dendrite at the edge (upper right), the morphology of the dendrites x5000 (lower left), and x10000 (lower right).

7.6 Conclusion

Syntheses of three new types of HBC that could be used as primers, were done successfully using different approaches. The first model synthesized (**45**, HBC-3,5PhCF$_3$) contains only bulky trifluoromethyl groups at its periphery whereas the last two of these latest series of molecules (HBC-OCF$_3$ and HBC-SCF$_3$) could be seen as promising primers because they bear either oxygen or sulfur groups at their ends. These two last atoms allow their corresponding molecules to bind chemically to the substrate on one hand, while their HBC central cores act as a template for π-bonding of other HBC derivatives onto them, on the other hand. Nonetheless, cyclodehydrogenation was found to be the problem because it doesn’t take place when electron withdrawing groups are present in the para position of the hexaphenyl moiety, which prevents the synthesis of some HBC derivatives. Preliminary SEM investigation of deposited sulfur containing HBC **71** revealed the formation of a homogeneous thin film of this latter on Si(100) substrate grown in a well-organized columnar dendritic morphology.

8. HBCs bearing long perfluorinated chains

8.1 Introduction

As indicated in chapter 5.1, HBCs decorated with long perfluorinated chains should excel the ones synthesized so far bearing aliphatic alkyl chains in the domain of organic materials. Alkyl substituted HBCs have shown very good properties, such as, high electron mobility[13, 104], high degree of order in columnar stacking[106, 192], and in addition, their relative ease of synthesis and purification. The main drawback in an application such as FED, however, remains in the lateral interaction between the stacks caused by the strong Van der Waals bonding between the aliphatic chains; a phenomenon that decreases drastically the chance of isolated columnar stacks and hence the electronic emission to such extent that field emission will then require much higher field strengths to take place[143]. Additionally, most of HBCs bearing aliphatic chains are liquid crystalline at room temperature, which constitutes a second drawback since this causes a drastic decrease of their electronic conductivity[14]. On the other hand, HBCs carrying perfluorinated chains at their periphery are expected to be promising molecules overcoming these disadvantages because the existence of the perfluorinated groups will considerably decrease any lateral interaction between different HBCs stacks. Thus, formation of isolated columns by π-stacking of the HBC cores should be possible as dispersed nanoemitters due to this isolating perfluorinated ‘mantle’. These molecules would therefore be prominent candidates to replace the commercially available FED metallic tips, used nowadays, and known to have many disadvantages like, for example, their short life time and the high fields required for their operation[135].

8.2 HBC with R = $PhRf_6$

Based on the reported higher order of the columnar stacking for HBCs bearing phenyl substituents[196], the first target molecule to be synthesized was HBC derivative **73** (HBC-$PhRf_6$). Its synthesis consists of inserting a perfluorinated hexyl chain in the para position of the biphenyl building block which, after many steps further, is expected to afford the HBC-$PhRf_6$ target bearing perfluorinated chains on an intercalated phenyl group.

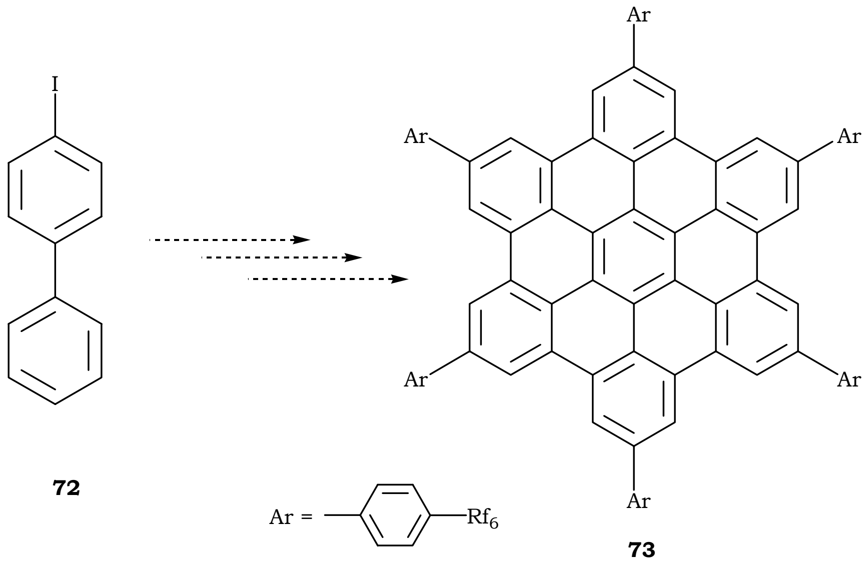

Figure 8.1. Synthetical approach of HBC-PhRf$_6$.

Nevertheless, all the previous attempts[290, 291], using several strategies, have failed to obtain the target HBC **73** or even its hexaphenyl benzene derivative. Even the best approach chosen reached only the tolane step **79** (To-PhRf$_6$) and this as an inseparable mixture with the homocoupling by-products of **75** and **78**. The diacetylene by-product causes a real complication when present in the reaction medium for the trimerization reaction, because both of its reactive acetylene moieties can react, leading to the formation of numerous by-products and, in addition, reduced catalytic activity of the cobalt species.

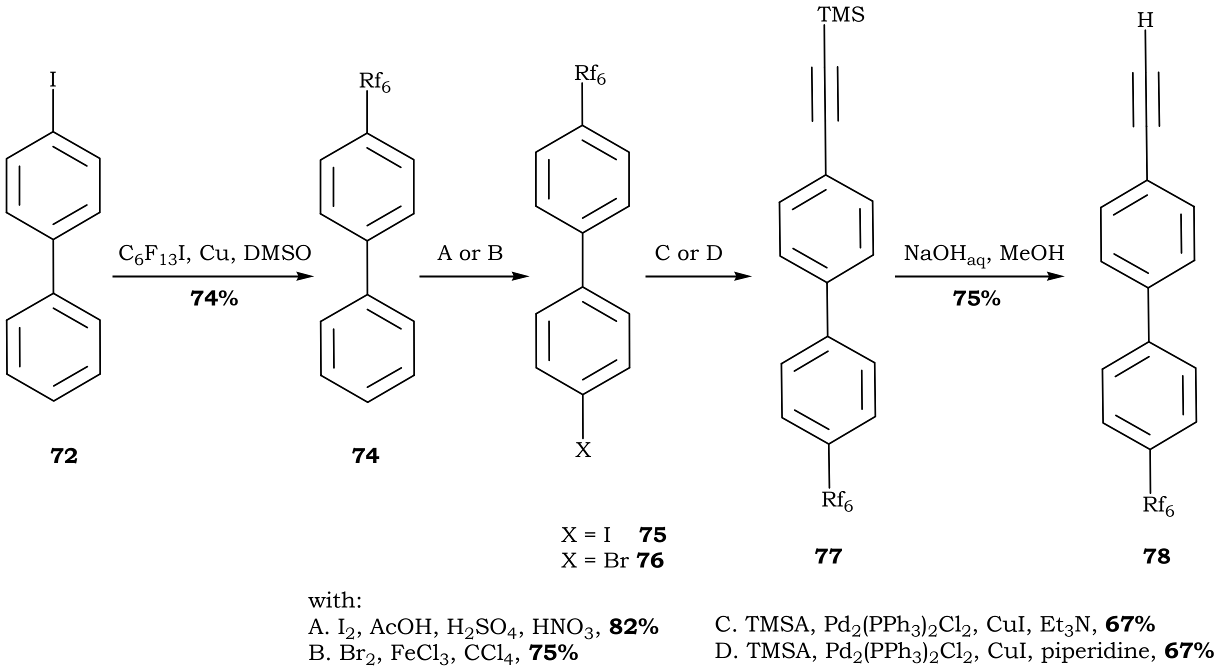
I
72
C6F13I, Cu, DMSO
74%
Rf6
74
A or B
Rf6
X
X = I 75
X = Br 76
C or D
TMS
Rf6
77
NaOHaq, MeOH
75%
H
Rf6
78
with:
A. I2, AcOH, H2SO4, HNO3, 82%
B. Br2, FeCl3, CCl4, 75%
C. TMSA, Pd2(PPh3)2Cl2, CuI, Et3N, 67%
D. TMSA, Pd2(PPh3)2Cl2, CuI, piperidine, 67%

Figure 8.2. Synthesis of the acetylene building block **78** by Sonogashira coupling.

All attempts to synthesize **75** and its corresponding acetylene derivative **77**, on a larger scale, employing the procedures described by P. Folly[290] gave much lower yields and many side products. For these reasons, and to avoid the formation of the homocoupling side product during the tolane formation, we replaced iodine with bromine[292] during the halogenation reaction of **74**. The former halogen is known to be a better leaving group than the latter one but its high reactivity causes the formation of many by-products.

Table 11. Perfluorination and halogenation of **72**.

Entry	Substrate (eq.)	Reagent 1 (eq.)	Reagent2 (eq.)	Solvent	Temp. (°C)	t (hrs)	Product (%Yld)
1	72 (1)	$C_6F_{13}I$ (1.2)	Cu (3.3)	DMSO[a]	130	24	**74** (74)
2	74 (1)[b]	I_2 (0.6)	HNO_3 (9)	H_2SO_4/AcOH	RT-40°C	2	**75** (82)
3	74 (1)	Br_2 (1)	$FeCl_3$(0.25)	CCl_4	RT	72	**76** (75)

a: reaction was done under argon. b: reaction was done on a 1 mmol scale.

As it can be noticed from figure 8.3, the exchange of iodine with bromine suppresses the formation of the homocoupling product **80** without affecting the yields of the following reaction steps.

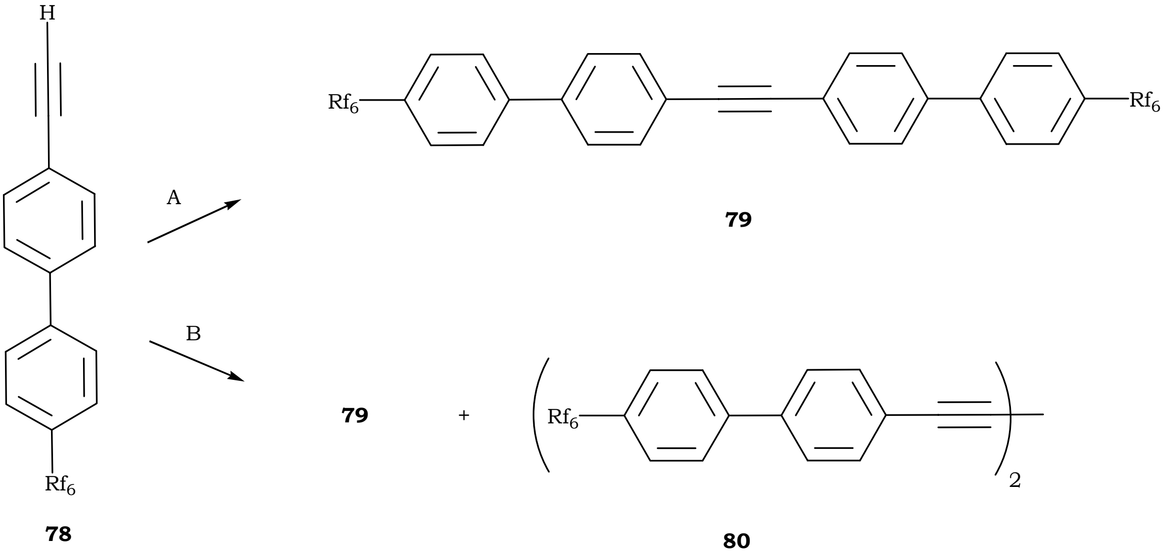

with:
A. **71**,Pd(PPh$_3$)$_4$, CuI, piperidine, 80°C, **58%**
B. **70**, Pd(PPh$_3$)$_4$, CuI, Et$_3$N, Toluene, RT

Figure 8.3. Different synthetical routes to produce perfluorinated tolane **79**.

Table 12 on the next page shows the different Sonogashira reactions conditions applied to get the desired tolane To-PhRf$_6$: entry 3 recalls the mixture of **79** & **80** which was obtained from standard reaction conditions. Replacing the base with a secondary cyclic one doesn't bring any remarkable change (entry 4). All purification attempts in these two trials (entries 3 & 4) have failed to separate To-PhRf$_6$ from the homocoupling product. Nevertheless, when the brominated derivative **76** is employed using the conditions mentioned in entry 5, the desired tolane **79** is obtained in 58%. We should note that the solubility of To-PhRf$_6$ is very weak in common organic solvent, THF and dioxane being poorest.

Table 12. Synthesis of tolane[a] **79**.

Entry	Substrate (eq.)	Reagent (eq.)	Catalyst (Mol%)	Co-cat. (Mol%)	Base	T (°C)	t (h)	Pdt (%Yld)
1	75 (1)	TMSA (1.6)	Pd(PPh$_3$)$_2$Cl$_2$ (7)	CuI (10)	Et$_3$N[b]	RT	3	**77** (67)
2	76 (1)	TMSA (1.3)	Pd(PPh$_3$)$_2$Cl$_2$[c] (3)	CuI (6)	Piperidine[b]	80	24	**77** (67)
3	78 (1)	70 (1)	Pd(PPh$_3$)$_4$ (6)	CuI (3)	Et$_3$N[b]	RT	24	**79, 80**
4[d]	78 (1)	75 (1)	Pd(PPh$_3$)$_4$ (6)	CuI (3)	Pyrolidine	RT	24	**79, 80**
5	78 (1)	76 (1)	Pd(PPh$_3$)$_4$ (6)	CuI (15)	Piperidine	85	48	**79** (58)

a: reactions were done under argon atmosphere. b: base used as solvent too. c: 6 mol% of PPh$_3$ were added d: base in a 1:5 mixture with toluene.

The trimerization of To-PhRf$_6$ was then achieved by reacting this latter with a cobalt catalyst shown in table 13. The moderate yield obtained (48%) can be explained by the low solubility of To-PhRf$_6$ in the appropriate solvent as well as by the electron withdrawing effect of the perfluorinated chain. Contrarily to the starting tolane **79**, the trimer derivative **81** (HPB-PhRf$_6$) is soluble in common organic solvents as a reason of its non-planarity caused by the steric hindrance of the phenyl groups.

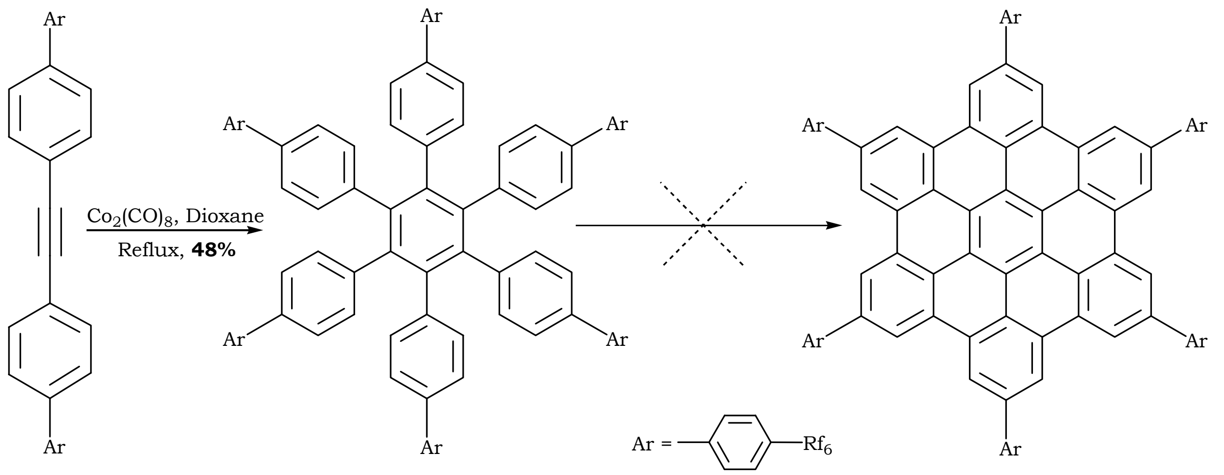

79 **81** **73**

Figure 8.4. Synthetical attempt to produce HBC-PhRf$_6$.

The cyclodehydrogenation reaction has been carried out using the conditions displayed in table 13 below. The employment of $FeCl_3/CH_3NO_2$ combination doesn't afford the HBC moiety either at room temperature (entry 2) or at reflux (entry 3). The replacement of $FeCl_3/CH_3NO_2$ with the more powerful $AlCl_3/Cu(OTf)_2$ reagent mixture doesn't improve the reaction: neither HBC-$PhRf_6$ nor the partially oxidized products have been detected (entry 4).

Table 13. Trimerization of To-$PhRf_6$ and cyclodehydrogenation of **81**^{a}.

Entry	Reagent (nb. eq/ H)	Additive	Solvent	Temp. (°C)	Time (h)	Product (%Yld)
1	$Co_2(CO)_8$^{b}	-	Dioxane	reflux	48	**81** (48)
2	$FeCl_3$(6)	CH_3NO_2	CH_2Cl_2	RT	32^c	**no rxn**
3	$FeCl_3$(6)	CH_3NO_2	CH_2Cl_2	reflux	24	**no rxn**
4	$AlCl_3$(3.3)^d	$Cu(OTf)_2$	CS_2	35°C	24	**no rxn**

a: all the reactions were done under argon. b: cobalt used catalytically (5 mol%).
c: argon was bubbled for 22 hours. d: equimolar amount of Al/Cu.

The good solubility of HPB-$PhRf_6$ leaves only one possible explanation for this failure: the high electron-withdrawing effect of the perfluorinated chain that prevents the oxidation reaction to take place. This strongly corroborates the results obtained during the trials to cyclodehydrogenate HBCs with R = CF_3 and R = 3,5-Bis-(trifluoromethyl)phenyl groups (products **39** and **45** in sections 7.2 and 7.3 respectively). HPB-CF_3 doesn't oxidize to afford HBC-CF_3 either upon using $FeCl_3$ or when employing $AlCl_3/Cu(OTf)_2$ and this can be only explained by the high electron-withdrawing effect of the trifluoromethyl group in the para position, whereas HPB-3,5PhCF_3 cyclodehydrogenates to give HBC-3,5PhCF_3 only when the strong $AlCl_3/Cu(OTf)_2$ conditions are used. A correlation between these data and the result we have obtained herein reveals that the phenyl spacer has a minor intercalating effect during the oxidation reaction when the group attached to it, in para position, has a too high electronegativity. The fact that HPB-3,5PhCF_3 bears the trifluoromethyl groups in the meta position, which doesn't have a strong influence on the reactive carbon, is the major reason why HBC-3,5PhCF_3 is obtained. Therefore we can draw out from all these data the importance of decreasing the electron-withdrawing effect of the perfluorinated side chains, when they are present in the para position as a key step to succeed in obtaining their desired HBCs derivatives.

9. Perfluorinated HBCs with alkyl intercalators

9.1 HBC with R = $Rf_{2,8}$ and $PhRf_{2,8}$

9.1.1 Synthetical strategy

To circumvent the problem we have encountered during the initial trials to synthesize HBC-$PhRf_6$, we have thought about intercalating an aliphatic spacer between HBC and the perfluorinated chains. The main task was therefore to find a suitable way to insert this chain into the aryl moiety in a good yield and in sufficiently high purity to continue the reactions steps further on. For this reason, we have bypassed the different Ullmann reaction conditions that use copper reagents due to their low reactivity with perfluorinated substrates[293]. Concerning coupling conditions that use lithium, the yield is also very low and many isomers form[294]. On the other hand, Kumada and Negishi conditions that use Grignard reagents of magnesium and zinc respectively, under suitable palladium catalysis, employ very harsh conditions affording products from low to moderate yields[295, 296]. Also, standard Heck reactions between halogenated aryls and ethylene containing molecules afford, under palladium catalysis, low yields in this particular case[295]. Nevertheless, Heck reaction conditions using a diazonium salt as a leaving group instead of halogens or triflates has been proven to be most reactive[297-301]. We have used the same conditions to synthesize the alkylated perfluoroalkyl starting materials we needed by using conditions that have been recently employed to synthesize a variety of alkylated perfluoroalkyl aryl compounds[302].

Aniline derivatives **82** and **83** are conveniently transformed to their arenediazonium salts[303] and isolated in a high yield. These latter are reacted in a subsequent step with an appropriate commercially available perfluoroalkene, in the presence of a catalytical amount of palladium species and under ligandless conditions, affording the fluorinated alkene compound **86** and **87** in quantitative yields after few minutes of reaction. Both products are then hydrogenated using the mild rhodium on charcoal catalyst under 50 atmosphere of hydrogen. It must be pointed out that product **85** has been obtained after bromination of 4-nitrobiphenyl[304] followed by a reduction of this latter to the amino group[305]. Perfluoroalkylated decene was given preference above all from other fluorinated alkenes because products bearing shorter chains are volatile and hence their isolation is very difficult while the insertion of chains longer than decene decreases the solubility significantly[302].

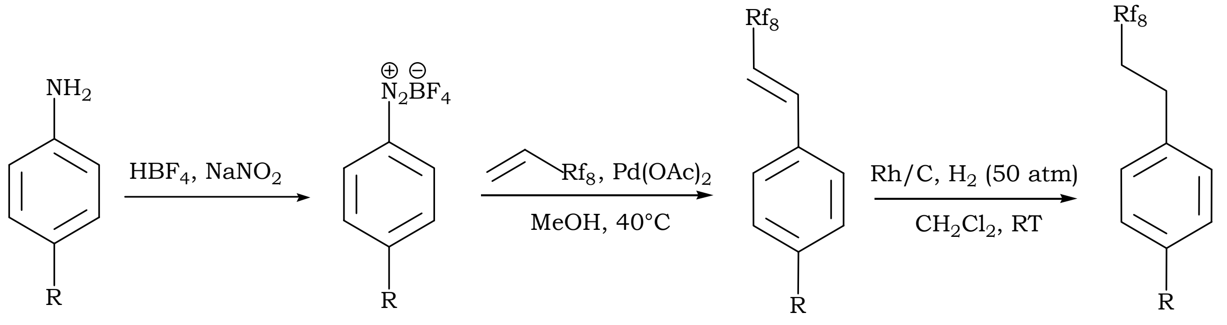
NH2
R
HBF4, NaNO2
N2BF4
R
Rf8, Pd(OAc)2
MeOH, 40°C
Rf8
R
Rh/C, H2 (50 atm)
CH2Cl2, RT
Rf8
R

R= Br **82**
R= *p*-PhBr **83**

R= Br (82%) **84**
R= *p*-PhBr (92%) **85**

R= Br (96%) **86**
R= *p*-PhBr (96%) **87**

R= Br (100%)**88**
R= *p*-PhBr (98%) **89**

Figure 9.1. Synthesis of bromo-perfluoroalkylated building blocks **88** and **89**.

The general mechanism of the Heck coupling[306, 307] reaction is analogous to both the Sonogashira and Suzuki ones since the same four general steps take place: 1) generation of an active Pd(0) species, 2) oxidative addition, 3) insertion, and 4) regeneration of the catalyst. Scheme X below shows the general mechanism omitting the internal steps that could occur depending on different parameters[286, 308].

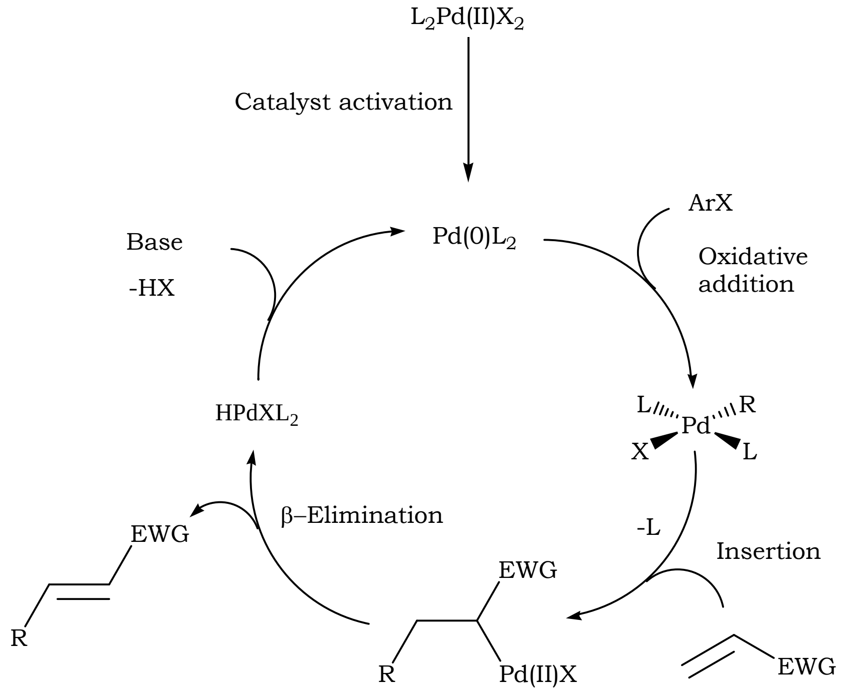
L2Pd(II)X2
Catalyst activation
Pd(0)L2
ArX
Oxidative addition
L
Pd
R
X
L
-L
Insertion
EWG
EWG
R
Pd(II)X
β–Elimination
EWG
R
HPdXL2
Base
-HX

Scheme X. General mechanism of the Heck cross-coupling reaction.

It must be pointed out; however, in our case that a diazonium salt was used as a leaving group and palladium acetate as a catalyst in methanol at 40°C. Thus, a different mechanism must be operating in our case since neither a phosphine ligand is present to reduce palladium(II) acetate, nor a base to regenerate the catalyst. However, we can assume that both roles are accomplished by the solvent, methanol. This latter is believed to act as a reductant too yielding heterogeneous Pd(0) clusters that will carry out the Heck reaction. As a qualitative proof, we must note that we have always obtained a black precipitate during the work-up of these reactions. In addition, it has been proven recently that polymer-supported Pd(0) is produced by simply allowing a solution of $Pd(OAc)_2$ in methanol to stand on a suitable substrate. The former will give two molecules of acetic acid while the latter will be oxidized to formaldehyde[309]. At the same time, the solvent in question acts as a base too because, the HBF_4 formed during the reaction is more acidic than methanol and can therefore protonate it (scheme XI).

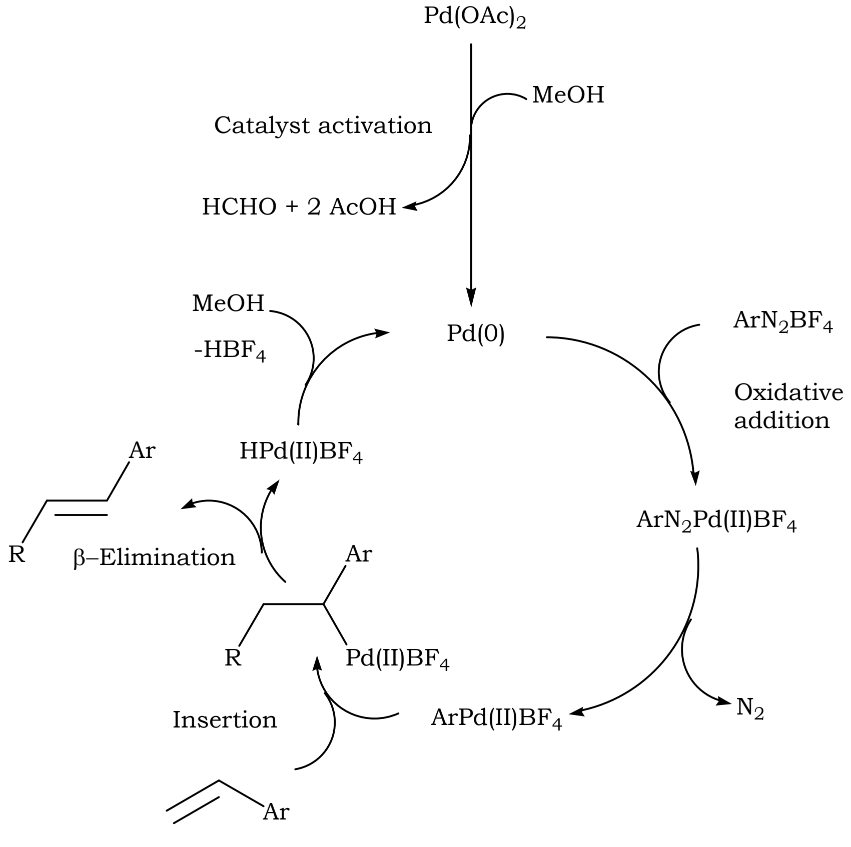
Pd(OAc)2
MeOH
Catalyst activation
HCHO + 2 AcOH
MeOH
-HBF4
Pd(0)
ArN2BF4
Oxidative addition
Ar
HPd(II)BF4
R
β–Elimination
ArN2Pd(II)BF4
Ar
R
Pd(II)BF4
Insertion
ArPd(II)BF4
N2
Ar

Scheme XI. Proposed mechanism of the Heck cross-coupling reaction when using arene diazonium salts.

Products **88** and **89** have been reacted with TMSA under Sonogashira reaction conditions (figure 9.2) yielding the trimethylsilylated acetylene derivatives, which after deprotection, were reacted again with the brominated species **88** and **89** to yield the desired tolanes. The deprotection steps of products **90** & **91** required optimization before reaching the best procedure whose conditions figure in table 14 on the next page.

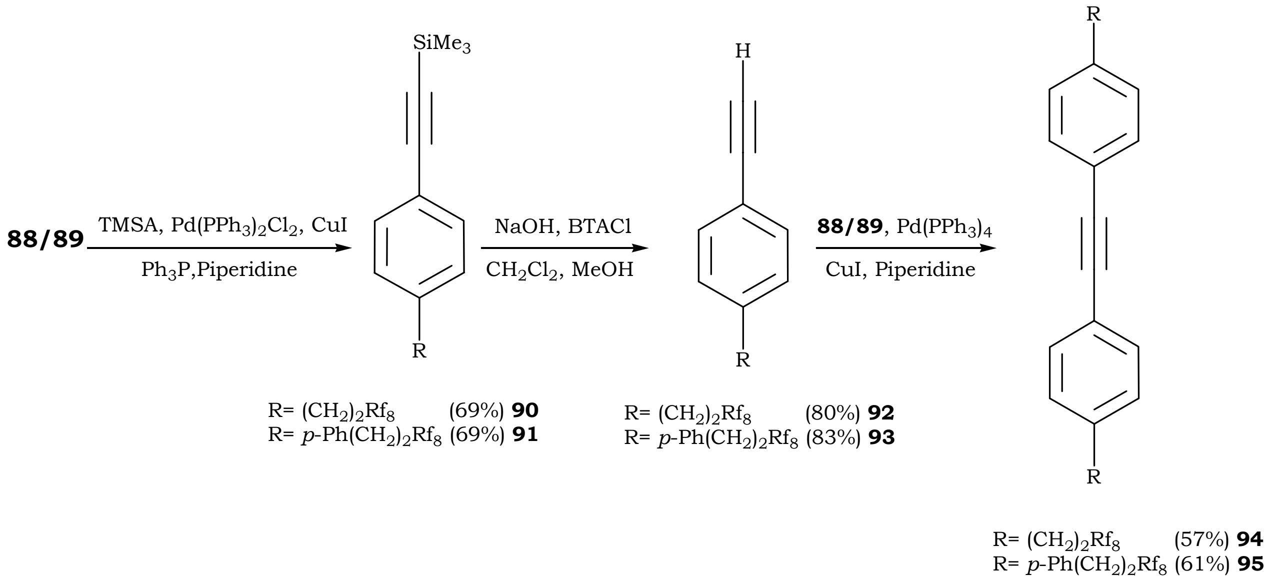
88/89
TMSA, $Pd(PPh_3)_2Cl_2$, CuI
Ph_3P,Piperidine
$SiMe_3$
R
NaOH, BTACl
CH_2Cl_2, MeOH
H
R
88/89, $Pd(PPh_3)_4$
CuI, Piperidine
R
R
R= $(CH_2)_2Rf_8$ (69%) **90**
R= *p*-$Ph(CH_2)_2Rf_8$ (69%) **91**
R= $(CH_2)_2Rf_8$ (80%) **92**
R= *p*-$Ph(CH_2)_2Rf_8$ (83%) **93**
R= $(CH_2)_2Rf_8$ (57%) **94**
R= *p*-$Ph(CH_2)_2Rf_8$ (61%) **95**

Figure 9.2. Synthesis of perfluoroalkylated tolane species **94** and **95**.

It is important to mention that, no matter what solvent used, products **90** & **91** have the same retention factor as compared to their respective deprotected derivatives forming therefore inseparable mixtures. Consequently, an optimization of the reaction conditions to obtain a quantitative conversion was crucial to carry on the subsequent reaction steps. In a first trial, the employment of potassium fluoride as base in a 1:1 methanol/DMF mixture at room temperature has only afforded a 2:1 mixture of **93** with the starting material **91** even after ~1 week of reaction (entry 1). Changing the base to sodium hydroxide and employing methanol only as a solvent yielded only the starting material (entry 2). A slight change of these latter conditions by adding DMF has yielded a 1:1 mixture of **91** and **93** (entry 3) which upon reacting for a longer time (~3 days) has afforded the deprotected species **93** in 82% yield (entry 5). However, employing these conditions to hydrolyze **90** have provided only 25% conversion even after a reaction time of one week (entry 6). Thus, as entry 7 shows, the addition of a minimum amount of CH_2Cl_2, sufficient to dissolve the starting material, decreases the reaction time drastically and affords now a 99% conversion even after two additional days of reaction. The use of BTACl, in two fold excess with respect to the starting material, affords a complete conversion of **93** on one hand, and decreases the reaction time to deprotect **91** even in the absence of DMF on the other hand (entries 8 and 9 respectively).

Table 14. Deprotection of **90** and **91**[a].

Entry	**Substrate**	**Base**	**Additive (eq)**	**Solvent**	**Time**	**Product (%Yld)**
1	91	KF	-	MeOH/ DMF (1:1)	6.5d	**93** (67) **91** (33)
2	91	$NaOH_{aq}$[b]	-	MeOH	6h	**91**
3	91	$NaOH_{aq}$[b]	-	MeOH/DMF (1:1)	14h	**93** (50) **91** (50)
4	91	$NaOH_{aq}$[b]	-	MeOH/DMF (1:1)	33h	**93** (75) **91** (25)
5	91	$NaOH_{aq}$[b]	-	MeOH /DMF (1:1)	3d	**93** (82)
6	91	$NaOH_{aq}$[b]	-	MeOH /DMF (1:1)	7d	**92** (25) **90** (75)
7	91	$NaOH_{aq}$[b]	-	MeOH /CH_2Cl_2/DMF (5:2:1)	1d	**93** (89)[c]
8	91	$NaOH_{aq}$[b]	BTACl (2)	MeOH/CH_2Cl_2 (2.5:1)	2d	**93** (83)
9	90	$NaOH_{aq}$[b]	BTACl (2)	MeOH/CH_2Cl_2 (5:1)	2d	**92** (80)

a: all the reactions were done at RT. b: ~10 M NaOH. c: ^{1}H NMR showed a 99% purity.

Table 15 summarizes the different reaction conditions employed for the coupling steps to produce the tolane derivatives **94** (To-$Rf_{2,8}$) and **95** (To-$PhRf_{2,8}$). The first two entries show that coupling TMSA with **88** and **89** afford products **90** and **91**, respectively, both in 69% yield. Applying the same conditions to obtain the tolane derivative **95** afford this latter in 41% yield only (entry 3). Whereas upon using $Pd(PPh_3)_4$, the yield increases to 61% (entry 4). Employing these conditions on substrates **88** and **92** afford, again, the tolane moiety To-$Rf_{2,8}$ in a moderate yield (entry 5).

Table 15. Syntheses of tolane derivatives **94** and **95**[a].

Entry	Substrate (eq.)	Reagent (eq.)	Catalyst (Mol%)	Co-cat. (Mol%)	Base[b]	T (°C)	t (h)	Pdt (%Yld)
1	88 (1)	TMSA (1.3)	$Pd(PPh_3)_2Cl_2$ (6)[c]	CuI (6)	Piperidine	80	22	**90** (69)
2	89 (1)	TMSA (1.3)	$Pd(PPh_3)_2Cl_2$ (6)[c]	CuI (6)	Piperidine	80	7	**91** (69)
3	93 (1)	89 (1)	$Pd(PPh_3)_2Cl_2$ (6)[d]	CuI (15)	Piperidine	85	49	**95** (41)
4	93 (1)	89 (1)	$Pd(PPh_3)_4$ (6)	CuI (15)	Piperidine	85	29	**95** (61)
5	92 (1)	88 (1)	$Pd(PPh_3)_4$ (6)	CuI (15)	Piperidine	80	29	**94** (57)

a: reactions were done under argon atmosphere. b: as solvent. c: 6 mol% of PPh_3 were added.
d: 12 mol% of PPh_3 were added

Despite the low solubility of To-$Rf_{2,8}$, it was found sufficiently soluble to perform ^1H NMR measurements. Combining this latter with EI-MS results, reveals the presence of the desired tolane species in good purity and confirms the absence of any trace of homocoupling products. On the other hand, the rigid rod-like structure of To-$PhRf_{2,8}$ renders its characterization with ^1H NMR more difficult since the spectrum shows signals of low intensities even after very long accumulation periods; therefore EI-MS was used as the only technique of characterization. The low solubility of both products has prompted us to perform ^{13}C solid state NMR (^{13}C SS-NMR); three different methods have been employed using magic angle spinning (MAS): High-power ^1H-decoupling (hpdec), cross-polarization (CP) and, non-quaternary suppression (NQS). Figure 9.3 on the next page shows the hpdec spectrum of To-$PhRf_{2,8}$: extreme broadening prevents the detection of the alkyne carbon atoms. Therefore, no conclusion can be drawn out from this spectrum besides the fact that aromatic and aliphatic carbons are present.

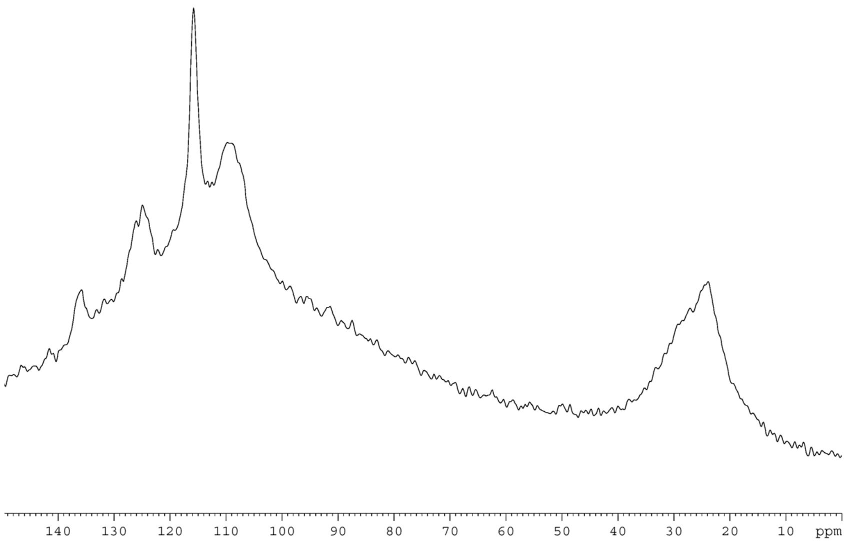

Figure 9.3. ^{13}C-MAS (hpdec) of To-PhRf$_{2,8}$.

The broadening encountered with the hpdec technique was suppressed by measuring the sample with CP-MAS where a better resolution is obtained: the single alkyne peak at ~89 ppm can easily be perceived in addition to the peaks in the aromatic region that are highly overlapped as a reason of their similar chemical shifts (figure 9.4).

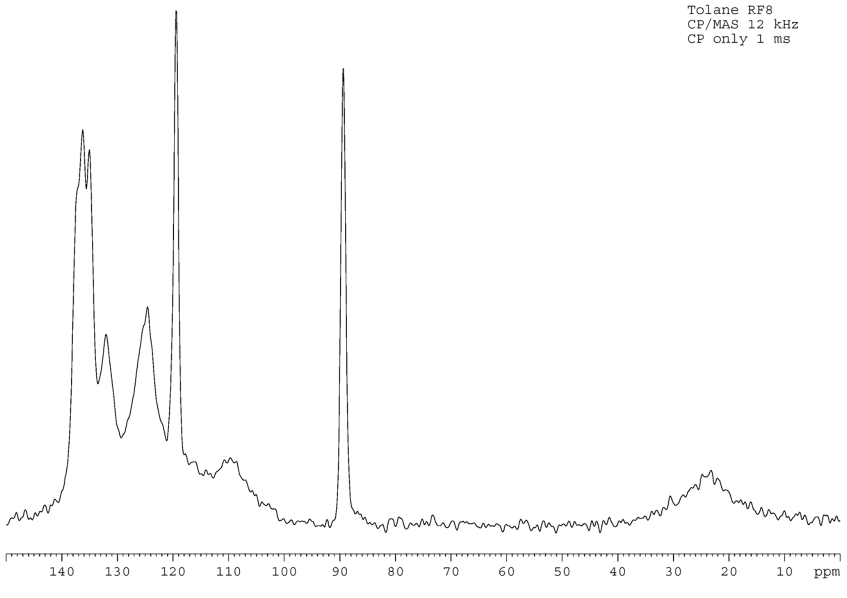

Figure 9.4. CP-MAS of To-PhRf$_{2,8}$.

One way to 'clear' the aromatic region from some overlapped peaks is to measure the sample with the CP-NQS technique that only shows quaternary carbons and exclude all the carbons carrying hydrogens. Figure 9.5 shows the result obtained using this method with which the attribution of the peaks to their corresponding carbons becomes easier.

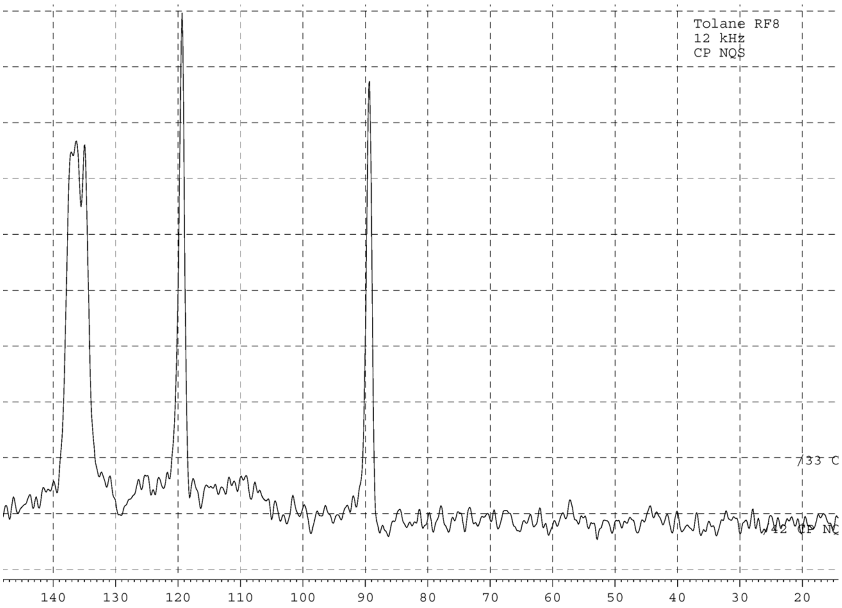

Figure 9.5. CP-NQS of To-PhRf$_{2,8}$.

Surprisingly, all of the SS-NMR techniques shown previously failed to provide the spectra of the tolane derivative To-Rf$_{2,8}$ showing only very broad peaks throughout the spectral region even after many parameter optimization attempts (from those we note, relaxation time, pulse length, power level and CP decay). The first explanation was that a paramagnetic source, resulting from an impurity like the catalytic species used during synthesis, might be present in the medium and is, therefore, responsible of this broadening. To prove this, commercially available tolane (diphenyl acetylene), whose ^{13}C-NMR in solution was performed, was measured with SS-NMR and the resulting spectra showed nearly the same broadening as in ToRf$_{2,8}$. This result renders the cause of the spectrum broadening of such type of tolane derivatives more ambiguous especially that the only difference between To-PhRf$_{2,8}$ and To-Rf$_{2,8}$ (or tolane) is the additional phenyl spacer it bears.

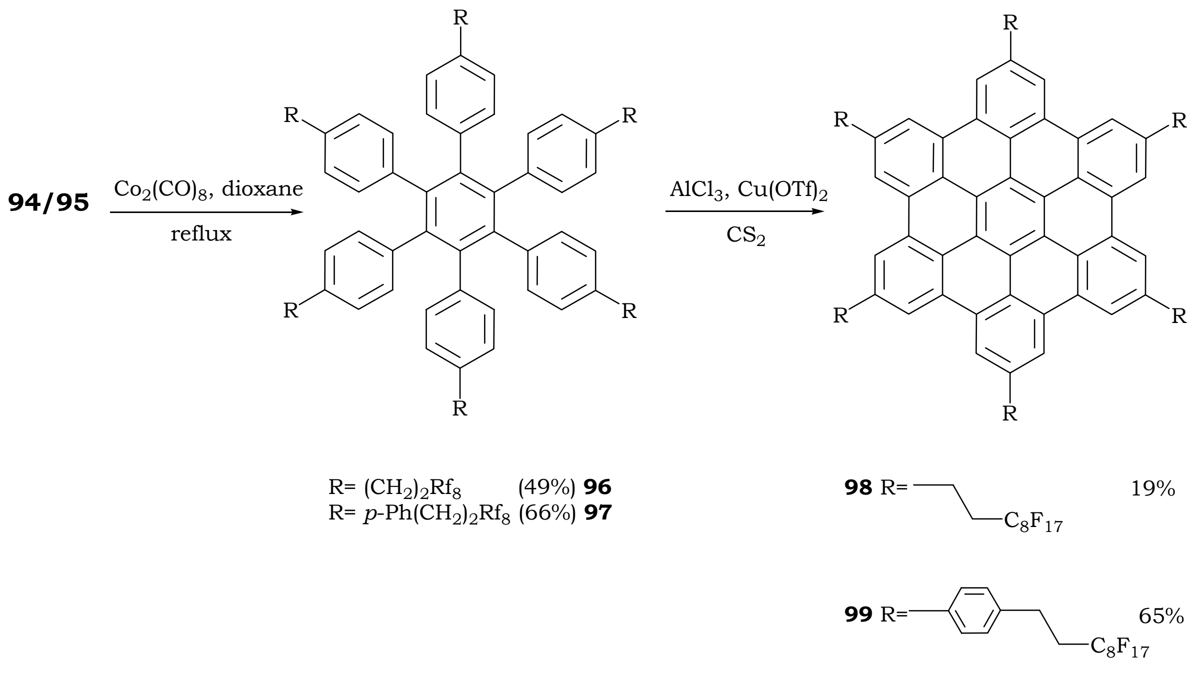

Figure 9.6. Syntheses of the perfluoroalkylated HBC species **98** and **99**.

Trimerization of the tolane species **94** and **95** have been done successfully affording their corresponding hexaphenyl benzene derivatives HPB-$Rf_{2,8}$ and HPB-$PhRf_{2,8}$ in moderate yields (entries 1 and 2 in table 16). This modest conversion is most probably due to the relatively low solubility of the tolane species in refluxing dioxane, as well as in THF, since some starting materials were always recovered.

Table 16. Trimerization reactions of To-$Rf_{2,8}$ & To-$PhRf_{2,8}$ and cyclodehydrogenation of their respective products[a].

Entry	**Substrate**	**Reagent (nb. eq/ H)**	**Additive**	**Solvent**	**Temp. (°C)**	**Time (h)**	**Product (%Yld)**
1	94	$Co_2(CO)_8$[b]	-	Dioxane	reflux	48	**96** (49)
2	95	$Co_2(CO)_8$[b]	-	Dioxane	reflux	72	**97** (66)
3	96	$FeCl_3$(6)	CH_3NO_2	CH_2Cl_2	RT	34[c]	**no rxn**
4	96	$AlCl_3$(3.3)[d]	$Cu(OTf)_2$	CS_2	35°C	24	**98**(19)
5	97	$FeCl_3$(6)	CH_3NO_2	CH_2Cl_2	RT-reflux	18[e]	**97,99,...**
6	97	$AlCl_3$(3.3)[d]	$Cu(OTf)_2$	CS_2	35°C	24	**99**(65)

a: all the reactions were done under argon. b: cobalt used catalytically (5 mol%). c: argon was bubbled for 24 hours. d: equimolar amount of Al/Cu. e: argon was bubbled for 17 hours followed by reflux for 1 hour.

Cyclodehydrogenation of HPB-$Rf_{2,8}$ using $FeCl_3/CH_3NO_2$ affords starting material only (entry 3) revealing that the electron withdrawing effect of the perfluorinated chain remains high even in presence of an ethylene spacer. The replacement of $FeCl_3/CH_3NO_2$ with the stronger combination of $AlCl_3/Cu(OTf)_2$ affords the desired HBC-$Rf_{2,8}$ product in 19% yield (entry 4). On the other hand, entry 5 shows that employing mild conditions on HPB-$PhRf_{2,8}$ affords mainly the starting material along with small amount of HBC-$PhRf_{2,8}$ besides many partially cyclodehydrogenated products. This result strongly agrees with the results obtained during the oxidation of the hexaphenyl derivatives HBC-CF_3 and HBC-$PhRf_6$ and shows once and for all that phenyl group is not a very good intercalator that inhibit the electron-withdrawing effect. Nonetheless, the employment of the Al(III)/Cu(II) combination of reagents for oxidation reactions, affords HBC-$PhRf_{2,8}$ in 65% yield (entry 7). It must be mentioned that upon using the $AlCl_3/Cu(OTf)_2$ combination, migration of the side chains may occur as we have cited earlier (section 6). But as a reason of their very low solubility, we can't prove analytically that the structure of the HBC moieties has changed under the influence of the strong Friedel-Crafts reagent $AlCl_3$ since only MALDI-TOF technique was employed to detect the presence of the HBC derivatives. However we do believe that the chain is sufficiently inert towards Friedel-Crafts reactions, many published works studying the reactivity of such intercalated alkylated perfluoroalkyl chains support this suggestion too[293, 310, 311].

9.1.2 DSC investigation of HBC-$Rf_{2,8}$ and HBC-$PhRf_{2,8}$

Differential scanning calorimetry (DSC) of both products **98** and **99** have been done as table 17 depicts. However, it is worthwhile to note that the term D is used in this work as a simplification to describe both the unknown mesomorphic phases (that could be nematic or columnar) and the columnar ones as given in the literature[14] even though the term D, which means discotic, is not the most appropriate one to use[60]. By comparing entries 1 and 2, we can easily notice that HBC-$Rf_{2,8}$ has four liquid crystalline phases whereas the fully alkylated HBC-C_{10} has only one mesomorphic phase whose transition temperature has nearly the same value as the first transition temperature observed for HBC-$Rf_{2,8}$ (124°C). A more interesting observation is the fact that HBC-C_{10} shows a crystalline phase transition, while HBC-$Rf_{2,8}$ doesn't, indicating, therefore, an amorphous state of the hitherto unknown product; a phenomenon that is presumably caused by the perfluorinated chains since they reduce the interactions between the different neighboring molecules. Last but not least, the insertion of a phenyl group between the HBC core and the alkylated perfluoroalkyl chains HBC-$PhRf_{2,8}$ increases the liquid phase transition temperature by ~100°C as compared to HBC-$Rf_{2,8}$ (entry 3) but still the DSC trace doesn't show any crystalline phase transition peak.

Table 17. Phase transition temperatures, enthalpy changes and structural assignments for different HBC derivatives[a,b].

Entry	Compound	Phase Transition temperature (°C)	ΔH ($KJ\ mol^{-1}$)	Phase width (°C)	Assignment
		heating/cooling	heating/cooling		
1	**HBC-C_{10}**	69/(c)	9/(c)	-	$K_1 \rightarrow K_2$
		124/97	64/71	55	$K_2 \leftrightarrow D_h$
2	**HBC-$Rf_{2,8}$ (98)**	122/114	1.4/1.2	-	$D_1 \leftrightarrow D_2$
		138/128	37.2/36	16	$D_2 \leftrightarrow D_3$
		180/173	7.7/6.5	42	$D_3 \leftrightarrow D_4$
3[d]	**HBC-Ph$Rf_{2,8}$ (99)**	227/223	66.4/60.5	-	$D_1 \leftrightarrow D_2$
		236/235	19.8/14.2	9	$D_2 \leftrightarrow D_3$

a: isotropic liquid wasn't formed below 360°C, decomposition occurs above ~250°C. b: rate of heating & cooling is 20°C/min. c: not determined. d: two peaks were obtained upon heating. With K: crystalline, D_h: discotic hexagonal, D: discotic.

9.2 HBC with R = $Rf_{4,8}$ and $Rf_{6,6}$

9.2.1 Synthetical approach

As it could be noticed from the previous section, even the insertion of an ethylene spacer didn't remove the electron withdrawing effect of the perfluorinated which is high and is still influencing the oxidation step that doesn't take place unless harsher conditions are employed. In addition, the starting materials leading to HBC-$Rf_{2,8}$ and HBC-Ph$Rf_{2,8}$ show a relatively high insolubility and are very difficult to remove during the following steps. These reasons have led us to divert to the synthesis of some new HBC derivatives bearing longer aliphatic intercalators. These latter are expected to enhance the solubility of the intermediate products, mainly tolane and the hexaphenyl benzene moieties which, upon cyclodehydrogenation will yield again insoluble HBC derivatives that can be isolated by simple filtration from the reaction medium. Moreover, the intercalators aren't expected to alter the isolating effect of the peripheral perfluorinated chains long enough to prevent any lateral interaction between HBCs. To achieve this, the synthesis of perfluorinated chains bearing four and six methylene groups have been done after improving the procedures found in the literature[312, 313]. We must mention that unless a high purity is obtained during the isolation of each of the intermediate products leading to **108** ($BrRf_{4,8}$) and **109** ($BrRf_{6,6}$), the later coupling reaction steps won't occur or many side products are isolated instead. Therefore, the known procedures employed herein have been improved by applying additional purification techniques, mainly filtration of the crude products over a short silica gel plug under reduced pressure with different solvents (hexane, pentane) in such a way to remove the less polar side products first followed by the elution of the pure product with a more polar solvent at last. As it can be noticed from Figure 9.7, commercially available 3-butenoic acid **100** and 5-hexen-1-ol **101** are reacted with perfluorooctyl iodide **102** and perfluorohexyl iodide **103** respectively in presence of a palladium catalyst[314] to yield the coupled chain products **104** and **105**. These latter are then reduced in presence of $LiAlH_4$ to afford the perfluoalkyl alcohols **101** and **107** which are converted to their halogen derivatives $BrRf_{4,8}$ and $BrRf_{6,6}$ respectively after refluxing with hydrobromic acid in presence of Aliquat 336® as PTC.

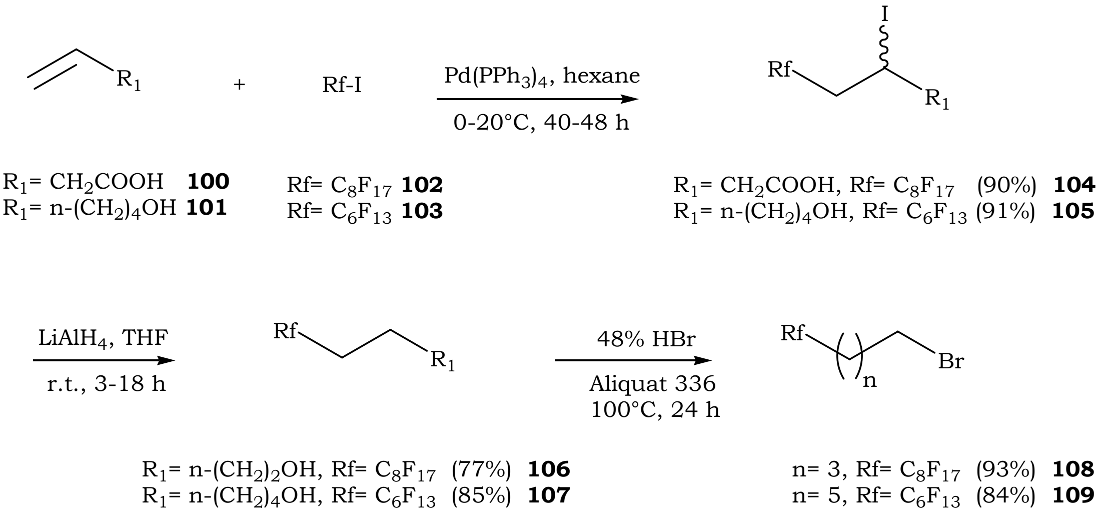
R1
+
Rf-I
Pd(PPh3)4, hexane
0-20°C, 40-48 h
I
Rf
R1
R1= CH2COOH 100
R1= n-(CH2)4OH 101
Rf= C8F17 102
Rf= C6F13 103
R1= CH2COOH, Rf= C8F17 (90%) 104
R1= n-(CH2)4OH, Rf= C6F13 (91%) 105
LiAlH4, THF
r.t., 3-18 h
Rf
R1
48% HBr
Aliquat 336
100°C, 24 h
Rf
n
Br
R1= n-(CH2)2OH, Rf= C8F17 (77%) 106
R1= n-(CH2)4OH, Rf= C6F13 (85%) 107
n= 3, Rf= C8F17 (93%) 108
n= 5, Rf= C6F13 (84%) 109

Figure 9.7. Syntheses of alkylated perfluoroalkyl chains.

The alkylated perfluoroalkyl chains $BrRf_{4,8}$ and $BrRf_{6,6}$ were reacted with dibromotolane **36** (figure 9.8) under Kumada[315] and Negishi[316] cross-coupling reaction conditions that consist of employing an organomagnesium species for the former, and an organozinc moiety for the latter, in presence of a halogenated aryl derivative and a suitable catalyst. When mild reaction conditions are needed, both cross-coupling reaction types use nickel complexes[317-320], such as Ni(dppp)Cl_2 and Ni(dppe)Cl_2, whereas palladium complexes are employed when harsher conditions are required[321] and the most frequently used catalyst for that purpose is Pd(dppf)Cl_2. Nevertheless, the Negishi coupling reaction has a wider spectrum of applications than Kumada because different types of substrates can be used, such as, alkyls, benzyls, vinyls, allyls, and aryls[322]. Recently, many reports have disclosed new methods to generate alkylzinc derivatives from inactivated alkyl bromides[323, 324]. Nonetheless, the major drawback upon using Negishi conditions is the fact that organozinc derivatives must be generated in situ since they can't be isolated. The mechanism of both coupling reactions is similar to Sonogashira and Suzuki ones that we have shown previously (schemes V and VII) employing organometallic derivatives and consisting of four main steps: 1) generation of an active Pd(0) species, 2) oxidative addition, 3) transmetallation, and 4- reductive elimination.

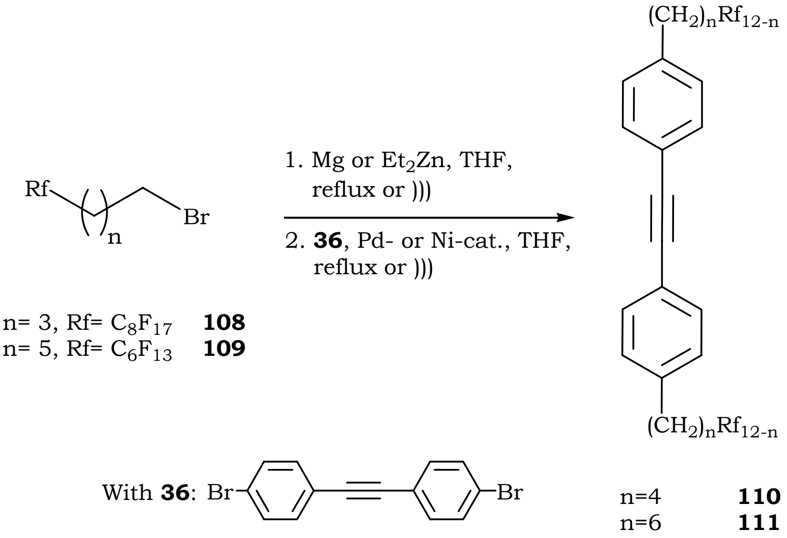
Rf
n
Br
n= 3, Rf= C_8F_{17} **108**
n= 5, Rf= C_6F_{13} **109**
1. Mg or Et_2Zn, THF, reflux or)))
2. **36**, Pd- or Ni-cat., THF, reflux or)))
$(CH_2)_nRf_{12-n}$
$(CH_2)_nRf_{12-n}$
With **36**: Br
Br
n=4 **110**
n=6 **111**

Figure 9.8. Syntheses of alkylated perfluoroalkyl tolanes by Kumada and Negishi couplings.

Table 18 on the next page shows the different attempts we have done to obtain the alkylated perfluoroalkyl tolane derivatives **110** (To-$Rf_{4,8}$) and **111** (To-$Rf_{6,6}$). We have first performed the reactions using the perfluorinated chain $BrRf_{6,6}$ because it bears an alkyl tail long enough to prevent the deactivating influence of the perfluorinated groups. The less reactive chain $BrRf_{4,8}$ has undergone coupling reaction only after optimizing the reaction conditions of $BrRf_{6,6}$.

Table 18. Kumada and Negishi cross-coupling reactions with **36**[a].

Entry	pdt	Grignard reaction					C-C Coupling reaction				Pdt (%Yld)
		Pdt (eq)	*Reagent (eq)*	*Sol.*	*T (°C)*	*t (d)*	*Catalyst (mol%)*	*Sol.*	*T (°C)*	*t (d)*	
1	36	109 (4)	Mg (4)	THF	80	1	Ni(dppp)Cl_2 (6)	THF	80	1	**no rxn**
2	36	109 (4)	Mg (4)	Et_2O	45	1	Ni(dppp)Cl_2 (6)	THF	80	1	**no rxn**
3	36	109 (4)	Mg (4)	THF	75	2	Ni(dppp)Cl_2 (10)	THF	75	1	**no rxn**
4	36	109 (4)	Mg (4)	THF	75	2	Ni(dppe)Cl_2 (6)	THF	75	1	**no rxn**
5	36	109 (4)	Et_2Zn(1), cat.CuCl, cat.$FeCl_3$[b]	THF	RT	1	Pd(dppf)Cl_2 (10)	THF	-50-75	1	**no rxn**
6	36	109 (4)	Mg (4)	THF	75	1	Pd(dppf)Cl_2 (6)	THF	)))	2	**111** (24)
7	36	109 (4)	Mg (4)	THF	75	1	Pd(dppf)Cl_2 (6)	THF:FC-72 (2:1)	70	2	**111** (45)
8	36	109 (4)	Mg (4)	THF	75	1	Pd(dppf)Cl_2 (10)	THF	75	3	**111** (65)
9	36	109 (4)	Mg (4)	THF	75	1	Pd(dppf)Cl_2 (10)	THF:FC-72 (2:1)	75	3	**111** (69)
10	36	108 (4)	Mg (4)	THF	75	1	Pd(dppf)Cl_2 (10)	THF	75	3	**110** (46)
11	36	108 (4)	Mg (4)	THF	75	1	Pd(dppf)Cl_2 (15)	THF	75	6	**110** (75)

a: number of equivalents is calculated with respect to 36. b: 5 mol% $FeCl_3$ and 3 mol% CuCl.

As the first four entries of table 18 show, the use of common Kumada reaction conditions that employ mild nickel complexes as catalysts were found to be inefficient; only the starting material **36** has been recovered. The same result was obtained when Negishi coupling conditions were used. These latter require the use of diethyl zinc and catalytical amounts of $FeCl_3$ and CuCl[324] to form the corresponding organozinc species of **109** first, followed by the coupling with **36** under Pd(dppf)Cl_2 catalysis (entry 5). Carrying the reaction in an ultrasonic bath for 2 days, using Kumada reaction conditions with Pd(dppf)Cl_2 as catalyst, however, has yielded 24% of the desired tolane derivative To-$Rf_{6,6}$ (entry 6). By addition of a perfluorinated co-solvent to the reaction medium, the yield was increased to 45% (entry 7). Nevertheless, entries 8 and 9 show clearly that yield of the reaction is mainly time dependent and that a perfluorinated co-solvent doesn't significantly affect the reaction. The same conditions of entry 9 were applied on **108** which afforded 46% of its corresponding tolane derivative **110**. Doubling the reaction time to six days, finally, yields 75% of To-Rf$_{4,8}$ (entry 11).

Trimerization of the tolane derivatives to their corresponding hexaphenylbenzene products followed by cyclodehydrogenation of these latter have been done as shown in figure 9.9. Reacting products To-Rf$_{4,8}$ and To-Rf$_{6,6}$ in presence of the dicobalt carbonyl catalyst, in refluxing dioxane, afford trimers **112** (HPB-Rf$_{4,8}$) and **113** (HPB-Rf$_{6,6}$) in 70 and 80% yield respectively (entries 1 and 2 in table 19).

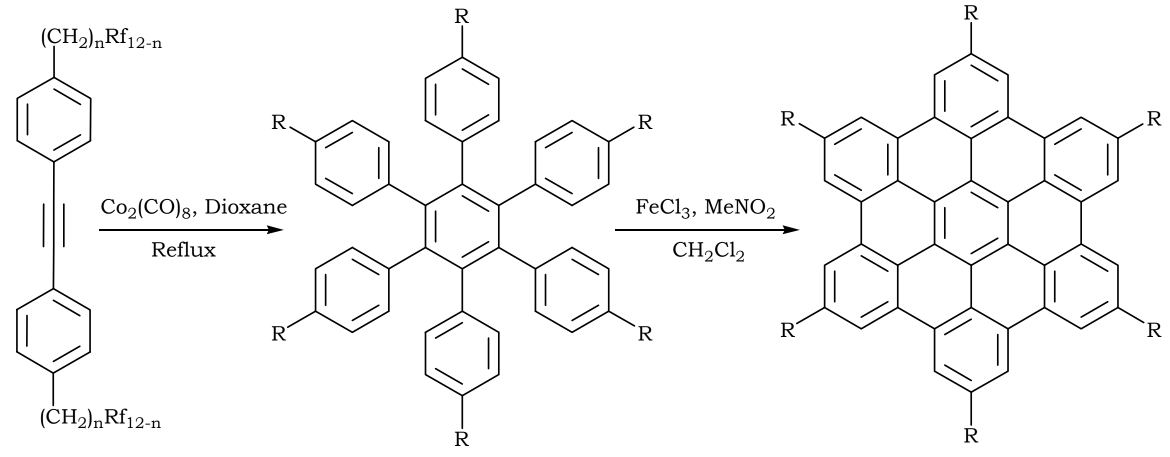

n=4 **110**
n=6 **111**

With R = $(CH_2)_nRf_{12-n}$
n=4 (70%) **112**
n=6 (80%) **113**

With R = $(CH_2)_nRf_{12-n}$
n=4 (35%) **114**
n=6 (87%) **115**

Figure 9.9. Syntheses of alkylated perfluoroalkyl HBC derivatives **114** and **115**.

Entry 3 in table 19 shows that cyclodehydrogenation reaction conditions using $FeCl_3/CH_3NO_2$ combination affords the HBC derivative **114** (HBC-Rf$_{4,8}$) in a modest yield (35%), both starting material HPB-Rf$_{4,8}$ and partially cyclodehydrogenated products were also isolated during the purification step implying that a longer reaction time would increase the yield of HBC-Rf$_{4,8}$. The relatively slow reaction is due to the low solubility of HPB-Rf$_{4,8}$ in CH_2Cl_2 and not to the electron-withdrawing effect of the alkylated perfluoroalkyl chain because if it was the case, the reaction wouldn’t take place at all as we have seen in the previous sections. Applying the same oxidation reaction conditions on HPB-Rf$_{6,6}$ (entry 4) provides the HBC derivative **115** (HBC-Rf$_{6,6}$), bearing six methylene spacer units in 87%. This higher yield than the one of HBC-Rf$_{4,8}$ can be explained by the relatively good solubility of HPB-Rf$_{6,6}$ in CH_2Cl_2.

Table 19. Trimerization of To-Rf$_{4,8}$ & To-Rf$_{6,6}$ and cyclodehydrogenation of their respective products^{a}.

Entry	Substrate	Reagent (nb. eq/ H)	Additive	Solvent	Temp. (°C)	Time (h)	Product (%Yld)
1	110	$Co_2(CO)_8$^{b}	-	Dioxane	reflux	48	**112** (70)
2	111	$Co_2(CO)_8$^{b}	-	Dioxane	reflux	48	**113** (80)
3	112	$FeCl_3$ (6)	CH_3NO_2	CH_2Cl_2	RT	10^{c}	**114** (35)
4	113	$FeCl_3$ (6)	CH_3NO_2	CH_2Cl_2	RT	5^{c}	**115** (87)
5	HPB/**108**^{d}	$FeCl_3$ (~2)^{e}	CH_3NO_2	CH_2Cl_2	RT	12	-

a: all the reactions were done under argon.. b: 5 mol% of cobalt. c: argon was bubbled throughout the reaction.. d: HBP/108 in 1:9 ratio e: $FeCl_3$ in CH_3NO_2 is added dropwise onto the reaction mixture.

Although all synthetical strategies we have used so far to produce the perfluorinated HBC derivatives permit the characterization of each product formed, they represent a major drawback because at each time a new perfluorinated group is to be introduced on the HBC core, the whole reaction sequence must be restarted from scratch which is time consuming. To circumvent this problem we have thought about reducing the number of linear reaction steps by attempting the one pot synthesis illustrated in figure 9.10. The trial has been performed by adding dropwise a solution of $FeCl_3$ in CH_3NO_2 on a mixture of Br-Rf$_{4,8}$ and the commercially available hexaphenylbenzene (HPB) in CH_2Cl_2. The reaction was carried out for 12 hours at room temperature and argon was bubbled through the medium during the whole reaction. Unfortunately, only the starting materials were recovered in addition to a small amount of a mixture of partially dehydrogenated hexaphenylbenzenes. This result can be explained by the fact that we have used a primary brominated chain which is less reactive towards Friedel-Crafts alkylation than the very specific tertiary alkyl group, t-BuCl, employed by Rathore et al.[197]. For this purpose more powerful Friedel-Crafts reagents must be explored in the future in such a way to generalize this reaction on all the HBC derivatives which, once succeeded, can considerably reduce the reaction sequences.

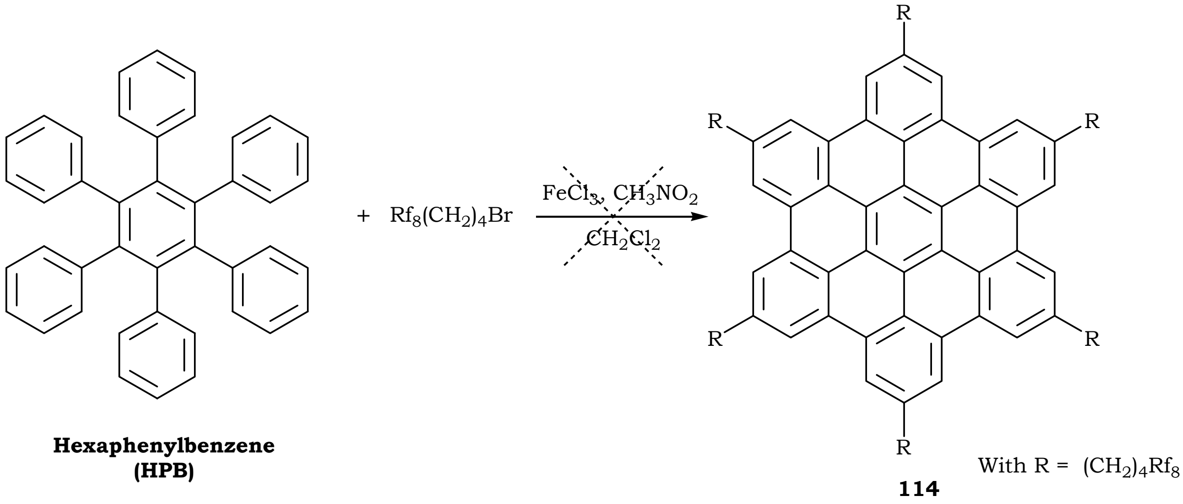

Hexaphenylbenzene (HPB)

114

Figure 9.10. One-pot synthetical attempt of HBC-$Rf_{4,8}$.

Figures 9.11 and 9.12 show the MALDI-TOF mass spectrum of HBC-$Rf_{4,8}$ and the UV-Vis spectrum of HBC-$Rf_{6,6}$, respectively. The analyses done with the MALDI-TOF technique on **114** and **115** have shown no trace of either the starting material or the partially cyclodehydrogenated products indicating, therefore, a high purity.

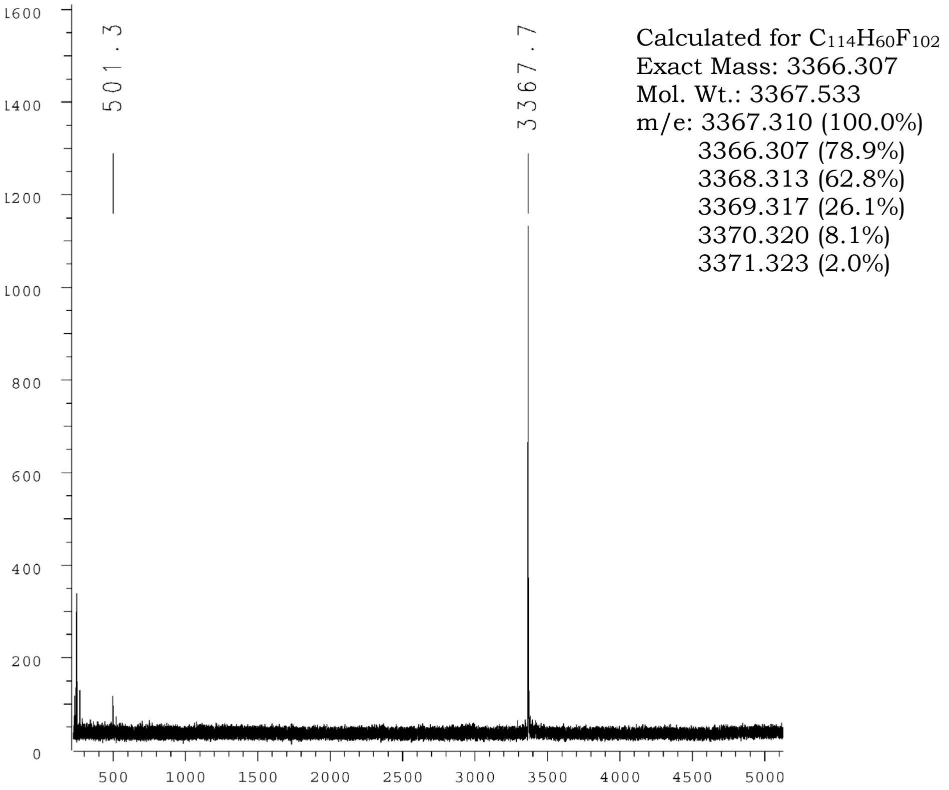

Calculated for $C_{114}H_{60}F_{102}$
Exact Mass: 3366.307
Mol. Wt.: 3367.533
m/e: 3367.310 (100.0%)
3366.307 (78.9%)
3368.313 (62.8%)
3369.317 (26.1%)
3370.320 (8.1%)
3371.323 (2.0%)

Figure 9.11. MALDI-TOF of HBC-$Rf_{4,8}$.

The UV-Vis spectrum of HBC-Rf$_{6,6}$ shows the three characteristic peaks of HBC core at 368, 394 and 421 nm, the shape of the spectrum obtained reveals that the product is present in the medium as an aggregate rather than being totally dissolved in 1,2,4-TCB. Additionally, the low solubility of the product doesn't permit a precise analytical calculation of the concentration because during the sample preparation, the suspension obtained is filtered over Millipore®, and the high boiling point of the solvent used (b.p. 214°C) doesn't allow to weigh analytically the precipitate remaining on the filter. Therefore, the molar absorption coefficient value of the maximum peak (ε ~ 114000 M^{-1} cm^{-1}) was taken from literature[193] and used to estimate the concentration which was found to be around $1.7x10^{-7}$ M (figure 9.12). The low solubility of HBC-Rf$_{4,8}$ in 1,2,4-TCB, on the other hand, didn't allow its investigation either by UV-Vis or by luminescence.

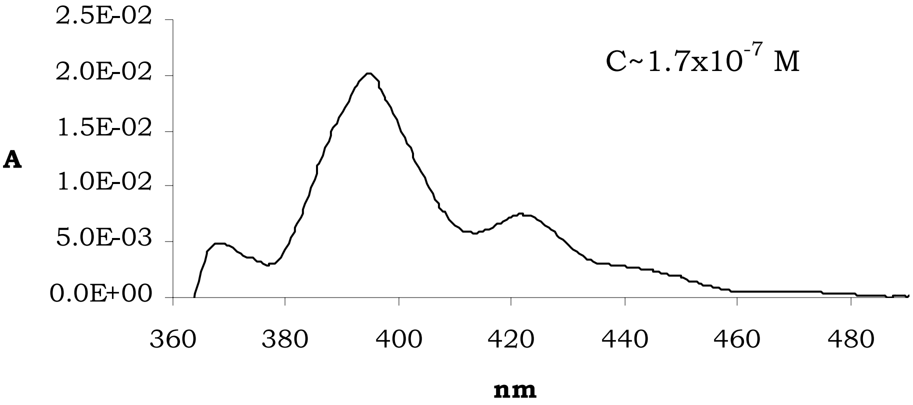

Figure 9.12. UV-Vis spectrum of HBC-Rf$_{6,6}$.

9.2.2 Calorimetric analyses of HBC-Rf$_{4,8}$ and HBC-Rf$_{6,6}$

Few publications describe the behavior change of some liquid crystalline materials upon replacing their lateral alkyl chains with perfluorinated ones: during their studies on small liquid crystalline molecules, that self-assemble by hydrogen bonding interactions, such as, cyano- and aminobiphenyl derivatives that form nematic and smectic phases for the former and the latter respectively, Fialkov et al. noted the disappearance of the liquid crystalline phases after replacing the lateral alkyl chains with perfluorinated ones[325]. Recently, Shimizu and co-workers showed that the replacement of lateral alkyl chains of triphenylene derivatives, owing either hexagonal columnar (Col$_h$) or hexagonal columnar plastic (Col$_p$) mesophases, with perfluorinated or alkylated perfluoroalkyl chains having the same length of their alkylated homologues, causes a better molecular arrangement that leads to homeotropic alignment of the discs on a series of suitable substrates[326, 327].

In order to study the behavior change brought by the perfluorinated chains to the HBC moiety, DSC measurements of both products HBC-$Rf_{4,8}$ and HBC-$Rf_{6,6}$ were compared to the well-known HBC derivatives bearing fully alkylated n-decyl and n-dodecyl chains[14], HBC-C_{10} and HBC-C_{12}, respectively. The calorimetric analyses have revealed the presence of at least one liquid crystalline phase for each perfluorinated HBC, as it can be noticed from entries 3 and 4 in table 20 on the next page. By comparing entries 1 and 2, we can easily notice that upon increasing the length of the fully alkylated chain by two methylene groups, the phase transition temperature decreases by ~19°C on one hand, but more energy is needed for liquid crystalline phase transition to take place, on the other hand, as a direct result of a higher crystalline order brought about by these additional alkyl groups. Concerning HBC-$Rf_{4,8}$ and HBC-$Rf_{6,6}$ (entries 3 and 4); the phase transition temperature of the latter is lower by ~30°C as a reason of the presence of two additional methylene carbons that make the molecule more flexible. On top of that, another important conclusion can be deduced from data in table 20, the enthalpy changes for both HBC-$Rf_{4,8}$ and HBC-$Rf_{6,6}$ to pass to liquid-crystalline phases, are lower to those with alkyl chains, and this can be explained by the fact that due to the steric hindrance caused by the fluorine atoms, perfluorinated chains have low crystallization packing and they maintain a helical conformation which doesn't necessitate a much high transition energy whereas the zig-zag conformation of the well packed crystallized alkyl chains requires more energy for liquid-crystalline phase to occur[328].

Table 20. Phase transition temperatures, enthalpy changes and structural assignments for different HBC derivatives.

Entry[a,b]	**Compound**	**Phase Transition temperature (°C)**	**ΔH (KJ mol^{-1})**	**Phase width (°C)**	**Assignment**
		heating/cooling	**heating/cooling**		
1	**HBC-C$_{10}$**	69/(c)	9/(c)	-	$K_1 \rightarrow K_2$
		124/97	64/71	55	$K_2 \leftrightarrow D_h$
2	**HBC-C$_{12}$**	42/(c)	10/(c)	-	$K_1 \rightarrow K_2$
		105/86	78/(c)	63	$K_2 \leftrightarrow D_h$
3	**HBC-Rf$_{4,8}$ (114)**	82/(c)	6/(c)	-	$K_1 \rightarrow K_2$
		120/103	58/52.6	38	$K_2 \leftrightarrow D_1$
		190/171	8.5/7.8	70	$D_1 \leftrightarrow D_2$
4[d]	**HBC-Rf$_{6,6}$ (115)**	50/(c)	4.6/(c)	-	$K_1 \rightarrow K_2$
		109/98	48/46	18	$K_2 \leftrightarrow D_1$

a: isotropic liquid wasn't formed below 360°C, decomposition occurs above ~250°C. b: rate of heating & cooling is 20°C/min. c: not determined. d: two peaks were obtained upon heating. With K: crystalline, D_h: discotic hexagonal, D: discotic.

9.2.3 Optical microscopy study of HBC-Rf$_{4,8}$ and HBC-Rf$_{6,6}$

Polarized optical microscopy (POM) investigation of HBC-Rf$_{4,8}$ and HBC-Rf$_{6,6}$ revealed their high viscosities that prevent the formation of definite textures. After a long time of heating, only 'schlieren' textures were seen (Figure 9.13). Nevertheless, we must point out that the same observations have been made by Shimizu and co-workers[326] on the perfluorinated triphenylene derivatives where only after the employment of suitable substrates, they observed a homeotropic alignment. Thus, we can assume that HBC-Rf$_{4,8}$ and HBC-Rf$_{6,6}$ would act in the same way when deposited on suitable substrates especially since their alkylated homologue HBC-C$_{12}$ has the same mesophase as the alkylated triphenylene i.e. hexagonal columnar[93]. To prove this, more characterization techniques should be carried out, such as, X-ray powder diffraction at the mesophase temperatures, as well as, a more in depth POM investigation of HBC-Rf$_{4,8}$ and HBC-Rf$_{6,6}$ derivatives.

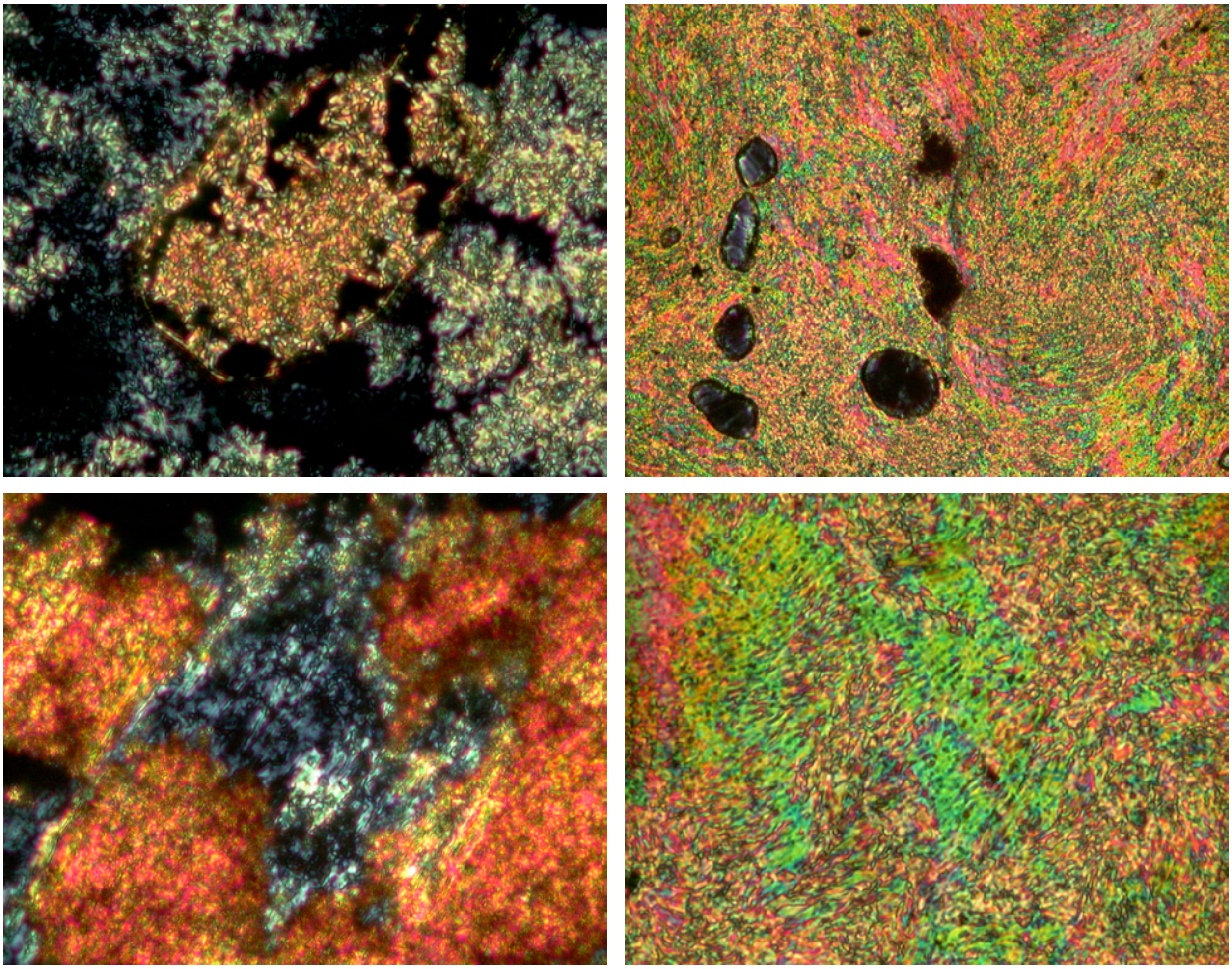

Figure 9.13. POM schlieren textures at different transition temperatures: HBC-Rf$_{4,8}$ at 193°C (upper left), HBC-Rf$_{6,6}$ at 242°C (upper right), 152°C (lower left) and 294°C (lower right).

An interesting phenomenon was observed during POM investigation of HBC-Rf$_{4,8}$; the yellowish powdered precipitate transforms rapidly to long needle-like structures when reaching the temperature of ~110°C (figure 9.14). These well-ordered columnar arrangements vanish when reaching the mesomorphic transition phase (~120 °C) and hardly reappear when cooling down the sample. It is important to note that this particular organization of product HBC-Rf$_{4,8}$ in the solid phase upon heating is the first reported so far for an HBC moiety and it proves the high tendency of this latter product to self-organize in well-defined columnar architectures.

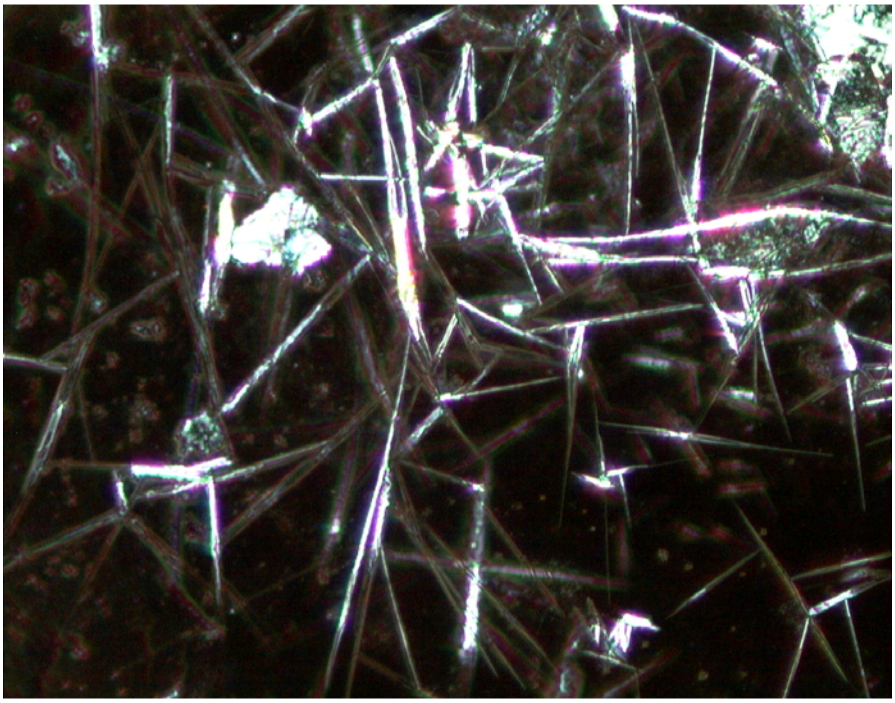

Figure 9.14. POM micrograph of the needles-like crystals of **114** formed at 110°C.

9.2.4 SEM investigation of HBC-Rf$_{4,8}$ and HBC-Rf$_{6,6}$

To better understand this structural arrangement, we have carried out the same experiment using an SEM equipped with a heating source where the precipitate of HBC-Rf$_{4,8}$ was placed on an Al support first which was then transferred to the SEM analyzing chamber to be characterized at reduced pressure and without sputtering. Figure 9.15 depicts the morphology of the latter product at room temperature showing an agglomerate structure composed of micrometer-sized needles which, upon warming up at 50°C don’t show any change.

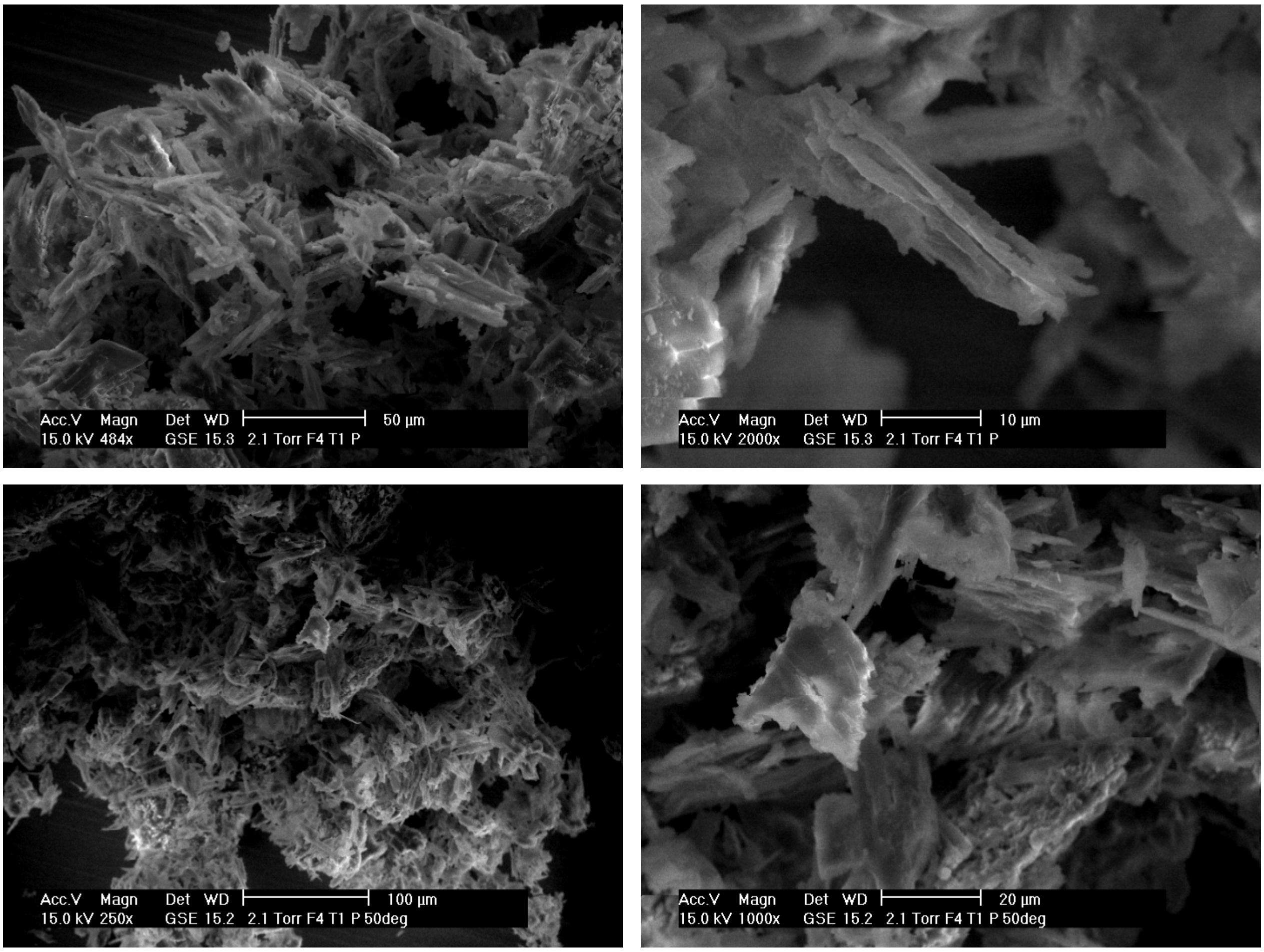
Acc.V Magn Det WD 50 µm
15.0 kV 484x GSE 15.3 2.1 Torr F4 T1 P
Acc.V Magn Det WD 10 µm
15.0 kV 2000x GSE 15.3 2.1 Torr F4 T1 P
Acc.V Magn Det WD 100 µm
15.0 kV 250x GSE 15.2 2.1 Torr F4 T1 P 50deg
Acc.V Magn Det WD 20 µm
15.0 kV 1000x GSE 15.2 2.1 Torr F4 T1 P 50deg

Figure 9.15. SEM micrographs of HBC-$Rf_{4,8}$ at room temperature showing an agglomerate composed of micrometer-sized needles (upper left), magnification of $2x10^3$ (upper right), heating at 50°C (lower left), and magnification of 10^3 at the same temperature (lower right).

Upon heating the sample at 70°C, slight changes of its morphology are observed especially at the interface with the heating source. The needles start to sinter when reaching 80°C, a temperature that is 40°C less than the liquid crystalline transition point (120°C) indicating that the change is taking place in the solid phase (figure 9.16).

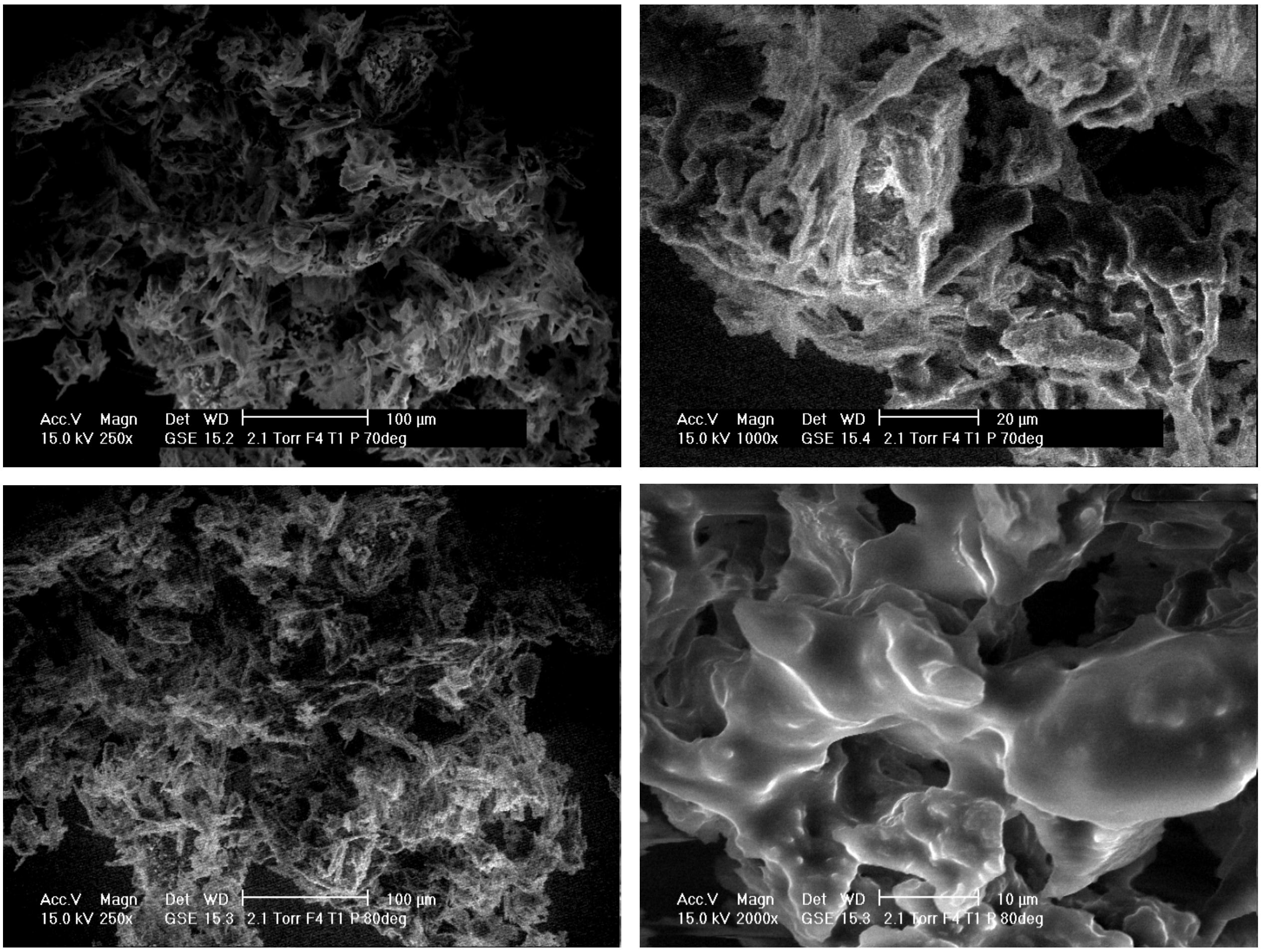
Acc.V Magn Det WD 100 µm
15.0 kV 250x GSE 15.2 2.1 Torr F4 T1 P 70deg
Acc.V Magn Det WD 20 µm
15.0 kV 1000x GSE 15.4 2.1 Torr F4 T1 P 70deg
Acc.V Magn Det WD 100 µm
15.0 kV 250x GSE 15.3 2.1 Torr F4 T1 P 80deg
Acc.V Magn Det WD 10 µm
15.0 kV 2000x GSE 15.3 2.1 Torr F4 T1 P 80deg

Figure 9.16. SEM micrographs of $\text{HBC-Rf}_{4,8}$ upon heating at 70°C (upper left), magnification of 10^3 at the same temperature (upper right), morphology change at 80°C (lower left), and the magnification of $2\text{x}10^3$ at the same temperature revealing the beginning of sintering process (lower right).

When the heating temperature reaches 90°C, the majority of the sample in contact with the susceptor smoothens whereas the largest agglomerates start to sinter at 115°C. The heating was stopped at this latter temperature to prevent the sample from reaching the liquid crystalline transition point. During the cooling stage, the morphology of the surface remains the same even at 70°C (figure 9.17).

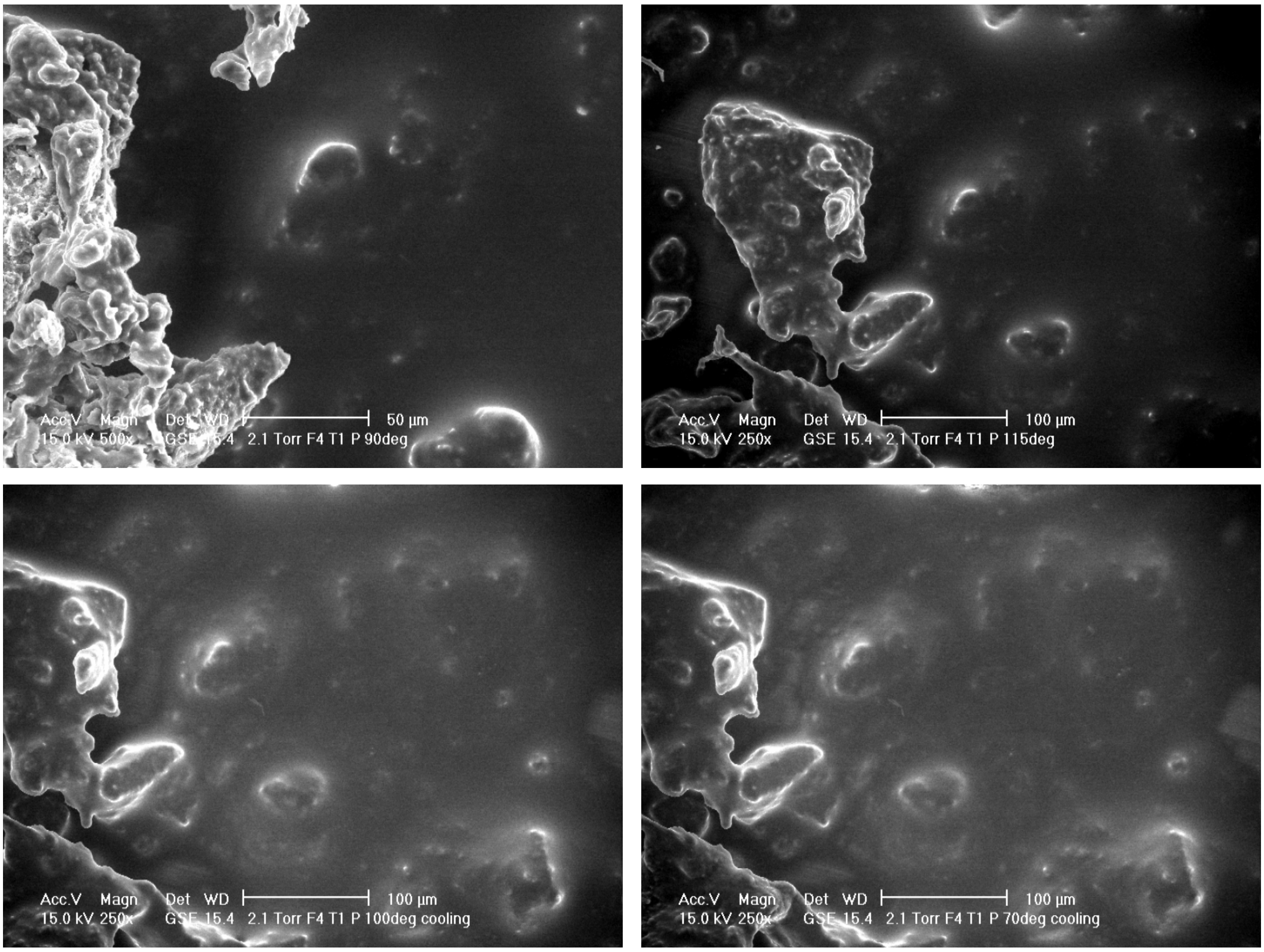
Acc.V Magn Det WD 50 µm
15.0 kV 500x GSE 15.4 2.1 Torr F4 T1 P 90deg
Acc.V Magn Det WD 100 µm
15.0 kV 250x GSE 15.4 2.1 Torr F4 T1 P 115deg
Acc.V Magn Det WD 100 µm
15.0 kV 250x GSE 15.4 2.1 Torr F4 T1 P 100deg cooling
Acc.V Magn Det WD 100 µm
15.0 kV 250x GSE 15.4 2.1 Torr F4 T1 P 70deg cooling

Figure 9.17. SEM micrographs of HBC-$Rf_{4,8}$ upon heating at 90°C (upper left), complete sintering at 115°C (upper right), the surface morphology upon cooling at 100°C (lower left), and at 70°C (lower right).

Figure 9.18 shows that when the cooling temperature attains 50°C, the surface becomes rough and small tips appear. The magnification of the surface shows a continuous film constituted by bundles of columnar structures that persist even when reaching room temperature and revealing, therefore, the high degree of HBC-$Rf_{4,8}$ to self-organize in columnar like structures even in solid state.

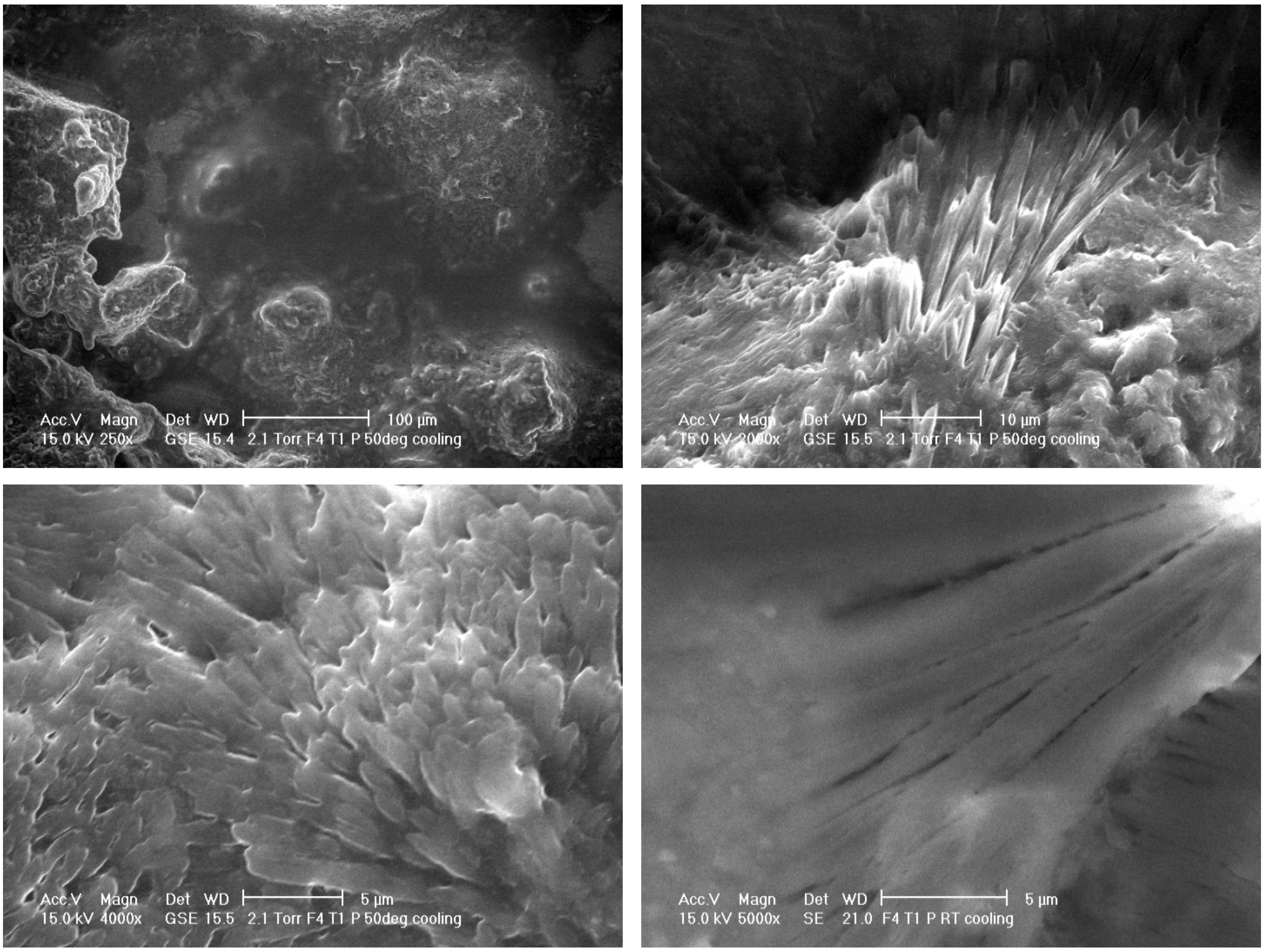
Acc.V Magn Det WD 100 µm
15.0 kV 250x GSE 15.4 2.1 Torr F4 T1 P 50deg cooling
Acc.V Magn Det WD 10 µm
15.0 kV 2000x GSE 15.5 2.1 Torr F4 T1 P 50deg cooling
Acc.V Magn Det WD 5 µm
15.0 kV 4000x GSE 15.5 2.1 Torr F4 T1 P 50deg cooling
Acc.V Magn Det WD 5 µm
15.0 kV 5000x SE 21.0 F4 T1 P RT cooling

Figure 9.18. SEM micrographs of HBC-$Rf_{4,8}$ on Al upon cooling. At 50°C showing rough surface (upper left), magnification of $2x10^3$ revealing a bundle-like morphology (upper right), magnification of $4x10^3$ showing the columns formed (lower left), and at room temperature (lower right).

The same structural arrangement is observed when cooling a 3 x 10^{-4} M solution of HBC-$Rf_{4,8}$ in 1,2,4-TCB after heating it for one hour at 90-120°C. This has led us to investigate these needles by SEM: a 3 x 10^{-4} M solution of HBC-$Rf_{4,8}$ in 1,2,4-TCB was heated at 120°C for ~2 hours and the solution was cooled whereupon cloudy yellowish fiber-like structures started to form at 80°C. A droplet of this suspension was then put on an Al substrate and the wafer was placed in a vacuum chamber to evaporate the 1,2,4-TCB under ~10^{-4} Torr first, followed by the sputtering of the remaining product with gold in order to cover it with a ~5-10 nm thick conducting film. As it can be noticed from the SEM micrographs in figure 9.19, very long columnar structures were detected over a large area of the substrate. The size of these rectangular-like micrometer columns were found to be homogeneous where all the stacks have a length of ~150 µm and a width varying between 2.2-2.7 µm, the thickness was also found to be in the range of 1.6-1.9

µm. The magnification (8 x 10^4) of these rectangular-columnar structures reveals that each ‘column’ is constituted of many nanometer-sized sheets whose lateral assembly forms this particular structure. Another important characteristic of these columns is that they don’t coagulate. It is important to mention, however, that we weren’t able to detect smaller HBC stacks. This brings us to suppose that by the time the solvent was evaporating, the dissolved stacks in 1,2,4-TCB self-assembled into larger columnar structures or they have simply added to the existing ones.

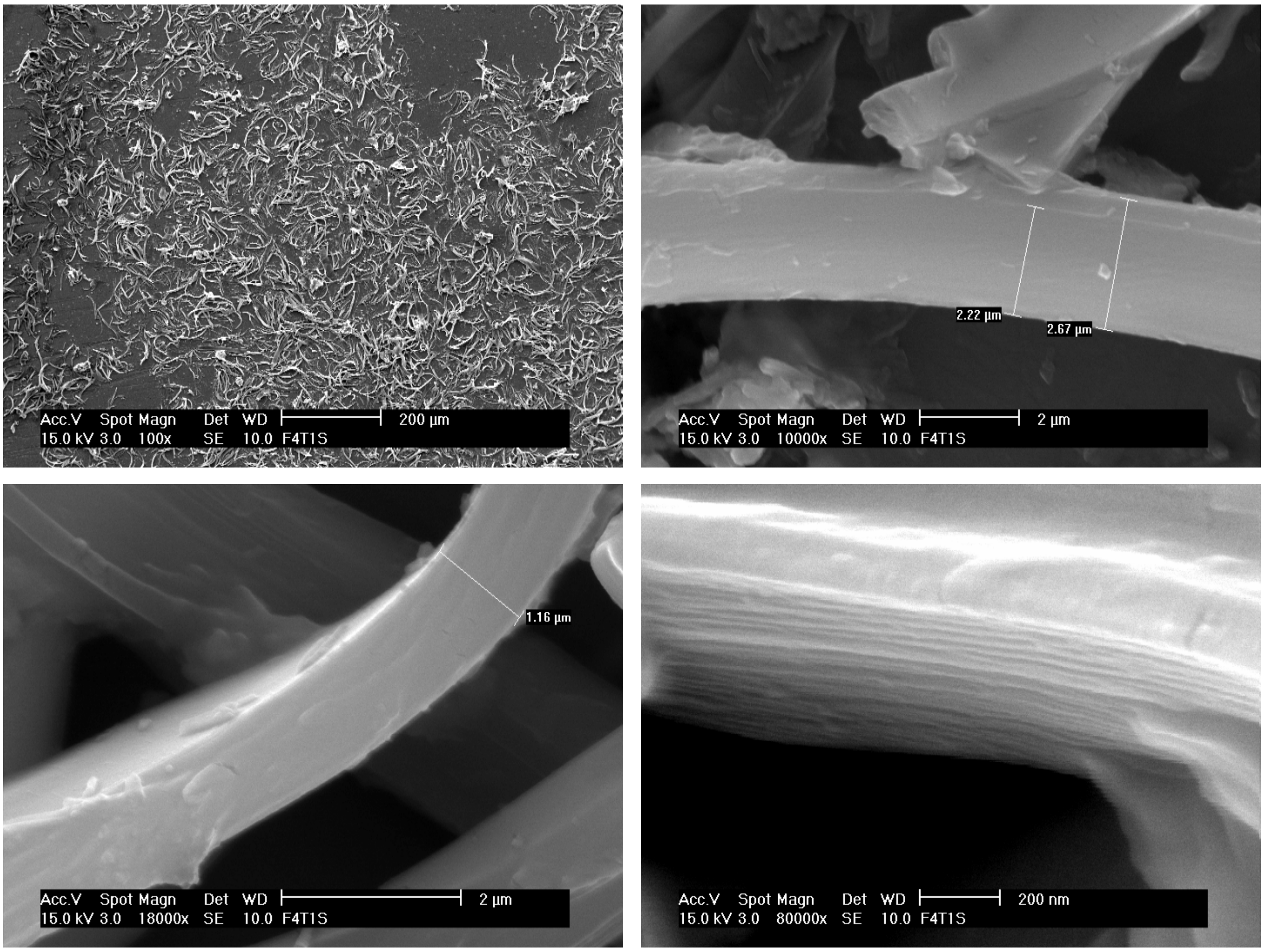
Acc.V Spot Magn Det WD 200 µm
15.0 kV 3.0 100x SE 10.0 F4T1S
2.22 µm
2.67 µm
Acc.V Spot Magn Det WD 2 µm
15.0 kV 3.0 10000x SE 10.0 F4T1S
1.16 µm
Acc.V Spot Magn Det WD 2 µm
15.0 kV 3.0 18000x SE 10.0 F4T1S
Acc.V Spot Magn Det WD 200 nm
15.0 kV 3.0 80000x SE 10.0 F4T1S

Figure 9.19. SEM micrographs of an evaporated ~3×10^{-4} M solution of HBC-$Rf_{4,8}$ on Al showing the columnar structures at the centre of the substrate (upper left), the column width (upper right), the column thickness (lower left), and the magnification of 8 x 10^4 of a single column (lower right).

In order to detect the presence of these solvated HBCs, we have performed a new SEM technique: Cryo-SEM. This technique is based on the freezing of the solution very rapidly to liquid N_2 temperatures (-196°C) under a 10^{-4} Torr vacuum. We expect under these conditions the solvated HBC nanometer-sized stacks to be prevented to self-assemble in micrometer sized columns or even to add on the long fiber-like structures. Additionally, this procedure permits, for instance, in the case of presence of water, to form the amorphous ice since it prevents a volume increase during solidification. In order to be able to notice any changing, we have taken a sample from the same suspension we have investigated previously. Therefore, a droplet of the 3 x 10^{-4} M suspension of HBC-$Rf_{4,8}$ in 1,2,4-TCB was frozen at -195°C under 10^{-4} Torr then it was transferred under vacuum to the cryo-transfer system where the solidified solvents were sublimed at about -95°C under a ~10^{-6} Torr vacuum. At the end of sublimation, the remaining product was sputtered with platinum in order to form a ~10 nm conducting film and then cooled to -130°C. Figures 9.20 and 9.21 show the preliminary results we have obtained by using this method: We can easily distinguish two types of columnar structures, the first ones resemble in their morphology to the ones we have observed with POM (figure 9.14) upon evaporating the 1,2,4-TCB (figure 9.19) while the second are nanometer-sized long filaments. Contrarily to what we have seen upon evaporating the solvent at room temperature, the columnar stacks in the cryo preparation are deposited in a near vertical position all along the crucible. In addition, these columnar structures are homogeneous in their distribution all over the surface of the substrate and they have uniform dimensions forming long tubular-like configurations. On the other hand, the nanometer-sized filaments were also detected all over the substrate and even on the surface of the micrometer tubes. The dimensions of these 'nano-columns' are very homogeneous both in their length (~750 nm) and their diameter (~30 nm), but the real size of these structures can't be estimated at present because the sample was sputtered with a film of Pt (theoretically 10 nm). However, we can suppose that the nano-sized filaments are nothing but the solvated HBC fibers in 1,2,4-TCB which, upon freezing and evaporating this latter, weren't able to aggregate in micrometer-sized columnar bundles.

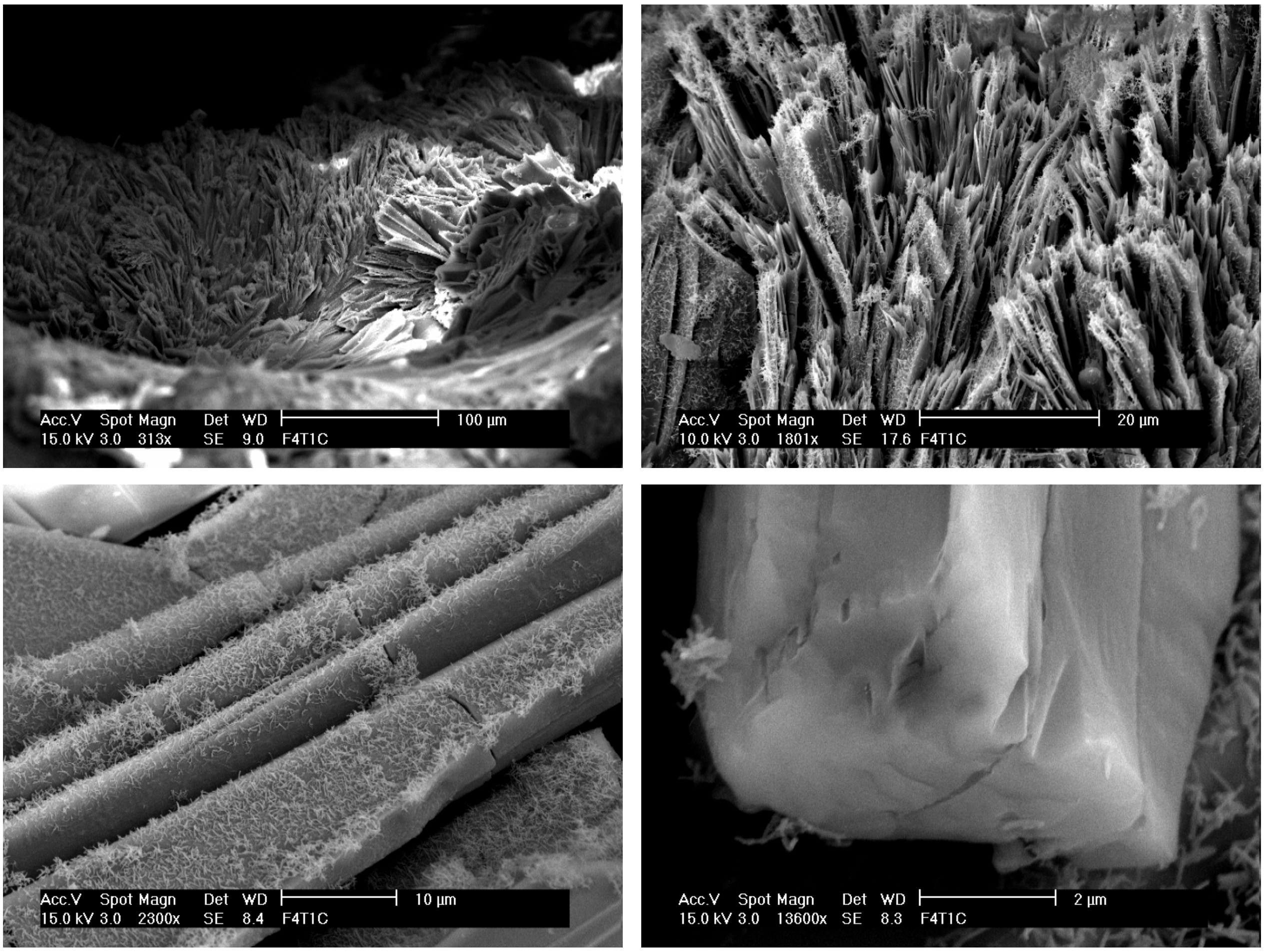
Acc.V Spot Magn Det WD 100 µm
15.0 kV 3.0 313x SE 9.0 F4T1C
Acc.V Spot Magn Det WD 20 µm
10.0 kV 3.0 1801x SE 17.6 F4T1C
Acc.V Spot Magn Det WD 10 µm
15.0 kV 3.0 2300x SE 8.4 F4T1C
Acc.V Spot Magn Det WD 2 µm
15.0 kV 3.0 13600x SE 8.3 F4T1C

Figure 9.20. Cryo-SEM micrographs of HBC-Rf$_{4,8}$ at -130°C deposited on an Al substrate showing the general morphology of the columnar structures in the crucible (upper left), the vertical order of the columns (upper right), the tubular-like structures (down).

Another type of micrometer-sized fibers was also detected, in some areas of the sample, having a length in the range of ~1,5-2 µm, a diameter of ~100-150 nm, and a well-defined texture (figure 9.20, lower left). Additionally, these fibers are very sensitive under the electron beam, contrarily to the nanometer-sized filaments of HBC-Rf$_{4,8}$ that resist when focusing the electron beam on one of them in order to detect it in a higher resolution. These observations show clearly that the nature of the micrometer-sized fibers is different from the nanometer-sized filaments, revealing, therefore, that the former might be the remaining traces of the solvent. This assumption was supported after measuring 1,2,4-TCB under the same conditions showing an identical morphology and behaving similarly under the electron beam (figure 9.21, lower right).

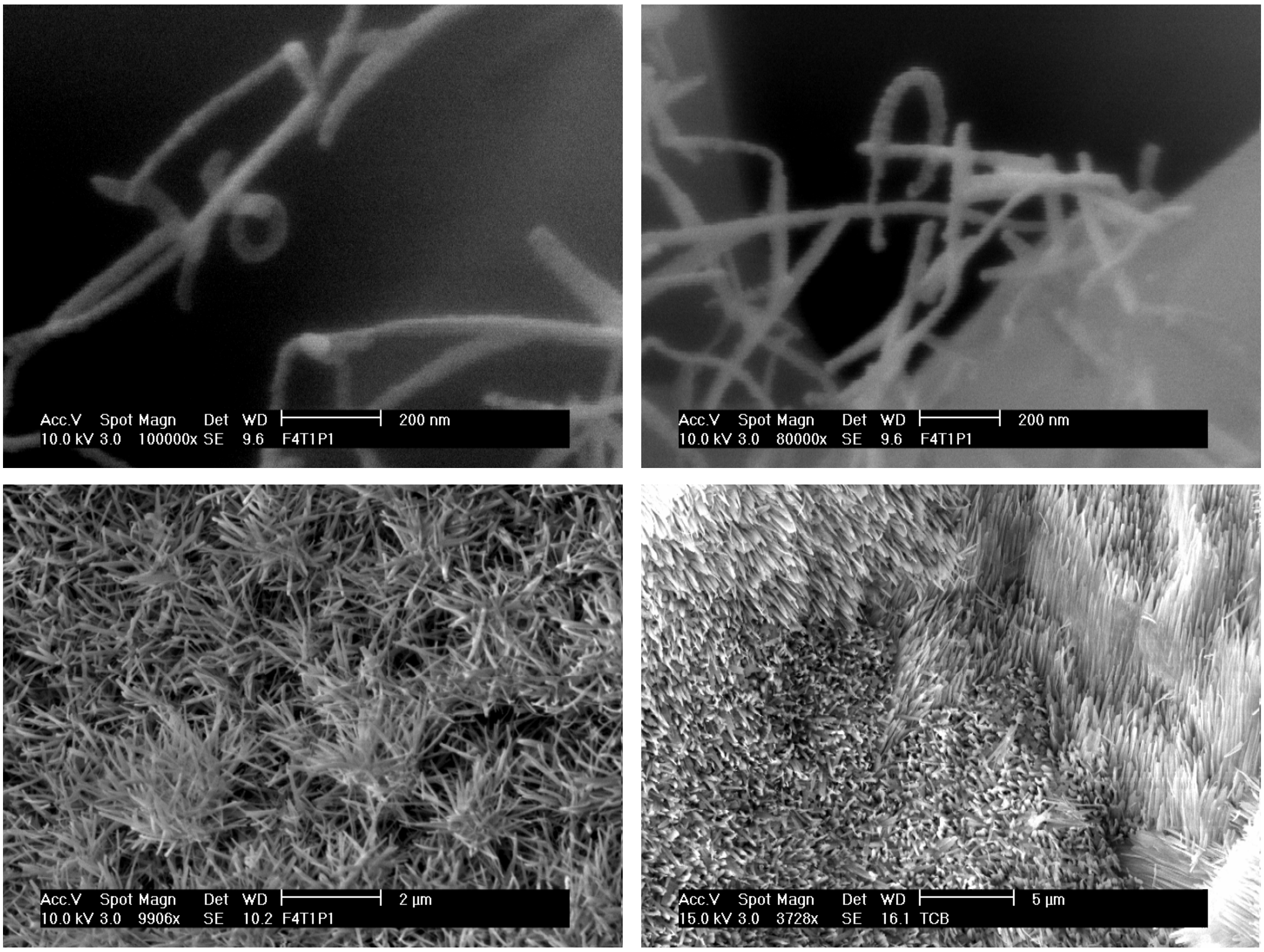
Acc.V Spot Magn Det WD 200 nm
10.0 kV 3.0 100000x SE 9.6 F4T1P1
Acc.V Spot Magn Det WD 200 nm
10.0 kV 3.0 80000x SE 9.6 F4T1P1
Acc.V Spot Magn Det WD 2 µm
10.0 kV 3.0 9906x SE 10.2 F4T1P1
Acc.V Spot Magn Det WD 5 µm
15.0 kV 3.0 3728x SE 16.1 TCB

Figure 9.21. Cryo-SEM micrographs at -130°C showing the filament structures of HBC-$Rf_{4,8}$ (up), and the columnar-like structures of 1,2,4-TCB present with the medium (lower left) and when measuring it alone.

The previous experiments prompted us to attempt a preliminarily deposition of HBC-$Rf_{4,8}$ on a smooth well-oriented substrate by solvent evaporation. For this reason, a 3 x 10^{-4} M solution of HBC-$Rf_{4,8}$ in 1,2,4-TCB was heated overnight then cooled at room temperature and allowed to settle for two days. The resulting solution was then filtrated to remove the fiber-like structures. A droplet from the faint yellow solution was placed on a Si(100) substrate and the resulting wet wafer was then put in a vacuum chamber to evaporate the solvent, followed by sputtering the surface with a ~5 nm film of gold to make the sample conducting. SEM investigation has showed the formation of a thin homogenous film that covers a large surface of the silicon wafer. Nevertheless, the film contains uniformly dispersed notches all along the deposition area (figure 9.22). The diameters of these button-like structures were found to be ~150-200 nm.

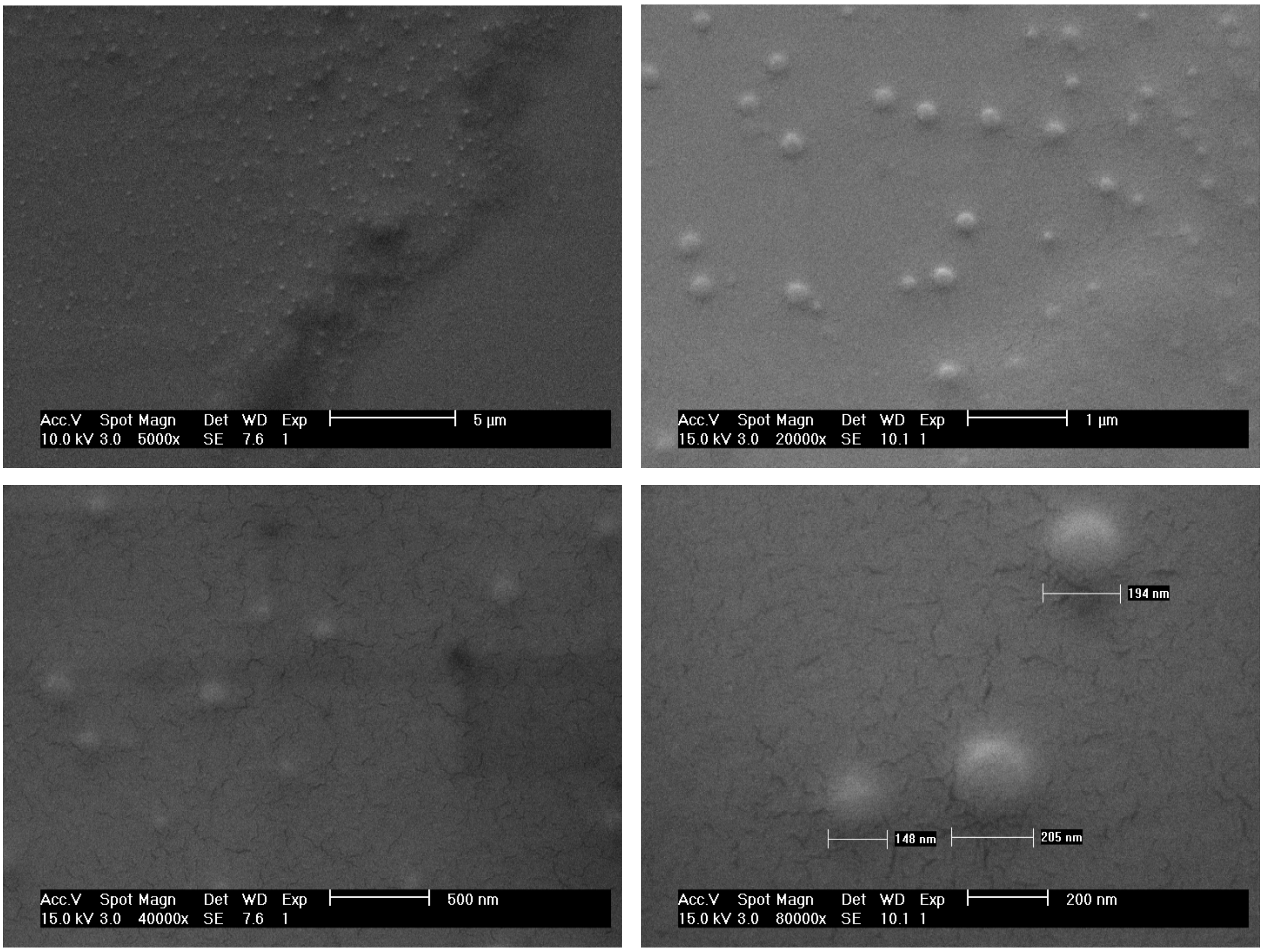
Acc.V Spot Magn Det WD Exp 5 µm
10.0 kV 3.0 5000x SE 7.6 1
Acc.V Spot Magn Det WD Exp 1 µm
15.0 kV 3.0 20000x SE 10.1 1
Acc.V Spot Magn Det WD Exp 500 nm
15.0 kV 3.0 40000x SE 7.6 1
194 nm
148 nm
205 nm
Acc.V Spot Magn Det WD Exp 200 nm
15.0 kV 3.0 80000x SE 10.1 1

Figure 9.22. SEM micrographs of an evaporated clear solution of HBC-Rf$_{4,8}$ on Si(100) showing the film morphology at the centre of the substrate (upper left), the morphology of the tips x 20000 (upper right), and x 40000 (lower left), and their diameters (lower right).

The same experiment was performed using a ~1.7x10^{-7} M solution of HBC-Rf$_{6,6}$ in 1,2,4-TCB. Surprisingly, the deposited product was present as a film with poor adherence on the substrate as the many cracks in the film reveal (figure 9.23). Nonetheless, upon moving away from the center of the deposited film to the edges, we can notice the existence of highly ordered columnar dendrites from the inner-side of the evaporated droplet. On the other hand, many nano-sized needles-like arrays, having a length of ~1 µm, are present in the outer-side of the dendrites. The detection of these latter is very hard since they move upon trying to focus the electron beam on them in order to measure them in a higher resolution.

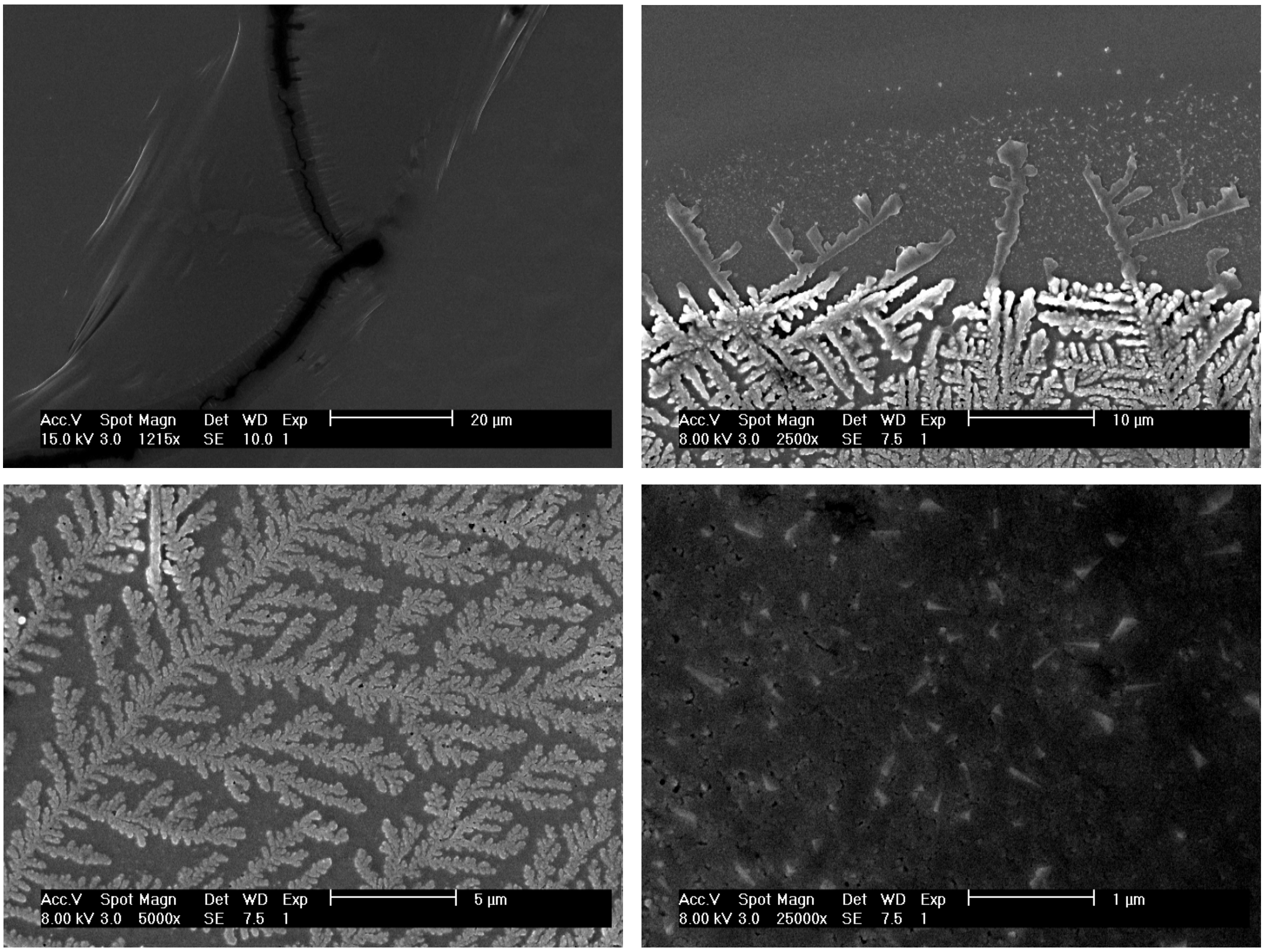
Acc.V Spot Magn Det WD Exp 20 µm
15.0 kV 3.0 1215x SE 10.0 1
Acc.V Spot Magn Det WD Exp 10 µm
8.00 kV 3.0 2500x SE 7.5 1
Acc.V Spot Magn Det WD Exp 5 µm
8.00 kV 3.0 5000x SE 7.5 1
Acc.V Spot Magn Det WD Exp 1 µm
8.00 kV 3.0 25000x SE 7.5 1

Figure 9.23. SEM micrographs of an evaporated ~1.7x10^{-7} M solution of HBC-$Rf_{6,6}$ on Si(100) showing the film formation at the centre of the substrate (upper left), the presence of dendrites at the edges (upper right), the highly ordered columnar dendrites (lower left), and the morphology of the nano-sized needles (lower right).

The results herein allow us to draw out two important conclusions: the first is the high dendritic order in which product HBC-$Rf_{6,6}$ deposits on well-oriented silicon substrates without forming a continuous uniform thin film that covers a large area of the substrate and adheres on it efficiently as the sulfur-containing HBC-SCF_3 does, and the second important deduction is the fact that very different behavior between HBC-$Rf_{4,8}$ and HBC-$Rf_{6,6}$ are seen upon their deposition on the same substrate under the same conditions. It is worth mentioning that these products only differ by the ratio of the perfluorinated/aliphatic lateral sections of the chains they bear.

10. HBCs with perfluoroalkyl alkoxy side chains

10.1 Synthetical attempt of HBC with R = $ORf_{4,8}$

We have tried to synthesize this HBC derivative although it has been published that the attempts to produce an HBC bearing alkoxy chains fail leading to the formation of quinonoids rather than HBCs[288] as we have mentioned in section 7.4. The reason of this trial can be seen as a logical extension to the HBC-OCF_3 (**65**) i.e. to see whether the electron-withdrawing effect of the peripheral perfluorooctyl chain will influence the alkyl spacer and, hence would prevent the quinone formation affording the desired HBC derivative instead. The synthetical approach consisted of synthesizing the brominated phenoxy perfluoro building block first, followed by a step-by-step Sonogashira coupling reaction to get the tolane species **119** (To-$ORf_{4,8}$) as shown in figure 10.1.

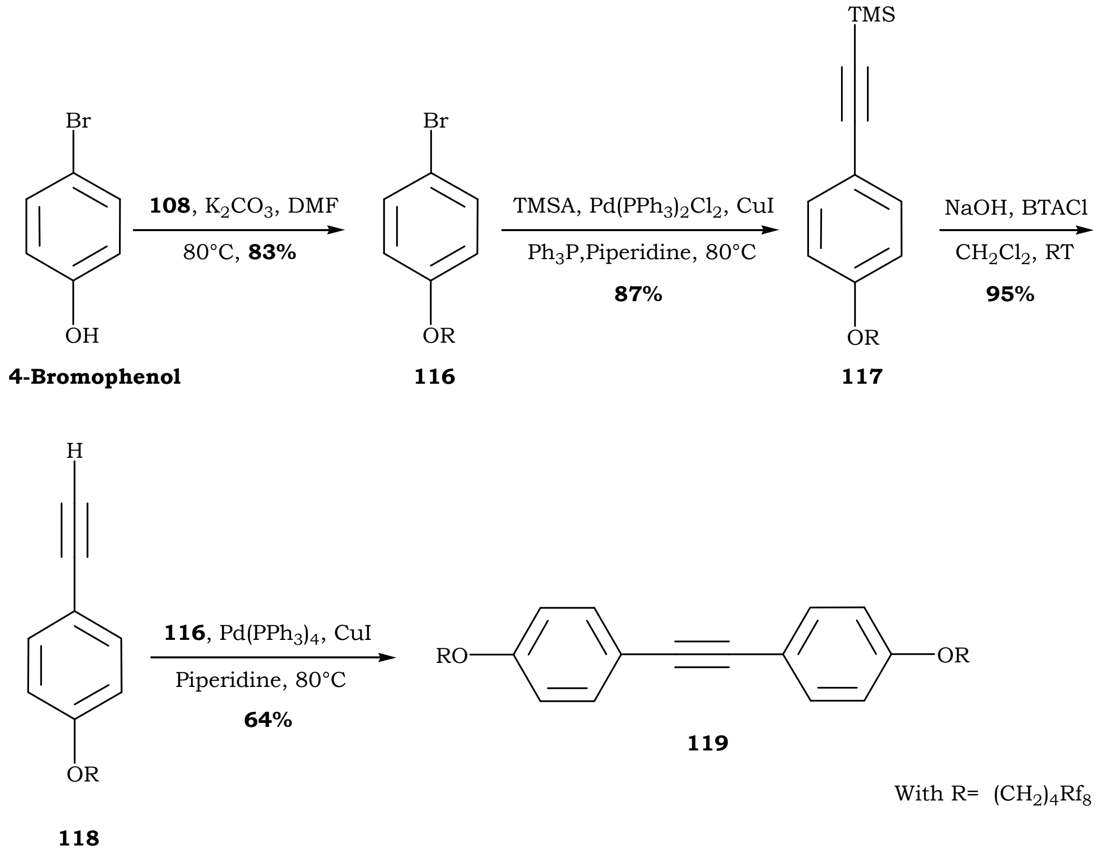
Br
OH
4-Bromophenol
108, K_2CO_3, DMF
80°C, **83%**
Br
OR
116
TMSA, $Pd(PPh_3)_2Cl_2$, CuI
Ph_3P,Piperidine, 80°C
87%
TMS
OR
117
NaOH, BTACl
CH_2Cl_2, RT
95%
H
OR
118
116, $Pd(PPh_3)_4$, CuI
Piperidine, 80°C
64%
RO
OR
119
With R= $(CH_2)_4Rf_8$

Figure 10.1. Synthesis of tolane bearing perfluoroalkyl-alkoxy chains.

Table 21 below shows the conditions used for the different reactions leading to To-ORf$_{4,8}$. Slight improvements of the work-up have allowed obtaining **116** in a good yield (83%). The first Sonogashira reaction affords the trimethylsilyl acetylene species **117** in 87% yield, whereas the second Sonogashira coupling reaction affords the tolane derivative in a moderate yield (64%).

Table 21. Syntheses of tolane derivatives **119**^{a}.

Entry	**Substrate (eq.)**	**Reagent (eq.)**	**Catalyst (Mol%)**	**Co-cat. (Mol%)**	**Base**	**T (°C)**	**t (h)**	**Pdt (%Yld)**
1	4-Bromo-phenol (1)	108 (1.3)	-	-	K_2CO_3 (3)^{b}	80	24	**116** (83)
2	116 (1)	TMSA (1.2)	$Pd(PPh_3)_2Cl_2$ (3)^{c}	CuI (6)	Piperidine^{d}	80	25	**117** (87)
3	118 (1)	116 (1)	$Pd(PPh_3)_4$ (6)	CuI (15)	Piperidine^{d}	80	48	**119** (64)

a: reactions were done under argon atmosphere. b: DMF as solvent. c: 6 mol% of PPh_3 were added. d: base used as solvent too.

Trimerization of To-ORf$_{4,8}$ has been done affording the hexaphenyl benzene derivative **120** (HPB-ORf$_{4,8}$) which has undergone cyclodehydrogenation reaction with $FeCl_3/CH_3NO_2$ reagents combination affording the quinonoid **121** as figure 10.2 depicts.

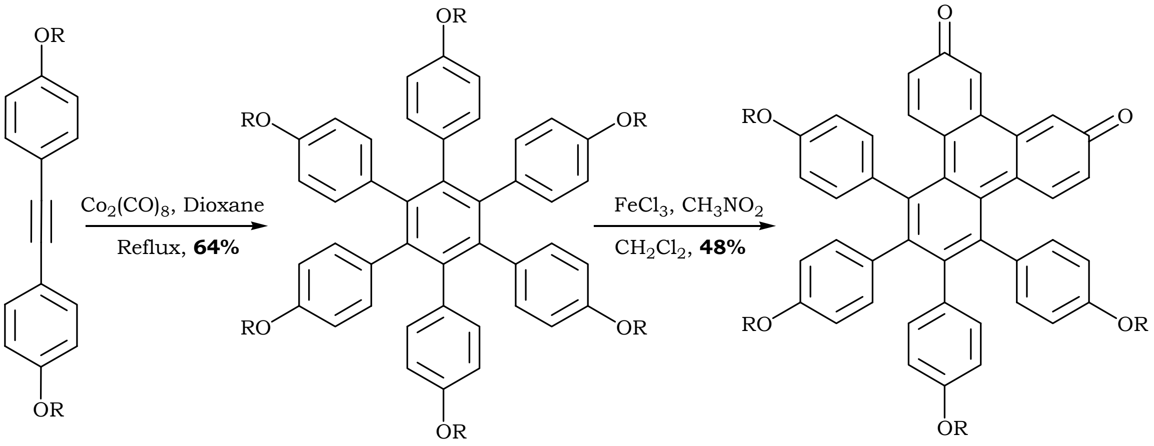

With R = $(CH_2)_4Rf_8$

119 **120** **121**

Figure 10.2. Oxidation of HPB-ORf$_{4,8}$ to quinonoid derivative.

Table 22. Trimerization and cyclodehydrogenation of **119** and **120**, respectively[a].

Entry	**Substrate**	**Reagent (nb. eq/ H)**	**Additive**	**Solvent**	**Temp. (°C)**	**Time (h)**	**Product (%Yld)**
1	119	$Co_2(CO)_8$[b]	-	Dioxane	reflux	48	**120** (64)
2	120	$FeCl_3$(3)	CH_3NO_2	CH_2Cl_2	RT	24[c]	**121** (48)

a: all the reactions were done under argon.. b: 5 mol% of cobalt. c: argon was bubbled for 19 hours.

Scheme XII illustrates a possible mechanism that we propose for the quinonoid formation. The mesomeric structures of the radical cation intermediate **120.2** lead to the cleavage of the alkylated perfluoroalkyl chain forming, therefore, the first quinone group. Additional oxidation followed by the removal of a cationic proton affords intermediate **120.4** which, after being subjected to the same preceding steps, yields the quinonoid **121**.

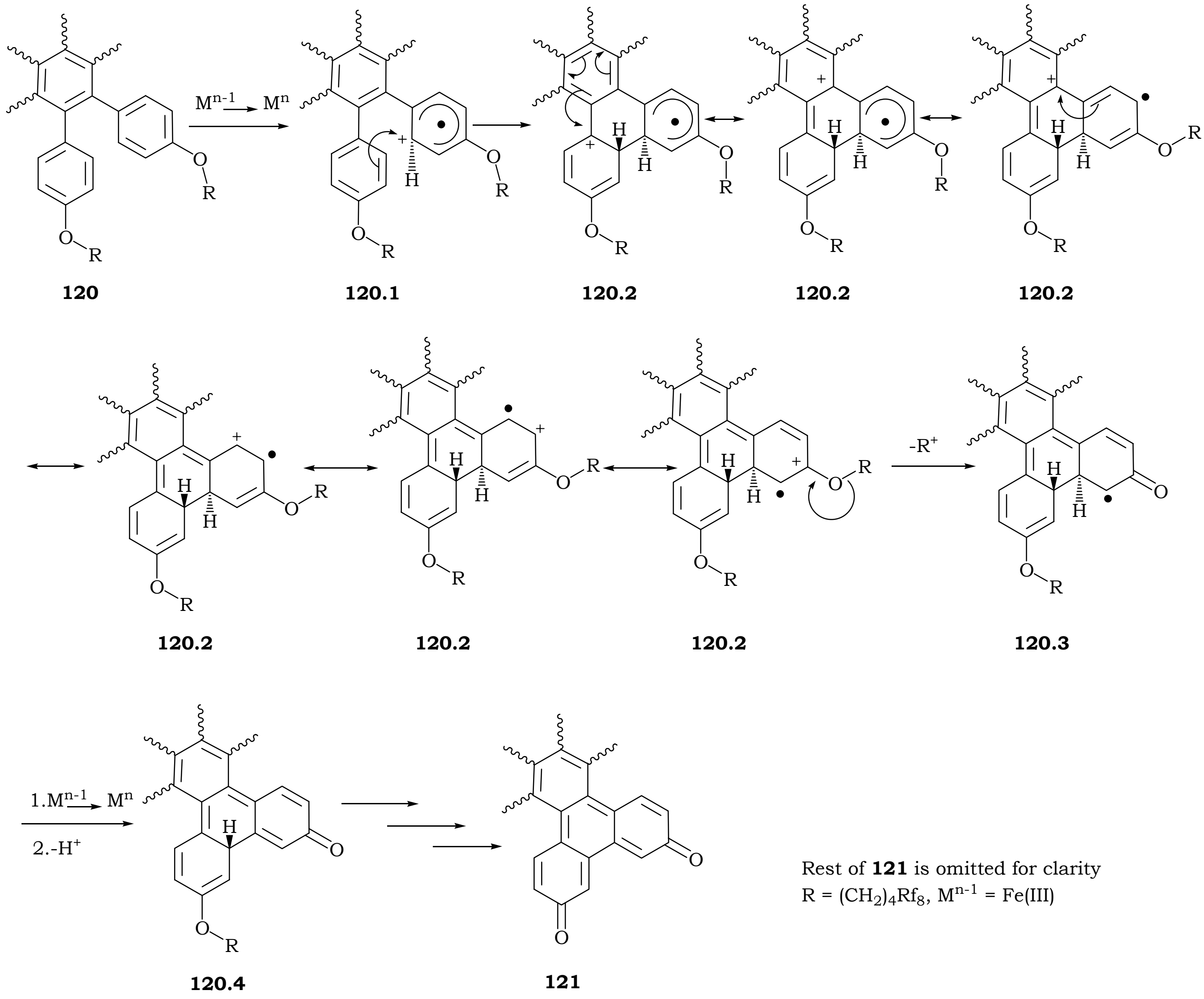
$M^{n-1} \rightarrow M^n$
120
120.1
120.2
120.2
120.2
120.2
120.2
120.2
$-R^+$
120.3
1.$M^{n-1} \rightarrow M^n$
2.$-H^+$
120.4
121

Rest of **121** is omitted for clarity
R = $(CH_2)_4Rf_8$, M^{n-1} = Fe(III)

Scheme XII. Quinonoid formation during cyclodehydrogenation step.

10.2 HBCs with phenoxy alkylated perfluoroalkyl substituents

10.2.1 Introduction

To circumvent the difficulty we have encountered during the attempted synthesis of HBC bearing alkylated perfluoroalkyl ethereal chains, we have envisaged intercalating these latter from the HBC core with a phenyl group to avoid the quinonoid formation. Tolane building blocks have been synthesized by two main synthetical routes: the first using Suzuki and Kumada cross-coupling reactions of the corresponding alkylated perfluoroalkyl phenyl derivatives with 4,4'-dibromotolane **36** building block whereas the second synthetical pathway uses Sonogashira reaction approach.

10.2.2 Tolane synthesis via Kumada and Suzuki cross-coupling.

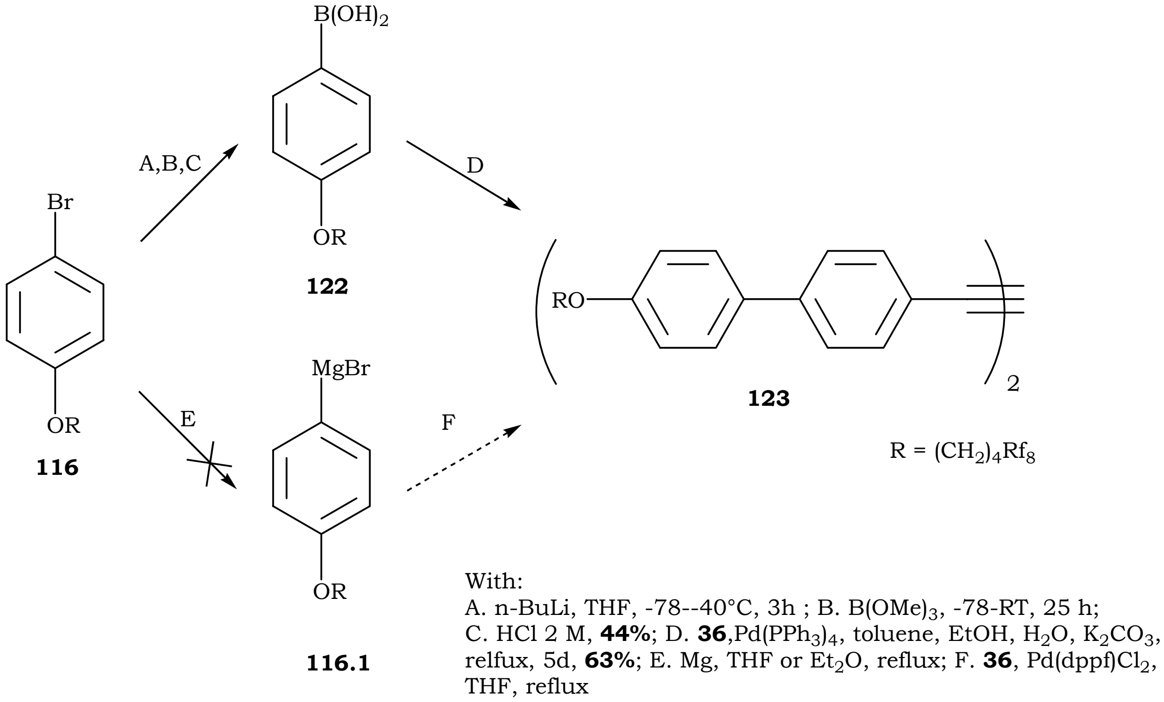

With:
A. n-BuLi, THF, -78--40°C, 3h ; B. $B(OMe)_3$, -78-RT, 25 h;
C. HCl 2 M, **44%**; D. **36**,$Pd(PPh_3)_4$, toluene, EtOH, H_2O, K_2CO_3, relfux, 5d, **63%**; E. Mg, THF or Et_2O, reflux; F. **36**, $Pd(dppf)Cl_2$, THF, reflux

Figure 10.3. 123 synthetical attempts using Kumada and Suzuki conditions.

As it can be noticed from figure 10.3, only Suzuki reaction conditions were successful whereas Kumada ones weren't. Entry 1 in table 23 shows that the boronic acid **122** was reacted with 4,4'-dibromotolane **36** under the Suzuki cross-coupling conditions to yield the desired tolane building block **123** (To-$PhORf_{4,8}$) in 63%. On the other hand, as it can be noticed from entry 2, we believe that the failure to obtain To-$PhORf_{4,8}$ via the Kumada reaction is due to the high difficulty to form the perfluoroalkoxy phenyl Grignard reagent **116.1**, necessary to continue the reaction further on. To prove that, many reactions were carried out under different conditions to see if the Grignard reagent forms but neither the replacement of heating with sonication (entry 4) nor the changing of the solvent from THF to diethyl ether (entries 5 and 6) were successful: after quenching all the reaction mixtures with H_2O, only the starting material **116** was found. We presume that this difficulty is due to the electron donating effect of the alkoxy group that deactivates the phenyl ring preventing, therefore, the formation of **116.1**.

Table 23. Suzuki and Kumada cross-coupling reactions with **36**.

Entry	product	Boronic acid/Grignard reactions					C-C Coupling reaction				Pdt
		Pdt (eq)	*Reagent (eq)*	*Sol.*	*T (°C)*	*t (d)*	*Catalyst (mol%)*	*Sol.*	*T (°C)*	*t (d)*	*(%Yld)*
1	36[a]	122 (2.4)	K_2CO_3 (16)	-	-	-	$Pd(PPh_3)_4$ (10)	toluene/ H_2O/EtOH[b]	80	5	**123** (63)
2	36[a]	116 (8)	Mg (8)	THF	75	5	$Pd(dppf)Cl_2$ (20)	THF	75	5	-
3	-	116 (1)	Mg (1.2)	THF	75	2	-	-	-	-	-
4	-	116 (1)	Mg (1.2)	THF	)))	1	-	-	-	-	-
5	-	116 (1)	Mg (1.2)	Et_2O	45	1	-	-	-	-	-
6	-	116 (1)	Mg (1.2)	Et_2O	)))	1	-	-	-	-	-

a: number of equivalents is calculated with respect to 36. b: solvent ratio 3:2:1.

10.2.3 Tolane synthesis via Sonogashira cross-coupling.

As figure 10.4 on the next page illustrates, the major starting materials **124** and **125** have been synthesized, in good yields, by reacting the commercially available 4-(4-bromophenyl)-phenol with the alkylated perfluoroalkyl chains $BrRf_{4,8}$ and $BrRf_{6,6}$. Two different pathways using Sonogashira cross-coupling reaction conditions have been attempted to synthesize the tolane species bearing dodecyl ethereal chains with four and six alkyl spacers To-$PhORf_{4,8}$ and To-$PhORf_{6,6}$ (**130**), respectively.

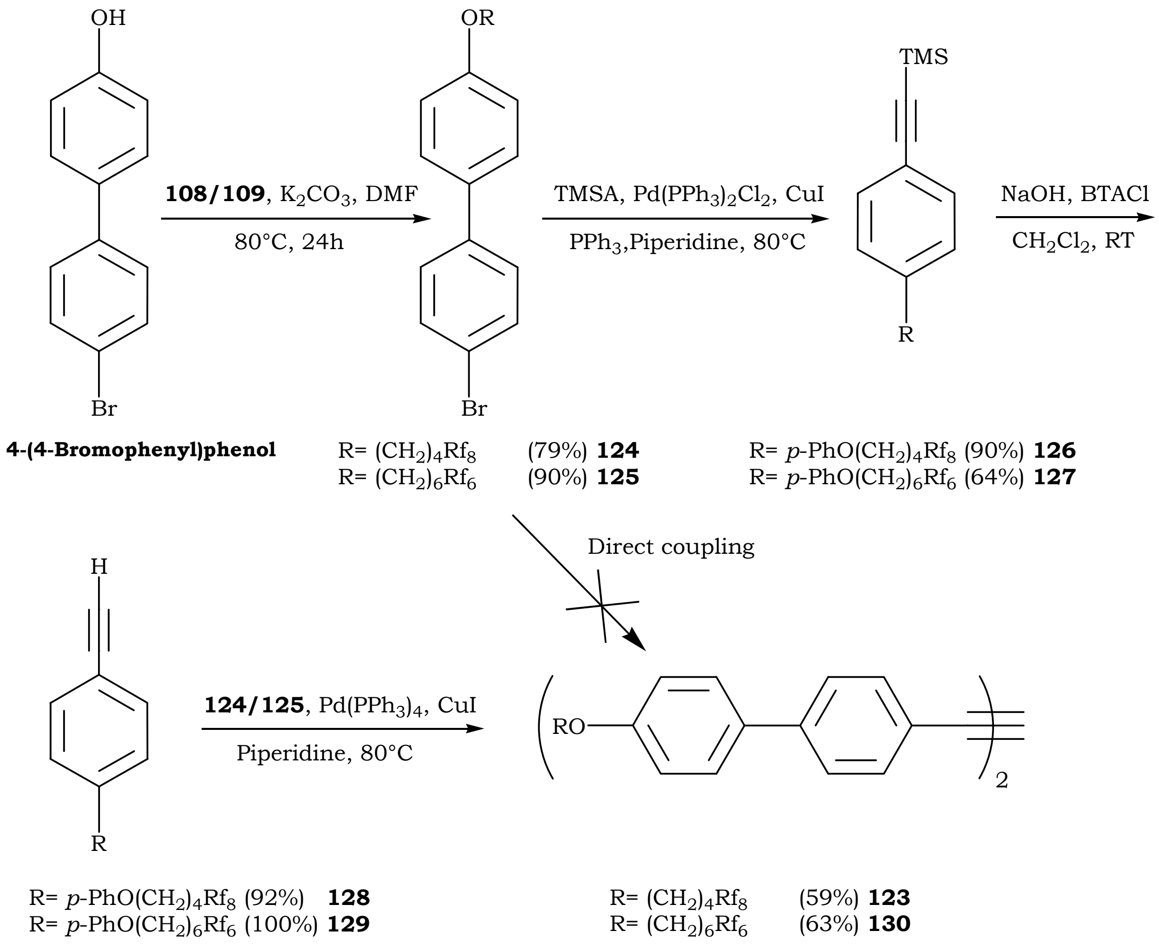
OH
OR
TMS
108/109, K$_2$CO$_3$, DMF
80°C, 24h
TMSA, Pd(PPh$_3$)$_2$Cl$_2$, CuI
PPh$_3$,Piperidine, 80°C
NaOH, BTACl
CH$_2$Cl$_2$, RT
R
Br
Br
4-(4-Bromophenyl)phenol
R= (CH$_2$)$_4$Rf$_8$ (79%) 124
R= (CH$_2$)$_6$Rf$_6$ (90%) 125
R= *p*-PhO(CH$_2$)$_4$Rf$_8$ (90%) 126
R= *p*-PhO(CH$_2$)$_6$Rf$_6$ (64%) 127
Direct coupling
H
124/125, Pd(PPh$_3$)$_4$, CuI
Piperidine, 80°C
RO
2
R
R= *p*-PhO(CH$_2$)$_4$Rf$_8$ (92%) 128
R= *p*-PhO(CH$_2$)$_6$Rf$_6$ (100%) 129
R= (CH$_2$)$_4$Rf$_8$ (59%) 123
R= (CH$_2$)$_6$Rf$_6$ (63%) 130

Figure 10.4. Syntheses of tolane derivatives **123** & **130** via Sonogashira coupling.

Table 24 reveals the reaction conditions for the different experiments we have done to obtain To-PhORf$_{4,8}$ and To-PhORf$_{4,8}$. The one-pot Sonogashira reaction by bubbling acetylene in a piperidine solution containing **124** and in presence of catalytical amounts of palladium and copper at 80°C (entry 3) has yielded decomposition products. Increasing the amount of the catalytical species (entry 4) hasn't brought any significant change. Entries 5 and 6 show that upon reacting the brominated perfluoroalkoxy derivative **124** and **125** with TMSA under the conditions mentioned below, the trimethylsilylated acetylene derivatives **126** and **127** are produced in 90% and 64% yields, respectively. Hydrolysis of these latter products has yielded the acetylene derivatives **128** and **129**, respectively, in virtually quantitative yields. Reaction of these latter products with their corresponding brominated derivatives **124** and **125**, afford the desired tolane species To-PhORf$_{4,8}$ and To-PhORf$_{6,6}$ in moderate yield (entries 7 & 8). Even though the step-by-step Sonogashira pathway requires one more step than the Suzuki one, the higher overall yield obtained of To-PhORf$_{4,8}$ is still higher (40% vs. 28%).

Table 24. Syntheses of tolane species **123** and **130**[a].

Entry	**Substrate (eq.)**	**Reagent (eq.)**	**Catalyst (Mol%)**	**Co-cat. (Mol%)**	**Base**	**T (°C)**	**t (h)**	**Pdt (%Yld)**
1	4-(4-BrPh)-phenol (1)	108 (1.1)	-	-	K_2CO_3 (3)[b]	80	24	**124** (79)
2	4-(4-BrPh)-phenol (1)	109 (1.1)	-	-	K_2CO_3 (3)[b]	80	24	**125** (90)
3	124	acetylene[c]	$Pd(PPh_3)_2Cl_2$ (4)[d]	CuI (6)	Piperidine[e]	80	48	-
4	124	acetylene[c]	$Pd(PPh_3)_2Cl_2$ (6)[f]	CuI (9)	Piperidine[g]	80	53	-
5	124	TMSA (1.3)	$Pd(PPh_3)_2Cl_2$ (3)[d]	CuI (6)	Piperidine[e]	80	24	**126** (90)
6	125	TMSA (1.3)	$Pd(PPh_3)_2Cl_2$ (3)[d]	CuI (6)	Piperidine[e]	80	16	**127** (64)
7	128 (1)	124 (1)	$Pd(PPh_3)_4$ (6)	CuI (15)	Piperidine[e]	80	48	**123** (59)
8	129 (1)	125 (1)	$Pd(PPh_3)_4$ (6)	CuI (15)	Piperidine[e]	80	48	**130** (63)

a: reactions were done under argon atmosphere. b: DMF as solvent. c: acetylene was bubbled in the reaction medium for 5 hours. d: 6 mol% of PPh_3 were added. e: as solvent. f: 9 mol% of PPh_3 were added. g:1:1 THF/piperidine solvent mixture.

10.2.4 Trimerization and cyclodehydrogenation of **123** and **130**.

Both perfluoroalkoxy tolane derivatives To-PhORf$_{4,8}$ and To-PhORf$_{6,6}$ have undergone trimerization reactions using dicobalt carbonyl as catalyst as shown in figure 10.5 on the next page. Cyclodehydrogenation reaction of the corresponding hexaphenyl benzene moieties **131** (HPB-PhORf$_{4,8}$) and **132** (To-PhORf$_{6,6}$), using the mild $FeCl_3/CH_3NO_2$ combination, has also been performed affording the desired HBC products **133** (HBC-PhORf$_{4,8}$) and **134** (HBC-PhORf$_{6,6}$).

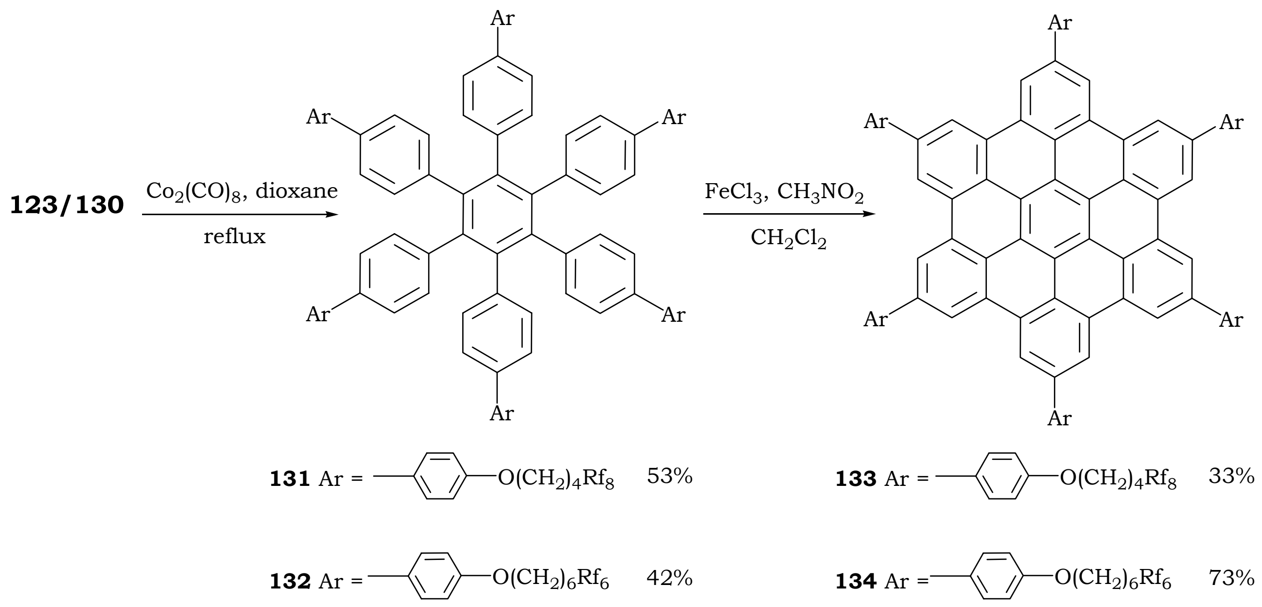

Figure 10.5. Syntheses of HBC-PhORf$_{4,8}$ and HBC-PhORf$_{6,6}$.

As it is mentioned in table 25 below, trimerization of the tolane species bearing four methylene spacers To-PhORf$_{4,8}$ affords the hexaphenyl benzene moiety HPB-PhORf$_{4,8}$ in 53% (entry 1) whereas the tolane species bearing six methylene spacers To-PhORf$_{6,6}$ affords 28% yield only (entry 2) of the hexaphenylbenzene derivative HPB-PhORf$_{6,6}$. The yield of this latter can be improved to 42% by increasing the reaction time (entry 3). The moderate yields obtained for both products are most probably due to the low solubility of the starting material in dioxane because these latter were always recovered during the work-up.

Table 25. Trimerization of To-PhORf$_{4,8}$ & To-PhORf$_{6,6}$ and cyclodehydrogenation of their respective products[a].

Entry	Substrate	Reagent (nb. eq/ H)	Additive	Solvent	Temp. (°C)	Time (h)	Product (%Yld)
1	123	$Co_2(CO)_8$[b]	-	Dioxane	reflux	48	**131** (53)
2	130	$Co_2(CO)_8$[c]	-	Dioxane	reflux	48	**132** (28)
3	130	$Co_2(CO)_8$[c]	-	Dioxane	reflux	66	**132** (42)
4	131	$FeCl_3$(6)	CH_3NO_2	CH_2Cl_2	RT	9[d]	**133** (33)
5	132	$FeCl_3$(6)	CH_3NO_2	CH_2Cl_2	RT	8[d]	**134** (73)

a: all the reactions were done under argon.. b: 10 mol% of cobalt. c: 5 mol% of cobalt. d: argon was bubbled throughout the reaction.

Shown in table 25, the HBC derivative bearing four methylene spacers is obtained in a lower yield than the one bearing six methylene intercalators. This can be only explained by the fact that HPB-PhORf$_{4,8}$ has a lower solubility in CH_2Cl_2 than HPB-PhORf$_{6,6}$, which leads to a slower reactivity. Increasing the reaction time is therefore the best solution to overcome this problem especially that the unreacted starting material is recovered from the medium. Both products have undergone many purification steps by washing repeatedly the crude material with hot solvents, known to dissolve the starting material and the partially cyclodehydrogenated products, until no trace of these latter was found in the mother liquor. Both HBC-PhORf$_{4,8}$ and HBC-PhORf$_{6,6}$ were characterized by MALDI-TOF mass spectrometry showing the corresponding desired peaks (figures 10.6 and 10.7), within the spectrometer margin error (~1-3 ppm), in addition to a mass corresponding to M + 32 in both spectra, an additional mass which is most probably caused by the matrix used (see experimental section for more details).

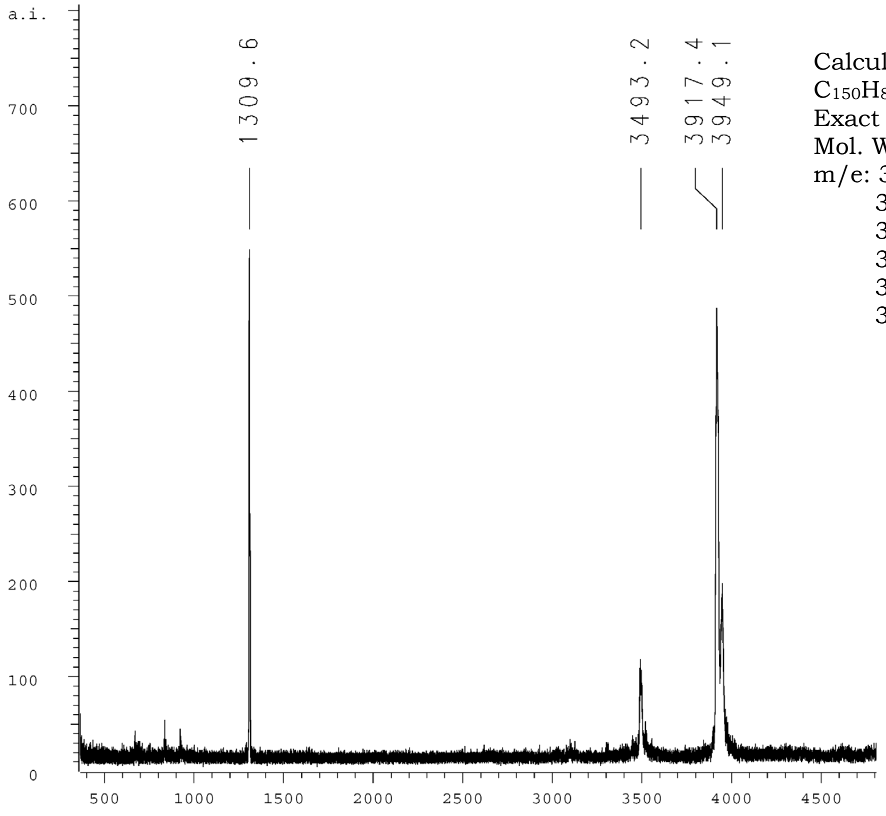

Calculated for $C_{150}H_{84}F_{102}O_6$
Exact Mass: 3918.464
Mol. Wt.: 3920.105
m/e: 3919.467 (100.0%)
3920.471 (83.1%)
3918.464 (59.9%)
3921.474 (45.5%)
3922.477 (18.6%)
3923.481 (6.0%)

Figure 10.6. MALDI-TOF of HBC-PhORf$_{4,8}$.

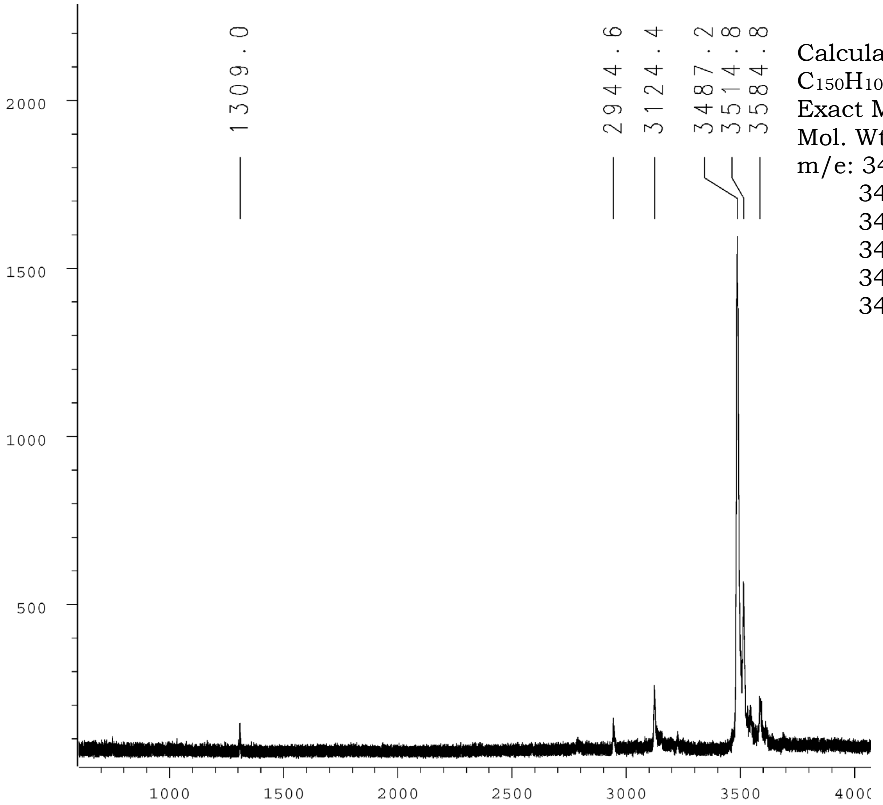

Calculated for
$C_{150}H_{108}F_{78}O_6$
Exact Mass: 3486.690
Mol. Wt.: 3488.334
m/e: 3487.693 (100.0%)
3488.697 (82.9%)
3486.690 (59.9%)
3489.700 (45.5%)
3490.703 (18.6%)
3491.707 (6.1%)

Figure 10.7. MALDI-TOF of HBC-PhORf$_{6,6}$.

HBC-PhORf$_{6,6}$ has also been measured by UV-Vis spectrometry showing the desired peaks, at 369, 395 and 453 nm (figure 10.8). Additionally, the molar absorption coefficient values taken from literature[193] have permitted to estimate the concentration which was found to be around 6x10^{-6} M in 1,2,4-TCB. On the other hand, characterization of HBC-PhORf$_{4,8}$ by the same technique wasn't possible due to its low solubility. This has led us to measure the fluorescence spectrum of this latter excited at the maximum wavelength of the UV-Vis spectrum found for HBC, i.e. 389 nm, which yielded a mirror image to the UV-Vis spectrum of HBC-PhORf$_{6,6}$ as it can be seen from figure 10.9. Both spectra show relatively broad peaks which reveals that the HBC derivatives are present in the solvent as stacked aggregates rather than being totally dissolved in 'monomeric' forms.

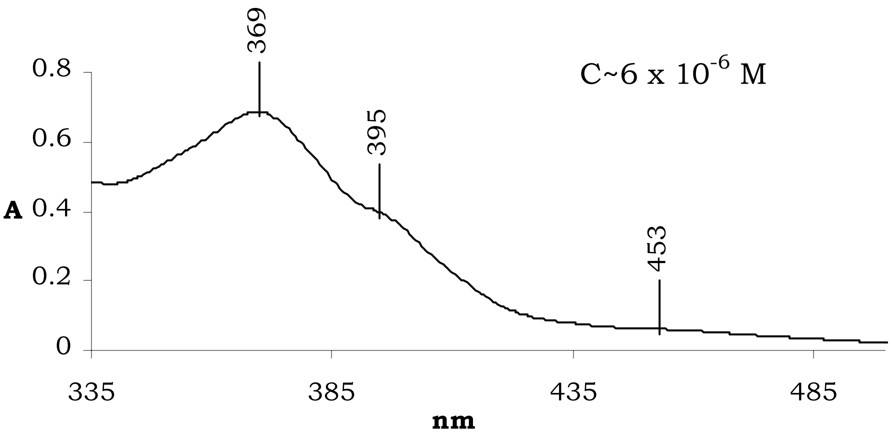

Figure 10.8. UV-Vis of HBC-PhORf$_{6,6}$.

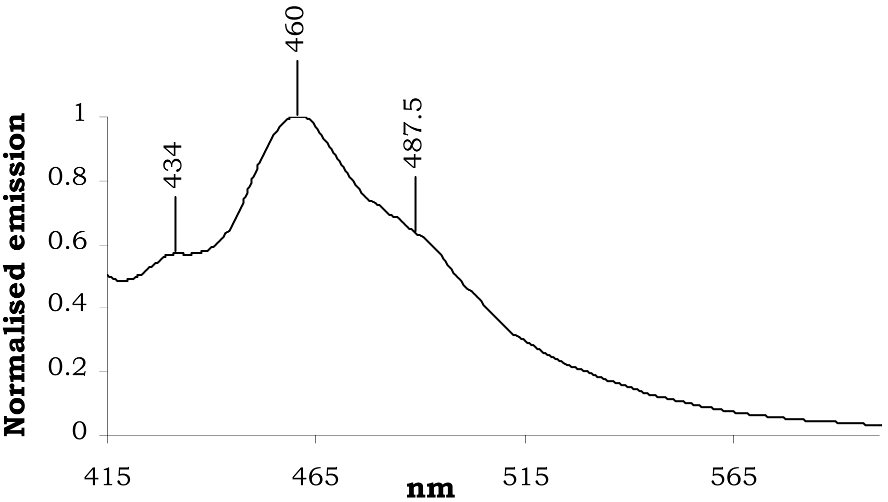

Figure 10.9. Emission spectrum of HBC-PhORf$_{4,8}$ excited at 389nm.

10.2.5 DSC investigation of HBC-PhORf$_{4,8}$ and HBC-PhORf$_{6,6}$

DSC measurements of both HBC-PhORf$_{4,8}$ and HBC-PhORf$_{6,6}$ have been performed to evaluate the changes brought about by the ethereal side chains. The first entry in table 26 shows that HBC-PhORf$_{4,8}$ has comparably high transition temperatures of 216 and 222°C. This can be explained by the low flexibility of both the lateral phenyl spacer and the oxygen group besides the fact that eight out of twelve methylene carbons are perfluorinated which increases the stiffness of the molecule. Surprisingly, upon decreasing the ratio of the perfluorinated groups to the methylene spacers, the product doesn’t show any liquid crystalline phase. The reason of this is still unclear especially that we do expect that the increase of the aliphatic side chain will decrease the transition temperature as we have seen in the previous section with products HBC-$Rf_{4,8}$ and HBC-$Rf_{6,6}$.

Table 26. Phase transition temperatures, enthalpy changes and structural assignments for HBC-$PhORf_{4,8}$ and HBC-$PhORf_{6,6}$.

Entry[a,b]	Compound	Phase Transition temperature (°C)	ΔH (KJ mol^{-1})	Phase width (°C)	Assignment
		heating/cooling	heating/cooling		
1	**HBC-$PhORf_{4,8}$ (133)**	182/(c) 216/207 222/215	3/(c) 18.7/19 6.3/25.6	- 34 6	$K_1 \leftrightarrow K_2$ $K_2 \leftrightarrow D_1$ $D_1 \leftrightarrow D_2$
2	**HBC-$PhORf_{6,6}$ (134)**	-	-	-	-

a: isotropic liquid was not formed below 360°C, decomposition occurs above ~300°C. b: rate of heating & cooling is 20°C. c: not determined. With K: crystalline, D: discotic.

10.3 Conclusion

On the synthetical level, we proved in this section the importance of cyclodehydrogenation as a key reaction to obtain HBC derivatives. Therefore, any synthetical strategy to design new HBCs must take into account the high sensitivity of this reaction step toward the electron withdrawing effect of substituents which have the ability to prevent the oxidation reaction to occur. We also proved that the insertion of a phenyl spacer between hexaphenylbenzene and the perfluorinated chain doesn't sufficiently decrease the electron withdrawing effect to such an extent that cyclodehydrogenation would occur. On the other hand, several HBCs bearing perfluorinated lateral chains were synthesized successfully with moderate to high yields, depending on the nature and the length of the spacer separating the perfluorinated part from the central aromatic core. Nevertheless, we showed that the spacing with an ethylene or a phenyl ethylene requires the use of harsh oxidation conditions using $AlCl_3/Cu(OTf)_2$ to afford the desired products HBC-$Rf_{2,8}$ and HBC-$PhRf_{2,8}$. On the other hand, upon using a butyl or a hexyl spacer, the cyclodehydrogenation reaction occurs with the mild $FeCl_3/CH_3NO_2$ reagent yielding HBC-$Rf_{4,8}$ in moderate yield and HBC-$Rf_{6,6}$ in very good yield. The same previous combination is sufficiently powerful to synthesize

HBC-PhORf$_{4,8}$ and HBC-PhORf$_{6,6}$ that bear alkylated perfluoroalkyl ethereal side chains spaced from the HBC core with a phenyl group. The presence of this aromatic spacer is crucial because otherwise quinonoid products will be obtained, as we have demonstrated for **121** which has been obtained instead of the desired HBC.

On the experimental level, many unusual observations have been gathered and studied for some of these HBCs. From these we note the self-organization of HBC-Rf$_{4,8}$ in the solid state and in solution into long micrometer-sized columnar structures. Different SEM techniques were used to investigate preliminarily this observation that revealed the homogeneity of these long columns and their probable composition of nano-sized filaments. On the other hand, cryo-SEM technique reveals the presence of homogeneous nano-sized columns besides the micrometer-sized ones we mentioned earlier. Preliminary studies of film deposition of HBC-Rf$_{4,8}$ and HBC-Rf$_{6,6}$ on Si(100) by solution evaporation have also been done; the former forms a uniform thin film containing homogeneously dispersed notches whereas the latter shows a poor adherence on the substrate but it grows in highly ordered columnar dendritic structure.

11. Nitrogen-containing polycondensed aromatic systems

11.1 Introduction

As we have noted previously (section 5.2), the synthesis of an HBC-like disc-shaped molecule bearing a nitrogen atom in its center was envisaged because it was expected that the presence of this latter will enhance the electron donating property of such molecules due to the free electron pair the nitrogen atom contains. Computational investigations of the stacking behavior of both candidates[329] **22** and **23**, whose structures are depicted in figure 11.1, have clearly confirmed that the symmetry of the former doesn't influence or improve the π- stacking very much, because the molecules are more favorable to an off-centered arrangement rather than an ordered columnar-like one; therefore, the less there are atoms at the edges, the better the stacking will be allowing more freedom to the peripheral sp^2 carbons to arrange. For all these reasons, product **23** was believed to be a promising candidate as well as its synthesis was expected to be less problematic than the more symmetrical product **22**.

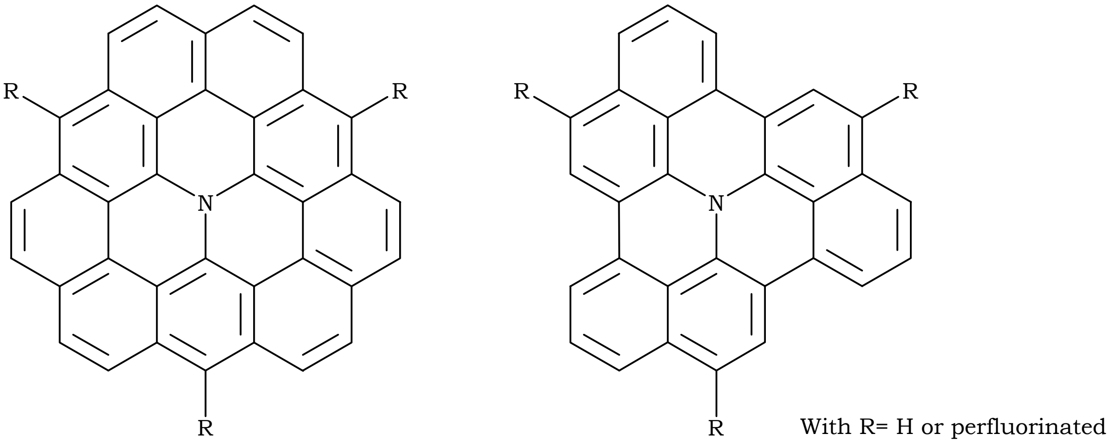

With R= H or perfluorinated chain

22 **23**

Figure 11.1. N-containing disc shaped aryls.

There is no known synthetical strategy for getting such types of unknown molecules; consequently, we thought about proceeding nearly in the same manner as we have done to synthesize the HBC derivatives: a closer look to **23** shows that its synthesis can be achieved by the cyclodehydrogenation of a corresponding trinaphthyl amine moiety **135** as shown in figure 11.2 on the next page. Hence, the synthesis of this latter was believed to be crucial since it constitutes the starting material for making the disc shaped aromatic moiety **23**.

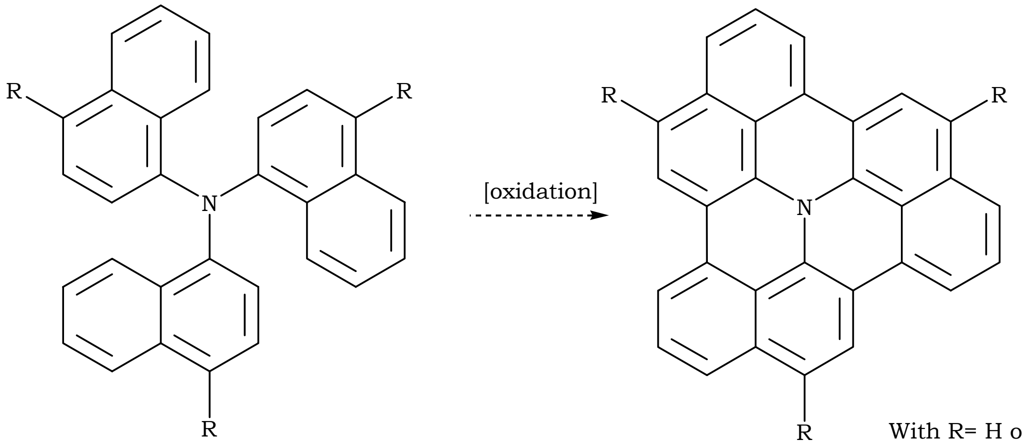

135 **23**

With R= H or perfluorinated chain

Figure 11.2. Oxidation of trinaphthyl amine to N-containing aryl disc shaped moiety.

There are many synthetical approaches to obtain triaryl amine derivatives, most of which employ an aryl amine and an aryl halide in presence of a transition metal reagent that could be present either stoichiometrically or catalytically. However, listing all these synthetical methods exceeds the aim of this work and for this reason we will only mention the most commonly used reactions. Copper-mediated Ullmann[330, 331] condensation reactions are the most famous using generally a stoichiometric amount of copper, a large excess of the aryl halide, with respect to the aryl amine, in presence of a base[332-334]. However, the limited choice of substrates, the high amounts of aryl halides and copper species required, besides the need for elevated temperatures have limited the use of these reactions. Recently, milder Ullmann-type reactions have been reported using catalytical amounts of copper species, a suitable ligand and, an appropriate base[335-339]. Nevertheless, the major drawback using these new methods is the fact that many additives are required in addition to the use of relatively expensive ligands and bases. Buchwald[340-343] and Hartwig[344, 345] have widely investigated the palladium-catalyzed couplings of amines. The general procedure [346] employs an equimolar mixture of the aryl amine and the aryl halide or triflate, a palladium catalyst, a suitable phosphine ligand and a mild organic base at low to medium temperatures under an inert atmosphere. Many improvements have been brought to this type of reaction: The syntheses of new phosphine ligands[276] have allowed the use of the inexpensive aryl chlorides instead of iodides and bromides species. Recently, the air-sensitive phosphine ligands was replaced by the air-stable imidazolium salts permitting a wider use of this reaction[347, 348]. Additionally, the use of low-cost nickel catalysts has also been found to be satisfactory for mild triaryl amine condensation reactions[349]. By comparing the two main N-C coupling reactions we can deduce that Ullmann condensation reactions require harsher and more sluggish conditions than the Buchwald-Hartwig conditions besides the fact that the latter reaction type has a wider scope concerning the choice of substrates. Therefore, we have favored the use of the latter procedure over the former. However, the mechanism of the palladium-catalyzed amination has a quite different behavior and is more complicated than the other palladium-catalyzed mechanisms we have showed so far. Many mechanistic propositions are presented in the literature from which we can conclude that the variations in these are dependent of many parameters such as the oxidation state of the palladium species[350, 351], the type of ligand used, and whether the amine is primary, secondary, aliphatic or aromatic[352, 353]. Nevertheless, we present, in scheme XIII below, the mechanism which was found to be most likely in our case i.e. upon using aromatic substrates.

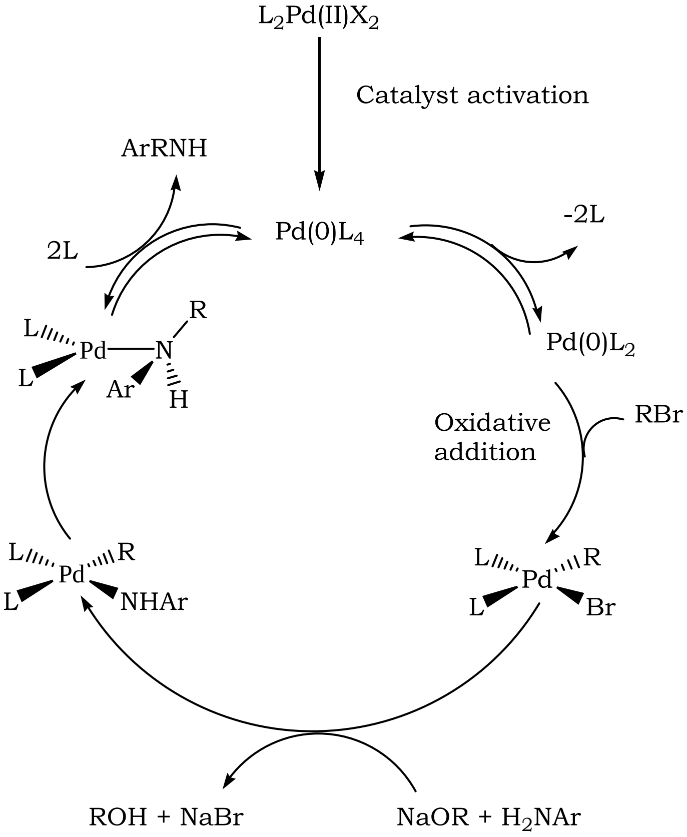

Scheme XIII. Mechanism of the Buchwald-Hartwig reaction.

11.2 Synthesis of the perfluoroalkyl substituted precursors

Synthesis of bromo- and aminonaphthalene derivatives bearing a perfluorinated chain with two methylene spacers has been performed using a similar procedure to that described in section 9.1. Figure 11.3 below, illustrates the different reaction steps required for this purpose: the diazotization of **136** and **137** has been done successfully[354] yielding the stable tetrafluoroborate diazonium salts **138** and **139** respectively. Heck cross-coupling reaction of these latter with the commercially available perfluorinated olefinic chain yields the corresponding perfluoroalkenyl naphthalene moieties **140** and **141** in good yields.

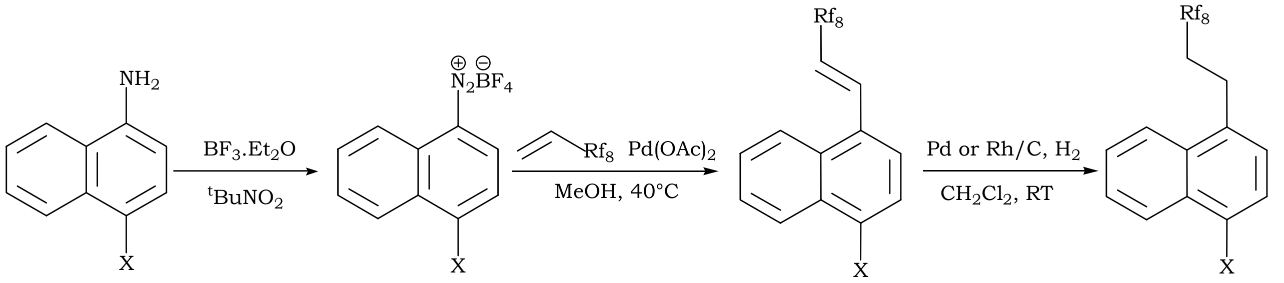

X= Br **136**
X= NO_2 **137**

X= Br (100%) **138**
X= NO_2 (99%) **139**

X= Br (76%) **140**
X= NO_2 (90%) **141**

X= Br (91%) **142**
X= NH_2 (94%) **143**

Figure 11.3. Syntheses of perfluorinated naphthalene derivatives **142** & **143**.

As it can be noticed from table 27 on the next page, the hydrogenation of **140** using the Rh/C catalyst under 50 bar hydrogen pressure affords the alkylated perfluoroalkyl naphthalene species **142** in very good yield (entry 1), whereas only the starting material is recovered upon applying the same conditions on the nitronaphthalene derivative **141** (entry 2). This could be explained by the mildness of Rhodium as a hydrogenation catalyst on one hand, and the fact that the nitro group has a deactivating influence as a reason of its electron withdrawing effect on the other hand. Consequently, we have tried to reduce the nitro group to the amino derivative in a first step followed by the hydrogenation of the olefinic double bond. Nevertheless, upon employing tin/hydrochloric acid conditions, only the staring material was recovered even after increasing both the amount reagents and the reaction time (entries 3 and 4). The replacement of Sn/HCl by $ZrCl_4/NaBH_4$ combination[355] yields decomposition products only (entry 5). On the other hand, the reaction of **141** under 1 bar of hydrogen in presence of Pd/C as catalyst yields 87% of the desired product (entry 6) which is improved to 94% yield upon increasing the hydrogen pressure to 3 bar (entry 7).

Table 27. Hydrogenation reactions of **140** and **141**.

Entry	**Substrate (eq.)**	**Reagent (eq.)**	**Catalyst (Mol%)**	**Solvent**	**T (°C)**	**t (h)**	**Pdt (%Yld)**
1	140 (1)	H_2 (50 bar)	Rh/C (2)	CH_2Cl_2	RT	24	**142** (91)
2	141 (1)	H_2 (50 bar)	Rh/C (2)	CH_2Cl_2	RT	24	**no rxn**
3	141 (1)	Sn (2)	-	HCl_{aq}	130	4	**no rxn**
4	141 (1)	Sn (25)	-	HCl_{aq}	130	24	**no rxn**
5	141 (1)	$ZrCl_4$(1.2)/ $NaBH_4$(4.8)	-	THF	0 - 75	20	**Decomp.**
6	141 (1)	H_2 (1 bar)	Pd/C (5)	MeOH/ THF (1:1)	RT	24	**143** (87)
7	141 (1)	H_2 (3 bar)	Pd/C (5)	MeOH/ THF (1:1)	RT	24	**143** (94)

11.3 Synthetical attempts of the perfluoroalkyl substituted trinaphthyl amine

11.3.1 Via a one-pot reaction

In a first place, we have attempted to obtain the desired trinaphthyl amine derivative **135** in a one-pot synthesis by reacting the aminonaphthalene moiety **143** with two fold excess of the brominated naphthalene compound **142** using the general reaction scheme depicted in figure 11.4.

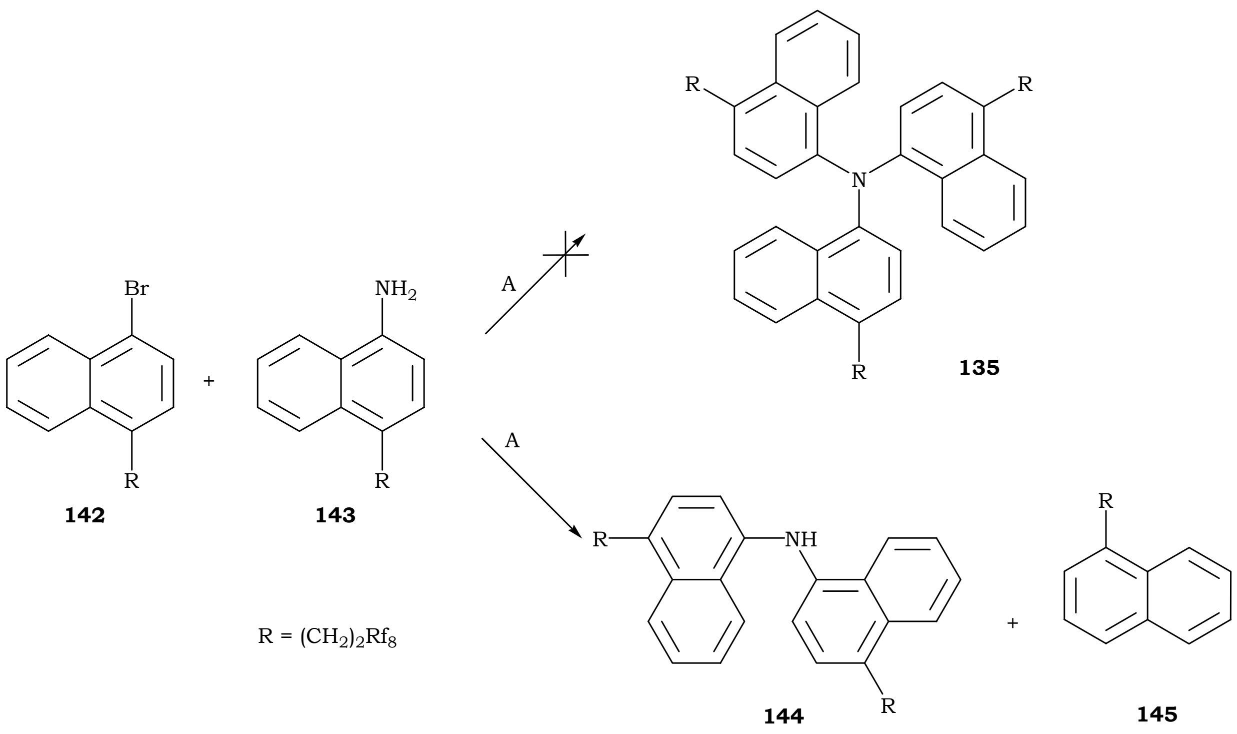

R = $(CH_2)_2Rf_8$

With A. $Pd(OAc)_2$, $t\text{-}Bu_3P$, NaOt-Bu, Xylene, 120°C

Figure 11.4. One-pot Pd-catalyzed amination reaction.

Table 28 on the next page shows the results of the series of trials we have done to obtain **135**. No trace of this latter product was found, only the binaphthyl amine species **144** was isolated in 35% yield after one day; the unreacted starting materials were recovered at the end of the reaction (entry 1). Increasing the reaction time (entry 2) has only increased the yield of **144** and afforded traces of perfluorinated naphthalene derivative **145**, resulting from the debromination of **142**. This latter product indicates that even though the formation of the binaphthyl amine intermediate **144** occurs, the reaction is not carrying on towards a second C-N coupling but instead of this, the metallated bromonaphthalene intermediate is cleaving and forms **145** which reveals that the reaction is somewhat hindered. To prove this assumption, an equimolar mixture of **142** and **143** has been reacted, under the same conditions used previously, affording the binaphthyl amine **144** in 83% yield (entry 3) and indicating a good reactivity when a 1:1 mixture of both starting materials is present.

Table 28. One-pot reaction attempts of perfluorinated trinaphthyl amine derivative **135**[a,b].

Entry	143 (eq.)	142 (eq.)	$Pd(OAc)_2$ (Mol%)	$t\text{-}Bu_3P$ (Mol%)	NaOt-Bu (eq)	T (°C)	t (h)	Pdt (%Yld)
1	1	2.3	5	20	3.5	120	24	**144** (35)
2	1	2.5	5	20	4	120	46	**144** (63), **145** (traces)
3	1	1	5	20	1.5	125	48	**144** (83)

a: reactions were done under argon atmosphere. b: xylene was used as solvent.

11.3.2 Using binaphthyl amine **144** as starting material

An alternative explanation to the sterical hindrance, we mentioned in the previous paragraph, preventing the binaphthyl amine species **135** to couple with an additional naphthalene group, could be the possible degradation of the palladium complex whose activity becomes critical, after affording the binaphthyl amine species. The acidity of the secondary proton can’t be suspected since it is well-known that the pK_a of aryl amines are known to drop upon the addition of a second aryl group, hence we expect that the secondary amine’s proton is more reactive than the primary one. Consequently, many attempts have been done to investigate the reaction: first, by using the binaphthyl amine species **135** as the starting material, instead of the aminonaphthalene derivative **143**, to overcome the possible erosion of the different palladium complexes during the reaction. In a second attempt, we have increased the activity of the binaphthyl amine by employing stronger bases and by exchanging its acidic proton by the more reactive lithium ion affording the amide species **144.1** that is reacted with **142** under different reaction conditions[356-358] (Figure 11.5).

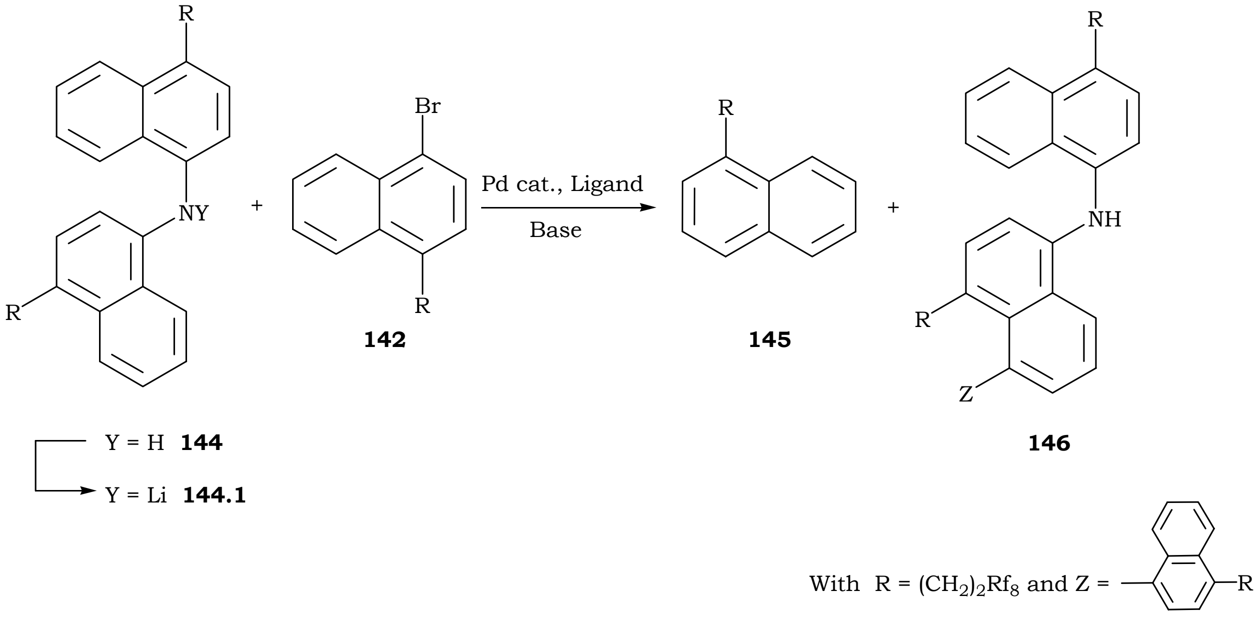

Figure 11.5. Using binaphthyl amine (or amide) as a starting material.

Table 29 on the next page, depicts the different reactions conditions applied and their corresponding results. Upon employing the classical conditions that we have used lately in the one-pot reactions attempts (table 27), both the debrominated product **145** and the C-C coupled product **146** were isolated in 10 and 32% respectively (entry 1). This result has prompted us to investigate the reaction at different temperatures assuming that a probable competition between thermodynamically and kinetically favored products is taking place. But when carrying out the reaction at room temperature for three days, only the starting materials are recovered (entry 2). The same result is also obtained after running the reaction at 70°C for two days and at 110°C for one day (entry 3 and 4 respectively). We have also noticed that the reaction doesn't take place even after approximately two days of reaction at 120°C which indicates a very low reactivity (entry 5) probably caused by the relatively weak base employed. Therefore, we have replaced sodium-tert-butoxide with the more basic cesium carbonate but the reaction didn't progress at room temperature (entry 6) and when carrying out the same reaction conditions at 120°C, again traces of the homocoupling product **146** are detected, by ^{1}H NMR spectroscopy, after two days of reaction (entry 7). This latter product can be isolated in 5% yield when carrying out the reaction for three days (entry 8). We have also noticed that if the catalyst and the ligand amounts are increased, the debrominated product is isolated in a significant yield (entry 9). Therefore, we can assume that the proton, needed for the debromination to occur, is afforded either by the acetate moiety or by the butyl group but to prove this, more investigations should be carried out by doing separate reactions that employ, in a first set of experiments, new Pd(II) and Pd(0) sources and, in a second series of experiments, different ligands than tert-butyl phosphine.

Table 29. Attempted synthesis of **135** using binaphthyl amine derivative **144** (or amide **144.1**) and bromonaphthalene **142**[a,b].

Entry	Substrate (eq.)	142 (eq.)	Catalyst (Mol%)	Ligand (Mol%)	Base (eq)	T (°C)	t (h)	Pdt (%Yld)
1	144 (1)	1	$Pd(OAc)_2$ (5)	$t\text{-}Bu_3P$ (20)	NaOt-Bu (1.5)	125	72	**145** (10) **146** (32)
2	144 (1)	1	$Pd(OAc)_2$ (10)	$t\text{-}Bu_3P$ (40)	NaOt-Bu (1.5)	RT	75	**no rxn**
3	144 (1)	1	$Pd(OAc)_2$ (10)	$t\text{-}Bu_3P$ (40)	NaOt-Bu (1.5)	70	48	**no rxn**
4	144 (1)	1	$Pd(OAc)_2$ (10)	$t\text{-}Bu_3P$ (40)	NaOt-Bu (1.5)	110	24	**no rxn**
5	144 (1)	1	$Pd(OAc)_2$ (10)	$t\text{-}Bu_3P$ (40)	NaOt-Bu (1.5)	120	40	**no rxn**
6	144 (1)	1	$Pd(OAc)_2$ (5)	$t\text{-}Bu_3P$ (20)	Cs_2CO_3 (1.5)	RT	120	**no rxn**
7	144 (1)	1	$Pd(OAc)_2$ (5)	$t\text{-}Bu_3P$ (20)	Cs_2CO_3 (1.5)	120	48	**146** (traces)[c]
8	144 (1)	1	$Pd(OAc)_2$ (5)	$t\text{-}Bu_3P$ (20)	Cs_2CO_3 (1.5)	120	72	**146** (5)[c]
9	144 (1)	1	$Pd(OAc)_2$ (25)	$t\text{-}Bu_3P$ (100)	Cs_2CO_3 (3)	120	120	**145** (82)
10	144 (1)	1	$Pd(OAc)_2$ (5)	$t\text{-}Bu_3P$ (20)	Cs_2CO_3 (3)	130	48	**145** (36)[c] **146** (16)
11	144 (1)	1	$Pd(OAc)_2$ (5)	$t\text{-}Bu_3P$ (20)	$NaOH_{aq}$ (12M)[d]	125	48	**decomp. pdts**
12	144 (1)	1	$Pd(OAc)_2$ (5)	$t\text{-}Bu_3P$ (20)	NaOH (2.2)[e]	100	52	**145** (40)[c] **146** (22)
13	144.1 (1)[f]	1	$Pd[(o\text{-}tol)_3P]_2Cl_2$ (5)	$(o\text{-}tol)_3P$ (20)	-	90	18	**no rxn**
14	144.1 (1)[g]	1	Pd_2dba_3 (2.5)	$(o\text{-}tol)_3P$ (20+15)	-	90	24	**145** (13)[c]
15	144.1 (1)[h]	1	$Pd[(o\text{-}tol)_3P]_2$ (20)	$(o\text{-}tol)_3P$ (60)	-	90	24	**no rxn**
16	144.1 (1)[h]	1	Pd_2dba_3 (2.5)	$t\text{-}Bu_3P$ (20)	-	90	46	**145** (42)[c]

a: reactions were done under argon. b: xylene or toluene were used as solvent. c: NMR yield. d: 2eq.of TBABr were used as a PTC. e: dioxane was used as solvent. f: n-BuLi, pentane, RT, 16hrs. g: n-BuLi, Et_2O, -50°C- RT, 24hrs. h: n-BuLi, THF, -90°C- RT, 24hrs.

Surprisingly, upon increasing the reaction temperature to 130°C, both products **145** and **146** are detected (entry 10). This reveals that a competition takes place between debromination, which is kinetically more favored, and homocoupling, which is thermodynamically more favored. The substitution of cesium carbonate with a hydroxylic base yields decomposition products, when a concentrated aqueous solution of sodium hydroxide is used in presence of tetrabutyl ammonium bromide (TBABr) as phase transfer catalyst (entry 11). On the other hand, the addition of powdered sodium hydroxide to the medium affords both **145** and **146** (entry 12).

In summary, all the trials to activate the aminic proton by using stronger bases or conducting the reaction at different temperatures turned out to be unsuccessful. Accordingly, we have tried to overcome the problem by exchanging the proton with a better reacting group, i.e. lithium ion: all the amide derivatives were synthesized in situ by ion exchange with n-BuLi and then reacted, in a next step, with the brominated species **142** in presence of a suitable palladium complex. Nevertheless, the reactions using the commercially available $Pd[(o\text{-}tol)_3P]_2Cl_2$ and $Pd[(o\text{-}tol)_3P]_2$, which was prepared according to literature[359], were found to be inefficient (entries 13 and 15 respectively). On the other hand, the use of Pd_2dba_3, with either an aromatic or an aliphatic phosphine, affords the alkylated perfluoroalkyl naphthalene product **145** (entries 14 and 16 respectively). The combination of these last two trials with the result obtained in entry 9, reveals that the proton source needed for debromination are most probably the substituents of the phosphine ligand.

In conclusion, neither the replacement of sodium tert-butoxide with stronger bases nor the proton exchange with a lithium ion, nor the usage of a series of different palladium/ligand combinations, have afforded the desired trinaphthyl amine derivative **135**. This allows only one remaining assumption to stand for true and that is the steric hindrance caused by the two bulky naphthyl groups preventing, consequently, the third naphthalene moiety to bind to the nitrogen atom. It is also worthwhile to note that only few patents were found in the literature describing the synthesis of the parent trinaphthyl amine[360, 361] which was characterized by mass spectrometry and GC/MS without being analyzed by any viable technique that reveals the structure of this molecule, like NMR for example, since the molar mass of both the C-C- coupled product and the trinaphthyl amine is identical.

11.3.3 Oxidative cyclization of binaphthyl amine **144**

To overcome the formation of homocoupling and debromination by-products **145** and **146**, as a direct reason of the steric hindrance of the binaphthyl amine moiety **144**, we thought about attempting a regioselective oxidative cyclization of this latter to its six-membered aza-benzo chrysene derivative **147** as illustrated in figure 11.6 below. The advantage of this latter product is the fact that its rigid aromatic group has a stronger electronic stabilizing effect than two naphthalene groups which will enhance the acidity of the amine's proton. Additionally, the aromatic core will allow more space for an additional naphthalene moiety to add on. The combination of both expected results should, therefore afford the product **148** obtained via a C-N coupling reaction without any problem. On top of that, the advantage of having this latter product is that, upon oxidative cyclization, it can only afford the disc shaped **23** due to the lack of any other possibility of oxidation.

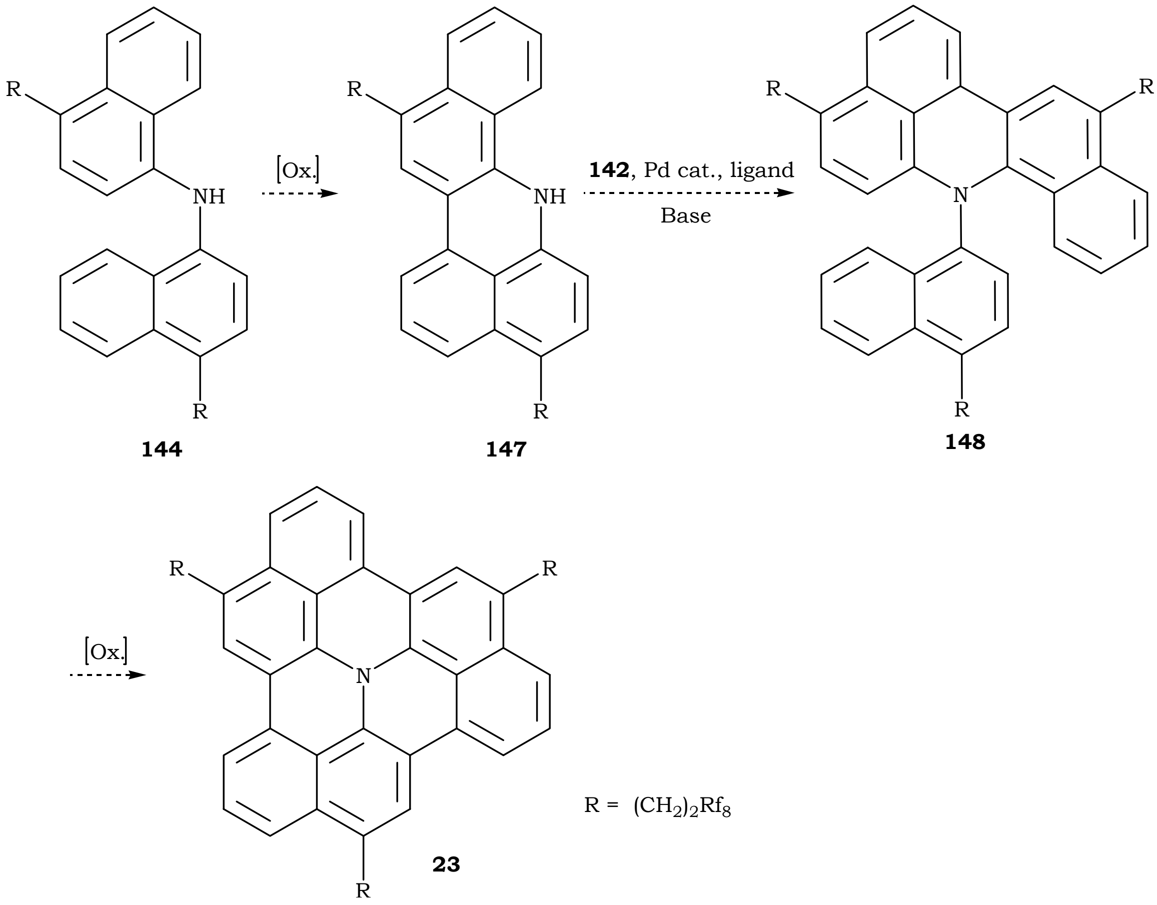

Figure 11.6. New approach using cyclized product **147** as a starting building block.

It is worthwhile to point out that two main cyclodehydrogenation reactions of diarylamine derivatives that are reported in literature: the first uses photochemical reaction conditions[362-364] while the second employs palladium(II) species as an oxidant[365, 366]. Nevertheless, both methods lead exclusively to the formation of the five-membered ring carbazole derivatives. Consequently, this has led us to explore reagents that have never been used previously on this type of particular substrate, such as, the conditions employed previously to aromatize hexaphenylbenzene into HBC or the hypervalent iodide reagent, [bis(trifluoro-acetoxy)iodo]benzene (PIFA), well-known for cyclization reactions of nitrogen containing products[367-369]. Preliminary oxidative cyclization reactions have been performed using the conditions depicted in figure 11.7 below.

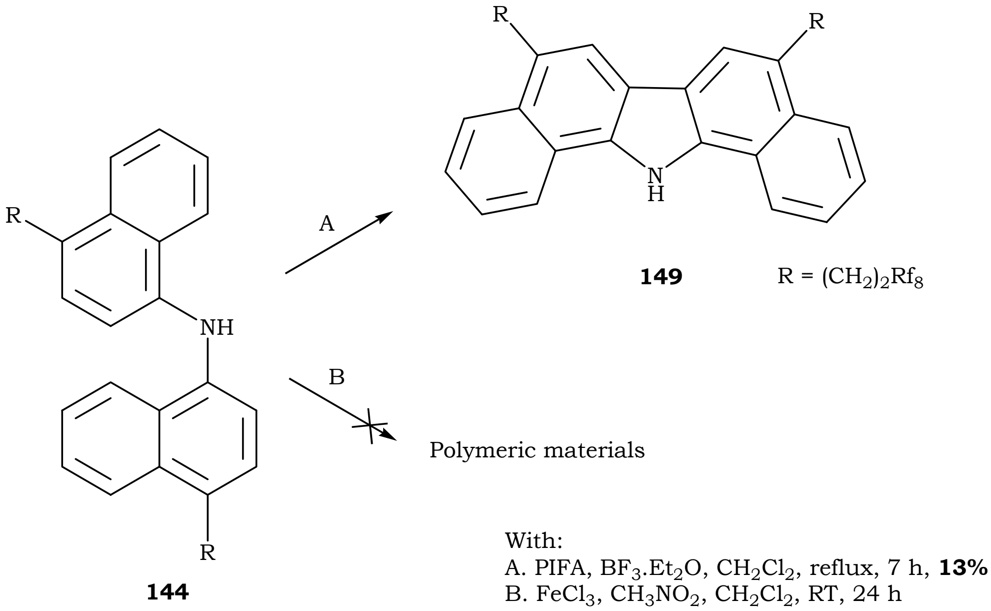

149 R = $(CH_2)_2Rf_8$

144

With:
A. PIFA, $BF_3.Et_2O$, CH_2Cl_2, reflux, 7 h, **13%**
B. $FeCl_3$, CH_3NO_2, CH_2Cl_2, RT, 24 h

Figure 11.7. Oxidative cyclization of binaphthyl amine species **139**.

As listed in table 30 on the next page, the cyclodehydrogenation of the binaphthyl amine moiety **144**, using $FeCl_3/CH_3NO_2$ combination of reagents, leads to the formation of a tarry product whose ESI-MS spectrum shows the formation of unidentified decomposition products (entry 1). On the other hand, the use of $PIFA/BF_3.Et_2O$ combinations leads to the formation of the carbazole **149** in 13% yield (entry 2).

Table 30. Oxidative cyclization of **144**^{a}.

Entry	Substrate	Reagent	Additive	Solvent	Temp. (°C)	Time (h)	Product (%Yld)
1	144	$FeCl_3$(12.5)	CH_3NO_2	CH_2Cl_2	RT	24^{b}	**decomp. pdts**
2	144	PIFA(1.2)	$BF_3.Et_2O^{c}$	CH_2Cl_2	reflux	9	**149** (13)

a: all the reactions were done under argon.. b: argon was bubbled for 4 hours. c: 2:1 ratio of $BF_3.Et_2O$/PIFA.

Even though the above preliminary reactions aren't sufficiently conclusive, a deepened study of the reaction done with $FeCl_3/CH_3NO_2$ could be excluded due to the decomposition products isolated at the end of the reaction. Nevertheless, a more exhaustive study must be carried out when using the PIFA reagent, because in the trial we present herein (entry 2, table 30), refluxing the medium could have forced the reaction toward a kinetic pathway to afford the carbazole **149** by-product instead of the desired six-membered ring product **147**. Hence, a thorough exploration of the reaction conditions, more specifically the study of the temperature effect on the product formation, should be done to see whether **147** product could be obtained via this route.

To prove that steric hindrance is the main reason for not obtaining the trinaphthyl amine derivative **23**, we have replaced the bromonaphthalene species **142** with its phenyl homologue **88** as well as with the commercially available 4,4'-dibromobiphenyl **150** (figure 11.8) and carried out the same reaction conditions that have been applied so far.

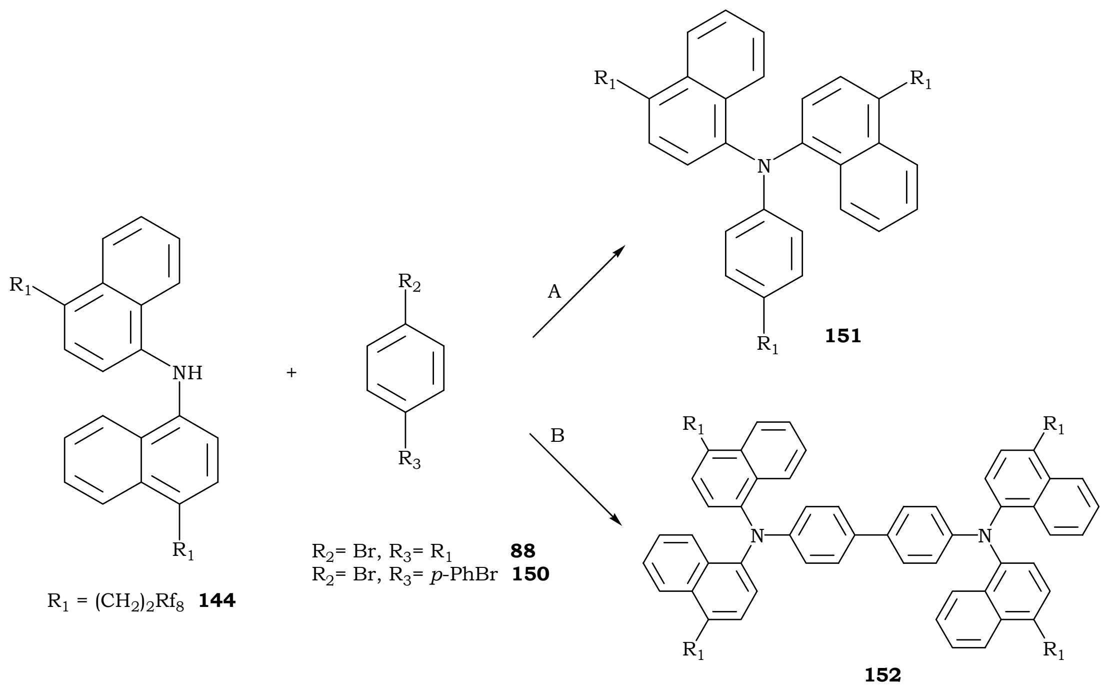

With: A. $Pd(OAc)_2$, t-Bu_3P, NaOt-Bu, toluene 120°C, 3d, **64%**; B. $Pd(OAC)_2$, t-Bu_3P, NaOt-Bu, toluene, 120°C, 10d, **50%**

Figure 11.8. Pd-catalyzed reaction of binaphthyl amine **144** with bromophenyl **88** and 4,4'-diromobiphenyl **150**.

Table 31, lists the different trials carried out to obtain **151** and **152**: The reaction between the binaphthyl amine derivative **144** and the alkylated perfluoroalkyl bromobenzene **88**, affords the triaryl amine moiety **151** in a relatively low yield (24%) even after six days of reaction in presence of Pd_2dba_3 (entry 1). Nevertheless, we were able to improve the yield significantly (64%) and in a shorter reaction time by replacing the so far used palladium(0) catalyst with $Pd(OAc)_2$ (entry 2). On the other hand, the reaction between binaphthyl amine derivative **144** and 4,4'-dibromobiphenyl **150** in presence of Pd_2dba_3 affords the desired alkylated perfluoroalkyl tetranaphthylbenzidine species **152** in 28% and 38% yield after four and six days of reaction, respectively (entry 3 and 4). Similarly to the reaction affording **151**, the use of $Pd(OAc)_2$ instead of Pd_2dba_3 improves the yield to 50% after a one week reaction time. The relatively long reaction times required to form both **151** and **152** prove clearly that steric hindrance is the main reason for preventing a third naphthalene species to bind to the nitrogen atom.

Table 31. Synthetical attempts of alkylated perfluoroalkyl triaryl amine[a-c].

Entry	**Substrate (eq.)**	**139 (eq.)**	**Catalyst (Mol%)**	**Ligand (Mol%)**	**NaOt-Bu (eq)**	**t (d)**	**Pdt (%Yld)**
1	88 (1)	1	Pd_2dba_3 (2.5)	t-Bu_3P (10)	1.5	6	**151** (24)
2	88 (1)	1	$Pd(OAc)_2$ (5)	t-Bu_3P (20)	1.5	3.5	**151** (64)
3	150 (1)	2	Pd_2dba_3 (10)	t-Bu_3P (80)	3	4	**152** (28)
4	150 (1)	2	Pd_2dba_3 (2.5)	t-Bu_3P (20)	3	6	**152** (38)
5	150 (1)	2	$Pd(OAc)_2$ (10)	t-Bu_3P (40)	3	7	**152** (50)

a: reactions were done under Ar. b: toluene was used as solvent. c: all the reactions were heated at 120°C.

Triarylamines are well-known as hole transporting materials and they have found applications[370] in many thin layer electroluminescence (EL) devices such as Organic Light Emitting Diodes (OLED), Organic Field Effect Transistors (OFET), and solar cells, besides their wide use in electrophotographic devices like photocopiers and laser printers. This wide application is due to the easily accessible oxidation potential of the nitrogen atom which, on hole injection, forms a free electron and generates a stable amine radical cation necessary for the hoping mechanism. However, the wide fields of applications we have mentioned above require from the triarylamine products many essential properties such as high thermal stability, electrochemical reversibility, high glass transition temperatures (T_g) to avoid any morphological change and last but not least, the ability to form amorphous phases. Listing the numerous triarylamines that have been synthesized and tested for this purpose exceeds the aim of this work; therefore, we provide herein some references describing the different groups of triarylamines that have been synthesized and explored so far[331, 333, 334, 336, 346, 356, 371-373].

Interestingly, the triaryl amine derivative **151**, isolated as a transparent waxy solid, was found to produce fibers even at room temperature. Polarized optical microscope observation of a fiber drawn at room temperature reveals a long homogenous structure that also shows clearly aligned features as illustrated in figure 11.9.

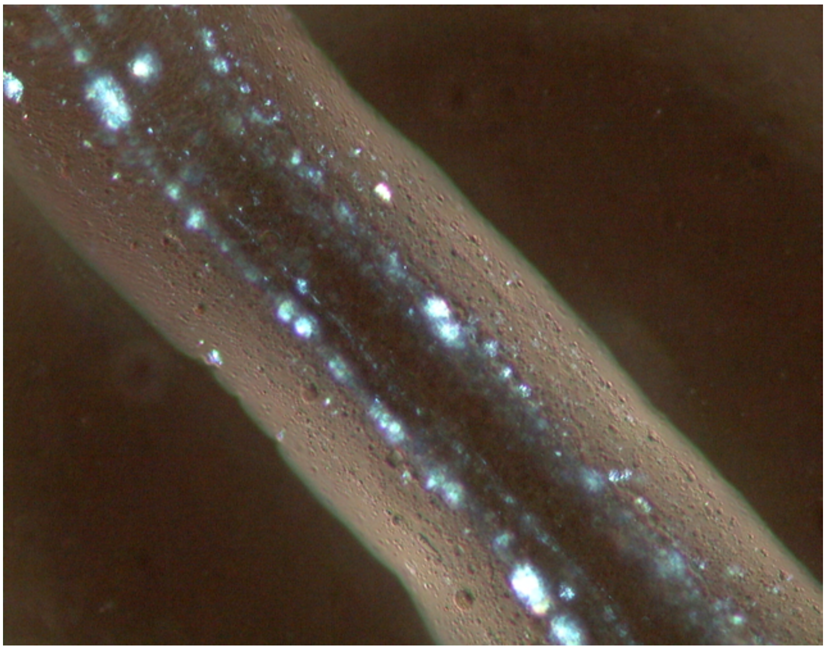

Figure 11.9. POM micrograph (x 100) of a fiber of **151** drawn at room temperature.

DSC measurements of these compounds have revealed promising properties because the calorimetric traces of both products showed no mesophases and high melting points: the former product doesn’t melt even at 450°C, while the latter has a melting point of 242°C. Upon cooling the samples from the liquid phase and heating them again at a rate of 20°C/min, they didn’t show any exothermic crystallization peak which reveals the amorphous nature of both **151** and **152**. This could be explained by the disordered packing of the molecules due to the perfluorinated chains they bear at their periphery. Significant thermal stability was also observed since the products were allowed to run many times at elevated temperatures. Upon cooling **152** from the liquid phase, two exothermic peaks at 198°C and 210°C appear, revealing that two different crystallites are present at least. This observation can be only explained by a contribution of the different structural conformations product **152** possess and which is caused by the planar chirality of the product since four atropisomers having different energies can form, leading to several physically different crystallites. Figure 11.10 on the next page depicts the some of these possible conformations that could be present.

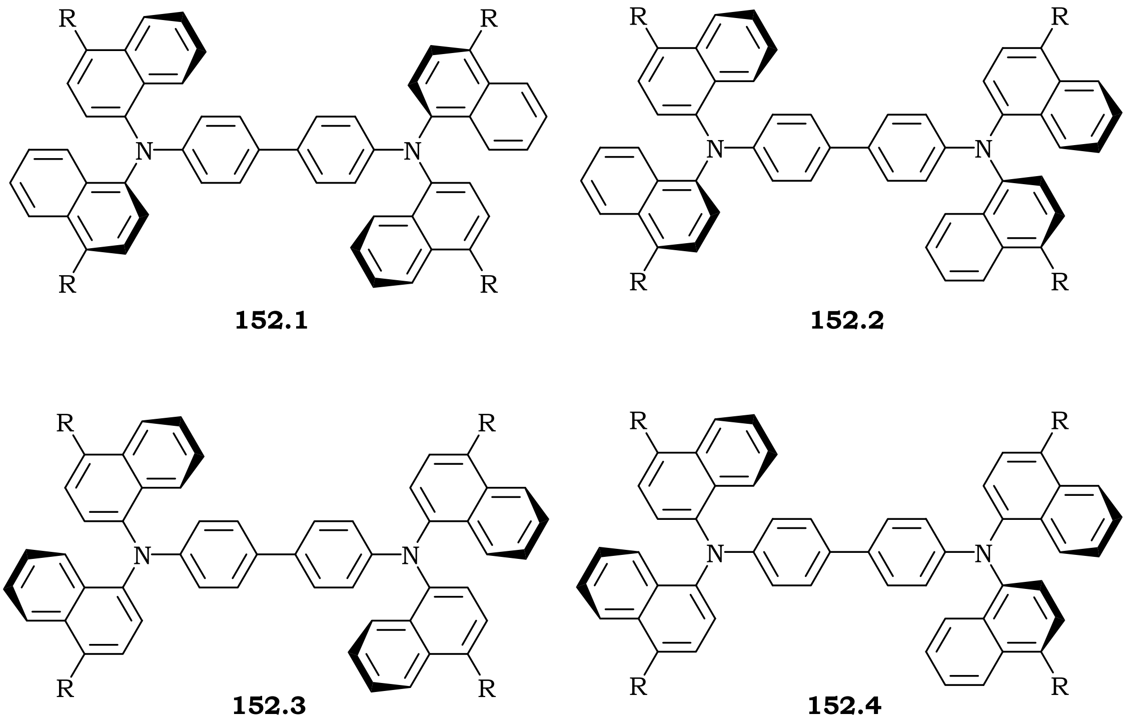

152.1 **152.2**

152.3 **152.4**

R = $(CH_2)_2Rf_8$

Figure 11.10. Possible conformations of **152**.

11.4 Conclusion

Synthesis of the disc-shaped naphth-annelated cyclazine bearing peripheral perfluorinated chains **23** was not possible due to the extreme difficulty to synthesize the key intermediate trinaphthyl amine **135** that upon oxidation, was expected to afford the desired product. Many reaction conditions have been examined to synthesize **135** but none of the trials were successful. We also prove in this project that steric hindrance is the main reason for not being able to form the trinaphthyl amine moiety **135** because the addition of a third naphthalene group to the binaphthyl amine **144** is diverted from nitrogen to carbon, while the addition of phenyl or biphenyl groups affords the corresponding triaryl amines **151** and **152**. Moreover, preliminary oxidative cyclization attempts of the binaphthyl amine **144** have afforded the five-membered carbazole derivative **149** instead of the required six-membered aryl amine **147** exclusively. On the other hand, preliminary investigation of the triarylamine products **151** and **152** show that they could be promising candidates as hole transporting materials especially on the background that two recent patents[361, 374] describe the utility of some tetranaphthyl benzidine derivatives.

III. Conclusions and outlooks

12.1 HBCs bearing perfluorinated groups

Syntheses of several HBC derivatives bearing different perfluorinated and mixed perfluoroalkylated alkyl groups, ranging from short to long tails, have been done successfully. The cyclodehydrogenation was found to be the key reaction in the production of any new HBC molecule. All hexaphenyl benzene starting materials with directly attached perfluorinated aliphatic chains couldn't be aromatized to their corresponding HBCs as a reason of the high electronegativity of the perfluorinated chains.

Additionally, smoother reaction conditions were found to be sufficient when increasing the aliphatic spacers between the hexaphenyl benzene and the lateral perfluoroalkylated alkyl chains. Moreover, the synthesis of HBC targets decorated with ethereal side chains, was made possible either when using a perfluoromethyl group (HBC-OCF$_3$) or upon employing a phenyl intercalator between the oxygen atom and the central aromatic core (HBC-PhORf$_{4,8}$ & HBC-PhORf$_{6,6}$). The use of one of these alternatives prevents the oxidation of the hexaphenylbenzene derivatives, bearing directly attached ethereal chains, to their quinonoid products.

Two out of three HBC primers (HBC-OCF$_3$ & HBC-SCF$_3$) designed for this purpose are expected to be valid candidates. Each of them is a ditopic molecule where the aromatic disk is surrounded by six heteroatoms (O or S) well-known for their good adhesion on metallic and intermetallic substrates. Preliminary SEM investigations have thus revealed promising and unusual observations: the deposition of HBC-SCF$_3$ on Si(100) forms a thin, smooth film that covers the surface of the substrate homogenously whereas HBC-Rf$_{6,6}$ deposits in well-organized columnar dendrites.

On the other hand, when depositing a dilute solution of HBC-Rf$_{4,8}$, in 1,2,4-TCB, a film forms that shows notches whose origin is still unclear, whereas a high concentration of the same product leads to the formation of non-coagulated micrometer-sized columnar structures homogenous in size, shape, and morphology. The observation of these structures at a high magnification reveals that they are made up of layers.

The investigation of the same concentrated solution of HBC-Rf$_{4,8}$ with cryo-SEM allowed the detection of two types of self-organized stacks: besides the micrometer sized columns we mentioned previously, nanometer-sized filaments were observed whose length and diameter is in the order of 750 nm and 30 nm, respectively. These nano-filaments can be regarded as a direct and a reliable proof on the possibility of obtaining free-standing, self-assembled singular columnar stacks when employing a perfluoroalkylated alkyl HBC derivative with a right match of alkyl and perfluoroalkyl chains.

The solid state investigation of the same product (HBC-$Rf_{4,8}$) under a POM and an SEM revealed a structural organization upon heating: the same micrometer-sized fibers were clearly observed under the optical microscope whereas a bundle-like morphology has been detected under the electronic microscope. One possible application of these micrometer-sized self-organized columns might be their employment as molecular wires.

Nevertheless, more has to be done in the future in order to build a functional field emission tip based on self-assembled HBC columns. One task will be to find a suitable technique to deposit a first layer of equally dispersed HBC primers on a substrate. A second hurdle to overcome will be to find the optimal conditions that afford single columnar architectures of the perfluorinated HBCs: one way to investigate would be the addition of a non-solvent to the solution of HBC columns in 1,2,4-TCB which will only mix with the latter solvent causing an increase of the dilution between the HBC stacks but without dissolving them into isolated molecules.

A deeper investigation of the HBCs bearing ethereal groups (HBC-OCF_3, HBC-$PhORf_{4,8}$ & HBC-$PhORf_{6,6}$) would be also of interest to see whether these groups introduce special features to the π-stacked columns, such as helicity. The synthesis of new HBC molecules decorated laterally with branched and cyclic perfluorinated groups might bring a better teflon-isolation effect of the central aromatic core from its surroundings in addition to a possible formation of helical stacks.

12.2 N-containing PAH

The synthesis of such type of molecules is believed to be of potential interest for electronic application because of the low oxidation potential the nitrogen atom has with respect to a carbon atom. None the less, the attempted synthesis of the perfluoroalkylated disc-shaped naphth-annelated cyclazine **23** couldn't be achieved as a reason of the impossibility to produce the trinaphthyl amine starting material **135**. Steric hindrance is the main reason for not being able to synthesize the desired product by addition of a third naphthalene substituent to the binaphthyl amine **144**.

A better strategy, however, would be to couple two naphthalene derivatives through a C-C bond first, followed by cyclization via the formation of a C-N bond affording, therefore, the six-membered aza-benzo chrysene derivative **147** whose nitrogen atom is less sterically hindered than the binaphthyl amine derivative **144**, which should permit a third naphthalene group to bind without any major difficulties.

Nevertheless, the synthesis of two alkyl perfluoroalkylated triaryl amine derivatives **151** and **152** was successful. Both products appear to be very good candidates for an application like OLED because they fulfill most of the requirements for such type of devices, from these we note, a high viscosity, a good thermal stability over a wide range, and an amorphous state.

IV. Experimental part

13. Analytical tools for characterizing PAHs

13.1 Optical spectroscopy

Because of its extended aromatic core, HBC has characteristic absorption bands that allow its analysis with optical spectroscopy. Nevertheless, the very low solubility of HBC in common organic solvents, as well as in inorganic ones, prohibited the exploit of such types of analytical methods until Clar and coworkers[193] found that TCB is a fair solvent for HBC. An undetermined concentration of HBC in TCB has been measured in a 100 cm cell affording a spectrum that reveals three characteristic peaks at 342.5, 360, and 387.5 nm. Samori and coworkers[92] have reported the formation of a saturated solution of HBC at a 10^{-4} M concentration in 1,2,4-TCB, by heating the solution at 100°C for 12 hours followed by filtration of the yellow solution through a Millipore® filter with pores of 200 nm diameter. We have further improved this method by sonicating the solution for 2 hours instead of heating it overnight which allowed reaching a ten fold excess of saturation in the same solvent (~10^{-3} M). Figure 13.1 below shows a typical spectrum of HBC in 1,2,4-TCB.

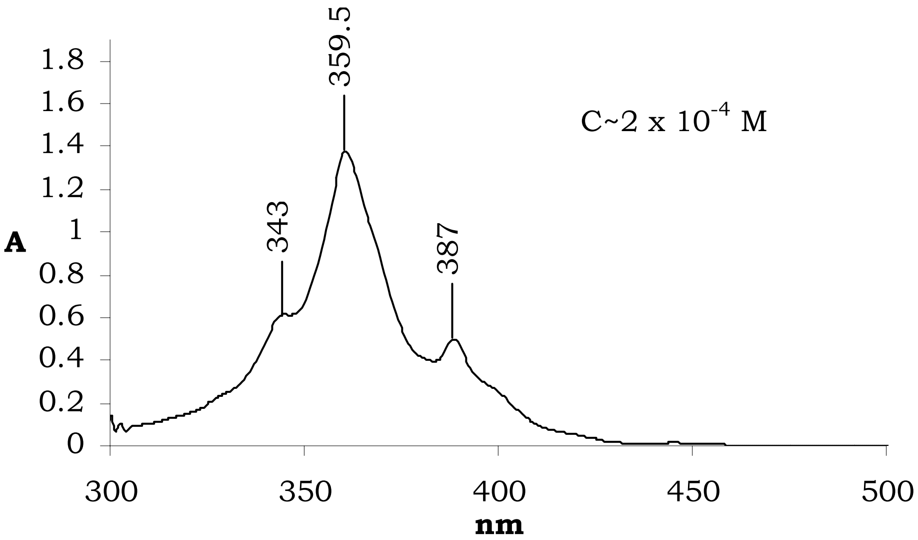

Figure 13.1. UV-Vis spectrum of HBC in 1,2,4-TCB.

Recently, Fleming and coworkers[98] have reported the effect of concentration on the luminescence and luminescence-excitation spectra of two soluble HBC derivatives whose structures are shown in figure 13.2 on the next page. Interestingly, the report proves that the previously published UV-VIS spectra of all the HBC derivatives (figure 13.2), are the ones of aggregation products and not the isolated HBC molecules. Furthermore, the study shows that different spectra of both products are obtained at low, medium, and high concentrations.

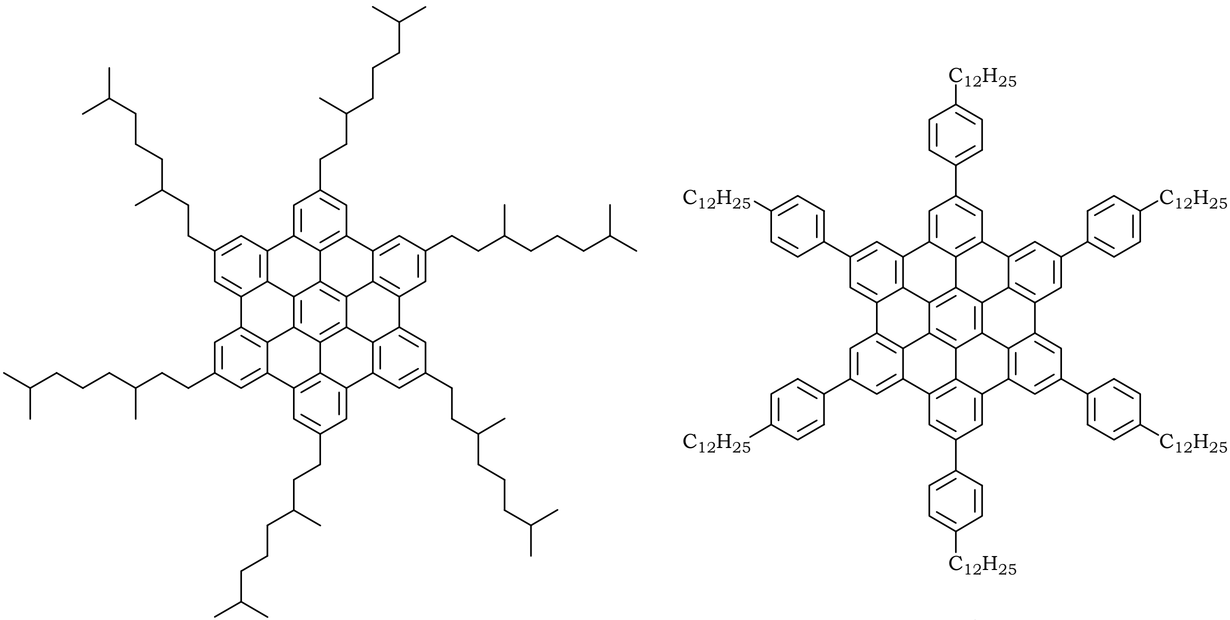

HBC-$C_{8,2}$ **HBC-PhC_{12}**

Figure 13.2. Structures of HBC-$C_{8,2}$ and HBC-PhC_{12}

At very low concentrations (10^{-15} – 10^{-9} M) both products are present in the solvent as isolated molecules. The additional phenyl groups of HBC-PhC_{12} don't contribute to the π-conjugation since no significant red-shift was observed. Instead, an inhomogeneous broadening of the spectrum, brought about by the tilting of the *exo*-phenyl groups, is detected (figure 13.3).

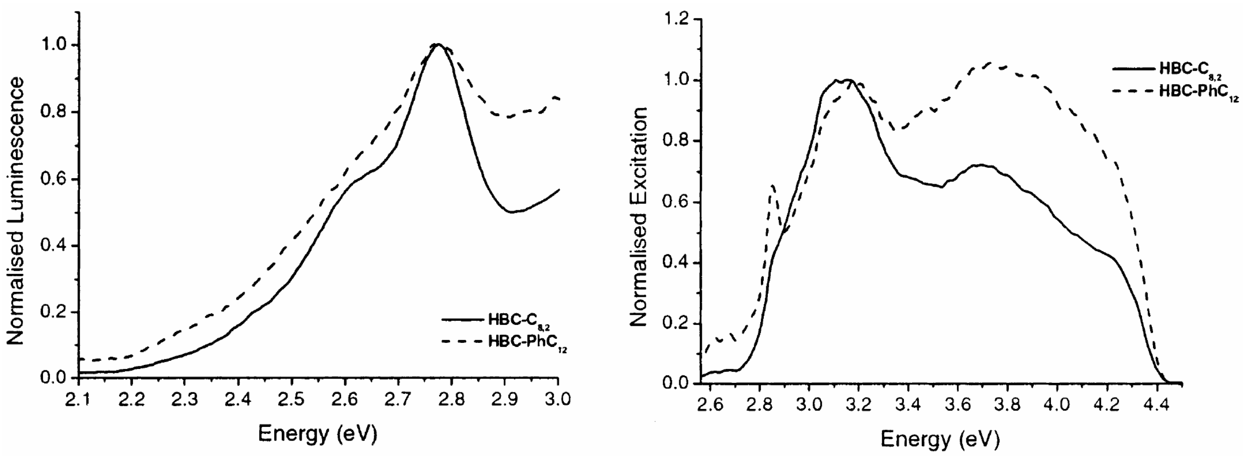

Figure 13.3. Normalized low concentration luminescence (left) and normalized low concentration luminescence-excitation (at 10^{-13} M).

At intermediate concentrations (~10^{-9} - 10^{-8} M) aggregates of both products can be seen in the spectra but HBC-$C_{8,2}$ is more blue shifted and is better resolved than HBC-PhC_{12} indicating, therefore, a superior aggregation of the former over the latter. At higher concentrations (≥1.4 x 10^{-6} M) the peaks of the isolated HBC-$C_{8,2}$ molecules disappear, and the luminescence spectrum is narrowed by ~20% with respect to the intermediate concentration spectrum revealing, therefore, a complete aggregation. On the other hand, the spectra of HBC-PhC_{12} show, at the same concentrations, a broadening of both its excitation as well as its luminescence spectra by 87% and 38%, respectively. Knowing that the aggregates emission is seen in the range of 2.1-2.6 eV whereas the single molecules emission is observed in the region of 2.6-3.0 eV, the luminescence-excitation spectrum of HBC-PhC_{12} was collected at 2.69 eV showing clearly the presence of monomeric molecules even at high concentration (inset in figure 13.4).

This direct observation of the free HBC-PhC_{12} molecules even at high concentrations is in contradiction to the interpretation of the data collected from different ^{1}H-SS-NMR measurements, which correlated with simulated data, were supposing an enhancement of the π-stacking brought by the *exo*-phenyl groups leading, consequently, to much closely packed columns than the alkylated HBCs[196].

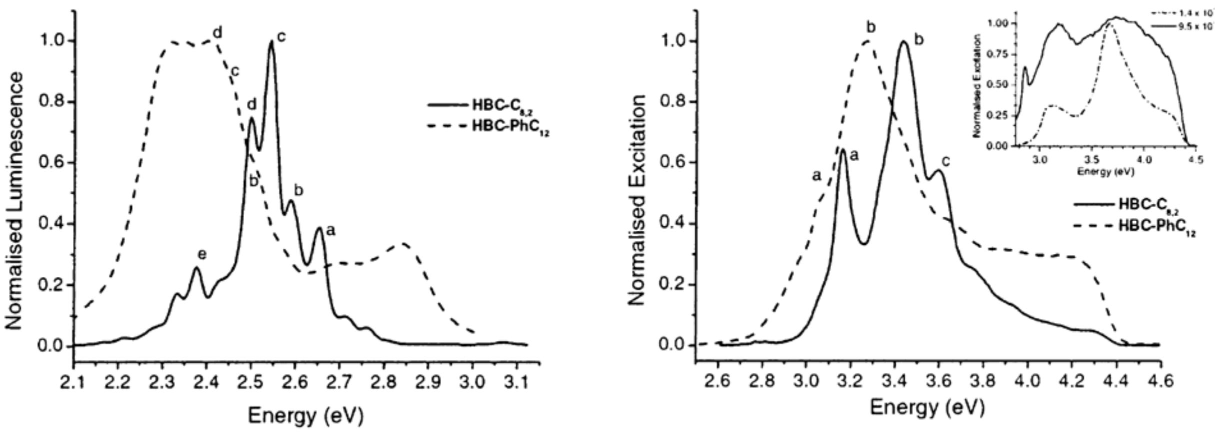

Figure 13.4. Normalized high concentration luminescence (left) and normalized high concentration luminescence-excitation (at 1.4 x 10^{-6} M). Inset: comparison of excitation collected at 2.69 eV of isolated molecules at 10^{-13} M and noncoupled molecules at 1.4 x 10^{-6} M (dashed dotted line).

In summary, optical spectroscopy is a helpful tool for an immediate detection of HBCs after performing a reaction. Additionally, it permits a direct observation and study of the aggregation phenomenon. In spite of the high insolubility of the HBC derivatives bearing perfluorinated chains, we were able to characterize many of them either by UV spectroscopy or by the more sensitive fluorescence.

13.2 MALDI-TOF mass spectrometry

PAHs are very good candidates for matrix-assisted laser desorption ionization and time-of-flight (MALDI-TOF) analysis since most of them absorb at the laser wavelength (337nm in the case of N_2). Nevertheless, the high insolubility of PAHs has always been the main reason for not analyzing them with MALDI-TOF mass spectrometry since this technique requires a high dilution and a good molecular distribution of the analyte in the matrix. Räder and coworkers[375, 376], have circumvented this hurdle by elaborating a new dry sample preparation that consists of mechanically mixing one part of the analyte with a 500 fold excess of the matrix and grinding them together while cooling with liquid nitrogen to assure a good homogeneity. The mixture is then suspended in a non-solvent (H_2O or cyclohexane), sonicated, and finally deposited on the sample holder for analysis. The choice of the matrix is of high importance and it was proven that good electron acceptors are the best matrices for such type of analytes since most of the PAH derivatives are detected as oxidized radical cations ($M^{\bullet+}$). Räder et al. have used the well-known electron acceptor product 7,7,8,8-tetracyanoquinodimethane (TCNQ) as a matrix, while we preferred to employ trans-2-[3-(4-tert-butylphenyl)-2-methyl-2-propenyliden]-malononitrile (DCTB), a recently introduced ‘magic’ matrix.

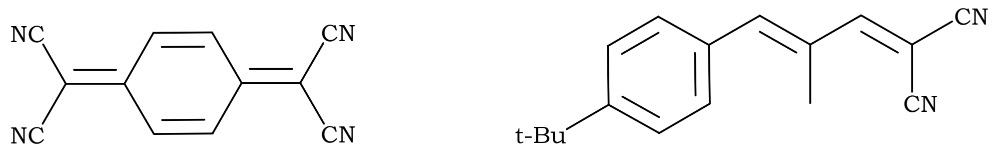

TCNQ **DCTB**

Figure 13.5. Structures of TCNQ & DCTB.

The dry sample method has revealed its efficiency even for the high molecular weight PAHs like, for example, the one depicted in figure 13.6 where the detected peaks match exactly the isotopic patterns, a fact that wouldn’t take place if the mass differed by one additional hydrogen only.

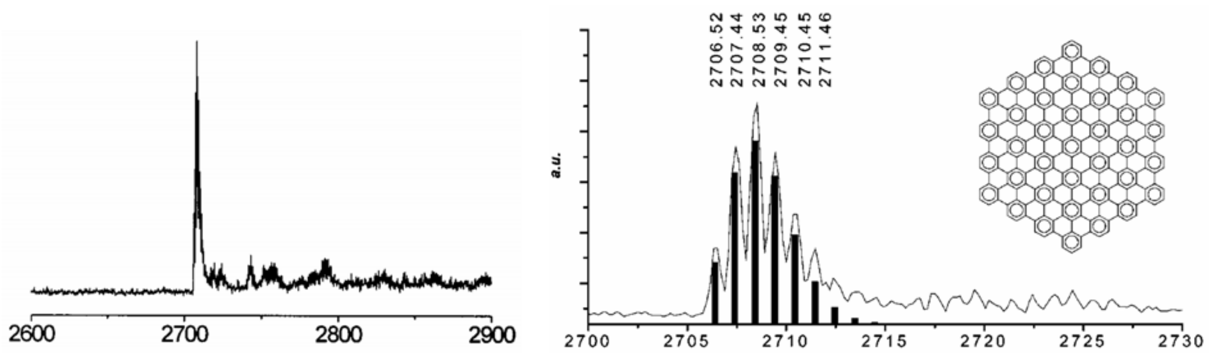

Figure 13.6. MALDI-TOF spectrum obtained by applying the dry sample preparation method using TCNQ as matrix (left) yielding the isotopically resolved MALDI-TOF spectrum of PAH $C_{222}H_{42}$ (right); the bars underneath represent the calculated spectrum[213].

However, the low volatility of the PAHs represents a serious problem since it causes a major decrease of their corresponding signal intensities. This was proven by analyzing a 1:1 mixture of the PAH $C_{222}H_{42}$ (figure 13.6) with its cyclodehydrogenated side products: the mass spectrum is illustrated in figure 13.7 showing that the signal intensity of the side-products is 285 times greater than the desired PAH one. This clearly reveals a much lower desorption and ionization efficiency of the cyclic aromatic product with respect to the partially dehydrogenated and the chlorinated products whose minor presence will be detected by MALDI-TOF spectrometry as the major product.

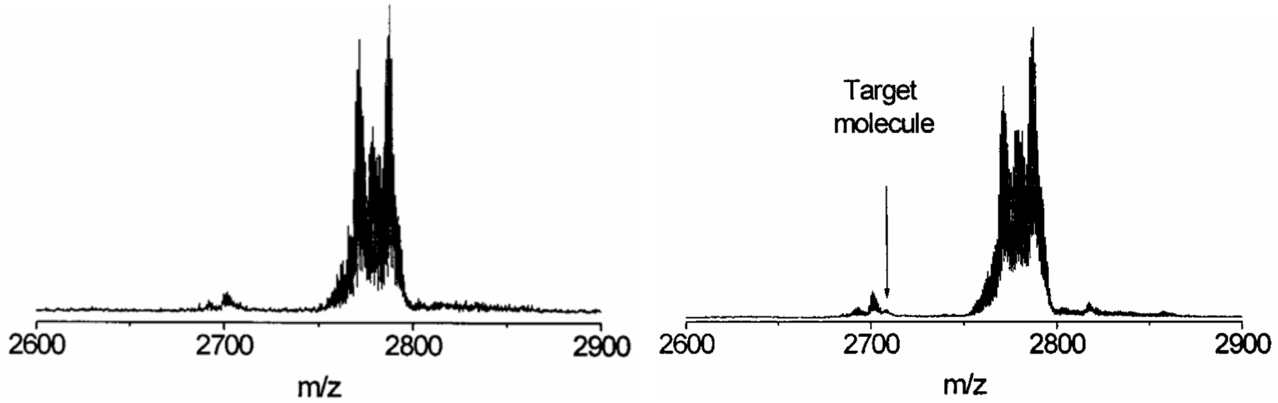

Figure 13.7. Sample containing only side products (left) and a 1:1 mixture of these latter with the desired PAH[375].

MALDI-TOF mass spectrometry analyses of the different HBCs bearing perfluorinated chains have revealed the same aspect as reported by Räder and coworkers, where for a nearly pure sample of HBC-PhRf$_{2,8}$, the presence of trace amounts of the unreacted hexaphenyl benzene starting material (HPB-PhRf$_{2,8}$) is detected with higher signal intensity with respect to the target molecule as figure 13.8 depicts.

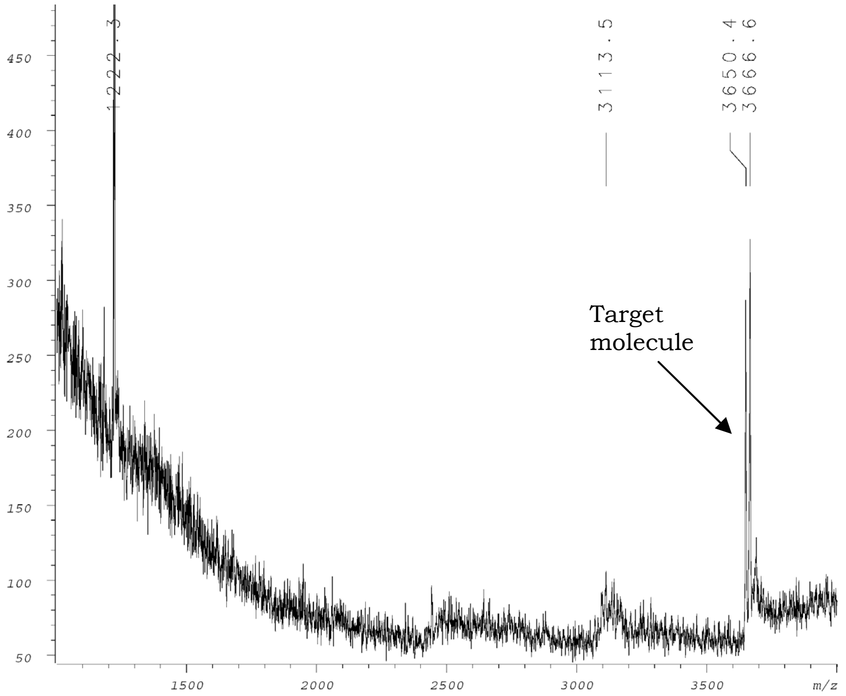

Figure 13.8. MALDI-TOF spectrum HBC-PhRf$_{2,8}$ containing traces of HPB-PhRf$_{2,8}$.

Exhaustive washings of this product with suitable solvents remove the traces of residual starting materials and afford the target molecule HBC-PhRf$_{2,8}$. It is noteworthy that the error of the instrument is estimated to be 3 ppm at maximum.

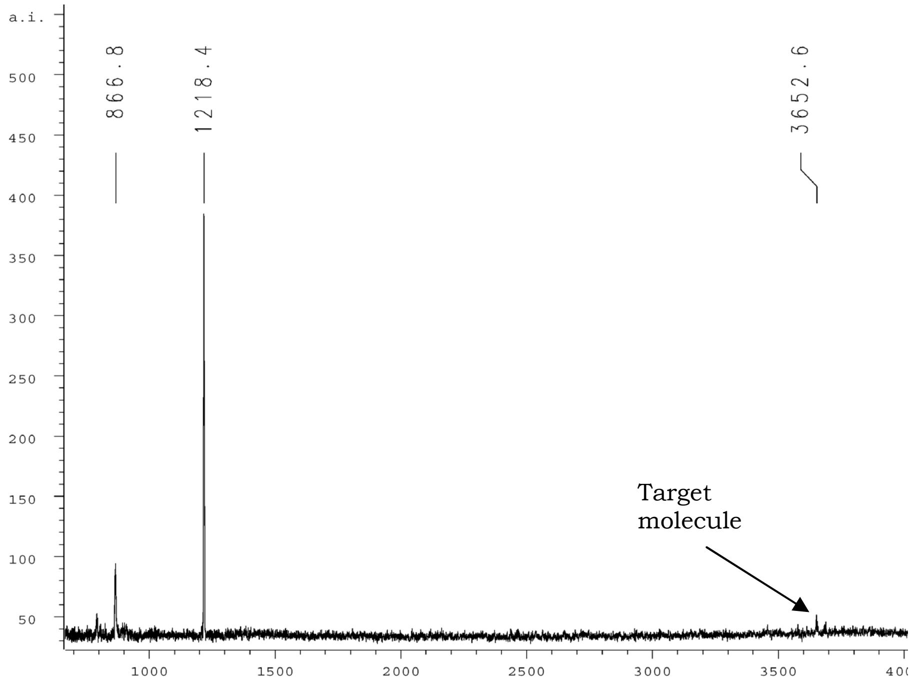

Figure 13.9. MALDI-TOF spectrum of HBC-PhRf$_{2,8}$.

Additionally, many MALDI-TOF mass spectra of products which were isolated after performing unsuccessful cyclodehydrogenation reactions reveal the presence of the starting material as a $(M + 60)^{\bullet+}$ peak as shown in figure 13.10. Likewise, some mass spectra of successful oxidation reactions reveal the presence of the HBC derivatives as $(M + 32)^{\bullet+}$. The structures of these products are still unknown but it is most probably caused by either the sample preparation or an interaction of the products with the matrix.

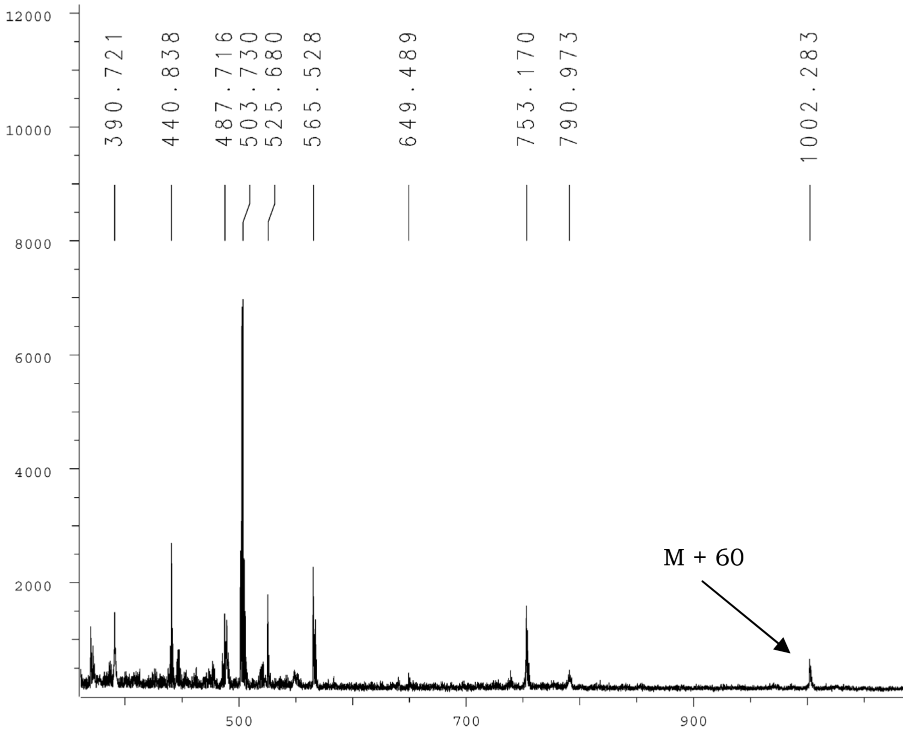

Figure 13.10. MALDI-TOF spectrum of the hexaphenyl benzene HPB-CF_3 as $(M + 60)^{\bullet+}$.

Nonetheless, most of the MALDI-TOF measurements performed on the perfluorinated HBCs have shown very good peak intensities as well as masses matching (albeit unresolved) perfectly the isotopic patterns.

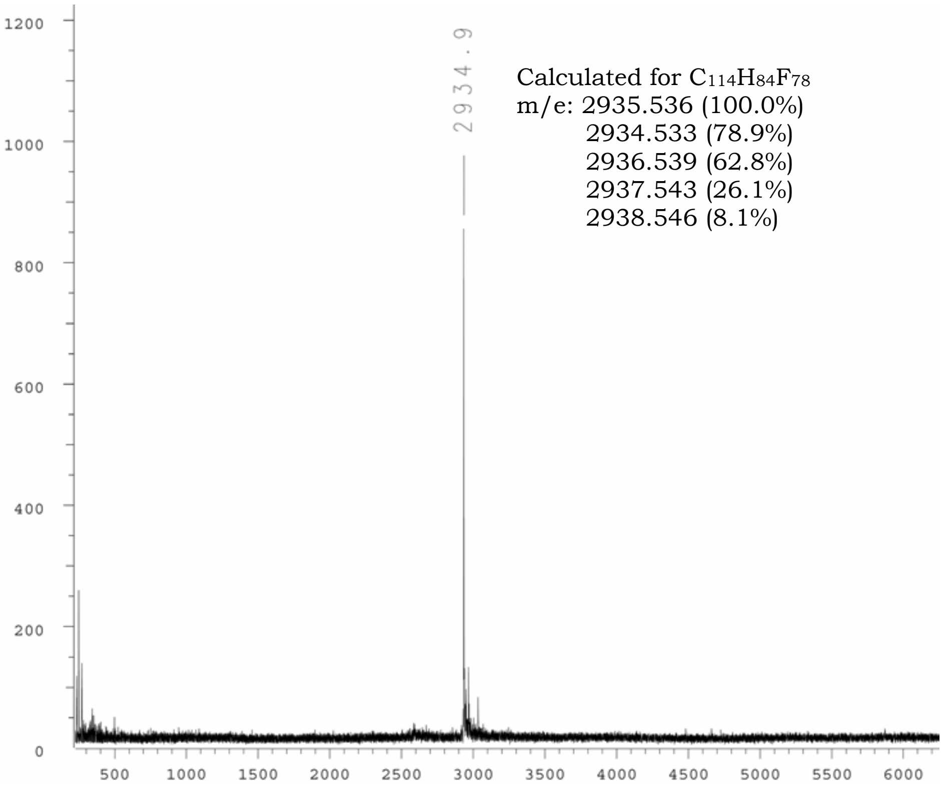

Calculated for $C_{114}H_{84}F_{78}$
m/e: 2935.536 (100.0%)
2934.533 (78.9%)
2936.539 (62.8%)
2937.543 (26.1%)
2938.546 (8.1%)

Figure 13.11. MALDI-TOF spectrum of HBC-$Rf_{6,6}$.

Interestingly, we noticed in many cases mass peaks corresponding to two or three time the molecular weight of the HBC derivatives. This reveals, therefore, that this technique is able to detect the π-stacked aggregates too.

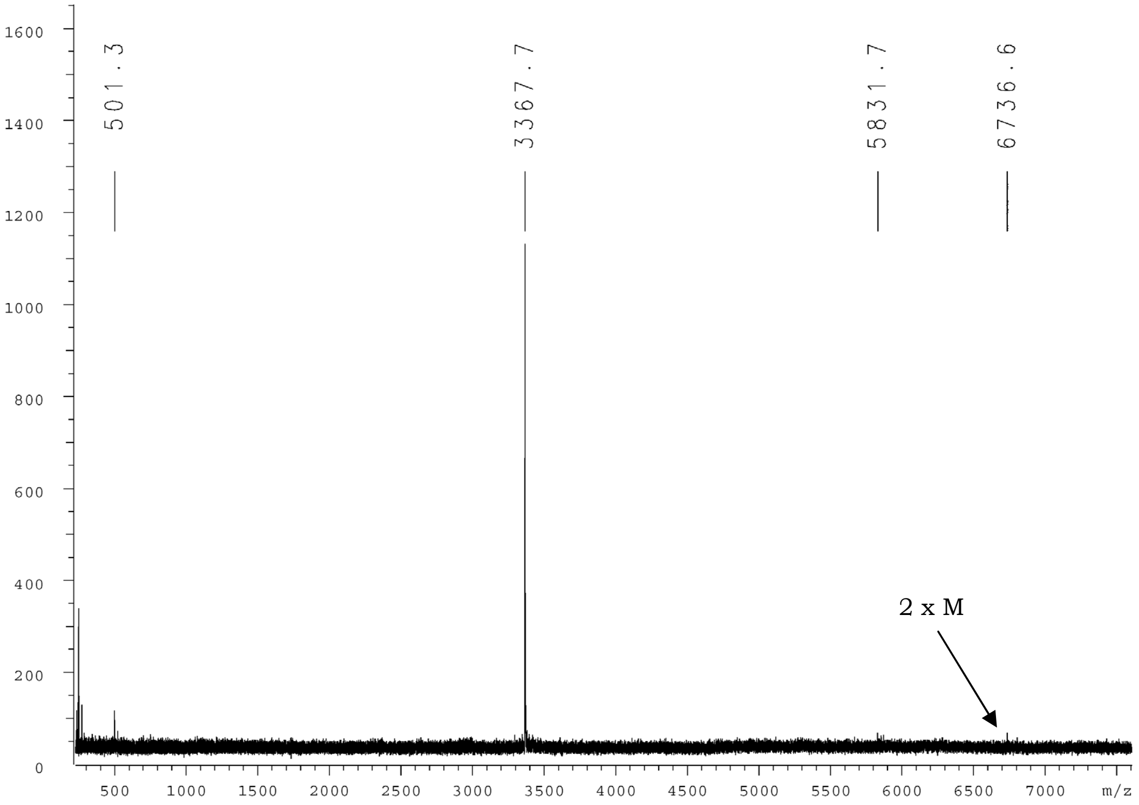

Figure 13.12. MALDI-TOF spectrum of HBC-Rf$_{4,8}$ showing also the (2 x M)$^{\bullet+}$ peak.

This has prompted us to analyze the non-alkylated HBC with the same technique. The MALDI-TOF mass spectrum of this latter product reveals clearly the mass peaks that belong to π-stacked HBCs showing up to six stacked molecular columns as illustrated in figure 13.13.

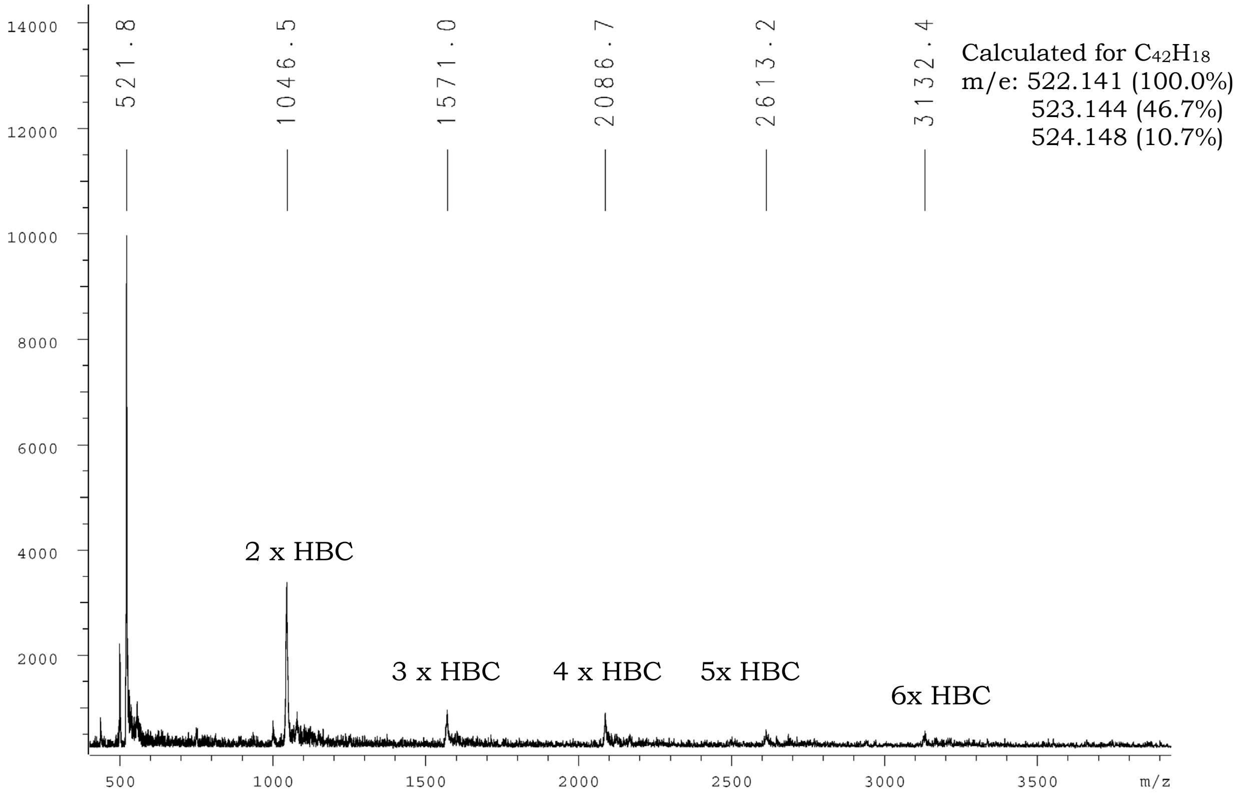

Figure 13.13. MALDI-TOF spectrum of HBC showing the peaks of its columnar stacks up to $(6 \text{ x } M)^{\bullet +}$.

In summary, MALDI-TOF technique is a very efficient tool for characterizing high molecular weight PAHs with low solubility like the ones we have synthesized. However, traces of the starting material or side products present in the medium show up with very high intensity. Additionally, special care must be applied during the sample preparation otherwise the desired peaks won't be detected. Some artifact peaks whose origin is still unknown are present in some of the spectra. Surprisingly, many spectra revealed the presence of dimers and oligomers implicating the possibility of detecting small columnar stacks.

13.3 Solid-state NMR

Few reports describe the use of special ^{1}H-SS-NMR techniques for characterizing and elucidating the degree of order in columnar stacking for different HBCs molecules[195, 377]. Presenting these methods will exceed the aim of this work, however, the authors interpreted the data they have obtained supposing that the HBC derivatives bearing *exo*-phenyl groups have a superior degree of order in columnar stacking that excels the ones that lack these extra phenyls, a conclusion that turned out to be in contradiction to the optical measurements study mentioned in section 13.1. Nevertheless, ^{13}C-CP-MAS can be used as a useful method to detect the presence of HBC derivatives as shown in figure 13.14.

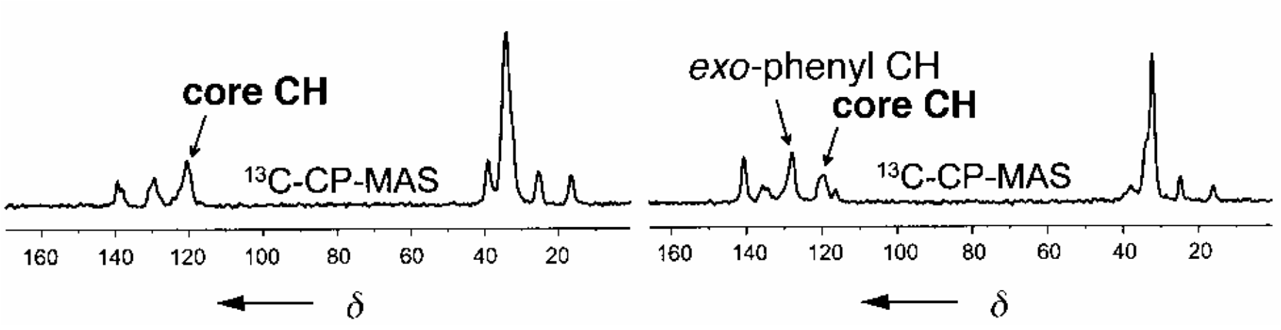

Figure 13.14. ^{13}C-CP-MAS spectra of HBC-C_{12} and HBC-PhC_{12}[196].

Nonetheless, the problems we have encountered when carrying out different SS-NMR experiments to measure the tolane derivative **94** (To-$Rf_{2,8}$), as well as the relatively high amounts required to perform such type of analysis (~150-200 mg), have prevented us from exploring this technique more in depth.

14. General remarks

All the chemical reagents were purchased from Acros, Aldrich, Fluka and Strem unless otherwise specified. Solvents were dried by passing them, under an argon atmosphere, through a special purification system similar to the one proposed by Grubbs and coworkers[378]. The solvents were saturated with argon for 15-30 minutes prior to use. Thin layer chromatography (TLC) analyses were done using aluminum sheets coated with silica gel 60 F_{254}. Column chromatography was carried out using Merck silica gel 60 (0.04-0.063, 230-400 mesh).

NMR spectra were measured with Bruker Avance DRX 500 (^{1}H: 500 & ^{13}C: 125.77 MHz) and Bruker Avance DPX 360 (^{1}H: 360 & ^{13}C: 90.55 MHz) spectrometers using $CDCl_3$, THF-d_8, and C_6D_6 as solvents. Chemical shifts are referred to tetramethyl silane (TMS) as an internal standard. Solid state NMR (SS-NMR) measurements were performed on a Bruker Avance 300 MAS (^{13}C: 75.5 MHz) spectrometer. Electron impact (EI) and electrospray ionization (ESI) mass spectra (MS) were recorded on a Vacuum Generators Micromass VG 70/70E spectrometer and on a FT/ICR mass spectrometer Bruker 4.7T BioApex II, whereas MALDI-TOF spectra were performed on a Bruker Reflex spectrometer with DCTB as matrix. UV-Vis spectra were recorded on a Perkin-Elmer Lambda 40 diode array spectrophotometer using 1,2,4 trichlorobenzene as solvent unless otherwise specified; λ_{max} (logε). GC-MS: ThermoQuest TraceGC 2000/Voyager. IR: FTIR Uicam Mattson 5000 spectrometer.

Differential scanning calorimetry traces were recorded using a Mettler Toledo DSC822e, calibrated with indium (m.p. = 156.6°C, ΔH_f = 28.45 KJ mol^{-1}) before each series of measurements. The samples were placed in an aluminum crucible and analyzed, under a stream of helium and nitrogen, with a heating/cooling rate of 20°C min^{-1}. Polarization optical microscopy (POM) was carried out using an Axioscope Zeiss microscope equipped with a Linkam THMS 600 platinum heating plate connected to a Linkam TMS 93 processor, the photographs were taken with a Fujix Digital camera HC-300Z. Scanning electron microscopy micrographs were recorded using a Philips ESEM FEG XL30 and a Gatan ALTO 2500 Cryo system.

15. Synthesis of the HBC primers

15.1 HBC with R = CF_3

15.1.1 Trimethyl{[4-(trifluoromethyl)phenyl]ethynyl}silane **40**

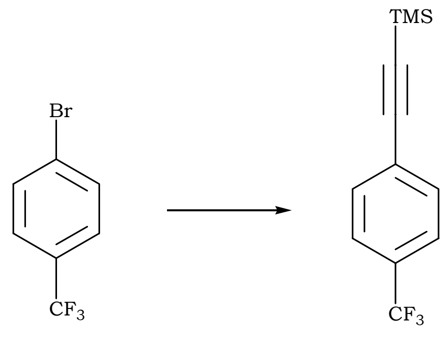

38 **40**

Method A. In a 100 ml two-necked round bottomed flask a solution of 1-bromo-4-(trifluoromethyl)benzene **38** (1.37 ml, 9 mmol), triphenylphosphine (143 mg, 0.54 mmol), CuI (103 mg, 0.54 mmol), and trans-dichlorobis(triphenylphosphine) palladium(II) (193 mg, 0.27 mmol) in piperidine (30 ml) was heated at 80°C, under an argon atmosphere. Trimethylsilylacetylene (TMSA) (1.7 ml, 12 mmol) was then added dropwise under a positive stream of argon and the mixture was stirred at the mentioned temperature for 24 hours. The brown solution was extracted with a saturated solution of NH_4Cl and methylenedichloride (3 x 50 ml), the combined organic layer was then washed with distilled water (3 x 50 ml), dried over Na_2SO_4 and filtered. After removal of the solvent, the residual brown oily product was then purified by flash column chromatography (SiO_2, pentane/hexane 1:1) to yield **40** (2.1 g, 96%) as a faint yellow liquid. TLC (SiO_2, pentane/hexane 1:1): $R_f = 0.71$. ^{1}H-NMR (360 MHz, $CDCl_3$): δ 7.55 (*m*, 4H, Ph), 0.26 (*m*, 9H, TMS). EI-MS: *m/z* 242 ($M^{\bullet+}$, 35%), 227 ($[M-CH_3]^{\bullet+}$, 100%), 223 ($[M-F]^{\bullet+}$, 18%), 197 ($[M-C_2H_6]^{\bullet+}$, 25%).

15.1.2 1-Ethynyl-4-(trifluoromethyl)benzene **41**

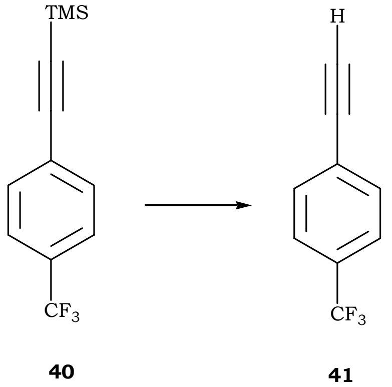

Method B. To a solution of **40** (~0.65 ml, 2.66 mmol), and benzyltriethylammonium chloride (BTACl) (1.4 g, 6 mmol) in dichloromethane (5 ml) was added 20 ml of a 10 M solution of $NaOH_{aq}$ The biphasic solution was then stirred at room temperature for 18 hours. The brown solution was extracted with ether (3 x 25 ml) and the combined organic layer was then washed with distilled water (3 x 25 ml), dried over Na_2SO_4 and filtered. After removal of the solvent, the residual colorless oil was purified by filtration over a short silica gel plug, under reduced pressure, using pentane as eluent affording **41** (0.33 g, 73%). Colorless liquid. TLC (SiO_2, pentane): R_f = 0.77. ^{1}H-NMR (360 MHz, $CDCl_3$): δ 7.59 (*m*, 4H, Ph), 3.2 (*s*, 1H, acetylene).

15.1.3 1-(trifluoromethyl)-4-{[(4-trifluoromethyl)phenyl]ethynyl}benzene **42**

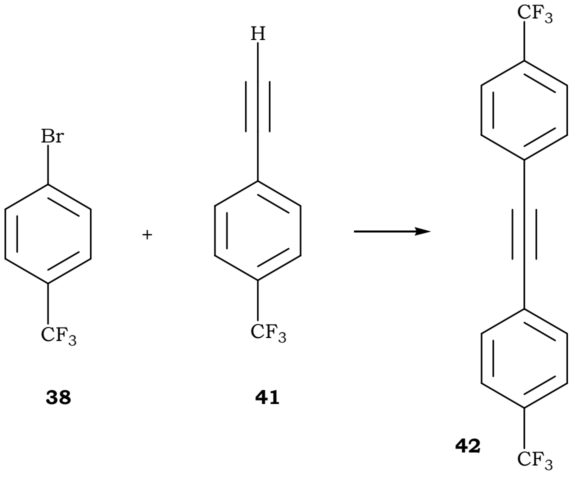

The reaction was done following method A: **38** (0.4 ml, 2.8 mmol), **41** (0.49 g, 2.8 mmol), triphenylphosphine (90 mg, 0.34 mmol), CuI (64 mg, 0.34 mmol), trans-dichlorobis(triphenylphosphine) palladium(II) (120 mg, 0.17 mmol), and piperidine (15 ml). Reaction time: 48 hours. Purification was carried out by filtration over a short silica gel plug, under reduced pressure, using pentane as eluent to yield **42** (0.31 g, 35%) as a white solid. TLC (SiO_2, pentane/methylene dichloride (1:1): $R_f = 0.77$. ^{1}H-NMR (360 MHz, $CDCl_3$): δ 7.64 (*m*, 8H, Ph). ^{13}C-NMR (90.55 MHz, $CDCl_3$): δ 132.1 (Ph), 130.79-130.42 (*q*, ^2J(C, F) = 33 Hz, Ph), 126,49 (Ph), 125.52 (Ph), 119.45-128.47 (*q*, ^1J(C, F) = 272 Hz, CF_3), 90.25 (acetylene). EI-MS: *m/z* 314 ($M^{\bullet+}$, 100%), 295 ($[M-F]^{\bullet+}$, 30%), 264 ($[M-CF_2]^{\bullet+}$, 20%), 225 ($[M-2(C_2F_5) + H]^{\bullet+}$, 16%).

15.1.4 Hexakis[4-(trifluoromethyl)phenyl]benzene **43**

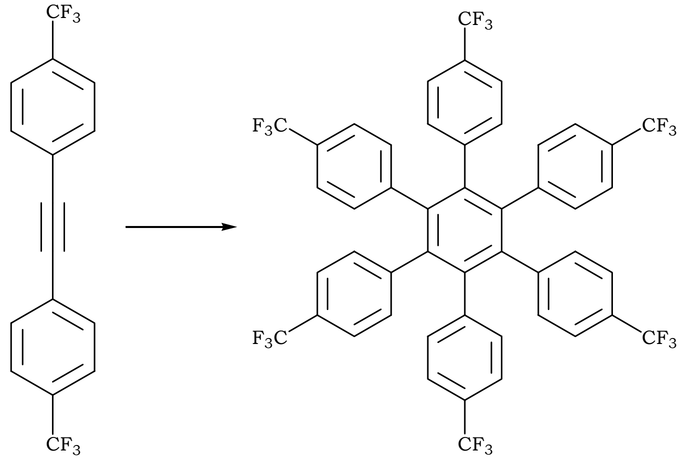

42 **43**

Method C. In a dry 50 ml two-necked round bottomed flask, fitted with a reflux condenser, a suspension of **42** (0.29 g, 0.9 mmol) in dioxane (15 ml) was purged with argon for 30 minutes before $Co_2(CO)_8$ (34 mg, 90 µmol) was then added under a positive stream of argon and the reaction mixture was refluxed for 24 hours. After evaporation of the solvent, the black metallic species were removed by filtration over a short silica gel plug, under reduced pressure, using THF as eluent. The solvent was removed and the residual off-white precipitate was suspended in pentane and collected by suction filtration over Millipore® (404 mg, 67%). ^{1}H-NMR (360 MHz, $CDCl_3$): δ 7.18-7.20 (*m*, 12H, Ph), 6.9-7.93 (*m*, 12H, Ph). ^{13}C-NMR (90.55 MHz, $CDCl_3$): δ 142.55 (Ph), 139.77 (Ph), 131.15 (Ph), 129.31-128.23 (*q*, ^2J(C, F) = 33 Hz, Ph,), 124.26-124.38 (*m*, Ph), 119.2-131.45 (*q*, ^1J(C, F) = 271.4 Hz, CF_3). EI-MS: *m/z* 942 ($M^{\bullet+}$, 100%), 923 ($[M-F]^{\bullet+}$, 10%), 873 ($[M-CF_3]^{\bullet+}$, 8%).

15.1.5 Cyclodehydrogenation of hexakis-[4-(trifluoromethyl)phenyl]benzene **43**

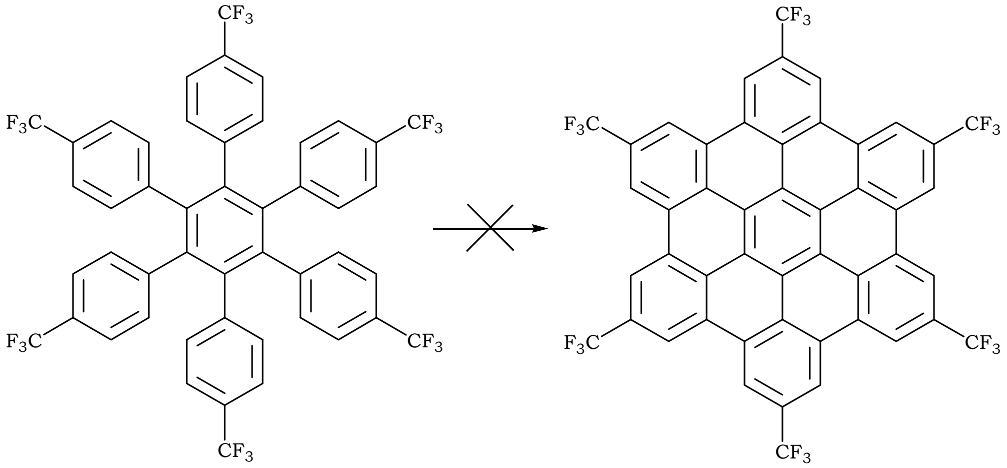

43 **39**

Method D. Copper(II) triflate (1.34 g, 3.6 mmol) was charged in a 50 ml two-necked round bottomed flask and dried completely under vacuum and heating. After reaching room temperature, $AlCl_3$ (0.48 g, 3.6 mmol), **43** (942 mg, 0.1 mmol), and CS_2 (50 ml) were added under an argon atmosphere and the reaction was heated at 30°C for 24 hours followed by quenching the medium with MeOH (50 ml). The residue was then collected by suction filtration over Millipore®, washed successively with NH_4OH_{aq} (10%, 100 ml), HCl_{aq} (1 M, 100ml), H_2O (3 x 50 ml), and ether (100 ml). The yellowish-brown residue was finally dried in vacuum. Yellow solid (12 mg, ~10%). MALDI-TOF: *m/z* 1002 ($[M+72]^{\bullet+}$, 18%), 936 ($[M-6]^{\bullet+}$, 9%), 503 (100%).

15.2 Tolane with R = *p*-PhCF$_3$

15.2.1 Trimethyl{[4'-(trifluoromethyl)-1,1'-biphenyl-4-yl]ethynyl}silane **53**

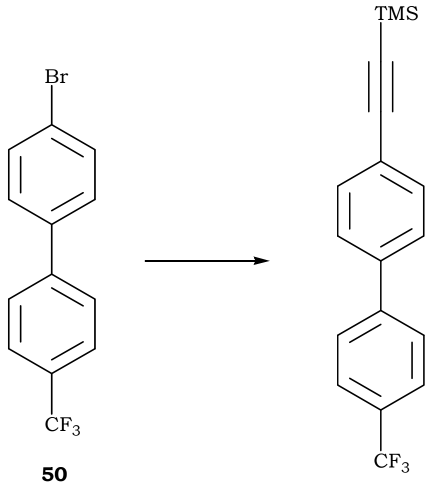

50

53

The reaction was carried out employing method A: 4-bromo-4'-(trifluoromethyl)-1,1'-biphenyl[259, 325] **50** (1.05 g, 3.5 mmol), TMSA (0.65 ml, 4.55 mmol), triphenylphosphine (56 mg, 0.21 mmol), CuI (40 mg, 0.21 mmol), trans-dichlorobis(triphenylphosphine) palladium(II) (75 mg, 0.1 mmol), and piperidine (10 ml). Purification was carried out by filtration over a short silica gel plug, under reduced pressure, using pentane as eluent to yield **53** (0.83 g, 75%) as a white solid. TLC (SiO$_2$, pentane: R$_f$ = 0.65). ^{1}H-NMR (360 MHz, CDCl$_3$): δ 7.69 (*br. s*, 4H, Ph), 7.52-7.58 (*m*, 4H, Ph), 0.27 (*s*, 9H, TMS).

15.2.2 4-Ethynyl-4'-(trifluoromethyl)-1,1'-biphenyl **54**

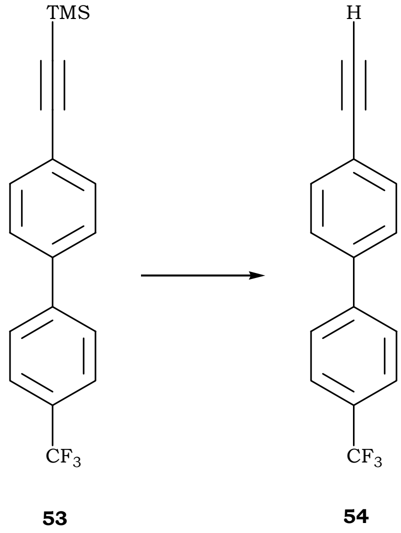

Applying method B: **53** (0.83 g, 2.61 mmol), BTACl (1.2 g, 5.22 mmol), $NaOH_{aq}$ (10 M, 20 ml), CH_2Cl_2 (3 ml). Filtration over a short silica gel plug, under reduced pressure, with pentane as eluent afforded **54** (0.53 g, 83%) as a white solid. TLC (SiO_2, pentane: R_f = 0.62. ^{1}H-NMR (360 MHz, $CDCl_3$): δ 7.67-7.72 (*m*, 4H, Ph), 7.55-7.61 (*m*, 4H, Ph), 3.16 (*s*, 1H, acetylene).

15.2.3 4-(Trifluotomethyl)-4'-{[4'-(trifluoromethyl)-1,1'-biphenyl-4-yl]ethynyl}-1,1'-biphenyl **55**

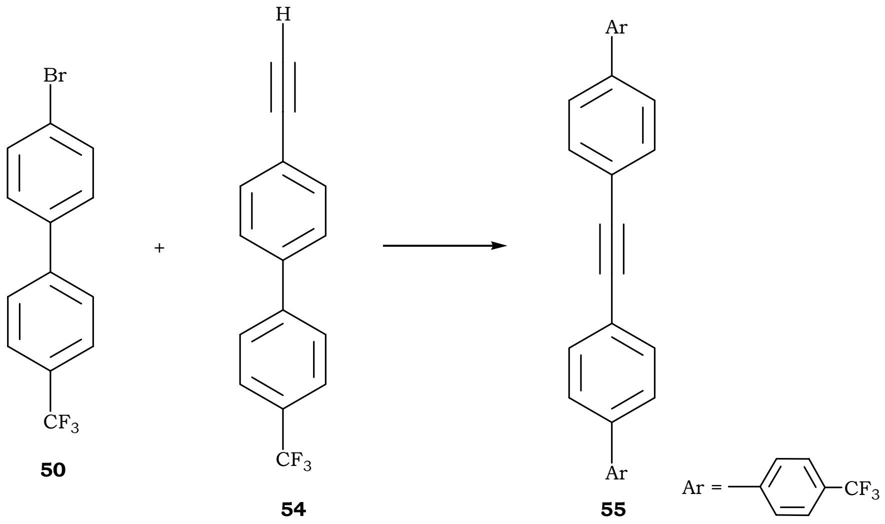

Method E. 4-Bromo-4'-(trifluoromethyl)-1,1'-biphenyl **50** (0.3 g, 1 mmol), **54** (0.25 ml, 1 mmol), tetrakis(triphenylphosphine) palladium(0) (70 mg, 60 µmol), and CuI (40 mg, 0.15

mmol) were placed in a 100 ml two-necked round bottomed flask fitted with a reflux condenser and dried under vacuum. Piperidine (10 ml) was then injected in the medium and the solution was reacted at 85°C for 24 hours, under an argon atmosphere. The orange-brown suspension was extracted with a saturated solution of NH_4Cl and methylenedichloride (3 x 50 ml), the combined organic layer was then washed with distilled water (3 x 50 ml), condensed to the fifth of its volume and the white precipitate was collected by vacuum filtration over Millipore® affording **55** (0.3 g, 65%). EI-MS: *m/z* 466 ($M^{\bullet +}$, 100%), 227 ($[M\text{-}CF_3+H]^{\bullet +}$, 9%).

15.3 HBC with R = 3,5-Ph(CF_3)$_2$

15.3.1 4’-{[3’, 5’-bis(trifluoromethyl)-1,1’-biphenyl-4-yl]ethynyl}-3,5-bis(trifluoromethyl)-1,1’-biphenyl **58**

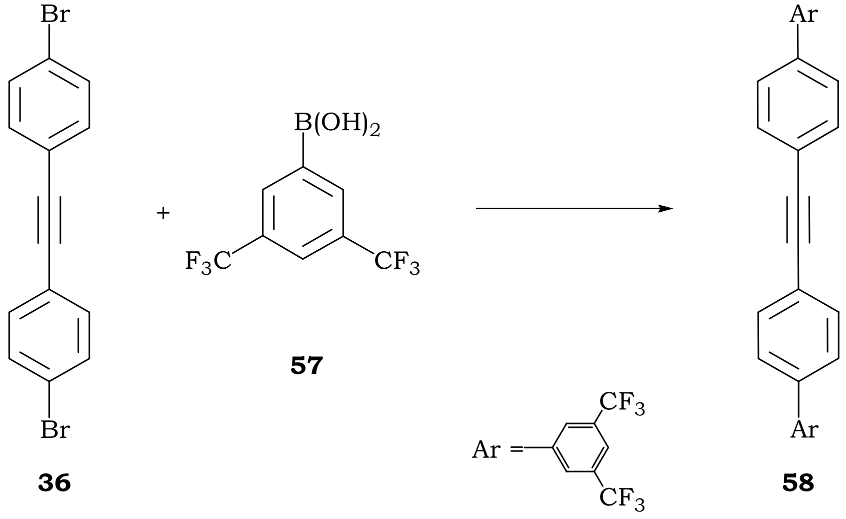

Method F. In a 100 ml two-necked round bottomed flask fitted with a reflux condenser, 4,4’-dibromotolane[221] **36** (0.34 g, 1 mmol), the boronic acid derivative **57** (0.53 g, 2 mmol), tetrakis(triphenylphosphine) palladium(0) (116 mg, 0.1 mmol), and K_2CO_3 (2.23 g, 16 mmol) were placed under an argon atmosphere. A solution mixture constituted of toluene (16.8 ml), ethanol (4.2 ml) and H_2O (8.4 ml) was injected in the medium and the resulting biphasic solution was reacted at reflux for 48 hours, under an argon atmosphere. The dark brown biphasic solution was then extracted with $NH_4Cl_{sat.}$ and methylenedichloride (3 x 50 ml). The combined organic layer was washed with H_2O (3 x 50 ml), dried over Na_2SO_4, and filtered. Removal of the solvent yielded a black solid which was filtered over a short silica gel plug, under reduced pressure, using a 4:1 mixture of pentane/CH_2Cl_2 in order to eliminate the metallic species. The residual yellow solid was then recrystallized from chloroform (or hexane) yielding **58** (0.36 g, 60%) as a faint yellow liquid. ^{1}H-NMR (360 MHz, $CDCl_3$): δ 8.04 (*s*, 2H, Ph), 7.88 (*s*, 1H, Ph), 7.69-7.71 (*d*, ^3J(H,H) = 8.17 Hz , 2H, Ph), 7.63-7.65 (*d*, ^3J(H,H) = 8.17 Hz, 2H, Ph). ^{13}C-NMR (90.55 MHz, $CDCl_3$): δ 142.78 (Ph), 138.45 (Ph), 132.93 (Ph), 132.15-133.25 (*q*, ^2J(C, F) = 37 Hz, Ph), 127.64 (Ph), 127.47 (Ph), 122.21 (Ph), 121.67 (Ph), 119.2-128.23 (*q*, ^1J(C, F) = 272.8 Hz, CF_3), 90.79 (acetylene). EI-MS: *m/z* 602 ($M^{\bullet +}$, 42%), 583 ($[M-F]^{\bullet +}$, 5%), 390 ($[M-Ph(CF_3)_2+H]^{\bullet +}$, 100%).

15.3.2 Hexakis{4-[3’,5’-bis(trifluoromethyl)]-1,1’-biphenyl}benzene **59**

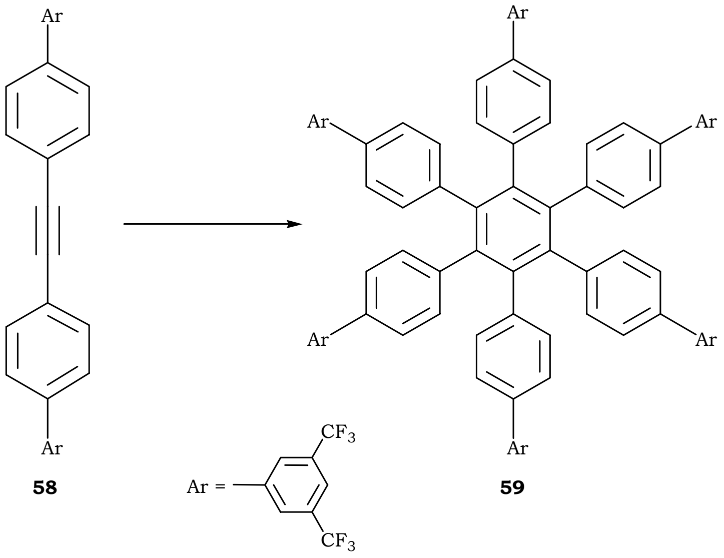

The reaction was done according to method C: **58** (0.27 g, 0.46 mmol), $Co_2(CO)_8$ (17.3 mg, 46 µmol) and dioxane (10 ml). After removal of the solvent, the resulting black precipitate was suspended in THF and washed successively with HCl_{aq} (1 M, 2 x 50 ml) and H_2O (3 x 50 ml). The organic layer was evaporated and the resulting beige product was suspended in ether and collected by suction filtration over Millipore®. The white precipitate was isolated after exhaustive washings with ether and CH_2Cl_2 (0.23 g, 83%). EI-MS: *m/z* 1806 ($M^{•+}$, 10%), 1595 ($[M\text{-}Ph(CF_3)_2+H]^{•+}$, 100%). MALDI-TOF: *m/z* 1808 ($M^{•+}$, 30%), 752 (100%).

15.3.3 2,5,8,11,14,17-Hexakis[3,5-bis(trifluoromethyl)phenyl]hexabenzo[*bc,ef,hi,kl,no,qr*]-coronene **45**

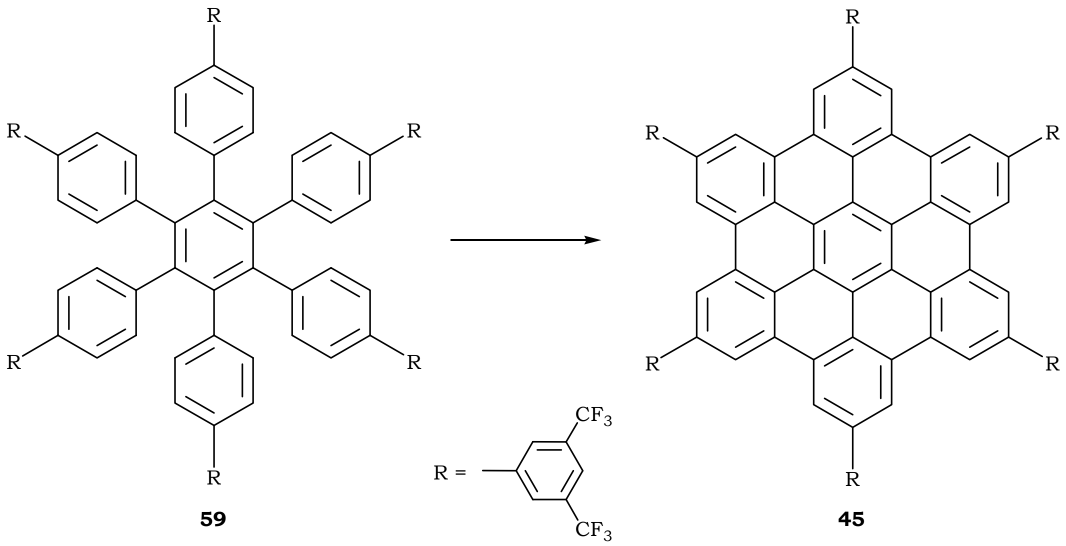

The cyclodehydrogenation reaction was carried out employing method D: **59** (100 mg, 55 µmol), $Cu(OTf)_2$ (0.82 g, 2.19 mmol), $AlCl_3$ (0.3 g, 2.19 mmol) and CS_2 (140 ml). Time of reaction: 39 hours at 35°C. The residue was collected by suction filtration over Millipore®, washed successively with NH_4OH_{aq} (10%, 60 ml), HCl_{aq} (1 M, 60ml), H_2O (60 ml) and ethanol (100 ml). The brown precipitate was washed subsequently with CH_2Cl_2 (160 ml), ether (60 ml), chloroform (60 ml) and finally THF (150 ml) and the resulting yellow precipitate was dried in vacuum (90 mg, 90%). MALDI-TOF: *m/z* 1797 ($M^{\bullet +}$, 20%), 747 (50%), 498 (100%).

15.4 HBC with R = OCF_3

15.4.1 Trimethyl{[4-(trifluoromethoxy)phenyl]ethynyl}silane **61**

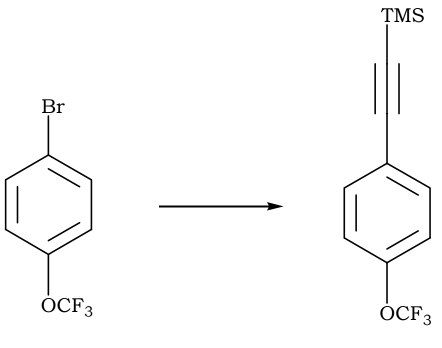

60 **61**

The trimethylsilylated acetylene derivative was synthesized using method A: **60** (1.35 ml, 9 mmol), TMSA (1.73 ml, 12 mmol), $Pd(PPh_3)_2Cl_2$ (0.19 g, 0.27 mmol), Ph_3P (143 mg, 0.54 mmol), CuI (102 mg, 0.54 mmol) and piperidine (30 ml). Purification was carried out by passing the product, twice, through a short silica gel plug, under reduced pressure, using pentane as eluent to yield **61** with trace amount of **60** (1.39 g, 60% with 95% purity (from ^{1}H-NMR spectrum)) as a faint yellow liquid. TLC (SiO_2, hexane: R_f = 0.76). ^{1}H-NMR (360 MHz, $CDCl_3$): δ 7.54-7.57 (*m*, 2H, Ph), 7.13-7.15 (*m*, 2H, Ph), 0.25 (*s*, 9H, TMS).

15.4.2 1-ethynyl-4-(trifluoromethoxy)benzene **62**

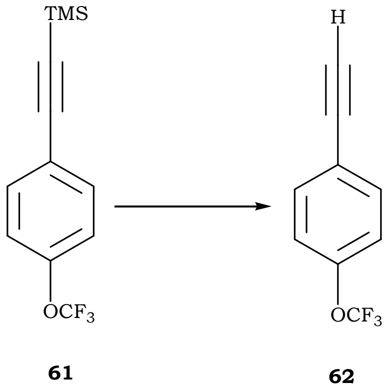

61 **62**

Deprotection was done using method B: **61** (0.58 g, 2.1 mmol), BTACl (1 g, 4.2 mmol), $NaOH_{aq}$ (15 ml, 10 M), and CH_2Cl_2 (5 ml). Filtration over a short silica gel plug, under reduced pressure, with pentane as eluent afforded **62** (0.53 g, 65%) as a faint yellow liquid. TLC (SiO_2, hexane: $R_f = 0.76$). ^{1}H-NMR (360 MHz, $CDCl_3$): δ 7.5-7.53 (*d*, ^3J(H,H) = 8.64 Hz, 2H, Ph), 7.16-7.18 (*d*, ^3J(H,H) = 8.64 Hz, 2H, Ph), 3.1 (*s*, 1H, acetylene).

15.4.3 1-(trifluoromethoxy)-4-{[4-(trifluoromethoxy)phenyl]ethynyl}benzene **63**

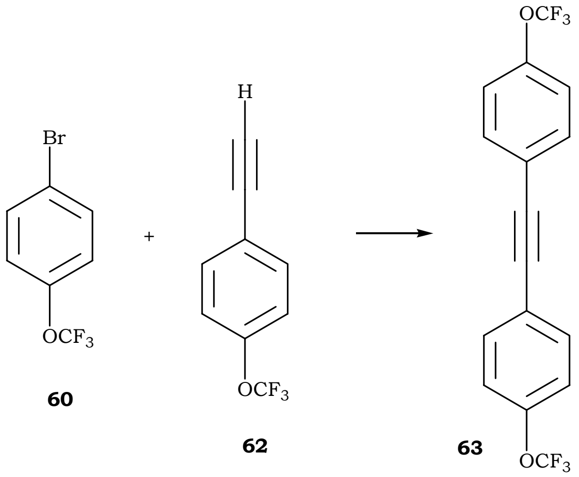

The cross-coupling reaction was carried out employing method E: **60** (0.54 g, 2.2 mmol), **62** (0.41 g, 2.2 mmol), $Pd(PPh_3)_4$ (154 mg, 0.13 mmol), CuI (63 mg, 0.33 mmol), and piperidine (20 ml). The solution was purged with argon for 30 minutes before carrying out the reaction at 85°C for 48 hours. The dark solution was then extracted with $NH_4Cl_{sat.}$ and methylenedichloride (3 x 25 ml). The combined organic layer was washed with H_2O (3 x 25 ml), dried over Na_2SO_4, and filtered. Removal of the solvent yielded a yellowish oily product which was purified by column chromatography using pentane as eluent yielding **63** (0.31 g, 41%) as a faint white solid. TLC (SiO_2, pentane: $R_f = 0.75$). ^{1}H-NMR (360 MHz, $CDCl_3$): δ 7.56-7.52 (*m*, 2H, Ph), 7.21-7.19 (*br. d*, 2H, Ph). ^{13}C-NMR (90.55 MHz, $CDCl_3$): δ 149.47 (Ph), 133.48-133.57 (Ph), 122.03 (Ph), 121.15 (Ph), 116.52-125.07 (*q*, ^1J(C, F) = 257.6 Hz, CF_3), 89.09 (acetylene). EI-MS: *m/z* 346 ($M^{\bullet+}$, 100%), 277 ($[M-CF_3]^{\bullet+}$, 45%).

15.4.4 Hexakis[4-(trifluoromethoxy)phenyl]benzene **64**

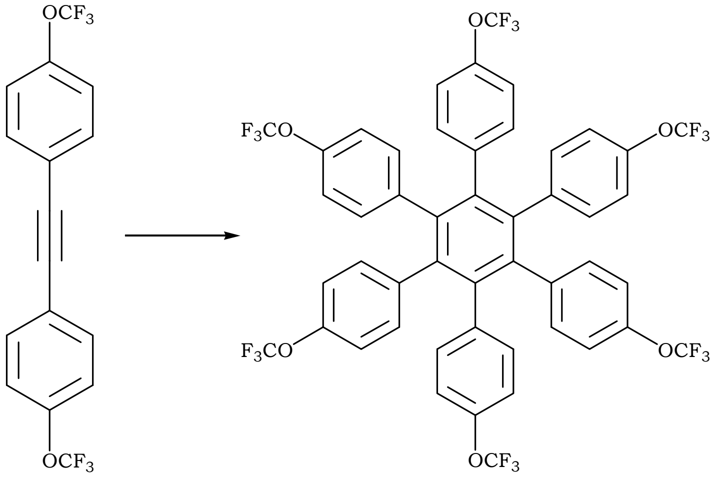

63 **64**

The trimerization reaction was done according to method C: **63** (0.31 g, 0.87 mmol), $Co_2(CO)_8$ (16.5 mg, 44 µmol) and dioxane (15 ml). The black precipitate was filtered over a short silica gel plug, under reduced pressure, using THF as solvent and the resulting yellow-brown solid was suspended in pentane and collected by suction filtration over Millipore®. The off-white precipitate was isolated after several washings with pentane (0.21 g, 71%). ^{1}H-NMR (360 MHz, $CDCl_3$): δ 6.88-6.9 (*br. d*, 12H, Ph), 6.8-6.83 (*br. d*, 12H, Ph). ^{13}C-NMR (90.55 MHz, $CDCl_3$): δ 147.78 (Ph), 140.29 (Ph), 138.75 (Ph), 132.85 (Ph), 120.23 (Ph), 116.44-124.93 (*q*, ^1J(C, F) = 256.28 Hz, CF_3). EI-MS: *m/z* 1038 ($M^{\bullet +}$, 100%), 954 ($[M-OCF_3+H]^{\bullet +}$, 10%), 867 ($[M-2(OCF_3)+2H)]^{\bullet +}$, 5%), 346 (42%).

15.4.5 2,5,8,11,14,17-Hexakis(trifluoromethoxy)hexabenzo[*bc,ef,hi,kl,no,qr*]coronene **65**

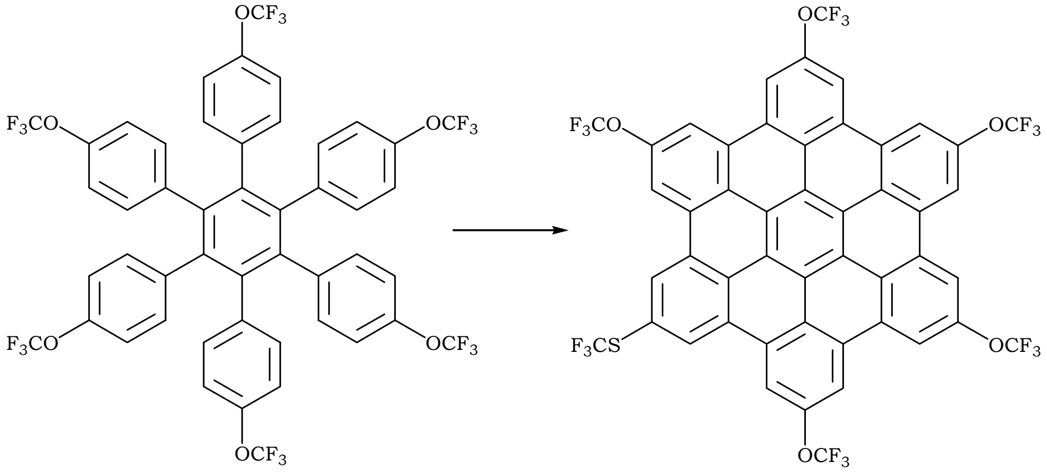

64 **65**

The oxidation reaction was carried out following method D: **64** (104 mg, 0.1 mmol), $Cu(OTf)_2$ (1.49 g, 4 mmol), $AlCl_3$ (0.54 g, 4 mmol) and CS_2 (130 ml). The green-brown residue was collected by suction filtration over Millipore®, washed successively with HCl_{aq} (1 M, 50ml), H_2O (50 ml), NH_4OH_{aq} (10%, 50 ml), H_2O (50 ml), ethanol (50 ml), CS_2 (50 ml), and CH_2Cl_2 (50 ml). The resulting yellow-green precipitate was dried in vacuum (14 mg, 14%). MALDI-TOF: *m/z* 1026 ($M^{\bullet+}$, 6%), 564 ($[M-3(OCF_3)-3(CF_3)]^{\bullet+}$, 100%). UV-Vis: 361 (5.2), 389 (5.06), 423.49 (4.76).

15.5 HBC with R = SCF_3

15.5.1 1-[(trifluoromethyl)thio]-4-({4-[(trifluoromethyl)thio]phenyl}ethynyl)benzene **69**

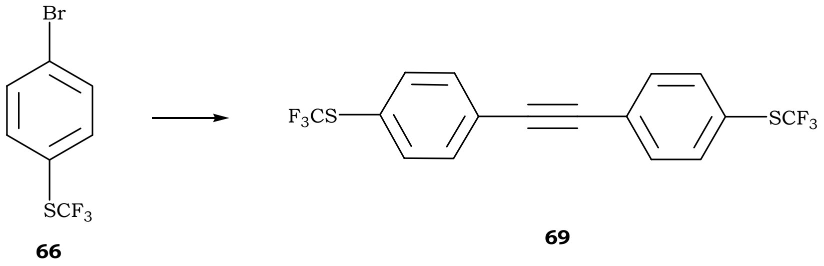

A dry three-necked round bottomed flask, kept under an argon atmosphere was charged with **66** (0.45 ml, 3 mmol), $Pd(PPh_3)_2Cl_2$ (43 mg, 60 µmol), Ph_3P (24 mg, 90 µmol), CuI (17 mg, 90 µmol), and piperidine (10 ml). The argon balloon was replaced by a bubbler and the solution was then purged with acetylene for 20 minutes at room temperature followed by heating the solution at 80°C. The acetylene stream was stopped after 6 hours and the reaction was run at the same temperature for 18 additional hours, under an argon atmosphere (total reaction time: 24 hours). The dark brown solution was extracted with $NH_4Cl_{sat.}$ and CH_2Cl_2 (3 x 25 ml). The combined organic layer was washed with H_2O (3 x 25 ml), dried over Na_2SO_4, and filtered. Removal of the solvent yielded a yellowish oily product which was purified by filtration, under reduced pressure, over a short silica gel plug using pentane as solvent affording **69** (0.32 g, 57%) as a white solid. TLC (SiO_2, pentane: R_f = 0.84). ^{1}H-NMR (360 MHz, $CDCl_3$): δ 7.64-7.66 (*d*, ^3J(H, H) = 8.172 Hz, 4H, Ph), 7.56-7.58 (*d*, ^3J(H, H) = 8.172 Hz, 4H, Ph). ^{13}C-NMR (90.55 MHz, $CDCl_3$): δ 136.11 (Ph), 132.53 (Ph), 125.47 (Ph), 124.91-133.86 (*q*, ^1J(C, F) = 251 Hz, CF_3), 89.09 (acetylene). EI-MS: *m/z* 378 ($M^{\bullet +}$, 100%), 309 ($[M-CF_3]^{\bullet +}$, 55%), 240 ($[M-2CF_3]^{\bullet +}$, 30%), 208 ($[M-CF_3-SCF_3]^{\bullet +}$, 11%).

15.5.2 Hexakis{4-[(trifluoromethyl)thio]phenyl}benzene **70**

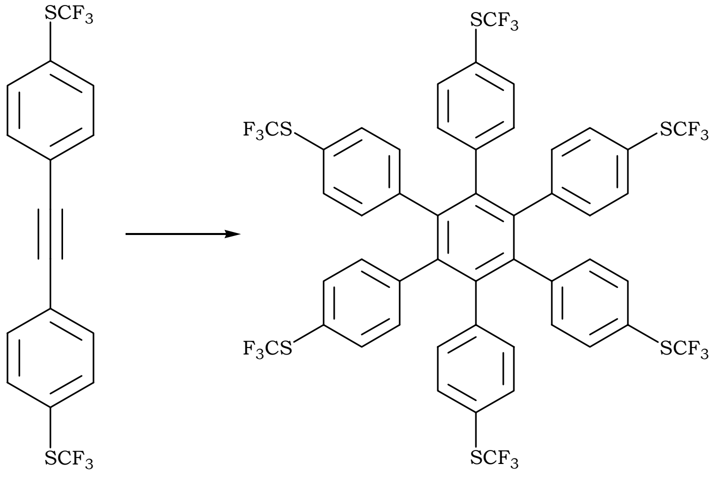

69

70

The reaction was done employing method C: **69** (0.29 g, 0.77 mmol), $Co_2(CO)_8$ (15 mg, 38 µmol) and dioxane (15 ml). After removal of the solvent, the resulting black metallic species were removed by filtration, under reduced pressure, over a short silica gel plug using THF as eluent. The yellow-orange filtrate was evaporated and the resulting orange product was suspended in pentane and collected by suction filtration over Millipore® (0.25 g, 86%). ^{1}H-NMR (360 MHz, $CDCl_3$): δ 7.19-7.26 (*d*, ^3J(H, H) = 8.172 Hz, 12H, Ph), 6.81-6.84 (*d*, ^3J(H, H) = 8.172 Hz, 12H, Ph). ^{13}C-NMR (90.55 MHz, $CDCl_3$): δ 141.77 (Ph), 139.59 (Ph), 135.19 (Ph), 131.87 (Ph), 124.12-134.33 (*q*, ^1J(C, F) = 308 Hz, CF_3), 122.71 (Ph). EI-MS: *m/z* 1134 ($M^{\bullet +}$, 100%), 932 ($[M-2SCF_3]^{\bullet +}$, 10%).

15.5.3 2,5,8,11,14,17-Hexakis[(trifluoromethyl)thio]hexabenzo[*bc,ef,hi,kl,no,qr*]coronene **71**

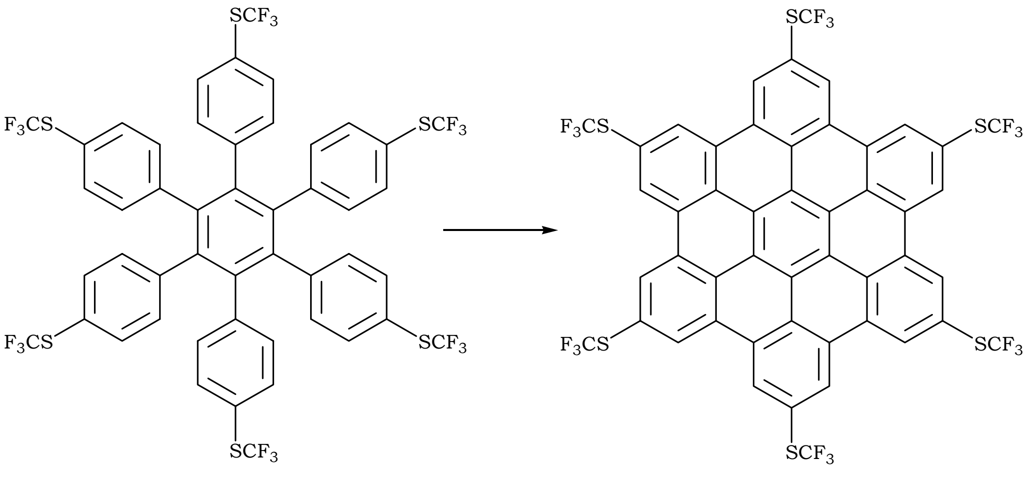

70 **71**

Method G. To a solution of **70** (114 mg, 0.1 mmol) in dry methylene dichloride (30 ml) was added, a degassed solution of anhydrous iron (III) chloride (1.5 g, 9 mmol) in nitromethane (7 ml) during a period of 5-10 minutes. The brown suspension was purged with a steady stream of argon throughout the entire reaction. After stirring for 6 hours, the reaction was quenched with methanol (25 ml) and the resulting yellow suspension was extracted with H_2O and methylene dichloride (3 x 25 ml). The combined organic layer was then evaporated and the bright yellow solid was suspended in pentane, refluxed for 24 hours, and collected by suction filtration over Millipore®. Yellow precipitate (74 mg, 66%). MALDI-TOF: *m/z* 750 ($[M\text{-}3SCF_3\text{-}CF_3]^{\bullet+}$, 8%), 649 ($[M\text{-}4SCF_3\text{-}CF_3]^{\bullet+}$, 35%), 564 (71%), 520 (100%). UV-Vis: 351.49 (4.46), 391.52 (5.07), 422 (4.8).

16. Synthesis of the HBCs with long perfluorinated chains

16.1 Attempted synthesis of HBC with R = *p*-PhC$_6$F$_{13}$

16.1.1 Trimethyl{[4’-(tridecafluorohexyl)-1,1’-biphenyl-4-yl]ethynyl}silane **77**

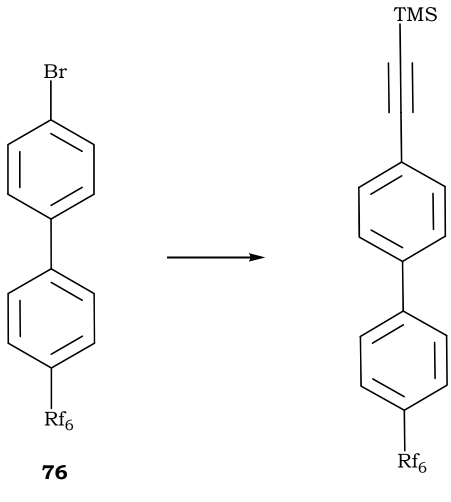

76 **77**

The Sonogashira cross-coupling reaction was carried out according to method A: 4-bromo-4’-(tridecafluorohexyl)-1,1’-biphenyl[325] **76** (2.5 ml, 4.53 mmol), TMSA (0.86 ml, 6.04 mmol), Pd(PPh$_3$)$_2$Cl$_2$ (0.1 g, 0.14 mmol), Ph$_3$P (75 mg, 0.27 mmol), CuI (52 mg, 0.27 mmol) and piperidine (22 ml). Purification by column chromatography using pentane as eluent afforded **77** (1.72 g, 67%) as a white solid. TLC (SiO$_2$, hexane: $R_f = 0.4$). ^{1}H-NMR (360 MHz, CDCl$_3$): δ 7.65-7.73 (*m*, 4H, Ph), 7.56 (*br. s*, 4H, Ph), 0.28 (*s*, 9H, TMS).

16.1.2 4-Ethynyl-4’-(tridecafluorohexyl)-1,1’-biphenyl **78**

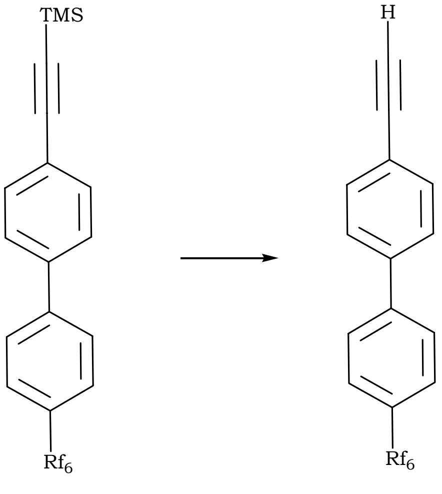

77 **78**

To a solution of **77** (1.72 g, 3.02 mmol) in methanol (170 ml) was added an aqueous solution of NaOH (34 ml, 1 M) and the reaction mixture was stirred overnight at room temperature. After extracting the solution with ether, the organic layer was dried over Na_2SO_4. Recrystallization from methanol yielded **78** as a white solid (1.12 g, 2.26 mmol). ^{1}H-NMR (360 MHz, $CDCl_3$): δ 7.66-7.73 (*m*, 4H, Ph), 7.56-7.62 (*m*, 4H, Ph), 3.17 (*s*, 1H, acetylene).

16.1.3 4-(Tridecafluorohexyl)-4’-{[4’-(tridecafluorohexyl)-1,1’-biphenyl-4-yl]ethynyl}-1,1’-biphenyl **79**

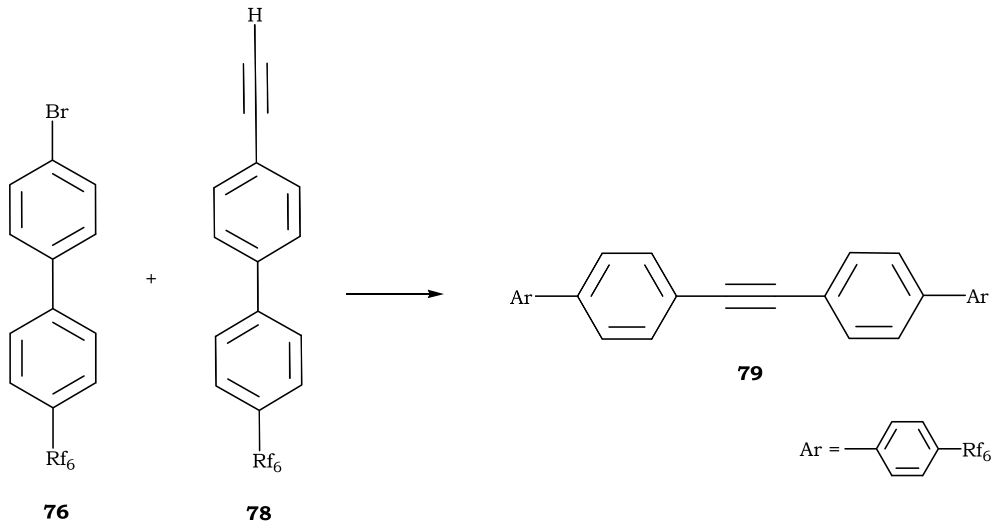

The tolane derivative **79** was synthesized as per method E: **76** (1.2 g, 2.21 mmol), **78** (1.1 g, 2.21 mmol), $Pd(PPh_3)_4$ (154 mg, 0.13 mmol), CuI (63 mg, 0.33 mmol), and piperidine (25 ml). The reaction was carried out at 85°C for 48 hours. The dark solution was then extracted with $NH_4Cl_{sat.}$ and ether (2 x 50 ml). The beige precipitate suspended in the combined organic layer was collected by filtration and refluxed in pentane (60 ml). The resulting off-white precipitate was collected by suction filtration (1.23 g, 58%). ^{1}H-NMR (360 MHz, $CDCl_3$): δ 7.74-7.76 (*d*, 4H, Ph), 7.65-7.7 (*m*, 12H, Ph). EI-MS: *m/z* 966 ($M^{\bullet+}$, 100%), 277 ($[M-(CF_2)_4CF_3]^{\bullet+}$, 85%), 428 ($[M-2(CF_2)_4CF_3]^{\bullet+}$, 18%), 214 (18%).

16.1.4 Hexakis{4-[4'-(tridecafluorohexyl)]-1,1'-biphenyl}benzene **81**

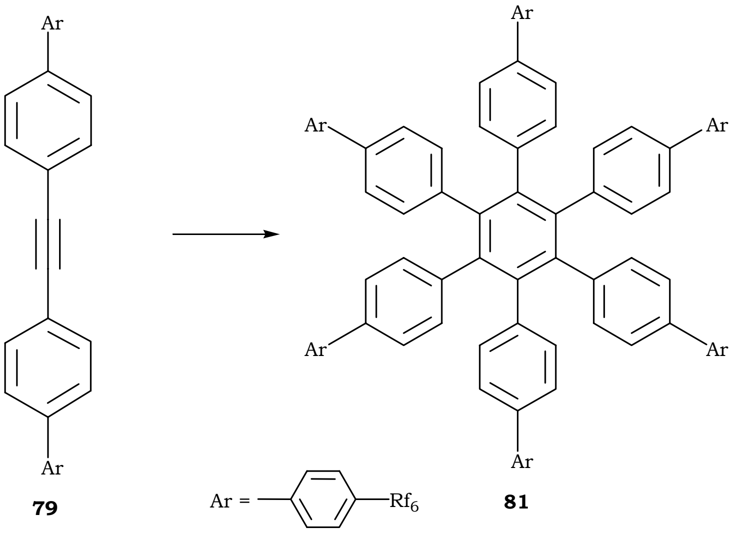

The trimerization reaction was done applying method C: **79** (0.4 g, 0.41 mmol), $Co_2(CO)_8$ (8 mg, 21 µmol) and dioxane (50 ml). After removal of the solvent, the resulting black precipitate was extracted with HCl_{aq} (1 M, 50 ml) and ether (3 x 50 ml). The combined organic layer was washed with H_2O (3 x 50 ml) and concentrated to the fifth of its volume before filtering it on a short silica gel plug, under reduced pressure, in order to remove the residual metallic species. The ethereal layer was evaporated and the resulting white product was suspended in pentane, collected by suction filtration over Millipore® and washed exhaustively with pentane (0.18 g, 48%). ^1H-NMR (360 MHz, $CDCl_3$): δ 7.54 (*br. s*, 24H, Ph) 7.20-7.22 (*d*, ^3J(H, H) = 8.17 Hz, 12H, Ph), 7 -7.03 (*d*, ^3J(H, H) = 8.17 Hz, 12H, Ph). EI-MS: *m/z* 2899 ($M^{•+}$, 100%). MALDI-TOF: *m/z* 2898 ($M^{•+}$, 100%).

16.2 HBC with R = $(CH_2)_2C_8F_{17}$

16.2.1 {[4-(3,3,4,4,5,5,6,6,7,7,8,8,9,9,10,10-heptadecafluorodecyl)phenyl]ethynyl} (trimethyl) silane **90**

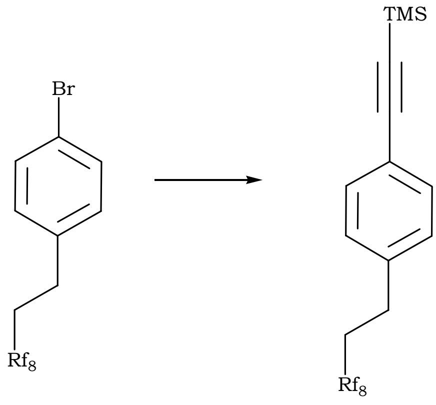

88 **90**

The trimethylsilylated derivative acetylene was synthesized using method A: 4-bromo-perfluorinated derivative[302] **88** (1.35 g, 7.5 mmol), TMSA (1.41 ml, 10 mmol), $Pd(PPh_3)_2Cl_2$ (0.16 g, 0.22 mmol), Ph_3P (0.12 mg, 0.45 mmol), CuI (86 mg, 0.45 mmol) and piperidine (20 ml). Reaction time: 22 hours. Purification was carried out by filtration over column chromatography using pentane as eluent. White solid (3.19 g, 69%). TLC (SiO_2, pentane: $R_f = 0.81$). ^{1}H-NMR (360 MHz, $CDCl_3$): δ 7.41-7.43 (*br. d*, 2H, Ph), 7.14-7.16 (*br. d*, 2H, Ph), 2.88-2.93 (*m*, 2H, $\mathit{CH_2}CH_2Rf_8$), 2.33-2.38 (*m*, 2H, $CH_2\mathit{CH_2}Rf_8$), 0.25 (*s*, 9H, TMS).

16.2.2 1-Ethynyl-4-(3,3,4,4,5,5,6,6,7,7,8,8,9,9,10,10-heptadecafluorodecyl)benzene **92**

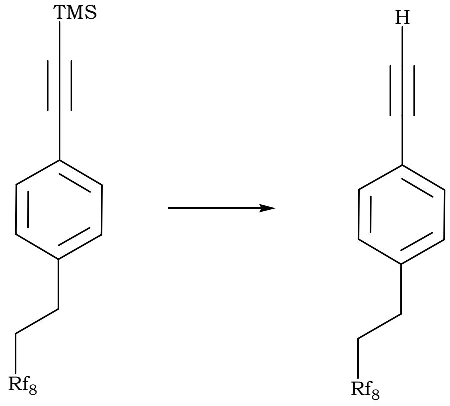

90 **92**

Deprotection was done following method B: **90** (4 g, 6.45 mmol), BTACl (3 g, 13 mmol), $NaOH_{aq}$ (25 ml, 10 M), MeOH (20), CH_2Cl_2 (4 ml). Filtration by column chromatography using pentane as eluent afforded **92** (2.73 g, 80%). TLC (SiO_2, pentane: R_f = 0.76). ^{1}H-NMR (360 MHz, $CDCl_3$): δ 7.44-7.47 (*d*, ^3J(H,H) = 8.17 Hz, 2H, Ph), 7.17-7.19 (*d*, ^3J(H,H) = 8.17 Hz, 2H, Ph), 3.07 (*s*, 1H, acetylene), 2.9-2.94 (*m*, 2H, $\mathit{CH_2}CH_2Rf_8$), 2.29-2.44 (*m*, 2H, $CH_2\mathit{CH_2}Rf_8$).

16.2.3 1-(3,3,4,4,5,5,6,6,7,7,8,8,9,9,10,10-Heptadecafluorodecyl)-4-{[4-(3,3,4,4,5,5,6,6,7,7,8,8,9,9,10,10-heptadecafluorodecyl)phenyl]ethynyl}benzene **94**

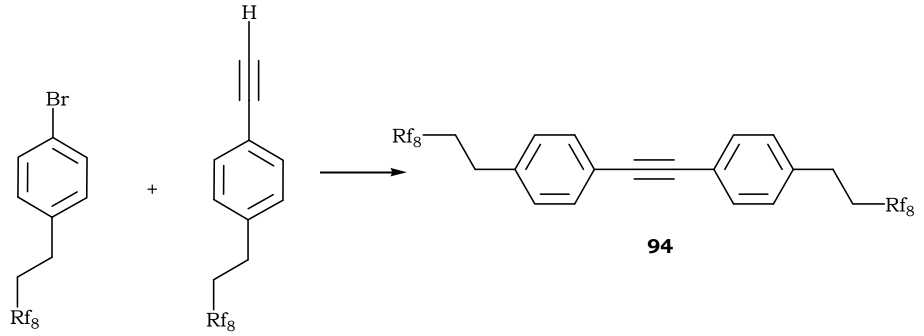

94

88 **92**

The Sonogashira cross-coupling reaction to synthesize the tolane derivative **79** was performed using method E: **88** (1.1 g, 1.8 mmol), **92** (1 g, 1.8 mmol), $Pd(PPh_3)_4$ (117 mg, 0.11 mmol), CuI (52 mg, 0.27 mmol), and piperidine (12 ml). The reaction was carried out at 80°C for 29 hours. The dark solution was extracted with $NH_4Cl_{sat.}$ and pentane (2 x 50 ml) followed by combining the organic layer and washing it with H_2O (2 x 50 ml). The suspended white precipitate was collected by filtration and washed exhaustively with

pentane yielding a white solid (1.17 g, 57%). ^{1}H-NMR (360 MHz, CDCl$_3$): δ 7.48-7.5 (*d*, ^3J(H,H) = 8.17 Hz, 4H, Ph), 7.2-7.22 (*d*, ^3J(H,H) = 8.17 Hz, 4H, Ph), 2.91-2.96 (*m*, 4H, *CH$_2$*CH$_2$Rf$_8$), 2.35-2.5 (*m*, 4H, CH$_2$*CH$_2$*Rf$_8$). EI-MS: *m/z* 1070 (M$^{\bullet+}$, 52%), 637 ([M-CH$_2$(CF$_2$)$_7$CF$_3$]$^{\bullet+}$, 100%), 204 (42%).

16.2.4 Hexakis[4-(3,3,4,4,5,5,6,6,7,7,8,8,9,9,10,10-heptadecafluorodecyl)phenyl] benzene **96**

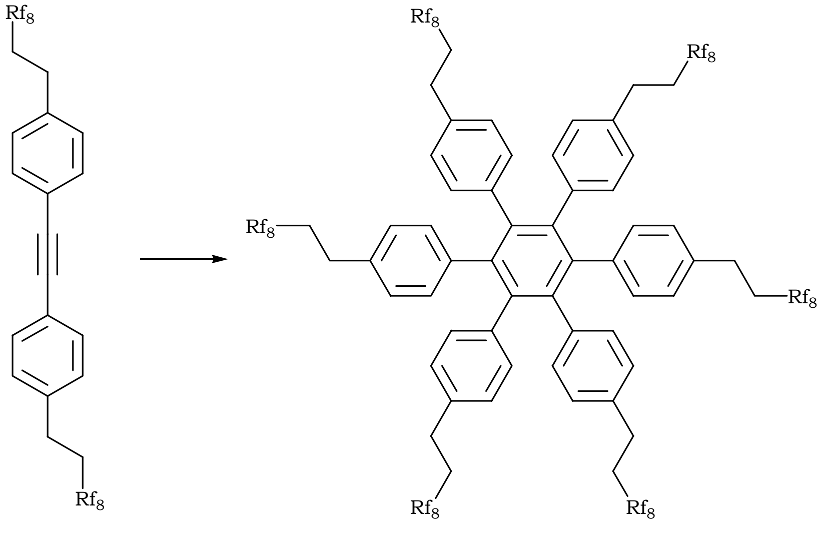

94 **96**

The synthesis of the hexaphenyl benzene derivative **96** was carried out applying method C: **94** (0.4 g, 0.37 mmol), Co$_2$(CO)$_8$ (7 mg, 19 µmol) and dioxane (50 ml). After removal of the solvent, the resulting black precipitate was extracted with HCl$_{aq}$ (1 M, 50 ml) and ether (3 x 50 ml). The combined organic layer was washed with H$_2$O (3 x 50 ml). The ethereal layer was evaporated and the resulting bright orange product was suspended in chloroform to be finally collected by suction filtration over Millipore®. The off-white precipitate was isolated after several washings with ether (194 mg, 49%). ^{1}H-NMR (360 MHz, CDCl$_3$): δ 6.67-6.73 (*m*, 24H, Ph), 2.64-2.68 (*m*, 12H, *CH$_2$*CH$_2$Rf$_8$), 2.06-2.19 (*m*, 12H, CH$_2$*CH$_2$*Rf$_8$). EI-MS: *m/z* 3211 ([M+H]$^+$, 100%). MALDI-TOF: *m/z* 3211 [(M+H]$^+$, 100%), 2839 (78%), 2774 (60%), 2431 (66%), 1725 (77%).

16.2.5 2,5,8,11,14,17-Hexakis(3,3,4,4,5,5,6,6,7,7,8,8,9,9,10,10-heptadecafluorodecyl) hexabenzo[*bc,ef,hi,kl,no,qr*]coronene **98**

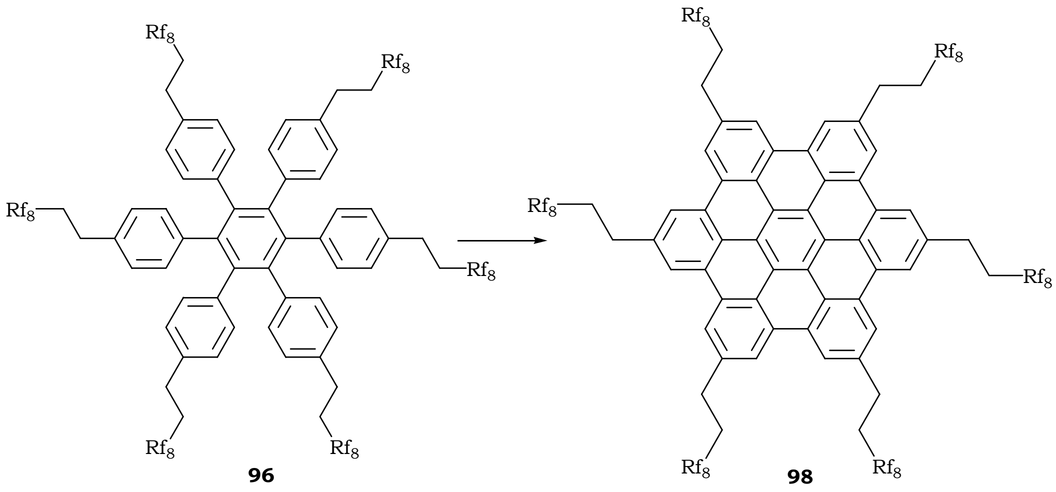

The cyclodehydrogenation reaction was done as per method D: **96** (115 mg, 36 µmol), $Cu(OTf)_2$ (0.53 g, 1.42 mmol), $AlCl_3$ (0.19 g, 1.42 mmol) and CS_2 (120 ml). Reaction time: 24 hours at 30°C. The green residue was collected by suction filtration over Millipore®, washed successively with NH_4OH_{aq} (10%, 60 ml), H_2O (50 ml), HCl_{aq} (1 M, 60ml), ethanol (50 ml), CH_2Cl_2 (60 ml), and $CHCl_3$ (80 ml). The resulting yellow precipitate was suspended in $CHCl_3$ (50 ml) and refluxed for 3 hours. The bright yellow precipitate was collected by suction filtration over Millipore® and washed with a hot solution of $CHCl_3$ (50 ml) followed by an exhaustive washing with THF yielding **98** (21 mg, 19%). MALDI-TOF: *m/z* 3199 ($M^{\bullet+}$, 100%).

16.3 Tolane with R = *p*-Ph(CH$_2$)$_2$C$_8$F$_{17}$

16.3.1 4'-Bromo-1,1'-biphenyl-4-diazonium tetrafluoroborate **85**

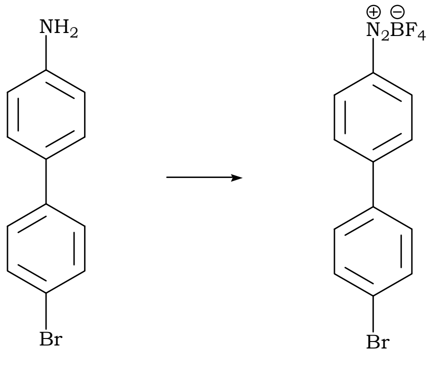

83 **85**

To a cooled solution of 4'-Bromo-biphenyl-4-ylamine[304] **83** (1.3 g, 5 mmol) in tetrafluoroboric acid (8 M, 1.6 ml) and H$_2$O (4 ml) at 0°C, was added dropwise a saturated aqueous solution of sodium nitrite (0.42 g, 6 mmol) during a period of 10 minutes and the reaction mixture was stirred at the same temperature for additional 30 minutes. The precipitate that formed was collected by suction filtration and washed, successively, with chilled solutions of HBF$_4$ (5%, 20 ml), MeOH (20 ml) and ether (20 ml). The off-white precipitate **85** (1.58 g, 92%) was allowed to dry in air overnight and used without characterization.

16.3.2 4-Bromo-4'-[(1*E*)- 3,3,4,4,5,5,6,6,7,7,8,8,9,9,10,10-heptadecafluorodec-1-enyl]-1,1'-biphenyl **87**

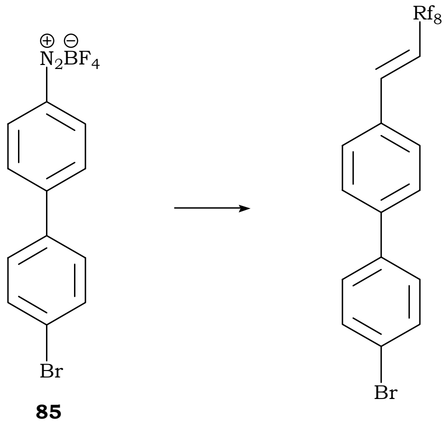

85 **87**

Method H. To a stirred suspension of the diazonium salt **85** (5.9 g, 17 mmol) and palladium acetate (38 mg, 0.17 mmol) in methanol (45 ml), was added dropwise

3,3,4,4,5,5,6,6,7,7,8,8,9,9,10,10-heptadecafluorodec-1-ene (4.7 ml, 17 ml) during 10-15 minutes. The reaction mixture was then warmed at 40°C and allowed to react for additional 90 minutes. After removal of the solvent, the resulting grey product was passed through a silica gel column chromatography using a 4:1 mixture of CH_2Cl_2/pentane as eluent affording **87** (11.02 g, 96%) as a white solid. ^{1}H-NMR (360 MHz, $CDCl_3$): δ 7.54-7.61 (*m*, 6H, Ph), 7.46-7.48 (*br. d*, 2H, Ph), 7.18-7.23 (*d*, 1H, *CH*=$CHRf_8$), 6.19-6.3 (*q*, 1H, CH=*CH*Rf_8). EI-MS: *m/z* 676 ($M^{\bullet+}$, 13%), 307 ($[M-(CF_2)_6CF_3]^{\bullet+}$, 10%), 228 (100%).

16.3.3 4-Bromo-4'-(3,3,4,4,5,5,6,6,7,7,8,8,9,9,10,10-heptadecafluorodecyl)-1,1'-biphenyl **89**

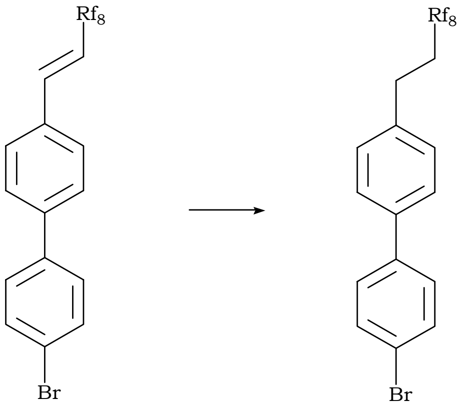

87 **89**

Method I. A solution of **87** (11.6 g, 17 mmol) and Rh/C (0.7 g, 0.34 mmol) in degassed methylene dichloride (60 ml) was placed under 50 atm. of H_2 and the reaction mixture was stirred at room temperature for 40 hours. The solvent was evaporated and the residual black solid was then purified by filtration over silica gel column chromatography using a 4:1 mixture of CH_2Cl_2/pentane as eluent affording **87** (11.37 g, 98%). TLC (SiO_2, pentane: R_f = 0.92). ^{1}H-NMR (360 MHz, $CDCl_3$): δ 7.54-7.57 (*d*, ^3J(H,H) = 8.17 Hz, 2H, Ph), 7.5-7.53 (*d*, ^3J(H,H) = 7.7 Hz, 2H, Ph), 7.43-7.45 (*d*, ^3J(H,H) = 8.17 Hz, 2H, Ph), 7.28-7.3 (*d*, ^3J(H,H) = 7.7 Hz, 2H, Ph), 2.94-2.99 (*m*, 2H, *CH*$_2$$CH_2Rf_8$), 2.33-2.48 (*m*, 2H, CH_2*CH*$_2$$Rf_8$).

16.3.4 {[(3,3,4,4,5,5,6,6,7,7,8,8,9,9,10,10-Heptadecafluorodecyl)-1,1'-biphenyl-4-yl] ethynyl}(trimethyl)silane **91**

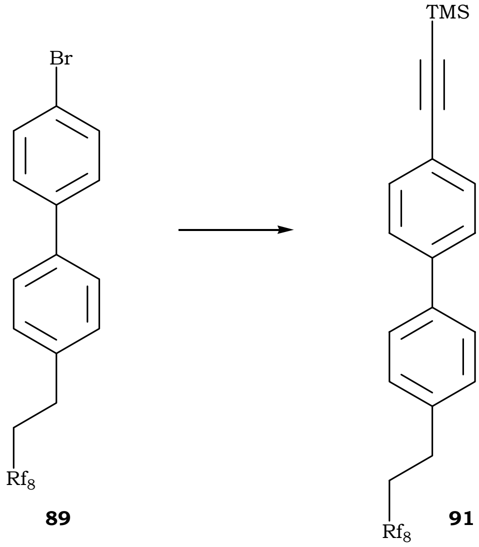

89 **91**

The Sonogashira cross-coupling reaction was done following method A: **89** (2.1 g, 3 mmol), TMSA (0.57 ml, 4 mmol), Pd(PPh$_3$)$_2$Cl$_2$ (65 mg, 90 µmol), Ph$_3$P (50 mg, 0.18 mmol), CuI (35 mg, 0.18 mmol) and piperidine (15 ml). Reaction time: 7 hours. Purification was carried out by column chromatography using pentane as eluent affording **91** (1.43 g, 69%) as a white solid. TLC (SiO$_2$, pentane: R_f = 0.52). ^{1}H-NMR (360 MHz, CDCl$_3$): δ 7.53-7.56 (*m*, 6H, Ph), 7.28-7.3 (*d*, 2H, Ph), 2.94-2.99 (*m*, 2H, *CH$_2$*CH$_2$Rf$_8$), 2.33-2.48 (*m*, 2H, CH$_2$*CH$_2$*Rf$_8$), 0.26 (*s*, 9H, TMS).

16.3.5 4-Ethynyl-4'-(3,3,4,4,5,5,6,6,7,7,8,8,9,9,10,10-heptadecafluorodecyl)-1,1'-biphenyl **93**

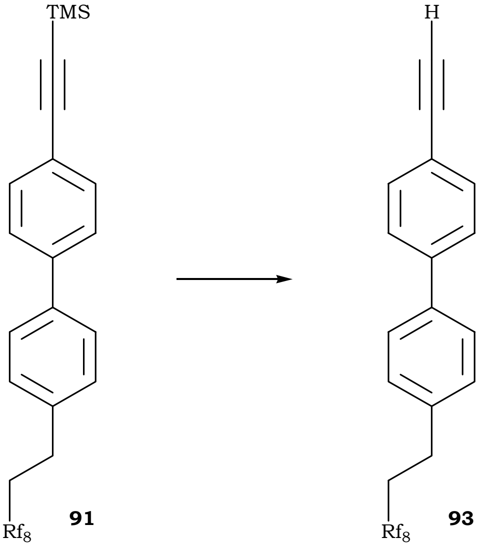

Deprotection was performed according to method B: **91** (1.29 g, 1.85 mmol), BTACl (0.85 g, 3.7 mmol), $NaOH_{aq}$ (10 M, 40 ml), MeOH (20 ml), CH_2Cl_2 (5 ml). Filtration by column chromatography using pentane as eluent afforded **93** (0.96 g, 83%). ^{1}H-NMR (360 MHz, $CDCl_3$): δ 7.53-7.55 (*m*, 6H, Ph), 7.29-7.31 (*d*, 2H, Ph), 3.13 (*s*, 1H, acetylene), 2.94-2.99 (*m*, 2H, $\mathit{CH_2}CH_2Rf_8$), 2.33-2.48 (*m*, 2H, $CH_2\mathit{CH_2}Rf_8$).

16.3.6 4-(3,3,4,4,5,5,6,6,7,7,8,8,9,9,10,10-Heptadecafluorodecyl)-4'-{[4'-(3,3,4,4,5,5,6,6,7,7,8,8,9,9,10,10-heptadecafluorodecyl)-1,1'-biphenyl-4-yl]ethynyl}-1,1'-biphenyl **95**

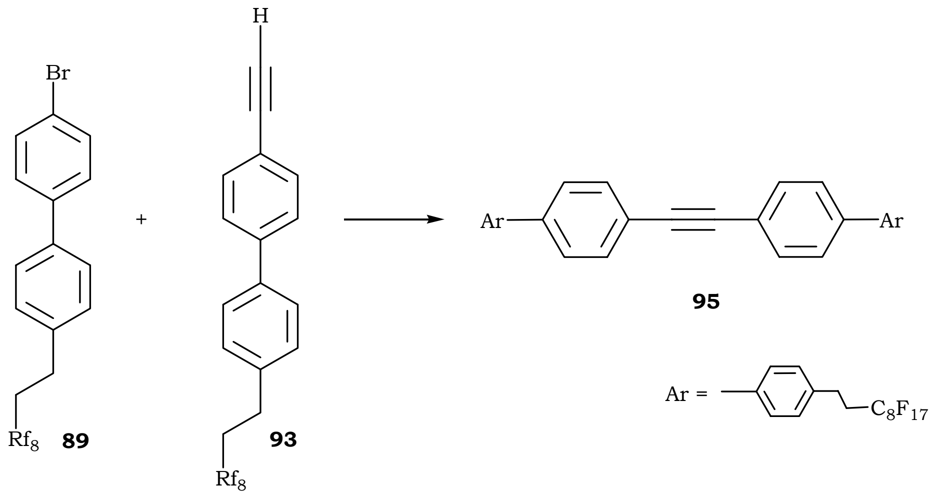

The tolane derivative **95** was synthesized employing method E: **89** (0.95 g, 1.4 mmol), **93** (0.87 g, 1.4 mmol), $Pd(PPh_3)_4$ (0.1 g, 84 µmol), CuI (40 mg, 0.21 mmol), and piperidine (15 ml). The reaction was carried out at 85°C for 29 hours. The brown suspension was then extracted with $NH_4Cl_{sat.}$ and CH_2Cl_2 (3 x 50 ml). The off-white precipitate suspended in the combined organic layer was collected by suction filtration and washed exhaustively with ether then allowed to dry affording **95** (1.04 g, 61%) as a white solid. ^{1}H-NMR (360 MHz, $CDCl_3$): δ 7.57-7.64 (*m*, 14H, Ph), 7.3-7.33 (*d*, 2H, Ph), 2.94-3 (*m*, 4H, $\mathit{CH_2}CH_2Rf_8$), 2.35-2.45 (*m*, 4H, $CH_2\mathit{CH_2}Rf_8$). ^{13}C-SSNMR (75.5 MHz, solid state): 125-136 (*br.*, Ph), 119 (Ph), 110 (Ph), 89 (acetylene), 15-35 (CH_2). EI-MS: *m/z* 1222 ($M^{\bullet+}$, 100%), 1203 ($[M-F]^{\bullet+}$, 5%), 789 ($[M-CH_2(CF_2)_7CF_3]^{\bullet+}$, 58%), 369 (22%).

16.3.7 Hexakis{4-[4'-(3,3,4,4,5,5,6,6,7,7,8,8,9,9,10,10-heptadecafluorodecyl)]-1,1'-biphenyl} benzene **97**

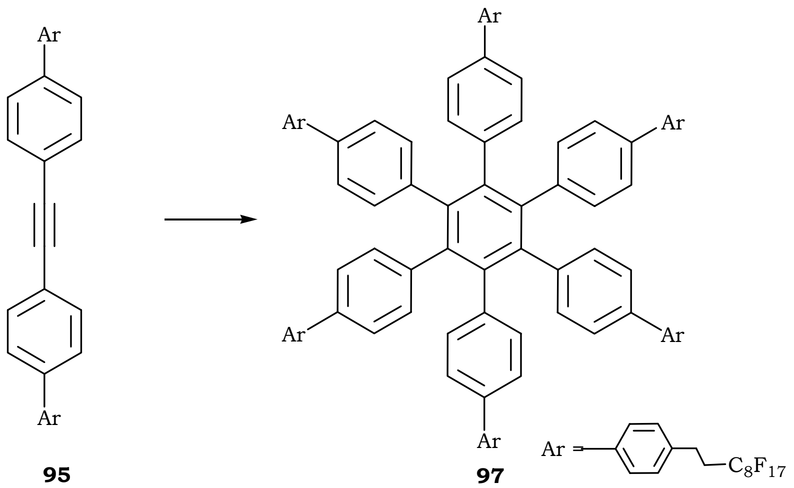

95 **97**

The trimerization reaction was done as per method C: **95** (0.34 g, 0.27 mmol), $Co_2(CO)_8$ (5 mg, 14 µmol) and dioxane (40 ml). Reaction time: 72 hours. Removal of the solvent yielded a greenish product which was extracted with HCl_{aq} (2 M, 25 ml) and CH_2Cl_2 (2 x 50 ml). The combined organic layer was washed with H_2O (3 x 50 ml) and concentrated to the fifth of its volume. The suspended solid was, therefore, collected by suction filtration over Millipore® and washed with CH_2Cl_2 (80 ml). The resulting white precipitate was refluxed in THF (20 ml) for 1.5 hours, collected by suction filtration over Millipore® and washed with hot THF (60 ml) followed by diethyl ether (5 ml) and dried under vacuum to yield **97** (0.22 g, 66%). MALDI-TOF: *m/z* 3666 ($M^{\bullet+}$, 25%), 3360 (73%), 3163 (85%), 2963 (66%), 2760 (66%), 2442 (100%).

16.3.8 2,5,8,11,14,17-Hexakis[4-(3,3,4,4,5,5,6,6,7,7,8,8,9,9,10,10-heptadecafluorodecyl) phenyl]hexabenzo[*bc,ef,hi,kl,no,qr*]coronene **99**

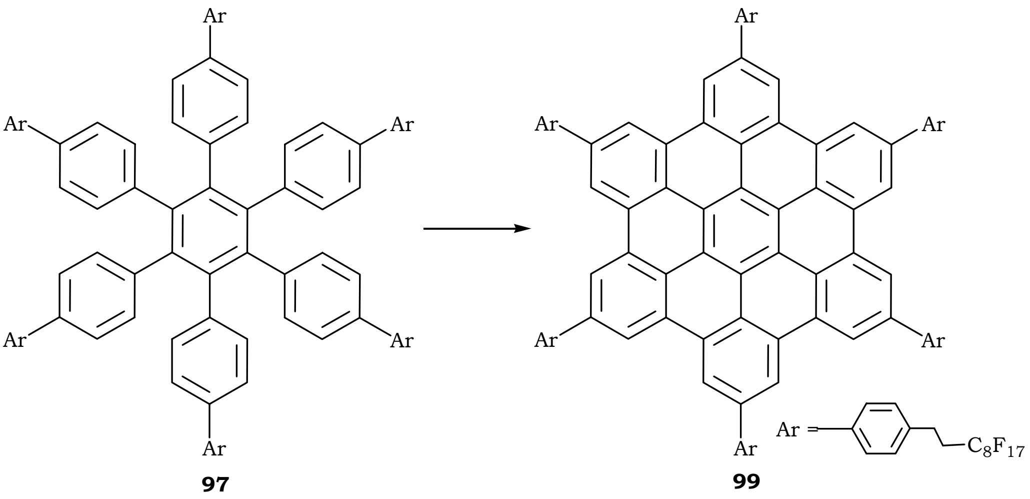

The oxidative cyclization reaction was carried out following method D: **97** (0.1 g, 27 μmol), $Cu(OTf)_2$ (0.41 g, 1.1 mmol), $AlCl_3$ (0.15 g, 1.1 mmol) and CS_2 (100 ml). The green residue was collected by suction filtration over Millipore®, washed successively with NH_4OH_{aq} (10%, 60 ml), H_2O (50 ml), HCl_{aq} (10%, 60ml), H_2O (60 ml), ethanol (60 ml), CH_2Cl_2 (60 ml), and ether (60 ml). The faint brown solid was then refluxed in dioxane (50 ml) for 4.5 hours and the resulting suspended yellow product was then collected by suction filtration of the hot solution over Millipore® followed by washing the precipitate with hot dioxane (55 ml) to afford **99** as a bright yellow solid (64 mg, 65%). MALDI-TOF: *m/z* 3688 (50%), 3653 ($M^{•+}$, 100%).

16.4 HBC with R = (CH$_2$)$_4$C$_8$F$_{17}$

16.4.1 1-(5,5,6,6,7,7,8,8,9,9,10,10,11,11,12,12,12-heptadecafluorododecyl)-4-{[4-(5,5,6,6,7, 7,8,8,9,9,10, 10,11,11,12,12,12-heptadecafluorododecyl)phenyl]ethynyl} benzene **110**

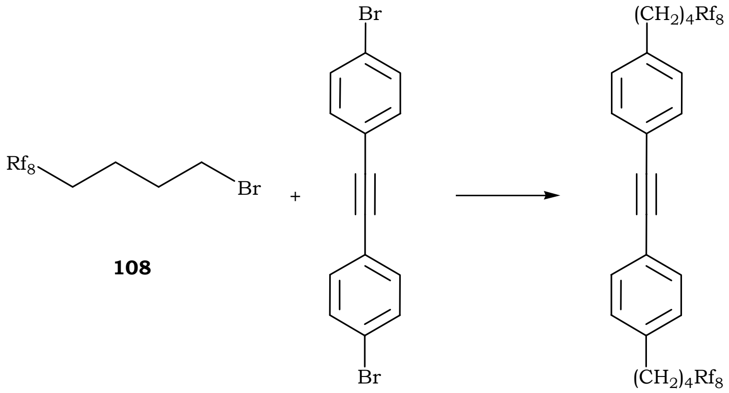

108

36

110

Method J. To a Schlenk vessel containing freshly activated magnesium turnings (50 mg, 2 mmol) was added a solution of the perfluoroalkylated alkyl chain derivative[313] **108** (1.11 g, 2 mmol) in degassed THF (1.5 ml) and the mixture was refluxed for 24 hours. The resulting solution of the Grignard reagent was then transferred via a cannula to a Schlenk flask containing a suspension of dibromotolane **36** (168 mg, 0.5 mmol) and Pd(dppf)Cl$_2$ (61 mg, 75 µmol) in degassed THF (2.5 ml) and the red mixture was refluxed for 6 days. The reaction was quenched with methanol (7.5 ml) and the suspended beige solid was collected by filtration and washed successively with a solution of NH$_4$Cl$_{sat.}$ (25 ml), H$_2$O (100 ml) and CH$_2$Cl$_2$ (75 ml). White solid (0.42 g, 75%). ^{1}H-NMR (360 MHz, CDCl$_3$): δ 7.44-7.46 (*d*, ^3J(H,H) = 7.7 Hz, 4H, Ph), 7.14-7.16 (*d*, ^3J(H,H) = 7.7 Hz, 4H, Ph), 2.65-2.69 (*br. t*, 4H, *CH$_2$*CH$_2$CH$_2$CH$_2$Rf$_8$), 2.02-2.16 (*m*, 4H, CH$_2$CH$_2$CH$_2$*CH$_2$*Rf$_8$), 1.61-1.77 (*m*, 8H, CH$_2$*CH$_2$CH$_2$*CH$_2$Rf$_8$). EI-MS: *m/z* 1126 (M$^{•+}$, 70%), 1207 ([M-F]$^{•+}$, 16%), 665 ([M-(CF$_2$)$_7$CF$_3$]$^{•+}$, 100%), 204 (36%).

16.4.2 Hexakis[4-(5,5,6,6,7,7,8,8,9,9,10,10,11,11,12,12,12-heptadecafluorododecyl) phenyl] benzene **112**

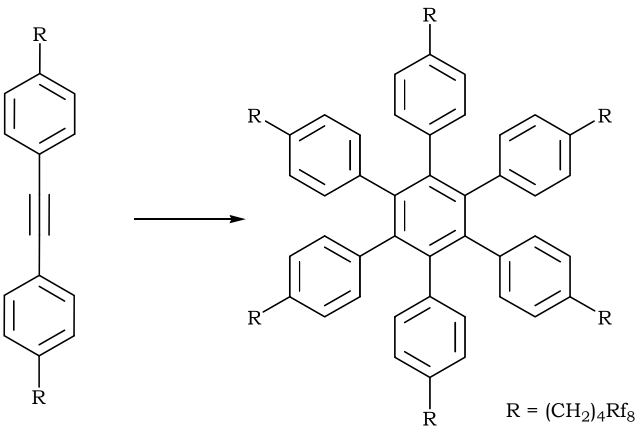

110 **112**

The reaction was carried out applying method C: **110** (0.24 g, 0.21 mmol), $Co_2(CO)_8$ (4 mg, 11 µmol) and dioxane (30 ml). Removal of the solvent yielded a grey product which was extracted with HCl_{aq} (2 M, 20 ml) and ether (2 x 25 ml). The combined organic layer was washed with H_2O (2 x 25 ml) and the greenish solution was filtered over Millipore® to remove the insoluble metallic species. The yellowish ethereal solution was then passed through a short silica gel plug under reduced pressure. Evaporation of the solvent gave an off-white solid which was suspended in pentane (10 ml) and collected by suction filtration over Millipore®. The precipitate was washed successively with pentane (10 ml) and ether (2 ml) yielding **112** (169 mg, 70%). ^{1}H-NMR (360 MHz, $CDCl_3$): δ 6.67-6.69 (*d*, ^3J(H,H) = 8.17 Hz, 12H, Ph), 6.61-6.63 (*d*, ^3J(H,H) = 8.17 Hz, 12H, Ph), 2.37-2.41 (*br. t*, 12H, *CH2*CH2CH2CH2Rf8), 1.89-2.04 (*m*, 12H, CH2CH2CH2*CH2*Rf8), 1.33-1.54 (*m*, 24H, CH2*CH2CH2*CH2Rf8). EI-MS: *m/z* 3379 ([M+H]$^+$, 100%), 714 (18%).

16.4.3 2,5,8,11,14,17-Hexakis(5,5,6,6,7,7,8,8,9,9,10,10,11,11,12,12,12-heptadecafluorododecyl)hexabenzo[*bc,ef,hi,kl,no,qr*]coronene **114**

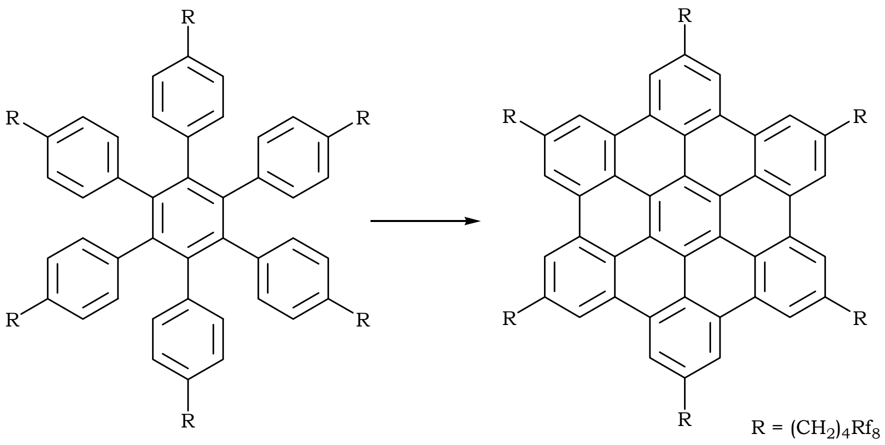

112 **114**

The cyclodehydrogenation reaction was performed following method G: **112** (90 mg, 27 µmol), $FeCl_3$ (0.32 g, 1.92 mmol), CH_3NO_2 (5 ml), CH_2Cl_2 (35 ml). Reaction time: 10 hours. The yellow-brown suspension was extracted with HCl_{aq} (2 M, 20 ml) and methylene dichloride (3 x 25 ml). The combined organic layer was then washed with H_2O (2 x 25 ml) and the solvent was evaporated affording a bright yellow solid which was suspended in ether (20 ml), refluxed for 22 hours, and collected by suction filtration over Millipore®. Exhaustive washings of the precipitate with ether (120 ml) and CH_2Cl_2 (25 ml) afforded **114** as a yellow solid (31 mg, 35%). MALDI-TOF: *m/z* 3367 ($M^{\bullet +}$, 100%), 501 (11%).

16.5 HBC with R = $(CH_2)_6C_6F_{13}$

16.5.1 1-(7,7,8,8,9,9,10,10,11,11,12,12,12-tridecafluorododecyl)-4-{[4-(7,7,8,8,9,9,10,10,11,11,12,12,12-tridecafluorododecyl)phenyl]ethynyl}benzene **111**

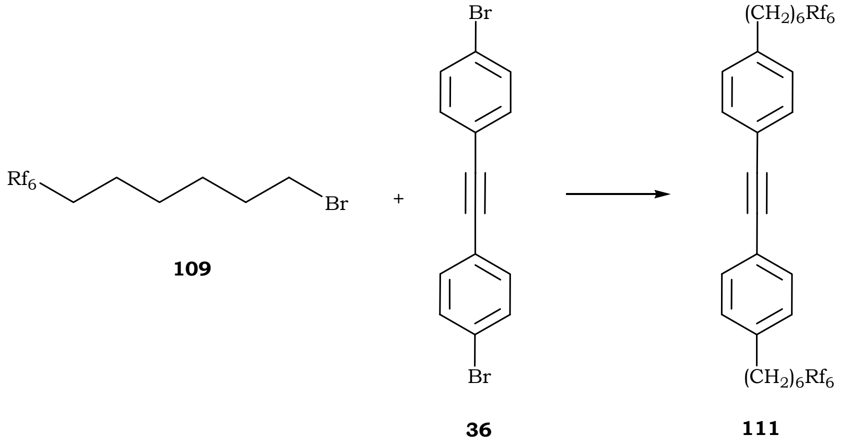

The Kumada cross-coupling reaction was carried out as per method J: The partially perfluorinated chain derivative[312] **109** (1.02 g, 2 mmol), Mg (50 mg, 2 mmol), **36** (168 mg, 0.5 mmol), Pd(dppf)Cl_2 (41 mg, 50 µmol), and THF (5 ml). Reaction time: 72 hours. The dark red suspension was extracted with $NH_4Cl_{sat.}$ and CH_2Cl_2 (2 x 50 ml). The combined organic layer was washed with H_2O (2 x 25 ml), dried over Na_2SO_4, and filtered. Removal of the solvent yielded an orange product which was filtered over a short silica gel plug under reduced pressure using a 9:1 mixture of hexane/CH_2Cl_2. After the evaporation of the solvent, the white solid was suspended in cyclohexane and the precipitate was collected by suction filtration over Millipore® affording **111** (321 mg, 65%). TLC (SiO_2, 9:1 hexane/CH_2Cl_2: $R_f = 0.32$). ^{1}H-NMR (360 MHz, $CDCl_3$): δ 7.43-7.45 (*d*, ^3J(H,H) = 8.17 Hz, 4H, Ph), 7.14-7.16 (*d*, ^3J(H,H) = 8.17 Hz, 4H, Ph), 2.6-2.64 (*br. t*, 4H, $\mathit{CH_2}(CH_2)_5Rf_6$), 1.97-2.12 (*m*, 4H, $CH_2(CH_2)_4\mathit{CH_2}Rf_6$), 1.36-1.68 (*m*, 16H, $CH_2\mathit{(CH_2)_4}CH_2Rf_6$). ^{13}C-NMR (90.55 MHz, $CDCl_3$): δ 142.79 (Ph), 131.55 (Ph), 128.43 (Ph), 120.8 (Ph), 116-120 (*m*, CF_2), 88.96 (acetylene), 35.76 (CH_2), 28.82-30.96 (overlapped peaks, CH_2), 20.08 (CH_2). EI-MS: *m/z* 982 ($M^{\bullet+}$, 20%), 714 (13%), 593 ($[M-(CH_2)_5(CF_2)_7CF_3]^{\bullet+}$, 100%), 204 (45%).

16.5.2 Hexakis[4-(7,7,8,8,9,9,10,10,11,11,12,12,12-tridecafluorododecyl)phenyl] benzene **113**

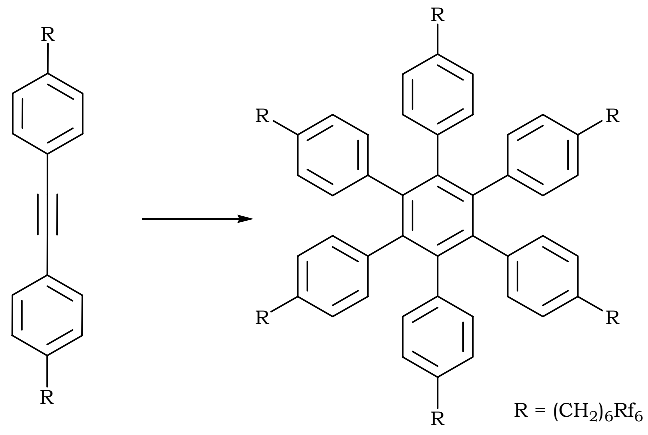
R = $(CH_2)_6Rf_6$

111 **113**

The cyclotrimerization reaction was carried out applying method C: **111** (0.31 g, 0.31 mmol), $Co_2(CO)_8$ (6 mg, 16 µmol) and dioxane (40 ml). Removal of the solvent yielded a dark product which was filtered under reduced pressure over a short silica gel plug using THF as solvent. Evaporation of THF yielded a yellow product which was suspended in cyclohexane (4 ml) and collected by suction filtration over Millipore® to afford **113** (0.25 g, 80%) as a white product. ^{1}H-NMR (500 MHz, $CDCl_3$): δ 6.67-6.68 (*d*, ^3J(H,H) = 8.25 Hz, 12H, Ph), 6.6-6.61 (*d*, ^3J(H,H) = 8.25 Hz, 12H, Ph), 2.33-2.36 (*br. t*, 12H, $\mathit{CH_2}(CH_2)_5Rf_6$), 1.95-2.06 (*m*, 12H, $CH_2(CH_2)_4\mathit{CH_2}Rf_6$), 1.5-1.56 (*m*, 12H, $(\mathit{CH_2})_4\mathit{CH_2}CH_2Rf_6$), 1.38-1.44 (*m*, 12H, $CH_2\mathit{CH_2}(CH_2)_4Rf_6$), 1.26-1.33 (*m*, 12H, $(CH_2)_3\mathit{CH_2}CH_2CH_2Rf_6$), 1.11-1.17 (*m*, 12H, $CH_2CH_2\mathit{CH_2}(CH_2)_3Rf_6$). ^{13}C-NMR (90.55 MHz, $CDCl_3$): δ 140.38 (Ph), 138.76 (Ph), 138.53 (Ph), 131.57 (Ph), 126.55 (Ph), 107-122 (*m*, CF_2), 35.22 (CH_2), 30.73-31.21 (overlapped peaks, CH_2), 29.11 (CH_2), 28.45 (CH_2), 20.18(CH_2). EI-MS: *m/z* 2947 ($[M+H]^+$, 100%).

16.5.3 2,5,8,11,14,17-Hexakis(7,7,8,8,9,9,10,10,11,11,12,12,12-tridecafluorododecyl) hexabenzo[*bc,ef,hi,kl,no,qr*]coronene **115**

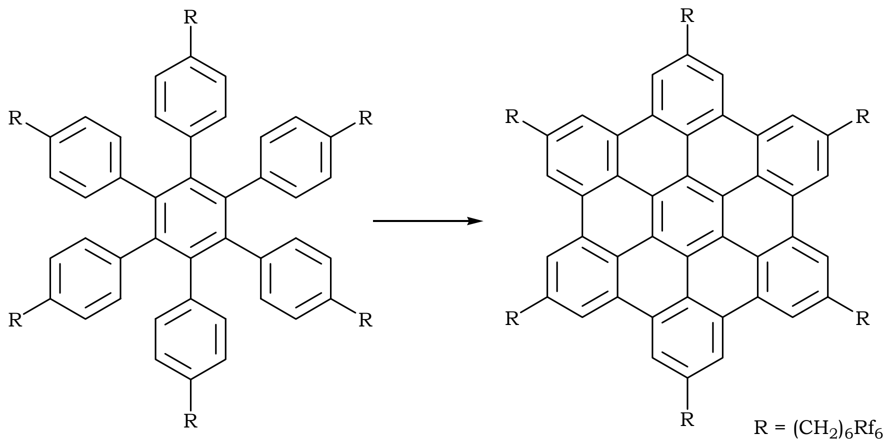

113 **115**

The oxidative cyclization reaction was done using method G: **113** (0.1 g, 34 µmol), $FeCl_3$ (0.4 g, 2.45 mmol), CH_3NO_2 (5 ml), CH_2Cl_2 (30 ml). Reaction time: 5 hours. The yellow-brown suspension was extracted with HCl_{aq} (2 M, 25 ml) and methylene dichloride (3 x 25 ml). The combined organic layer was then washed with H_2O (50 ml) and the solvent was evaporated affording a bright yellow solid which was suspended in $CHCl_3$ (5 ml), sonicated for 5-10 minutes, and collected by suction filtration over Millipore®. After several washings of the precipitate with $CHCl_3$, **115** was isolated as a yellow solid (87 mg, 87%). MALDI-TOF: *m/z* 2934 ($M^{\bullet+}$, 100%). UV-Vis: 368 (4.46), 394.5 (5.07), 421.5 (4.64).

16.6 Attempted synthesis of HBC with R = $O(CH_2)_4C_8F_{17}$

16.6.1 1-Bromo-4-[(5,5,6,6,7,7,8,8,9,9,10,10,11,11,12,12,12-heptadecafluorododecyl)-oxy]benzene **116**

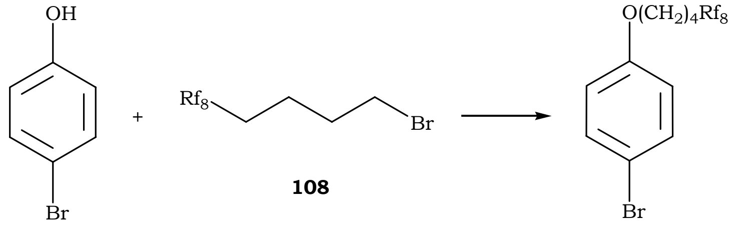

108

4-Bromophenol

116

Method K. A solution of 4-bromophenol (0.7 g, 4 mmol), **108** (2.44 g, 4.4 mmol), and K_2CO_3 (1.68 g, 12 mmol) in degassed DMF (60 ml) was reacted, under argon, at 80°C for 24 hours. The yellowish suspension was extracted with H_2O and ether (3 x 25 ml). The combined organic layer was then washed with a saturated aqueous solution of NaCl (2 x 50 ml), dried over Na_2SO_4, filtered and the solvent was evaporated to give a faint orange solid which was recrystallized from ethanol affording **116** (2.16 g, 83%). ^{1}H-NMR (360 MHz, $CDCl_3$): δ 7.35-7.39 (*br. d*, 2H, Ph), 6.76-6.79 (*br. d*, 2H, Ph), 3.94-3.98 (*br. t*, 2H, $O\mathit{CH_2}CH_2CH_2CH_2Rf_8$), 2.08-2.23 (*m*, 2H, $OCH_2CH_2CH_2\mathit{CH_2}Rf_8$), 1.76-1.92 (*m*, 4H, $OCH_2\mathit{CH_2CH_2}CH_2Rf_8$). ^{13}C-NMR (90.55 MHz, $CDCl_3$): δ 158.3 (Ph), 132.69 (Ph), 116.63 (Ph), 113.36 (Ph), 67.82 (*s*, $O\mathit{CH_2}CH_2CH_2CH_2Rf_8$), 30.82-31.3 (*m*, $OCH_2CH_2CH_2\mathit{CH_2}Rf_8$), 29.01 (*s*, $OCH_2\mathit{CH_2}CH_2CH_2Rf_8$), 17.62-17.71 (*m*, $OCH_2CH_2\mathit{CH_2}CH_2Rf_8$). EI-MS: *m/z* 648 ($[M+H]^+$, 16%), 646 ($[M+H]^+$, 17%), 173 ($[M+H-(CH_2)_4Rf_8]^{\bullet+}$, 100%), 171 ($[M+H-(CH_2)_4Rf_8]^{\bullet+}$, 97%).

16.6.2 ({4-[(5,5,6,6,7,7,8,8,9,9,10,10,11,11,12,12,12-Heptadecafluorododecyl)oxy]-phenyl}ethynyl)(trimethyl)silane **117**

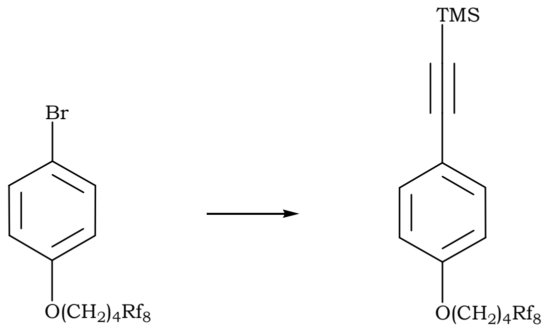

116 **117**

The Sonogashira cross-coupling reaction was done applying method A: **116** (0.8 g, 1.2 mmol), TMSA (0.21 ml, 1.5 mmol), $Pd(PPh_3)_2Cl_2$ (26 mg, 36 µmol), Ph_3P (20 mg, 72 µmol), CuI (13 mg, 72 µmol) and piperidine (7.5 ml). Reaction time: 25 hours. Purification was carried out by filtration over a short silica gel plug, under reduced pressure, using a 9:1 pentane/ether mixture as the eluent affording **117** (0.67 g, 87%). TLC (SiO_2, 9:1 pentane/ether: R_f = 0.8). ^{1}H-NMR (360 MHz, $CDCl_3$): δ 7.41-7.39 (*br. d,* 2H, Ph), 6.79-6.81 (*br. d*, 2H, Ph), 3.98-4 (*br. t*, 2H, $OCH_2CH_2CH_2CH_2Rf_8$), 2.1-2.25 (*m*, 2H, $OCH_2CH_2CH_2CH_2Rf_8$), 1.79-1.9 (*m*, 4H, $OCH_2CH_2CH_2CH_2Rf_8$), 0.23 (*s*, 9H, TMS).

16.6.3 1-Ethynyl-4-[(5,5,6,6,7,7,8,8,9,9,10,10,11,11,12,12,12-heptadecafluorododecyl)-oxy]benzene **118**

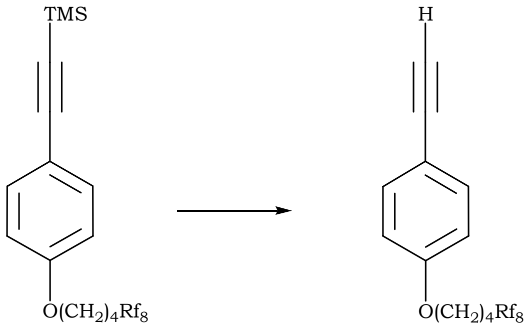

117 **118**

The deprotection was done using method B: **117** (0.68 g, 1 mmol), BTACl (0.47 g, 2 mmol), $NaOH_{aq}$ (7.5 ml, 10 M), CH_2Cl_2 (5 ml). Filtration over a short silica gel plug, under reduced pressure, using a 98:2 mixture of pentane/ether yielded **117** (0.56 g, 95%). TLC (SiO_2, 98:2 pentane/ether: R_f = 0.64). ^{1}H-NMR (360 MHz, $CDCl_3$): δ 7.39-7.41 (*d*, ^3J(H,H) =

8.64 Hz, 2H, Ph), 6.79-6.81 (*d*, ^3J(H,H) = 8.64 Hz, 2H, Ph), 3.98-4.01 (*br. t*, 2H, O*CH₂*CH₂CH₂CH₂Rf₈), 2.99 (*s*, 1H, acetylene), 2.09-2.23 (*m*, 2H, OCH₂CH₂CH₂*CH₂*Rf₈), 1.79-1.92 (*m*, 4H, OCH₂*CH₂CH₂*CH₂Rf₈). ^{13}C-NMR (90.55 MHz, $CDCl_3$): δ 159.58 (Ph), 133.9-134.02 (Ph), 114.82 (Ph), 108-119 (*m*, CF_2), 83.95 (acetylene), 76.14 (acetylene), 67.25-67.93 (*t*, O*CH₂*CH₂CH₂CH₂Rf₈), 30.78-31.28 (*m*, OCH₂CH₂CH₂*CH₂*Rf₈), 30.12 (*s*, OCH₂*CH₂*CH₂CH₂Rf₈), 17.63 (*br. s*, OCH₂CH₂*CH₂*CH₂Rf₈). EI-MS: *m/z* 592 ($M^{\bullet+}$, 10%), 118 ($[M-(CH_2)_4Rf_8]^{\bullet+}$, 100%).

16.6.4 1-[(5,5,6,6,7,7,8,8,9,9,10,10,11,11,12,12,12-heptadecafluorododecyl)oxy]-4-({4-[(5,5,6,6,7,7,8,8,9,9,10,10,11,11,12,12,12-heptadecafluorododecyl)oxy]phenyl}ethynyl)-benzene **119**

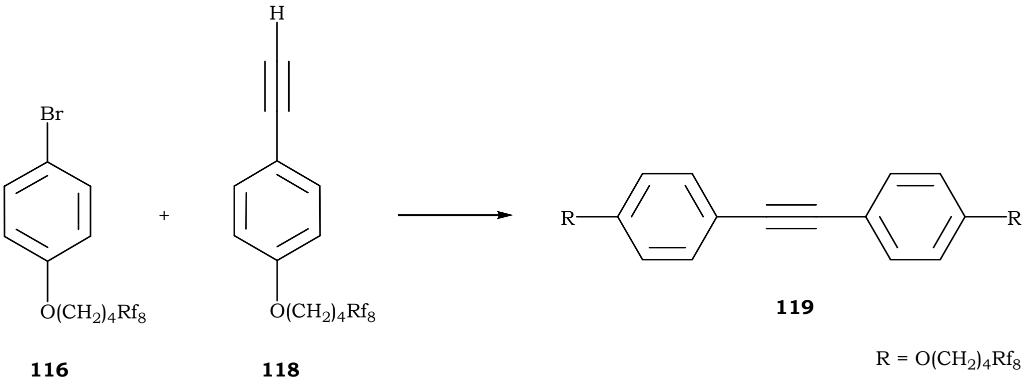

The Sonogashira cross-coupling reaction was done employing method E: **116** (0.15 g, 0.23 mmol), **118** (0.14 g, 0.23 mmol), $Pd(PPh_3)_4$ (16.5 mg, 14 µmol), CuI (7 mg, 35 µmol), and piperidine (5 ml). The reaction was carried out at 85°C for 48 hours. The brown suspension was then extracted with $NH_4Cl_{sat.}$ and CH_2Cl_2 (3 x 50 ml). The combined organic layer was washed with H_2O (2 x 25 ml) and the white suspended precipitate was collected by suction filtration. The organic layer was evaporated and the residue was passed through a short silica gel plug, under reduced pressure, using CH_2Cl_2. Recrystallization of the residual product from chloroform and its combination with the white precipitate collected at first afforded **119** (0.17 g, 64%). ^{1}H-NMR (360 MHz, $CDCl_3$): δ 7.43-7.45 (*br. d*, 4H, Ph), 6.84-6.86 (*br. d*, 4H, Ph), 4-4.03 (*br. t*, 4H, O*CH₂*CH₂CH₂CH₂Rf₈), 2.99 (*s*, 1H, acetylene), 2.1-2.3 (*m*, 4H, OCH₂CH₂CH₂*CH₂*Rf₈), 1.82-1.93 (*m*, 8H, OCH₂*CH₂CH₂*CH₂Rf₈). EI-MS: *m/z* 1158 ($M^{\bullet+}$, 32%), 684 ($[M+H-(CH_2)_4Rf_8]^{\bullet+}$, 25%), 210 (100%).

16.6.5 Hexakis({4-[(5,5,6,6,7,7,8,8,9,9,10,10,11,11,12,12,12-heptadecafluorododecyl)-oxy]phenyl}benzene **120**

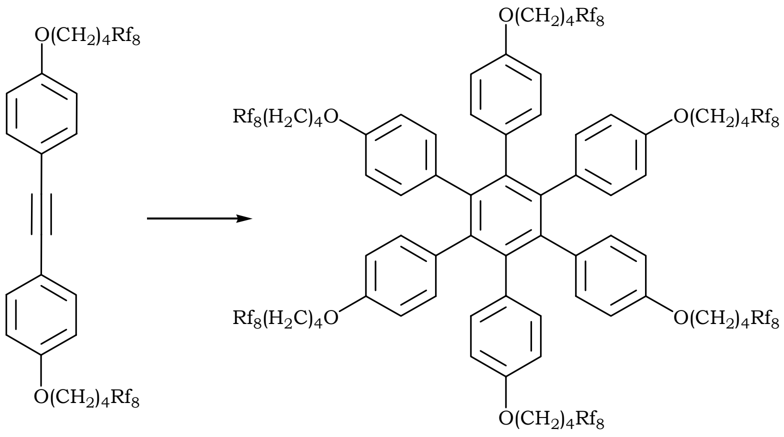

119

120

The hexaphenyl benzene derivative was synthesized according to method C: **119** (0.24 g, 0.2 mmol), Co$_2$(CO)$_8$ (4 mg, 10 µmol) and dioxane (20 ml). Removal of the solvent yielded a dark product which was filtered under reduced pressure over a short silica gel plug using THF as solvent. Evaporation of THF yielded a yellow product which was suspended in ether (7 ml), sonicated, and collected by suction filtration over Millipore® to afford **120** (0.15 g, 64%) as a white glassy solid. ^{1}H-NMR (360 MHz, CDCl$_3$): δ 6.65-6.68 (*br. d,* 12H, Ph), 6.39-6.42 (*br. d*, 12H, Ph), 3.78-3.8 (*br. t*, 12H, O$\mathit{CH_2}$CH$_2$CH$_2$CH$_2$Rf$_8$), 2.04-2.14 (*m*, 12H, OCH$_2$CH$_2$CH$_2$$\mathit{CH_2}Rf_8$), 1.75 (*br. s*, 24H, OCH$_2$$\mathit{CH_2}$$\mathit{CH_2}CH_2Rf_8$). ^{13}C-NMR (90.55 MHz, CDCl$_3$): δ 156.38 (Ph), 140.58 (Ph), 134.12 (Ph), 132.88 (Ph), 113.22 (Ph), 67.22 (*s*, O$\mathit{CH_2}$CH$_2$CH$_2$CH$_2$Rf$_8$), 31.02 (*m*, OCH$_2$CH$_2$CH$_2$$\mathit{CH_2}Rf_8$), 29.02 (*s*, OCH$_2$$\mathit{CH_2}CH_2CH_2Rf_8$), 17.55 (*s*, OCH$_2CH_2$$\mathit{CH_2}CH_2Rf_8$). EI-MS: *m/z* 3474 (M$^{\bullet+}$, 100%).

16.6.6 5,6,7,8-Tetrakis{4-[(5,5,6,6,7,7,8,8,9,9,10,10,11,11,12,12,12-heptadecafluorododecyl)oxy]phenyl}triphenylene-2,11-dione **121**

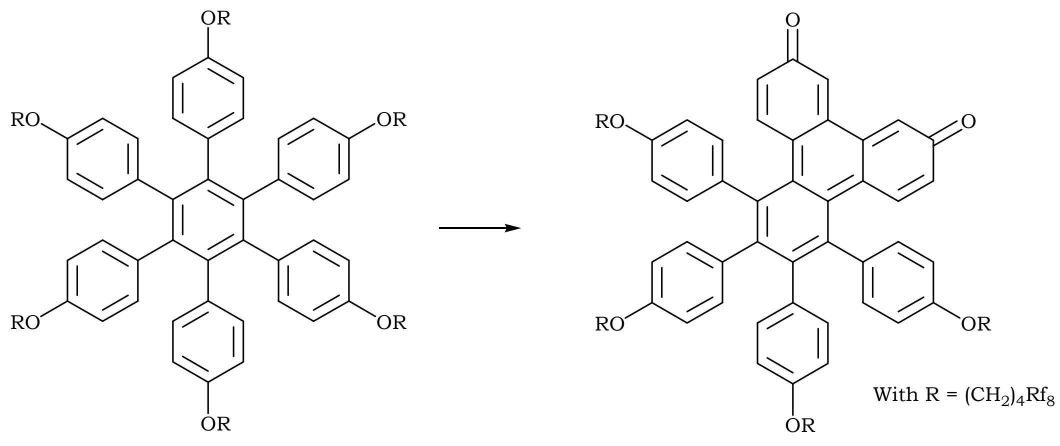

120 **121**

The reaction was carried out following method G: **120** (60 mg, 17 µmol), $FeCl_3$ (0.1 g, 0.62 mmol), CH_3NO_2 (1 ml), CH_2Cl_2 (15 ml). Reaction time: 24 hours including 5 hours of purging with argon. The red-brown suspension was extracted with H_2O and ether (3 x 25 ml). Evaporation of the organic layer afforded a brown solid which was suspended in ether (10 ml) and collected by suction filtration over Millipore®. Exhaustive washings of the precipitate with ether (50 ml) yielded **121** as a brown solid (21 mg, 48%). ^{1}H-NMR (500 MHz, $CDCl_3$): δ 7.17-7.18 (*br. d*, 4H, Ph), 6.88-6.9 (*br. d*, 4H, Ph), 6.55-6.58 (*dd*, 2H, *o*-quinone), 6.52-6.54 (*br. d*, 4H, Ph), 6.50-6.51 (*d*, 2H, *o*-quinone), 6.28-6.29 (*d*, 2H, *m*-quinone), 6.12-6.14 (*dd*, 4H, Ph), 4.06-4.09 (*br. t*, 4H, $\mathrm{O}\mathit{CH_2}\mathrm{CH_2CH_2CH_2Rf_8}$), 3.83-3.7 (*t*, 4H, $\mathrm{O}\mathit{CH_2}\mathrm{CH_2CH_2CH_2Rf_8}$), 2.2-2.32 (*m*, 4H, $\mathrm{OCH_2CH_2CH_2}\mathit{CH_2}\mathrm{Rf_8}$), 2.03-2.15 (*m*, 4H, $\mathrm{OCH_2CH_2CH_2}\mathit{CH_2}\mathrm{Rf_8}$), 1.86-1.97 (*m*, 8H, $\mathrm{OCH_2}\mathit{CH_2CH_2}\mathrm{CH_2Rf_8}$), 1.7-1.81 (*m*, 8H, $\mathrm{OCH_2}\mathit{CH_2CH_2}\mathrm{CH_2Rf_8}$). IR [cm^{-1}]: 3060 (w), 1662 [$(CO)_{\mathrm{stretch.}}$], 1612 (m), 1490 [$(C{=}C)_{\mathrm{arene}}$], 1243 [(Ar-O-R)], 1207 (m), 1149 (m), 704 (s). MALDI-TOF: *m/z* 2524 ($M^{\bullet+}$, 100%).

16.7 HBC with R = *p*-PhO$(CH_2)_4C_8F_{17}$

*Tolane derivative **123** via a Suzuki cross-coupling reaction*

16.7.1 4-[(5,5,6,6,7,7,8,8,9,9,10,10,11,11,12,12,12-heptadecafluorododecyl)oxy]phenylboronic acid **122**

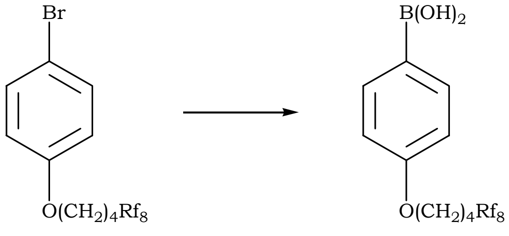

116 **122**

n-BuLi (1.5 mmol, 1 ml, 1.6 M in hexanes) was injected dropwise to a solution of **116** (0.39 g, 0.6 mmol) in degassed THF (5 ml) at -85°C. The reaction was allowed to warm at -40°C over a period of 50 minutes and it was stirred for 130 minutes (total reaction time: 3 hours). After cooling the solution once again at -85°C, $B(OMe)_3$ (0.34 ml, 3 mmol) was injected and the reaction was stirred for 1 hour at -60°C, then it was warmed at room temperature overnight. HCl_{aq} (2 M, 15 ml) was finally added and the reaction was stirred at room temperature for 20 hours. The solution was extracted with HCl_{aq} (2 M, 25 ml) and CH_2Cl_2 (3 x 25 ml). After washing the combined organic layers with H_2O (3 x 25 ml) and distilling off CH_2Cl_2, the faint yellow solid was suspended in ether an the white precipitate was collected by suction filtration over Millipore® (0.162 g, 44%). ^{1}H-NMR (360 MHz, $CDCl_3$): δ 8.15-8.18 (*d*, ^3J(H,H) = 8.6 Hz, 2H, Ph), 6.99-7.01 (*d*, ^3J(H,H) = 8.6 Hz, 2H, Ph), 4.07-4.15 (*br. t*, 2H, $OCH_2$$CH_2CH_2CH_2Rf_8$), 2.12-2.25 (*m*, 2H, $OCH_2CH_2CH_2CH_2Rf_8$), 1.86-1.94 (*m*, 4H, $OCH_2CH_2CH_2CH_2Rf_8$).

16.7.2 4-[(5,5,6,6,7,7,8,8,9,9,10,10,11,11,12,12,12-Heptadecafluorododecyl)oxy]-4'-({4'-[(5,5,6,6,7,7,8,8,9,9,10,10,11,11,12,12,12-heptadecafluorododecyl)oxy]1,1'-biphenyl-4-yl}ethynyl)-1,1'-biphenyl **123**

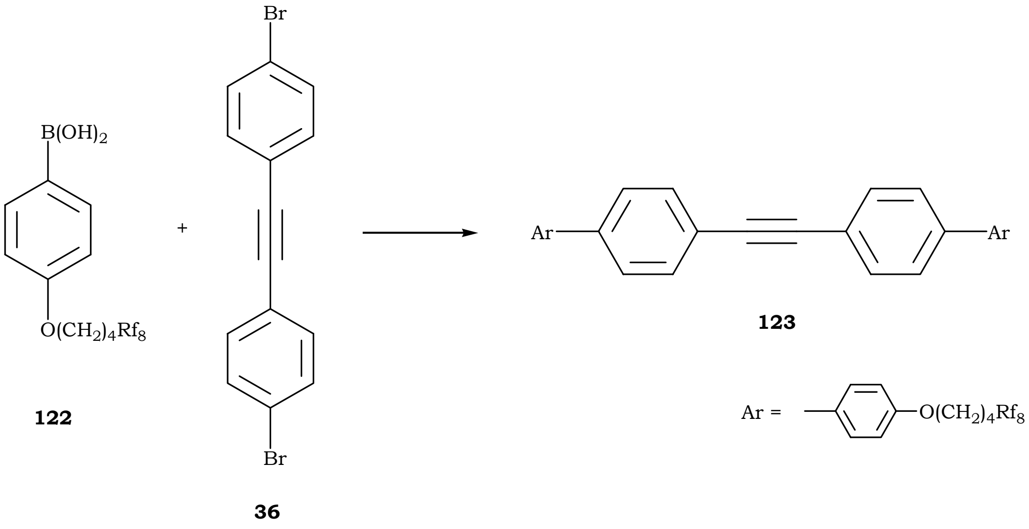

The Suzuki cross-coupling reaction was done as per method F: 4,4'-dibromotolane[221] **36** (26 mg, 79 µmol), **122** (120 mg, 0.19 mmol), $Pd(PPh_3)_4$ (10 mg, 7.9 µmol), and K_2CO_3 (176 mg, 1.26 mmol), toluene (1.5 ml), ethanol (0.5 ml) and H_2O (1 ml). Reaction time: 5 days. The dark brown biphasic solution was then extracted with $NH_4Cl_{sat.}$ and methylenedichloride (50 ml). The suspended precipitate in the organic layer was collected by suction filtration and washed exhaustively with CH_2Cl_2 yielding a white solid (65 mg, 63%). EI-MS: *m/z* 1310 ($M^{\bullet+}$, 100%), 1291 ($[M-F]^{\bullet+}$, 5%), 836 ($[M-(CH_2)_4Rf_8]^{\bullet+}$, 43%), 362 ($[M-2(CH_2)_4Rf_8]^{\bullet+}$, 32%).

*Tolane derivative **123** via a step by step Sonogashira cross-coupling reaction*

16.7.3 4-Bromo-4’-[(5,5,6,6,7,7,8,8,9,9,10,10,11,11,12,12,12-heptadecafluorododecyl)-oxy]-1,1’-biphenyl **124**

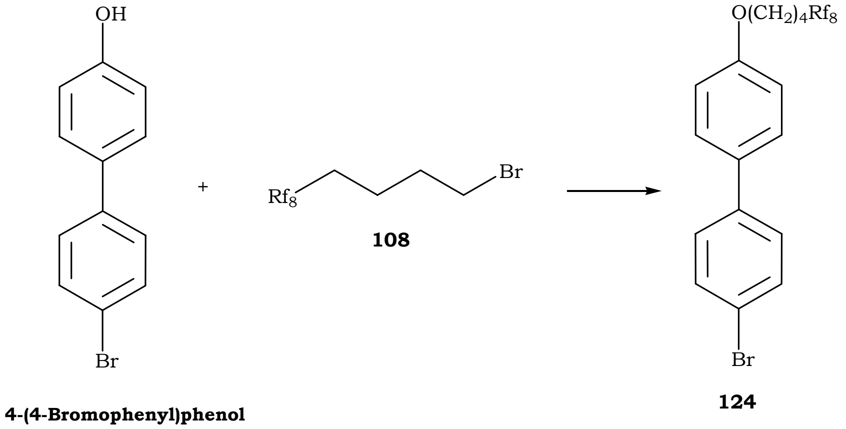

The reaction was carried out following method K: 4-(4-bromophenyl)phenol (1.01 g, 4 mmol), **108** (2.44 g, 4.4 mmol), K_2CO_3 (1.68 g, 12 mmol), and degassed DMF (60 ml). The yellowish product was suspended in pentane (30 ml), sonicated and allowed to settle then it was collected by suction filtration and washed with ether (5 ml) affording **124** (2.28 g, 79%). ^{1}H-NMR (360 MHz, $CDCl_3$): δ 7.52-7.54 (*br. d*, 2H, Ph), 7.47-7.49 (*d*, ^3J(H,H) = 8.6 Hz, 2H, Ph), 7.4-7.42 (*d*, ^3J(H,H) = 8.6 Hz, 2H, Ph), 6.95-6.97 (*br. d*, 2H, Ph), 4.03-4.06 (*br. t*, 2H, $O\mathit{CH_2}CH_2CH_2CH_2Rf_8$), 2.13-2.25 (*m*, 2H, $OCH_2CH_2CH_2\mathit{CH_2}Rf_8$), 1.8-1.95 (*m*, 4H, $OCH_2\mathit{CH_2CH_2}CH_2Rf_8$). ^{13}C-NMR (90.55 MHz, $CDCl_3$): δ 159.03 (Ph), 140.1 (Ph), 133.06 (Ph), 132.2 (Ph), 128.7 (Ph), 128.4 (Ph), 121.23 (Ph), 115.25 (Ph), 67.69 (*s*, $O\mathit{CH_2}CH_2CH_2CH_2Rf_8$), 30.82-31.35 (*m*, $OCH_2CH_2CH_2\mathit{CH_2}Rf_8$), 29.1 (*s*, $OCH_2\mathit{CH_2}CH_2CH_2Rf_8$), 17.71 (*br. s*, $OCH_2CH_2\mathit{CH_2}CH_2Rf_8$). EI-MS: *m/z* 724 ($M^{\bullet+}$, 18%), 724 ($M^{\bullet+}$, 22%), 249 ($[M-(CH_2)_4Rf_8]^{\bullet+}$, 97%), 247 ($[M-(CH_2)_4Rf_8]^{\bullet+}$, 100%).

16.7.4 ({4’-[(5,5,6,6,7,7,8,8,9,9,10,10,11,11,12,12,12-heptadecafluorododecyl)oxy]-1,1’-biphenyl-4-yl}ethynyl)(trimethyl)silane **126**

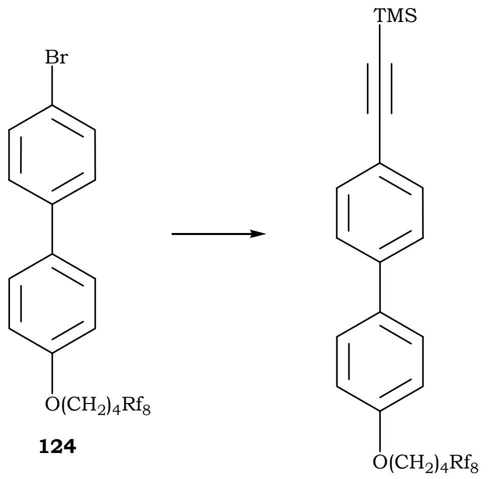

124

126

The Sonogashira cross-coupling reaction was done using method A: **124** (0.13 g, 0.41 mmol), TMSA (80 µl, 0.54 mmol), $Pd(PPh_3)_2Cl_2$ (9 mg, 13 µmol), Ph_3P (7 mg, 25 µmol), CuI (5 mg, 25 µmol) and piperidine (10 ml). Purification was carried out by filtration over a short silica gel plug, under reduced pressure, using a 4:1 pentane/CH_2Cl_2 mixture as the eluent affording **126** (0.275 g, 90%). TLC (SiO_2, 4:1 pentane/ CH_2Cl_2: $R_f = 0.83$). ^{1}H-NMR (360 MHz, $CDCl_3$): δ 7.47-7.53 (*m*, 6H, Ph), 6.94-6.97 (*d*, 2H, Ph), 4.03-4.06 (*br. t*, 2H, $O\mathit{CH_2}CH_2CH_2CH_2Rf_8$), 2.13-2.25 (*m*, 2H, $OCH_2CH_2CH_2\mathit{CH_2}Rf_8$), 1.81-1.93 (*m*, 4H, $OCH_2\mathit{CH_2}\mathit{CH_2}CH_2Rf_8$), 0.26 (*s*, 9H, TMS).

16.7.5 4-Ethynyl-4'-[(5,5,6,6,7,7,8,8,9,9,10,10,11,11,12,12,12-heptadecafluorododecyl)-oxy]-1,1'-biphenyl **128**

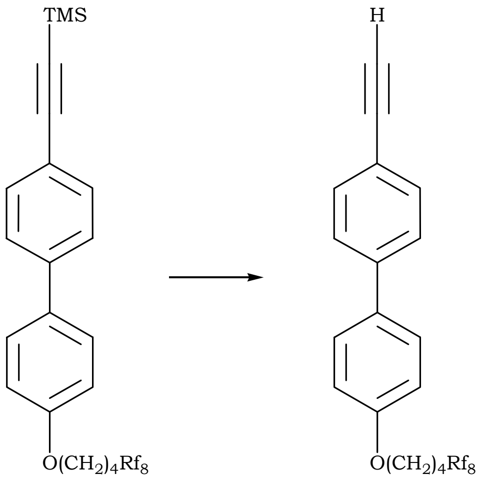

126 **128**

The elimination of the trimethylsilylated group was performed applying method B: **127** (275 mg, 0.37 mmol), BTACl (174 mg, 0.75 mmol), $NaOH_{aq}$ (5 ml, 10 M), CH_2Cl_2 (12 ml). Filtration over a short silica gel plug, under reduced pressure, using pentane/CH_2Cl_2 (4:1) yielded **128** (226 mg, 92%). TLC (SiO_2, 4:1 pentane/CH_2Cl_2: $R_f = 0.83$). ^{1}H-NMR (360 MHz, $CDCl_3$): δ 7.51-7.57 (*m*, 6H, Ph), 6.97-6.99 (*d*, 2H, Ph), 4.04-4.07 (*br. t*, 2H, $O\mathit{CH_2}CH_2CH_2CH_2Rf_8$), 3.13 (*s*, 1H, acetylene), 2.13-2.25 (*m*, 2H, $OCH_2CH_2CH_2\mathit{CH_2}Rf_8$), 1.81-1.93 (*m*, 4H, $OCH_2\mathit{CH_2}\mathit{CH_2}CH_2Rf_8$). ^{13}C-NMR (90.55 MHz, $CDCl_3$): δ 159.12 (Ph), 141.53 (Ph), 133.28 (Ph), 132.94 (Ph), 128.53 (Ph), 126.87 (Ph), 120.72 (Ph), 115.23 (Ph), 84.04 (acetylene), 77.91 (acetylene), 67.69 (*s*, $O\mathit{CH_2}CH_2CH_2CH_2Rf_8$), 30.85-31.34 (*m*, $OCH_2CH_2CH_2\mathit{CH_2}Rf_8$), 29.1 (*s*, $OCH_2\mathit{CH_2}CH_2CH_2Rf_8$), 17.72 (*br. s*, $OCH_2CH_2\mathit{CH_2}CH_2Rf_8$).

16.7.6 4-[(5,5,6,6,7,7,8,8,9,9,10,10,11,11,12,12,12-Heptadecafluorododecyl)oxy]-4’-({4’-[(5,5,6,6,7,7,8,8,9,9,10,10,11,11,12,12,12-heptadecafluorododecyl)oxy]1,1’-biphenyl-4-yl}ethynyl)-1,1’-biphenyl **123**

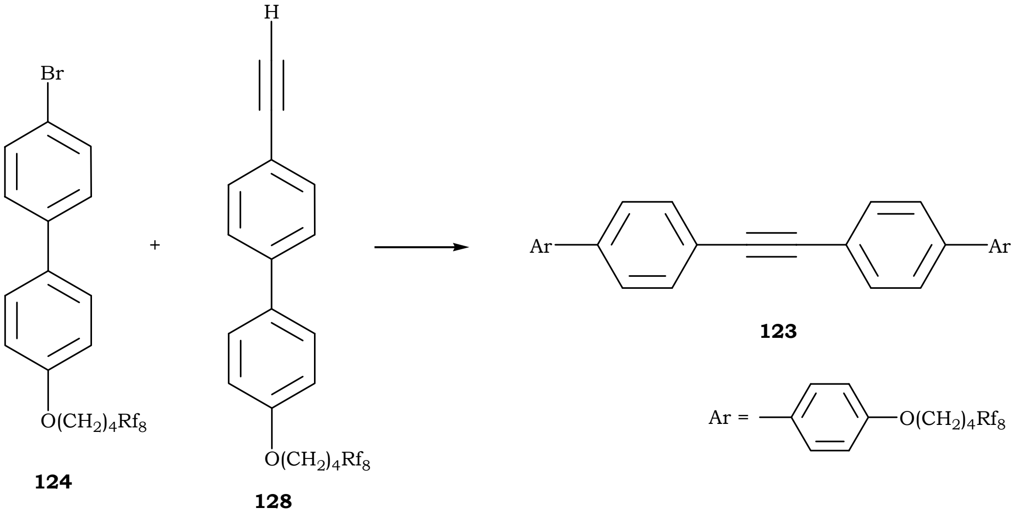

The Sonogashira cross-coupling reaction was done as per method E: **124** (216 mg, 0.3 mmol), **128** (0.2 g, 0.3 mmol), $Pd(PPh_3)_4$ (21 mg, 18 µmol), CuI (9 mg, 45 µmol), and piperidine (15 ml). The reaction was carried out at 80°C for 48 hours. The brown suspension was then extracted with $NH_4Cl_{sat.}$ and CH_2Cl_2 (3 x 50 ml). The combined organic layer was washed with H_2O (25 ml) and the white suspended precipitate was collected by suction filtration affording **123** (232 mg, 59%). EI-MS: *m/z* 1310 ($M^{•+}$, 100%), 836 ($[M-(CH_2)_4Rf_8]^{•+}$, 7%), 362 ($[M-2(CH_2)_4Rf_8]^{•+}$, 15%).

16.7.7 Hexakis(4-{4'-[(5,5,6,6,7,7,8,8,9,9,10,10,11,11,12,12,12-heptadecafluorododecyl)-oxy]-1,1'-biphenyl})benzene **131**

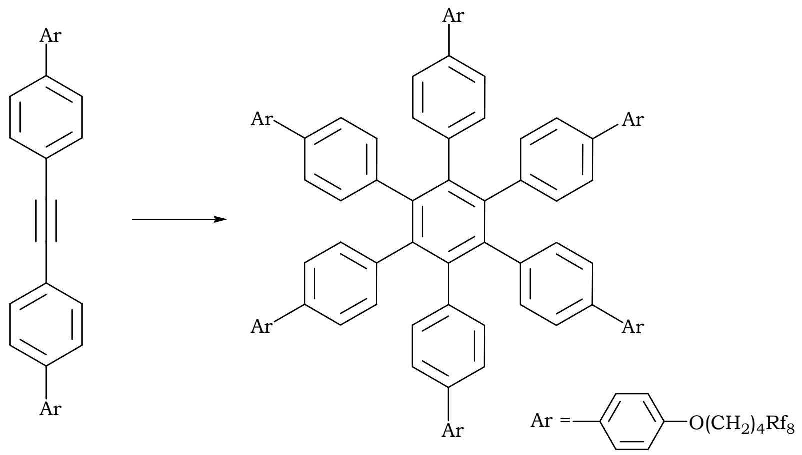

123 **131**

The hexaphenyl benzene derivative was synthesized according method C: **123** (215 mg, 0.16 mmol), $Co_2(CO)_8$ (6 mg, 16 µmol) and dioxane (60 ml). After distilling off the solvent, the grey product was suspended in ether (15 ml), sonicated for 5-10 minutes, and collected by suction filtration over Millipore® yielding **131** (115 mg, 53%) as an off-white solid. ^{1}H-NMR (360 MHz, THF-d_8): δ 7.34 (*br. s*, 12H, Ph), 7.14 (*br. s*, 12H, Ph), 6.82-6.95 (*br. d*, 24H, Ph), 3.98 (*br. s*, 12H, $\mathrm{O}\mathit{CH_2}\mathrm{CH_2CH_2CH_2Rf_8}$), 2.25 (*m*, 12H, $\mathrm{OCH_2CH_2CH_2}\mathit{CH_2}\mathrm{Rf_8}$), 1.82 (*br. s*, 24H, $\mathrm{OCH_2}\mathit{CH_2CH_2}\mathrm{CH_2Rf_8}$). (360 MHz, $CDCl_3$): δ 7.85 (*br. s*, 12H, Ph), 7.1 (*br. s*, 12H, Ph), 6.82-6.95 (*br. d*, 24H, Ph), 3.98 (*br. s*, 12H, $\mathrm{O}\mathit{CH_2}\mathrm{CH_2CH_2CH_2Rf_8}$), 2.25 (*m*, 12H, $\mathrm{OCH_2CH_2CH_2}\mathit{CH_2}\mathrm{Rf_8}$), 1.82 (*br. s*, 24H, $\mathrm{OCH_2}\mathit{CH_2CH_2}\mathrm{CH_2Rf_8}$). EI-MS: *m/z* 3930 ($M^{\bullet+}$, 100%), 1310 (70%).

16.7.8 2,5,8,11,14,17-Hexakis{4-[(5,5,6,6,7,7,8,8,9,9,10,10,11,11,12,12,12-heptadecafluorododecyl)oxy]phenyl}hexabenzo[*bc,ef,hi,kl,no,qr*]coronene **133**

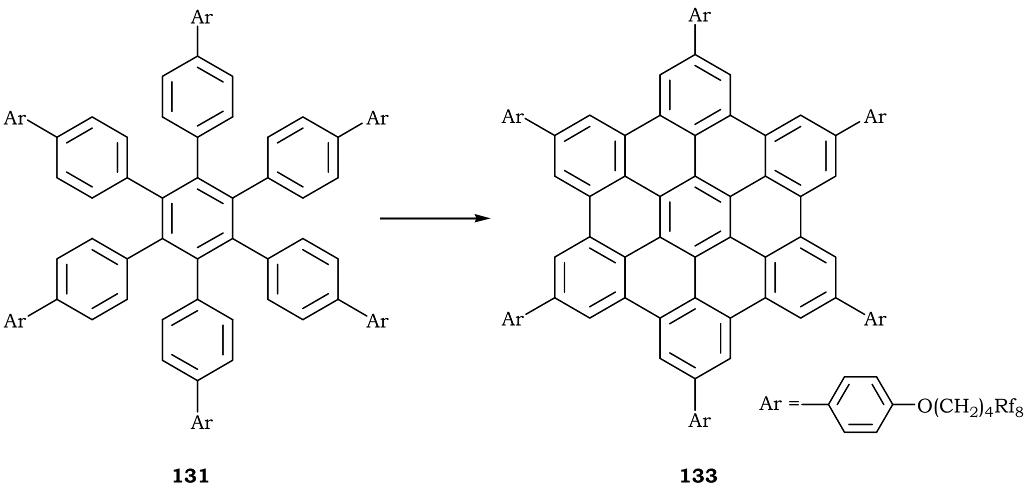

The oxidative cyclization reaction was done using method G: **131** (101 mg, 26 µmol), $FeCl_3$ (0.31 g, 1.85 mmol), CH_3NO_2 (5 ml), CH_2Cl_2 (30 ml). Reaction time: 9 hours. The yellow-brown suspension was extracted with $NH_4Cl_{sat.}$ (25 ml) and methylene dichloride (3 x 25 ml). The combined organic layer was then washed with H_2O (2 x 50 ml) and the solvent was evaporated affording a brown-yellow solid which was suspended in THF (30 ml), refluxed for 2 hours, and collected by suction filtration over Millipore®. After several washings of the precipitate with hot THF (60 ml), **133** was isolated as a yellow solid (33 mg, 33%). MALDI-TOF: *m/z* 3949 (36%), 3917 ([M-H]$^{\bullet+}$, 90%), 1309 (100%).

16.8 HBC with R = *p*-PhO$(CH_2)_6C_6F_{13}$

16.8.1 4-Bromo-4’-[(7,7,8,8,9,9,10,10,11,11,12,12,12-tridecafluorododecyl)oxy]-1,1’-biphenyl **125**

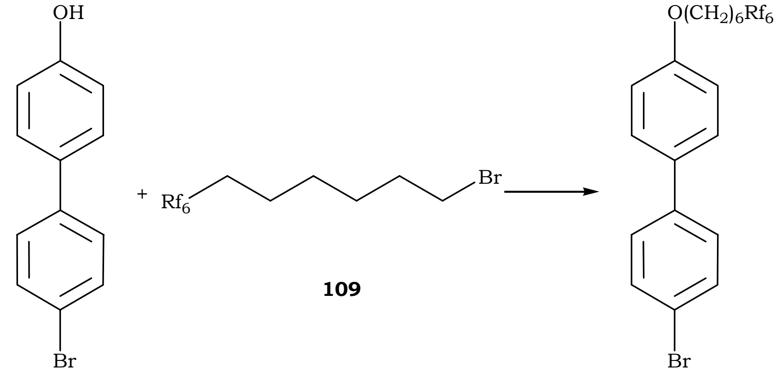

109

4-(4-Bromophenyl)phenol

125

The reaction was carried out using method K: 4-(4-bromophenyl)phenol (0.75 g, 3 mmol), **109** (1.59 g, 3.3 mmol), K_2CO_3 (1.24 g, 9 mmol), and degassed DMF (45 ml). Reaction time: 28 hours. The yellowish product was suspended in hexane, then it was collected by suction filtration affording **125** (1.76 g, 90%). ^{1}H-NMR (360 MHz, $CDCl_3$): δ 7.52-7.54 (*br. d*, 2H, Ph), 7.47-7.49 (*br. d*, 2H, Ph), 7.4-7.42 (*br. d*, 2H, Ph), 6.94-6.97 (*br. d*, 2H, Ph), 3.99-4.02 (*br. t*, 2H, O*CH*$_2$$(CH_2)_4CH_2Rf_6$), 2-2.15 (*m*, 2H, O$(CH_2)_5$*CH*$_2Rf_6$), 1.4-1.87 (*br. m*, 8H, OCH_2*(CH*$_2$*)*$_4$$CH_2Rf_6$). ^{13}C-NMR (90.55 MHz, $CDCl_3$): δ 159 (Ph), 139.9 (Ph), 132.54 (Ph), 131.93 (Ph), 128.42 (Ph), 128.11 (Ph), 120.9 (Ph), 114 (Ph), 67.92 (*s*, O*CH*$_2$$(CH_2)_4CH_2Rf_6$), 30.95 (*m*, $OCH_2(CH_2)_4$*CH*$_2$Rf$_6$), 29-29.15 (overlapped peaks, CH_2), 25.92 (CH_2), 20.23 (CH_2). EI-MS: *m/z* 652 ($[M+H]^+$, 38%), 650 ($[M+H]^+$, 34%), 249 ($[M-(CH_2)_6Rf_6]^{\bullet +}$, 100%), 247 ($[M-(CH_2)_6Rf_6]^{\bullet +}$, 97%).

16.8.2 Trimethyl({4’-[(7,7,8,8,9,9,10,10,11,11,12,12,12-tridecafluorododecyl)oxy]-1,1’-biphenyl-4-yl}ethynyl)silane **127**

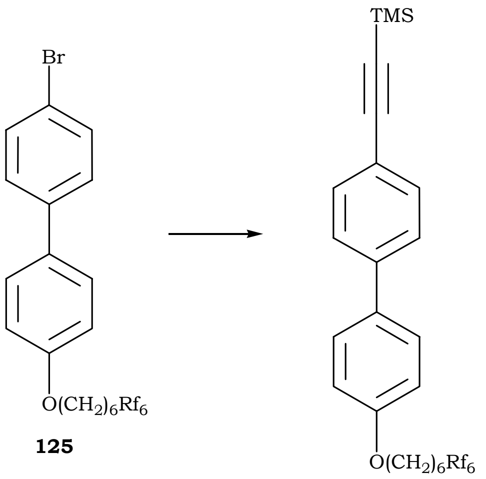

125

127

The reaction was done applying method A: **125** (325 mg, 0.5 mmol), TMSA (90 µl, 0.65 mmol), $Pd(PPh_3)_2Cl_2$ (10.5 mg, 15 µmol), Ph_3P (7.8 mg, 30 µmol), CuI (5.7 mg, 30 µmol) and piperidine (25 ml). Reaction time: 16 hours. Purification was carried out by filtration over a short silica gel plug, under reduced pressure, using pentane/CH_2Cl_2 (4:1) affording **127** (0.21 g, 64%). TLC (SiO_2, 4:1 pentane/ CH_2Cl_2: $R_f = 0.71$). ^{1}H-NMR (360 MHz, $CDCl_3$): δ 7.5-7.53 (*m*, 6H, Ph), 6.95-6.97 (*d*, 2H, Ph), 3.99-4.02 (*br. t*, 2H, $O\mathit{CH_2}(CH_2)_4CH_2Rf_6$), 2.01-2.15 (*m*, 2H, $OCH_2(CH_2)_4\mathit{CH_2}Rf_6$), 1.81-1.93 (*m*, 2H, $O(CH_2)_4\mathit{CH_2}CH_2Rf_6$), 1.61-1.79 (*m*, 6H, $OCH_2\mathit{(CH_2)_3}CH_2Rf_6$), 0.26 (*s*, 9H, TMS).

16.8.3 4-Ethynyl-4’-[(7,7,8,8,9,9,10,10,11,11,12,12,12-tridecafluorododecyl)oxy]-1,1’-biphenyl **129**

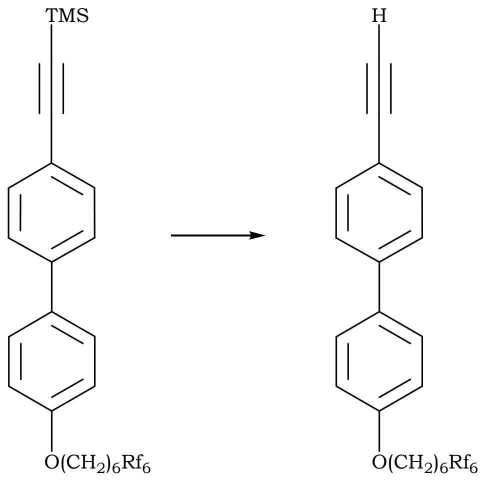

127 **129**

The deprotection reaction was carried out employing method B: **127** (472 mg, 0.69 mmol), BTACl (313 mg, 1.37 mmol), $NaOH_{aq}$ (9.5 ml, 10 M), CH_2Cl_2 (24 ml). Filtration over a short silica gel plug, under reduced pressure, using pentane/CH_2Cl_2 (4:1) yielded **129** (416 mg, 100%). TLC (SiO_2, 4:1 pentane/CH_2Cl_2: R_f = 0.71). ^{1}H-NMR (360 MHz, $CDCl_3$): δ 7.49-7.53 (*m*, 6H, Ph), 6.95-6.98 (*d*, 2H, Ph), 3.99-4.02 (*br. t*, 2H, $O\mathit{CH_2}(CH_2)_4CH_2Rf_6$), 3.11 (*s*, 1H, acetylene), 2.01-2.15 (*m*, 2H, $OCH_2(CH_2)_4\mathit{CH_2}Rf_6$), 1.81-1.93 (*m*, 2H, $O(CH_2)_4\mathit{CH_2}CH_2Rf_6$), 1.61-1.79 (*m*, 6H, $OCH_2\mathit{(CH_2)_3}CH_2Rf_6$). ^{13}C-NMR (90.55 MHz, $CDCl_3$): δ 158.98 (Ph), 141.22 (Ph), 132.54 (Ph), 128.09 (Ph), 126.48 (Ph), 120.27 (Ph), 114.86 (Ph), 93.71 (acetylene), 83.68 (acetylene), 67.79 (*s*, $O\mathit{CH_2}(CH_2)_4CH_2Rf_6$), 30.78-31.28 (*m*, $OCH_2(CH_2)_4\mathit{CH_2}Rf_6$), 29.02 ($CH_2$), 28.86 ($CH_2$), 25.79 ($CH_2$), 20.11 ($CH_2$). EI-MS: *m/z* 596 ($M^{\bullet+}$, 54%), 194 ($[M+H-(CH_2)_6Rf_6]^{\bullet+}$, 100%).

16.8.4 4-[(7,7,8,8,9,9,10,10,11,11,12,12,12-Tridecafluorododecyl)oxy]-4'-({4'-[(7,7,8,8, 9,9,10,10,11,11,12,12,12-tridecafluorododecyl)oxy]-1,1'-biphenyl-4-yl}ethynyl)-1,1'-biphenyl **130**

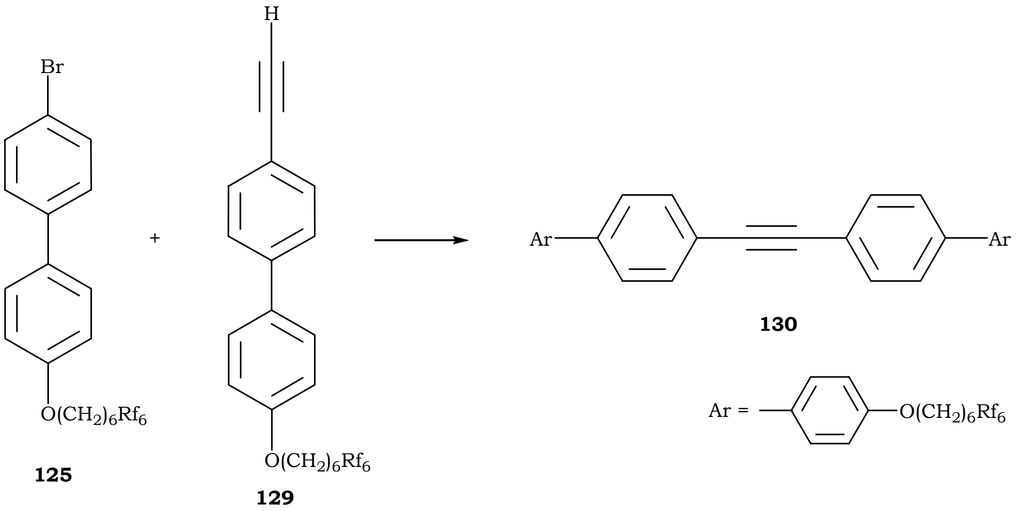

The tolane derivative **130** was synthesized as per method E: **125** (249 mg, 0.38 mmol), **129** (228 mg, 0.38 mmol), $Pd(PPh_3)_4$ (26 mg, 23 µmol), CuI (11 mg, 57 µmol), and piperidine (15 ml). The reaction was carried out at 80°C for 48 hours. The suspension was extracted with H_2O and CH_2Cl_2 (3 x 50 ml) and the suspended product in the combined organic layer was collected by suction filtration over Millipore®. The product was further purified by sonication in $CHCl_3$ (15 ml) for 5-10 minutes followed by collecting the precipitate by suction filtration over Millipore® affording **130** (266 mg, 63%). EI-MS: *m/z* 1166 ($M^{\bullet+}$, 100%), 764 ($[M+H-(CH_2)_6Rf_6]^{\bullet+}$, 4%), 362 ($[M+H-2(CH_2)_6Rf_6]^{\bullet+}$, 22%).

16.8.5 Hexakis(4-{4'-[(7,7,8,8, 9,9,10,10,11,11,12,12,12-tridecafluorododecyl)oxy]-1,1'-biphenyl})benzene **132**

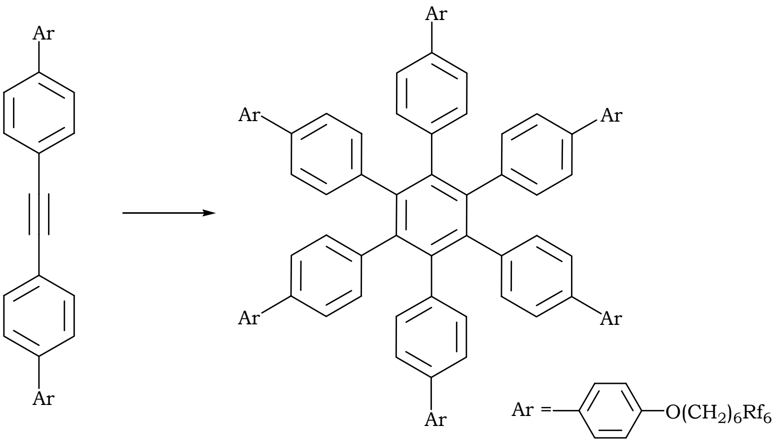

130 **132**

The trimerization reaction was carried out using method C: **130** (156 mg, 0.13 mmol), $Co_2(CO)_8$ (2.5 mg, 6.7 µmol) and dioxane (20 ml). After distilling off the solvent, the greenish product was dissolved in $CHCl_3$ and filtered over a short silica gel plug under reduced pressure to discard the metallic species. The organic layer was evaporated and the residual product was suspended in hexane (10 ml), sonicated for 10 minutes and the precipitate was collected by filtration over Millipore®, under reduced pressure. **132** (66 mg, 42%) as an off-white solid. ^{1}H-NMR (360 MHz, $CDCl_3$): δ 7.33-7.36 (*br. d*, 12H, Ph), 7.08-7.11 (*d*, ^3J(H,H) = 8.17 Hz, 12H, Ph), 6.9-6.92 (*d*, ^3J(H,H) = 8.17 Hz, 12H, Ph), 6.82-6.84 (*br. d*, 12H, Ph), 3.92-3.95 (*br. t*, 12H, $O\mathit{CH_2}(CH_2)_5Rf_6$), 2-2.15 (*m*, 12H, $O(CH_2)_5\mathit{CH_2}Rf_6$), 1.74-1.8 (*m*, 12H, $O(CH_2)_4\mathit{CH_2}CH_2Rf_6$), 1.58-1.67 (*m*, 12H, $OCH_2\,\mathit{CH_2}(CH_2)_4Rf_6$), 1.43-1.53 (*m*, 24H, $O(CH_2)_2\mathit{CH_2CH_2}(CH_2)_2Rf_6$). ^{13}C-NMR (90.55 MHz, $CDCl_3$): δ 158.29 (Ph), 140.31 (Ph), 139.18 (Ph), 137.1 (Ph), 133.29 (Ph), 131.93 (Ph), 127.72 (Ph), 124.77 (Ph), 114.56 (Ph), 67.73 (*s*, $O\mathit{CH_2}(CH_2)_5Rf_6$), 31.83 (*m*, $O(CH_2)_5\mathit{CH_2}Rf_6$), 29 (*s*, CH_2), 28.84 (CH_2), 25.75 (CH_2), 20.08 (CH_2). MALDI-TOF: *m/z* 3600 (18%), 3501 ($M^{\bullet+}$, 100%), 3142 (19%), 3017 (21%), 2350 (13%).

16.8.6 2,5,8,11,14,17-Hexakis{4-[(7,7,8,8,9,9,10,10,11,11,12,12,12-tridecafluoro-dodecyl)oxy]phenyl}hexabenzo[*bc,ef,hi,kl,no,qr*]coronene **134**

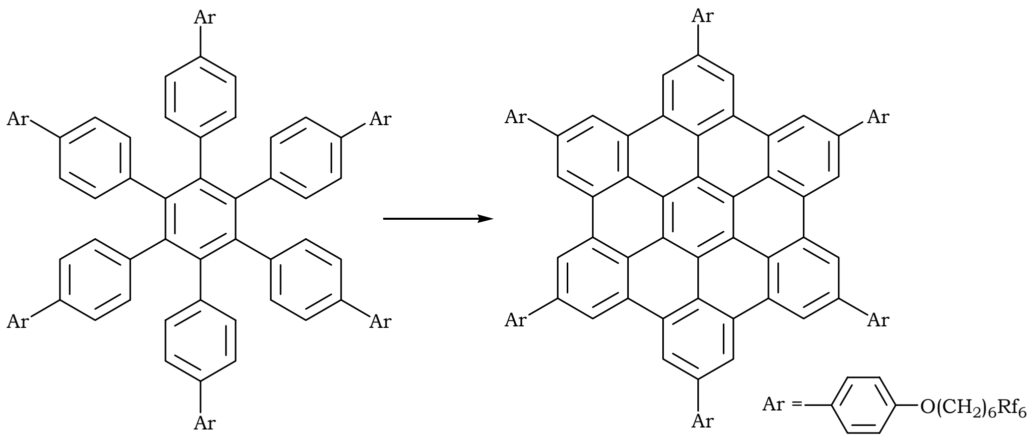

132 **134**

The HBC derivative synthesis was done applying method G: **132** (103 mg, 29 µmol), $FeCl_3$ (0.35 g, 2.12 mmol), CH_3NO_2 (5 ml), CH_2Cl_2 (40 ml). Reaction time: 8 hours. The yellow-brown suspension was extracted with $NH_4Cl_{sat.}$ (25 ml) and methylene dichloride (3 x 25 ml). The combined organic layer was then washed with H_2O (3 x 50 ml) and the solvent was evaporated affording a brown-yellow solid which was suspended in CH_2Cl_2 (30 ml), sonicated for 15 minutes, and collected by suction filtration over Millipore®. The precipitate was then washed successively CH_2Cl_2 (60 ml), H_2O (60 ml), ether (60 ml), and finally $CHCl_3$ (60 ml). **134** was isolated as a bright yellow solid (75 mg, 73%). MALDI-TOF: *m/z* 3514 (36%), 3487 ($M^{\bullet+}$, 100%), 3124 (17%). UV-Vis: 369.5 (5.06), 395 (4.8), 453 (4.01).

17. Attempted synthesis of nitrogen-containing PAH

17.1 Synthesis of the perfluorinated binaphthyl amine compound 144

17.1.1 4-Bromonaphthalene-1-diazonium tetrafluoroborate **138**

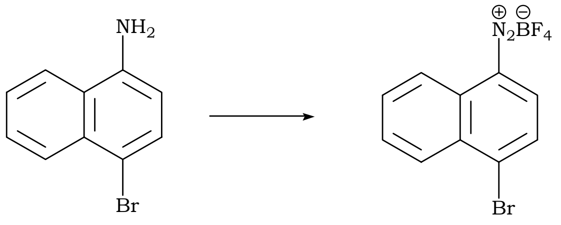

136 **138**

Method L. $BF_3.Et_2O$ (2.5 ml, 19.5 mmol) was placed in a three-necked round bottomed flask equipped with an addition funnel, a septum, and a reflux condenser. The temperature was decreased to -15°C and a solution of 4-bromonaphthylamine **136** (3 g, 13 mmol) in dimethoxy ethane (DME, 15 ml) was added dropwise first, followed by the addition of a solution of $^tBuNO_2$ (2.1 ml, 15.6 mmol) in DME (25 ml), at the same temperature, during 15 minutes. After stirring the reaction at -15°C for 20 minutes, the temperature was raised to 5°C over a period of 20 minutes. Pentane (50 ml) was then added and the suspended compound was collected by suction filtration, washed with ether (50 ml at 0°C, and 50 ml at RT) yielding a kaki solid (4.16 g, 100%).

17.1.2 1-Bromo-4-[(1*E*)-3,3,4,4,5,5,6,6,7,7,8,8,9,9,10,10-heptadecafluorodec-1-enyl]-naphthalene **140**

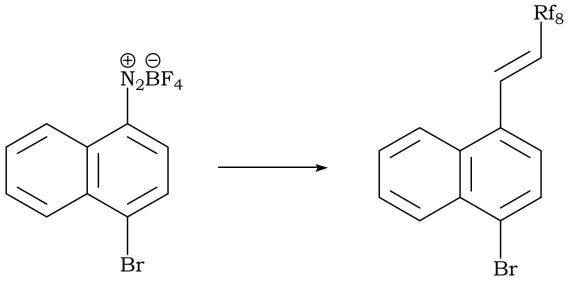

138 **140**

The Heck cross-coupling reaction was carried out following method H: diazonium salt **138** (0.32 g, 1 mmol), 3,3,4,4,5,5,6,6,7,7,8,8,9,9,10,10-heptadecafluorodec-1-ene (0.28

ml, 1 mmol), $Pd(OAc)_2$ (11.2 mg, 50 µmol), MeOH (3 ml). Reaction time: 3 hours. Purification by filtration over a short silica gel plug using pentane/CH_2Cl_2 (4:1) afforded **140** (0.495 g, 76%) as a yellow solid. TLC (SiO_2, hexane: R_f = 0.73). ^{1}H-NMR (360 MHz, $CDCl_3$): δ 8.34-8.31 (*br. d*, 1H, aromatic), 8.04-8.02 (*br. d*, 1H, aromatic), 7.9-7.95 (*br. d*, 1H, C*H*=*C*HRf$_8$), 7.8-7.82 (*d*, 1H, aromatic), 7.62-7.68 (*m*, 2H, aromatic), 7.47-7.49 (*d*, 1H, aromatic) 6.22-6.33 (*q*, 1H, CH=*CH*Rf$_8$).

17.1.3 1-Bromo-4-(3,3,4,4,5,5,6,6,7,7,8,8,9,9,10,10-heptadecafluorodecyl)naphthalene **142**

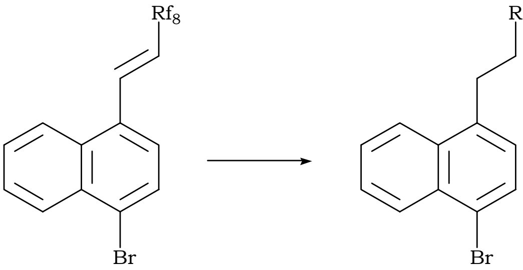

140 **142**

The hydrogenation reaction was done employing method I: **140** (4.43 g, 6.7 mmol), Rh/C (0.28 g, 0.13 mmol), and degassed CH_2Cl_2 (35 ml). Reaction time: 24 hours. The product was purified by filtration over silica gel column chromatography with CH_2Cl_2 as eluent (4 g, 91%). TLC (SiO_2, pentane: R_f = 0.62). ^{1}H-NMR (360 MHz, $CDCl_3$): δ 8.31-8.34 (*m*, 1H, aromatic), 7.94-7.98 (*m*, 1H, aromatic), 7.72-7.74 (*d*, 1H, aromatic), 7.61-7.66 (*m*, 2H, aromatic) 7.22-7.24 (*d*, 1H, aromatic), 3.34-3.38 (*m*, 2H, *CH*$_2$CH$_2$Rf$_8$), 2.4-2.55 (*m*, 2H, CH$_2$*CH*$_2$Rf$_8$). ^{13}C-NMR (90.55 MHz, $CDCl_3$): δ 135.2 (aromatic), 132.62 (aromatic), 132.35 (aromatic), 129.71 (aromatic), 128.4 (aromatic), 127.38 (aromatic), 127.3 (aromatic), 126.75 (aromatic), 123.33 (aromatic), 122.26 (aromatic), 31.87-32.36 (*m*, CH$_2$*CH*$_2$Rf$_8$), 23.5-23.6 (*m*, *CH*$_2$CH$_2$Rf$_8$).

17.1.4 4-Nitronaphthalene-1-diazonium tetrafluoroborate **139**

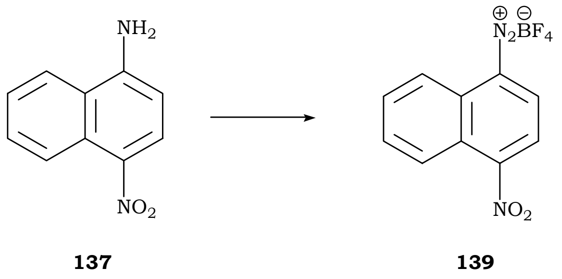

The diazotization reaction was carried out applying method L: **137** (2.52 g, 13 mmol), $BF_3.Et_2O$ (2.5 ml, 19.5 mmol), $^tBuNO_2$ (2.1 ml, 15.6 mmol), and DME (65 ml). Bright yellow solid (3.82 g, 99%).

17.1.5 1-[(1*E*)- 3,3,4,4,5,5,6,6,7,7,8,8,9,9,10,10-Heptadecafluorodec-1-enyl]]-4-nitro-naphthalene **141**

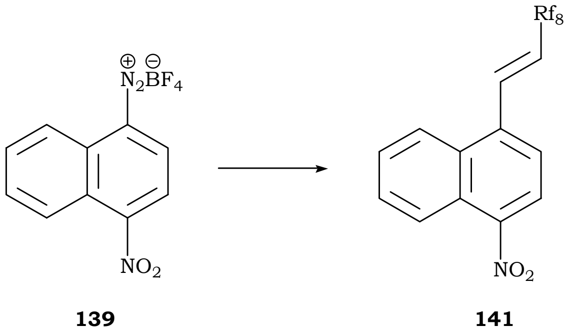

The cross-coupling reaction was performed as per method H: diazonium salt **139** (1.7 g, 5.9 mmol), 3,3,4,4,5,5,6,6,7,7,8,8,9,9,10,10-heptadecafluorodec-1-ene (1.56 ml, 5.9 mmol), $Pd(OAc)_2$ (66.5 mg, 0.3 mmol), MeOH (20 ml). Reaction time: 3 hours. Silica gel column chromatography using pentane/CH_2Cl_2 (4:1) yielded **141** (3.27 g, 90%) as a yellow solid. TLC (SiO_2, 4:1 pentane/CH_2Cl_2: R_f = 0.61). ^{1}H-NMR (360 MHz, $CDCl_3$): δ 8.58-8.55 (*d*, ^3J(H,H) = 8.17 Hz, 1H, aromatic), 8.18-8.2 (*d*, ^3J(H,H) = 8.17 Hz, 1H, aromatic), 8.1-8.13 (*d*, 1H, ^3J(H,H) = 8.17 Hz, aromatic), 7.95-7.99 (*br. d*, 1H, C*H*=CHRf$_8$), 7.72-7.81 (*m*, 2H, aromatic), 7.67-7.69 (*d*, 1H, aromatic) 6.3-6.41 (*q*, 1H, CH=*CH*Rf$_8$).

17.1.6 4-(3,3,4,4,5,5,6,6,7,7,8,8,9,9,10,10-heptadecafluorodecyl)-1-naphthylamine **143**

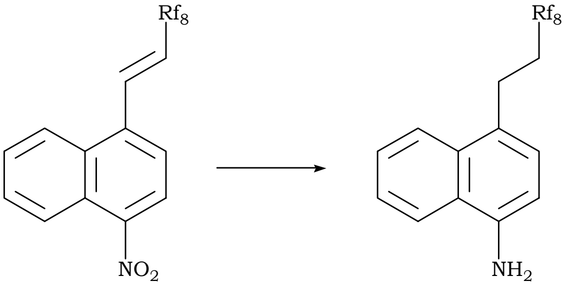

141 **143**

The reaction was done applying method I: **141** (0.93 g, 1.5 mmol), Pd/C (0.08 g, 75 µmol, 10% Pd), and degassed THF/MeOH (1:1, 15 ml) under 3 atm. of H_2. Reaction time: 24 hours. The product was purified by silica gel column chromatography with pentane/CH_2Cl_2 (2:1) as eluent (0.83 g, 94%). TLC (SiO_2, 2:1 pentane/CH_2Cl_2: R_f = 0.21). ^{1}H-NMR (360 MHz, C_6D_6): δ 7.74-7.76 (*d*, ^3J(H,H) = 8.17 Hz, 1H, aromatic), 7.49-7.51 (*d*, ^3J(H,H) = 8.17 Hz, 1H, aromatic), 7.2-7.35 (*m*, 2H, aromatic), 6.81-6.83 (*d*, ^3J(H,H) = 7.74 Hz, 1H, aromatic), 6.29-6.31 (*d*, ^3J(H,H) = 7.74 Hz, 1H, aromatic), 3.3 (*br. s*, 2H, NH), 3.06-3.1 (*m*, 2H, *CH_2*CH_2Rf_8), 2.12-2.24 (*m*, 2H, CH_2*CH_2*Rf_8).

17.1.7 *N,N*-Bis[4-(3,3,4,4,5,5,6,6,7,7,8,8,9,9,10,10-heptadecafluorodecyl)-1-naphthyl]-amine **144**

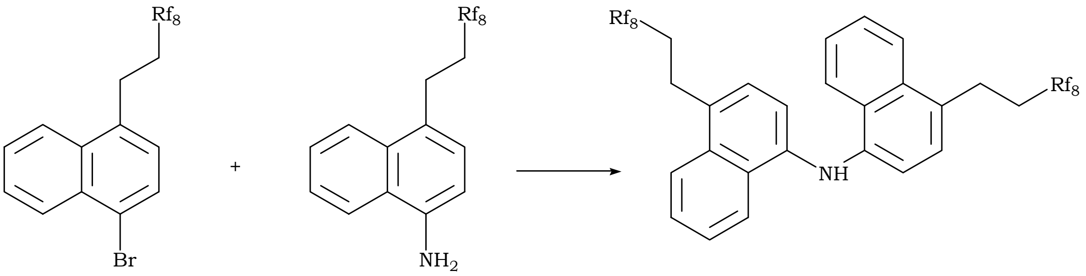

142 **143** **144**

Method M. A Schlenk flask was charged with **142** (130 mg, 0.2 mmol), **143** (118 mg, 0.2 mmol), $Pd(OAc)_2$ (2.2 mg, 10 µmol), $^tBu_3P$ (8.1 mg, 10 µmol), NaO^tBu (30 mg, 0.3 mmol), and degassed toluene or xylene (2 ml). The reaction was carried out at 125°C for 48 hours under an argon atmosphere. The dark brown solution was extracted with $NH_4Cl_{sat.}$ and ether (3 x 25 ml). The combined organic layer was washed with H_2O (3 x 25 ml), dried over K_2CO_3, and filtered. Removal of the solvent yielded a brown product which was chromatographed using a mixture of pentane/CH_2Cl_2 (9:1) to afford **144** (191 mg, 83%)

as a faint yellow product. TLC (SiO_2, 9:1 pentane/CH_2Cl_2: R_f = 0.41). ^{1}H-NMR (500 MHz, C_6D_6): δ 7.94-7.95 (*d*, 2H, aromatic), 7.82-7.83 (*d*, 2H, aromatic), 7.23-7.38 (*m*, 4H, aromatic), 6.81-6.82 (*d*, 2H, aromatic), 6.76-6.77 (*d*, 2H, aromatic), 5.8 (*br. s*, 1H, NH), 3.1-3.13 (*m*, 4H, $\mathit{CH_2}CH_2Rf_8$), 2.17-2.27 (*m*, 4H, $CH_2\mathit{CH_2}Rf_8$).). ^{13}C-NMR (125.77 MHz, C_6D_6): δ 140.3 (aromatic), 132.73 (aromatic), 131.91 (aromatic), 128.15 (aromatic), 126.82 (aromatic), 126.8 (aromatic), 125.66 (aromatic), 123.71 (aromatic), 123.31 (aromatic), 115.73 (aromatic), 31.4 (*m*, $CH_2\mathit{CH_2}Rf_8$), 23.34 (*m*, $\mathit{CH_2}CH_2Rf_8$). ESI-MS (HCOOH/THF): *m/z* 1206 ($[M+CO_2]^{\bullet +}$, 35%), 1162 ($[M+H]^+$, 100%), 288 (22%).

17.2 Attempted syntheses of the *N,N,N*-tris[4-(3,3,4,4,5,5,6,6,7,7,8,8,9,9,10,10-heptadecafluorodecyl)-1-naphthyl]amine 135

17.2.1 Using the binaphthylamine derivative **144**

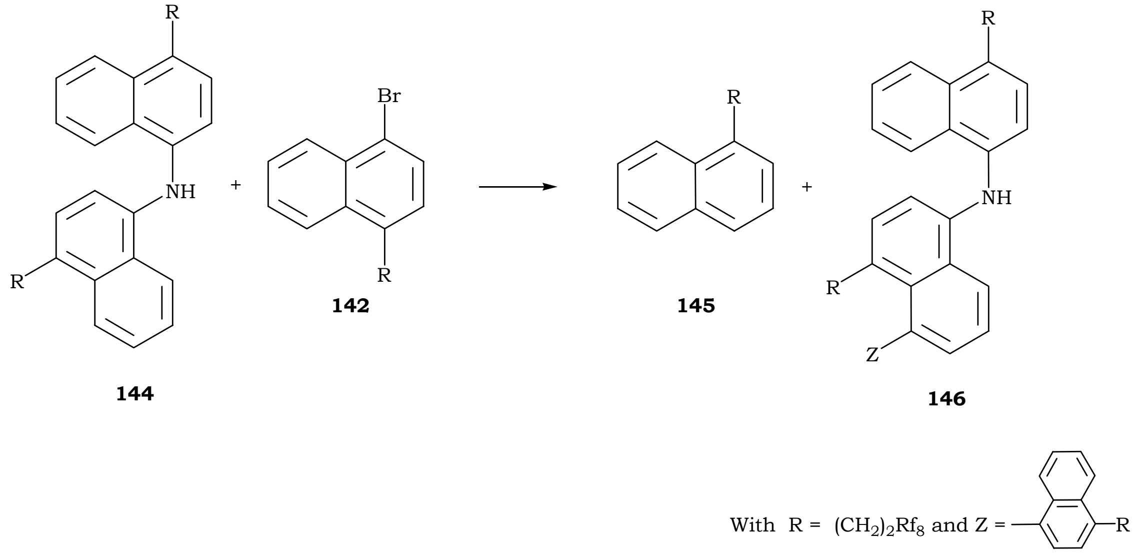

The reaction was carried out following method M: **144** (116 mg, 0.1 mmol), **142** (66 mg, 0.1 mmol), $Pd(OAc)_2$ (1.12 mg, 5 µmol), $^tBu_3P$ (4 mg, 20 µmol), Cs_2CO_3 (100 mg, 0.3 mmol), and degassed xylene (10 ml). **145** (21 mg, 36% partially determined from ^1H NMR spectrum), **146** (27 mg, 16%).

145: ^1H-NMR (500 MHz, C_6D_6): δ 7.72-7.74 (*m*, 1H, aromatic), 7.64-7.66 (*m*, 1H, aromatic), 7.54-7.56 (*br. d*, 1H, aromatic), 7.24-7.28 (*m*, 2H, aromatic), 7.14-7.17 (*br. d*, 1H, aromatic), 6.87-6.89 (*br. d*, 1H, aromatic), 3.06-3.1 (*m*, 2H, $\mathit{CH_2}CH_2Rf_8$), 2.09-2.2 (*m*, 2H, $CH_2\mathit{CH_2}Rf_8$). ^{13}C-NMR (125.77 MHz, C_6D_6): δ 135.09 (aromatic), 134.46 (aromatic), 131.85 (aromatic), 129.33 (aromatic), 128.29 (aromatic), 126.64 (aromatic), 126.44 (aromatic), 125.98 (aromatic), 125.75 (aromatic), 123.04 (aromatic), 111.06-120.80 (*m*, CF_2), 31.9-31.3 (*m*, $CH_2\mathit{CH_2}Rf_8$), 23.58 (*br. s*, $\mathit{CH_2}CH_2Rf_8$). EI-MS: *m/z* 574 ($M^{\bullet+}$, 100%).

146: ^1H-NMR (500 MHz, C_6D_6): δ 8.23-8.25 (*m*, 1H, aromatic), 7.92-7.94 (*d*, 1H, aromatic), 7.88-7.9 (*m*, 1H, aromatic), 7.72 (*br. s*, 1H, aromatic), 7.62-7.63 (*d*, 1H, aromatic), 7.52 (*br. s*, 1H, aromatic), 7.31-7.36 (*overlapped peaks*, 3H, aromatic), 7.2-7.25 (*m*, 4H, aromatic), 6.98-7.01 (*br. t*, 1H, aromatic), 6.63 (*br. s*, 2H, aromatic), 6.48-6.49 (*d*, 1H, aromatic), 5.96 (*s*, 1H, NH), 3.19-3.3 (*m*, 2H, $\mathit{CH_2}CH_2Rf_8$), 2.89-3.02 (*m*, 4H,

*CH_2*CH_2Rf_8), 2.31-2.39 (*m*, 2H, CH_2*CH_2*Rf_8), 1.94-2.07 (*m*, 4H, CH_2*CH_2*Rf_8). EI-MS: *m/z* 1733 ($M^{\bullet +}$, 70%), 1714 ($[M-F]^{\bullet +}$, 8%), 1300 ($[M-CH_2Rf_8]^{\bullet +}$, 100%), 156 (60%).

17.2.2 Starting from the perfluorinated binaphthyl amide derivative **144.1**

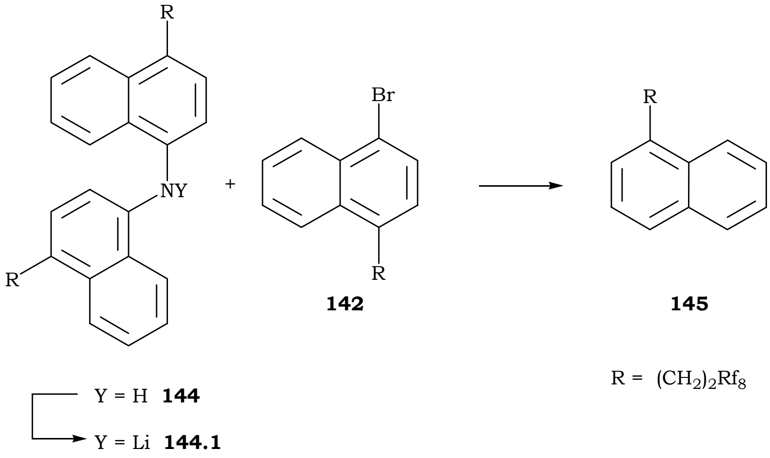

142

145

R = $(CH_2)_2Rf_8$

Y = H **144**

Y = Li **144.1**

n-BuLi (0.25 mmol, 0.16 ml, 1.6 M in hexanes) was injected dropwise to a solution of **144** (116 mg, 0.1 mmol) in degassed THF (5 ml) at -85°C and the reaction was carried out for 2 hours. After allowing the reaction to warm gently at room temperature, it was stirred for 22 hours under argon (total reaction time: 24 hours). The volume of THF was concentrated to ~0.5 ml and the solution was added, via cannula, to a solution of **142** (66 mg, 0.1 mmol), $Pd_2(dba)_3$ (2.3 mg, 2.5 µmol) and $^tBu_3P$ (4 mg, 20 µmol) in degassed toluene (6 ml) and the reaction was carried out at 90°C for 46 hours under an atmosphere of argon. The green-yellow solution was extracted with $NH_4Cl_{sat.}$ and ether (3 x 25 ml). The combined organic layer was washed with H_2O (3 x 25 ml), dried over Na_2SO_4, and filtered. Removal of the solvent afforded a yellow product which was passed through a silica gel column chromatography with hexane as eluent to yield a white solid (24 mg, 42%). TLC (SiO_2, 9:1 hexane: R_f = 0.66). ^{1}H-NMR (500 MHz, C_6D_6): δ 7.72-7.74 (*m*, 1H, aromatic), 7.64-7.66 (*m*, 1H, aromatic), 7.54-7.56 (*br. d*, 1H, aromatic), 7.24-7.28 (*m*, 2H, aromatic), 7.14-7.17 (*br. d*, 1H, aromatic), 6.87-6.89 (*br. d*, 1H, aromatic), 3.06-3.1 (*m*, 2H, *CH_2*CH_2Rf_8), 2.09-2.2 (*m*, 2H, CH_2*CH_2*Rf_8). ^{13}C-NMR (125.77 MHz, C_6D_6): δ 135.09 (aromatic), 134.46 (aromatic), 131.85 (aromatic), 129.33 (aromatic), 128.29 (aromatic), 126.64 (aromatic), 126.44 (aromatic), 125.98 (aromatic), 125.75 (aromatic), 123.04 (aromatic), 111.06-120.80 (*m*, CF_2), 31.9-31.3 (*m*, CH_2*CH_2*Rf_8), 23.58 (*br. s*, *CH_2*CH_2Rf_8). EI-MS: *m/z* 574 ($M^{\bullet +}$, 100%).

17.2.3 5,8-Bis(3,3,4,4,5,5,6,6,7,7,8,8,9,9,10,10-heptadecafluorodecyl)-13*H*-dibenzo[a,i]-carbazole **149**

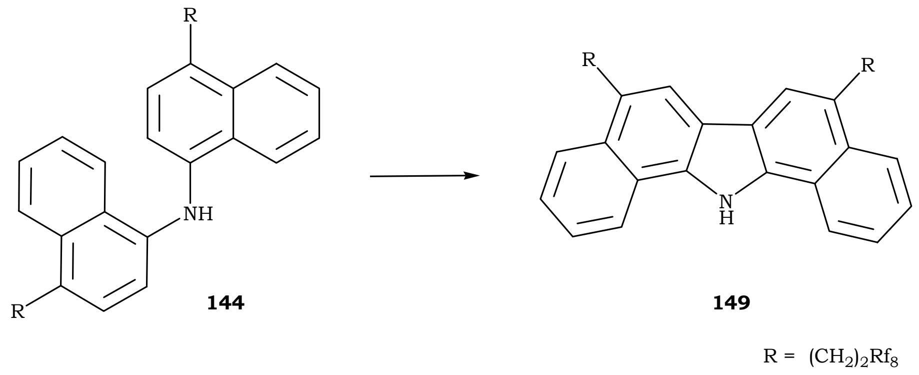

To a refluxed solution of the binaphthyl amine derivative **144** (116 mg, 0.1 mmol) in degassed CH_2Cl_2 (15 ml) was added, dropwise, a solution of [bis(trifluoro-acetoxy)iodo]benzene (PIFA, 53 mg, 0.12 mmol) and $BF_3.Et_2O$ (34 mg, 0.24 mmol) in CH_2Cl_2 (5 ml). The reaction was refluxed for 7 hours followed by stirring at room temperature overnight under argon. After evaporating the solvent, the starting material was removed by silica gel column chromatography using pentane/ether (4:1) and the fractions having an $R_f < 0.5$ were then collected and chromatographed using a 97.5:2.5 pentane/ethyl acetate mixture as eluent which afforded **149** (15 mg, 13%) as a white product. TLC (SiO_2, 9:1 pentane/ethyl acetate: $R_f = 0.32$). ^{1}H-NMR (360 MHz, $CDCl_3$): δ 8.8 (*br. s*, 1H, NH), 8-8.03 (*br. d*, 2H, aromatic), 7.88 (*s*, 2H, aromatic), 7.77-7.79 (*d*, 2H, aromatic), 7.41-7.48 (*m*, 4H, aromatic), 3.4-3.44 (*m*, 4H, $\mathit{CH_2}CH_2Rf_8$), 2.4-2.43 (*m*, 4H, $CH_2\mathit{CH_2}Rf_8$). EI-MS: *m/z* 1159 ($M^{\bullet+}$, 42%), 1140 ($[M-F]^{\bullet+}$, 8%), 726 ($[M-CH_2Rf_8]^{\bullet+}$, 100%), 293 (20%).

17.3 Synthesis of perfluorinated aryl amine derivatives

17.3.1 *N,N*-Bis[4-(3,3,4,4,5,5,6,6,7,7,8,8,9,9,10,10-heptadecafluorodecyl)-1-naphthyl]- *N*-[4-(3,3,4,4,5,5,6,6,7,7,8,8,9,9,10,10-heptadecafluorodecyl)phenyl]amine **151**

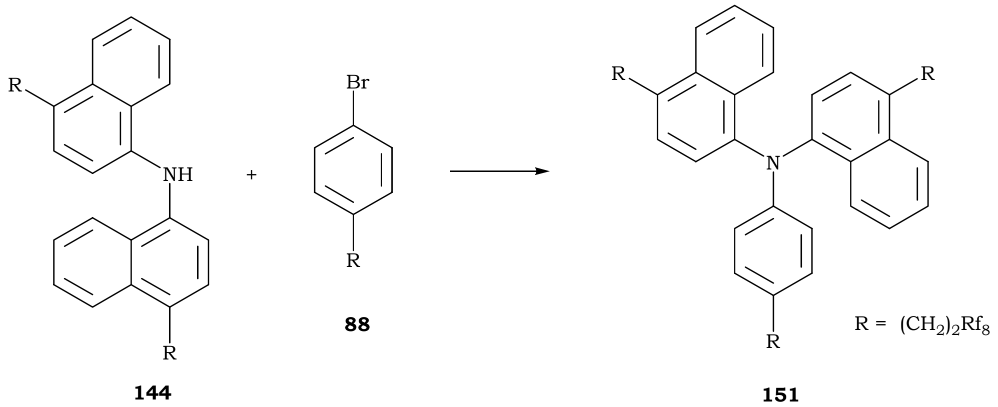

The reaction was done as per method M: **144** (116 mg, 0.1 mmol), **88** (60 mg, 0.1 mmol), $Pd(OAc)_2$ (1.12 mg, 5 µmol), $^tBu_3P$ (4 mg, 20 µmol), NaO^tBu (15 mg, 0.15 mmol), and degassed toluene (5 ml). Reaction time: 82 hours. **151** (108 mg, 64%) as a glassy colorless solid. TLC (SiO_2, 9:1 pentane/CH_2Cl_2: R_f = 0.65). ^{1}H-NMR (360 MHz, THF-d_8): δ 8.26-8.28 (*d*, ^3J(H,H) = 8.17 Hz, 2H, aromatic), 8.17-8.19 (*d*, ^3J(H,H) = 8.64 Hz, 2H, aromatic), 7.63-7.68 (*t*, ^3J(H,H) = 7.7 Hz, 2H, aromatic), 7.45-7.48 (*m*, 4H, aromatic and Ph), 7.25-7.27 (*d*, ^3J(H,H) = 7.7 Hz, 2H, Ph), 7.13-7.15 (*d*, ^3J(H,H) = 8.64 Hz, 2H, aromatic), 6.73-6.76 (*d*, ^3J(H,H) = 8.17 Hz, 2H, aromatic), 3.5-3.54 (*br. t*, 4H, $\mathit{CH_2}CH_2Rf_8$), 2.92-2.96 (*br. t*, 2H, $\mathit{CH_2}CH_2Rf_8$), 2.67-2.78 (*m*, 4H, $CH_2\mathit{CH_2}Rf_8$), 2.53-2.62 (*m*, 2H, $CH_2\mathit{CH_2}Rf_8$). ^{1}H-NMR (360 MHz, C_6D_6): δ 8.45-8.48 (*d*, ^3J(H,H) = 8.64 Hz, 2H, aromatic), 7.73-7.76 (*d*, ^3J(H,H) = 8.17 Hz, 2H, aromatic), 7.21-7.23 (*d*, 2H, aromatic), 7.09-7.17 (*m*, 4H, aromatic and Ph), 6.8-6.84 (*t*, 4H, aromatic), 6.62-6.64 (*d*, ^3J(H,H) = 8.17 Hz, 2H, aromatic), 3.05-3.09 (*br. t*, 4H, $\mathit{CH_2}CH_2Rf_8$), 2.49-2.53 (*br. t*, 2H, $\mathit{CH_2}CH_2Rf_8$), 2.08-2.23 (*m*, 4H, $CH_2\mathit{CH_2}Rf_8$), 1.83-1.98 (*m*, 2H, $CH_2\mathit{CH_2}Rf_8$). ^{13}C-NMR (90.55 MHz, C_6D_6): δ 133.92 (aromatic), 133.35 (aromatic), 131.45 (aromatic), 129.8 (aromatic), 127.28 (aromatic), 127.3 (aromatic), 127.13 (aromatic), 126.08 (aromatic), 125.27 (aromatic), 124.38 (aromatic), 33.3 (*br. s*, $CH_2\mathit{CH_2}Rf_8$), 32.51 (*br. s*, $CH_2\mathit{CH_2}Rf_8$), 23.95 (*br. s*, $\mathit{CH_2}CH_2Rf_8$). ESI-MS (HCOOH/THF): *m/z* 1732 ($[M+HCO_2]^{\bullet+}$, 55%), 1683 ($M^{\bullet+}$, 100%). EI-MS: *m/z* 1683 ($M^{\bullet+}$, 100%), 1664 ($[M-F]^{\bullet+}$, 40%), 1250 ($[M-CH_2Rf_8]^{\bullet+}$, 45%), 789 (10%).

17.3.2 *N,N,N',N'*-Tetrakis[4-(3,3,4,4,5,5,6,6,7,7,8,8,9,9,10,10-heptadecafluorodecyl)-1-naphthyl]-1,1'-biphenyl-4,4'-diamine **152**

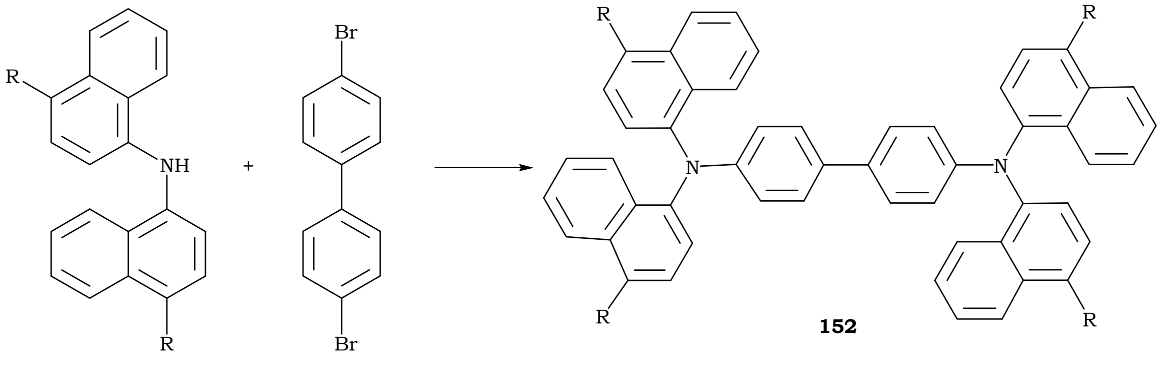

144 **150** **152**

The reaction was carried out applying method M: **144** (116 mg, 0.1 mmol), **150** (16 mg, 50 µmol), Pd(OAc)$_2$ (1.12 mg, 5 µmol), ^{t}Bu$_3$P (4 mg, 20 µmol), NaO^{t}Bu (15 mg, 0.15 mmol), and degassed toluene (5 ml). Reaction time: 7 days. After extraction, the off-white solid was suspended in CH$_2$Cl$_2$, sonicated for 15-20 minutes and collected by suction filtration over Millipore®. The precipitate was purified by successive washings with CH$_2$Cl$_2$ (60 ml) and ether (45 ml) affording **152** (62 mg, 50%) as a white solid. m.p.: 242°C. ^{1}H-NMR (360 MHz, THF-d$_8$): δ 8.16-8.18 (*d*, ^3J(H,H) = 8.64 Hz, 4H, aromatic), 8.05-8.07 (*d*, ^3J(H,H) = 8.6 Hz, 4H, aromatic), 7.51-7.55 (*t*, ^3J(H,H) = 7.27 Hz, 4H, aromatic), 7.34-7.37 (*m*, 8H, aromatic), 7.29-7.31 (*d*, ^3J(H,H) = 8.17 Hz, 4H, Ph), 6.65-6.67 (*d*, ^3J(H,H) = 8.17 Hz, 4H, Ph), 2.56-2.68 (*m*, 8H, CH$_2$*CH$_2$*Rf$_8$). ESI-MS (HCOOH/THF): *m/z* 2473 (M$^{\bullet+}$, 100%), 1957 (58%), 686 (48%). EI-MS: *m/z* 2473 (M$^{\bullet+}$, 100%).

V. Annexes

A.1 Calorimetric data from DSC measurements

Phase transition temperatures, enthalpy changes and structural assignments for perfluoroalkylated alkyl HBC derivatives[a,b].

Entry	Compound	Phase Transition temperature (°C)	ΔH (KJ mol^{-1})	Phase width (°C)	Assignment
		heating/cooling	heating/cooling		
1	**HBC-Rf$_{2,8}$ (98)**	122/114	1.4/1.2	-	$D_1 \leftrightarrow D_2$
		138/128	37.2/36	16	$D_2 \leftrightarrow D_3$
		180/173	7.7/6.5	42	$D_3 \leftrightarrow D_4$
2[c]	**HBC-PhRf$_{2,8}$ (99)**	227/223	66.4/60.5	-	$D_1 \leftrightarrow D_2$
		236/235	19.8/14.2	9	$D_2 \leftrightarrow D_3$
3	**HBC-Rf$_{4,8}$ (114)**	82/(d)	6/(d)	-	$K_1 \rightarrow K_2$
		120/103	58/52.6	38	$K_2 \leftrightarrow D_1$
		190/171	8.5/7.8	70	$D_1 \leftrightarrow D_2$
4[c]	**HBC-Rf$_{6,6}$ (115)**	50/(d)	4.6/(d)	-	$K_1 \rightarrow K_2$
		109/98	48/46	18	$K_2 \leftrightarrow D_1$
5	**HBC-PhORf$_{4,8}$ (133)**	182/(d)	3/(d)	-	$K_1 \leftrightarrow K_2$
		216/207	18.7/19	34	$K_2 \leftrightarrow D_1$
		222/215	6.3/25.6	6	$D_1 \leftrightarrow D_2$
6	**HBC-PhORf$_{6,6}$ (134)**	-	-	-	-

a: isotropic liquid wasn't formed below 360°C, decomposition occurs above ~250°C. b: rate of heating & cooling is 20°C/min. c: two peaks were obtained upon heating. With K: crystalline, D$_h$: discotic hexagonal, D: discotic. d: not determined.

A.2 SEM micrographs of HBC-SCF_3 (71)

A.2.1 Precipitate

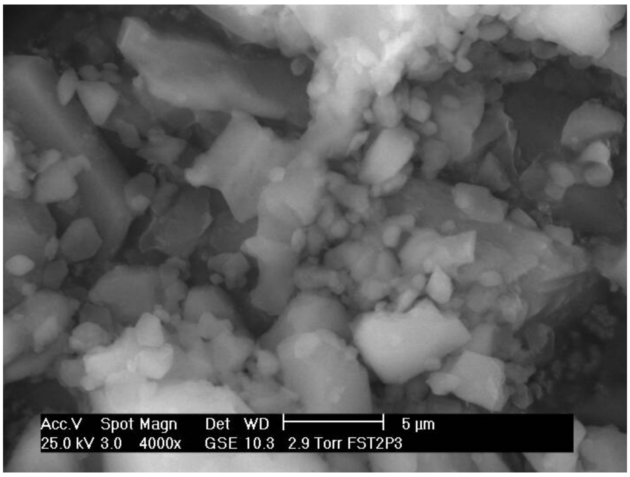
Acc.V Spot Magn Det WD 5 µm
25.0 kV 3.0 4000x GSE 10.3 2.9 Torr FST2P3

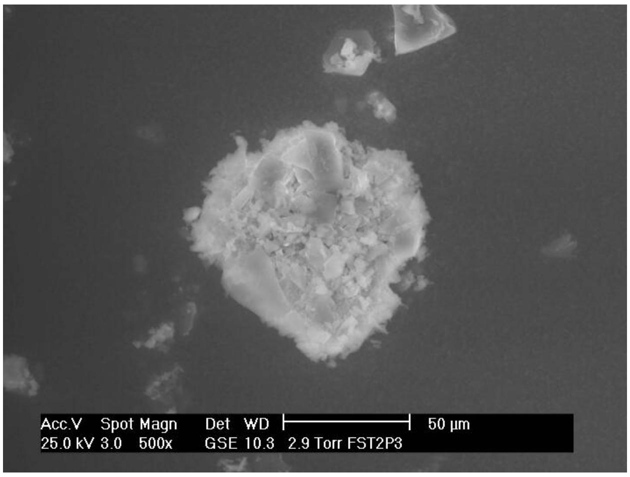
Acc.V Spot Magn Det WD 50 µm
25.0 kV 3.0 500x GSE 10.3 2.9 Torr FST2P3

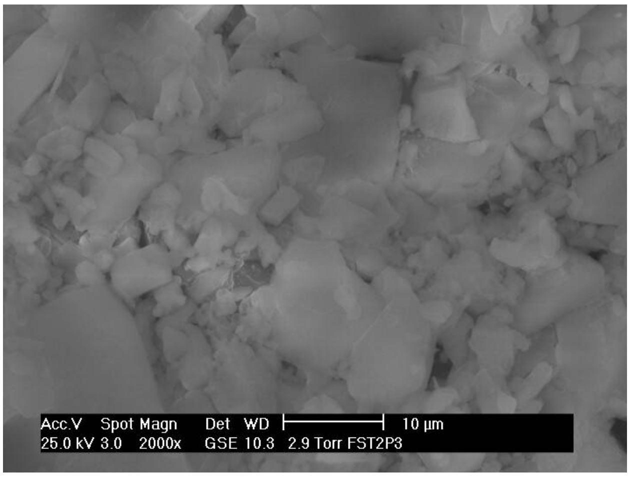
Acc.V Spot Magn Det WD 10 µm
25.0 kV 3.0 2000x GSE 10.3 2.9 Torr FST2P3

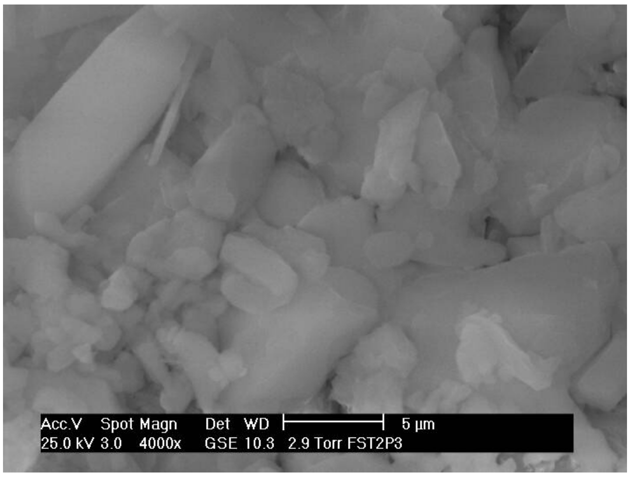
Acc.V Spot Magn Det WD 5 µm
25.0 kV 3.0 4000x GSE 10.3 2.9 Torr FST2P3

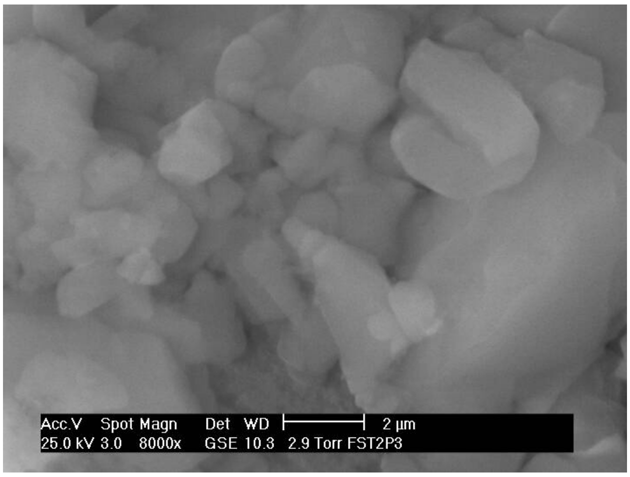
Acc.V Spot Magn Det WD 2 µm
25.0 kV 3.0 8000x GSE 10.3 2.9 Torr FST2P3

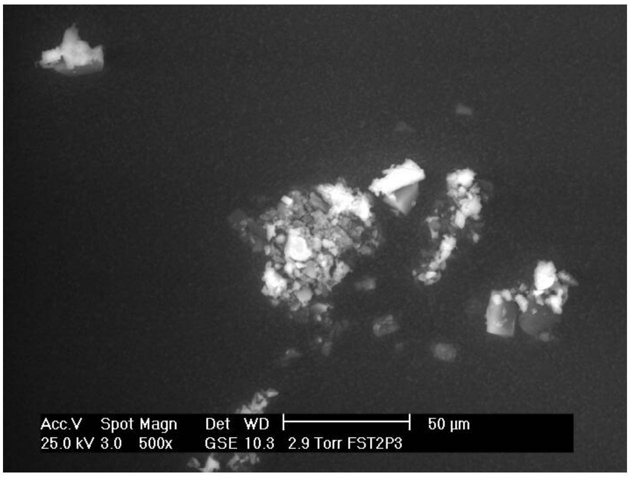
Acc.V Spot Magn Det WD 50 µm
25.0 kV 3.0 500x GSE 10.3 2.9 Torr FST2P3

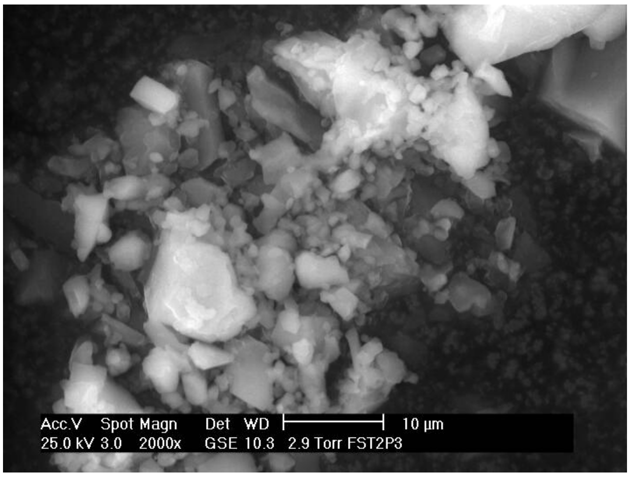
Acc.V Spot Magn Det WD 10 µm
25.0 kV 3.0 2000x GSE 10.3 2.9 Torr FST2P3

A.2.2 Deposited film from a dilute solution

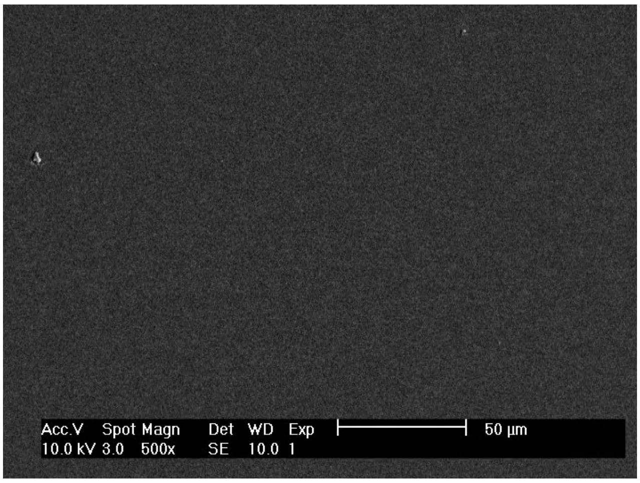
Acc.V Spot Magn Det WD Exp 50 µm
10.0 kV 3.0 500x SE 10.0 1

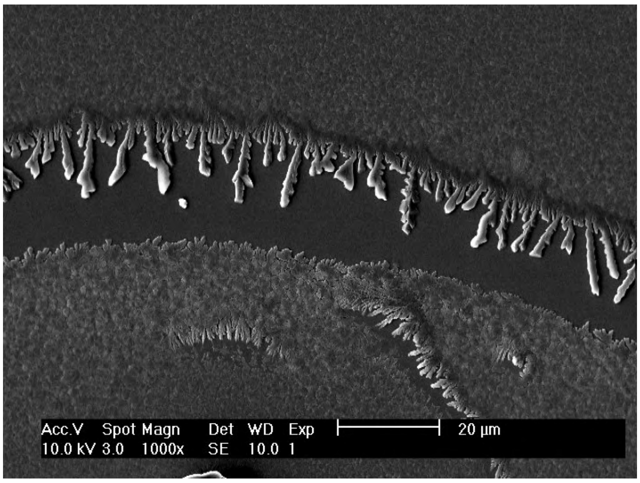
Acc.V Spot Magn Det WD Exp 20 µm
10.0 kV 3.0 1000x SE 10.0 1

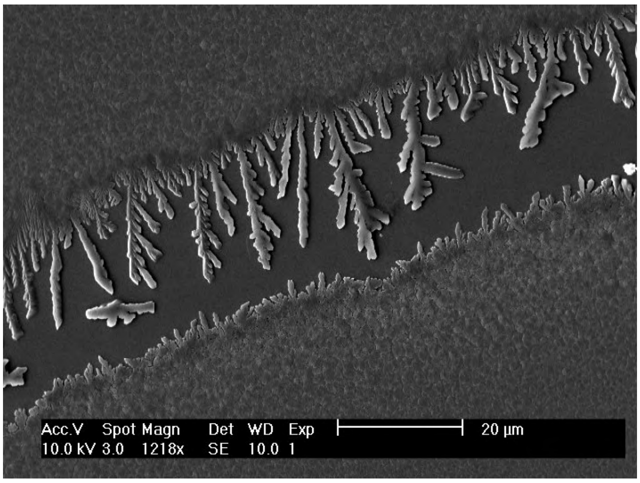
Acc.V Spot Magn Det WD Exp 20 µm
10.0 kV 3.0 1218x SE 10.0 1

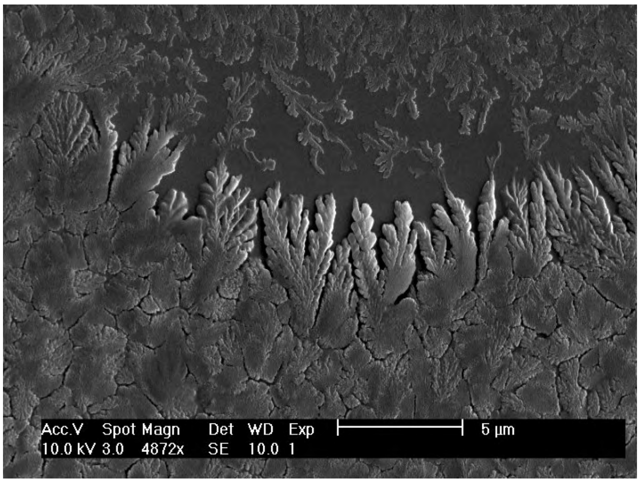
Acc.V Spot Magn Det WD Exp 5 µm
10.0 kV 3.0 4872x SE 10.0 1

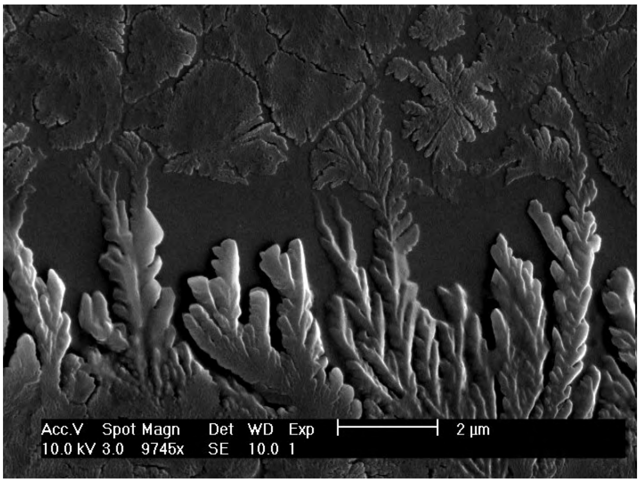
Acc.V Spot Magn Det WD Exp
2 µm
10.0 kV 3.0 9745x SE 10.0 1

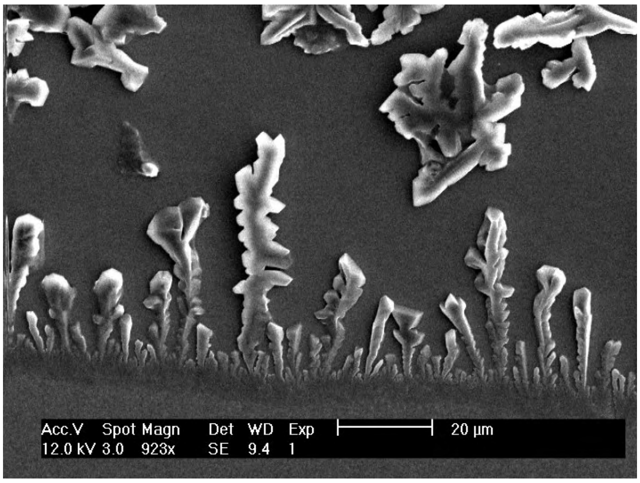
Acc.V Spot Magn Det WD Exp
20 µm
12.0 kV 3.0 923x SE 9.4 1

A.3 SEM micrographs of HBC-Rf$_{4,8}$ (114)

A.3.1 In-situ heating of the precipitate

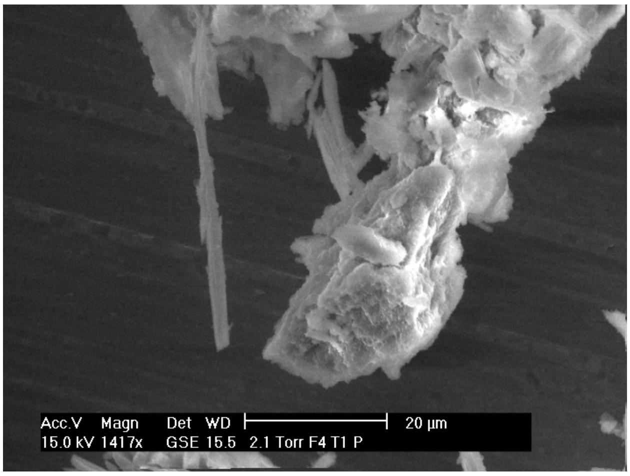
Acc.V Magn Det WD
20 µm
15.0 kV 1417x GSE 15.5 2.1 Torr F4 T1 P

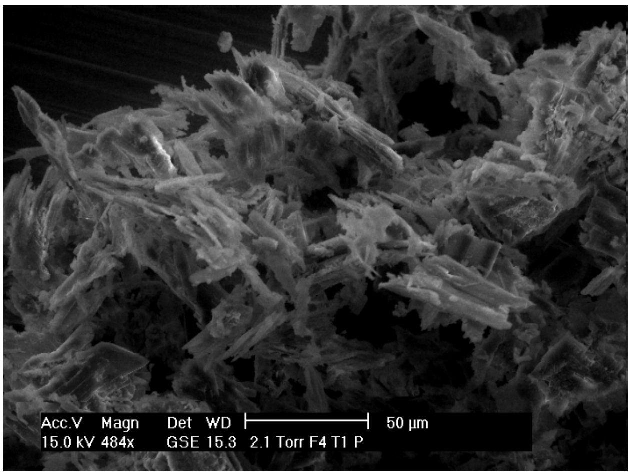
Acc.V Magn Det WD
50 µm
15.0 kV 484x GSE 15.3 2.1 Torr F4 T1 P

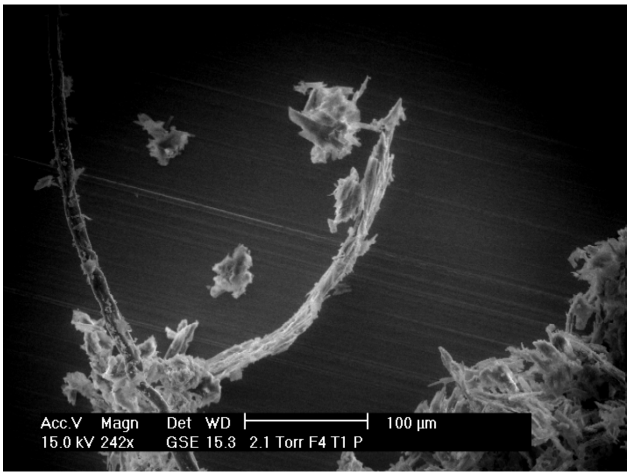
Acc.V Magn Det WD 100 µm
15.0 kV 242x GSE 15.3 2.1 Torr F4 T1 P

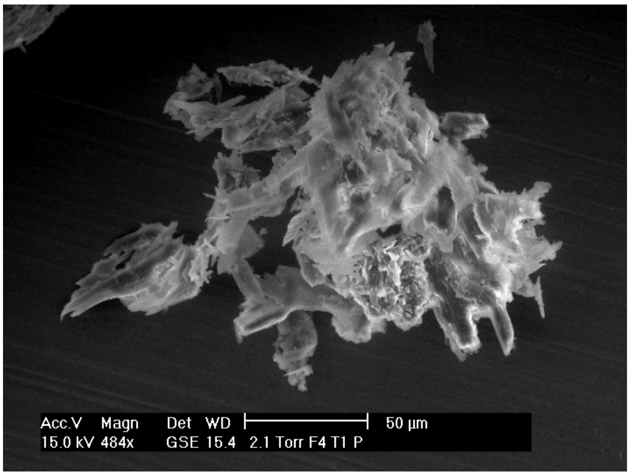
Acc.V Magn Det WD 50 µm
15.0 kV 484x GSE 15.4 2.1 Torr F4 T1 P

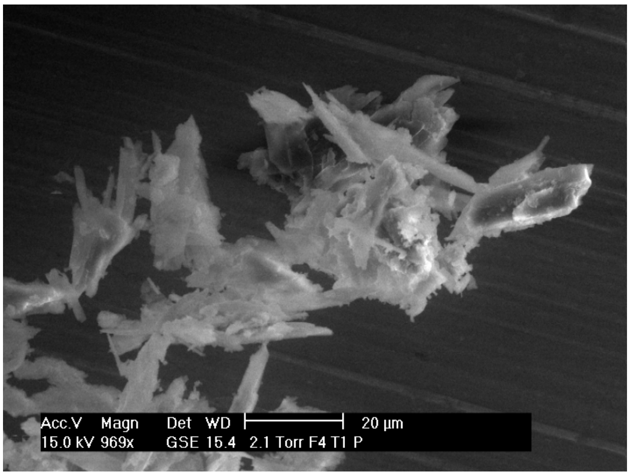
Acc.V Magn Det WD 20 µm
15.0 kV 969x GSE 15.4 2.1 Torr F4 T1 P

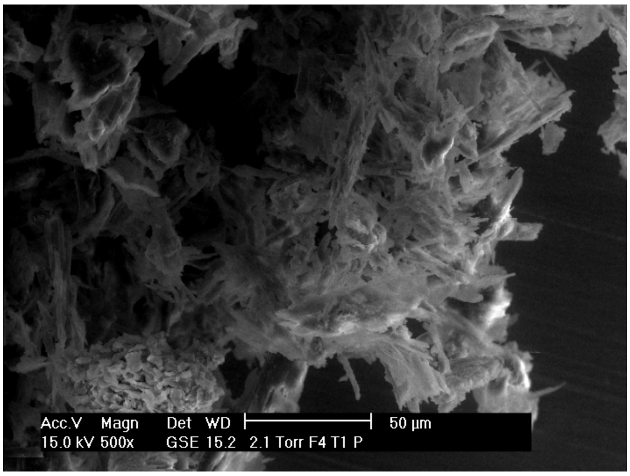
Acc.V Magn Det WD 50 µm
15.0 kV 500x GSE 15.2 2.1 Torr F4 T1 P

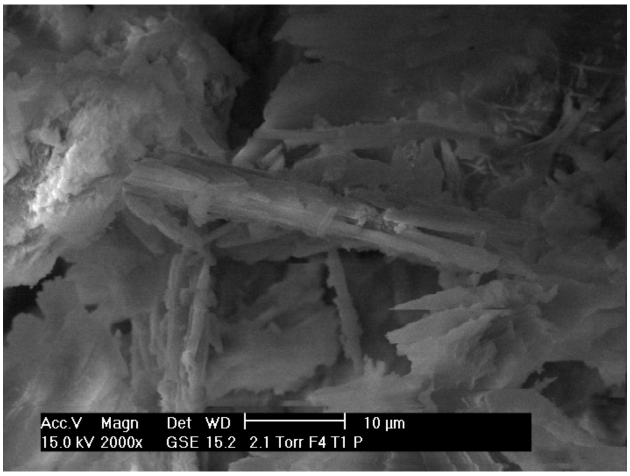
Acc.V Magn Det WD 10 µm
15.0 kV 2000x GSE 15.2 2.1 Torr F4 T1 P

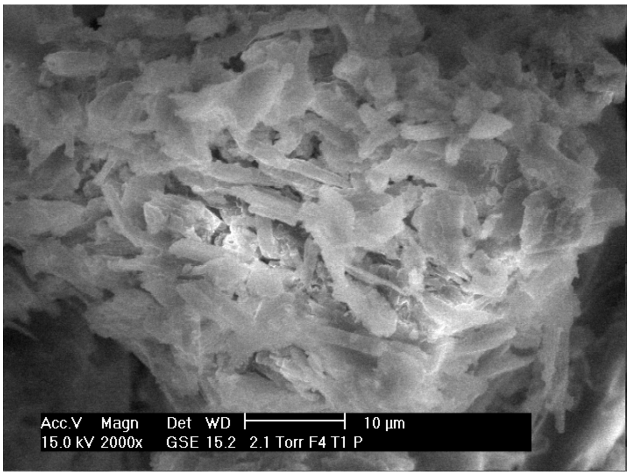
Acc.V Magn Det WD 10 µm
15.0 kV 2000x GSE 15.2 2.1 Torr F4 T1 P

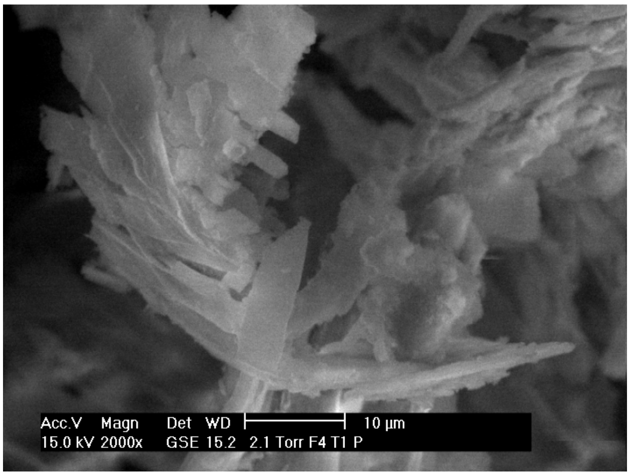
Acc.V Magn Det WD 10 µm
15.0 kV 2000x GSE 15.2 2.1 Torr F4 T1 P

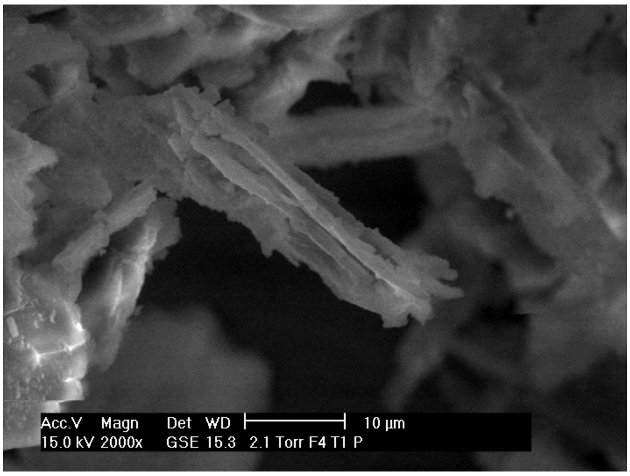
Acc.V Magn Det WD 10 µm
15.0 kV 2000x GSE 15.3 2.1 Torr F4 T1 P

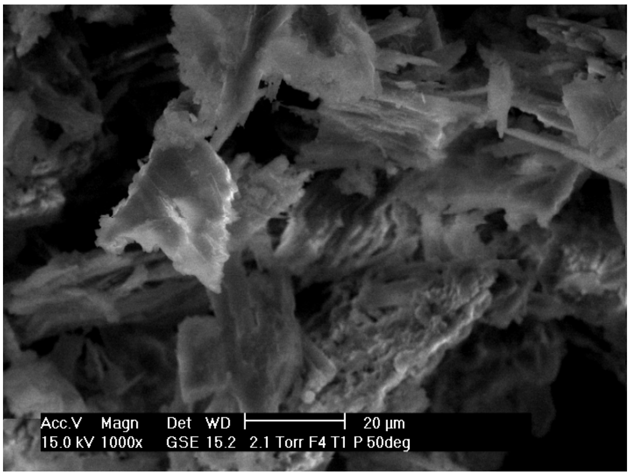
Acc.V Magn Det WD 20 µm
15.0 kV 1000x GSE 15.2 2.1 Torr F4 T1 P 50deg

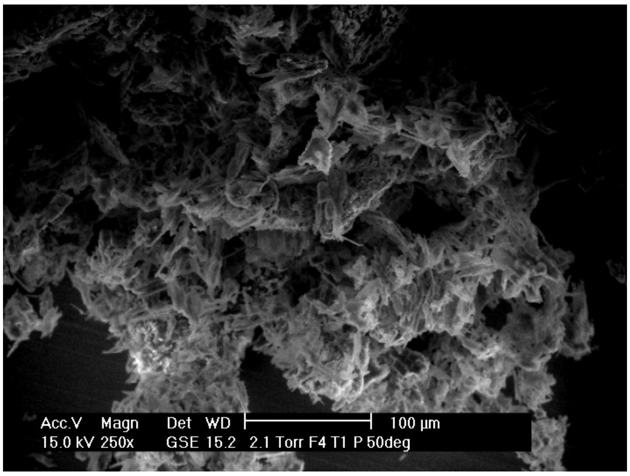
Acc.V Magn Det WD 100 µm
15.0 kV 250x GSE 15.2 2.1 Torr F4 T1 P 50deg

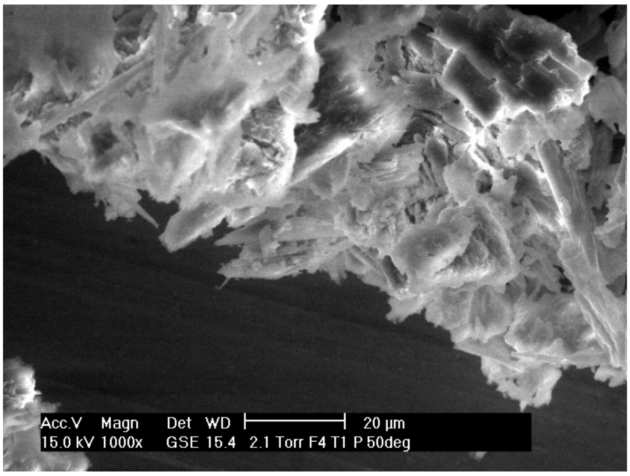
Acc.V Magn Det WD 20 µm
15.0 kV 1000x GSE 15.4 2.1 Torr F4 T1 P 50deg

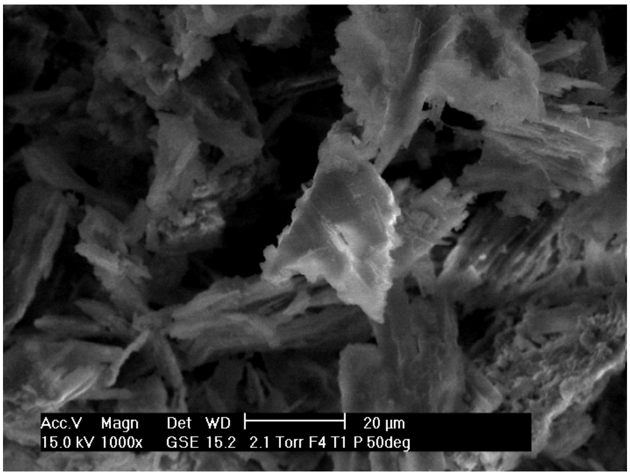
Acc.V Magn Det WD 20 µm
15.0 kV 1000x GSE 15.2 2.1 Torr F4 T1 P 50deg

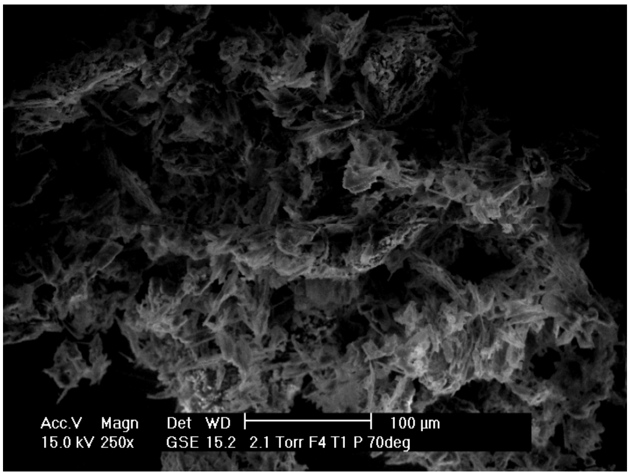
Acc.V Magn Det WD 100 µm
15.0 kV 250x GSE 15.2 2.1 Torr F4 T1 P 70deg

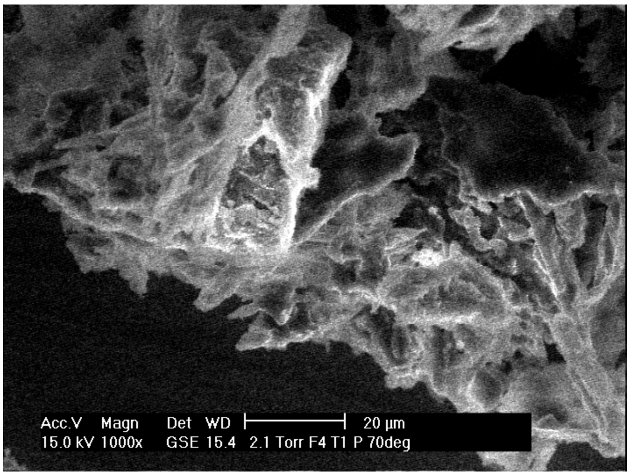
Acc.V Magn Det WD 20 µm
15.0 kV 1000x GSE 15.4 2.1 Torr F4 T1 P 70deg

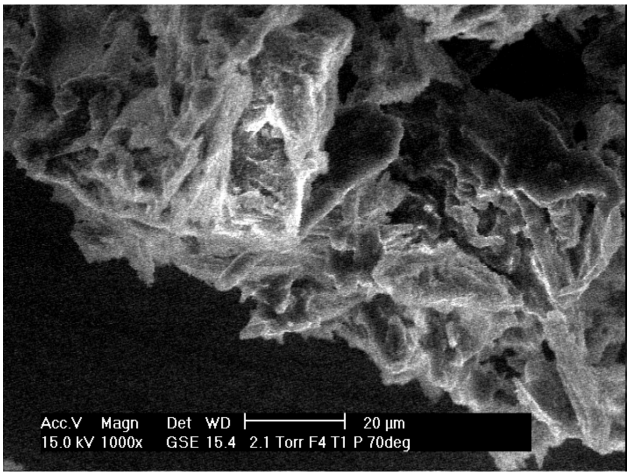
Acc.V Magn Det WD 20 µm
15.0 kV 1000x GSE 15.4 2.1 Torr F4 T1 P 70deg

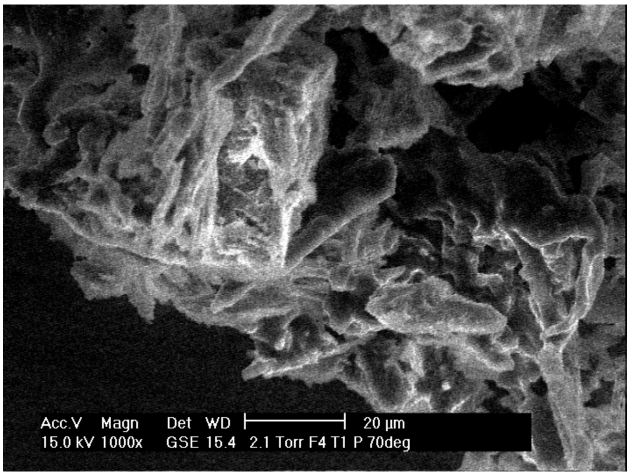
Acc.V Magn Det WD 20 µm
15.0 kV 1000x GSE 15.4 2.1 Torr F4 T1 P 70deg

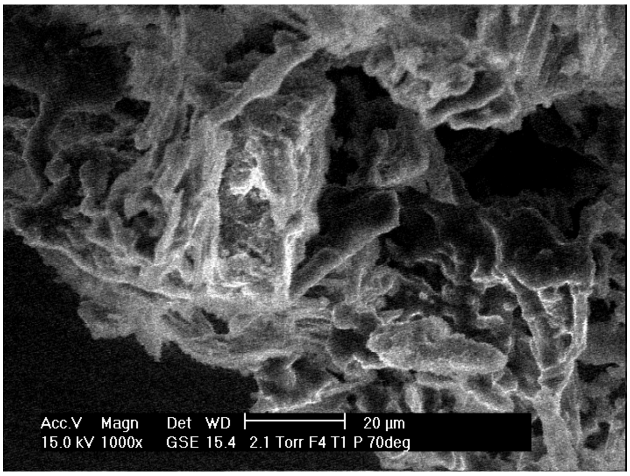
Acc.V Magn Det WD 20 µm
15.0 kV 1000x GSE 15.4 2.1 Torr F4 T1 P 70deg

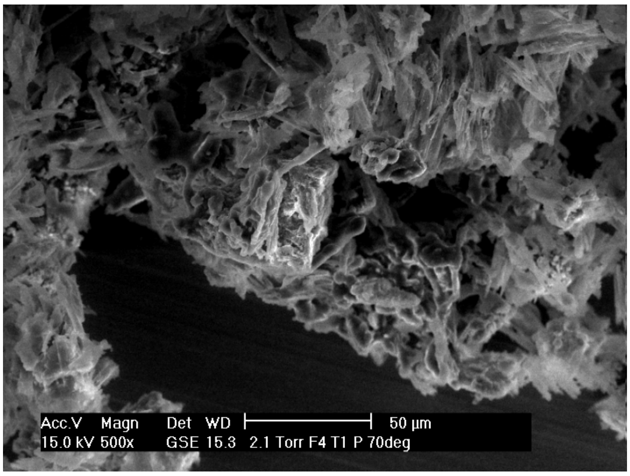
Acc.V Magn Det WD 50 µm
15.0 kV 500x GSE 15.3 2.1 Torr F4 T1 P 70deg

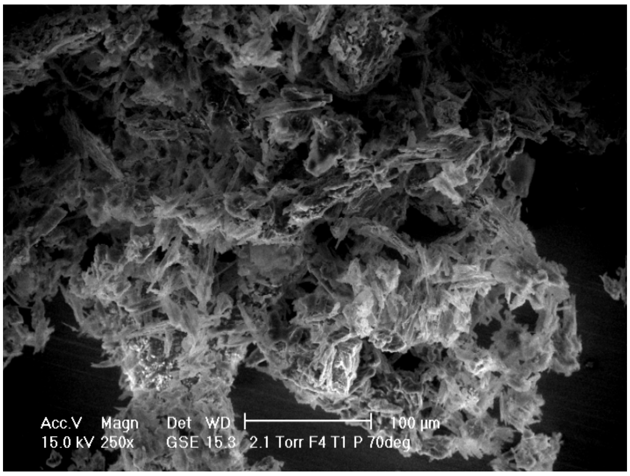
Acc.V Magn Det WD 100 µm
15.0 kV 250x GSE 15.3 2.1 Torr F4 T1 P 70deg

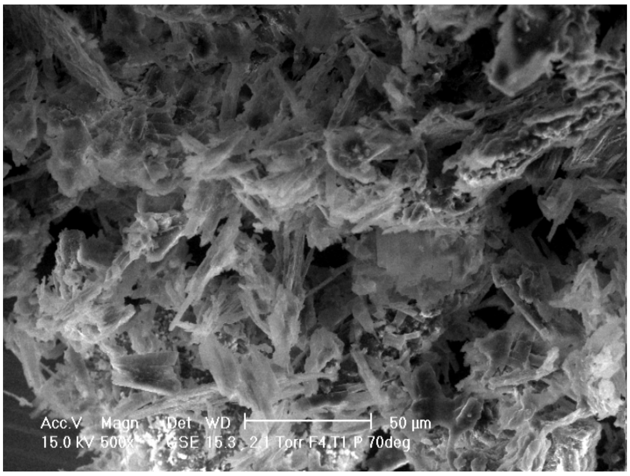
Acc.V Magn Det WD 50 µm
15.0 kV 500x GSE 15.3 2.1 Torr F4 T1 P 70deg

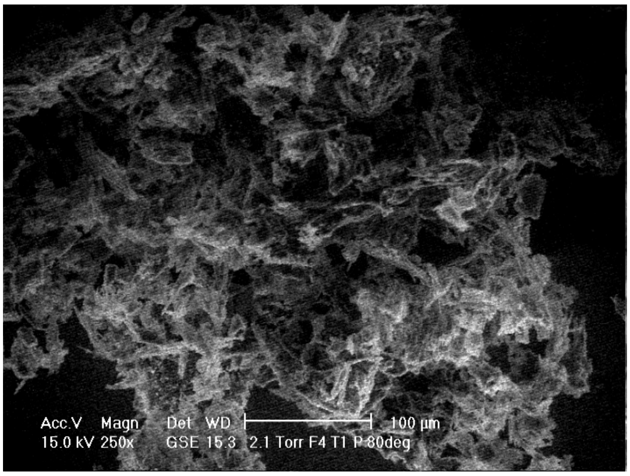
Acc.V Magn Det WD 100 µm
15.0 kV 250x GSE 15.3 2.1 Torr F4 T1 P 80deg

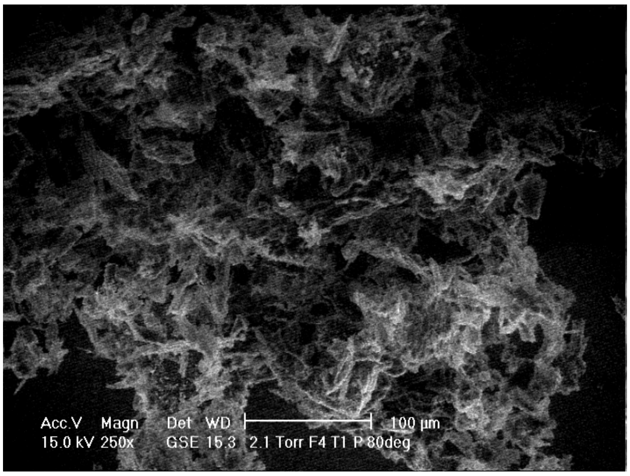
Acc.V Magn Det WD 100 µm
15.0 kV 250x GSE 15.3 2.1 Torr F4 T1 P 80deg

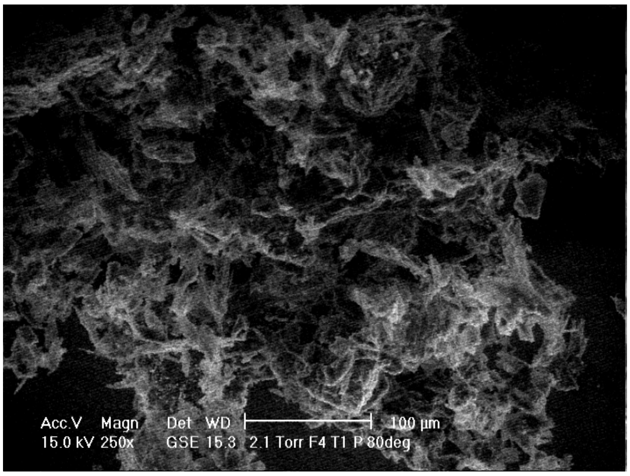
Acc.V Magn Det WD 100 µm
15.0 kV 250x GSE 15.3 2.1 Torr F4 T1 P 80deg

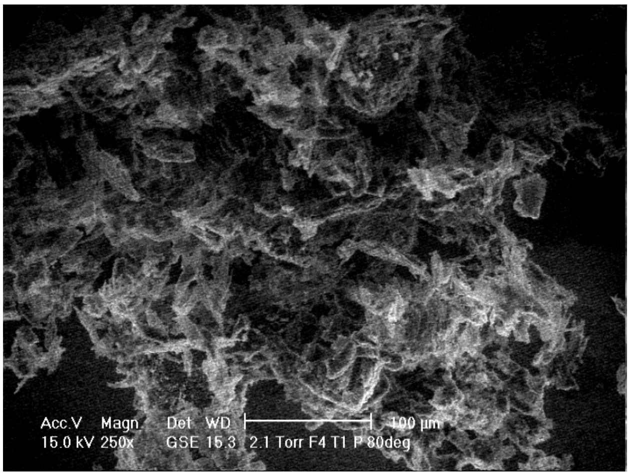
Acc.V Magn Det WD 100 µm
15.0 kV 250x GSE 15.3 2.1 Torr F4 T1 P 80deg

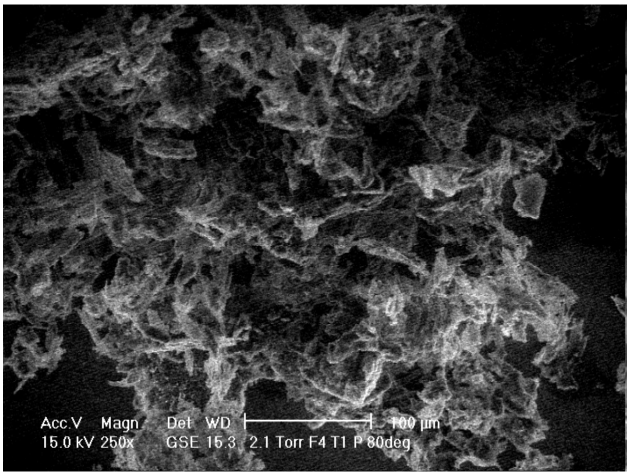
Acc.V Magn Det WD 100 µm
15.0 kV 250x GSE 15.3 2.1 Torr F4 T1 P 80deg

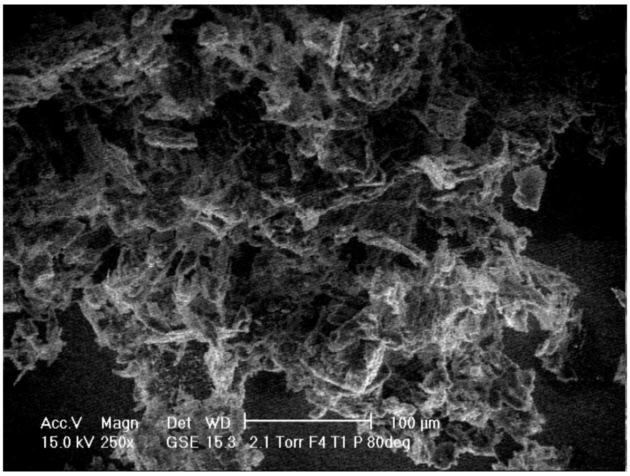
Acc.V Magn Det WD 100 µm
15.0 kV 250x GSE 15.3 2.1 Torr F4 T1 P 80deg

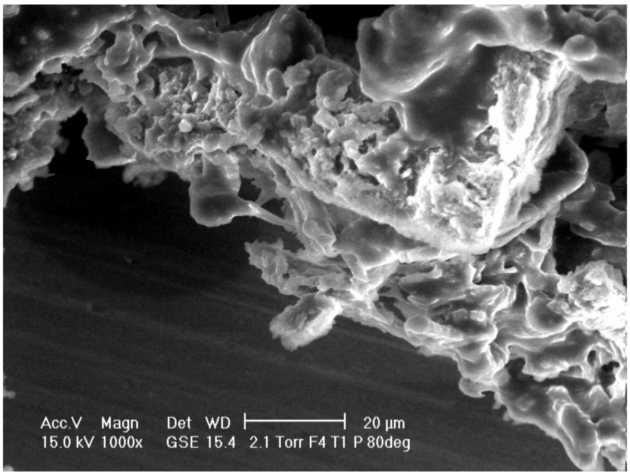
Acc.V Magn Det WD 20 µm
15.0 kV 1000x GSE 15.4 2.1 Torr F4 T1 P 80deg

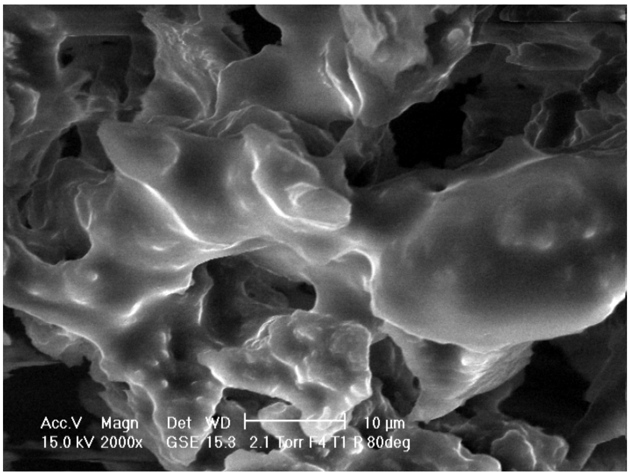
Acc.V Magn Det WD 10 µm
15.0 kV 2000x GSE 15.3 2.1 Torr F4 T1 P 80deg

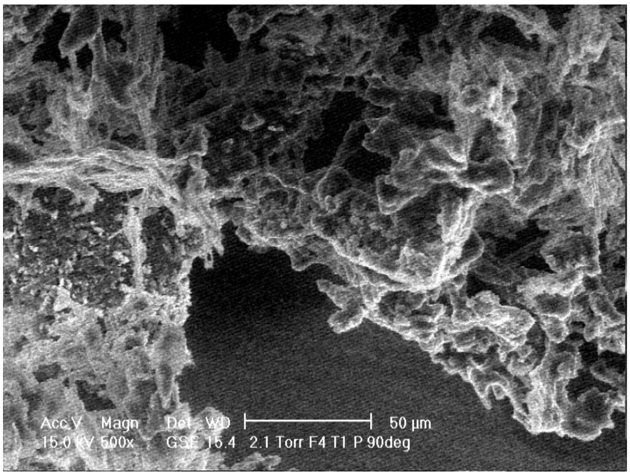
Acc.V Magn Det WD 50 µm
15.0 kV 500x GSE 15.4 2.1 Torr F4 T1 P 90deg

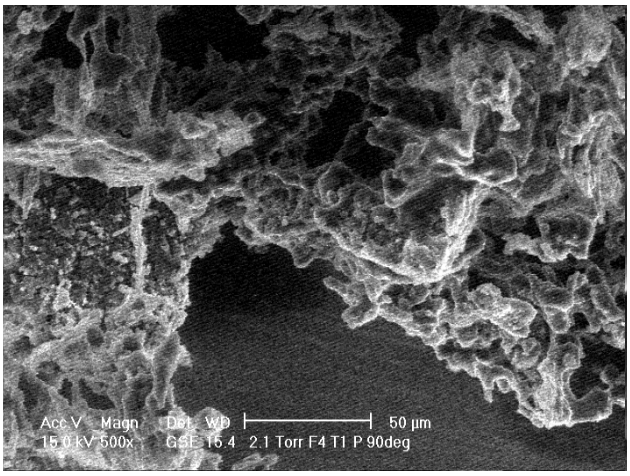
Acc.V Magn Det WD 50 µm
15.0 kV 500x GSE 15.4 2.1 Torr F4 T1 P 90deg

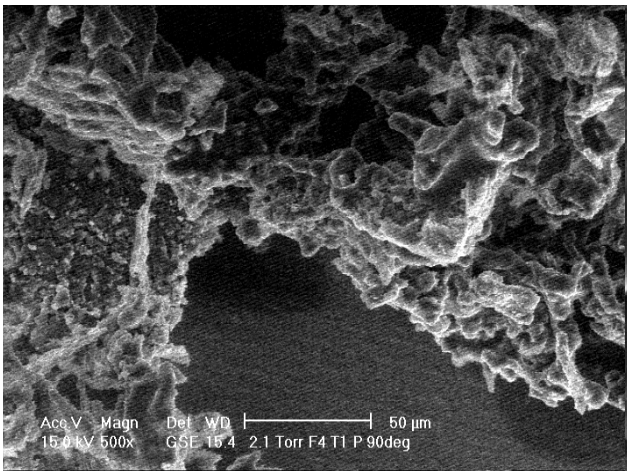
Acc.V Magn Det WD 50 µm
15.0 kV 500x GSE 15.4 2.1 Torr F4 T1 P 90deg

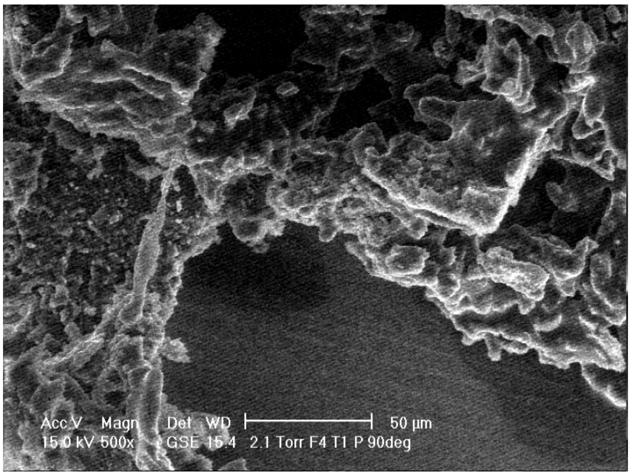
Acc.V Magn Det WD 50 µm
15.0 kV 500x GSE 15.4 2.1 Torr F4 T1 P 90deg

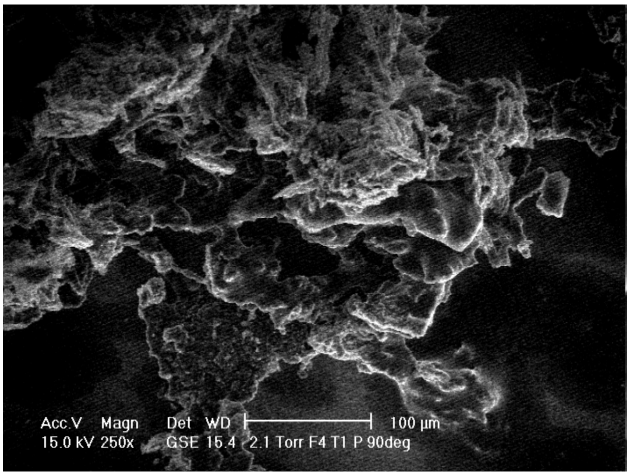
Acc.V Magn Det WD 100 µm
15.0 kV 250x GSE 15.4 2.1 Torr F4 T1 P 90deg

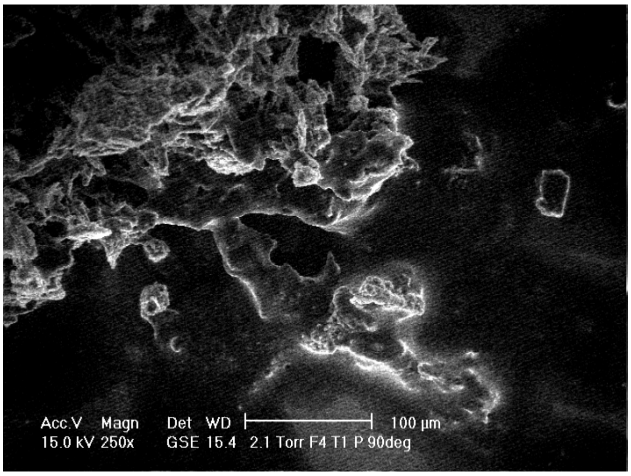
Acc.V Magn Det WD 100 µm
15.0 kV 250x GSE 15.4 2.1 Torr F4 T1 P 90deg

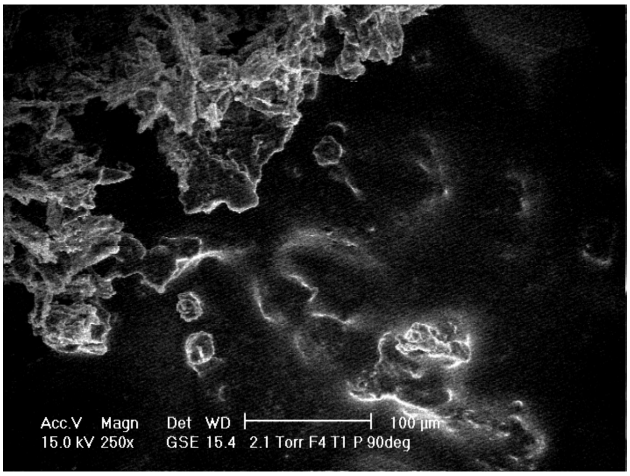
Acc.V Magn Det WD 100 µm
15.0 kV 250x GSE 15.4 2.1 Torr F4 T1 P 90deg

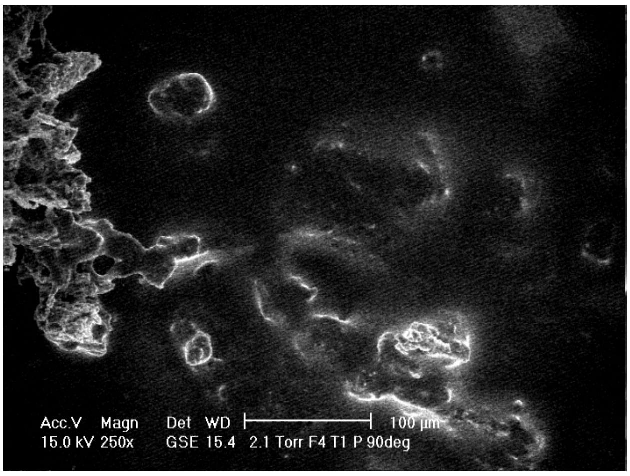
Acc.V Magn Det WD 100 µm
15.0 kV 250x GSE 15.4 2.1 Torr F4 T1 P 90deg

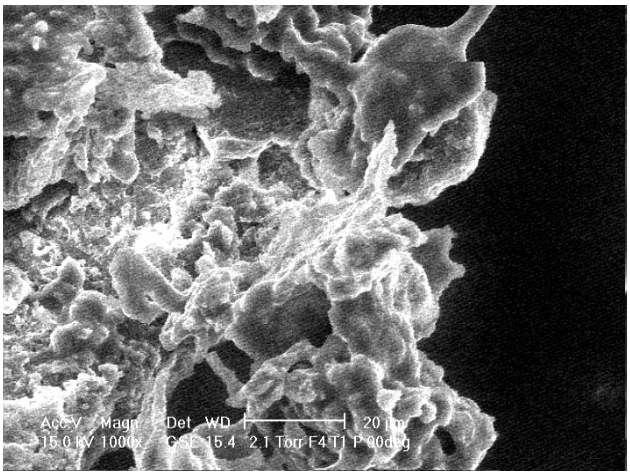
Acc.V Magn Det WD 20 µm
15.0 kV 1000x GSE 15.4 2.1 Torr F4 T1 P 90deg

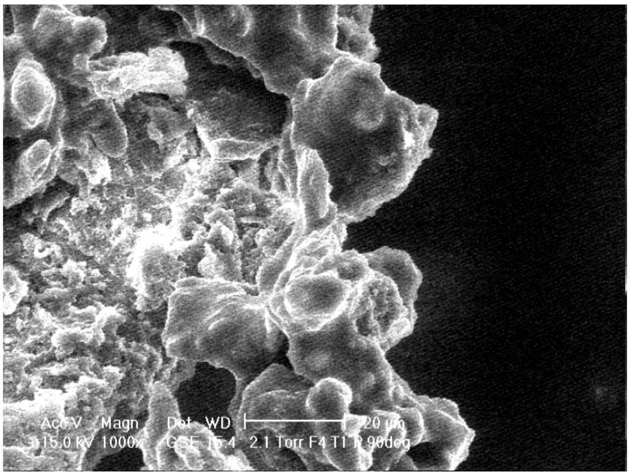
Acc.V Magn Det WD 20 µm
15.0 kV 1000x GSE 15.4 2.1 Torr F4 T1 P 90deg

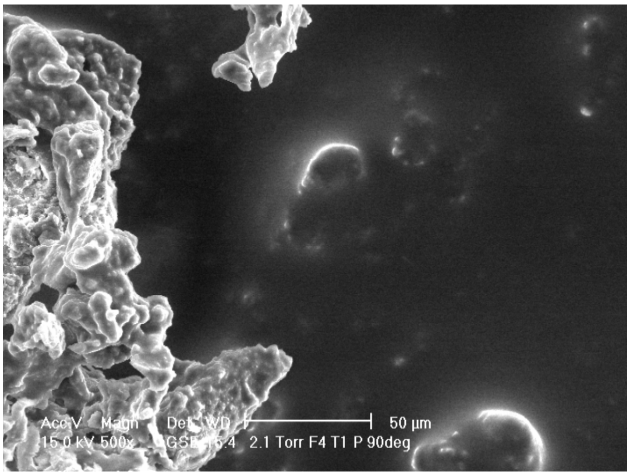
Acc.V Magn Det WD 50 µm
15.0 kV 500x GSE 15.4 2.1 Torr F4 T1 P 90deg

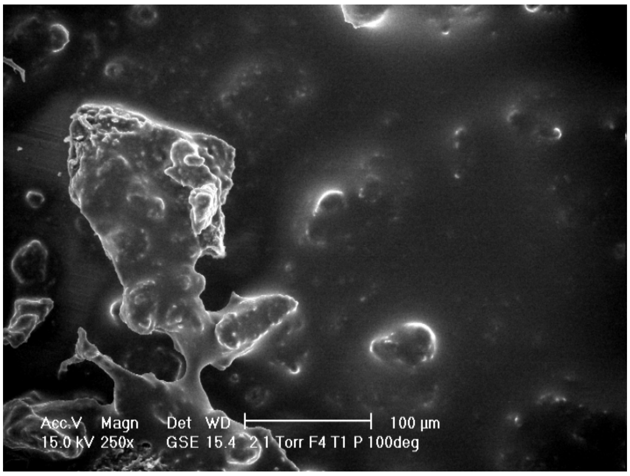
Acc.V Magn Det WD 100 µm
15.0 kV 250x GSE 15.4 2.1 Torr F4 T1 P 100deg

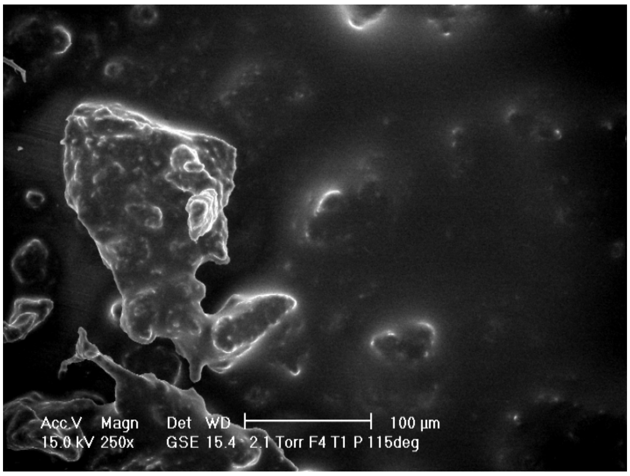
Acc.V Magn Det WD 100 µm
15.0 kV 250x GSE 15.4 2.1 Torr F4 T1 P 115deg

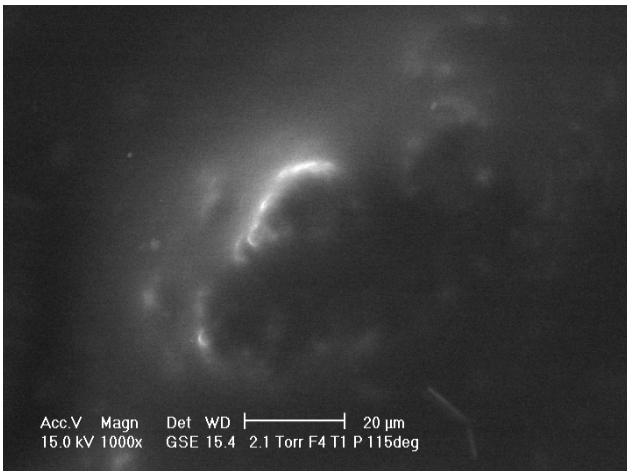
Acc.V Magn Det WD 20 µm
15.0 kV 1000x GSE 15.4 2.1 Torr F4 T1 P 115deg

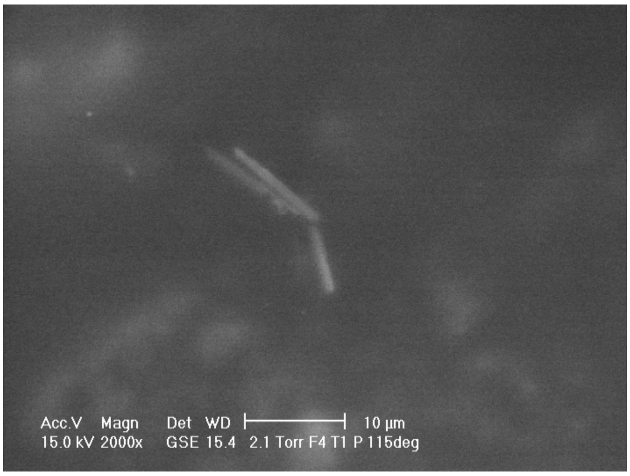
Acc.V Magn Det WD 10 µm
15.0 kV 2000x GSE 15.4 2.1 Torr F4 T1 P 115deg

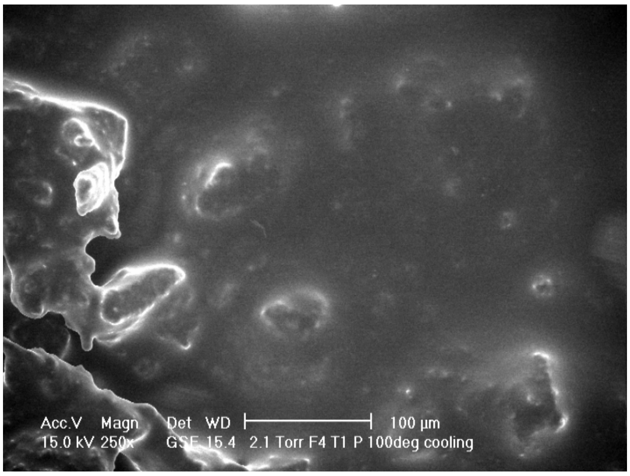
Acc.V Magn Det WD 100 µm
15.0 kV 250x GSE 15.4 2.1 Torr F4 T1 P 100deg cooling

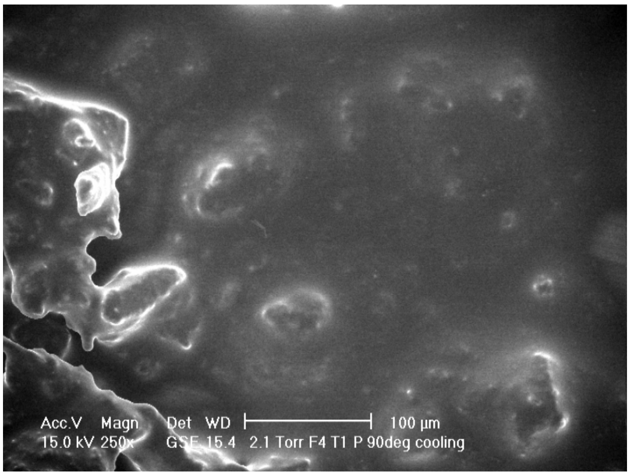
Acc.V Magn Det WD 100 µm
15.0 kV 250x GSE 15.4 2.1 Torr F4 T1 P 90deg cooling

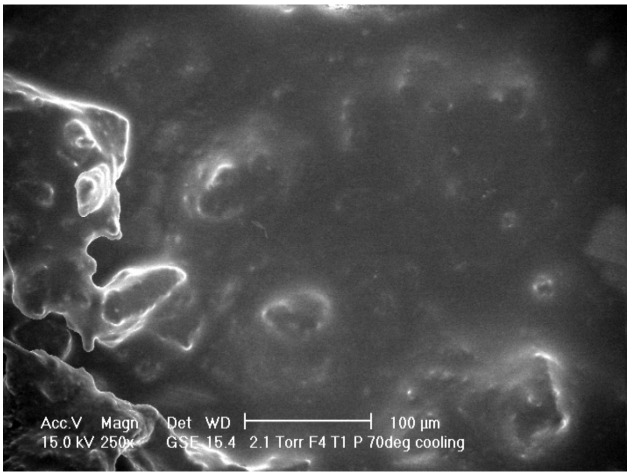
Acc.V Magn Det WD 100 µm
15.0 kV 250x GSE 15.4 2.1 Torr F4 T1 P 70deg cooling

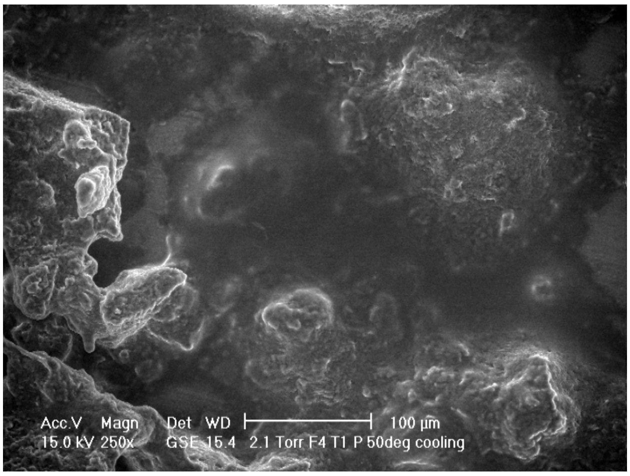
Acc.V Magn Det WD 100 µm
15.0 kV 250x GSE 15.4 2.1 Torr F4 T1 P 50deg cooling

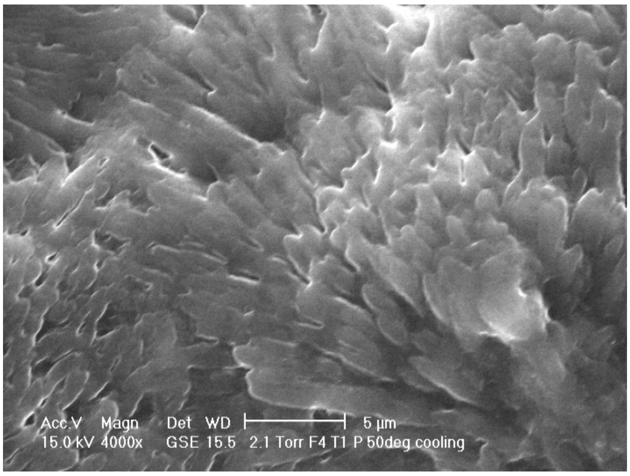
Acc.V Magn Det WD 5 µm
15.0 kV 4000x GSE 15.5 2.1 Torr F4 T1 P 50deg cooling

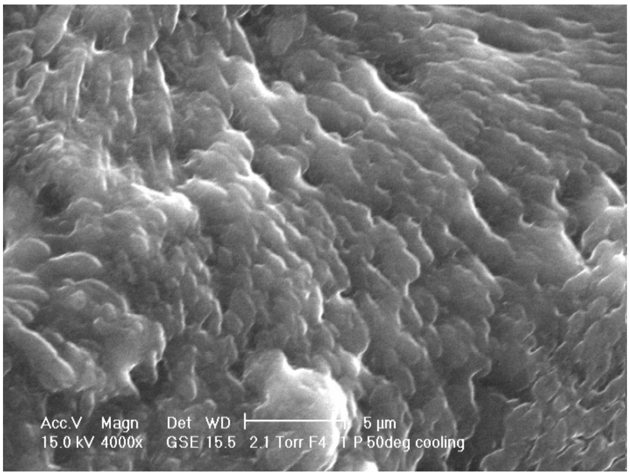
Acc.V Magn Det WD 5 µm
15.0 kV 4000x GSE 15.5 2.1 Torr F4 T1 P 50deg cooling

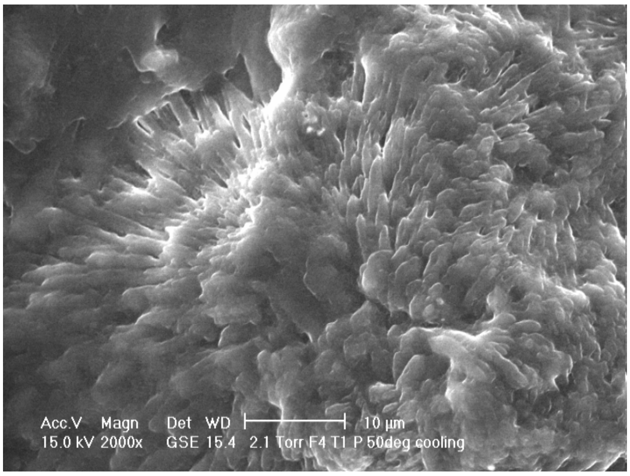
Acc.V Magn Det WD 10 µm
15.0 kV 2000x GSE 15.4 2.1 Torr F4 T1 P 50deg cooling

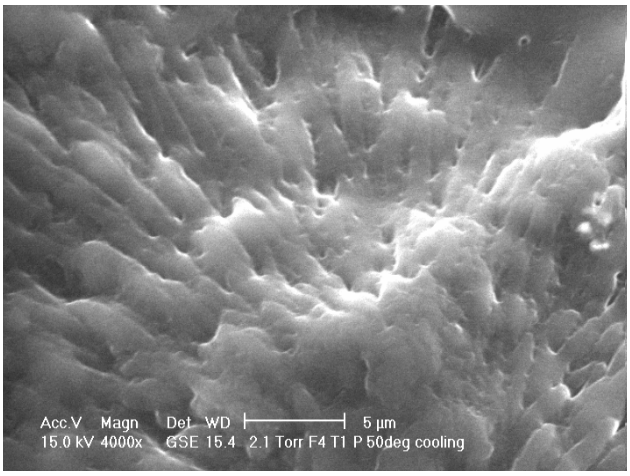
Acc.V Magn Det WD 5 µm
15.0 kV 4000x GSE 15.4 2.1 Torr F4 T1 P 50deg cooling

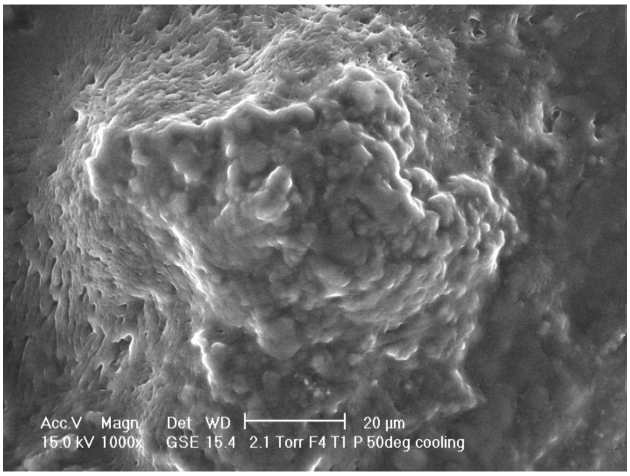
Acc.V Magn Det WD 20 µm
15.0 kV 1000x GSE 15.4 2.1 Torr F4 T1 P 50deg cooling

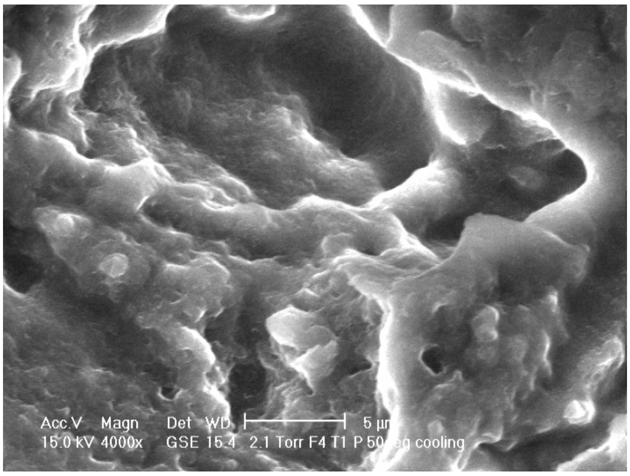
Acc.V Magn Det WD 5 µm
15.0 kV 4000x GSE 15.4 2.1 Torr F4 T1 P 50deg cooling

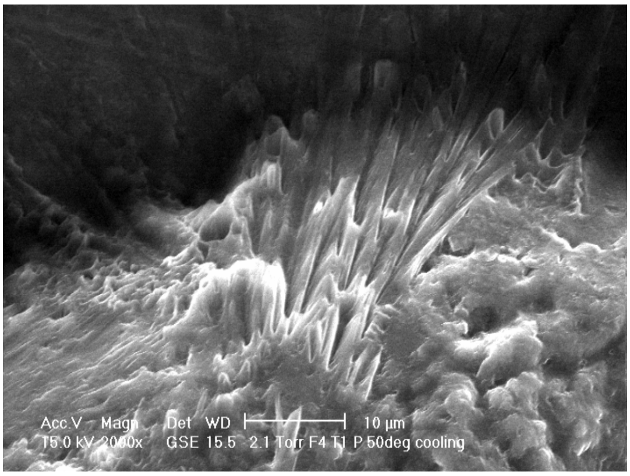
Acc.V Magn Det WD 10 µm
15.0 kV 2000x GSE 15.5 2.1 Torr F4 T1 P 50deg cooling

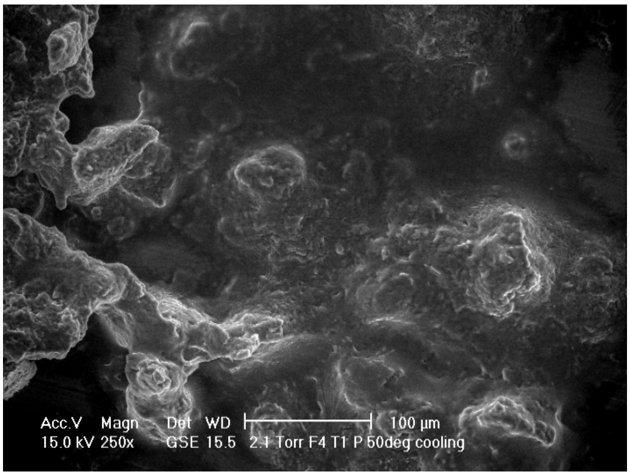
Acc.V Magn Det WD 100 µm
15.0 kV 250x GSE 15.5 2.1 Torr F4 T1 P 50deg cooling

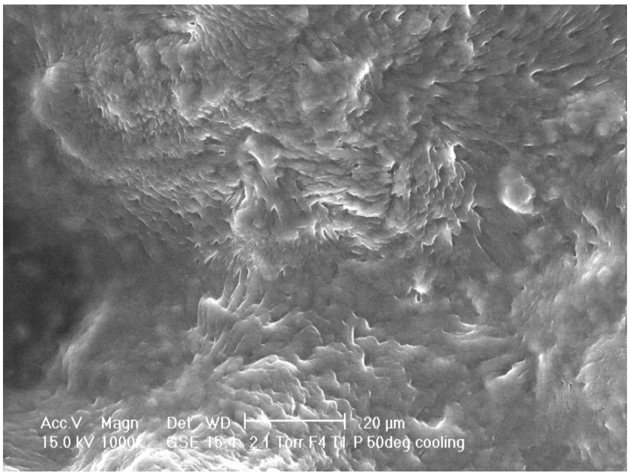
Acc.V Magn Det WD 20 µm
15.0 kV 1000x GSE 16.4 2.1 Torr F4 T1 P 50deg cooling

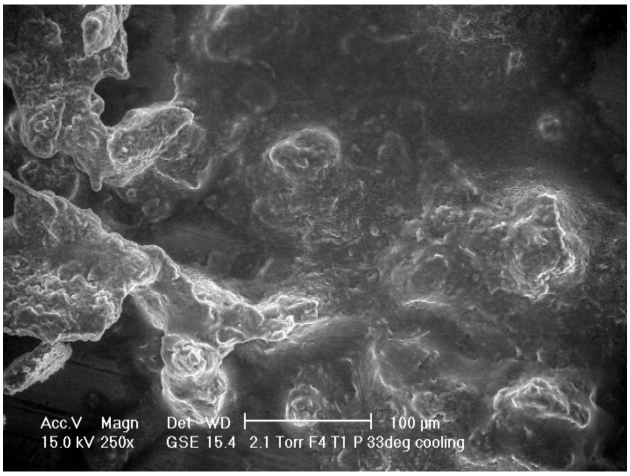
Acc.V Magn Det WD 100 µm
15.0 kV 250x GSE 15.4 2.1 Torr F4 T1 P 33deg cooling

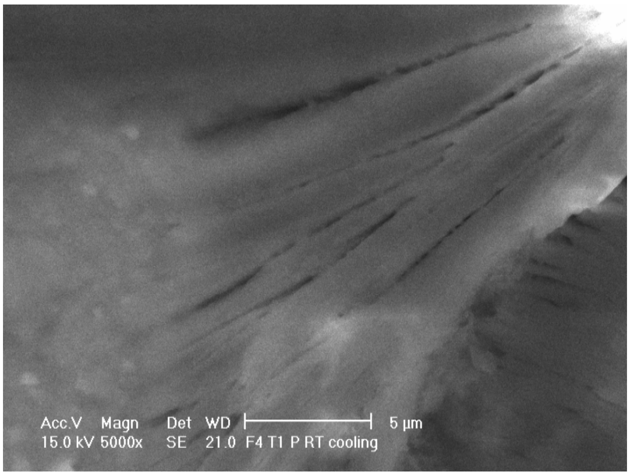
Acc.V Magn Det WD 5 µm
15.0 kV 5000x SE 21.0 F4 T1 P RT cooling

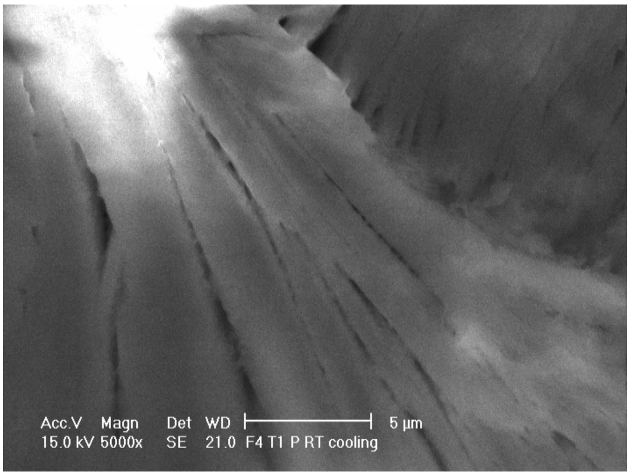
Acc.V Magn Det WD 5 µm
15.0 kV 5000x SE 21.0 F4 T1 P RT cooling

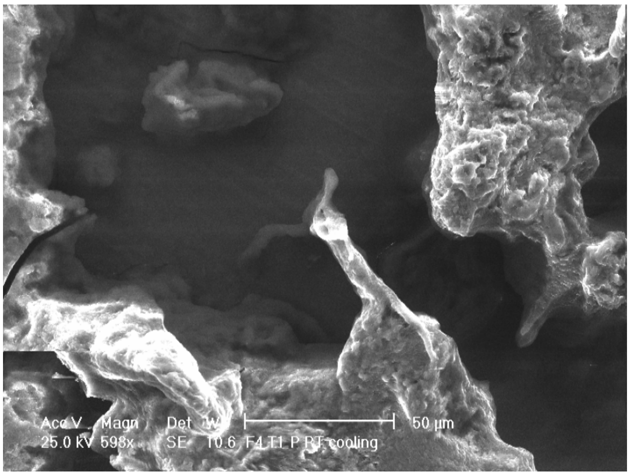
Acc.V Magn Det WD 50 µm
25.0 kV 598x SE 10.6 F4 T1 P RT cooling

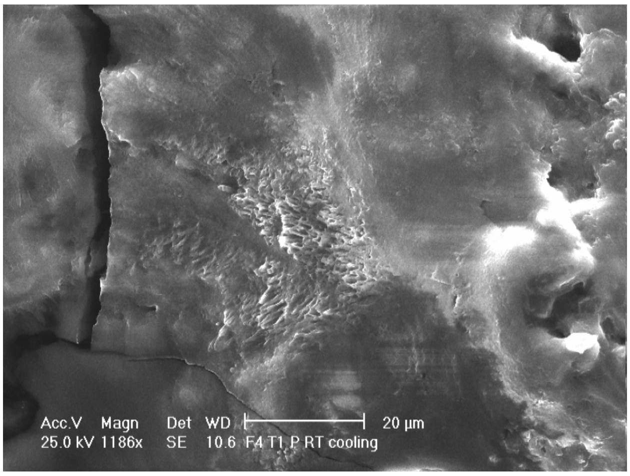
Acc.V Magn Det WD 20 µm
25.0 kV 1186x SE 10.6 F4 T1 P RT cooling

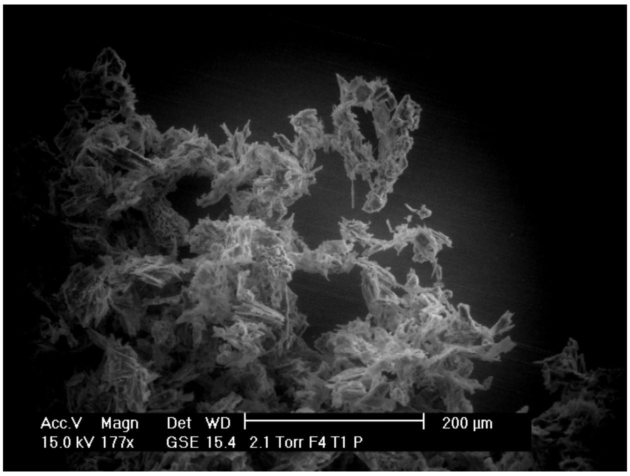
Acc.V Magn Det WD 200 µm
15.0 kV 177x GSE 15.4 2.1 Torr F4 T1 P

A.3.2 Evaporation of the concentrated solution

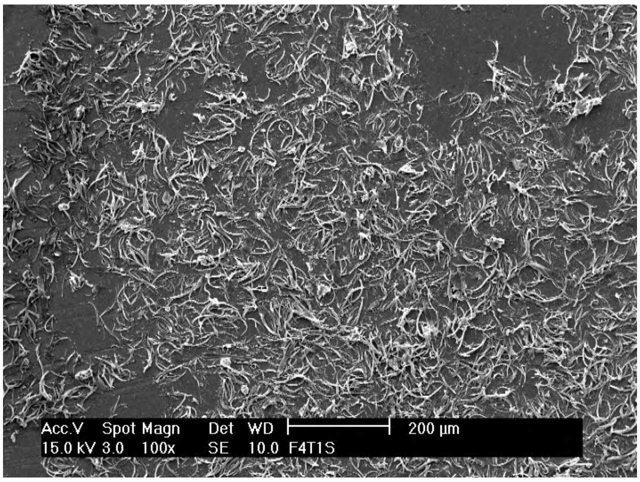
Acc.V Spot Magn Det WD 200 µm
15.0 kV 3.0 100x SE 10.0 F4T1S

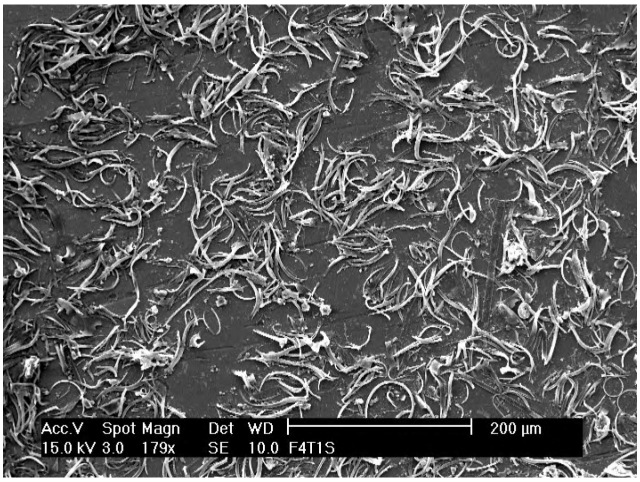
Acc.V Spot Magn Det WD 200 µm
15.0 kV 3.0 179x SE 10.0 F4T1S

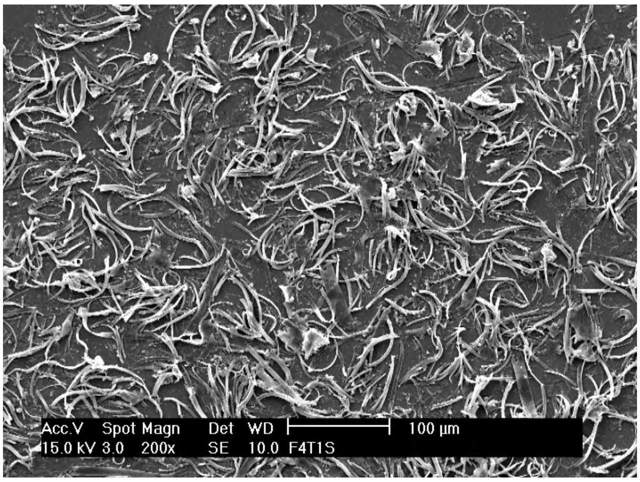
Acc.V Spot Magn Det WD 100 µm
15.0 kV 3.0 200x SE 10.0 F4T1S

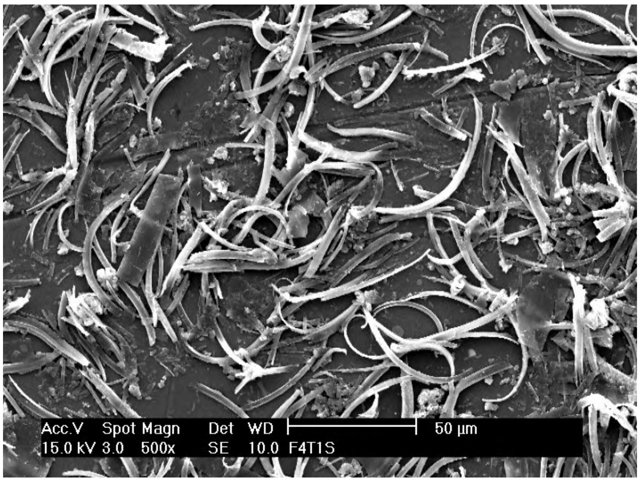
Acc.V Spot Magn Det WD 50 µm
15.0 kV 3.0 500x SE 10.0 F4T1S

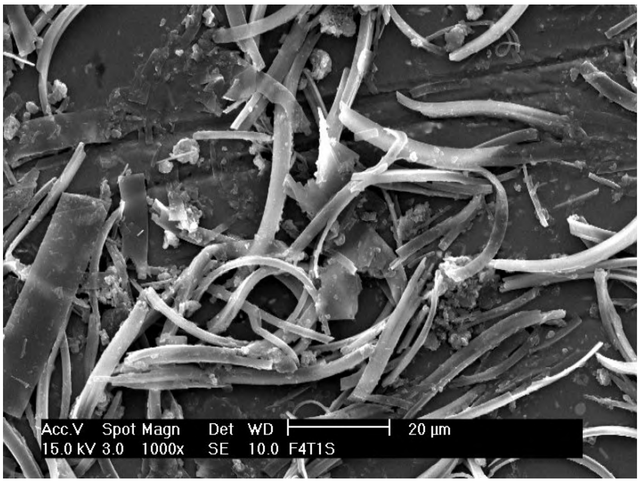
Acc.V Spot Magn Det WD
20 µm
15.0 kV 3.0 1000x SE 10.0 F4T1S

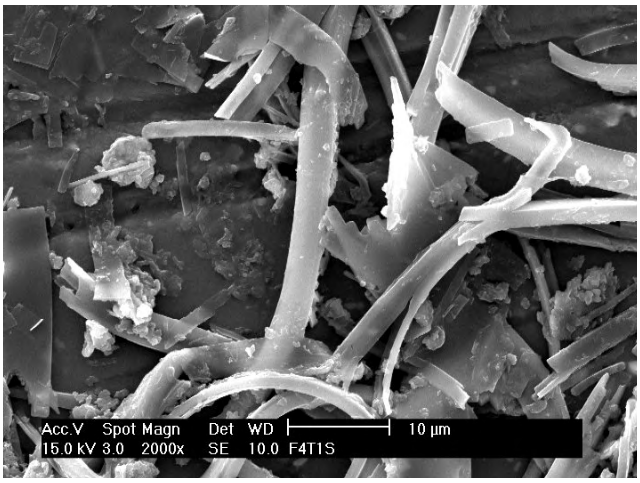
Acc.V Spot Magn Det WD
10 µm
15.0 kV 3.0 2000x SE 10.0 F4T1S

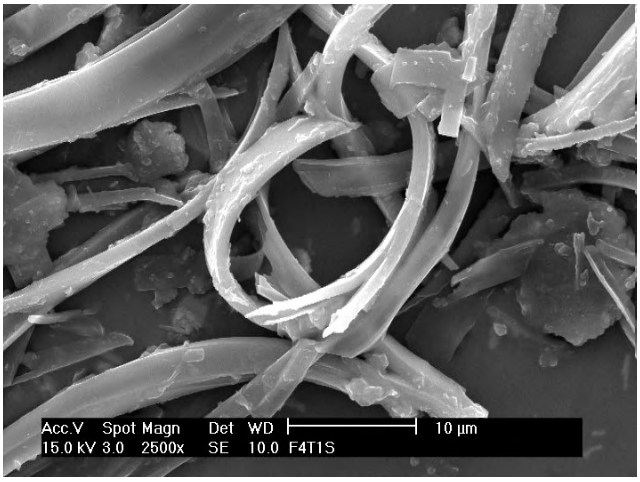
Acc.V Spot Magn Det WD
10 µm
15.0 kV 3.0 2500x SE 10.0 F4T1S

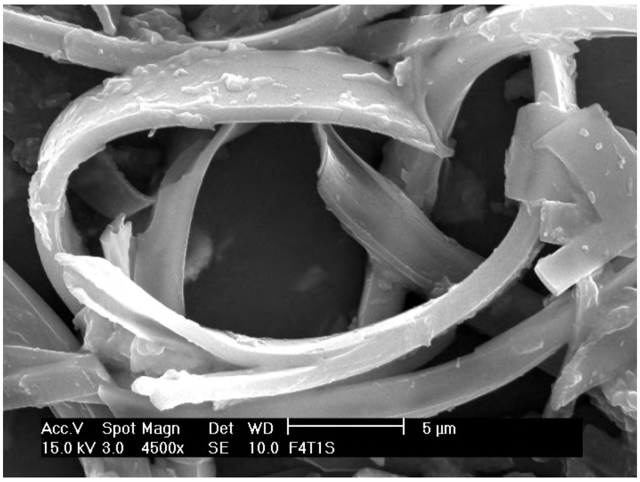
Acc.V Spot Magn Det WD
5 µm
15.0 kV 3.0 4500x SE 10.0 F4T1S

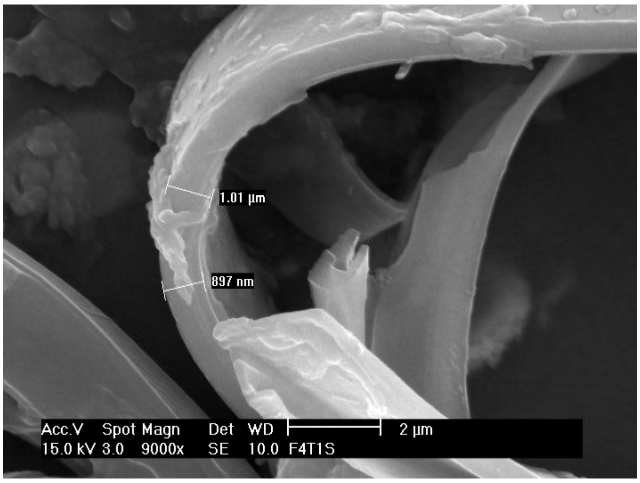
1.01 µm
897 nm
Acc.V Spot Magn Det WD
2 µm
15.0 kV 3.0 9000x SE 10.0 F4T1S

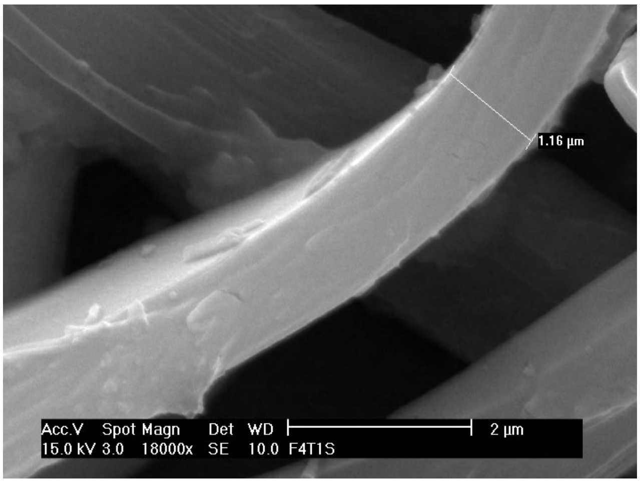
1.16 µm
Acc.V Spot Magn Det WD
2 µm
15.0 kV 3.0 18000x SE 10.0 F4T1S

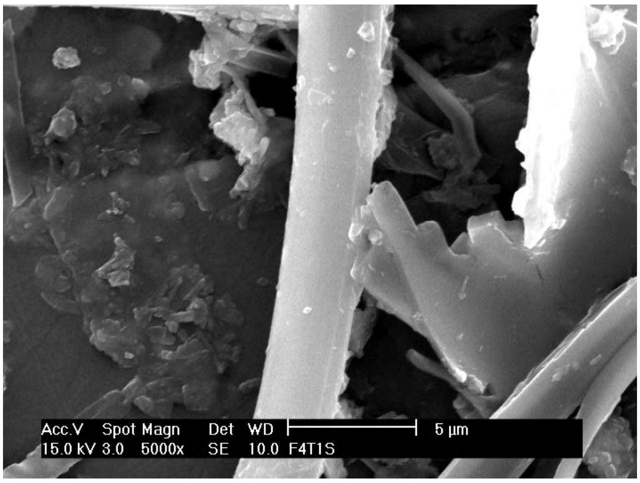
Acc.V Spot Magn Det WD 5 µm
15.0 kV 3.0 5000x SE 10.0 F4T1S

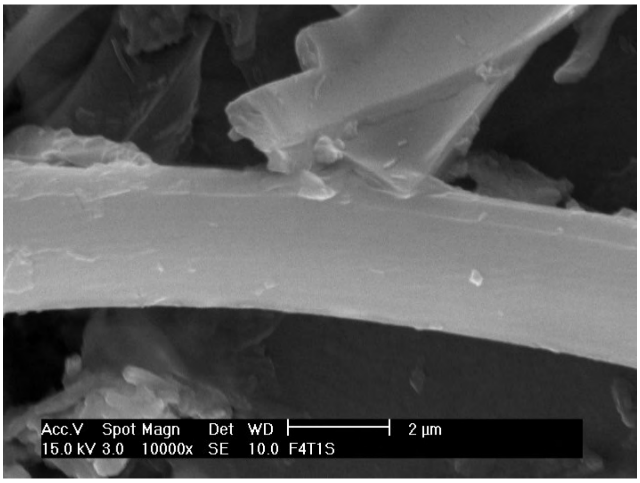
Acc.V Spot Magn Det WD 2 µm
15.0 kV 3.0 10000x SE 10.0 F4T1S

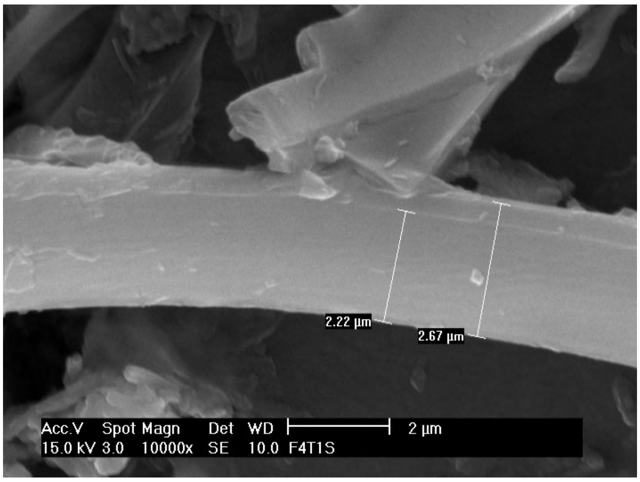
2.22 µm
2.67 µm
Acc.V Spot Magn Det WD 2 µm
15.0 kV 3.0 10000x SE 10.0 F4T1S

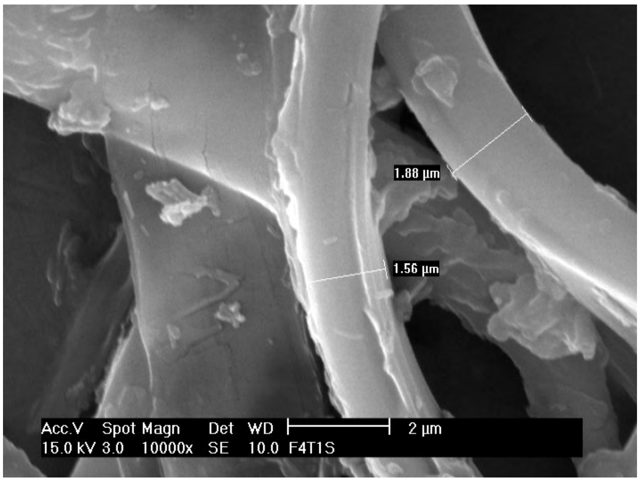
1.88 µm
1.56 µm
Acc.V Spot Magn Det WD 2 µm
15.0 kV 3.0 10000x SE 10.0 F4T1S

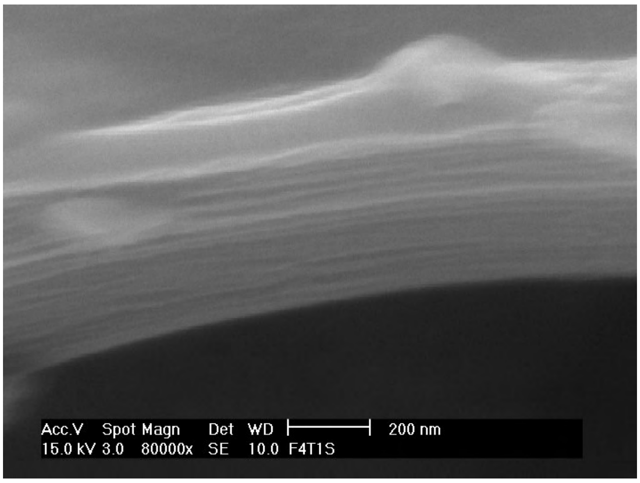
Acc.V Spot Magn Det WD 200 nm
15.0 kV 3.0 80000x SE 10.0 F4T1S

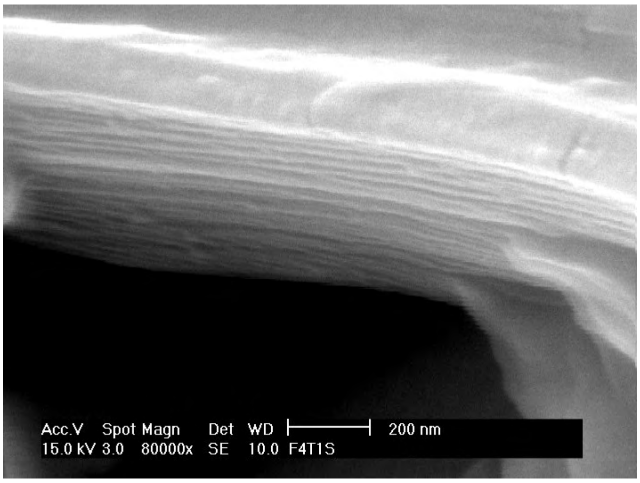
Acc.V Spot Magn Det WD 200 nm
15.0 kV 3.0 80000x SE 10.0 F4T1S

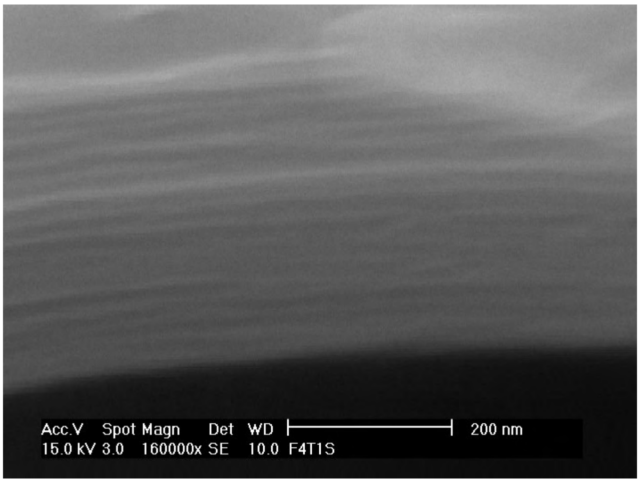
Acc.V Spot Magn Det WD 200 nm
15.0 kV 3.0 160000x SE 10.0 F4T1S

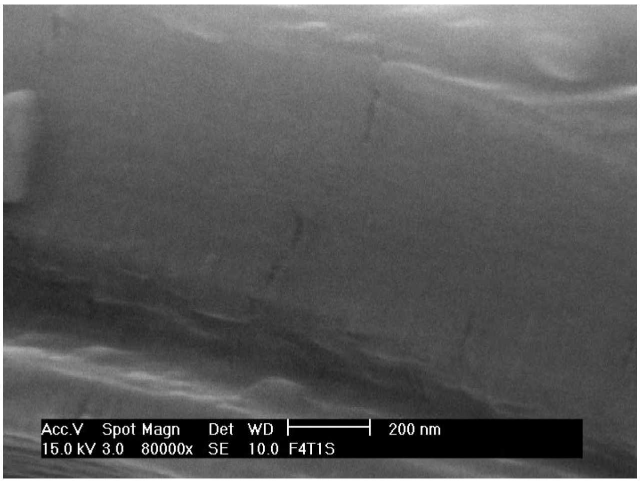
Acc.V Spot Magn Det WD 200 nm
15.0 kV 3.0 80000x SE 10.0 F4T1S

A.3.3 Cyro-SEM of the concentrated solution

Micrometer-sized columns

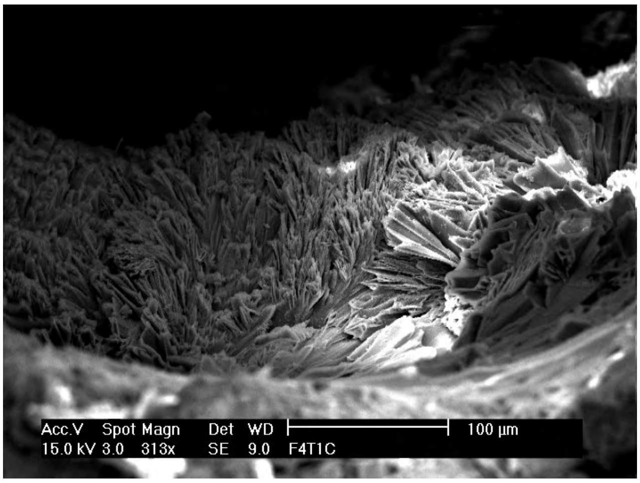
Acc.V Spot Magn Det WD 100 µm
15.0 kV 3.0 313x SE 9.0 F4T1C

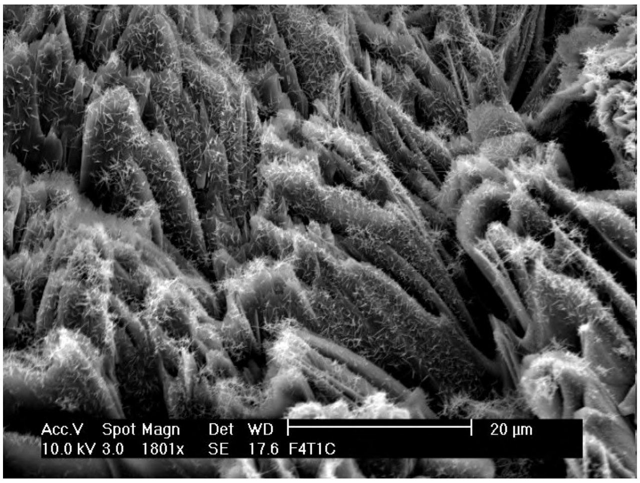
Acc.V Spot Magn Det WD 20 µm
10.0 kV 3.0 1801x SE 17.6 F4T1C

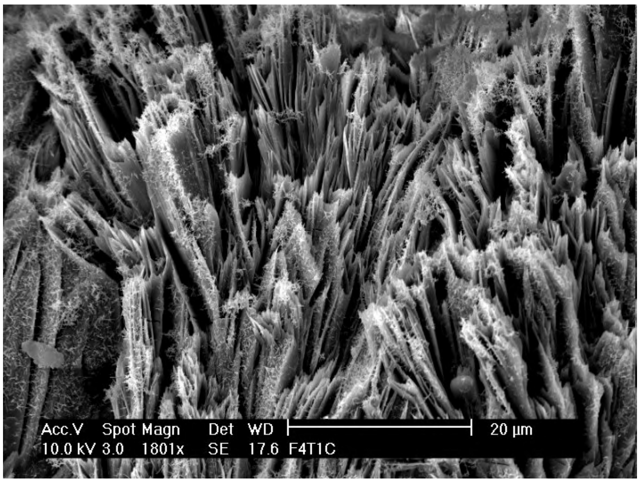
Acc.V Spot Magn Det WD 20 µm
10.0 kV 3.0 1801x SE 17.6 F4T1C

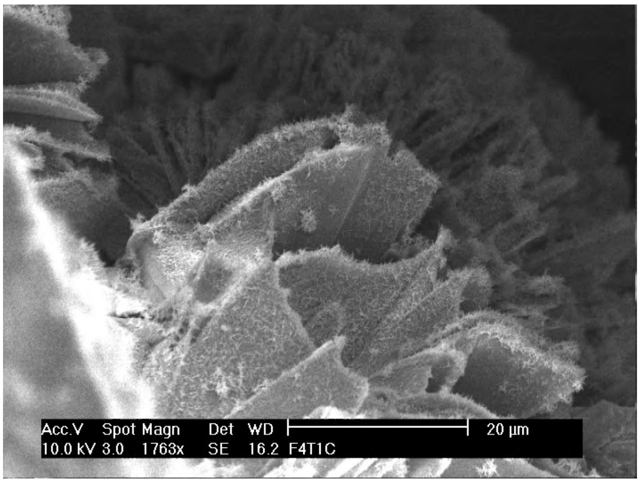
Acc.V Spot Magn Det WD 20 µm
10.0 kV 3.0 1763x SE 16.2 F4T1C

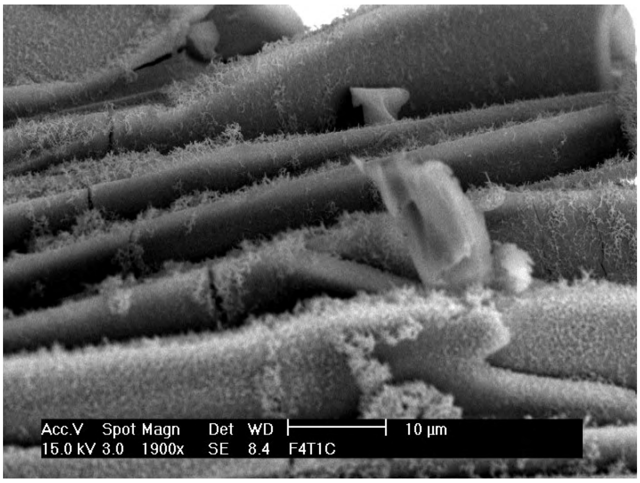
Acc.V Spot Magn Det WD 10 µm
15.0 kV 3.0 1900x SE 8.4 F4T1C

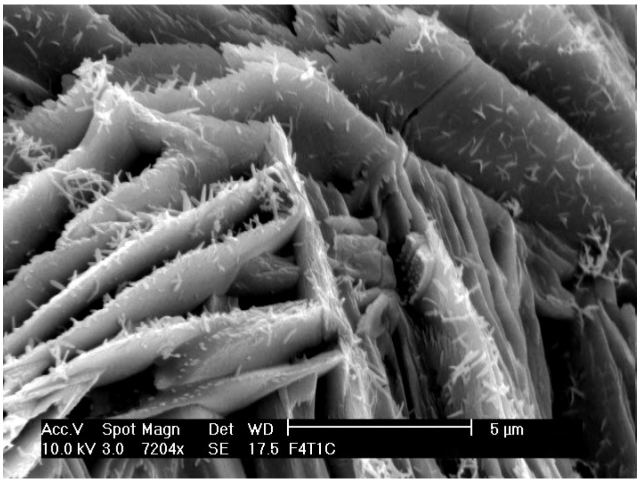
Acc.V Spot Magn Det WD 5 µm
10.0 kV 3.0 7204x SE 17.5 F4T1C

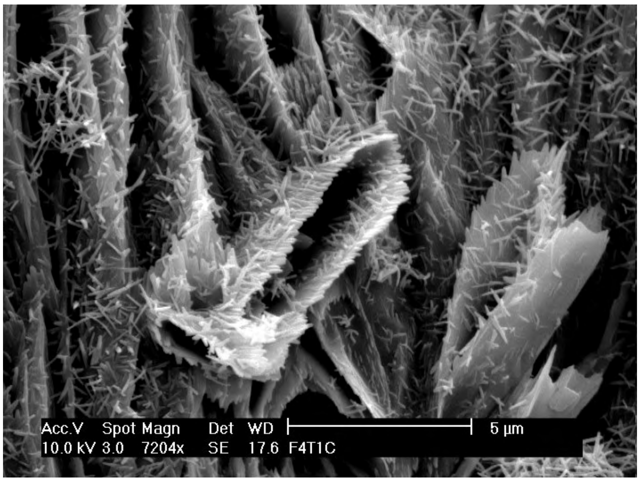
Acc.V Spot Magn Det WD 5 µm
10.0 kV 3.0 7204x SE 17.6 F4T1C

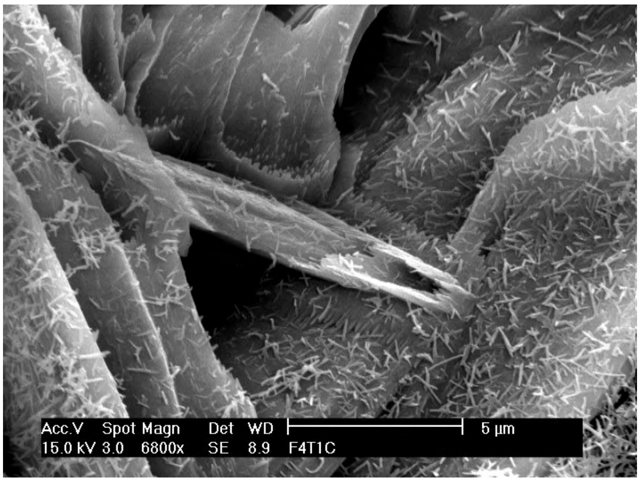
Acc.V Spot Magn Det WD 5 µm
15.0 kV 3.0 6800x SE 8.9 F4T1C

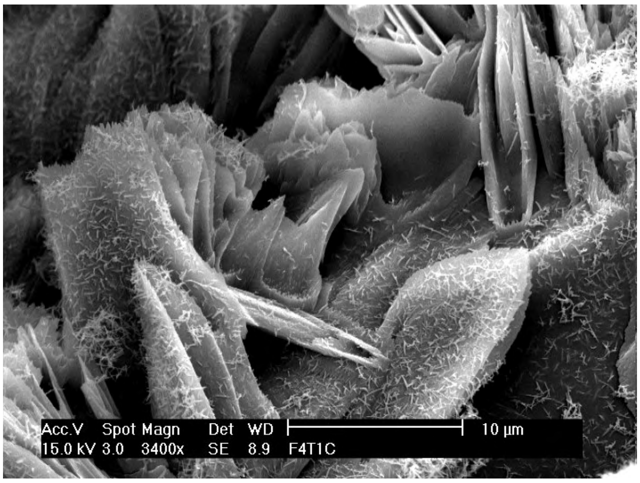
Acc.V Spot Magn Det WD 10 µm
15.0 kV 3.0 3400x SE 8.9 F4T1C

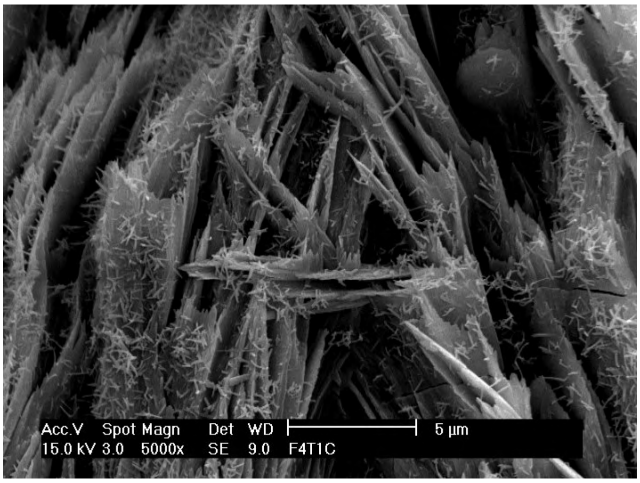
Acc.V Spot Magn Det WD 5 µm
15.0 kV 3.0 5000x SE 9.0 F4T1C

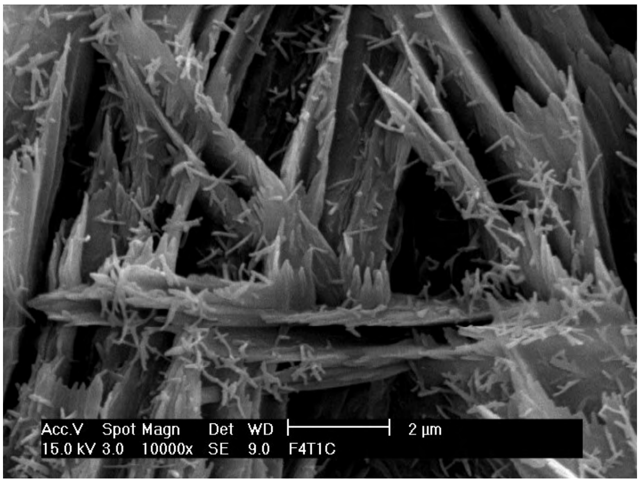
Acc.V Spot Magn Det WD 2 µm
15.0 kV 3.0 10000x SE 9.0 F4T1C

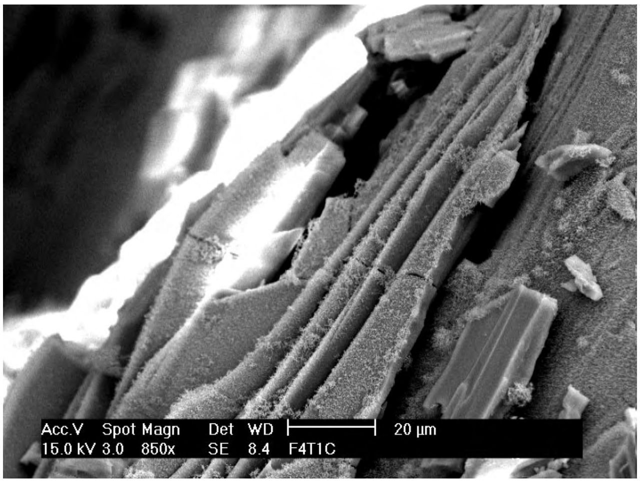
Acc.V Spot Magn Det WD 20 µm
15.0 kV 3.0 850x SE 8.4 F4T1C

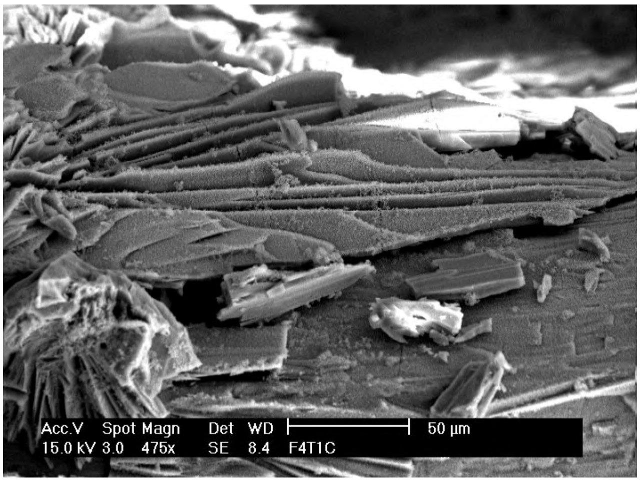
Acc.V Spot Magn Det WD 50 µm
15.0 kV 3.0 475x SE 8.4 F4T1C

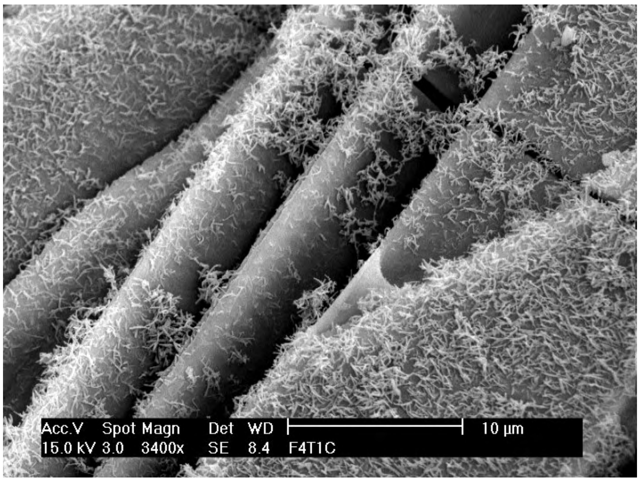
Acc.V Spot Magn Det WD 10 µm
15.0 kV 3.0 3400x SE 8.4 F4T1C

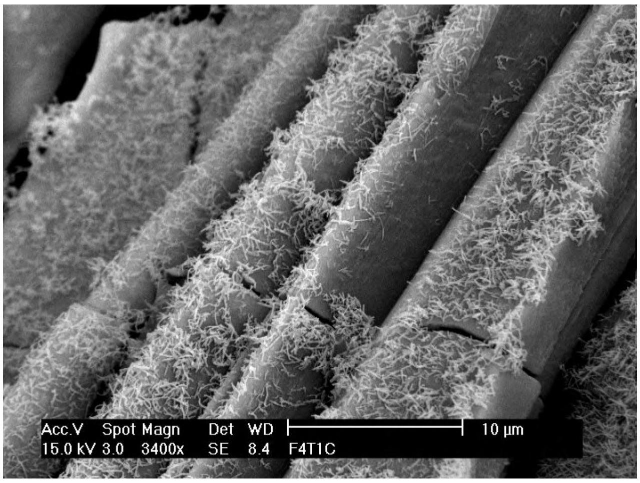
Acc.V Spot Magn Det WD 10 µm
15.0 kV 3.0 3400x SE 8.4 F4T1C

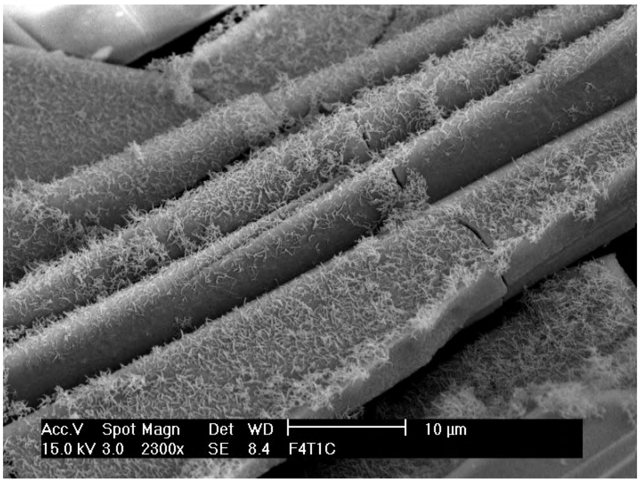
Acc.V Spot Magn Det WD 10 µm
15.0 kV 3.0 2300x SE 8.4 F4T1C

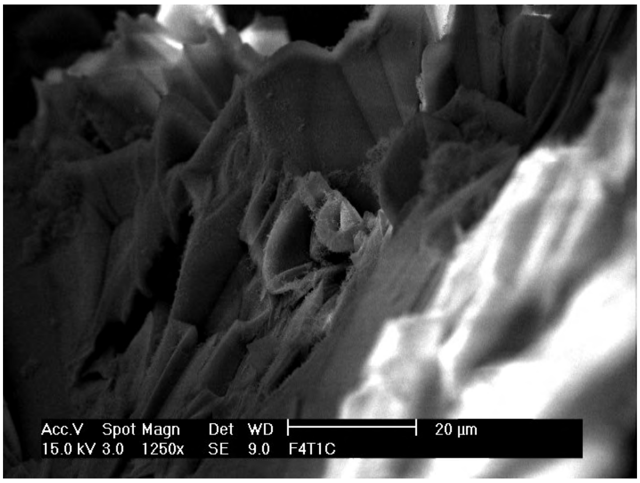
Acc.V Spot Magn Det WD 20 µm
15.0 kV 3.0 1250x SE 9.0 F4T1C

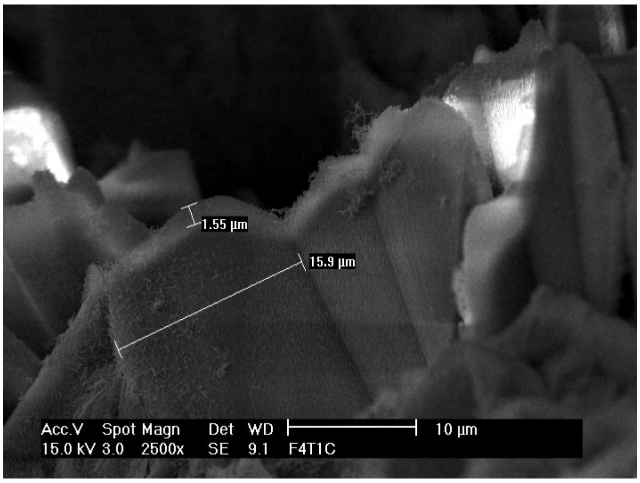
1.55 µm
15.9 µm
Acc.V Spot Magn Det WD 10 µm
15.0 kV 3.0 2500x SE 9.1 F4T1C

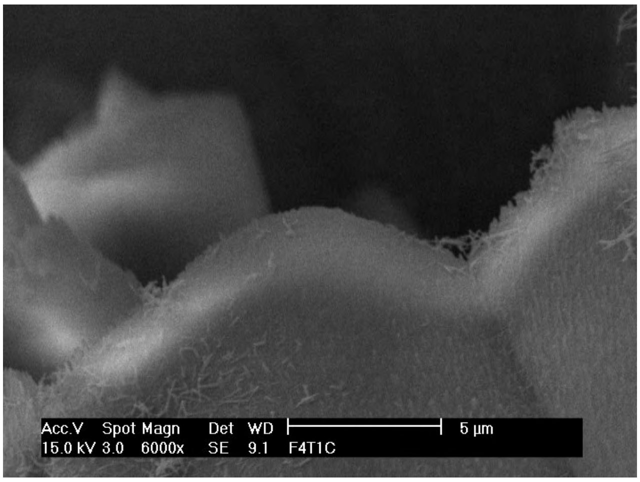
Acc.V Spot Magn Det WD 5 µm
15.0 kV 3.0 6000x SE 9.1 F4T1C

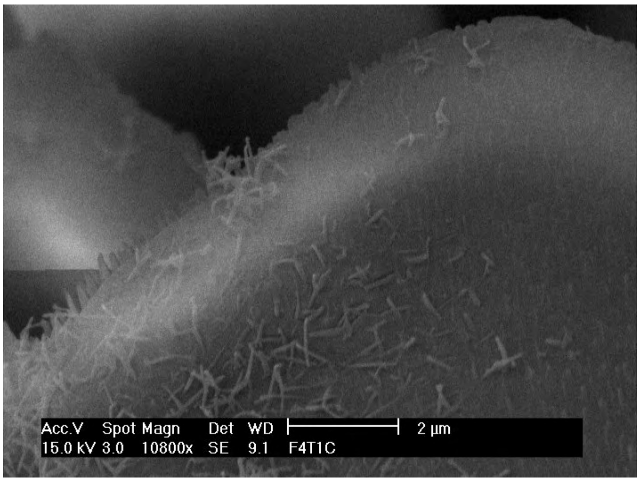
Acc.V Spot Magn Det WD 2 µm
15.0 kV 3.0 10800x SE 9.1 F4T1C

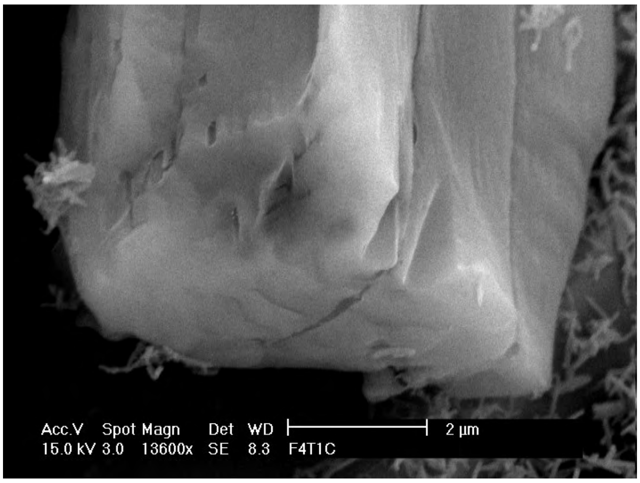
Acc.V Spot Magn Det WD 2 µm
15.0 kV 3.0 13600x SE 8.3 F4T1C

Nanometer-sized filaments

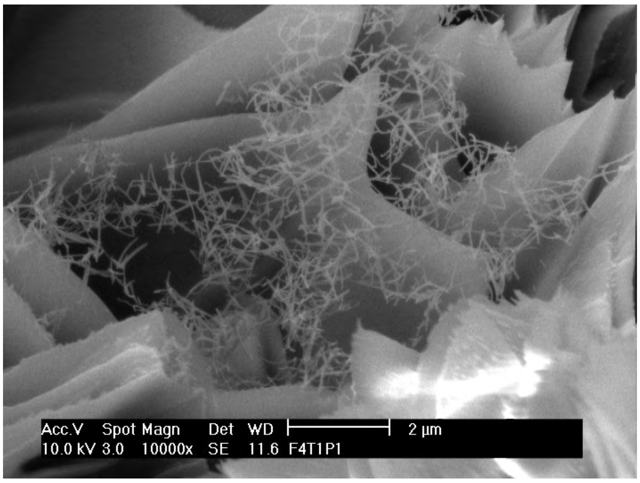
Acc.V Spot Magn Det WD 2 µm
10.0 kV 3.0 10000x SE 11.6 F4T1P1

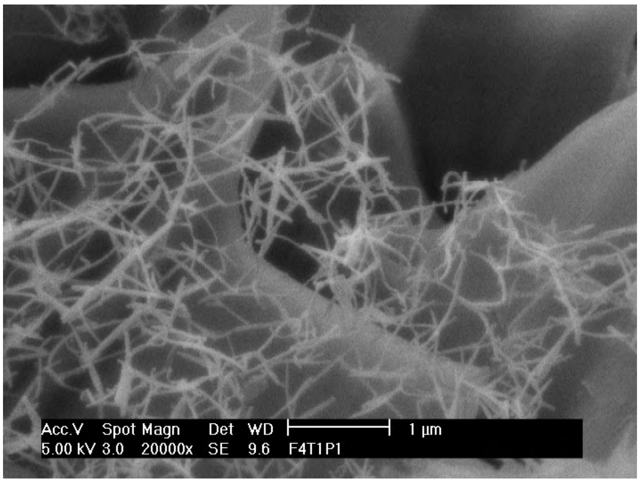
Acc.V Spot Magn Det WD 1 µm
5.00 kV 3.0 20000x SE 9.6 F4T1P1

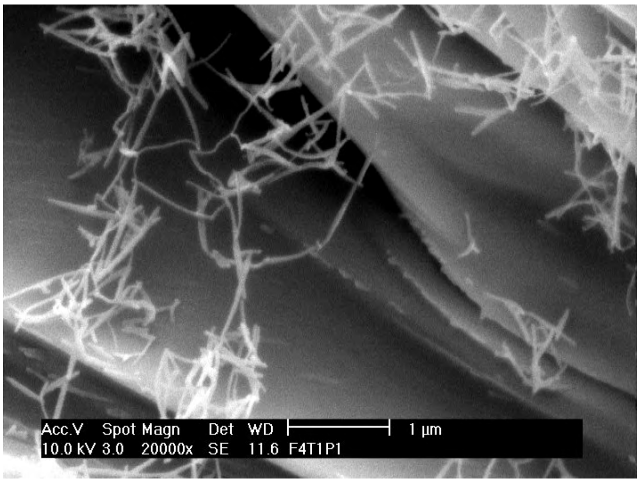
Acc.V Spot Magn Det WD 1 µm
10.0 kV 3.0 20000x SE 11.6 F4T1P1

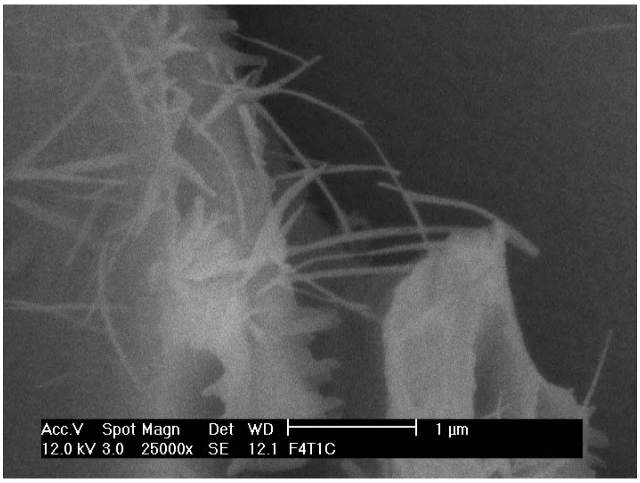
Acc.V Spot Magn Det WD 1 µm
12.0 kV 3.0 25000x SE 12.1 F4T1C

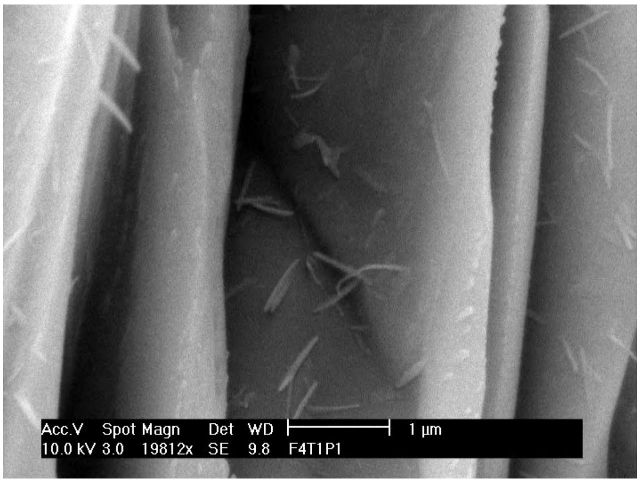
Acc.V Spot Magn Det WD 1 µm
10.0 kV 3.0 19812x SE 9.8 F4T1P1

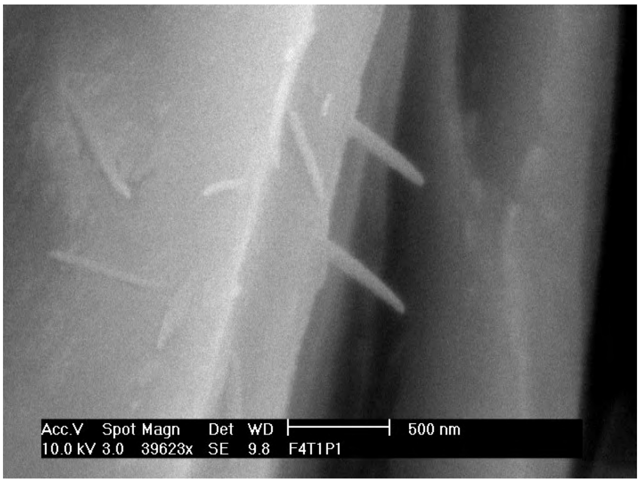
Acc.V Spot Magn Det WD 500 nm
10.0 kV 3.0 39623x SE 9.8 F4T1P1

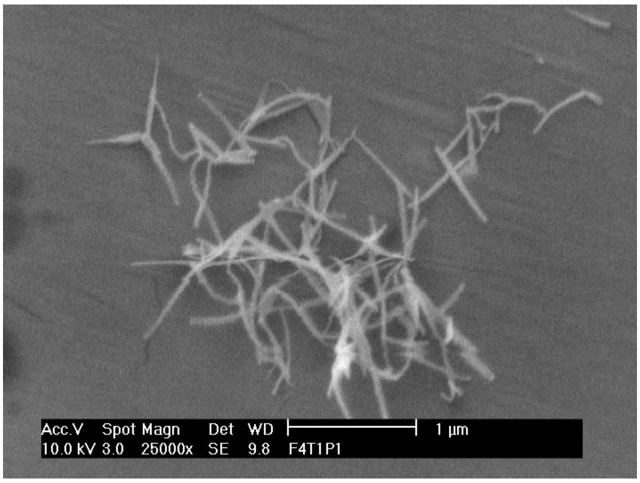
Acc.V Spot Magn Det WD
1 µm
10.0 kV 3.0 25000x SE 9.8 F4T1P1

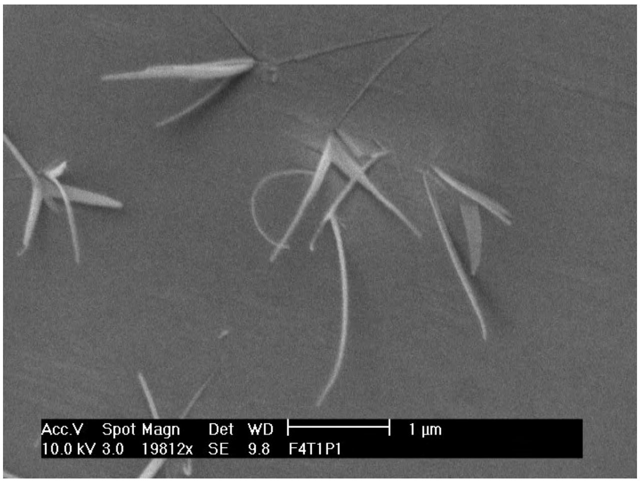
Acc.V Spot Magn Det WD
1 µm
10.0 kV 3.0 19812x SE 9.8 F4T1P1

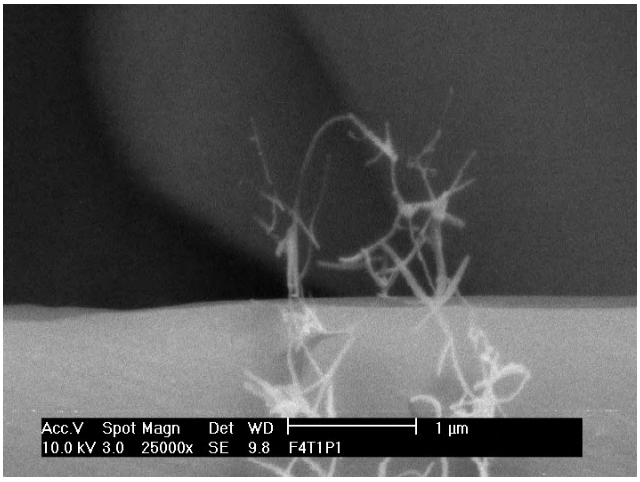
Acc.V Spot Magn Det WD
1 µm
10.0 kV 3.0 25000x SE 9.8 F4T1P1

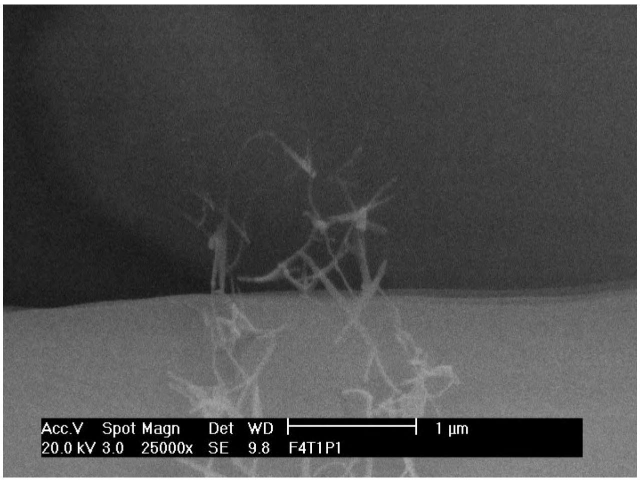
Acc.V Spot Magn Det WD
1 µm
20.0 kV 3.0 25000x SE 9.8 F4T1P1

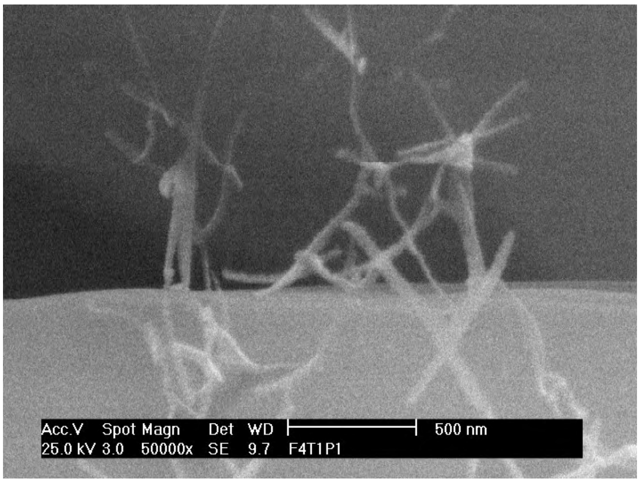
Acc.V Spot Magn Det WD
500 nm
25.0 kV 3.0 50000x SE 9.7 F4T1P1

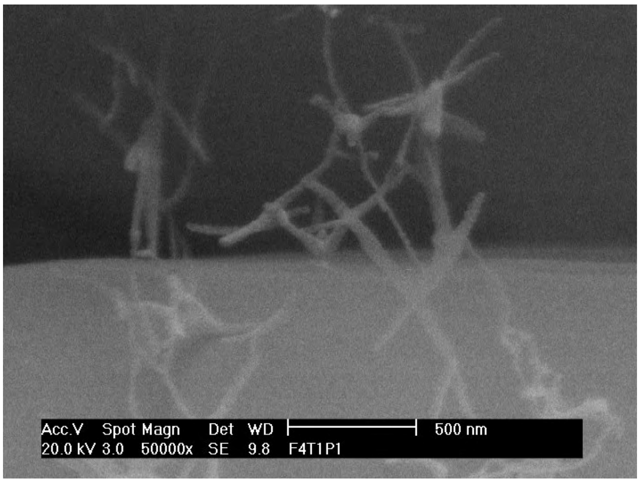
Acc.V Spot Magn Det WD
500 nm
20.0 kV 3.0 50000x SE 9.8 F4T1P1

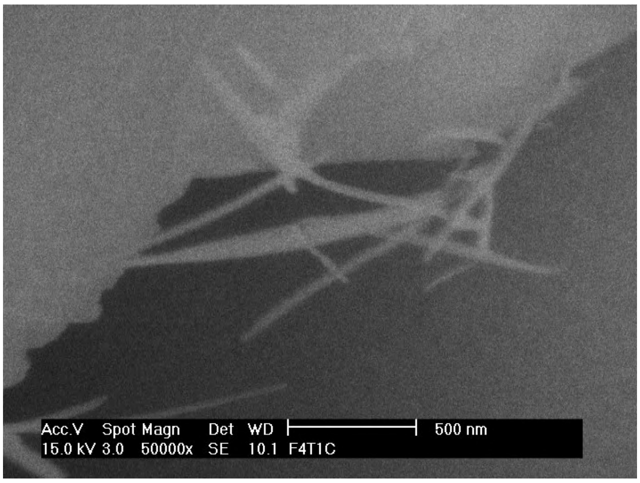
Acc.V Spot Magn Det WD 500 nm
15.0 kV 3.0 50000x SE 10.1 F4T1C

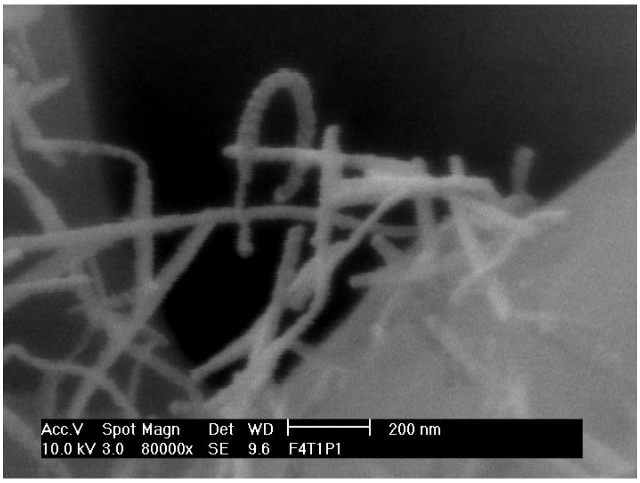
Acc.V Spot Magn Det WD 200 nm
10.0 kV 3.0 80000x SE 9.6 F4T1P1

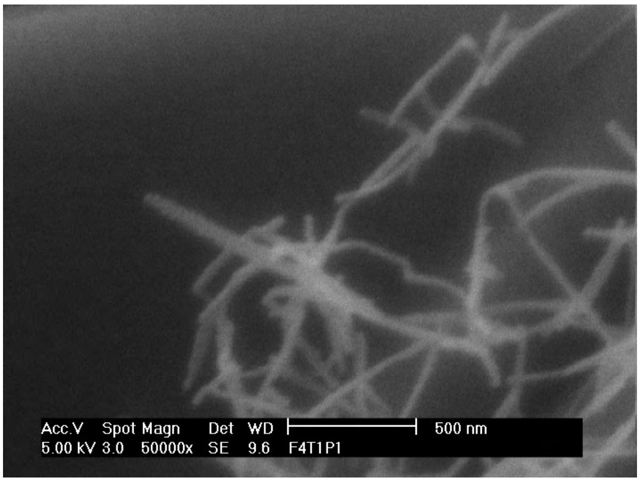
Acc.V Spot Magn Det WD 500 nm
5.00 kV 3.0 50000x SE 9.6 F4T1P1

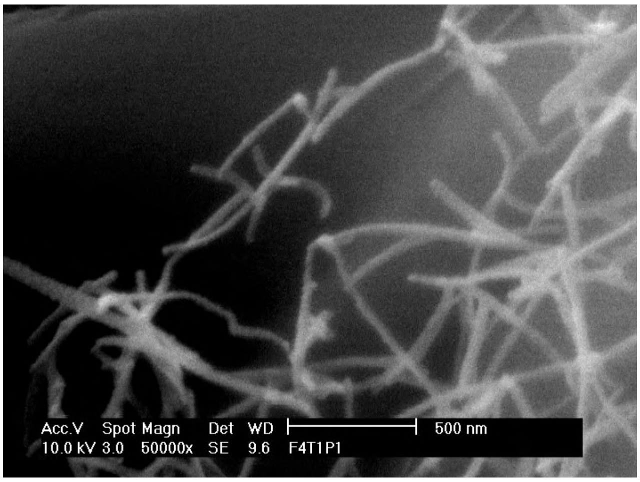
Acc.V Spot Magn Det WD 500 nm
10.0 kV 3.0 50000x SE 9.6 F4T1P1

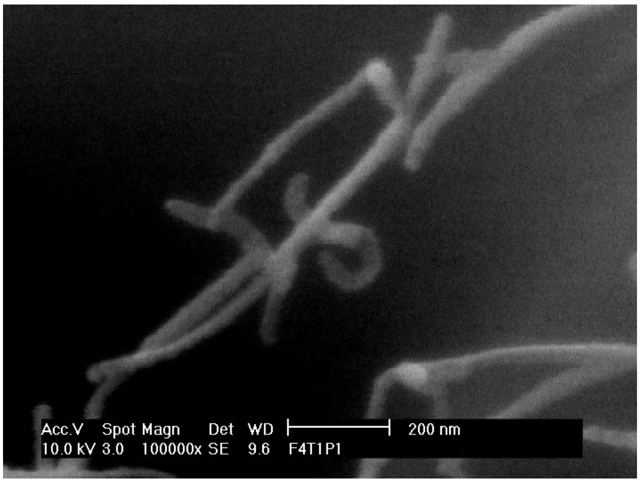
Acc.V Spot Magn Det WD 200 nm
10.0 kV 3.0 100000x SE 9.6 F4T1P1

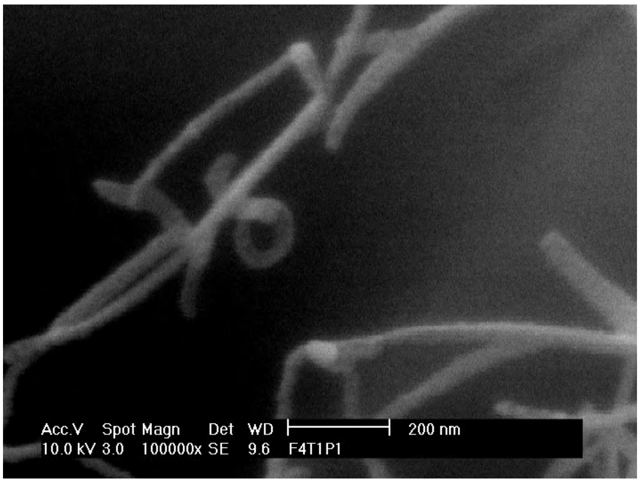
Acc.V Spot Magn Det WD 200 nm
10.0 kV 3.0 100000x SE 9.6 F4T1P1

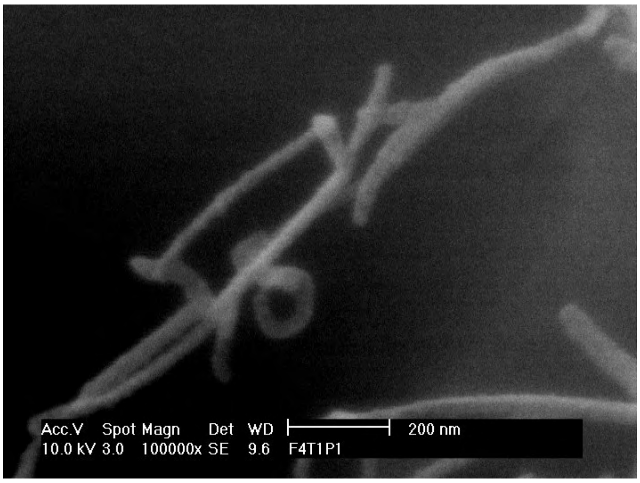
Acc.V Spot Magn Det WD 200 nm
10.0 kV 3.0 100000x SE 9.6 F4T1P1

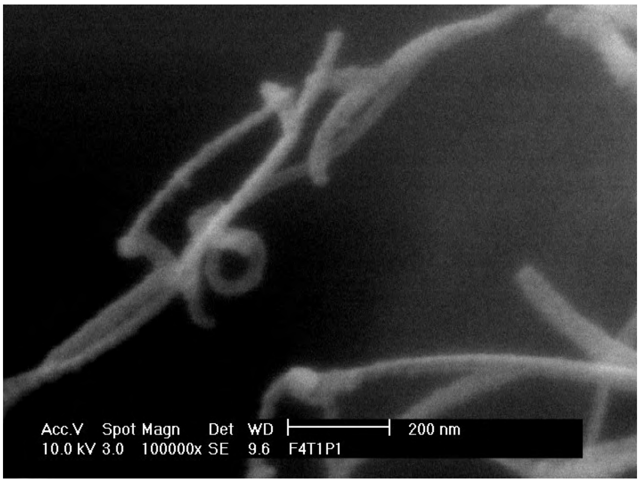
Acc.V Spot Magn Det WD 200 nm
10.0 kV 3.0 100000x SE 9.6 F4T1P1

Solvent’s residue

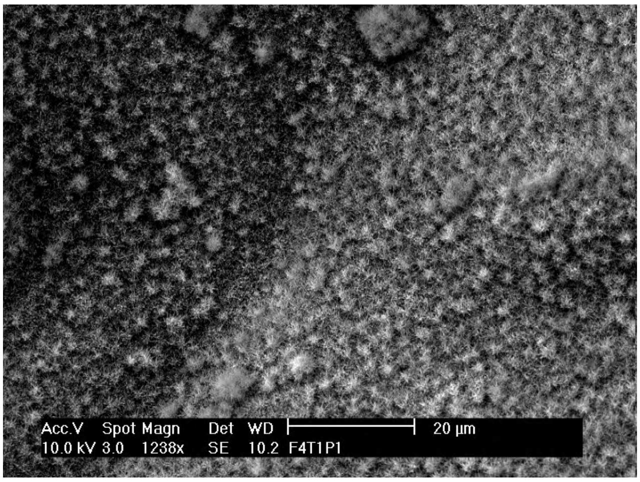
Acc.V Spot Magn Det WD 20 µm
10.0 kV 3.0 1238x SE 10.2 F4T1P1

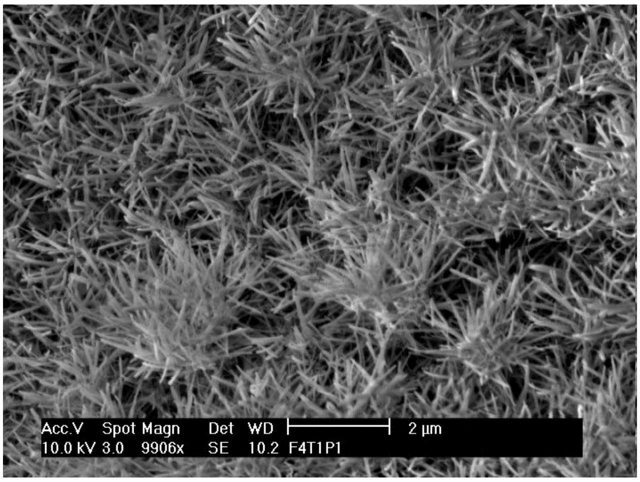
Acc.V Spot Magn Det WD 2 µm
10.0 kV 3.0 9906x SE 10.2 F4T1P1

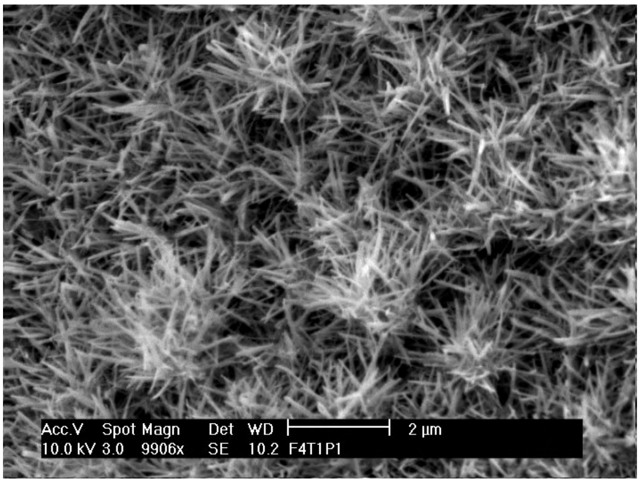
Acc.V Spot Magn Det WD 2 µm
10.0 kV 3.0 9906x SE 10.2 F4T1P1

Cryo-SEM micrographs of 1,2,4-TCB

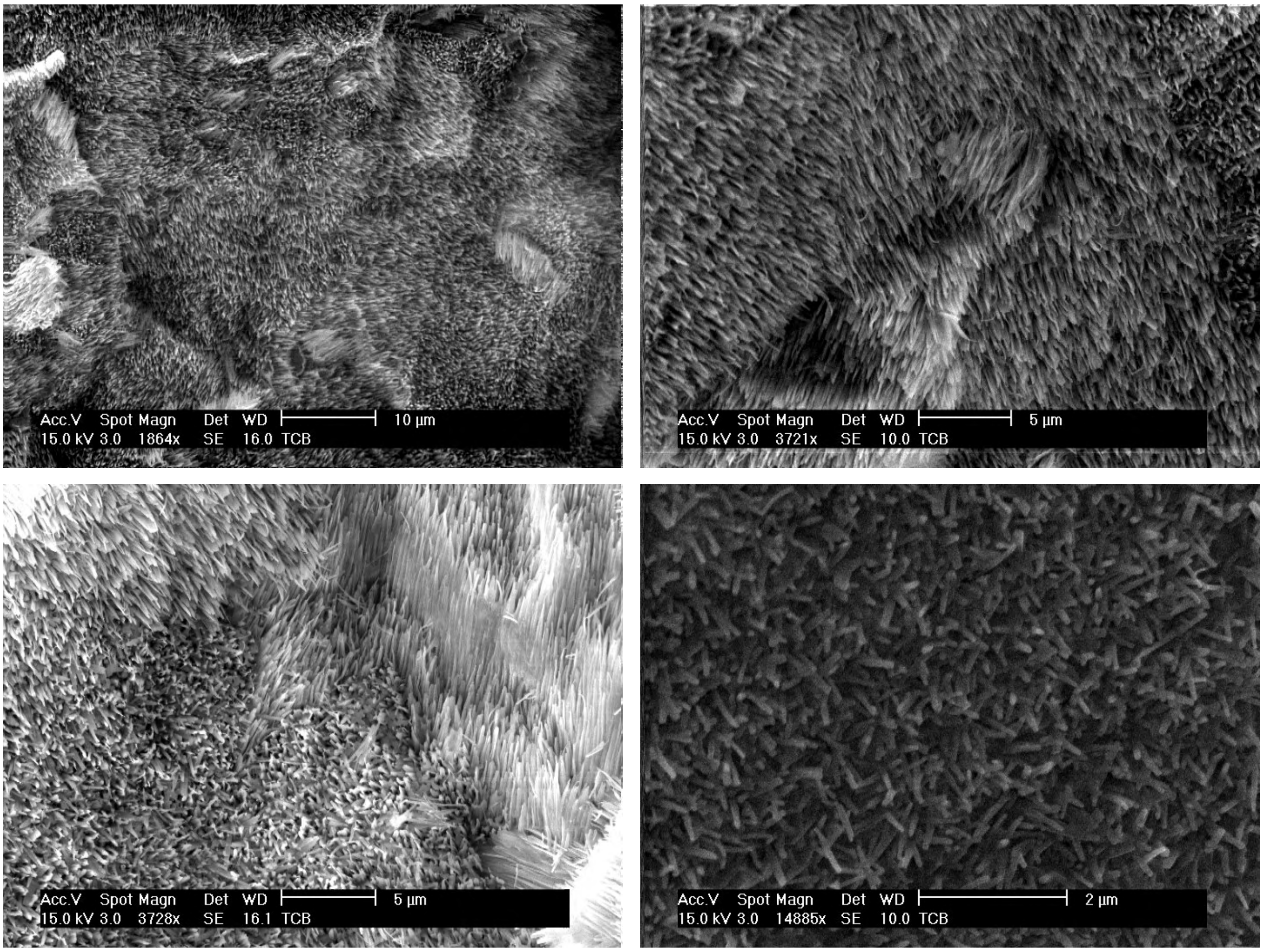
Acc.V Spot Magn Det WD 10 µm
15.0 kV 3.0 1864x SE 16.0 TCB
Acc.V Spot Magn Det WD 5 µm
15.0 kV 3.0 3721x SE 10.0 TCB
Acc.V Spot Magn Det WD 5 µm
15.0 kV 3.0 3728x SE 16.1 TCB
Acc.V Spot Magn Det WD 2 µm
15.0 kV 3.0 14885x SE 10.0 TCB

A.3.4 Deposited film from a dilute solution

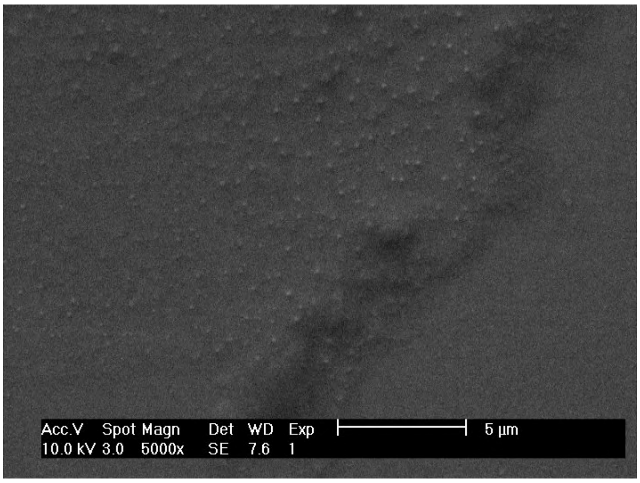
Acc.V Spot Magn Det WD Exp
10.0 kV 3.0 5000x SE 7.6 1
5 µm

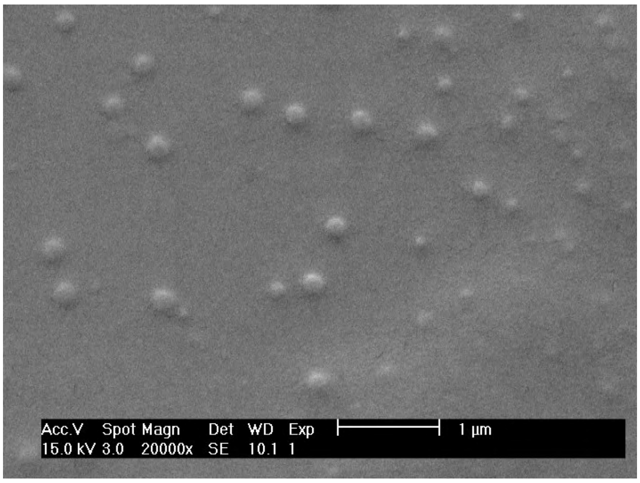
Acc.V Spot Magn Det WD Exp
15.0 kV 3.0 20000x SE 10.1 1
1 µm

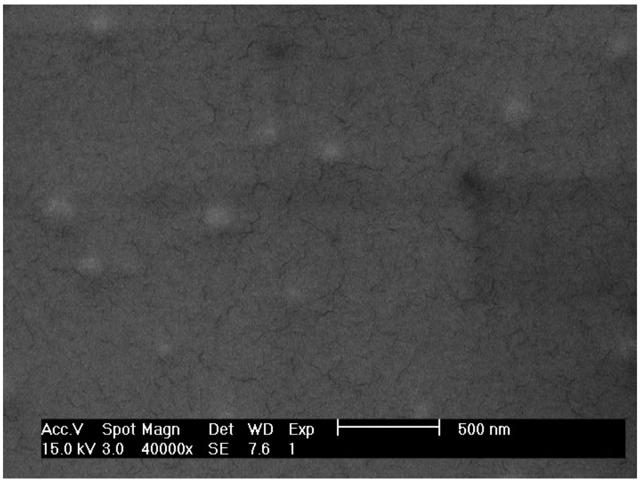
Acc.V Spot Magn Det WD Exp
15.0 kV 3.0 40000x SE 7.6 1
500 nm

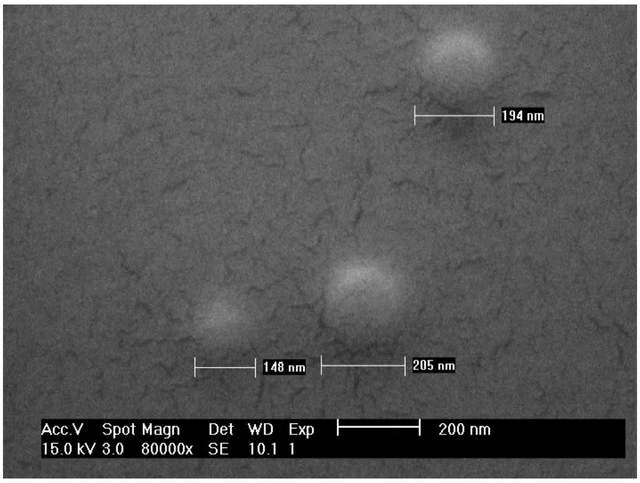
194 nm
148 nm
205 nm
Acc.V Spot Magn Det WD Exp
15.0 kV 3.0 80000x SE 10.1 1
200 nm

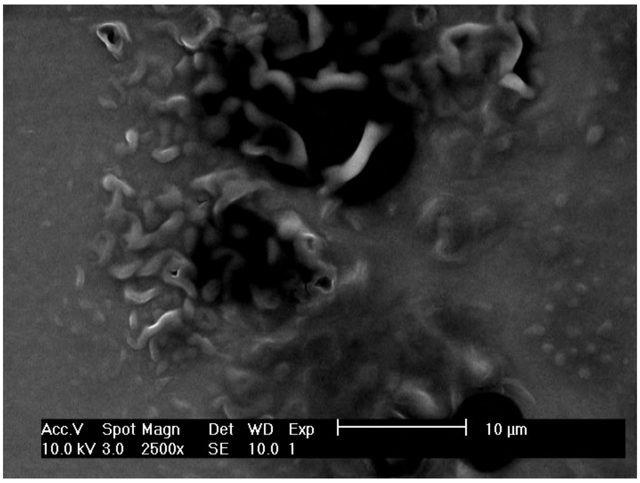
Acc.V Spot Magn Det WD Exp
10.0 kV 3.0 2500x SE 10.0 1
10 µm

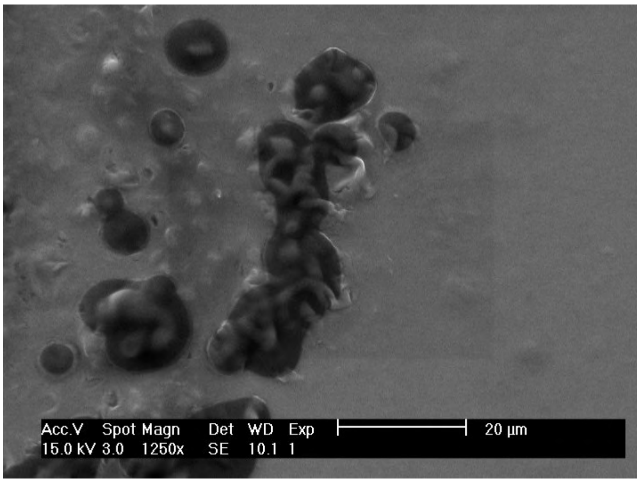
Acc.V Spot Magn Det WD Exp
15.0 kV 3.0 1250x SE 10.1 1
20 µm

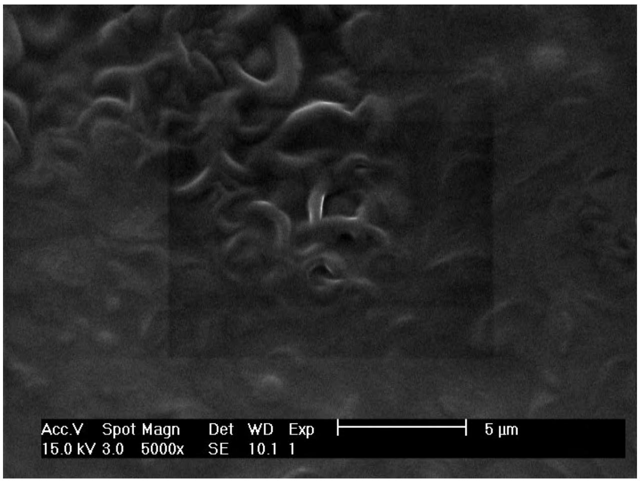
Acc.V Spot Magn Det WD Exp
15.0 kV 3.0 5000x SE 10.1 1
5 µm

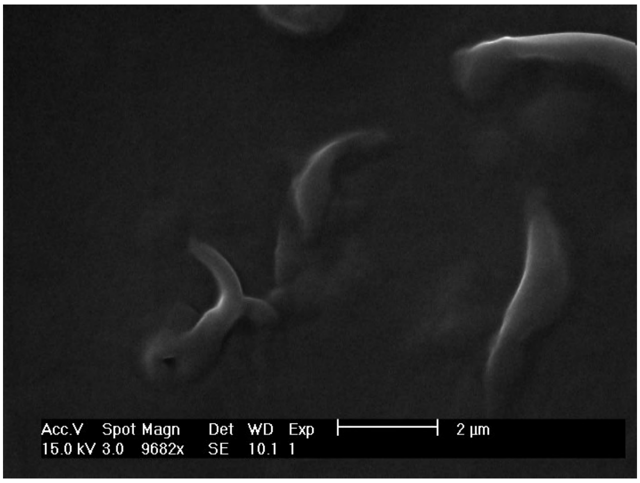
Acc.V Spot Magn Det WD Exp
15.0 kV 3.0 9682x SE 10.1 1
2 µm

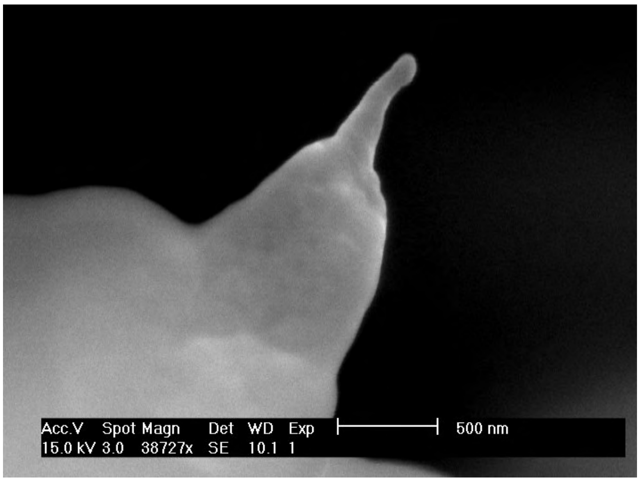
Acc.V Spot Magn Det WD Exp
15.0 kV 3.0 38727x SE 10.1 1
500 nm

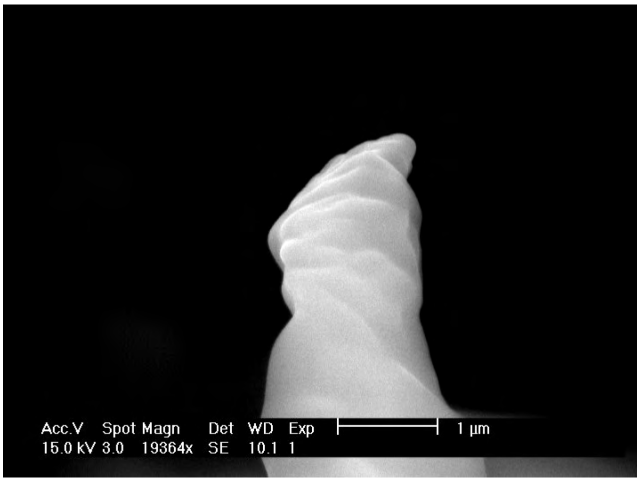
Acc.V Spot Magn Det WD Exp
15.0 kV 3.0 19364x SE 10.1 1
1 µm

A.4 SEM micrographs of HBC-Rf$_{6,6}$ (115)

A.4.1 Precipitate

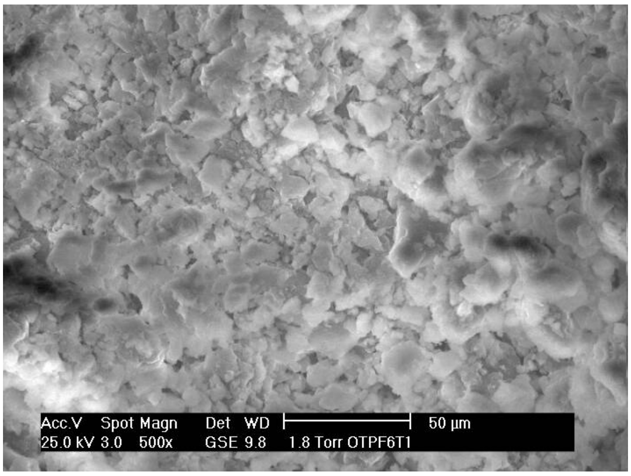
Acc.V Spot Magn Det WD 50 µm
25.0 kV 3.0 500x GSE 9.8 1.8 Torr OTPF6T1

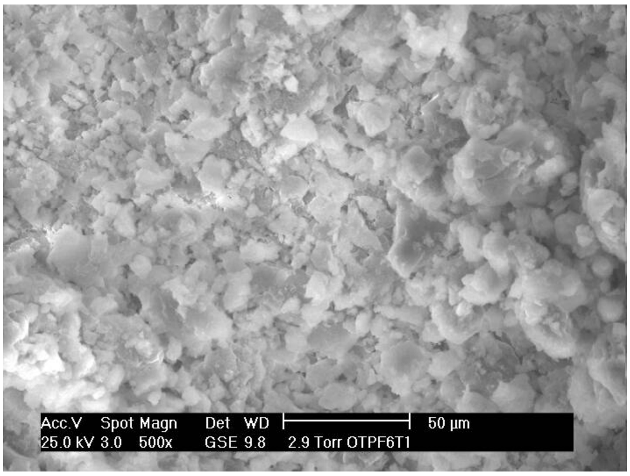
Acc.V Spot Magn Det WD 50 µm
25.0 kV 3.0 500x GSE 9.8 2.9 Torr OTPF6T1

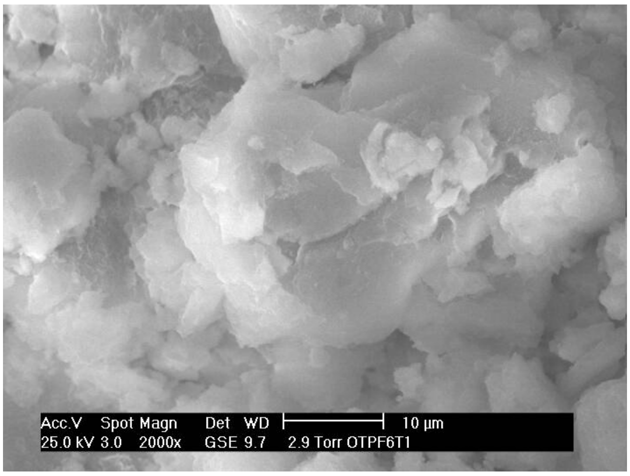
Acc.V Spot Magn Det WD 10 µm
25.0 kV 3.0 2000x GSE 9.7 2.9 Torr OTPF6T1

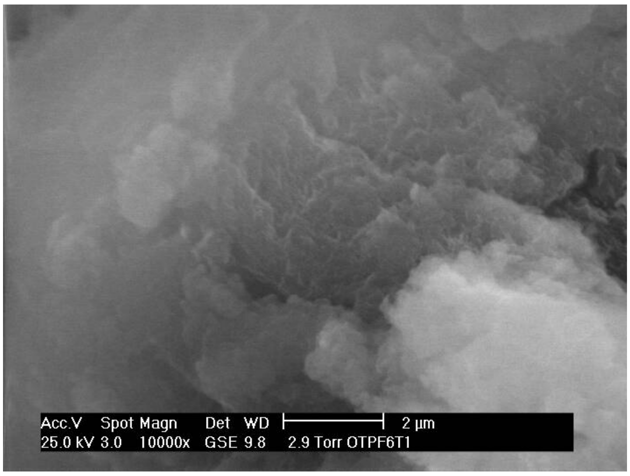
Acc.V Spot Magn Det WD 2 µm
25.0 kV 3.0 10000x GSE 9.8 2.9 Torr OTPF6T1

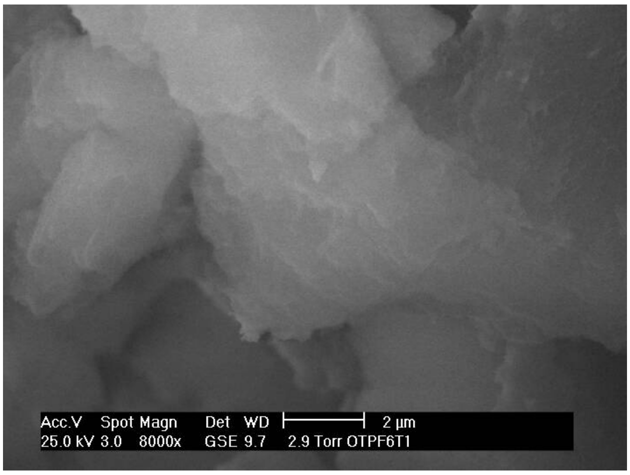
Acc.V Spot Magn Det WD 2 µm
25.0 kV 3.0 8000x GSE 9.7 2.9 Torr OTPF6T1

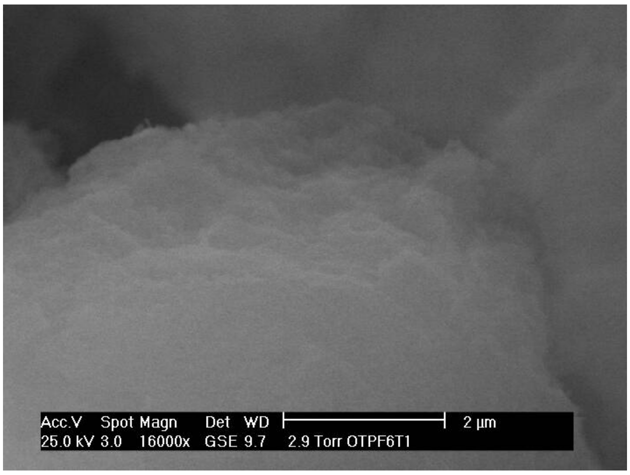
Acc.V Spot Magn Det WD 2 µm
25.0 kV 3.0 16000x GSE 9.7 2.9 Torr OTPF6T1

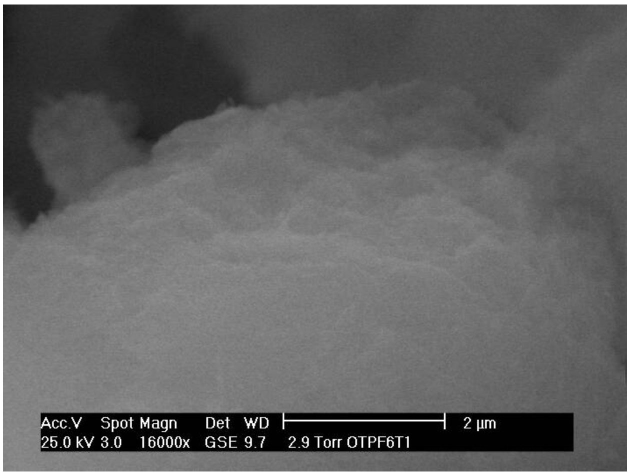
Acc.V Spot Magn Det WD 2 µm
25.0 kV 3.0 16000x GSE 9.7 2.9 Torr OTPF6T1

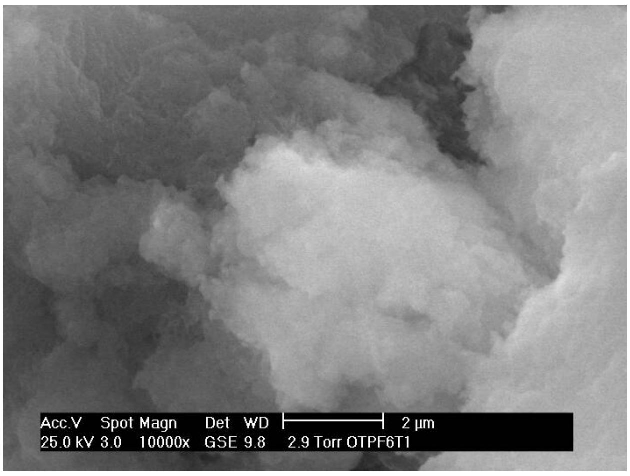
Acc.V Spot Magn Det WD 2 µm
25.0 kV 3.0 10000x GSE 9.8 2.9 Torr OTPF6T1

A.4.2 Deposited film from a dilute solution

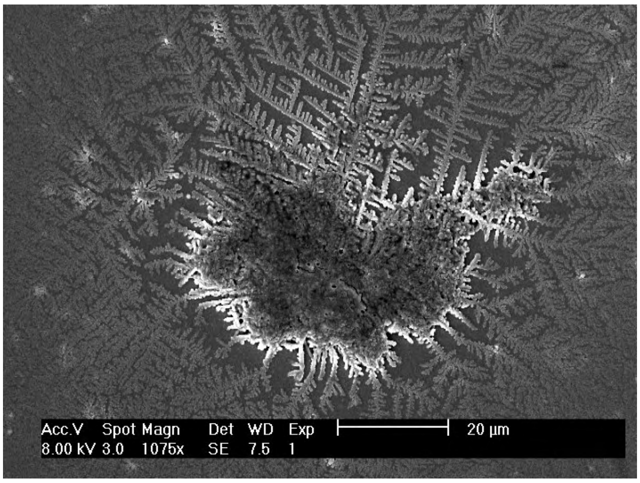
Acc.V Spot Magn Det WD Exp 20 µm
8.00 kV 3.0 1075x SE 7.5 1

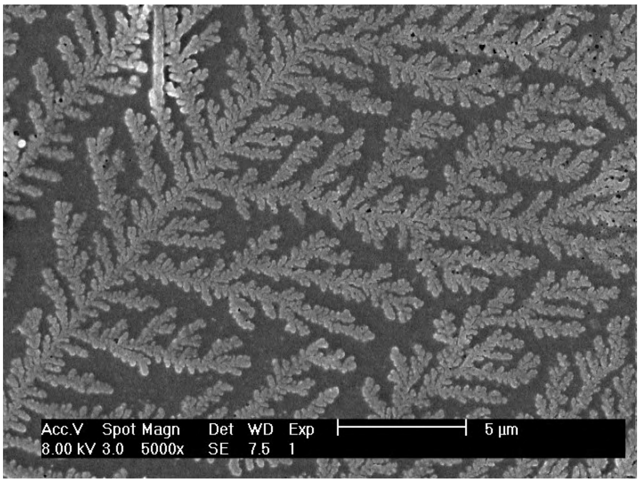
Acc.V Spot Magn Det WD Exp 5 µm
8.00 kV 3.0 5000x SE 7.5 1

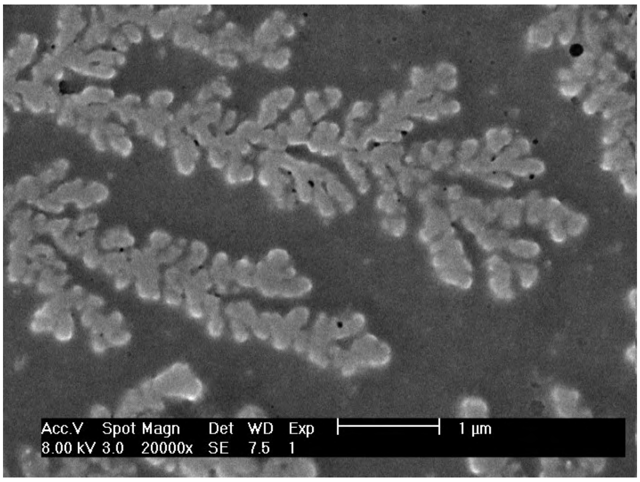
Acc.V Spot Magn Det WD Exp 1 µm
8.00 kV 3.0 20000x SE 7.5 1

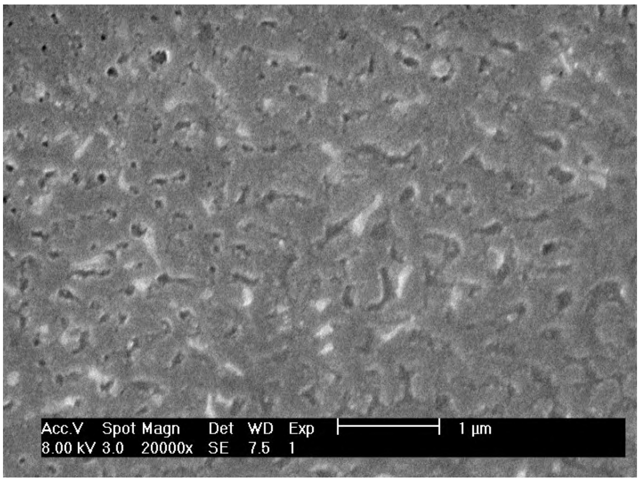
Acc.V Spot Magn Det WD Exp 1 µm
8.00 kV 3.0 20000x SE 7.5 1

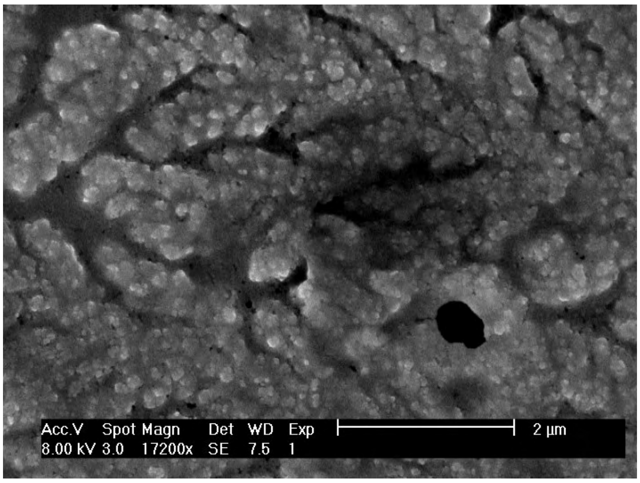
Acc.V Spot Magn Det WD Exp
8.00 kV 3.0 17200x SE 7.5 1
2 µm

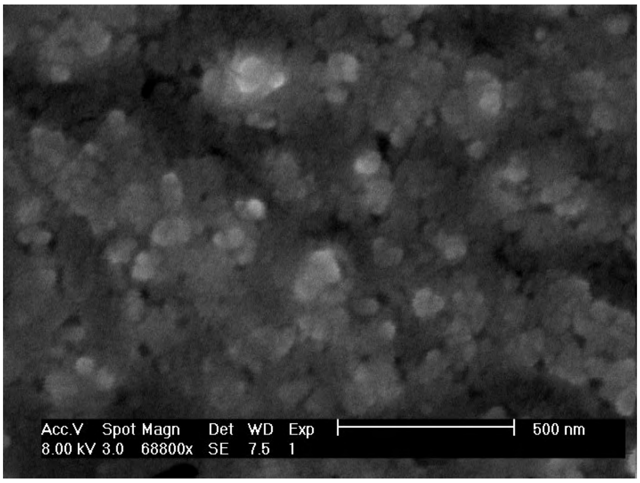
Acc.V Spot Magn Det WD Exp
8.00 kV 3.0 68800x SE 7.5 1
500 nm

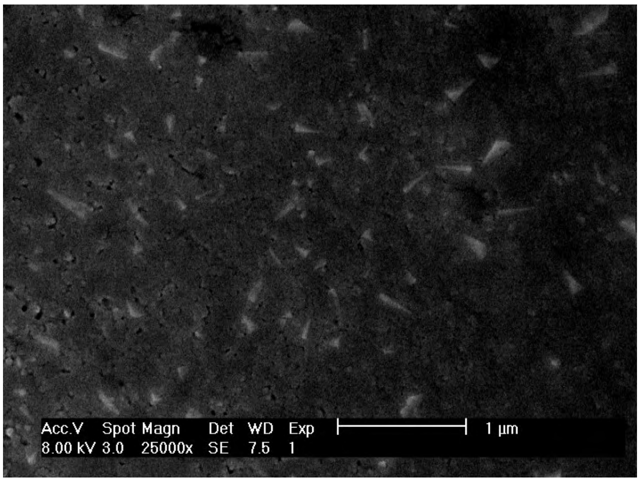
Acc.V Spot Magn Det WD Exp
8.00 kV 3.0 25000x SE 7.5 1
1 µm

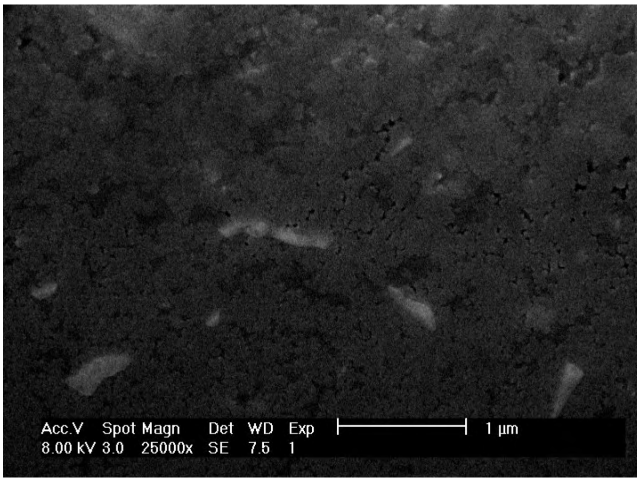
Acc.V Spot Magn Det WD Exp
8.00 kV 3.0 25000x SE 7.5 1
1 µm

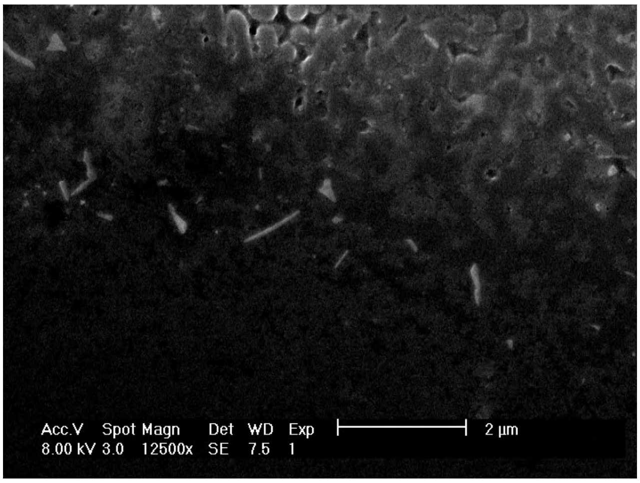
Acc.V Spot Magn Det WD Exp
8.00 kV 3.0 12500x SE 7.5 1
2 µm

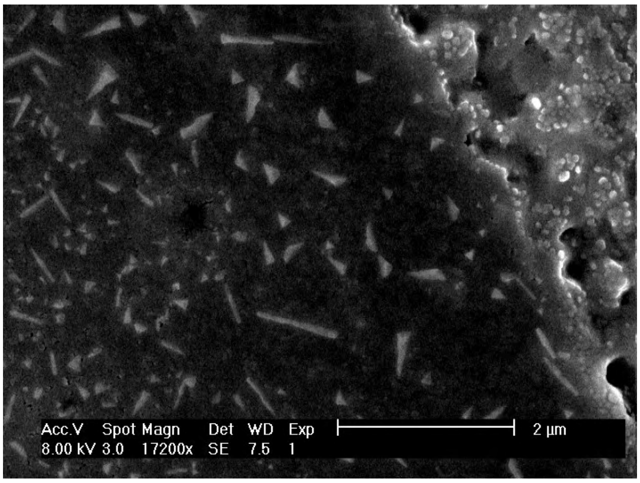
Acc.V Spot Magn Det WD Exp
8.00 kV 3.0 17200x SE 7.5 1
2 µm

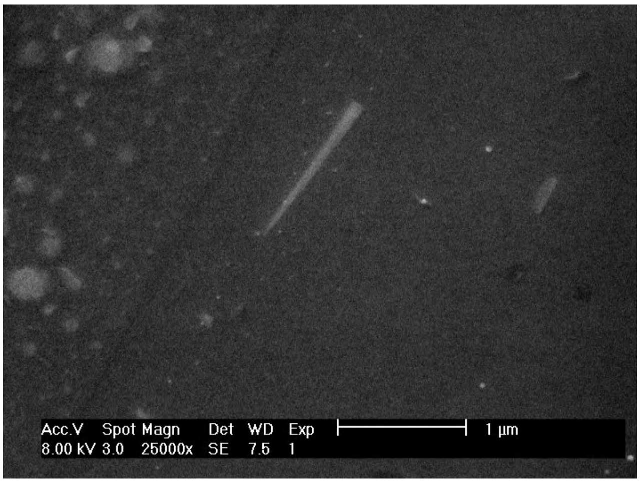
Acc.V Spot Magn Det WD Exp
8.00 kV 3.0 25000x SE 7.5 1
1 µm

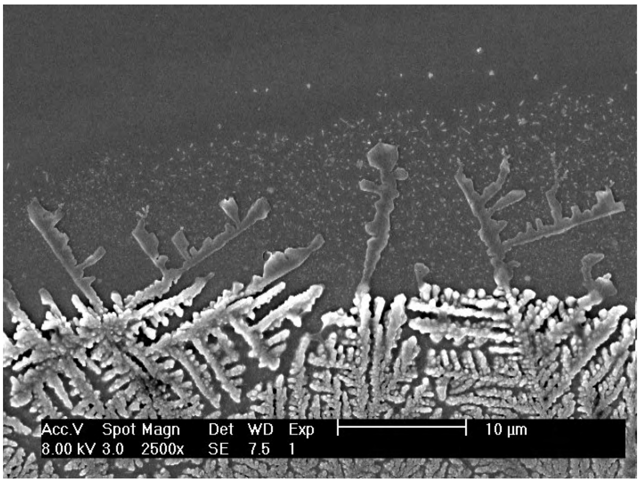
Acc.V Spot Magn Det WD Exp
8.00 kV 3.0 2500x SE 7.5 1
10 µm

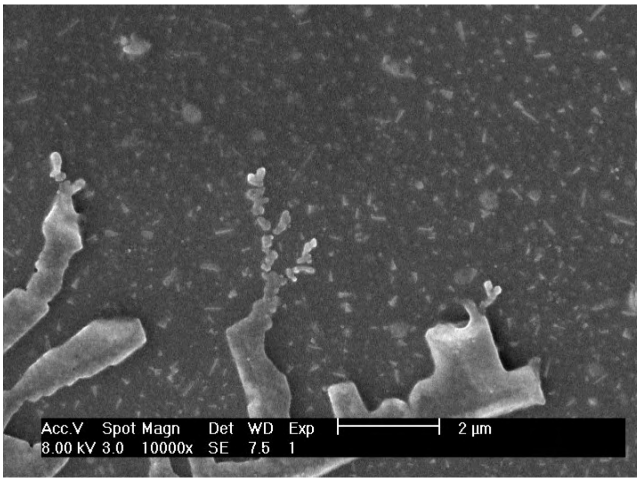
Acc.V Spot Magn Det WD Exp
8.00 kV 3.0 10000x SE 7.5 1
2 µm

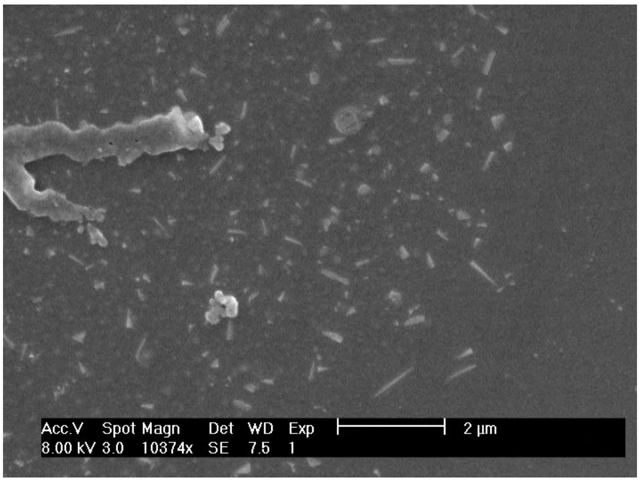
Acc.V Spot Magn Det WD Exp
8.00 kV 3.0 10374x SE 7.5 1
2 µm

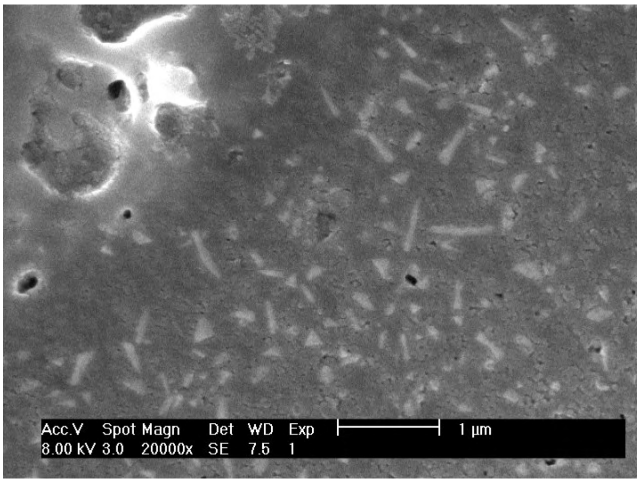
Acc.V Spot Magn Det WD Exp
8.00 kV 3.0 20000x SE 7.5 1
1 µm

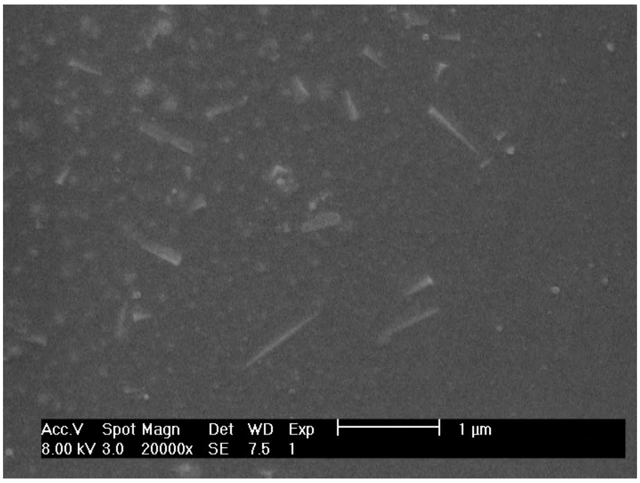
Acc.V Spot Magn Det WD Exp
8.00 kV 3.0 20000x SE 7.5 1
1 µm

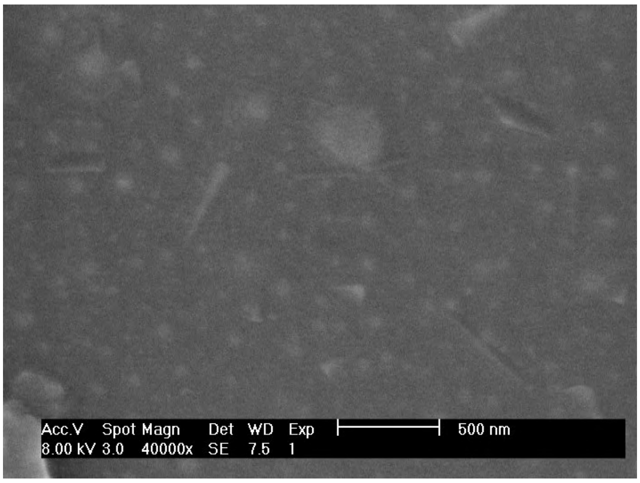
Acc.V Spot Magn Det WD Exp
500 nm
8.00 kV 3.0 40000x SE 7.5 1

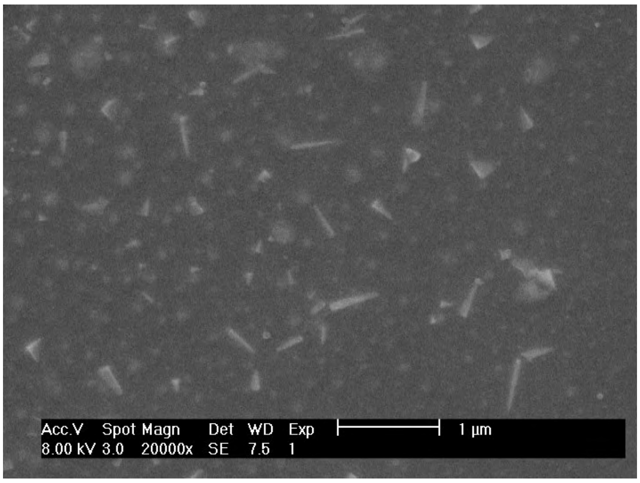
Acc.V Spot Magn Det WD Exp
1 µm
8.00 kV 3.0 20000x SE 7.5 1

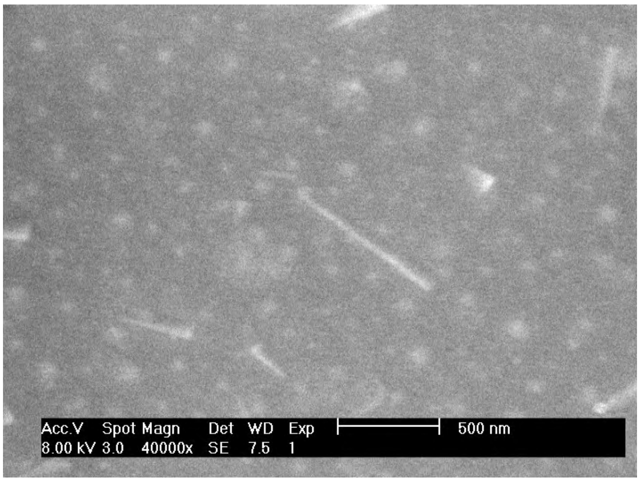
Acc.V Spot Magn Det WD Exp
500 nm
8.00 kV 3.0 40000x SE 7.5 1

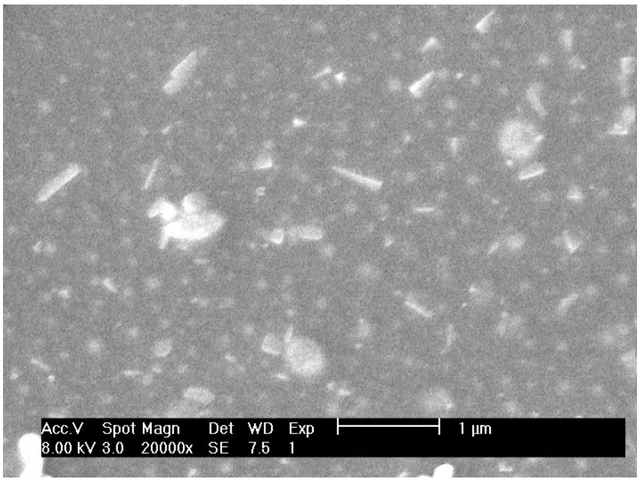
Acc.V Spot Magn Det WD Exp
1 µm
8.00 kV 3.0 20000x SE 7.5 1

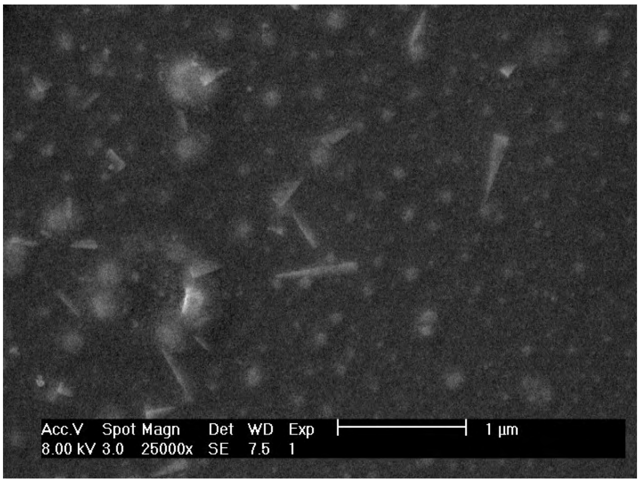
Acc.V Spot Magn Det WD Exp
1 µm
8.00 kV 3.0 25000x SE 7.5 1

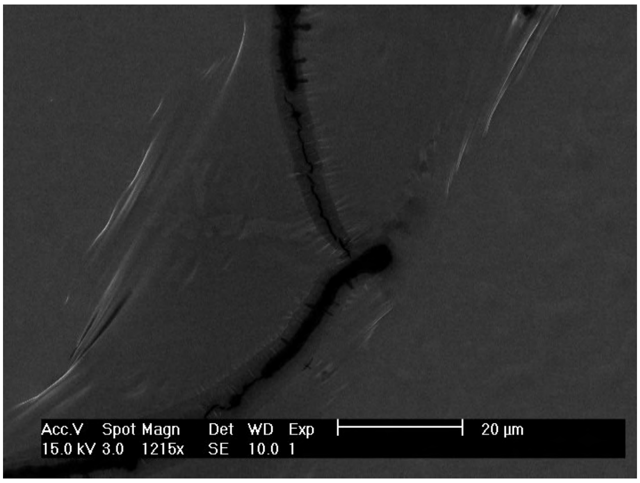
Acc.V Spot Magn Det WD Exp
20 µm
15.0 kV 3.0 1215x SE 10.0 1

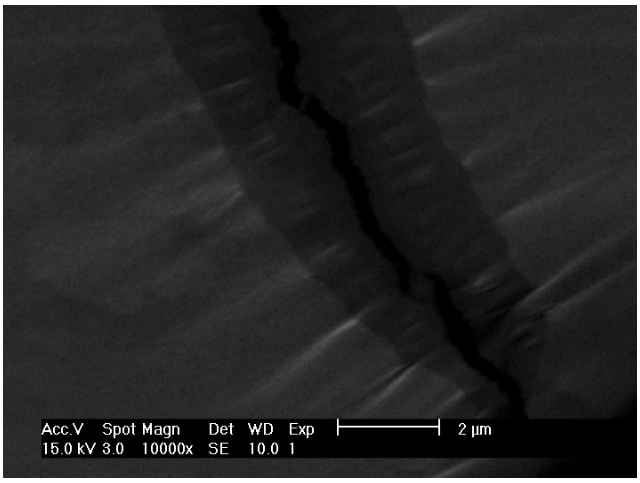
Acc.V Spot Magn Det WD Exp
15.0 kV 3.0 10000x SE 10.0 1
2 µm

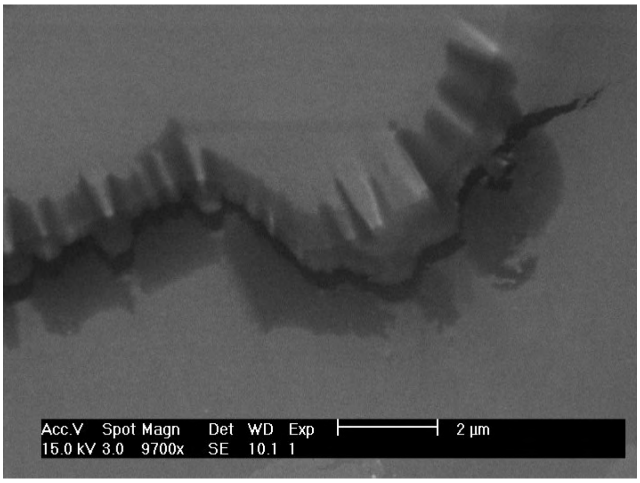
Acc.V Spot Magn Det WD Exp
15.0 kV 3.0 9700x SE 10.1 1
2 µm

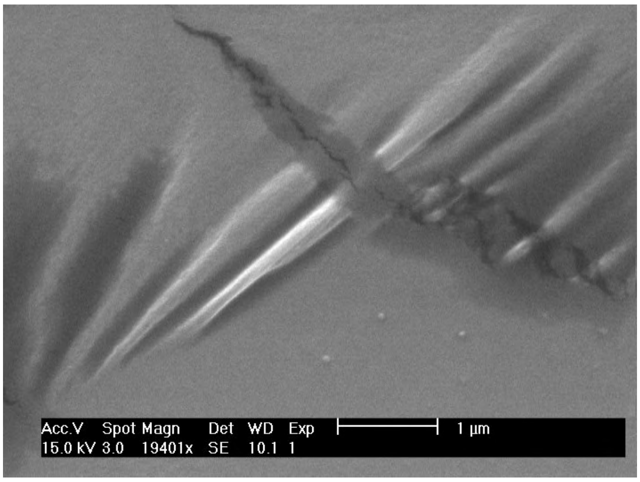
Acc.V Spot Magn Det WD Exp
15.0 kV 3.0 19401x SE 10.1 1
1 µm

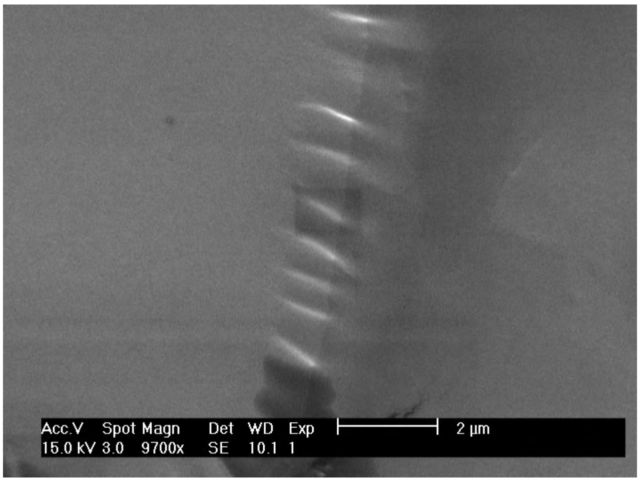
Acc.V Spot Magn Det WD Exp
15.0 kV 3.0 9700x SE 10.1 1
2 µm

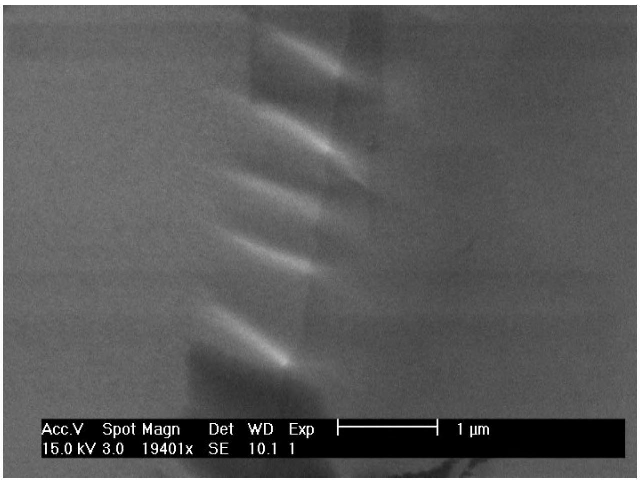
Acc.V Spot Magn Det WD Exp
15.0 kV 3.0 19401x SE 10.1 1
1 µm

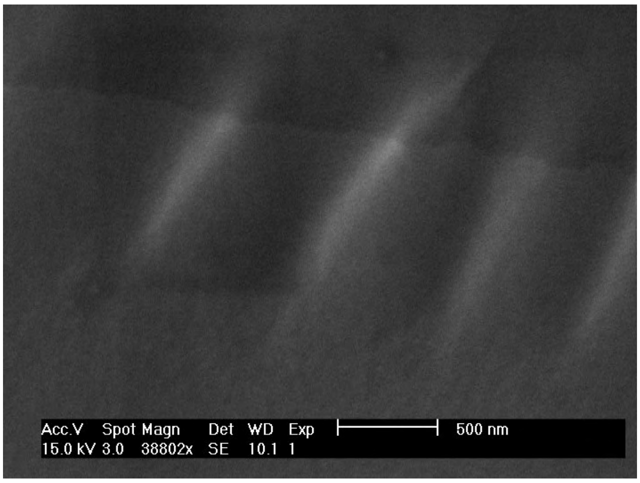
Acc.V Spot Magn Det WD Exp
15.0 kV 3.0 38802x SE 10.1 1
500 nm

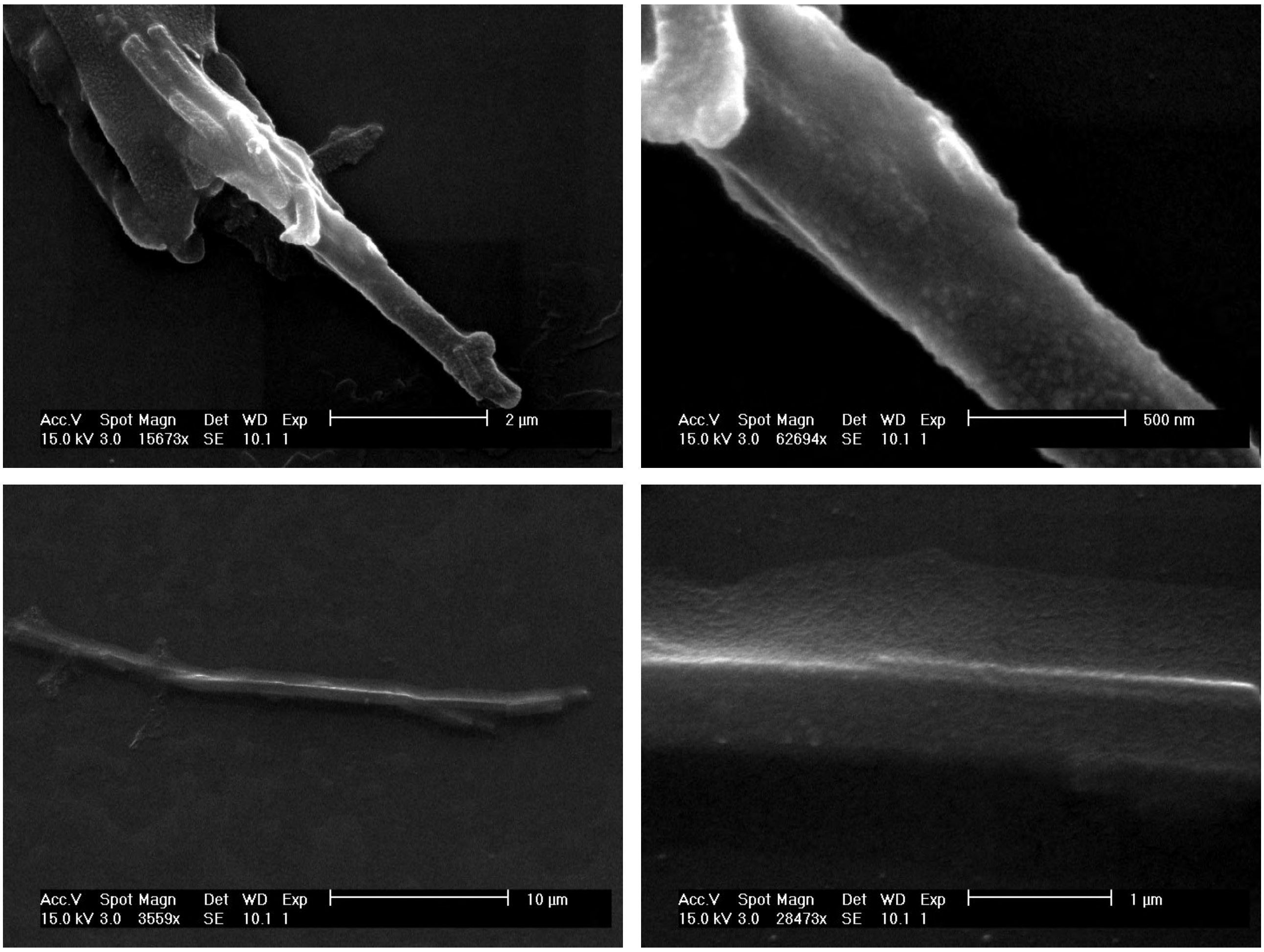
Acc.V Spot Magn Det WD Exp 2 µm
15.0 kV 3.0 15673x SE 10.1 1
Acc.V Spot Magn Det WD Exp 500 nm
15.0 kV 3.0 62694x SE 10.1 1
Acc.V Spot Magn Det WD Exp 10 µm
15.0 kV 3.0 3559x SE 10.1 1
Acc.V Spot Magn Det WD Exp 1 µm
15.0 kV 3.0 28473x SE 10.1 1

VI. References

[1] J.-M. Lehn, *Angew. Chem. Int. Ed.* **1988**, *27*, 89.

[2] J. S. Lindsey, *New J. Chem.* **1991**, *15*, 153.

[3] S. Mann, *Chem. Commun.* **2004**, *1*, 1.

[4] D. N. Reinhoudt, M. Crego-Calama, *Science* **2002**, *295*, 2403.

[5] R. F. M. Lange, M. Van Gurp, E. W. Meijer, *J. Polym. Sci. A* **1999**, *37*, 3657.

[6] J.-M. Lehn, *Science* **2002**, *295*, 2400.

[7] M. M. Conn, J. Rebek Jr., *J. Am. Chem. Soc.* **1997**, *97*, 1647

[8] C. G. Claessens, J. F. Stoddart, *J. Phys. Org. Chem.* **1997**, *10*, 254.

[9] L. Brunsveld, B. J. Folmer, E. W. Meijer, *MRS Bull.* **2000**, *25*, 49.

[10] L. Brunsveld, B. J. B. Folmer, E. W. Meijer, R. P. Sijibesma, *Chem. Rev.* **2001**, *101*, 4071.

[11] B. J. B. Folmer, R. P. Sijbesma, R. M. Versteegen, J. A. J. van der Rijt, E. W. Meijer, *Adv. Mater.* **2000**, *12*, 874.

[12] D. Adam, P. Schuhmacher, J. Simmerer, L. Haeussling, K. Siemensmeyer, K. H. Etzbach, H. Ringsdorf, D. Haarer, *Nature* **1994**, *371*, 141.

[13] A. Van de Craats, J. M. Warman, K. Müllen, Y. Geerts, J. D. Brand, *Adv. Mater.* **1998**, *10*, 36.

[14] A. Van de Craats, J. M. Warman, A. Fechtenkötter, J. D. Brand, K. Müllen, *Adv. Mater.* **1999**, *11*, 1469.

[15] G. M. Whitesides, J. P. Mathias, C. T. Seto, *Science* **1991**, *254*, 1312.

[16] S. Mann, *Nature* **1993**, *365*, 499.

[17] D. S. Lawrence, T. Jiang, M. Levett, *Chem. Rev.* **1995**, *95*, 2229.

[18] D. B. Amabilino, J. F. Stoddart, *Chem. Rev.* **1995**, *95*, 2725.

[19] F. M. Raymo, J. F. Stoddart, *Chem. Rev.* **1999**, *99*, 1643.

[20] S. Rucareanu, O. Mongin, A. Schuwey, N. Hoyler, A. Gossauer, W. Amrein, H.-U. Hediger, *J. Org. Chem.* **2001**, *66*, 4973

[21] L. J. Prins, D. N. Reinhoudt, P. Timmerman, *Angew. Chem. Int. Ed.* **2001**, *40*, 2382.

[22] D. C. Sherrington, K. A. Taskinen, *Chem. Soc. Rev.* **2001**, *30*, 83.

[23] K. Endo, T. Sawaki, M. Koyanagi, K. Kobayashi, H. Masuda, Y. Aoyama, *J. Am. Chem. Soc.* **1995**, *117*, 8341

[24] Y. Aoyama, K. Endo, T. Anzai, Y. Yamaguchi, T. Sawaki, K. Kobayashi, N. Kanehisa, H. Hashimoto, Y. Kai, H. Masuda, *J. Am. Chem. Soc.* **1996**, *118*, 5562

[25] T. Dewa, K. Endo, Y. Aoyama, *J. Am. Chem. Soc.* **1998**, *120*, 8933.

[26] M. Fujita, Y. J. Kwon, O. Sasaki, K. Yamaguchi, K. Ogura, *J. Am. Chem. Soc.* **1995**, *117*, 7287.

[27] J. Rebek Jr., *Acc. Chem. Res.* **1999**, *32*, 278

[28] J. N. Reek, J. A. Elemans, R. de Gelder, P. T. Beurskens, A. E. Rowan, R. J. Nolte, *Tett.* **2003**, *59*, 175.

[29] S. V. Kolotuchin, S. C. Zimmerman, *J. Am. Chem. Soc.* **1998**, *120*, 9092.

[30] J. L. Sessler, R. Wang, *Angew. Chem. Int. Ed.* **1998**, *37*, 1726.

[31] F. H. Beijer, H. Kooijman, A. L. Spek, R. P. Sijbesma, E. W. Meijer, *Angew. Chem. Int. Ed.* **1998**, *37*, 75.

[32] R. P. Sijbesma, E. W. Meijer, *Chem. Commun.* **2003**, 5.

[33] R. P. Sijbesma, F. H. Beijer, L. Brunsveld, B. J. B. Folmer, J. H. Hirschberg, R. F. Lange, J. K. Lowe, E. W. Meijer, *Science* **1997**, *278*, 1601.

[34] A. El-Ghayoury, E. Peeters, A. P. Schenning, *Chem. Commun.* **2000**, *19*, 1969.

[35] B. J. B. Folmer, E. Cavini, S. P. Sijbesma, E. W. Meijer, *Chem. Commun.* **1998**, *17*, 1847.

[36] P. S. Corbin, S. Perry, S. C. Zimmerman, *J. Am. Chem. Soc.* **1998**, *120*, 9710.

[37] C. Fouquey, J.-M. Lehn, A.-M. Levelut, *Adv. Mater.* **1990**, *2*, 254.

[38] M. Kotera, J.-M. Lehn, J. P. Vigneron, *Chem. Commun.* **1994**, *2*, 197.

[39] M. Kotera, J.-M. Lehn, J. P. Vigneron, *Tett.* **1995**, *51*, 1953.

[40] J. Y. Lee, P. C. Painter, M. M. Coleman, *Macromolecules* **1988**, *21*, 954.

[41] U. Kumar, T. Kato, J. M. Fréchet, *J. Am. Chem. Soc.* **1992**, *114*, 6630.

[42] T. Kato, *Supramol. Sci.* **1996**, *3*, 53.

[43] K.-I. Aoki, M. Nakagawa, K. Ichimura, *Chem. Lett.* **1999**, *28*, 1205.

[44] G. Ambrozic, M. Zigon, *Macromol. Rapid Commun.* **2000**, *21*, 53.

[45] M. Lee, B.-K. Cho, Y.-S. Kang, W.-C. Zin, *Macromolecules* **1999**, *32*, 8531.

[46] A. Singh, Y. Lvov, S. B. Qadri, *Chem. Mater.* **1999**, *11*, 3196.

[47] C. B. St. Pourcain, A. C. Griffin, *Macromolecules* **1995**, *28*, 4116.

[48] K. N. Wiegel, A. C. Griffin, *Polym. prep.* **1999**, *40*, 1136.

[49] C. P. Lillya, R. J. Baker, S. Hütte, H. H. Winter, Y.-G. Lin, J. Shi, L. C. Dickinson, J. C. W. Chien, *Macromolecules* **1992**, *25*, 2076.

[50] G. F. Swiegers, T. J. Malefetse, *Chem. Rev.* **2000**, *100*, 3483.

[51] O. Mamula, A. Von Zelewsky, *Coord. Chem. Rev.* **2003**, *242*, 87.

[52] J. P. Sauvage, J. P. Collin, J. C. Chambron, S. Guillerez, C. Coudret, V. Balzani, F. Barigelletti, L. D. Cola, L. Flamigni, *Chem. Rev.* **1994**, *94*, 993.

[53] H. Chen, J. A. Cronin, R. D. Archer, *Macromolecules* **1994**, *27*, 2174.

[54] H. Chen, J. A. Cronin, R. D. Archer, *Inorg. Chem.* **1995**, *34*, 2306.

[55] R. Knapp, A. Schott, M. Rehahn, *Macromolecules* **1996**, *29*, 478.

[56] C. Gorman, *Adv. Mater.* **1998**, *10*, 295.

[57] J. F. Modder, K. Vrieze, A. L. Spek, G. Challa, G. Van Koten, *Inorg. Chem.* **1992**, *31*, 1238.

[58] U. Michelsen, C. A. Hunter, *Angew. Chem. Int. Ed.* **2000**, *39*, 764.

[59] R. J. Bushby, C. Hardy, *J. Chem. Soc. Perkin Trans. 1* **1985**, *4*, 721.

[60] R. J. Bushby, O. R. Lozman, *Current Opinion in Colloid & Interface Science* **2002**, *7*, 343.

[61] T. Nakano, T. Yade, *J. Am. Chem. Soc.* **2003**, *125*, 15474.

[62] W. Wang, J. J. Han, L.-Q. Wang, L.-S. Li, W. J. Shaw, A. D. Q. Li, *Nano Lett.* **2003**, *3*, 455.

[63] T. Yatabe, M. A. Harbison, J. D. Brand, M. Wagner, K. Müllen, P. Samori, J. P. Rabe, *J. Mater. Chem.* **2000**, *10*, 1519.

[64] M. D. Watson, A. Fechtenchötter, K. Müllen, *Chem. Rev.* **2001**, *101*, 1267.

[65] N. Boden, R. J. Bushby, C. Hardy, F. Sixl, *Chem. Phys. Lett.* **1986**, *123*, 359.

[66] J. P. Gallivan, G. B. Schuster, *J. Org. Chem.* **1995**, *60*, 2423

[67] E. O. Arikainen, N. Boden, R. J. Bushby, O. R. Lozman, J. G. Vinter, A. Wood, *Angew. Chem. Int. Ed.* **2000**, *39*, 2333.

[68] N. Boden, R. J. Bushby, G. Cooke, O. R. Lozman, Z. Lu, *J. Am. Chem. Soc.* **2001**, *123*, 7915.

[69] N. Boden, R. J. Bushby, J. Clements, B. Movaghar, K. J. Donovan, T. Kreouzis, *Phy. Rev. B* **1995**, *52*, 13274.

[70] A. Van de Craats, M. P. de Haas, J. W. Warman, *Synthetic Metals* **1997**, *86*, 2125.

[71] A. Van de Craats, L. D. A. Siebbles, I. Bleyl, D. Haarer, Y. A. Berlin, A. A. Zhakhirov, J. W. Warman, *J. Phys. Chem. B.* **1998**, *102*, 9625.

[72] W. J. Schutte, M. Sluyters-Rehbach, J. H. Sluyters, *J. Phys. Chem.* **1993**, *97*, 6069.

[73] D. S. Terekhov, K. J. M. Nolan, C. R. McArthur, C. C. Leznoff, *J. Org. Chem.* **1996**, *61*, 3034

[74] W.-F. Law, K. M. Lui, D. K. P. Ng, *J. Mat. Chem.* **1997**, *7*, 2063

[75] E. J. Osburn, A. Schmidt, L. K. Chau, S. Y. Chen, P. Smolenyak, N. R. Armstrong, D. F. O'Brian, *Adv. Mater.* **1996**, *8*, 926.

[76] M. Kimura, T. Muto, H. Takimoto, K. Wada, K. Ohta, K. Hanabusa, H. Shirai, N. Kobayashi, *Langmuir* **2000**, *16*, 2078

[77] O. E. Sielcken, M. M. Van Tilborg, M. F. M. Roks, R. Hendriks, W. Drenth, R. J. M. Nolte, *J. Am. Chem. Soc.* **1987**, *109*, 4261

[78] N. Kobayashi, A. B. P. Lever, *J. Am. Chem. Soc.* **1987**, *109*, 7433

[79] H. Engelkamp, S. Middelbeek, R. J. M. Nolte, *Science* **1995**, *284*, 785.

[80] K. Kano, H. Minamizono, T. Kitae, S. Negi, *J. Phys. Chem. A.* **1997**, *101*, 6118

[81] L. Ruhlmann, A. Nakamura, J. G. Vos, J.-H. Fuhrhop, *Inorg. Chem.* **1998**, *37*, 6052

[82] J. H. Fuhrhop, C. Demoulin, C. Boettcher, J. Koening, U. Siggel, *J. Am. Chem. Soc.* **1992**, *114*, 4159

[83] J. Zhang, J. S. Moore, *J. Am. Chem. Soc.* **1994**, *116*, 2655

[84] S. Höger, V. Enkelmann, K. Bonrad, C. Tschierske, *Angew. Chem. Int. Ed.* **2000**, *39*, 2267.

[85] Y. Tobe, N. Utsumi, A. Nagano, K. Naemura, *Angew. Chem. Int. Ed.* **1998**, *37*, 1285.

[86] Y. Tobe, A. Nagano, K. Kawabata, M. Sonoda, K. Naemura, *Org. Lett.* **2000**, *2*, 3265

[87] V. Iyer, M. Wehmeier, J. D. Brand, M. A. Keegstra, K. Müllen, *Angew. Chem. Int. Ed. Engl.* **1997**, *36*, 1604.

[88] M. Müller, V. S. Iyer, C. Kübel, V. Enkelmann, K. Müllen, *Angew. Chem. Int. Ed.* **1997**, *36*, 1607.

[89] M. Müller, C. Kübel, K. Müllen, *Chem. Eur. J.* **1998**, *4*, 2099.

[90] A. J. Berresheim, M. Müller, K. Müllen, *Chem. Rev.* **1999**, *99*, 1747 and refernences therein.

[91] F. Dötz, J. D. Brand, S. Ito, L. Gherghel, K. Müllen, *J. Am. Chem. Soc.* **2000**, *122*, 7707.

[92] P. Samori, N. Severin, C. D. Simpson, K. Müllen, J. P. Rabe, *J. Am. Chem. Soc.* **2002**, *124*, 9454.

[93] P. Herwig, C. W. Kayser, K. Müllen, H. W. Spiess, *Adv. Mater.* **1996**, *8*, 510.

[94] S. Ito, M. Wehmeier, J. D. Brand, C. Kübel, R. Epsch, J. P. Rabe, K. Müllen, *Chem. Eur. J.* **2000**, *6*, 4327.

[95] M. Lee, J.-W. Kim, S. Peleshanko, K. Larson, Y.-S. Yoo, D. Vaknin, S. Markutsya, V. V. Tsukruk, *J. Am. Chem. Soc.* **2002**, *124*, 9121.

[96] A. Fechtenchötter, N. Tchebotareva, K. Watson, K. Müllen, *Tett.* **2001**, *57*, 3769.

[97] A. F. Thünemann, S. K. Kubowizc, C. Burger, M. D. Watson, N. Tchebotareva, K. Müllen, *J. Am. Chem. Soc.* **2003**, *125*, 352.

[98] A. J. Fleming, J. N. Coleman, A. B. Dalton, A. Fechtenkötter, M. D. Watson, K. Müllen, H. J. Byrne, W. J. Blau, *J. Phys. Chem. B.* **2003**, *107*, 37.

[99] A. Stabel, P. Herwig, K. Müllen, J. Rabe, *Angew. Chem. Int. Ed. Engl.* **1995**, *34*, 1609.

[100] C. Kübel, K. Eckhardt, V. Enkelmann, G. Wegner, K. Müllen, *J. Mater. Chem.* **2000**, *10*, 879.

[101] P. Ruffieux, O. Gröening, M. Bielman, C. Simpson, K. Müllen, L.Schlapbach, P. Gröening, *Phy. Rev. B* **2002**, *66*, 073409/1.

[102] J. Wu, M. D. Watson, K. Müllen, *Angew. Chem. Int. Ed.* **2003**, *42*, 5329.

[103] J. Wu, M. D. Watson, L. Zhang, Z. Wang, K. Müllen, *J. Am. Chem. Soc.* **2004**, *126*, 177.

[104] A. Van de Craats, J. M. Warman, *Adv. Mater.* **2001**, *13*, 130.

[105] L. Schmidt-Mende, A. Fechtenchötter, K.Müllen, E. Moons, R. H. Friend, J. D. MacKenzie, *Science* **2001**, *293*, 1119.

[106] A. Van de Craats, N. Stutzman, O. Bunk, M. M. Nielsen, M. Watson, K. Müllen, H. D. Chanzy, H. Sirringhaus, R. H. Friend, *Adv. Mater.* **2003**, *15*, 495.

[107] C.-Y. Liu, A. Fechtenkötter, M. D. Watson, K. Müllen, A. J. Bard, *Chem. Mater.* **2003**, *15*, 124.

[108] C. Nuckolls, T. J. Katz, L. Castellanos, *J. Am. Chem. Soc.* **1996**, *118*, 3767–3768.

[109] C. Nuckolls, T. J. Katz, G. Katz, P. J. Collings, L. Castellanos, *J. Am. Chem. Soc.* **1999**, *121*, 79.

[110] A. J. Lovinger, C. Nuckolls, T. J. Katz., *J. Am. Chem. Soc.* **1998**, *120*, 264–268.

[111] T. Verbiest, S. Van Elshocht, M. Karuanen, L. Hellemans, Snauwaert, C. Nuckolls, T. J. Katz, A. Persoons., *Science* **1998**, *282*, 913.

[112] C. Nuckolls, T. J. Katz., *J. Am. Chem. Soc.* **1998**, *120*, 9541–9544.

[113] L. A. Cuccia, J.-M. Lehn, J.-C. Homo, M. Schmutz, *Angew. Chem. Int. Ed.* **2000**, *39*, 233.

[114] T. J. Katz, *Angew. Chem. Int. Ed.* **2000**, *39*, 1921.

[115] J. C. Nelson, J. G. Saven, J. S. Moore, P. G. Wolynes, *Science* **1997**, *277*, 1793.

[116] R. B. Prince, J. G. Saven, P. G. Wolynes, J. S. Moore, *J. Am. Chem. Soc.* **1999**, *121*, 3114

[117] L. Brunsveld, R. B. Prince, E. W. Meijer, J. S. Moore, *Org. Lett.* **2000**, *2*, 1525

[118] L. Brunsveld, E. W. Meijer, R. B. Prince, J. S. Moore, *J. Am. Chem. Soc.* **2001**, *123*, 7978

[119] M. J. Mio, R. B. Prince, J. S. Moore, C. Kuebel, D. C. Martin, *J. Am. Chem. Soc.* **2000**, *122*, 6134

[120] V. Berl, M. J. Krische, I. Huc, J.-M. Lehn, M. Schmutz, *Chem. Eur. J.* **2000**, *6*, 1938.

[121] M. Lightfoot, F. S. Mair, R. G. Pritchard, J. E. Warren, *Chem. Commun.* **1999**, *19*, 1945.

[122] L. Brunsveld, A. P. Schenning, M. A. Broeren, H. M. Janssen, J. A. Vekemans, E. W. Meijer, *Chem. Lett.* **2000**, *3*, 292.

[123] A. R. Palmans, J. A. Vekemans, H. Fischer, R. A. Hikmet, E. W. Meijer, *Chem. Eur. J.* **1997**, *3*, 300.

[124] A. R. Palmans, J. A. Vekemans, E. E. Havinga, E. W. Meijer, *Angew. Chem. Int. Ed.* **1997**, *36*, 2648.

[125] L. Brunsveld, H. Zhang, M. Glasbeek, J. A. Vekemans, E. W. Meijer, *J. Am. Chem. Soc.* **2000**, *122*, 6175.

[126] L. Brunsveld, B. G. Lohmeijer, J. A. Vekemans, E. W. Meijer, *Chem. Commun.* **2000**, *23*, 2305.

[127] P. A. van der Schoot, M. A. J. M. Brunsveld, R. P. Sijbesma, A. Ramzi, *Langmuir* **2000**, *16*, 10076.

[128] J. H. K. K. B. Hirschberg, Luc; Ramzi, Aissa; Vekemans, Jef A. J. M.; Sijbesma, Rint P.; Meijer, E. W., *Nature* **2000**, *407*, 167.

[129] P. Jonkheijm, F. J. M. Hoeben, R. Kleppinger, J. van Herrikhuyzen, A.Schenning, E. W. Meijer, *J. Am. Chem. Soc.* **2003**, *125*, 15941

[130] P. Jonkheijm, A. Miura, M. Zdanowska, F. J. M. Hoeben, S. De Feyter, A. P. Schenning, F. C. De Schryver, E. W. Meijer, *Angew. Chem. Int. Ed.* **2004**, *43*, 74.

[131] K. S. Min, M. P. Suh, *Eur. J. Inorg. Chem.* **2001**, 449.

[132] A. Tsuda, S. Sakamoto, K. Yamaguchi, T. Aida, *J. Am. Chem. Soc.* **2003**, *125*, 15722

[133] G. N. Fursey, *Appl. sur. Sc.* **2003**, *215*, 113.

[134] C. A. Spindt, *J. Appl. Phys.* **1968**, *39*, 7.

[135] P. Groening, P. Ruffieux, L. Schlapbach, O. Groening, *Adv. Eng. Mat.* **2003**, *5*, 541.

[136] Hewlett-Packard, *Sci. Am.* **2000**, *may*, 50.

[137] J. W. Gadzuk, *Rev. Mod. Phys.* **1973**, *45*, 487.

[138] O. Gröning, R. Clergereaux, L. Nilsson, P. Ruffieux, P. Gröning, L. Schlapbach, *Chimia* **2002**, *56*, 553.

[139] P. R. Schwoebl, I. Brodie, *J. Vac. Sci. Tech. B* **1995**, *13*, 1391.

[140] R. H. Fowler, L. W. Nordheim, *Proc. Roy. Soc. London, Ser. A* **1928**, *119*, 173.

[141] L. W. Nordheim, *Proc. Roy. Soc. London, Ser. A* **1928**, *121*, 626.

[142] O. Gröning, O. M. Küttel, C. Emmenegger, P. Gröning, L.Schlapbach, *J. Vac. Sci. Tech. B* **2000**, *18*, 665.

[143] J.-M. Bonard, N. Weiss, H. Kind, T. Stöckli, L. Forró, K. Kern, A. Châtelain, *Adv. Mater.* **2001**, *13*, 184.

[144] N. S. Lee, D. S. Chung, I. T. Han, J. H. Kang, Y. S. Choi, H. Y. Kim, S. H. Park, Y. W. Jin, W. K. Yi, M. J. Yi, M. J. Yun, J. E. Jung, C. J. Lee, J. H. You, S. H. Jo, C. G. Lee, J. M. Kim, *Diam. & Rel. Mat.* **2001**, *10*, 265.

[145] K. Shoulders, *J. Appl. Phys.* **1968**, *39*, 3504.

[146] C. Spindt, *J. Appl. Phys.* **1968**, *39*, 3504.

[147] C. A. Spindt, I. Brodie, L. Humphrey, E. R. Wetsburg, *J. Appl. Phys.* **1976**, *47*, 5248.

[148] A. Ghis, R. Meyer, P. Rambaud, F. Levy, T. Leroux, *IEEE Trans Electron Dev* **1993**, *38*, 2320.

[149] A. A. Talin, K. A. Dean, J. E. Jaskie, *Solid-state electronics* **2001**, *45*, 963.

[150] J. H. Cho, A. R. Zouklarneev, J. W. Kim, J. P. Hong, J. M. Kim, in *Tech digest of the 10th Int Vac Microelectron Conf*, Kyongju, Korea, **1997**, p. 401.

[151] T. S. Fahlen, in *Technical digest of the 12th Int. Vac. Microelectron Conf.*, Darmstadt, Germany, **1999**, p. 56.

[152] S. Ito, in *Flat panel displays year book* (Eds.: Nikkei, Microdevices), InterLingua, Redondo beach, California, United States, **1999**, p. 171.

[153] A. v. Oostrom, *J. Appl. Phys.* **1962**, *33*, 2917.

[154] A. Mosely, *Displays* **1993**, *14*, 67.

[155] M. O'Neill, S. M. Kelly, *Adv. Mater.* **2003**, *15*, 1135.

[156] S. M. Kelly, M. O'Neill, *Handbook of advanced electronic and photonic materials, Vol. 1*, Academic press, San Diege, CA, **2000**.

[157] C. W. Tang, S. A. Van Slyke, *Appl. Phys. Lett.* **1987**, *51*, 913.

[158] J. H. Burroughes, D. D. C. Bradley, A. R. Brown, N. Marks, K. Mackay, R. H. Friend, P. L. Burn, A. B. Holmes, *Nature* **1990**, *347*, 539.

[159] A. Kraft, A. C. Grimsdale, A. B. Holmes, *Angew. Chem. Int. Ed.* **1998**, *37*, 403.

[160] Y. Yoshida, A. Ishizuka, H. Makishima, *Mat. Chem. Phys.* **1995**, *40*, 267.

[161] I. Brodie, C. Spindt, *Adv. Electronics Electron Phys.* **1992**, *83*, 6.

[162] B. C. Djubua, N. N. Chubun, *IEEE Trans Electron Dev* **1991**, *38*, 2314.

[163] M. W. Geis, N. N. Efremow, J. D. Woodhouse, M. D. McAleese, M. Marchywka, D. G. Socker, J. F. Hochedez, *IEEE Lett.* **1991**, *12*, 456.

[164] C. Wang, A. Garcia, D. C. Ingram, M. Lake, M. E. Krodesch, *Electron. Lett.* **1991**, *27*, 1459.

[165] N. S. Xu, Y. Tzeng, R. V. Lantham, *J. Phys. D: Appl. Phys.* **1993**, *26*, 1776.

[166] D. Hong, M. Aslam, *J. Vac. Sci. Tech. B* **1995**, *13*, 427.

[167] K. Okano, S. Koizumi, S. Ravi, P. Silva, G. A. J. Amaratunga, *Nature* **1996**, *381*, 140.

[168] O. Groening, O. Kuettel, P. Groening, L. Schlapbach, *App. Sur. Sc.* **1997**, *111*, 135.

[169] J. v. d. Weide., Z. Zhang, P. K. Baumann, M. G. Wemnsell, J. Bernholc, R. J. Nemanich, *Phys. Rev. B* **1994**, *50*, 5803.

[170] I. L. Krainsky, V. M. Asnin, G. T. Mearini, J. A. Dayton, *Phy. Rev. B* **1996**, *53*, 7650.

[171] I. L. Krainsky, V. M. Asnin, *Appl. Phys. Lett.* **1998**, *72*, 2574.

[172] G. A. J. Amaratunga, S. R. P. Silva, *Appl. Phys. Lett.* **1996**, *68*, 2529.

[173] M. W. Geis, J. C. Twichell, T. M. Lyszczarz, *J. Vac. Sci. Tech. B* **1996**, *14*, 2060.

[174] Z. H. Huang, P. H. Cuttler, N. M. Miskovsky, T. E. Sullivan, *Appl. Phys. Lett.* **1994**, *65*, 2562.

[175] O. Groning, L. Nilsson, P. Groning, L. Schlapbach, *Solid-state electronics* **2001**, *45*, 929.

[176] O. M. Küttel, O. Groening, L. Schlapbach, *J. Vac. Sci. Tech. A* **1998**, *16*, 3464.

[177] O. Groning, O. M. Kuttel, P. Groning, L. Schlapbach, *Appl. Phys. Lett.* **1997**, *71*, 2253.

[178] V. V. Zhirnov, O. M. Küttel, O. Gröning, A. N. Alimova, P. Y. Detkov, P. I. Belobrov, E. Maillard-Schaller, L. Schlapbach, *J. Vac. Sci. Tech. B* **1999**, *17*, 666.

[179] J. L. Davidson, W. P. Kang, A. Wisitsora-At, *Diam. & Rel. Mat.* **2003**, *12*, 429.

[180] T. Utsumi, *IEEE Trans Electron Dev* **1991**, *38*, 2276.

[181] W. A. de Heer, A. Châtelain, D. Ugarte, *Science* **1995**, *270*, 1179.

[182] A. G. Rinzler, J. H. Hafner, P. Nikolaev, L. Lou, S. G. Kim, D. Tomanek, P. Nordlander, D. T. Colbert, R. E. Smalley, *Science* **1995**, *269*, 1550.

[183] Y. Saito, S. Uemura, *Carbon* **2000**, *38*, 169.

[184] J. L. Kwo, C. C. Tsou, M. Yokoyama, I. N. Lin, C. C. Lee, W. C. Wang, F. Y. Chuang, *J. Vac. Sci. Tech. B* **2001**, *19*, 23.

[185] R. H. Baughman, A. A. Zakhidov, W. A. d. Heer, *Science* **2002**, *297*, 787.

[186] Y. Huh, J. Y. Lee, J. H. Lee, T. J. Lee, S. C. Lyu, C. J. Lee, *Chem. Phys. Lett.* **2003**, *375*, 388.

[187] L. Nilsson, O. Groening, O. Kuettel, P. Groening, L. Schlapbach, *J. Vac. Sci. Tech. B* **2002**, *20*, 326.

[188] L. Nilsson, O. Groening, O. Kuettel, P. Groening, L. Schlapbach, *Thin Solid Films* **2001**, *383*, 78.

[189] L. Nilsson, O. Groening, P. Groening, L. Schlapbach, *Appl. Phys. Lett.* **2001**, *79*, 1036.

[190] W. I. Milne, K. B. K. Teo, M. Chhowalla, G. A. J. Amaratunga, S. B. Lee, D. G. Hasko, H. Ahmed, O. Groening, P. Legagneux, L. Gangloff, J. P. Schnell, G. Pirio, D. Pribat, M. Castignolles, A. Loiseau, V. Semet, V. T. Binh, *Diam. & Rel. Mat.* **2003**, *12*, 422.

[191] K. B. K. Teo, S.-B. Lee, M. Chhowalla, V. Semet, V. T. Binh, O. Groening, M.Castignolles, A.Loiseau, G. Pirio, P. Legagneux, D. Pribat, D. G. Hasko, H. Ahmed, G. A. J. Amaratunga, W. I. Milne, *Nanotechnology* **2003**, *14*, 204.

[192] O. Bunk, M. M. Nielsen, T. I. Solling, A. Van de Craats, N. Stutzmann, *J. Am. Chem. Soc.* **2003**, *125*, 2252.

[193] E. Clar, C. T. Ironside, M. Zander, *J. Chem. Soc.* **1959**, *1*, 142.

[194] J. D. Dunitz, R. Taylor., *Chem. Eur. J.* **1997**, *3*, 89.

[195] S. P. Brown, I. Schnell, J. D. Brand, K. Müllen, H. W. Spiess, *J. Am. Chem. Soc.* **1999**, *121*, 6712.

[196] A. Fechtenkötter, K. Saalwächter, M. A. Harbison, K. Müllen, H. W. Spiess, *Angew. Chem. Int. Ed.* **1999**, *38*, 3039.

[197] R. Rathore, C. L. Burns, *J. Org. Chem.* **2003**, *68*, 4071.

[198] V. Iyer, K. Yoshimura, V. Enkelmann, R. Epsch, J. Rabe, K. Müllen, *Angew. Chem. Int. Ed. Engl.* **1998**, *37*, 2696.

[199] A. G. Brown, P. D. Edwards, *Tett. Lett.* **1990**, *31*, 6581.

[200] T. Biftu, B. G. Hazra, R. Stevenson, *J. Chem. Soc. Perkin Trans. 1* **1979**, *9*, 2276.

[201] M. A. Schwartz, P. T. K. Pham, *J. Org. Chem.* **1988**, *53*, 2318.

[202] P. Magnus, J. Schultz, T. Gallagher, *J. Am. Chem. Soc.* **1985**, *107*, 4984.

[203] L. Liu, B. Yang, T. J. Katz, M. K. Poindexter, *J. Org. Chem.* **1991**, *56*, 3769.

[204] P. G. Copeland, R. E. Dean, D. McNeil, *J. Chem. Soc.* **1960**, 1689.

[205] A. Halleux, R. H. Martin, *Helv. Chim. Acta* **1958**, *41*, 1177.

[206] C. F. H. Allen, F. P. Pingert, *J. Am. Chem. Soc.* **1942**, *64*, 1365.

[207] P. Kovacic, J. Oziomek, *J. Org. Chem.* **1964**, *29*, 100.

[208] P. Kovacic, A. Kyriakis, *J. Am. Chem. Soc.* **1963**, *85*, 454.

[209] L. A. Paquette, in *Encyclopedia of reagents for organic synthesis, Vol. 4*, John Wiley & Sons, **1995**, pp. 2875.

[210] P. Kovacic, F. W. Koch, *J. Org. Chem.* **1963**, *28*, 1864.

[211] P. Kovacic, C. Wu, *J. Polym. Sci.* **1960**, *47*, 45.

[212] P. Kovacic, C. Wu, *Am. Chem. Soc., Div. Polymer Chem., Preprints* **1960**, *1*, 60.

[213] C. D. Simpson, J. D. Brand, A. J. Berresheim, L. Pryzbilla, H. J. Räder, K. Müllen, *Chem. Eur. J.* **2002**, *8*, 1424.

[214] P. Kovacic, M. B. Jones, *Chem. Rev.* **1987**, *87*, 357.

[215] G. A. Clowes, *J. Chem. Soc. C* **1968**, *20*, 2519.

[216] A. J. Bard, A. Ledwith, H. Shine, *Adv. Phys. Org. Chem.* **1976**, *13*, 155.

[217] G. Baddeley, *J. Chem. Soc.* **1950**, 994.

[218] A. L. Rusanov, M. L. Keshtov, M. M. Begretov, I. A. Khotina, A. K. Mikitaev, *Russ. Chem. Bull.* **1996**, *45*, 1169.

[219] S. Takahashi, Y. Kuroyama, K. Sonogashira, N. Hagihara, *Synthesis* **1980**, 627.

[220] C.-J. Li, D.-L. Chen, C. W. Costello, *Organic Process Research & Development* **1997**, *1*, 325.

[221] R. M. Harisson, T. Brotin, B. C. Noll, J. Michel, *Organomet.* **1997**, *16*, 3401.

[222] M. J. Mio, L. C. Kopel, J. B. Braun, T. L. Gadikwa, K. L. Hull, R. G. Brisbois, C. J. Markworth, P. A. Grieco, *Org. Lett.* **2002**, *4*, 3199.

[223] J. A. Hyatt, *Oppi Briefs* **1991**, *23*, 460.

[224] H. Pepermans, R. Willem, C. Hoogzand, *Bull. Soc. Chim. Belg.* **1987**, *96*, 563.

[225] P. Quénéch, R. Rumin, F. Pétillon, *J. Organomet. chem.* **1994**, *479*, 93.

[226] K. Peter, C. Volhardt, R. G. Bergman, *J. Am. Chem. Soc.* **1974**, *96*, 4996.

[227] R. F. Funk, K. Peter, C. Volhardt, *J. Am. Chem. Soc.* **1980**, *102*, 5253.

[228] D. B. Denney, D. Z. Denney, C.-F. Ling, *J. Am. Chem. Soc.* **1976**, *98*, 6755.

[229] S. Saito, T. Kawasaki, N. Tsuboya, Y. Yamamoto, *J. Org. Chem.* **2001**, *66*, 796.

[230] J. Yang, J. G. Verkade, *Organom.* **2000**, *19*, 893.

[231] M. S. Yusybov, V. D. Filimonov, *synthesis* **1991**, 131.

[232] H. des Abbayes, J. Clement, J. Laurent, G. Tanguy, N. Thilmont, *Organometallics* **1988**, *7*, 2293.

[233] P. T. Herwig, V. Enkelmann, O. Schmelz, K. Müllen, *Chem. Eur. J.* **2000**, *6*, 1834.

[234] R. Rathore, C. L. Burns, M. I. Deselnicu, *Org. Lett.* **2001**, *3*, 2887.

[235] M. Pomrantz, A. Aviram, R. A. McCorkle, L. Li, A. G. Schrott, *Science* **1992**, *255*, 1115.

[236] T. David, J. K. Gimsewski, D. Purdie, R. R. Schlitter, *Phy. Rev. B* **1994**, *50*, 5810.

[237] R. E. Palmer, Q. Guo, *Phys. Chem. Chem. Phys.* **2002**, *4*, 4275.

[238] A. C. Hillier, G. A. Grasa, M. S. Viciu, H. M. Lee, C. Yang, S. P. Nolan, *J. Organomett. Chem.* **2002**, *653*, 69.

[239] R. A. Batey, M. Shen, A. J. Lough, *Org. Lett.* **2002**, *4*, 1411.

[240] P. Siemsen, R. C. L. Diederich, *Angew. Chem. Int. Ed.* **2000**, *39*, 2632.

[241] G. T. C. D. Turner, K. A. Stephens, *J. Organometall. Chem.* **1998**, *570*, 219.

[242] A. L. Casalnuovo, J. C. Calabrese, *J. Am. Chem. Soc.* **1990**, *112*, 4324

[243] M. M. Haley, M. L. Bell, S. C. Brand, D. B. Kimball, J. J. Pak, W. B. Wan, *Tett. Lett.* **1997**, *38*, 7483.

[244] J.-P. Genêt, E. Blart, M. Savignac, *Synlett* **1992**, *9*, 715.

[245] C. Amatore, E. Blart, J.-P.-. Genêt, A. Jutand, S. Lemaire-Audoire, M. Savignac, *J. Org. Chem.* **1995**, *60*, 6829.

[246] J.-P. Genêt, M. Savignac, *J. Organometall. Chem.* **1999**, *576*, 305.

[247] H.-F. Chow, C.-W. Wan, K.-H. Low, Y.-Y. Yeung, *J. Org. Chem.* **2001**, *66*, 1910.

[248] M. Alami, F. Ferri, G. Linstrumelle, *Tett. Lett.* **1993**, *34*, 6403.

[249] K. Sonogashira, *J. Organometall. Chem.* **2002**, *653*, 46.

[250] L. A. Paquette, in *Encyclopedia of reagents for organic synthesis, Vol. 6*, John Wiley & Sons, **1995**, pp. 3785.

[251] F. L. Bowden, A. P. B. Lever, *Organometal. Chem. Rev. Sect. A* **1968**, *3*, 227.

[252] R. S. Dickson, P. J. Fraser, *Adv. Organomet. Chem.* **1974**, *12*, 323.

[253] W. Hübel, U. Kruerke, *Chem. Ber.* **1961**, *94*, 2829.

[254] W. Hübel, in *Organic synthesis via metal carbonyls, Vol. 1* (Eds.: I. Wender, P. Pino), Interscience, New York, **1968**, p. 273.

[255] R. S. Dickson, D. B. W. Yawney, *Aust. J. Chem* **1969**, *22*, 533.

[256] M. A. Bennett, P. B. Donaldson, *Inorg. Chem.* **1978**, *17*, 1995.

[257] R. S. Dickson, P. J. Fraser, B. M. Gatehouse, *J. Chem. Soc., Dalton Trans.* **1972**, *20*, 2278.

[258] R. J. Kaufman, R. S. Sindhu, *J. Org. Chem.* **1982**, *47*, 4941.

[259] C. R. LeBlond, A. T. Andrews, Y. Sun, J. R. S. Jr., *Org. Lett.* **2001**, *3*, 1555.

[260] G. Marck, A. Villiger, R. Buchecker, *Tett. Lett.* **1994**, *35*, 3277.

[261] T. M. Miller, T. X. Neenan, R. Zayas, H. E. Bair, *J. Am. Chem. Soc.* **1992**, *114*, 1018.

[262] V. G. Chapoulaud, J. Audoux, N. Plé, A. Turck, G. Quéguiner, *Tett. Lett.* **1999**, *40*, 9005.

[263] P. Wipf, J.-K. Jung, *J. Org. Chem.* **2000**, *65*, 6319.

[264] L.-Z. Gong, Q.-S. Hu, L.-. Pu, *J. Org. Chem.* **2001**, *66*, 2358.

[265] J. K. Stille, *Angew. Chem. Int. Ed.* **1986**, *25*, 508.

[266] G. Y. Li, *J. Org. Chem.* **2002**, *67*, 3643.

[267] X. Bei, H. W. Turner, W. H. Weinberg, A. S. Guram, J. L. Petersen, *J. Org. Chem.* **1999**, *64*, 6797

[268] G. A. Molander, C.-S. Yun, *Tetrahedron* **2002**, *58*, 1465.

[269] M. R. Netherton, G. C. Fu, *Angew. Chem. Int. Ed.* **2002**, *41*, 3910.

[270] S. Sengupta, S. Bhattacharyya, *J. Org. Chem.* **1997**, *62*, 3405

[271] S. Darses, T. Jeffrey, J.-L. Brayer, J.-P. Demoute, J.-P. Genêt, *Bull. Chem. Soc. Chim. Fr.* **1996**, *133*, 1095.

[272] J. H. Kirchhof, M. R. Netherton, I. D. Hills, G. C. Fu, *J. Am. Chem. Soc.* **2002**, *124*, 13662.

[273] R. B. Bedford, C. S. Cazin, *Chem. Commun.* **2001**, 1540.

[274] C. A. Parrish, S. L. Buchwald, *J. Org. Chem.* **2001**, *66*, 3820.

[275] D. S. McGuinness, K. J. Cavell, *Organom.* **2000**, *19*, 741.

[276] J. P. Wolfe, S. L. Buchwald, *Angew. Chem. Int. Ed.* **1999**, *38*, 2413.

[277] W. A. Hermann, C.-P. Reising, M. Spiegler, *J. Organomet. chem.* **1998**, *557*, 93.

[278] D. Zim, V. R. Lando, J. Dupont, A. L. Monteiro, *Org. Lett.* **2001**, *3*, 3049.

[279] J.-C. Galland, M. Savignac, J.-P. Genêt, *Tett. Lett.* **1999**, *40*, 2323.

[280] T. I. W. M. Novak, *J. Org. Chem.* **1994**, *59*, 5034

[281] D. Badone, M. Baroni, R. Cardamone, A. Ielmini, U. Guzzi, **1997**, *62*, 7170

[282] G. W. Kabalka, V. Namboodiri, *Chem. Comm.* **2001**, 775.

[283] M. R. Netherton, G. C. Fu, *Org. Lett.* **2001**, *3*, 4295.

[284] N. E. Leadbeater, M. Marco, *Org. Lett.* **2002**, *4*, 2973.

[285] G. B. Smith, G. C. Dezeny, D. L. Hughes, A. O. King, T. R. Verhoeven, *J. Org. Chem.* **1994**, *59*, 8151

[286] J.-M. Campagne, D. Prim, *Les complexes de palladium en synthèse organique*, CNRS ed., CNRS Editions, Paris, **2001**.

[287] N. Miyaura, T. Yanagai, A. Suzuki, *Synth. Commun.* **1981**, *11*, 513.

[288] K. Weiss, G. Beernink, F. Dötz, A. Birkner, K. Müllen, C. Wöll, *Angew. Chem. Int. Ed.* **1999**, *38*, 3748.

[289] A. Bader, D. Arlt, in *United states patent, 5,185,454*, Bayer aktiengeselschaft, Germany, **1993**.

[290] P. Folly, Postdoc, University of Fribourg, chemistry departement, **2000**.

[291] R. Mariaca, Postdoc, University of Fribourg, chemistry departement, **2001**.

[292] Y. A. Fialkov, S. V. Shelyazhenko, L. M. Yagupol'skii, *Zh. Org. Kh.* **1983**, *19*, 1048.

[293] W. Chen, L. Xu, Y. Hu, A. M. B. Osuna, J. Xiao, *Tetrahedron* **2002**, *58*, 3889.

[294] T. Briza, J. Kvicala, P. Mysik, O. Paleta, J. Cermak, *Synlett* **2001**, *5*, 685.

[295] R. Shimizu, E. Yoneda, T. Fuchikami, *Tett. Lett.* **1996**, *37*, 557.

[296] T. Kitazume, N. Ishikawa, *Chem. Lett.* **1982**, 137.

[297] S. M. Dirk, D. W. P. Jr., S. Chanteau, D. V. Kosynkin, J. M. Tour, *Tetrahedron* **2001**, *57*, 5109.

[298] H. Brunner, N. le Cousturier de Courcy, J.-P. Genêt, *Synlett* **2000**, *2*.

[299] H. Brunner, N. le Cousturier de Courcy, J.-P. Genêt, *Tett. Lett.* **1999**, *40*, 4815.

[300] W. Yong, P. Yi, Z. Zhuangu, H. Hongwen, *synthesis* **1991**, 967.

[301] K. Kikukawa, K. Nagira, F. Wada, T. Matsuda, *Tett.* **1981**, *37*, 31.

[302] S. Darses, M. Pucheault, J.-P. Genêt, *Eu. J. Org. Chem.* **2001**, 1121.

[303] A. Roe, in *Organic Reactions, Vol. 5*, **1949**, pp. 193.

[304] R. J. W. Le Fevre, E. E. Turner, *J. Chem. Soc. Abstratcs* **1926**, 2041.

[305] M. Blanchard-Desce, B. Fosset, F. Guyot, L. Julien, S. Palacin, *Chimie organique expérimentale, Vol. Collection enseignement des sciences*, Paris, **1987**.

[306] M. Buback, T. Perkovic, S. R. d. Meijere, *Eu. J. Org. Chem.* **2003**, *13*, 2375.

[307] W. Cabri, I. Candiani, *Acc. Chem. Res.* **1995**, *28*, 2.

[308] I. P. Beletskaya, A. V. Cheprakov, *Chem. Rev.* **2000**, *100*, 3009.

[309] S. Hironao, I. Takashi, Y. Hiromi, T. Kozo, H.Kosaku, *Tett. Lett.* **2002**, *44*, 171.

[310] D. J. Adams, D. Gudmunsen, J. Fawcett, E. G. Hope, A. M. Stuart, *Tetrahedron* **2002**, *58*, 3827.

[311] C. Guillon, P. Vierling, *J. Organometall. Chem.* **1996**, *506*, 211.

[312] G. Johansson, V. Percec, G. Ungar, K. Smith, *Chem. Mater.* **1997**, *9*, 164.

[313] G. Johansson, V. Percec, G. Ungar, J. P. Zhou, *Macromolecules* **1996**, *29*, 646.

[314] Q.-Y. Chen, Z.-Y. Yang, Z.-M. Qiu, *J. Chem. Soc., Perkin Trans. I* **1988**, 563.

[315] K. Tamao, K. Sumitani, M. Kumada, *J. Am. Chem. Soc.* **1972**, *94*, 4374.

[316] N. Okukado, D. E. V. Horn, W. L. Klima, E.Negishi, *Tett. Lett.* **1978**, *19*, 1027.

[317] J. Terao, H. Watanabe, A. Ikumi, H. Kuniyasu, N. Kambe, *J. Am. Chem. Soc.* **2002**, *124*, 4222.

[318] F.-L. Qing, R. Wang, B. Li, X. Zheng, W.-D. Meng, *J. Fluorine. Chem.* **2003**, *120*, 21.

[319] Y. Uozumi, A. Tanahashi, S. Y. Lee, T. Hayashi, *J. Org. Chem.* **1993**, *58*, 1945.

[320] S. Sengupta, M. Leite, D. S. Raslan, C. Quesnelle, V. Snieckus, *J. Org. Chem.* **1992**, *57*, 4066.

[321] T. Hayashi, M. Konishi, Y. Kobori, M. Kumada, T. Higushi, K. Hirotsu, *J. Am. Chem. Soc.* **1984**, *106*, 158.

[322] E. Erdik, *Tett.* **1992**, *48*, 9577.

[323] S. Huo, *Org. Lett.* **2003**, *5*, 423.

[324] I. Klement, P. Knochel, K. Chau, G. Cahiez, *Tett. Lett.* **1994**, *35*, 1177.

[325] Y. A. Fialkov, S. V. Shelyazhenko, L. M. yagupol'skii, *Zh. Org. Kh. Engl. Ed.* **1983**, 933.

[326] N. Terasawa, H.Monobe, K. Kiyohara, Y. Shimizu, *Chem. Commun.* **2003**, 1678.

[327] N. Terasawa, H.Monobe, K. Kiyohara, Y. Shimizu, *Chem. Lett.* **2003**, *32*, 214.

[328] J. Visjager, T. A. Tervort, P. Smith, *Polymer* **1999**, *40*, 4533.

[329] F. Tran, B. Alameddine, T. A. Jenny, T. A. Wesolowski, **2004**, In Prep.

[330] J. Lindley, *Tett.* **1984**, *40*, 1433.

[331] Y. Shirota, T. Kobata, N. Noma, *Chem. Lett.* **1989**, *7*, 1145.

[332] T. Yamamoto, Y. Kurata, *Can. J. Chem.* **1983**, *61*, 86.

[333] M. Thelakkat, J. Hagen, D. Haarer, H.-W. Scmidt, *Synthetic Metals* **1999**, *102*, 1125.

[334] M. J. Plater, M. McKay, T. Jackson, *J. Chem. Soc., Perkin Trans. 1* **2000**, 2695.

[335] V. A. Tarasievich, S. M. Mikhalevskaya, N. G. Kozlov, *Russ. J. Org. Chem.* **1997**, *33*, 1100.

[336] H. B. Goodbrand, N.-X. Hu, *J. Org. Chem.* **1999**, *64*, 670.

[337] J. C. Antilla, S. L. Buchwald, *Org. Lett.* **2001**, *3*, 2077.

[338] S.-K. kang, D.-H. Kim, J.-N. Park, *Synlett* **2002**, 427.

[339] F. Y. Kwong, A. Klapars, S. Buchwald, *Org. Lett.* **2002**, *4*, 581.

[340] X. Huang, S. L. Buchwald, *Org. Lett.* **2001**, *3*, 3417.

[341] M. A. Ali, S. L. Buchwald, *J. Org. Chem.* **2001**, *66*, 2560.

[342] G. H. Yang, S. L. Buchwald, *J. Organometall. Chem.* **1999**, *576*, 125.

[343] J. P. Wolfe, S. Wagaw, J.-F. Marcoux, S. L. Buchwald, *Acc. Chem. Res.* **1998**, *31*, 805

[344] J. F. Hartwig, M. Kawatsura, S. I. Hauck, K. H. Shaughnessy, L. M. Alcazar-Roman, *J. Org. Chem.* **1999**, *64*, 5575.

[345] J. F. Hartwig, *Angew. Chem. Int. Ed.* **1998**, *37*, 2046.

[346] T. Yamamoto, M. Nishiyama, Y. Koie, *Tett. Lett.* **1998**, *39*, 2367.

[347] M. S. Viciu, R. M. Kissling, E. D. S. P. Nolan, *Org. Lett.* **2002**, *4*, 2229.

[348] G. A. Grasa, M. S. Viciu, J. Huang, S. P. Nolan, *J. Org. Chem.* **2001**, *66*, 7729.

[349] B. H. Lipshutz, H. Ueda, *Angew. Chem. Int. Ed.* **2000**, *39*, 4492.

[350] J. F. Hartwig, F. Paul, *J. Am. Chem. Soc.* **1995**, *117*, 5373.

[351] C. Amatore, A. Jutand, M. A. M'Barki, *Organometallics* **1992**, *11*, 3009

[352] U. K. Singh, E. R. Strieter, D. G. Blackmond, S. L. Buchwald, *J. Am. Chem. Soc.* **2002**, *124*, 14104.

[353] L. M. Alcazar-Roman, J. F. Hartwig, A. L. Rheingold, L. M. Liable-Sands, I. A. Guzei, *J. Am. Chem. Soc.* **2000**, *122*, 4618.

[354] M. P. Doyle, W. J. Bryker, *J. Org. Chem.* **1979**, *44*, 1572.

[355] K. P. Chary, S. R. Ram, D. S. Iyengar, *Synlett* **2000**, 683.

[356] J. Louie, J. F. Hartwig, *J. Am. Chem. Soc.* **1997**, *119*, 11695.

[357] J. F. Hartwig, F. E. Goodson, J. Louie, S. Hauck, in *Polym. Mat. Sc. and Eng., Vol. 80*, **1999**, pp. 41.

[358] J. F. Hartwig, *Polym. prep.* **2000**, *41*, 420.

[359] F. Paul, J. Patt, J. F. Hartwig, *Organometallics* **1995**, *14*, 3030.

[360] M. Tamano, S. Okutsu, in *US patent*, Toyo Ink Manaufacturing, United states, US005968675, **1999**.

[361] S. Xie, in *US patent 20030031893A1*, **2003**, p. 48.

[362] K. H. Grellmann, U. Schmitt, *J. Am. Chem. Soc.* **1982**, *104*, 6267.

[363] H. Weller, K. H. Grellmann, *J. Am. Chem. Soc.* **1983**, *105*, 6268.

[364] P. Bhattacharyya, S. S. Sagar, A. K. Dey, *Chem. Commun.* **1984**, *24*, 1668.

[365] M. Raposo, M. Manuela, A. Oliveira-Campos, P. Shanon, *J. Chem Res., Synop.* **1997**, *10*, 354.

[366] A. B. Mandal, F. Delgado, T. Joaquín, *Synlett* **1998**, *1*, 87.

[367] M. Moreno-Manas, R. Pleixats, S. Villaroya, *Synlett* **1999**, *12*, 1996.

[368] T. Wirth, U. S. Hirt, *synthesis* **1999**, *8*, 1271.

[369] R. S. Ward, D. D. Hughes, *Tetrahedron* **2001**, *57*, 5633.

[370] M. Thelakkat, *Macromol. Mater. Eng.* **2002**, *287*, 442.

[371] Y. Kuwabara, H. Ogawa, H. Inada, N. Noma, Y. Shirota, *Adv. Mater.* **1994**, *6*, 677.

[372] S. Sasaki, M. Iyoda, *Chem. Lett.* **1995**, 1011.

[373] H. Tanaka, S. Tokito, Y. Taga, A. Okada, *Chem. Commun.* **1996**, 2175.

[374] J. Shi, in *European Patent 1156536A2*, Germany, **2001**, p. 22.

[375] L. Pryzbilla, J.-D. Brand, K. Yoshimura, H. J. Räder, K. Müllen, *Anal. Chem.* **2000**, *72*, 4591.

[376] K. Yoshimura, L. Przybilla, S. Ito, J. D. Brand, M. Wehmeir, H. J. Rader, K. Mullen, *Macromol. Chem. Phys.* **2001**, *202*, 215.

[377] S. P. Brown, I. Schnell, J. D. Brand, K. Müllen, H. W. Spiess, *J. Mol. Str.* **2000**, *521*, 179.

[378] A. B. Pangborn, M. A. Giardello, R. H. Grubbs, R. K. Rosen, R. K., F. J. Timmers, *Organometallics* **1996**, *15*, 1518.

VII. Curriculum Vitae

BASSAM A. ALAMEDDINE

Osta Bldg. Tarik al jadida
Beirut
Lebanon
Tel.: +9611652684 / +9613814606 (Cellular phone)
Email: balameddine@hotmail.com

EDUCATION

University of Fribourg, Fribourg, Switzerland ▪ 2000 – 2004
Ph.D. in Natural Sciences, Organic and Metal organic Chemistry
Dissertation: “Synthesis and Investigation of New Large Self-Assembled Supramolecules as Potential Electron Emitters”.

Ecole Nationale Supérieure de Chimie - National Polytechnic Institute, Toulouse, France ▪ 1999 –2000
M. Sc. Degree, Materials Science and Engineering
Thesis: “Development of a Procedure for the Elaboration of Thin Quasicrystalline Films by Chemical Vapor Deposition”
Rank: First foreign student.

Beirut Arab University, Beirut, Lebanon ▪ 1995 –1999
B.Sc., Analytical chemistry
Degree: Very Good (Total of four years of studies).

AWARDS

- Swiss National Science Foundation (FNS), University of Fribourg, Switzerland 2000 – present.

WORK EXPERIENCE

- 1st March 2001 – present: **Assistant**; University of Fribourg, Organic Chemistry Department.
- 1st July – 14th September 1998: **Quality Control Department**; AR. Chamsin Est. for Beauty products fabrication – Beirut, Lebanon.
- 1st July – 3rd October 1997: **Training**; Itani medical laboratory – Beirut, Lebanon.
- 7th July – 2nd October 1996: **Training**; Jarkas Foundry – Beirut, Lebanon.
- 1997–1999: **Private Courses Teaching in Chemistry, Physics and Mathematics** for secondary classes’ students.

ADDITIONAL RELATED EXPERIENCE

- Advanced Techniques used in metal organic and organic syntheses for C-C cross-coupling (e.g. Suzuki, Sonogashira, Heck, Stille, Hartwig, Negishi, Kumada etc.).
- Formation on the different instrumental analysis techniques utilized in chemistry (NMR, Solid-state NMR, MS, GC, GC/MS, FT–IR, UV–VIS).
- Practical knowledge in the different electron microscopy techniques (SEM, TEM, AFM, EDX).
- Capacity of mounting and assembling the reactors used in the chemical vapor deposition technique (CVD).

PUBLICATIONS AND PARTICIPATIONS

- Alameddine, B.; Jenny, T. A. *"Synthesis and characterization of large self-assembled disc-shaped supramolecules: Potential conducting devices" Chimia* **2003**, *57*, 445.
- Alameddine, B.; Jenny, T. A.; Ruffieux, P.; Groening, O.; Groening, P.; L.Schlapbach *"Synthesis and Investigation of New Disc-Shaped Conducting Supramolecules" Chimia* **2002**, *56*, 357.
- Alameddine, B.; Jenny, T. A.; Ruffieux, P.; Groening, O.; Groening, P.; L.Schlapbach *"Electron Emission from Disc-Shaped Supramolecules for Flat Panel Displays"* In *SFC Eurochem*; SFC: Toulouse, **2002**, pp 3-1.
- Alameddine, B.; Jenny, T. A. *"Synthesis and Investigation of New Triaryl Amine Compounds" Chimia* **2001**, *55*, 638.
- *"Synthesis and Investigation of New Disc-Shaped Conducting Supramolecules"* Poster presented at the NFP47-FNS reunion, Bern, Switzerland ▪ **2001**.

LANGUAGES

Arabic – native language; **English and French** – speak fluently and read/write with high proficiency.

MEMBERSHIPS

New Swiss Chemical Society.

Lebanese Chemical Society.

HOBBIES

Psychology, Sociology, History and Culture.